THE JOURNAL
OF
CHEMICAL PHYSICS

VOLUME 20, NUMBER 8 AUGUST, 1952

Self-Diffusion in Solid Sodium. I

NORMAN H. NACHTRIEB, EDWARD CATALANO, AND JOHN A. WEIL
Institute for the Study of Metals, University of Chicago, Chicago, Illinois

(Received February 25, 1952)

Measurements are reported for the self-diffusion of solid sodium over the temperature range, 0°–95°C. The data fit the empirical equation $D=.242\exp(-10{,}450/RT)$ with an uncertainty of ± 300 cal mole^{-1} in the heat of activation. The entropy of activation calculated from the temperature coefficient of the elastic modulus is in agreement with the value based upon the vacancy mechanism.

THE diffusion measurements here reported are the first to result from a systematic study of diffusion phenomena among the alkali metals. Heretofore, no experimental attention has been directed to the kinetics of atom movement for this group of elements. The simplicity of their crystal structure (all are body-centered cubic), the accuracy with which their cohesive properties are known, and the comparative absence of ion-core interactions recommend their study in the search for a detailed mechanism of solid state atom mobility. It is probable, of course, that different mechanisms predominate in different solids, and a complete understanding of atomic movements in the open body-centered metals whose ions have the electron configurations of rare gases does not imply an equally full knowledge of diffusion phenomena in all solids. Huntington and Seitz,[1] in their theoretical appraisal of mechanisms of self-diffusion in copper, concluded that the vacancy model is energetically preferable to either the interstitial or direct interchange mechanisms. In sodium, however, Huntington[2] pointed out that interstitial atom movements might compete favorably with the mechanism based upon the Schottky-Wagner or Frenkel theories of equilibrium lattice vacancies.

More recently, the Bernal direct interchange mechanism has been extended by Zener[3] to the cooperative rotation of rings of 4 or more atoms with a lowering of the activation required in the case of copper. Paneth[4] has discussed the possibility that diffusion in sodium may arise through the crowding of an adventitious atom into a (111) array. The relaxation of the resulting linear dislocation would result in atom movements along the (111) directions. Paneth's estimate of the activation energy for self-diffusion in sodium by the "crowdion" mechanism is less than 7000 cal mole^{-1}.

[1] H. B. Huntington and F. Seitz, Phys. Rev. **61**, 315 (1942).
[2] H. B. Huntington, Phys. Rev. **61**, 325 (1942).
[3] C. Zener, Acta Cryst. **3**, 346 (1950).
[4] H. Paneth, Phys. Rev. **80**, 708 (1950).

EXPERIMENTAL

Metallic radioactive sodium was prepared[5] from a tracer $Na^{22}Cl$ solution[6] by means of the exchange reaction:

$$Na_{(l)}{}^{23}+Na^{22}Cl_{(s)}\rightarrow Na_{(l)}{}^{22}+Na^{23}Cl_{(s)}.$$

The resulting metal had an activity of about 800 disintegrations mg^{-1} min^{-1}, and since the isotope has a half-life of 2.6 years, no decay corrections were necessary. Cylinders of ordinary sodium and of radioactive sodium $\frac{1}{2}$ in. in diam and $\frac{1}{2}$ in. in length were prepared by pipetting an excess of molten metal into stainless steel dies* (Fig. 1) under paraffin oil. When the cylinders had solidified, they were compressed in their respective dies under 2000 psi in a hydraulic press. The adhering paraffin was then washed away with petroleum ether and the flashing of excess sodium was removed

[5] Nachtrieb, Weil, and Catalano, J. Am. Chem. Soc. **74**, 264 (1952).
[6] Supplied by the Isotopes Division, AEC, Oak Ridge, Tennessee.

* The dies were constructed with removable locating pins for the purpose of assembling them coaxially. The walls of the holes and the end surfaces were lapped to a mirror finish to avoid galling by sodium. The compression pin (see Fig. 1) diameter was 0.0005 in. less than the hole diameter. The screws and pins used for holding the dies together were of the same composition to avoid dimensional changes during immersion in liquid nitrogen. The authors are very much indebted to J. Getzholtz, E. Masny, and E. Blume for the construction of these precision dies.

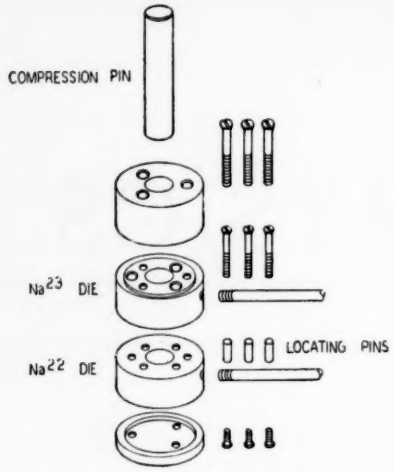

FIG. 1. Details of diffusion dies.

with a keen flat blade. In order to prevent oxidation of the clean metal surfaces this cutting operation was performed under liquid nitrogen. Sodium metal surfaces so prepared remained bright for hours at −196°C, even though no unusual precautions were taken to avoid the precipitation of ice in the liquid nitrogen from the moisture of the air. Oxide films were occasionally encountered, but were easily recognized from the abnormal shape of the resulting diffusion profile (vide infra). The dies were assembled under liquid nitrogen by means of locating pins and screws. They were then removed from the Dewar vessel and the cylinders pressure-welded together across their basal surfaces while still at essentially liquid nitrogen temperature. Compression at 5000 psi for one minute produced welds which would withstand tensile stresses high enough to cause visible reduction in area without failure. The dies were then transferred to an oil thermostat for the diffusion period (usually about 3 days). The thermostat temperature was controlled to within ±0.1°C.

Following the diffusion period the composite cylinder was sectioned with a hand microtome. The usual thickness of the slices was 0.05 mm (0.002 in.). Moisture in the xylene used for a protective lubricant, revealed the grain size by etching the metal surface. Usually the crystals were of the order of 5 mm in diameter. The slices were placed in weighed glass planchets (1 in. in diam×$\frac{1}{4}$ in. high) and allowed to decompose overnight to a mixture of sodium hydroxide and sodium carbonate. Dilute hydrochloric acid was then added and a uniform residue of sodium chloride formed by evaporation of the solutions under an infrared lamp. Thicknesses of the slices were calculated from the weights of the sodium chloride residues, and corrected for thermal expansion at the temperature of the experiments. The Na^{22} activity was determined with a helium-propane gas flow counter and a conventional scaler. At least 10^4 counts were obtained for the majority of samples. Corrections for coincidence counting were not made since they lay within the over-all experimental error for the counting rates involved.

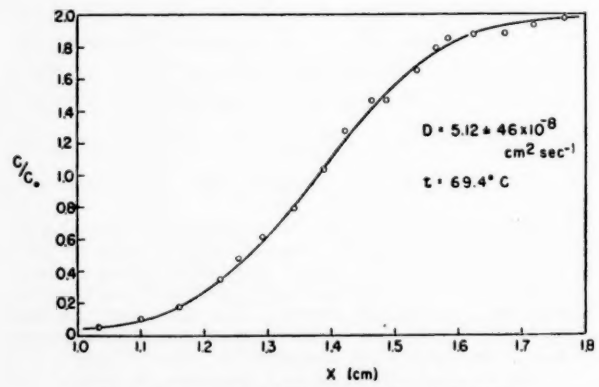

FIG. 2. Three-day diffusion profile at 69.4°C.

CALCULATIONS

The general one-dimensional differential equation which expresses the rate of diffusion is Fick's Law:

$$\frac{\partial c}{\partial t}=\frac{-\partial}{\partial x}\left(D\frac{\partial c}{\partial x}\right). \tag{1}$$

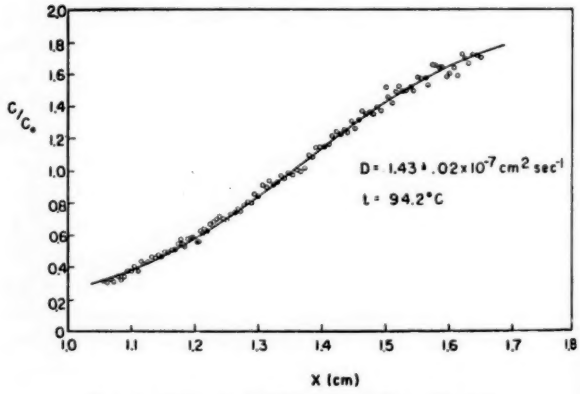

FIG. 3. Three-day diffusion profile at 94.2°C.

For the special case of self-diffusion the coefficient is independent of concentration, and the law may be more simply expressed as

$$\frac{\partial c}{\partial t}=-D\frac{\partial^2 c}{\partial x^2}. \tag{2}$$

The particular solution depends upon the geometry of the diffusion system. In the present case diffusion occurred across a plane separating two cylinders which were, for practical purposes, of infinite extent. If the original specific activity of the radioactive cylinder is designated as $2C_0$ and the specific activity at any point in the composite cylinder after a time t is represented by C, then the boundary conditions are

	$x<x_0$	$x>x_0$
for	$t=0,\ C=0$	$C=2C_0,$
for	$t>0,\ C=\phi(x,t)$	$C=\phi(x,t),$

where x_0-x is the distance from the interface. For these boundary conditions the solution of the differential equation is

$$\frac{C}{C_0}=1-\frac{2}{(\pi)^{\frac{1}{2}}}\int_0^{x_0-x/2(Dt)^{\frac{1}{2}}}\exp[-y^2]dy. \qquad (3)$$

Figures 2 and 3 show typical diffusion profiles from which, by the use of the time of the experiment and tables of the error integral, series of values of D were calculated as a function of x_0-x. The average values of D so obtained were used to construct the solid lines. Table I records the values of the self-diffusion coefficient obtained for temperatures ranging from 0°C to 95°C. Diffusion cylinders in which a barrier of oxide separated the two halves gave diffusion profiles for which the calculated values of D varied with distance from the boundary; in extreme cases the profile was almost discontinuous in the neighborhood of the boundary. The uncertainties in D given in Table I are the mean deviations from the average value of D for each profile.

TABLE I. Self-diffusion coefficients of sodium.

T (°K)	D (cm² sec⁻¹)
273.5	$9.22\times10^{-10}\pm2.47\times10^{-10}$
274.2	$9.66\times10^{-10}\pm2.15\times10^{-10}$
312.6	$1.31\times10^{-8}\pm0.02\times10^{-8}$
312.6	$1.24\times10^{-8}\pm0.06\times10^{-8}$
342.6	$5.26\times10^{-8}\pm0.46\times10^{-8}$
367.4	$1.43\times10^{-7}\pm0.02\times10^{-7}$

ACTIVATION ENERGY

The diffusion data given in Table I fit a simple Arrhenius rate expression, as Fig. 4 shows. The equation of the straight line is

$$D=0.242\exp(-10{,}450/RT). \qquad (4)$$

The uncertainty associated with the activation energy is estimated to be ±300 cal mole⁻¹ from lines drawn with maximum and minimum possible slope through the error ranges of the experimental points. To the authors' knowledge this is the lowest activation energy reported to date for solid metal diffusion, and is in accord with the qualitative correlation[7] between the activation energy for diffusion in a metal on the one hand and its melting point and hardness on the other. Calculation of the heat of activation from the Langmuir-Dushman semi-empirical equation:[8]

$$D=\frac{\Delta Ha^2}{Nh}\exp(-\Delta H/RT), \qquad (5)$$

where N = Avogadro's number and h = Planck's constant, gives the remarkably close value of 10,300 cal mole⁻¹. The value of D at 312.4°K was used for the calculation, and the unit cell parameter (4.28A) was taken for a.

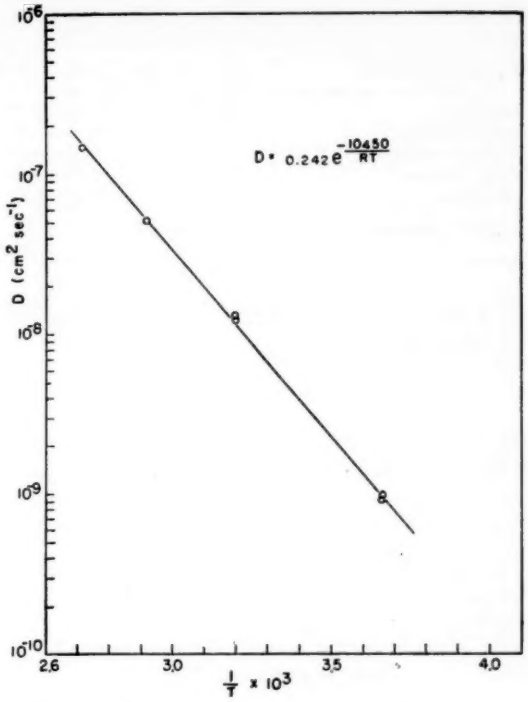

FIG. 4. Plot of log D *versus* $1/T$.

ENTROPY OF ACTIVATION

Evidence favoring the vacancy mechanism of diffusion in sodium may be adduced from calculations of the entropy of activation. The Arrhenius equation in the notation of diffusion,

$$D=D_0\exp(-\Delta H/RT), \qquad (6)$$

may be rewritten, as Zener has done,[9] by use of the second law of thermodynamics

$$\Delta F=\Delta H-T\Delta S. \qquad (7)$$

Thus,

$$D=D_0\exp(-\Delta F/RT)\exp(-\Delta S/R), \qquad (8)$$

where ΔF is the isothermal work required to move one gram atom of sodium atoms reversibly from equilibrium lattice sites to positions corresponding to the saddle configuration in the elementary diffusion act. ΔS is the associated entropy change of the system.

D may also be written quite generally as a random walk expression by

$$D=\tfrac{1}{6}\textstyle\sum_i\Gamma_i\delta_i^2, \qquad (9)$$

where Γ_i is the mean jump frequency, δ_i is the associated elementary jump distance, and the summation extends over all jump modes i. For an isotropic solid

[7] R. M. Barrer, *Diffusion in and through Solids* (Macmillan Company, New York, 1941), p. 302.
[8] I. Langmuir and S. Dushman, Phys. Rev. **20**, 113 (1922).
[9] C. Zener, J. Appl. Phys. **22**, 372 (1950).

TABLE II. Entropies of activation for self-diffusion in sodium.

Assumed mechanism		ΔS_{exp} (cal mole^{-1} deg^{-1})
Vacancy	1	7.31±0.80
Interstitial	$\frac{1}{6}$	10.86±0.80
Direct interchange	1	7.31±0.80
Ring (4 atom)	6	3.75±0.80
Crowdion	$\frac{1}{8}$	11.43±0.80
Elastic modulus	$\Delta S_{theor.}=7.70$	

Γ_i has a single value and is related to the characteristic lattice vibration frequency ν by

$$\Gamma_i=\nu\exp(-\Delta F/RT). \tag{10}$$

δ_i may be evaluated for any given structure by relating it to the unit cell parameter by defining

$$\tfrac{1}{6}\textstyle\sum_i\delta_i^2\equiv\gamma a^2. \tag{11}$$

γ is a coefficient which depends upon the unit cell geometry and the assumed jump mechanism. Combination of Eqs. (9), (10), and (11) gives

$$D=\gamma a^2\nu\exp(-\Delta F/RT), \tag{12}$$

and comparison of Eqs. (8) and (12) shows that

$$D_0=\gamma a^2\nu\exp(\Delta S/R). \tag{13}$$

The values of ΔS calculated from Eq. (13) are designated ΔS_{exp} since they depend upon the experimentally determined value of D_0.†

Zener has calculated the values of γ which are given in Table II for diffusion by vacancy, interstitial, and ring mechanisms in a b.c.c. lattice. γ for the crowdion mechanism may be calculated as follows: Γ denotes the frequency with which a crowdion advances by its minimum jump distance in a particular [111] direction.

According to Paneth a crowdion consists of about nine atoms compressed into the distance normally occupied by eight atoms in the (111) direction. As a crowdion relaxes, it therefore moves a distance $\delta=a\sqrt{3}/16$, and each of the eight atoms within the crowdion advances by this amount. The result is as though one atom had moved a distance $a\sqrt{3}/2$. Thus, from Eq. (11),

$$\gamma a^2=\tfrac{1}{6}(a\sqrt{3}/2)^2$$

and $\gamma=\frac{1}{8}$.

† ΔS_{exp} also depends upon the assumed diffusion mechanism, and the seemingly arbitrary designation "Experimental" is used to distinguish values so obtained from a "Theoretical" entropy to be calculated later from elastic moduli.

The values of ΔS_{exp} recorded in Table II were calculated from Eq. (13) with the appropriate γ's and with $\nu=3.33\times10^{12}$ sec^{-1} (calculated from the Debye critical temperature for sodium, $\theta_D=159°$K). The uncertainties assigned to the entropies arise from the experimental uncertainty in D_0 and ΔH. Each of the mechanisms leads to a positive entropy of activation, in accordance with Zener's argument.

Zener has also shown a correlation between the entropy of activation for diffusion and the temperature coefficient of the appropriate elastic modulus. Thus if all of the free energy of activation in self-diffusion goes into the elastic distortion of the lattice, the temperature coefficient of the elastic modulus should give the entropy of activation for diffusion:

$$\frac{1}{\Delta F_0}\frac{d\Delta F}{dT}=\frac{1}{\mu_0}\cdot\frac{d\mu}{dT}, \tag{14}$$

where ΔF_0 and μ_0 are the free energy and elastic modulus at the absolute zero, respectively. Since

$$(d\Delta F/dT)_P=-\Delta S, \tag{15}$$

Eq. (14) may be written

$$\Delta S=-\frac{\Delta F_0}{\mu_0}\cdot\frac{d\mu}{dT}. \tag{16}$$

ΔH varies only slightly, if at all, with temperature and may be used in place of ΔF_0. The quantity $1/\mu_0\cdot d\mu/dT$ was calculated to be 7.229×10^{-4} sec^{-1} from the precise data of Quimby and Siegel[10] for the S_{11} elastic modulus. $\Delta S_{theor.}$ so calculated has the value 7.70 cal mole^{-1} deg^{-1} and is in excellent agreement with ΔS_{exp} based upon the vacancy mechanism. ΔS_{exp} for the direct interchange mechanism has the same value, but diffusion by this process can probably be excluded on energetic considerations.

ACKNOWLEDGMENTS

The authors would like to express their appreciation to Professor C. Zener, Professor A. W. Lawson, and Professor C. S. Barrett for their continual interest and assistance, and to Dr. R. Gomer and Dr. A. Brooks for many helpful discussions. The work described was supported in part by the Air Materiel Command, Wright-Patterson Field, under United States Air Force Contract AF-33(038)-6534.

[10] S. L. Quimby and S. Siegel, Phys. Rev. **54**, 293 (1938).

Self-Diffusion in Solid Sodium. II. The Effect of Pressure

N. H. NACHTRIEB, J. A. WEIL, E. CATALANO, AND A. W. LAWSON
Institute for the Study of Metals, University of Chicago, Chicago, Illinois

(Received February 25, 1952)

Hydrostatic pressure is found to decrease the rate of self-diffusion in sodium. The free energy of activation is a linear function of the melting point, and the enthalpy of activation is proportional to the melting point. For sodium and for all cubic metals (except lead and tungsten) for which diffusion data exist the enthalpy of activation is related to the latent heat of fusion by the equation $\Delta H = 16.5\ L_m$. The change in D_0 for sodium with pressure is expressible in terms of the compressibility and the activation entropy change.

THERE are only a few recorded attempts to determine the effect of pressure on the rate of diffusion in metals. Johnston and Adams[1] made a passing reference to a study which indicated that hydrostatic pressures increase the mobility of atoms in solid metals. Radavich and Smoluchowski,[2] on the other hand, found the diffusion coefficient of Al in an Al—Cu alloy to decrease about 30 percent by application of a pressure of 7000 kg/cm² at 500°C. The alkalies are the most compressible of metals, so that relatively large effects of pressure on their rate of diffusion might be expected.

Such experiments are of interest because pressure should alter the concentration of crystals defects which may play a role in diffusion as well as reduce the mobility of the diffusing atoms. In diffusion by direct interchange or ring rotation mechanisms lattice imperfections are not involved, and the reduction of the atomic jump frequency by pressure is the controlling factor in the change in diffusion rate. If diffusion were to proceed by means of interstitial atoms or by the crowdion mechanism,[3] the decrease in jump frequency by pressure would be partially compensated or might possibly be over-compensated by an increase in the number of defects. Diffusion rates could conceivably increase with pressure if the latter mechanisms were operative. If, however, diffusion is controlled by the migration of atoms into vacant lattice sites, pressure should reduce the equilibrium concentration of vacancies as well as their volumes, and the diffusion rate should be reduced by these effects in addition to the reduction in jump frequency.

Unfortunately, at the present time direct experimental techniques are not available for separating the effect of jumping time from the effect of concentration of defects on the self-diffusion rate of metals. Nevertheless, experimental data on the pressure dependence of self-diffusion coupled with other evidence permit tentative and suggestive conclusions to be drawn concerning the mechanism of self-diffusion in sodium.

EXPERIMENTAL

The preparation of diffusion cylinders of sodium 23 and sodium 22 and the procedure followed in sectioning the diffusion couple have been described in the preceding paper.[4] The ½-in. diam.×1-in. long sodium cylinders were subjected to hydrostatic pressures in a hydraulic press of established design.[5] A silicone oil (Dow-Corning 200) or hexane were used as the hydraulic fluid. The high pressure bomb which contained the diffusion cylinders was immersed in an oil thermostat for temperatures up to 90°C. A cylindrical furnace surrounded the bomb for the 130° experiments. A continuous record of temperature was provided by a recording potentiometer with a chromel-alumel thermocouple inserted into a well in the bomb plug. A continuous record of pressure was provided by a manganin coil pressure gauge located in the hydraulic fluid in the upper cylinder of the press. The resistance of the gauge was measured with a Wheatstone bridge, an unbalance current in the bridge being used to operate a second recording potentiometer. The bomb was preheated before insertion of the diffusion cylinders in order that the "time at temperature" might be known to within 0.5 percent. On the average experiments were of the order of 2.5×10^5 seconds (3 days), but a few experiments at high pressure and low temperature were continued for as long as 10^6 seconds.

Densities of sodium which are necessary for the calculation of the distance of penetration were obtained by use of Hagen's formula[6] for the thermal coefficient of expansion and Bridgman's data[7] for the compressibility of sodium.

EXPERIMENTAL RESULTS

Three series of experiments are recorded in Table I. The first group comprises the 1 kg/cm² isobar earlier reported for the temperature range 0°–95°C. The second group provides a 90°C isotherm for pressures ranging from 1 kg/cm² to 12,000 kg/cm². The third group comprises an isobar at 8000 kg/cm² for the tem-

[1] Johnston and Adams, Z. anorg. u. allgem. Chem. **80**, 328 (1913).
[2] F. J. Radavich and R. Smoluchowski, Phys. Rev. **65**, 62 (1944).
[3] H. Paneth, Phys. Rev. **80**, 708 (1950).
[4] Nachtrieb, Catalano, and Weil, J. Chem. Phys. **20**, 1185 (1952).
[5] P. Bridgman, *Physics of Solids* (G. Bell and Sons, London, 1949).
[6] E. Hagen, Wied. Ann. Physik **19**, 436 (1883).
[7] P. W. Bridgman, Proc. Am. Acad. Arts Sci. **58**, 166 (1923).

TABLE I. Summary of sodium diffusion data.

P (kg/cm²)	T(°K)	T_m(°K)	T_m/T	D (cm² sec⁻¹)	ΔD
1	367.4	370.7	1.009	1.43×10^{-7}	$\pm0.02\times10^{-7}$
1	363.2	370.7	1.021	1.23×10^{-7}	$\pm0.02\times10^{-7}$
1	342.6	370.7	1.082	5.26×10^{-8}	$\pm0.46\times10^{-8}$
1	312.6	370.7	1.186	1.24×10^{-8}	$\pm0.06\times10^{-8}$
1	312.6	370.7	1.186	1.31×10^{-8}	$\pm0.02\times10^{-8}$
1	274.2	370.7	1.352	9.66×10^{-10}	$\pm2.15\times10^{-10}$
1	273.5	370.7	1.355	9.22×10^{-10}	$\pm2.47\times10^{-10}$
4030	363.2	402.5	1.111	2.89×10^{-8}	$\pm0.04\times10^{-8}$
7970	363.2	428.0	1.178	1.14×10^{-8}	$\pm0.11\times10^{-8}$
8060	363.2	428.0	1.178	1.03×10^{-8}	$\pm0.05\times10^{-8}$
8550	363.2	431.2	1.187	6.96×10^{-9}	$\pm0.23\times10^{-9}$
12000	363.2	450.4	1.240	3.09×10^{-9}	$\pm0.11\times10^{-9}$
8000	308.2	428.0	1.388	5.02×10^{-10}	$\pm0.07\times10^{-10}$
8000	329.2	428.0	1.300	1.48×10^{-9}	$\pm0.03\times10^{-9}$
8000	331.2	428.0	1.290	1.79×10^{-9}	$\pm0.06\times10^{-9}$
8000	405.1	428.0	1.057	4.42×10^{-8}	$\pm0.06\times10^{-9}$
8000	405.1	428.0	1.057	3.93×10^{-8}	$\pm0.06\times10^{-9}$

perature range 35°–130°C. The two isobars are fitted by the empirical equations

$$D_1=0.242\exp(-10{,}450/RT)(\text{cm}^2\ \text{sec}^{-1}), \quad (1)$$

$$D_{8000}=0.176\exp(-12{,}060/RT). \quad (2)$$

Table II lists the enthalpy, free energy, and entropy of activation of diffusion derived from the 90°C isotherm. Table III presents values of the activation volume calculated from the Clapeyron relationship and from the pressure variation of the isothermal diffusion coefficients. Table IV shows a comparison of the enthalpies of activation which have been reported for diffusion in other cubic metals with values calculated from the latent heat of fusion.

DISCUSSION

A. Heat and Free Energy of Activation

As stated in the introduction, no unique conclusions can be drawn concerning the mechanism of diffusion in metals from the pressure dependence of the diffusion rate alone. Such a decision must depend upon direct measurement of the mean jump frequency. Variation of the pressure does, however, permit the use of certain formal thermodynamic relationships with interesting consequences.

In a completely general way the diffusion coefficient for a cubic metal may be expressed by the equation

$$D=\gamma a^2\nu e^{-\Delta F/RT}, \quad (3)$$

where γ = a constant whose magnitude is determined by the lattice geometry and the assumed jump mechanism, a = the unit cell parameter, ν = the average vibration frequency of atoms in the direction of the elementary jump, and ΔF = the free energy of activation.* With equal generality Eq. (3) may be written as

$$D=\gamma a^2\nu e^{-\Delta H/RT}e^{\Delta S/R}, \quad (4)$$

where ΔH and ΔS are the associated enthalpy and entropy of activation. At constant pressure ΔH is given as the slope of a plot of $-R\ln D$ against $1/T$. Figure 1 shows such a plot for diffusion isobars at 1 kg/cm² and 8000 kg/cm², and the corresponding heats of activation are 10,450 and 12,060 cal mole⁻¹. The small variation of a and ν with temperature are neglected in the calculations of the heats of activation.

The free energy of activation may be obtained directly from Eq. (3) if a and ν are known as functions of pressure. The values of a in Table II were calculated from Bridgman's data[7] for the compressibility of sodium. The characteristic lattice frequency has been used to approximate ν,† and numerical values have been calculated (see Table II) by means of the Lindemann relation, $\theta_0=C(T_m/MV^{\frac{2}{3}})^{\frac{1}{2}}$, with $C=115$ for sodium.[8] Essentially the same numerical results are obtained if ν is calculated from the Grüneisen relation and the compressibilities. Table II lists the value for ΔF at atmospheric pressure and the values of ΔF calculated from the 90°C diffusion isotherm for pressures ranging up to 12000 kg/cm². ΔS is calculated from ΔF and ΔH for 1 kg/cm² and 8000 kg/cm² (the two pressures for which ΔH is known) by means of the second law of thermodynamics at 90°C (363.2°K). $d\Delta S/dP$ has the average value -9.10×10^{-5} cal mole⁻¹ deg⁻¹ atmos⁻¹ over this pressure range at 90°C.

TABLE II. Free energy, enthalpy, and entropy of activation at 90°C.

P(kg/cm²)	a(cm $\times10^8$)	ν(sec⁻¹ $\times10^{-12}$)	$D/\gamma a^2\nu$	ΔF(cal mole⁻¹)	ΔH(cal mole⁻¹)	ΔS(cal mole⁻¹ deg⁻¹)
1	4.310	3.330	1.99×10^{-5}	7800	10,450	7.31
4030	4.240	3.539	4.54×10^{-6}	8935		
7970			1.78×10^{-6}	9605		
8060	4.146	3.718	1.60×10^{-6}	9685	12,060	6.58
8550			1.09×10^{-6}	9968		
12000	4.078	3.872	4.80×10^{-7}	10,570		

* A more complete discussion of the significance of ΔF is deferred to Part B.

† Whether it is appropriate to employ the characteristic lattice frequency for ν depends upon the actual mechanism of diffusion. Presumably, it is satisfactory if diffusion proceeds by direct interchange of neighbors but would be somewhat too high for a Schottky mechanism and too low for an interstitial mechanism.

[8] F. Lindemann, Physik. Z. 11, 609 (1910).

TABLE III. Pressure dependence of volume and heat of activation.

P(kg/cm²)	T_m	ΔV_m(cm³/g atom)[a]	L_m(cal/g atom)[a]	ΔV_{act} (cm³/g atom)[b]	ΔV_{act}[c]	$\frac{\Delta V_{act}}{\Delta V_m}$[b]	ΔH_{calc}[d]	ΔH_{obs}
1	370.7	0.6410	636.2	12.25	12.36	19.11	10,440	10,450
1000	379.2	0.5877	633.0	11.55	11.12	19.65	10,685	
2000	387.2	0.5433	631.4	10.93	10.18	20.12	10,910	
3000	394.7	0.5067	629.7	10.42	9.65	20.56	11,120	
4000	402.1	0.4768	630.2	9.98	9.36	20.93	11,330	
5000	409.0	0.4526	633.4	9.59	9.10	21.19	11,530	
6000	415.7	0.4308	641.0	9.17	8.90	21.29	11,720	
7000	422.1	0.4117	650.7	8.76	8.63	21.28	11,895	
8000	428.0	0.3935	658.3	8.39	8.47	21.32	12,055	12,060
9000	434.2	0.3758	661.5	8.10	8.22	21.55	12,245	
10000	439.9	0.3578	660.9	7.81	8.12	21.83	12,395	
11000	445.4	0.3395	656.7	7.55	8.00	22.24	12,545	
12000	450.7	0.3215	650.7	7.31	7.87	22.74	12,710	

[a] P. W. Bridgman, Phys. Rev. **6** (2), 32 (1915).
[b] Calculated from $\Delta V_{act}=16.53RT_m\Delta V_m/L_m$.
[c] Obtained from $\Delta V_{act}=-RT\partial\left[\frac{\ln D/\gamma a^2\nu}{\partial P}\right]_{90°C}$.
[d] Obtained from $\Delta H=14.2/16.53\cdot\Delta V_{act}/\Delta V_m\cdot L_m$.

B. Relation between ΔF, ΔH, and ΔS and the Melting Point

An interesting relationship is found between ΔF and the melting point (a variable with pressure) if Fig. 1 is plotted in another way. Equation (3) may be written as

$$-R\ln D/\gamma a^2\nu=\Delta F/T. \tag{5}$$

Differentiation by T_m/T for $T_m=$ const gives

$$\left[\frac{d\ln D/\gamma a^2\nu}{dT_m/T}\right]_{T_m}=-\frac{1}{R}\cdot\frac{\Delta H}{T_m}. \tag{6}$$

Figure 2 shows plots of $\log D/\gamma a^2\nu$ against T_m/T for the 1 kg/cm² and 8000 kg/cm² isobars. The interesting observation to be noted is that the two straight lines are parallel with slopes equal to

$$-\Delta H(P)/RT_m=-14.2 \text{ independent of } T. \tag{7}$$

The heat of activation as a function of pressure is therefore proportional to the melting point. It should be remarked that there have been several efforts in the past to associate the enthalpy of activation for diffusion in metals with the melting point. Van Liempt[9] found that the equation $\Delta H=32T_m$ applied to a number of cubic metals, but Table IV shows that the calculated values are low for most metals but high for sodium. Van Liempt[10] and Braune[11] independently proposed an equation of the form $\Delta H=3b^2RT_m$ on the basis of the Lindemann theory of melting; here b depends upon the polarizability and radius of the atom and has a value of approximately 2 for some metals. More recently, Dienes[12] has found a rough correlation between $\Delta H/T_m$

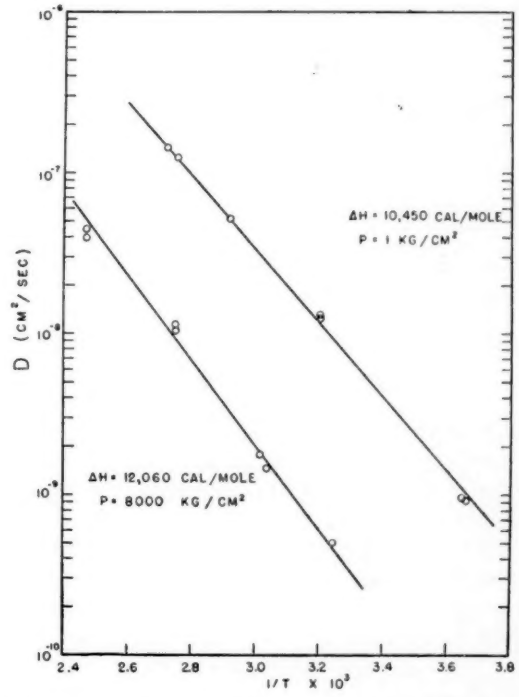

FIG. 1. Variation of D with $1/T$ at 1 kg/cm² and 8000 kg/cm².

TABLE IV. Heats of activation for self-diffusion of various cubic metals at 1 atmosphere.

Metal	T_m	L_m	ΔH_{calc}[a]	ΔH_{calc}[b]	ΔH_{obs}
Au	1336	3060	42,800	50,280	51,000
Ag	1234	2730	39,500	44,850	45,950
Cu	1357	3110	43,500	50,920	{54,000 / 48,000
W	3555	11,200	113,400	184,000	141,000
Pb	600.6	1190	19,200	19,550	27,900
Li	453	690	14,500	11,340	...
Na	370.7	636.2	11,840	10,450	10,450
K	336.8	571	10,800	9380	...
Rb	311.7	525	10,000	8625	...
Cs	301.7	500	9700	8215	...
Co	1751	3700	56,000	60,790	61,900
Fe	1808	3630	58,000	59,640	59,700

[a] $\Delta H=32\ T_m$ (Van Liempt's equation).
[b] $\Delta H=16.5\ L_m$.

[9] J. Van Liempt, Z. Physik **96**, 534 (1935).
[10] J. Van Liempt, Z. anorg. u. allgem. Chem. **195**, 366 (1931).
[11] H. Braune, Z. physik. Chem. **110**, 147 (1924).
[12] G. T. Dienes, J. Appl. Phys. **21**, 1189 (1950).

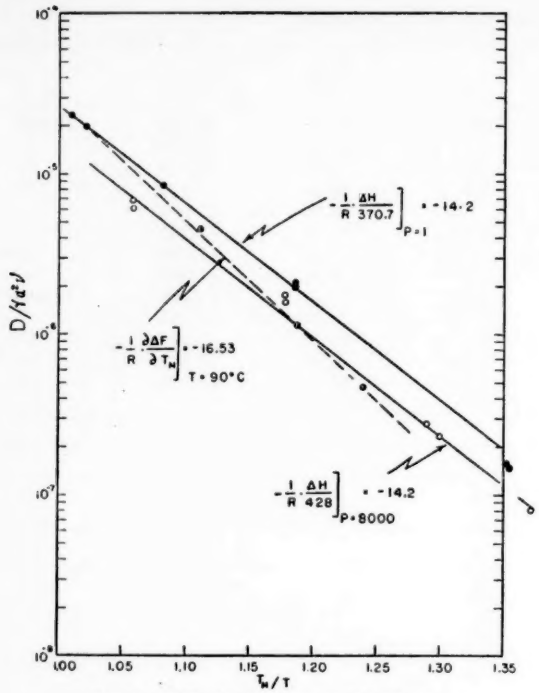

FIG. 2. Diffusion isobars and isotherm.

and $\ln D_0/a^2\nu$ for a large number of pure metals and alloys.

Differentiation of Eq. (3) by T_m/T for $T=$const (variable pressure), however, gives

$$\left.\frac{d\ln D/\gamma a^2\nu}{dT_m/T}\right]_T = -\frac{1}{R}\cdot\frac{d\Delta F}{dT_m}. \tag{8}$$

Thus, the slope of a plot of $\ln D/\gamma a^2\nu$ *versus* T_m/T for the 90°C isothermal data is equal to $-d\Delta F/RdT_m$. This isotherm is also straight and intersects the isobars at the points ($T=90$°C, $P=1$ kg/cm²) and ($T=90$°C, $P=8000$ kg/cm²). Hence, it follows that the free energy of activation is also a linear function of the melting point for a given temperature. For this 90°C isotherm the slope is

$$-d\Delta F/RdT_m = -16.53. \tag{9}$$

Integration of this equation and use of the free energy values and melting points of Tables I and II to evaluate the integration constant gives

$$\Delta F\Big]_{T=90°C} = 16.53RT_m - 4365. \tag{10}$$

Isothermal lines of ΔF at lower temperatures should cut the isobars with successively increasing slopes, since it is to be expected that ΔF approaches ΔH in the limit of absolute zero. Moreover, with a negative pressure great enough to make $T_m=0$°K, ΔH should equal zero. Figure 3 shows the relation of ΔH to ΔF and ΔS at 90°C as a function of the melting point. Substitution of ΔH and ΔF from Eqs. (7) and (10) into the second law gives the following relation for ΔS at 90°C as a function of the melting point:

$$\Delta S\Big]_{90°C} = -\frac{4.625T_m}{363.2} + \frac{4365}{363.2}. \tag{11}$$

The variation of entropy with pressure at this temperature is therefore given by

$$\left.\frac{d\Delta S}{dP}\right]_{T=90°C} = -\frac{4.625}{363.2}\cdot\frac{dT_m}{dP}. \tag{12}$$

C. The Activation Volume and the Clapeyron Equation

From Eq. (3) and the general thermodynamic relation

$$\left.\frac{d\Delta F}{dP}\right]_T = \Delta V, \tag{13}$$

it follows that

$$-RT\left.\frac{d\ln D/\gamma a^2\nu}{dP}\right]_T = \Delta V, \tag{14}$$

where ΔV may be called the volume of activation. The physical significance of this quantity is the change in volume attending the simultaneous movement of N atoms over their associated saddle configurations in an infinitely large crystal. No consideration of the detailed mechanism is involved in this interpretation. Figure 4 shows a plot of $-RT\ln D/\gamma a^2\nu$ for the 90°C isotherm *versus* pressure. Tangents to this curve provide the values of the activation volume which are plotted in Fig. 5. These values agree within the experimental error with those derived by application of the Clausius-Clapeyron equation. Differentiation of Eq. (10) by

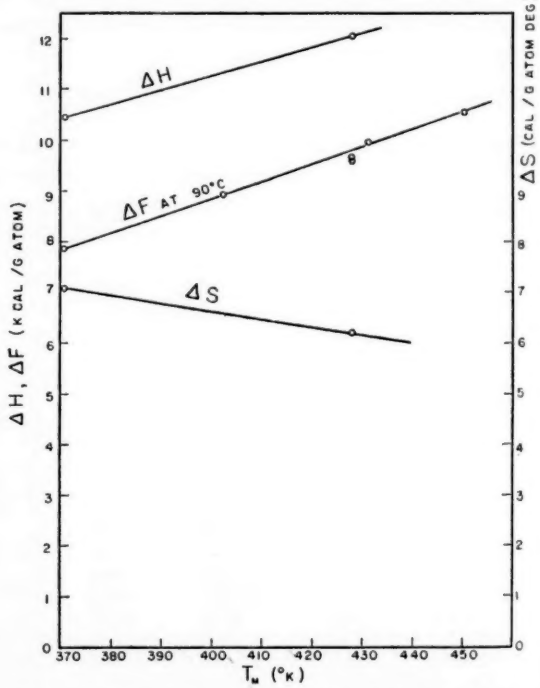

FIG. 3. Free energy, enthalpy, and entropy of activation *versus* melting point at 90°C.

pressure gives

$$\left.\frac{d\Delta F}{dP}\right]_T = \Delta V_{act} = 16.53R\frac{dT_m}{dP}. \quad (15)$$

The Clapeyron equation is

$$\frac{dT_m}{dP} = \frac{\Delta V_m}{\Delta S_m} = \frac{T_m \Delta V_m}{L_m}, \quad (16)$$

where ΔV_m, ΔS_m, and L_m are, respectively, the molar volume change on fusion, the entropy of fusion, and the latent heat of fusion. Elimination of dT_m/dP between Eqs. (15) and (16) gives the activation volume

$$\Delta V_{act} = \frac{16.53RT_m\Delta V_m}{L_m}. \quad (17)$$

Table III lists Bridgman's values for the quantities ΔV_m and L_m (derived from compressibilities), together with the values of the activation volume obtained by the two methods. The agreement serves to show the thermodynamic self-consistency of the diffusion data within the limits of experimental error.

Elimination of T_m from Eqs. (7) and (17) gives the relation

$$\Delta H(P) = \frac{14.2}{16.53}\cdot\frac{\Delta V_{act}}{\Delta V_m}\cdot L_m. \quad (18)$$

Table III shows that the ratio $\Delta V_{act}/\Delta V_m$ varies somewhat with pressure and in conjunction with Eq. (18) gives satisfactory agreement for ΔH at 1 kg/cm² and 8000 kg/cm².

It might be supposed that Eq. (18) would correlate the heats of activation with latent heats of fusion for other metals which have the same structure. This is approximately true if an initial value of 19.2 is taken for $\Delta V_{act}/\Delta V_m$. Then

$$\Delta H = 16.5L_m. \quad (19)$$

As Table IV indicates, the agreement is excellent for all cubic metals for which diffusion data are available, except tungsten and lead. It is not improbable that

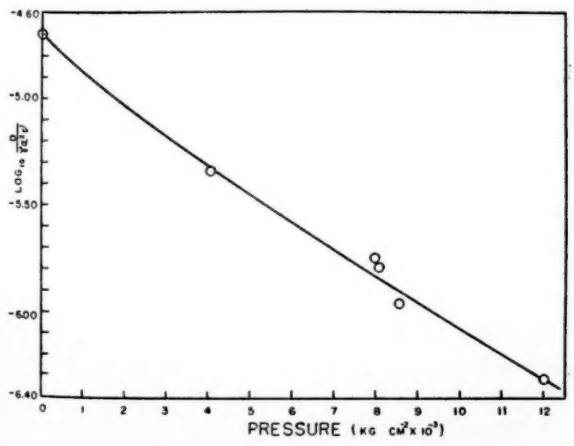

FIG. 4. Variation of $\log D/\gamma a^2\nu$ with pressure at 90°C.

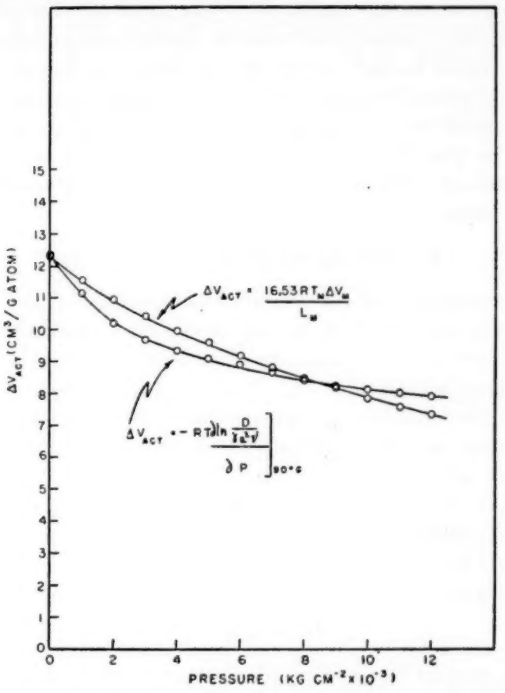

FIG. 5. Variation of activation volume with pressure at 90°C.

either the heat of activation or the latent heat of fusion of tungsten may be in error, but no explanation is offered for the discrepancy in lead.

D. Some Further Comments Concerning ΔF, ΔV, ΔH, and ΔS

No attempt has been made to interpret the results of these experiments in terms of a particular mechanism of diffusion up to this point. Certain formal thermodynamic identities have been employed to demonstrate the self-consistency of the data, and the question of the detailed mechanism of diffusion has had no relevance. Some speculations may be permitted, however.

If the direct interchange model is correct for sodium, the quantities ΔF, ΔH, ΔV, and ΔS are appropriately termed "activation" quantities and refer to changes in the state of an average atom between its position in a normal lattice site to a position midway to a neighboring normal site over a route of minimum work.

If, on the other hand, the correct model requires that lattice defects of a thermodynamic nature be formed as a necessary prelude to atom jumps, then each of the above quantities is comprised of two parts: (1) a free energy, enthalpy, volume, or entropy of *formation* of N defects at infinite dilution, and (2) activation quantities relating to the *movement* of N atoms or defects.

The most promising quantity for further consideration is probably the activation volume, since it offers the possibility of distinguishing the interstitial and vacancy cases. The volume of formation of vacancies must be positive, while the volume of formation of interstitialcies should be negative. In any case the volume change at-

tending atom movement should be positive. It is difficult to decide whether the volume change associated with movement should be numerically larger or smaller than the volume of formation, although in ionic crystals where it is possible to determine both, $\Delta V_{\text{form}} > \Delta V_{\text{movement}}$. If this be true in sodium, the observed positive activation volume is evidence in favor of the vacancy model for that metal.

E. The Effect of Pressure on D_0

Comparison of the empirical equations for diffusion at 1 kg/cm² and 8000 kg/cm² shows that pressure alters not merely the enthalpy of activation but the pre-exponential term as well. It is interesting to note that D_0 is decreased by pressure, while ΔH is increased. (In this same connection it may be remarked that metals for which ΔH is large have small D_0 values and the converse.) The major part of the decrease in D_0 arises from the decrease in the entropy of activation, as may be seen from the following:

Differentiation of

$$D_0 = \gamma a^2 \nu e^{\Delta S/R} \tag{20}$$

with respect to pressure at constant temperature gives

$$\left.\frac{d \ln D_0}{dP}\right]_T = \frac{2d \ln a}{dP} + \frac{d \ln \nu}{dP} + \frac{1}{R}\cdot\frac{d\Delta S}{dP}. \tag{21}$$

The first and third terms of Eq. (21) are inherently negative and lead to a decrease of D_0 with increasing pressure. The second term is positive, but the characteristic frequency does not increase sufficiently with pressure to overcome the other two. It is readily shown that the first term is equal to $-2/3\beta$, where β is the compressibility of sodium. The second term may be evaluated by means of the Grüneisen relation and has the value of $\alpha\beta$, where $\alpha = 1.25$ is the Grüneisen constant for sodium.

Bridgman's data[7] extrapolated to 90°C for the compressibility of sodium are fitted by the equation,

$$\beta = 1.732\times10^{-5} - 1.334\times10^{-9}P + 7.62\times10^{-14}P^2, \tag{22}$$

within 0.3 percent over the range 1 to 8000 kg/cm² and permit integration of Eq. (21). The entropy values at the two pressures are obtained from the corresponding ΔF and ΔH values and are listed in Table II. The value of the ratio D_0^{8000}/D_0^1 so calculated is 0.737, in good agreement with the observed ratio, $0.176/0.242 = 0.727$.

ACKNOWLEDGMENT

This work was supported in part by the Air Materiel Command, Wright-Patterson Field, under United States Air Force Contract AF-33(038)-6534.

THE JOURNAL OF CHEMICAL PHYSICS VOLUME 20, NUMBER 8 AUGUST, 1952

Photochemistry of Ferrous Ions in Aqueous Solution

TYSON RIGG AND JOSEPH WEISS
University of Durham, King's College, Newcastle upon Tyne, England

(Received January 21, 1952)

The photochemistry of ferrous ions in aqueous solutions has been investigated, and it has been confirmed that irradiation in the quartz ultraviolet, in the absence of oxygen, leads to the formation of ferric salt and molecular hydrogen. It has been concluded further that the primary absorption of a light quantum results in the formation of excited ions, $(Fe^{2+}\cdot H_2O)^*$, a considerable proportion of which undergo processes of deactivation, while the remaining (about one-tenth) dissociate according to

$$(Fe^{2+}\cdot H_2O)^* \rightarrow Fe^{3+} + OH^- + H,$$

leading to the formation of hydrogen atoms. The latter can undergo back reactions of the type

$$Fe^{3+} + H \rightarrow Fe^{2+} + H^+.$$

Investigation of the pH dependence of the quantum yield has led to the assumption that hydrogen atoms can also react according to

$$H + H^+_{(hydr)} \rightleftharpoons H_2^+{}_{(hydr)},$$

leading to the formation of hydrated hydrogen molecular ions which intervene in this process according to the reaction

$$Fe^{2+} + H_2^+ \rightarrow Fe^{3+} + H_2.$$

Other experimental evidence and some theoretical considerations which have led to the assumption of $H_2^+{}_{(hydr)}$ in aqueous solution are referred to.

ACCORDING to Franck and Scheibe[1] and Franck and Haber,[2] the ultraviolet absorption spectrum of simple negative ions in aqueous solution corresponds to an electron affinity spectrum, i.e., the transfer of an electron from the central ion to the water molecules in the hydration shell.

Subsequently, this basic concept was extended to simple positive ions, and it was suggested, e.g., in the

[1] J. Franck and G. Scheibe, Z. physik. Chem. **A139**, 22 (1928).
[2] J. Franck and F. Haber, Sitzber. preuss. Akad. Wiss. 250 (1931).

case of ferrous ions, that the absorption of a light quantum of suitable energy gives rise to the process[3]

$$Fe^{2+}HOH+h\nu \rightarrow Fe^{3+}+OH^{-}+H.$$

In agreement with this view it could be shown that irradiation of ferrous salt solutions in the near ultraviolet leads to the formation of ferric salt and molecular hydrogen.[3,4]

The mechanism of these photochemical processes was taken up later by Farkas and Farkas[5] who suggested that in the case of, e.g., iodide ions the photochemical reaction takes place only if the (negative) primary complex ($I \cdot H_2O^{-}$), formed by the absorption of a light quantum, reacts with hydrogen ions, and that, therefore, the quantum yield should increase with decreasing *p*H, while, on the other hand, these authors suggested that in the case of *positive ions* the quantum yield should be independent of the hydrogen ion concentration.

The earlier experimental work on ferrous ions,[4] which was confined to solutions containing from $0.2N$ to $0.5N$ H_2SO_4, appeared to confirm this. In the present investigation these measurements have been extended over a much wider range of *p*H, and it has been found that the quantum yield shows a very marked dependence on the hydrogen ion concentration. This has led to a modification of the mechanism of these reactions, which is discussed below.

EXPERIMENTAL

The source of radiation was a full wave low pressure mercury arc of 550 watts, supplied from a voltage stabilizer (Ferranti). Unfiltered radiation was used under conditions of complete absorption. The apparatus was on conventional lines. A spherical silica flask, filled with triply distilled water, was used as a condenser. In this way, and with a small centrifugal blower, the temperature in the reaction vessel could be kept constant at 20°±1°C.

ACTINOMETRY

The total light output in the ultraviolet region was measured actinometrically by means of monochloracetic acid. This was chosen since its absorption spectrum shows a good overlap with that of ferrous ions in aqueous solution and the error involved should not amount to more than about 10 percent which was adequate for the purpose of the present investigation.

A $0.1M$ solution of monochloracetic acid was used which gave practically complete absorption at $\lambda \sim 210$ mμ in a 2 cm thickness. The Cl^{-} ions were estimated by the Volhard method: the Cl^{-} was precipitated by $N/50$ $AgNO_3$, the precipitate separated by centrifuging, and back-titration with $N/50$ KCNS then carried out.

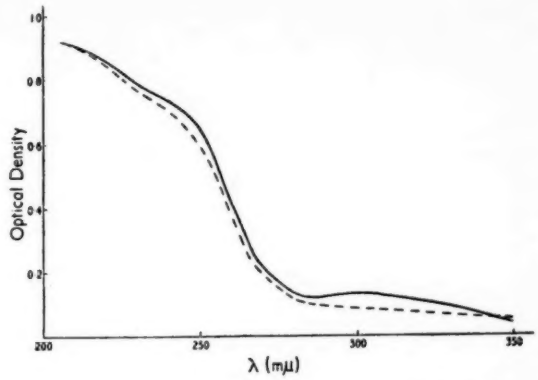

FIG. 1. Absorption spectrum of ferrous sulfate ($0.03M$) in sulfuric acid ($0.1M$). Broken line for solution containing sodium fluoride ($7.5\times10^{-3}M$). Optical density determined in a quartz cell of 1 cm thickness.

The output of the light source with the stabilizer was found to remain very constant over a period of several months. The value of 0.62 ± 0.04 which was used for the quantum efficiency of monochloracetic acid photolysis is taken from the recent work of Kuechler and Pick[6] who carried out a very careful investigation of this reaction.

PREPARATION OF THE SOLUTIONS

The water used was triply distilled (ordinary distilled water redistilled from permanganate and finally from dilute phosphoric acid). It was boiled out in a stream of carbon dioxide, and after cooling in the gas stream it was siphoned into the reaction vessel which contained the required amount of ferrous sulfate and sulfuric acid. In this way autoxidation of the ferrous salt was completely avoided.

$0.1M$ $FeSO_4$ solutions were employed to ensure complete absorption. The ferric salt produced in the reaction has a much greater absorption coefficient than the ferrous ions; thus to avoid any appreciable "inner-filter" effect the reaction was carried on only up to conversions of generally less than one percent. The ferrous sulfate had also to be initially free from ferric salt.

DE-AERATION OF THE SOLUTIONS

All experiments were carried out in evacuated solutions. The solutions were de-aerated either with oxygen-free carbon dioxide or with pure nitrogen followed by pumping out with a "Hyvac" oil pump *via* a liquid air trap. This procedure was then repeated, and the evacuation was finally completed and checked on the gas analysis apparatus where the solutions were evacuated by means of a Toepler pump.

The vapor phase in equilibrium with the solutions was also tested for oxygen by means of a trypaflavine gel, and it was shown that the oxygen pressure did not exceed 10^{-5} mm Hg.

[3] J. Weiss, Nature **136**, 794 (1935).
[4] Potterill, Walker, and Weiss, Proc. Roy. Soc. (London) **A156**, 561 (1936); J. Weiss, Trans. Faraday Soc. **37**, 463 (1941).
[5] A. Farkas and L. Farkas, Trans. Faraday Soc. **34**, 1113 (1938).
[6] L. Kuechler and H. Pick, Z. physik. Chem. **B45**, 116 (1939).

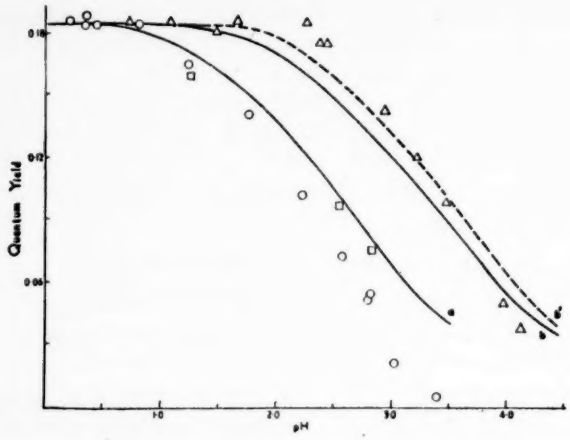

FIG. 2. pH—dependence of the quantum yield of the photochemical formation of hydrogen in vacuum. (○) = experiments with ferrous sulfate solutions (0.1M). (△) = with added fluoride ($7.5\times10^{-3}M$). (□) = in the presence of sodium sulfate (0.25M). For constant time of irradiation (14 min).

No effects due to residual oxygen could be observed in any of the experiments after using the above routine.

GAS ANALYSIS

The quantum yields were determined by measuring the gas liberated during the irradiation. This was shown to be *hydrogen* by diffusing it through a heated paladium tube after no contraction had been observed on passing it over a heated platinum spiral.

The hydrogen was collected by means of a semi-automatic Toepler pump and its volume measured.

Special precautions had to be taken to avoid autoxidation during the preparation of the experiments which were carried out in the presence of fluoride ($7.5\times10^{-3}M$). For this purpose the solution containing the ferrous salt was first of all thoroughly de-aerated and the fluoride added afterwards by means of a small silica tube which was dropped into the solution from one of the side arms of the radiation vessel.

All chemicals used were Analar except the sodium fluoride which was of puriss grade.

EXPERIMENTAL RESULTS

(a) Absorption Spectra

The absorption spectrum of ferrous ions was known from the earlier investigations.[4] For the experiments in the presence of fluoride it was necessary to establish whether the absorption spectrum of ferrous ions was changed. For this purpose a solution containing 0.03M $FeSO_4$, 0.1M H_2SO_4, and $7.5\times10^{-3}M$ NaF was examined. Although the ratio of fluoride to ferrous concentration is higher than the one used in the actual experiments, the absorption spectrum was found to be virtually unchanged (see Fig. 1).

(b) Photochemical Experiments

In view of the "inner filter effect" of the ferric salt formed in the reaction it was only possible to work up to very low concentrations of ferric salt, which could not be analyzed accurately in the presence of the large excess of ferrous salt, and therefore the reaction was followed by measuring the amount of hydrogen gas produced.

Figure 2, curve (a), shows the dependence of the quantum yield on pH, in vacuum; there is a very marked decrease of the quantum yield with increasing pH. The addition of fluoride which, as is well known, forms a strong complex with ferric ions leads to an increase in the quantum yield (Fig. 2, curve (b)) indicating that the lower quantum yields may be due to a back reaction involving ferric ions.

Figures 3 and 4 show the amount of photochemically formed ferric salt which is equivalent to the hydrogen gas produced at constant light intensity for different times of irradiation.

Although, in both cases the dependence is in general not linear, at the lower pH, the experimental results are represented by a straight line for short times of irradiation (see Fig. 3).

MECHANISM

According to the theory of Farkas and Farkas,[5] the quantum yield of the ferrous ion photolysis should be independent of the hydrogen ion concentration; however, this is not in agreement with the experimental facts as shown in Fig. 2.

On the other hand, the assumption of a photoexcited complex, as an intermediate, appears to be in general agreement with the results. Furthermore, in the case of positive ions the existence of an excited state is also to be expected on theoretical grounds.

The reaction can be described by the following equations:

$$\text{light absorption}\quad Fe^{2+}\cdot H_2O + h\nu \rightarrow (Fe^{2+}\cdot H_2O)^*, \quad (0)$$
$$\text{excited state}$$

I_a, number of quanta absorbed per unit of time.

$$\text{deactivation}\quad (Fe^{2+}\cdot H_2O)^* \rightarrow Fe^{2+}\cdot H_2O + \text{energy}\ (k_1), \quad (1)$$

$$(Fe^{2+}\cdot H_2O)^* \rightarrow Fe^{3+} + OH^- + H\ (k_2). \quad (2)$$

The excited ion could be formulated as $(Fe^{3+}\cdot H_2O^-)$ similar to the suggestion of Farkas and Farkas;[5] however, this point is not important for the present discussion.

As suggested previously, the hydrogen atoms formed in reaction (2) can undergo the back reaction

$$Fe^{3+} + H \rightarrow Fe^{2+} + H^+\ (k_3) \quad (3)$$

and the recombination process

$$2H \rightarrow H_2\ (k_4). \quad (4)$$

On the basis of the above reactions the quantum yield would be independent of *p*H, which, however, as pointed out above is not the case.

This and other experimental facts to be described below can be explained by the assumption that hydrogen atoms can also act as oxidizing agents, particularly under conditions of low *p*H.

The dehydrogenating effect of hydrogen atoms is well known in homolytic reactions, e.g., $RH+H\rightarrow R+H_2$, but has only recently been considered in an ionic mechanism.[7] The latter possibility arises if one assumes the equilibrium

$$H+H^+_{(hydr)} \underset{(k_5')\leftarrow}{\overset{(k_5)\rightarrow}{\rightleftharpoons}} H_2^+{}_{(hydr)} \qquad (5)$$

which leads to the formation of hydrated hydrogen molecular ions, capable of oxidizing ferrous ions according to

$$Fe^{2+}+H_2^+\rightarrow Fe^{3+}+H_2. \quad (k_6) \qquad (6)$$

In agreement with this, the curves (a) and (b) in Fig. 2 converge towards the same limiting quantum yield which should be twice that resulting from the initiating reaction (2).

From the well-known equilibrium[8]

$$Fe^{3+}+H_2O\rightleftharpoons FeOH^{2+}+H^+$$
(equilibrium constant, $K_h\sim 10^{-3}$ at 25°C) (7)

it follows that $FeOH^{2+}$ may also be of some importance, particularly at the lower hydrogen ion concentrations. In fact, the results indicate that in general the reaction

$$FeOH^{2+}+H\rightarrow Fe^{2+}+H_2O \qquad (8)$$

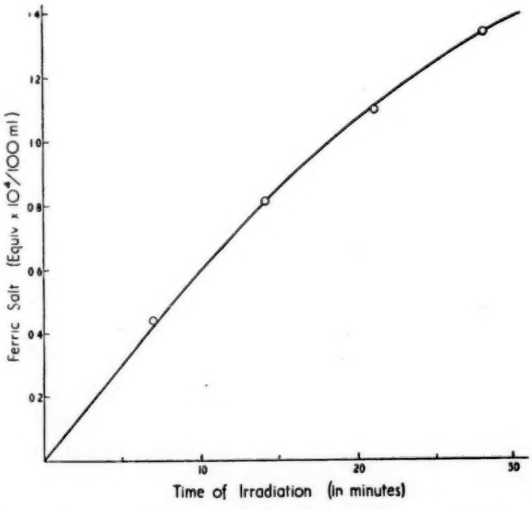

FIG. 3. Dependence of ferrous salt oxidized on time of irradiation at constant light intensity. Ferrous sulfate (0.1*M*) in sulfuric acid (0.5*M*) in vacuum.

[7] J. Weiss, Nature **165**, 728 (1950).

[8] A. B. Lamb and A. G. Jacques, J. Am. Chem. Soc. **60**, 1215 (1938); E. Rabinowitsch and W. H. Stockmeyer, J. Am. Chem. Soc. **64**, 335 (1942); M. G. Evans and N. Uri, Trans. Faraday Soc. **45**, 230 (1949).

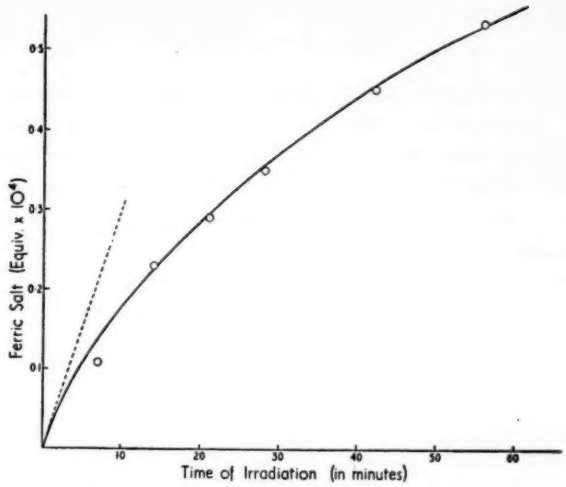

FIG. 4. Dependence of ferrous salt oxidized on time of irradiation at constant light intensity. Ferrous sulfate (0.1*M*) at *p*H = 2.80 in vacuum.

has to be taken into account.

For the stationary state one has

$$\frac{d((Fe^{2+}\cdot H_2O)^*)}{dt}=0$$
$$=I_a-(k_1+k_2)[(Fe^{2+}\cdot H_2O)^*], \qquad (9a)$$

$$\frac{d(H)}{dt}=0=k_2[(Fe^{2+}\cdot H_2O)^*]-k_3[Fe^{3+}][H]$$
$$-k_8[FeOH^{2+}][H]-k_5[H][H^+]+k_5'[H_2^+], \qquad (9b)$$

$$\frac{d(H_2^+)}{dt}=k_5[H][H^+]-k_5'[H_2^+]-k_6[Fe^{2+}][H_2^+], \qquad (9c)$$

with all the above reactions except the recombination reaction (4) which can be neglected, as a first approximation, *unless* the ferric *and* hydrogen ion concentrations are very low.

Thus, for the rate of photochemical formation of ferric salt one obtains

$$\frac{d(Fe^{III})}{dt}=k_2[(Fe^{2+}\cdot H_2O)^*]-k_3[Fe^{3+}][H]$$
$$-k_8[FeOH^{2+}][H]+k_6[Fe^{2+}][H_2^+], \qquad (10)$$

where (Fe^{III}) represents the total (analytical) concentration of the ferric salt in the solution, and from the equilibrium (7) it follows that

$$[Fe^{3+}]=(Fe^{III})[H^+]/(K_h+[H^+]),$$
$$[FeOH^{2+}]=(Fe^{III})K_h/(K_h+[H^+]). \qquad (11)$$

Combining Eqs. (9)–(11) one obtains finally

$$\frac{d(Fe^{III})}{dt}=\frac{2I_a'AC[H^+]}{\{AC[H^+]+BD(Fe^{III})\}}, \qquad (12)$$

where

$$A=k_8k_6[Fe^{2+}], \qquad B=(k_5'+k_6[Fe^{2+}]),$$
$$C=(K_h+[H^+]), \qquad D=(k_8K_h+k_3[H^+]),$$

and

$$I_a' = I_a\{k_2/(k_1+k_2)\}.$$

As the ferrous and hydrogen ion concentrations may be regarded as practically constant under the conditions of these experiments, Eq. (12) can be integrated easily between the time limits 0 and t, which gives

$$(Fe^{III})_t = \Gamma\{[1+(4I_a't/\Gamma)]^{\frac{1}{2}}-1\}, \quad (13)$$

where

$$\Gamma = CK_1 10^{-pH}/\{1+K_2 10^{-pH}\}.$$

$$K_1 = A/BK_h k_8, \quad K_2 = k_3/K_h k_8.$$

The quantum yield γ is given from Eq. (13) by

$$\gamma = (Fe^{III})_t/(I_a t). \quad (14)$$

The whole course of the variation of the quantum yield with pH which is given by Fig. 2 can be represented satisfactorily by Eq. (13) with the following numerical constants:

$$K_1 \cong 120, \quad \text{and} \quad K_2 \cong 1.7\times 10^3,$$

which have been used for the calculation of the theoretical curve (fully drawn) in Fig. 2, curve (a).

In the experiments where fluoride was added to the solution the back reaction is obviously suppressed which is presumably due to the formation of a less reactive ferric complex, which can react according to

$$(Fe^{3+}\cdot \text{complex}) + H \rightarrow Fe^{2+} + H^+ + \cdots (k_{15}). \quad (15)$$

One now obtains by a similar procedure as above, replacing Eqs. (3) and (8) by Eq. (15), for the quantum yield ($\gamma_{(c)}$) the expression

$$\gamma_{(c)} = \frac{\Gamma_{(c)} 10^{-pH}}{(I_a t)}\{[1+(4I_a' t 10^{pH}/\Gamma_{(c)})]^{\frac{1}{2}}-1\}, \quad (16)$$

which contains only *one* arbitrary constant, the value of which can be deduced from the second set of experimental results in Fig. 2 giving

$$\Gamma_{(c)} = A/Bk_{15} \simeq 5\times 10^{-1},$$

where A and B have the same significance as above: the theoretical curve thus calculated and represented by curve (b), Fig. 2, is again in satisfactory agreement with the experimental results. The broken line (curve b')) has been calculated with $\Gamma_{(c)} \cong 7\times 10^{-1}$. The difference is practically within the limits of experimental error.

The numerical values of the constants K_1, K_2, and $\Gamma_{(c)}$ allow the estimation of the ratios of the velocity constants of the reactions (3), (8), and (15). Thus one finds

$$(k_3/k_8) \cong 1.7, \qquad (k_8/k_{15}) \cong 4.2,$$

which means that the rate constant for the reduction of ferric ions by hydrogen atoms is approximately 1.7 times faster than the corresponding reaction with $FeOH^{2+}$ and about 7 times faster than the corresponding reaction with the ferric fluoride complex.

For sufficiently low pH, i.e., if $(4I_a't/\Gamma) \ll 1$, Eq. (13) reduces to

$$(Fe^{III})_t \simeq 2I_a' t, \quad (17)$$

i.e., under these conditions the amount of ferric salt (at constant light intensity) should be a linear function of the time of irradiation. This is found to be the case as shown by the experiments in Fig. 3 which refers to pH$\sim$0.3. For larger doses the yield falls off as is to be expected also as a result of the "inner filter effect" of the strongly absorbing ferric ions produced in the reaction.

The slope of the linear portion in Fig. 3 can be used to evaluate I_a' which was found to be

$$I_a' \simeq 3.0\times 10^{-5} \text{ moles/min} \times 1000 \text{ ml.}$$

This quantity can also be calculated from the experimentally determined maximum quantum yield. From Eqs. (14) and (15) follow under conditions similar to those above

$$\gamma_{(max)} \sim 2(I_a'/I_a).$$

The total number of light quanta absorbed per minute as determined actinometrically gave

$$I_a \simeq 3.15\times 10^{-4} \text{ einstein/min} \times 1000 \text{ ml.}$$

Thus one obtains from the slope of the linear part of the curve shown in Fig. 3

$$(I_a'/I_a) \simeq (3.0\times 10^{-5}/3.15\times 10^{-4}) \simeq 0.95\times 10^{-1}$$

and from the experimentally determined maximum quantum yield (0.185) from Fig. 2

$$(I_a'/I_a) = (\gamma_{(max)}/2) \simeq 0.185/2 \simeq 0.93\times 10^{-1}.$$

It is obvious that physically the ratio

$$(I_a'/I_a) = k_2/(k_1+k_2) \sim 1/10$$

represents the fraction of the excited ions which dissociate, contributing towards the photochemical process, i.e., only about *one* out of *ten* excited ions dissociates while the rest are deactivated.

Under conditions of higher pH, the formation of H_2^+ will be disfavored and the yields should be lower because of the increased back reactions (3) and (8). This is fully supported by comparing Figs. 3 and 4.

As stated above the differential Eq. (12) cannot be applied at low ferric and hydrogen ion concentrations and has been derived on the assumption that in acid solution the recombination of the hydrogen atoms (Eq. 4) can be neglected. In this case the *initial slope* is given by

$$\left.\frac{d(Fe^{III})}{dt}\right|_{(Fe^{III})\rightarrow 0} \simeq 2I_a'$$

as follows from Eq. (12).

However, at *sufficiently low hydrogen ion concentrations* the H_2^+ formation can be neglected and initially, when there are practically no ferric ions present, the

recombination of the hydrogen atoms is predominant. For the stationary state one now has the equation

$$\frac{d(\mathrm{H})}{dt}\simeq \mathrm{I}_a' - k_3[\mathrm{Fe}^{3+}][\mathrm{H}] - k_8[\mathrm{FeOH}^{2+}][\mathrm{H}] - 2k_4[\mathrm{H}]^2 = 0. \quad (18)$$

From this, one obtains for the *initial* formation of ferric salt (or molecular hydrogen) the equation

$$\left.\frac{d(\mathrm{Fe}^{III})}{dt}\right|_{(\mathrm{Fe}^{III})\sim 0} = 2\left.\frac{d(\mathrm{H}_2)}{dt}\right|_{(\mathrm{Fe}^{III})\sim 0} \simeq \mathrm{I}_a',$$

for relatively high *p*H. Thus, the initial slope in very acid solutions should be theoretically twice the initial slope at relatively high *p*H. This is fully borne out by the experimental facts as the initial slope in Fig. 3 referring to 1*N* H_2SO_4, solutions is about 6×10^{-6} equiv/100 ml min, while the initial slope in Fig. 4 (referring to *p*H 2.8) is about 3×10^{-6} equiv/100 ml min; thus, experimentally the ratio is very nearly 2:1, in very good agreement with the theory.

This means that in acid solutions initially practically all the H atoms form H_2^+, which oxidize ferrous to ferric, while at high *p*H, initially, when practically no ferric is present, the H atoms recombine to give molecular hydrogen.

Normally, there is a considerable variation of the sulfate ion concentration in going from the high to the low *p*H experiments. We suspected that this could be one of the reasons for some of the observed deviations from the theoretical curve. This was confirmed by experiments carried out by adding sodium sulfate up to about 0.25*M*. Under these conditions much better agreement with the theory is obtained in the experiments at higher *p*H where normally only little sulfate is present (see Fig. 2). This is probably due to the fact that sulfate ions can form ferric ion complexes which are somewhat less reactive and inhibit the back reaction to some extent. One should take into account also the variation of the hydrolysis constant K_h with ionic strength; although full data regarding this are not available in the literature, there is some indication that this might also improve the agreement with theory.

Independent support for the view outlined above has been obtained from experiments on the irradiation of dilute aqueous solutions of ferrous sulfate by x-rays.[9] It is well known that in this case the primary effect occurs in the water and can be represented by the *net* process:[10] $H_2O\rightarrow H+OH$. After the reaction of the OH radicals according to $Fe^{2+}+OH\rightarrow Fe^{3+}+OH^-$, one should again have conditions in some respects very similar to those discussed above.

A recent study of this reaction[9] has shown that it can be described by a mechanism which is, apart from the primary processes, in every essential point the same as the one discussed above for the photochemical reaction.

The extent of this agreement is shown by the fact that the constants K_1, K_2, and $\Gamma_{(c)}$ deduced from the photochemical experiments are practically identical with those obtained from the radiation chemistry. (The constants K_1, Γ_v'', and $\Gamma_{(o)}$ given in this paper, when referred again to the proper units, as above, are to be multiplied by a factor of 10.) This also lends further support to the assumption of the formation of free hydrogen atoms in the photochemistry of ferrous ions in aqueous solutions.

In the reaction mechanism outlined above the hydrated hydrogen molecular ion has been assumed to play an important part. This assumption rests primarily on the indirect evidence from the reactions of hydrogen atoms in solution in various systems and under different *p*H conditions. The existence of $H_2^+{}_{hydr}$ in aqueous systems is fully compatible with thermodynamical and other theoretical considerations as has been shown elsewhere.[9]

The heat of hydration ($S_{H_2^+}$) of the H_2^+ ion can, under certain assumptions, be estimated to be within the following limits:

$$221 \text{ kcal} \leqslant S_{H_2^+} \leqslant 255 \text{ kcal}.$$

The lower limit is obtained from the equation:

$$\mathrm{H}+\mathrm{H}^+_{(hydr.)} = \mathrm{H}_2^+{}_{(hydr.)} + (D_{H_2^+} + S_{H_2^+} - S_{H^+}),$$

$D_{H_2^+}$ = bond energy of H_2^+ (61 kcal)

S_{H^+} = heat of hydration of the proton ($\sim$282 kcal)

$S_{H_2^+}$ = heat of hydration of the H_2^+ ion,

and assuming that this reaction is exothermal or thermoneutral, one obtains

$$(D_{H_2^+} + S_{H_2^+} - S_{H^+}) \geqslant 0.$$

The upper limit is obtained from the reactions:

$$\mathrm{Fe}^{2+}+\mathrm{H}^+ = \mathrm{Fe}^{3+}+\mathrm{H}-69 \text{ kcal}$$
$$\mathrm{H}_2^+ = \mathrm{H}^+ + \mathrm{H} - (S_{H_2^+} - 221) \text{ kcal}$$
$$2\mathrm{H} = \mathrm{H}_2 + 103 \text{ kcal},$$

leading to

$$\mathrm{Fe}^{2+}_{(hydr.)} + \mathrm{H}_2^+{}_{(hydr.)} = \mathrm{Fe}^{3+}_{(hydr.)} + \mathrm{H}_2 - (S_{H_2^+} - 255 \text{ kcal}),$$

and assuming again that this reaction is exothermal or thermoneutral one obtains

$$(S_{H_2^+} - 255 \text{ kcal}) \leqslant 0.$$

A similar previous calculation[9] was marred by an error in one of the signs, which is hereby corrected.

We wish to thank the Chemical Society (London) for a grant to cover the cost of some of the apparatus, and one of us (T. R.) expresses his thanks to the Cumberland Education Committee for a maintenance grant.

[9] Rigg, Stein, and Weiss, Proc. Roy. Soc. (London) **A211**, 375 (1952).

[10] J. Weiss, Nature **153**, 748 (1944).

Theory of Ion Exchange for Polyelectrolytes Undergoing Electrolytic Transference*

FREDERICK T. WALL AND PHILIP F. GRIEGER†
Noyes Chemical Laboratory, University of Illinois, Urbana, Illinois
(Received February 18, 1952)

It has been observed experimentally that polymeric ions generally have associated with them a large number of small ions of opposite charge. These smaller ions, which are considered bound to the polymeric ions, are capable of exchanging with free ions in solution. The rate of this exchange can be determined by certain electrolytic transference experiments involving the use of radioactive tracers. The theory of such transference experiments is worked out by formulating and solving appropriate differential equations subject to certain boundary conditions. It is then shown how results of these transference studies can be used for evaluating ion rate exchange constants.

INTRODUCTION

WHEN a solution of polyacrylic acid partially neutralized with sodium hydroxide is electrolyzed in a transference cell, it is experimentally observed that part of the sodium appears to move toward the anode, the rest moving in the normal way toward the cathode.[1] As a matter of fact, under appropriate conditions it is found that more sodium moves to the anode than to the cathode. This surprising observation can be explained by assuming that a portion of the sodium ions are either un-ionized or bound in some way to the polyacrylate ions. This binding, or incomplete ionization of the salt, presumably occurs because of the very large electrostatic forces that arise when a polymer of a high degree of polymerization undergoes appreciable ionization. It is evident that any sodium so bound to the anion will move to the anode during electrolysis just as any metal would move with a complex anion.

The sodium ions which are attached to the polyacrylate ions are, however, rather loosely bound and are readily capable of undergoing exchange with free ions in solution. It might be surmised that this exchange would be exceedingly rapid, but it actually turns out that the rate is measurably finite.

It is possible to learn something about the rate of exchange by means of experiments carried out as follows. An electrolytic cell divided into anode and cathode compartments is originally filled with polyacrylic acid partially neutralized with sodium hydroxide with a small amount of radioactive sodium ions added to one side, let us say to the cathode. As the electrolysis proceeds, sodium will tend to move in both directions, the direction depending upon whether the sodium is free or bound. Let us now consider the bound radioactive sodium originally in the cathode side that moves into the anode compartment. If the rate of exchange were zero, the net amount of radio sodium carried into the sodium compartment would obviously be a maximum and could be simply computed from a knowledge of the fraction of the sodium which is bound and the transference numbers of the different ionic species. Actually it is observed that the net amount of radio sodium carried into the anode compartment is less than one would calculate from the appropriate transference data assuming zero exchange rate. Accordingly it can be surmised that some of the radio sodium, upon entering the anode compartment, exchanges with the free nonradioactive species and is subsequently carried back toward the cathode from whence it came. Qualitatively it can be seen that a measure of the rate of exchange should be forthcoming from a knowledge of the net flow of radio sodium as a function of time for experiments of the type described above, providing the necessary transference and related data are known.

A theoretical interpretation of experiments of this kind is given in the present paper. In an accompanying article,[2] there are given actual experimental results for polyacrylic acid-sodium hydroxide mixtures. Accordingly, whenever it is helpful to consider a specific example, we shall refer to sodium and polyacrylate ions.

THE EXCHANGE PROCESS

In the interest of simplicity we shall consider only systems in which exchange takes place between two kinds of ions. Specifically, we will assume that in a particular solution of polyacrylic acid and sodium hydroxide there exist free sodium ions and a single polymer ion species of degree of polymerization s, containing p_2 bound sodium ions. The concentrations of free sodium ions and polymer ions will be designated as n_1 and n_2, respectively. Since we want to determine the rate of exchange of sodium ions between polymer and the unassociated species, a radioactive isotope of sodium ion is added to part of the system in trace concentration. It is assumed throughout that the two isotopes have identical properties except that one of them is radioactive.

Let us denote by ρ_1 and ρ_2 the fraction of free sodium

* This investigation was carried out under the sponsorship of the Reconstruction Finance Corporation, Synthetic Rubber Division.

† Present address: The Edison Laboratory, Thomas A. Edison, Inc., West Orange, New Jersey.

[1] Huizenga, Grieger, and Wall, J. Am. Chem. Soc. 72, 2636 (1950).

[2] Wall, Grieger, Huizenga, and Doremus, J. Chem. Phys. 20, 1206 (1952).

ions and the average fraction of bound sodium ions that are radioactive. Although all of the polymer ions are assumed to contain p_2 bound sodium ions, there will generally be a nonuniform distribution of radioactive sodium ions among them. Let $n_2(m)$ be the concentration of the polymer ions containing m radioactive and p_2-m nonradioactive sodium ions. Then to compute the rate at which polymer tends to gain or lose radioactive ions, we should consider the reactions

$$P(m)+Na^{+*}\rightarrow P(m+1)+Na^{+} \quad (1)$$

and

$$P(m)+Na^{+}\rightarrow P(m-1)+Na^{+*}, \quad (2)$$

where $P(m)$ denotes a polymer ion with m radioactive sodiums and Na^{+*} denotes the free radioactive ion. It now appears reasonable to assume that the rates of reaction (1) and (2) will be given, respectively, by

$$kn_1\rho_1 n_2(m)(p_2-m)$$

and

$$kn_1(1-\rho_1)m[n_2(m)],$$

where k is the appropriate specific reaction rate constant.[3] The over-all rate at which polymer gains Na^{+*} will be

$$\sum_{m=0}^{p_2}[kn_1\rho_1 n_2(m)(p_2-m)]-kn_1(1-\rho_1)m[n_2(m)]$$

$$=kn_1\sum_{m=0}^{p_2}\left(\rho_1-\frac{m}{p_2}\right)n_2(m)p_2$$

$$=kp_2n_1n_2(\rho_1-\rho_2).$$

A similar conclusion for the net rate of exchange can be obtained with a variable p_2, providing certain reasonable assumptions are made.

FORMULATION OF DIFFERENTIAL EQUATIONS

In the presence of an electric field, the exchange of bound with unbound sodium ions will be superimposed on electrical transference of the cations and anions.

The equations of continuity for tracer as free sodium ions and as ions bound to polymer are

$$-\partial(n_1\rho_1)/\partial t=\mathrm{div}J_1^{*}+kp_2n_1n_2(\rho_1-\rho_2)$$
$$-\partial(n_2p_2\rho_2)/\partial t=\mathrm{div}J_2^{*}-kp_2n_1n_2(\rho_1-\rho_2),$$

where J_1^{*} and J_2^{*} are the tracer currents attributable to free ion flow and bound ion flow. If the effect of ordinary diffusion is neglected, then for the one-dimensional case the flows are[4]

$$J_1^{*}=n_1v_1\rho_1 \quad \text{with} \quad v_1=e_1\omega_1E$$

and

$$J_2^{*}=n_2p_2v_2\rho_2 \quad \text{with} \quad v_2=e_2\omega_2E,$$

[3] The "k" used in reference 1 differs from that used in the present paper by the factor $n_1n_2p_2$.

[4] L. Onsager and R. M. Fuoss, J. Phys. Chem. **36**, 2689 (1932).

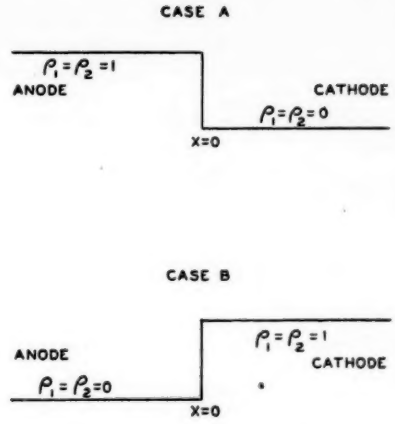

FIG. 1. Initial conditions of tracer concentration in transference cell for two cases described in text.

where, for example, e_1 and ω_1 are the charge and mobility of free sodium ions and E is the electric field strength. Then if we assume that n_1 and n_2 are constant space and time and that E as well as the ω's are constant in space, the equations of continuity can be written as

$$\begin{aligned}-\partial\rho_1/\partial t&=v_1\partial\rho_1/\partial x+n_2p_2k(\rho_1-\rho_2)\\ \partial\rho_2/\partial t&=-v_2\partial\rho_2/\partial x+n_1k(\rho_1-\rho_2).\end{aligned} \quad (3)$$

LIMITING CASES

As k becomes infinite,[1] $\rho_1\rightarrow\rho_2=\rho$, and Eqs. (3) become simply

$$-\partial\rho/\partial t=u\partial\rho/\partial x, \quad (3')$$

where $u=(n_1v_1+n_2p_2v_2)/(n_1+n_2p_2)$. The general solution of (3′) is

$$\rho=\rho(x-ut).$$

From this solution, it is evident that if the exchange rate is infinite, tracer will appear to move in only one direction, with a velocity u. (This conclusion depends, of course, on the assumption that ordinary diffusion is negligible.)

Let us now consider the case where initially $\rho_1=\rho_2=\rho_0$ for $x<0$ (anode), and $\rho_1=\rho_2=0$ for $x>0$ (cathode). Since v_1 and v_2 have opposite signs, tracer will appear to move past the point of original tracer discontinuity either in the direction of the cathode or anode, depending upon whether $|n_1v_1|$ is greater or less than $|n_2p_2v_2|$. For infinitely rapid exchange, with $u>0$, the flow of tracer into the region $x>0$ is

$$\rho(n_1+n_2p_2)u=\rho(n_1v_1+n_2p_2v_2)=J_1^{*}+J_2^{*}.$$

But this is precisely the flow of tracer that should be observed for any rate of exchange, providing ρ_1 and ρ_2 are initially made uniform throughout the system and equal to ρ. Therefore, if it is desired to obtain the net ion flow J_1+J_2 (where $J_1=n_1v_1$ and $J_2=n_2p_2v_2$) by means of transference experiments involving tracers,

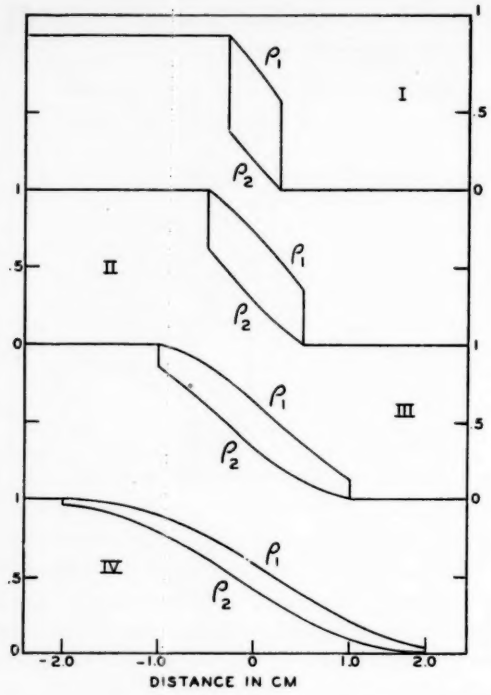

FIG. 2. Tracer concentrations for case A after various times of electrolysis assuming $v_1=-v_2$; I, $v_1t=0.25$ cm, II, $v_1t=0.5$ cm, III, $v_1t=1.0$ cm, and IV, $v_1t=2.0$ cm.

this can be done regardless of the exchange rate of tracer by simply making the tracer concentration uniform throughout.[1]

For $k=0$, Eqs. (3) are independent of each other. If $v_1>0$ and $v_2<0$, and if tracer is initially placed on the anode side only, then the flow of tracer towards the cathode will be $|n_1v_1|$. Conversely, if tracer is initially placed on the cathode side only, the flow towards the anode will be $|n_2p_2v_2|$. For finite values of k, tracer will appear to move in both directions, but the effect of exchange will be to make the magnitude of the flow smaller than $|n_1v_1|$ in the first instance and smaller than $|n_2p_2v_2|$ in the second. It is evident that by using a solution of Eqs. (3) it should be possible to evaluate k by means of appropriate transference experiments involving the initially discontinuous distribution of tracer defined above. The solution to this problem is given in the following sections.

GENERAL SOLUTION OF DIFFERENTIAL EQUATIONS

In the following treatment we shall always assume v_1 and v_2 to be constant. By making a change of variables to ξ and η where

$$\xi=kn_2p_2(x-v_2t)/(v_1-v_2)$$
$$\eta=-kn_1(x-v_1t)/(v_1-v_2),$$

Eqs. (3) reduce to

$$\partial\rho_1/\partial\xi=\rho_2-\rho_1$$
$$-\partial\rho_2/\partial\eta=\rho_2-\rho_1. \tag{4}$$

Elimination of ρ_2 from Eqs. (4) gives

$$\partial^2\rho_1/\partial\eta\partial\xi+\partial\rho_1/\partial\xi+\partial\rho_1/\partial\eta=0.$$

The variables are readily separable by use of a trial solution

$$\rho_1=S(\xi)N(\eta),$$

which yields

$$(1/S)dS/d\xi$$
$$=-(1/N)(dN/d\eta)/[(1/N)(dN/d\eta)+1]=\lambda-1,$$

where $\lambda-1$ has been written as the separation constant. The solutions of the separate ordinary differential equations give

$$S(\xi)=\exp(\lambda-1)\xi$$
$$N(\eta)=\exp(\lambda^{-1}-1)\eta,$$

and the general solution of (4) can be written as

$$\rho_1(\xi,\eta)=\sum_\lambda g(\lambda)\exp[(\lambda-1)\xi+(\lambda^{-1}-1)\eta]$$
$$\rho_2(\xi,\eta)=\sum_\lambda g(\lambda)\lambda\exp[(\lambda-1)\xi+(\lambda^{-1}-1)\eta], \tag{5}$$

where $g(\lambda)$ is any function of λ.

INITIAL AND BOUNDARY CONDITIONS

Both from the standpoint of computation and experiment, a particularly simple set of conditions involves the initial type of discontinuity in tracer concentration described above, using a long tube of uniform cross section. Except for the negligible effect of the addition of tracer, the stoichiometric concentrations of sodium hydroxide and polyacrylic acid are assumed to be uniform throughout. As will be seen below, it is advantageous to perform the experiments in pairs; for case A, tracer is initially added to the anode compartment; for case B, to the cathode side. For the sake of clarity, we shall outline the boundary conditions for both cases.

As might be expected, we shall ultimately require only relative values of the ρ's. Accordingly it is convenient to consider the initial ρ's to be unity on one side of the cell and zero on the other. The solution so obtained is perfectly general, however, because the equations of continuity are homogeneous in the ρ's. If the actual values of the ρ's are required, they are computed simply by multiplying the relative values by the true initial value of ρ in the initially radioactive side.

Throughout this discussion the electric field is assumed to point in the positive x direction. The initial conditions as shown in Fig. 1 can be written as follows:

Initial Conditions, $t=0$

Case A	Case B
$\rho_{1A}=\rho_{2A}=1$, $x<0$	$\rho_{1B}=\rho_{2B}=0$, $x<0$
$\rho_{1A}=\rho_{2A}=0$, $x>0$	$\rho_{1B}=\rho_{2B}=1$, $x>0$
$\rho_{1A}=1$, $\rho_{2A}=0$, $x=0$	$\rho_{1B}=0$, $\rho_{2B}=1$, $x=0$.

Since polyacrylate ion is negatively charged, $v_1 > v_2$. At any time t, there will be a region $v_2 t \leqslant x \leqslant v_1 t$, for which $\rho_1 \neq \rho_2$. Outside the region specified above, i.e., for $x < v_2 t$ or $x > v_1 t$, $\rho_1 = \rho_2 =$ initial value, for both cases A and B. Further boundary conditions can be summarized as follows:

Boundary Conditions

Case A

$$\rho_{2A} = 0 \quad \text{at} \quad x = v_1 t \quad \text{or} \quad \eta = 0, \quad \xi = k n_2 p_2 t = \bar{\xi}$$
$$\rho_{1A} = 1 \quad \text{at} \quad x = v_2 t \quad \text{or} \quad \xi = 0, \quad \eta = k n_1 t = \bar{\eta}$$

Case B

$$\rho_{2B} = 1 \quad \text{at} \quad x = v_1 t \quad \text{or} \quad \eta = 0, \quad \xi = k n_2 p_2 t = \bar{\xi}$$
$$\rho_{1B} = 0 \quad \text{at} \quad x = v_2 t \quad \text{or} \quad \xi = 0, \quad \eta = k n_1 t = \bar{\eta}.$$

If $v_1 < v_2$, the above conditions are altered simply by interchanging ξ and η and the subscripts 1 and 2.

SOLUTION FOR SPECIFIED CONDITIONS

Outside the region of disturbance $v_2 t \leqslant x \leqslant v_1 t$, the required solution is simply

$$\rho_{1A} = \rho_{2A} = 1 \quad \text{for} \quad x < v_2 t$$
$$\rho_{1A} = \rho_{2A} = 0 \quad \text{for} \quad x > v_1 t,$$

with a similar solution for case B. These equations, together with relations for ρ_1 and ρ_2 inside the region of disturbance satisfying the boundary conditions and the differential equations, constitute the solution to the problem. We require a function $g(\lambda)$ such that

$$\rho_{1A}(\xi, \eta) = \sum_{\lambda} g(\lambda) \exp[(\lambda - 1)\xi + (\lambda^{-1} - 1)\eta] \quad (5')$$

satisfies the boundary conditions; that is,

$$\rho_{1A} = 1 \quad \text{for} \quad \xi = 0, \quad \eta = \bar{\eta}.$$

Hence for all $\bar{\eta}$,

$$1 = \sum_{\lambda} g(\lambda) \exp(\lambda^{-1} - 1)\bar{\eta}$$
$$= \sum_{\lambda} g(\lambda) \sum_{i=0}^{\infty} (1/i!) \sum_{j=0}^{i} (-1)^j \lambda^{i-j} \binom{i}{j} (\bar{\eta})^i.$$

Therefore

$$\sum_{\lambda} g(\lambda) = 1,$$

and

$$\sum_{\lambda} g(\lambda) \sum_{j=0}^{i} (-1)^j \lambda^{i-j} \binom{i}{j} = 0 \quad i = 1, 2, 3, \cdots.$$

For $i = 1$

$$\sum_{\lambda} g(\lambda)(\lambda^{-1} + 1) = 0,$$

or

$$\sum_{\lambda} g(\lambda)\lambda^{-1} = 1.$$

Repeating this for $i = 2$, 3, etc., we find in general, since

$$\sum_{j=0}^{i} (-1)^j \binom{i}{j} = 0,$$

that

$$\sum_{\lambda} g(\lambda)\lambda^p = 1, \quad p = 0, -1, -2, \cdots. \quad (6)$$

Similarly from the other boundary condition,

$$0 = \sum_{\lambda} g(\lambda)\lambda \exp(\lambda - 1)\bar{\xi},$$

it turns out that

$$\sum_{\lambda} g(\lambda)\lambda^p = 0 \quad p = +1, +2, \cdots. \quad (7)$$

Combining (6) and (7) we note that

$$\sum_{\lambda} g(\lambda)(1 - \lambda)\lambda^p = 1, \quad p = 0$$
$$= 0 \quad p \neq 0. \quad (8)$$

$\rho_{1A}(\xi, \eta)$ can be written in a number of forms by using relations (6) and (7) in connection with (5'). For example, it can be given in terms of Laguerre polynomials $L_p(\eta)$, as

$$\rho_{1A}(\xi, \eta) = 1 - \xi e^{-\eta} \sum_{p=0}^{\infty} (-\xi)^p L_p(\eta)/(p+1)!p!,$$

where[5]

$$L_p(\eta) = \sum_{q=0}^{p} (-\eta)^q \binom{p}{q} p!/q!.$$

For time integration at the point $x = 0$ we shall use

$$\rho_{1A}(\xi, \eta) = 1 + \sum_{i=1}^{\infty} \sum_{j=0}^{i-1} (-1)^i \xi^{i-j} \eta^j \binom{i}{j} \binom{i-1}{j} \Big/ i!. \quad (9)$$

For purposes of illustration ρ_{1A} and ρ_{2A} have been computed and are shown graphically in Fig. 2 for four values of $v_1 t$, corresponding to the special case of $v_1 = -v_2$.

GENERAL RELATIONS AMONG THE ρ'S

If $\rho_{1A}(\xi, \eta)$ and $\rho_{2A}(\xi, \eta)$ are solutions, then so are

$$\rho_{2A}(\eta, \xi) = 1 - \rho_{1A}(\xi, \eta)$$
and (10)
$$\rho_{1A}(\eta, \xi) = 1 - \rho_{2A}(\xi, \eta).$$

Clearly Eqs. (10) satisfy the initial and boundary conditions and the transformed differential Eqs. (4):

$$\partial \rho_1(\eta, \xi)/\partial \eta = \rho_2(\eta, \xi) - \rho_1(\eta, \xi)$$
$$-\partial \rho_2(\eta, \xi)/\partial \xi = \rho_2(\eta, \xi) - \rho_1(\tau, \xi).$$

It should be noted that the exchange term in (3) is not the only one that would give rise to Eqs. (10). Thus the exchange term could be any function $f(\rho_1, \rho_2)$ such that

$$f(\rho_1, \rho_2) = f(1 - \rho_2, 1 - \rho_1),$$

for example, any function of $\rho_1 - \rho_2$.

[5] The notation is that of Courant and Hilbert, *Methoden der mathematischen Physik* (Julius Springer, Berlin, 1931), Vol. I, p. 79.

TABLE I. $-H(\eta_0, \alpha)$.

η_0 \ α	0	0.5	0.75	1	1.5	2	4
0.2	0.1814	0.1733	0.1695	0.1658	0.1588	0.1521	0.1290
0.5	0.3935	0.3578	0.3416	0.3263	0.2985	0.2737	0.1987
1.0	0.6321	0.5475	0.5103	0.4762	0.4164	0.3662	0.2335
2.0	0.8647	0.7324	0.6711	0.6135	0.5152	0.4348	0.2471
3.0	0.9502	0.8197	0.7494	0.6813	0.5596	0.4618	
4.0	0.9817	0.8697	0.7969	0.7224	0.5843		
5.0	0.9933	0.9016	0.8293	0.7509			
∞	1	1	1	1	0.6667	0.5000	0.2500

Similarly, if $\rho_{1A}(\xi, \eta)$ and $\rho_{2A}(\xi, \eta)$ are solutions, then so are

$$\rho_{1B}(\xi, \eta)=1-\rho_{1A}(\xi, \eta)$$
$$\rho_{2B}(\xi, \eta)=1-\rho_{2A}(\xi, \eta). \tag{10'}$$

Again Eqs. (10′) satisfy the initial and boundary conditions and the differential Eqs. (4). Also the exchange term in (3) is not the only one that would give rise to (10′). In fact the exchange term could be any function $F(\rho_1, \rho_2)$ such that

$$F(\rho_1, \rho_2)=-F(1-\rho_1, 1-\rho_2),$$

for example, any odd function of $\rho_1-\rho_2$.

Equations (10) and (10′) are important in the subsequent development. As will be shown below the validity of (10′) can be tested by direct experiments.

It is evident from Eqs. (10) and (10′) that if one of the ρ's is known, then the other three can be found at once.

THE FLOW INTEGRALS

The observable quantities of interest are the net amounts of radioisotope that are transferred from one compartment to the other in the course of an electrolysis experiment. After passage of current for time t the solution in the cell is divided into two parts corresponding to $x>0$ and $x<0$. The separate parts are mixed and the counting rates of aliquots of side $x>0$ in case A and side $x<0$ in case B are determined. Then the amount of tracer that passes the boundary $x=0$ in the two cases will be

$$q_A=\frac{\gamma_A V_I}{\gamma_A{}^0 V_{II}}\cdot rV_{II}=\frac{\gamma_A}{\gamma_A{}^0}\cdot rV_I,$$
$$q_B=\frac{\gamma_B V_{II}}{\gamma_B{}^0 V_I}\cdot rV_I=\frac{\gamma_B}{\gamma_B{}^0}\cdot rV_{II}, \tag{11}$$

where γ_A = counting rate per unit volume, side $x>0$, time $=t$; $\gamma_A{}^0$ = counting rate per unit volume, side $x<0$, time $=0$; γ_B = counting rate per unit volume, side $x<0$, time $=t$; $\gamma_B{}^0$ = counting rate per unit volume, side $x>0$, time $=0$; V_I = volume side $x>0$; V_{II} = volume side $x<0$; and r = stoichiometric sodium concentration.

Let us first compute the difference, q_A-q_B, which turns out to be simply related to the results of experiments in which tracer is initially made uniform throughout the cell. If A is the cross section of the cell, then

$$q_A=A\int_0^t [J_1\rho_{1A}(0, t)+J_2\rho_{2A}(0, t)]dt \tag{12}$$

and

$$q_B=-A\int_0^t [J_1\rho_{1B}(0, t)+J_2\rho_{2B}(0, t)]dt.$$

Making use of Eqs. (10′) we see that

$$q_A-q_B=A(J_1+J_2)t. \tag{13}$$

If Q' is the rate at which tracer moves in an experiment where the initial tracer concentration is uniform, then in accordance with the earlier discussion we see that

$$Q'=A(J_1+J_2) \tag{14}$$

and

$$q_A-q_B=Q't. \tag{15}$$

This equation provides us with a direct test of Eqs. (10′). In writing the above equations, as well as in the discussion that follows, it is assumed that, except for the initial tracer concentrations, the experimental conditions are identical in cases A, B, and that involving uniform tracer.

We can now evaluate q_A and q_B. For $x=0$,

$$\xi=kn_2p_2(x-v_2t)/(v_1-v_2)=-\frac{kn_2p_2v_2t}{v_1-v_2}=-KJ_2t=\xi_0, \tag{16}$$

$$\eta=-kn_1(x-v_1t)/(v_1-v_2)=\frac{kn_1v_1t}{v_1-v_2}=KJ_1t=\eta_0, \tag{17}$$

where

$$K=k/(v_1-v_2).$$

On substituting these values for ξ and η into Eqs. (9) and making use of the flow ratio[6]

$$\alpha=-J_2/J_1,$$

we obtain

$$\rho_{1A}(0, t)=1+\sum_{i=1}^{\infty}\sum_{j=0}^{i-1}(-KJ_1t)^i\alpha^{i-j}\binom{i}{j}\binom{i-1}{j}\Big/ i!.$$

Using Eqs. (10), we find

$$\rho_{2A}(0, t)=-\sum_{i=1}^{\infty}\sum_{j=1}^{i}(-KJ_1t)^i\alpha^{i-j}\binom{i}{j}\binom{i-1}{i-j}\Big/ i!.$$

On substituting these relations into (12) we find upon integration and simplification that

$$q_A/AJ_1t=1+\alpha\sum_{i=1}^{\infty}[(-KJ_1t)^i/i!]\sum_{j=0}^{i-1}\alpha^j\binom{i}{j}\binom{i}{j+1}\Big/ i.$$

[6] Separate experiments, of course, are required to determine α. For polyacrylic acid—sodium hydroxide mixtures we have already shown how the information needed to compute α can be obtained (see reference 1).

For simplicity, we let $h_i(\alpha)$ represent the polynomials in α,

$$h_i(\alpha)=\sum_{j=0}^{i-1}\alpha^j\binom{i}{j}\binom{i}{j+1}\Big/ i \quad i\geqslant 1, \tag{18}$$

and also define

$$H(\eta_0,\alpha)=\sum_{i=1}^{\infty}(-\eta_0)^i h_i(\alpha)/i!, \tag{19}$$

where η_0 was defined in Eq. (17). Then

$$q_A/AJ_1t=1+\alpha H(\eta_0,\alpha), \tag{20}$$

and by using Eq. (13),

$$q_B/AJ_1t=\alpha[1+H(\eta_0,\alpha)]. \tag{21}$$

THE LIMITS OF q_A and q_B

It follows from purely physical considerations that q_A and q_B will be largest when $k=0$ and smallest when k is infinite.

For $k=0$

$$H(\eta_0,\alpha)=H(0,\alpha)=0$$

and

$$\begin{aligned} q_A&=AJ_1t=Q't/(1-\alpha)\\ q_B&=\alpha q_A. \end{aligned} \tag{22}$$

From the discussion given under Limiting Case above, it follows that for k infinite and $\alpha\leqslant 1$,

$$H(\eta_0,\alpha)=H(\infty,\alpha)=-1,$$

so that

$$\begin{aligned} q_A&=Q't\\ q_B&=0. \end{aligned} \tag{23}$$

For k infinite and $\alpha\geqslant 1$, it follows that

$$H(\infty,\alpha)=-1/\alpha$$

and

$$\begin{aligned} q_A&=0\\ q_B&=Q't. \end{aligned} \tag{24}$$

Equations (23) and (24) would also apply if k were finite and $v_1=v_2$, a situation which could be encountered only if the ions had the same sign of charge. It should be noted that the present method is best adapted to measuring the rate of exchange between ions of opposite sign rather than those of like sign. Thus if v_1 and v_2 had the same sign and were of the same order of magnitude, their difference would be difficult to determine with accuracy.

COMPUTATION OF k

As it stands, Eq. (19) converges slowly for values of η_0 greater than 2 or 3; however, it can be expressed in such a way that it is easy to compute. The polynomials $h_i(\alpha)$ are the hypergeometric functions $F(-i,\ -i+1;\ 2;\ \alpha)$, where F is given by the series

$$F(A,B;C;\alpha)=1+\frac{A\cdot B}{1!C}\alpha+\frac{A(A+1)B(B+1)}{2!C(C+1)}\alpha^2+\cdots.$$

The polynomials h_i satisfy the recursion formula

$$(i+1)h_i=(2i-1)(1+\alpha)h_{i-1}-(i-2)(1-\alpha)^2h_{i-2}.$$

The computation of $H(\eta_0,\alpha)$ can be greatly simplified by expressing the function in another way, namely,

$$\begin{aligned} H(\eta_0,\alpha)=&-\frac{1}{1+\alpha}+\frac{\exp[-(1+\alpha)\eta_0]}{1+\alpha}\\ &\times\left\{1-\sum_{i=1}^{\infty}\left[\frac{\eta_0}{(1+\eta_0)^2}\right]^i b_{2i-1}\right.\\ &\left.\times\exp_{2i+1}[(1+\alpha)\eta_0]\right\}, \end{aligned} \tag{25}$$

where

$$b_n=\frac{4n}{n+3}\cdot\frac{4(n-2)}{n+1}\cdot\frac{4(n-4)}{n-1}\cdots\frac{4}{4}$$

and

$$\exp_n x=e^x-\sum_{j=0}^{n-1}x^j/j!.$$

The series in (25) converges much more rapidly than that in (17).

To expedite the computation of k, we have prepared a short table of $H(\eta_0,\alpha)$ [see Table I]. From (20) and (14) we see that

$$H(\eta_0,\alpha)=\frac{1}{\alpha}\left[\frac{q_A(1-\alpha)}{Q't}-1\right]. \tag{26}$$

Since α, q_A, Q', and t are all experimentally measureable quantities, it follows that η_0 can be determined by reference to Table I. A similar procedure can be followed using α, q_A, and q_B in conjunction with the equation obtained by combining (20) and (21), namely,

$$-H(\eta_0,\alpha)=\frac{1/\alpha-q_A/q_B}{1-q_A/q_B}. \tag{27}$$

The calculation of k might be done more directly by solving (20) for η_0 as a function of q_A and α. Unfortunately, the resulting series converges slowly so we have preferred to compute $H(\eta_0,\alpha)$.

EFFECT OF A FRIT IN THE CELL

In the above calculations we have assumed that the cell is of uniform cross section and that by means of a suitable mechanical device we can bring about an initial discontinuity in tracer concentration. Such an initial discontinuity can also be formed conveniently with the aid of a glass frit in the cell. If this is done, it turns out that the equations given above for q_A, q_B, and k still apply exactly, providing one side *and* the frit are initially filled with the solution containing tracer.

This can be shown as follows. Let the frit extend over the range $-L\leqslant x\leqslant 0$, and let us denote the cross sections of the frit and the tube parts of the cell by A'

and A, respectively. If we still regard the problem as one-dimensional, then the field strength in the frit is

$$E'=(A/A')E,$$

where, as before, E is the field strength in the tubular parts of the cell.

Let us designate the three regions of the cell by I, II, III, as follows: region I, $x>0$; region II, the frit; region III, $x<-L$. Consider case A, with initial conditions $\rho_1=\rho_2=1$ in regions II and III, and $\rho_1=\rho_2=0$ in region I. The differential equations are of the same form as Eq. (3) but with the velocities v appropriate to each region.

We make the following change of variables: ξ_I, η_I, ξ_{II}, and η_{II}, the same as ξ and η above but with appropriate v's;

$$\xi_{III}=n_2p_2[(x+L)-v_{2III}t']/(v_{1III}-v_{2III}).$$

$\eta_{III}=-kn_1\{(x+L)+(A'/A)L[1-(v_{1II}/v_{2II})]-v_{1III}t'\}/(v_{1III}-v_{2III})$, where $t'=t+(L/v_{2II})$. With the aid of this transformation and the fact that the ρ's must be continuous at $x=0$ and $x=-L$, it can be shown that in case A, ρ_{1I} and ρ_{2I} are identical with the ρ_{1A} and ρ_{2A} previously obtained. The details of this proof are straightforward but lengthy so we omit them here.

ACKNOWLEDGMENT

We wish to express our appreciation to Mr. Peter B. Hill for his help in computing Table I.

THE JOURNAL OF CHEMICAL PHYSICS VOLUME 20, NUMBER 8 AUGUST, 1952

Electrolytic Properties of Aqueous Solutions of Polyacrylic Acid and Sodium Hydroxide. III. The Rate of Sodium Ion Exchange between Polyacrylate and Free Sodium Ions*

FREDERICK T. WALL, PHILIP F. GRIEGER,† JOHN R. HUIZENGA,‡ AND ROBERT H. DOREMUS
Noyes Chemical Laboratory, University of Illinois, Urbana, Illinois

(Received February 18, 1952)

The exchange of free sodium ions with sodium ions bound to polyacrylate ion has been investigated by an electrolytic transference method. On the assumption that there is a single exchange process, rate constants have been computed and the theory has been found to provide a moderately good representation of the data. A much better correlation is obtained, however, if it is assumed that there are two exchange processes, one very rapid and the other very slow. Presumably the sodium ions that exchange rapidly belong to the polyacrylate ion atmosphere while those that exchange slowly are located within the coiled polymer ion. The distribution of sodium ions between these two groups has been computed.

INTRODUCTION

THE immediately preceding article[1] deals with the theory of bound ion exchange accompanying electrolytic transference experiments. The present paper, on the other hand, is concerned with some observed results of such experiments together with their interpretation. The actual transference-exchange measurements were made on polyacrylic acid—sodium hydroxide mixtures over a range of 35 percent to 80 percent neutralization; in this range, polyacrylate ions bind many sodium ions which are capable of exchanging with free sodium ions in solution.

The physical quantity of significance which we seek to measure is the specific exchange rate constant k, which was defined in the aforementioned article.[1] The actual total exchange rate is presumed to be given by $kn_1n_2p_2$, which was derived assuming that all sodium ions bound in the sphere of the polyelectrolyte anion can exchange with free ions with equal facility. Actually it is not unreasonable to suppose that the sodium ions bound near the interior of the coiled-up polymeric anion would exchange less rapidly than those near the surface. Accordingly, any exchange constant which might be evaluated assuming the above expression will be only an average value, and hence we can expect appreciable uncertainty in the magnitude of the constant k.

An alternative model for the polymer and its bound ions consists of the following. Let us suppose that the central core of the polymeric anion contains bound sodium ions which exchange infinitely slowly while the outer portion of the polymeric anion holds ions of opposite charge so loosely that they exchange at an infinite rate. Although this model is arbitrarily extreme, it lends itself to easy calculation without recourse to solution of any new differential equations. The interpretation of our experiments will therefore be made in each of two ways: first, assuming a uniform exchange rate, and second, assuming the extreme alternative model just defined.

* This investigation was carried out under the sponsorship of the Reconstruction Finance Corporation, Synthetic Rubber Division.

† Present address: The Edison Laboratory, Thomas A. Edison, Inc., West Orange, New Jersey.

‡ Present address: Argonne National Laboratory, P. O. Box 5207, Chicago 80, Illinois.

[1] F. T. Wall and P. F. Grieger, J. Chem. Phys. **20**, 1200 (1952).

APPARATUS AND PROCEDURE

The details pertaining to the transference apparatus, its operation, the preparation of materials, the methods of chemical analysis, the tracer counting technique, together with a discussion of sources of error, have already been given.[2] There are, however, a few new points in connection with the present experiments that should be mentioned. As before, the cell consisted of a straight horizontal tube about 22 cm long separated into two equal compartments by a sintered glass coarse Pyrex frit, 3 mm thick and 2 cm in diameter. The volumes of the anode and cathode compartments were both found to be 49 cm³ by weighing their respective volumes of water. Platinum electrodes were sealed into the cell at both ends. They consisted of disks whose areas were about one-half the cross section of the tube. The faces of the electrodes, which were 21 cm apart, were nearly parallel and normal to the long axis of the tube. Directly above and below the electrodes were tubes used for filling and emptying the cell. During electrolysis the tubes above the electrodes were left open to permit the escape of oxygen and hydrogen.

The experiments were invariably started as follows. Both end compartments and the frit were filled with a polyacrylic acid solution neutralized to a known extent with sodium hydroxide containing tracer.[3] The filling tube on one side was then closed and the opposite compartment was drained. The empty side was filled with an identical polyacrylic acid—sodium hydroxide mixture, except that it contained no tracer. This side was again drained to remove residual tracer and then refilled. The liquid levels in the filling tubes were adjusted visually. After opening the filling tube on the first side the current was started. In all experiments, one side and the frit were initially filled with solution containing tracer.

As might be expected, this simple technique of making a sharp boundary is not perfect, and nearly always a detectable amount of tracer either gets into, or is left in, the compartment that is supposed to be free of tracer. To get a measure of this effect, some duplicate "blank" experiments were carried out. In these experiments, the cell was filled as described above, and then allowed to stand for various times without passage of current. Upon taking radioactive counts of the "nonactive" side, it was found that the error attributable to mixing amounted to about one-fifth of the background count. A small correction for this effect was made in those instances where it appeared warranted.

By adjusting an external resistance the current was held constant throughout each electrolysis at 4 milliamperes. Not more than one-tenth of the total sodium was transported across a given boundary in any experiment, so it is safe to assume that the stoichiometric concentrations remained essentially constant in the neighborhood of the frit. Na^{22} was used as tracer in all the experiments listed in Table I.[4]

TABLE I. Transference experiments with initial discontinuity in tracer concentration for polyacrylic acid partially neutralized with sodium hydroxide.

Time, min	$q_A \times 10^5$, moles	$q_B \times 10^5$, moles	$(q_A - q_B) \times 10^5$, (moles) obs.	calc.
Series 1, 78.7% Neutralized, $C=0.0396N$ $Q'=-6.10\times10^{-7}$ moles/min., $\alpha=1.4$				
30	0.44	2.09	−1.65	−1.83
60	0.95	4.78	−3.83	−3.65
90	1.81	7.70	−5.89	−5.48
90		8.13	−6.32	
120	2.15	10.08	−7.93	−7.30
120		10.45	−8.30	
Series 2, 74.9% Neutralized, $C=0.0396N$ $Q'=-5.41\times10^{-7}$ moles/min, $\alpha=1.4$				
40	0.92	3.43	−2.51	−2.16
60	1.74	4.85	−3.11	−3.25
80	2.21	6.67	−4.46	−4.33
120	3.68	11.14	−7.46	−6.50
Series 3, 64.2% Neutralized, $C=0.0263N$ $Q'=-3.23\times10^{-7}$ moles/min, $\alpha=1.27$				
20	1.11	1.54	−0.43	−0.65
40	1.65	3.02	−1.37	−1.29
80	2.63	5.15	−2.52	−2.58
120	4.53	8.04	−3.51	−3.88
Series 4, 54.7% Neutralized, $C=0.0396N$ $Q'=0.34\times10^{-7}$ moles/min, $\alpha=0.92$				
30	0.93	0.56	0.37	0.10
60	1.79	1.21	0.58	0.21
90	2.85	2.44	0.41	0.31
120	3.48	3.33	0.15	0.41
Series 5, 47.2% Neutralized, $C=0.0396N$ $Q'=1.39\times10^{-7}$ moles/min, $\alpha=0.74$				
40	1.65	0.69	0.96	0.56
80	3.21	1.78	1.43	1.11
80	3.34	1.95	1.39	
120	5.50	3.63	1.87	1.67
Series 6, 39.7% Neutralized, $C=0.0263N$ $Q'=2.55\times10^{-7}$ moles/min, $\alpha=0.60$				
20	1.37			
40	2.42	0.81	1.61	1.02
40	2.53			
80	3.75	1.57	2.18	2.04
120	6.10	2.94	3.16	3.06
Series 7, 36.5% Neutralized, $C=0.0396N$ $Q'=4.46\times10^{-7}$ moles/min, $\alpha=0.48$				
40	3.15	1.29	1.86	1.78
60	3.68	1.31	2.37	2.68
80	5.37	1.53	3.84	3.57
120	7.69	2.62	5.07	5.35

RESULTS

In Table I are given the results of experiments on polyacrylic acid partially neutralized with sodium hydroxide over the range 37 percent to 79 percent.

[2] Huizenga, Greiger, and Wall, J. Am. Chem. Soc. **72**, 2636 (1950).

[3] The mixture of polyacrylic acid and sodium hydroxide containing tracer was allowed to stand for a few days (at least) before it was used in transference experiments. For these solutions then it is safe to assume that $\rho_1=\rho_2$.

[4] The tracer was obtained from Professor A. L. Hughes, Washington University, St. Louis, Missouri.

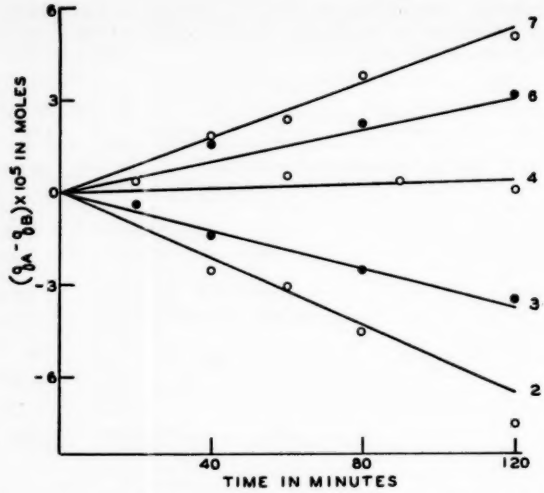

FIG. 1. Plots of $q_A - q_B$ *vs* time for various polyacrylic acid solutions. Circles and dots represent experimental points; lines are drawn with calculated slope.

Measurements were made at two polyacrylic acid concentrations, namely, $C = 0.0396$ and 0.0263 equivalents per liter. The number of equivalents, of course, is taken as the weight of polymer divided by the monomer molecular weight.

For each series of experiments the quantities Q' and α are listed. Q', as previously defined,[1] is the rate at which radioactive sodium is transported if the tracer concentration is initially uniform throughout the apparatus, the conditions of the experiment being otherwise identical to those of cases *A* and *B*. α is computed by using the equation

$$\alpha = -J_2/J_1 = (cp_2/s)\Lambda_p/rf\Lambda_{Na}, \qquad (1)$$

where s is the degree of polymerization, Λ_p and Λ_{Na} the equivalent conductances of the ions, r the stoichiometric sodium hydroxide concentration, and f the fraction of sodium ions that are not bound by polymer.

The α-values listed in Table I were computed from data already reported.[2] The various quantities appearing in Eq. (1) and defined earlier[2] depend upon the results of transference, conductance, and *p*H measurements; there is probably an uncertainty of 10 percent in the α-values listed in Table I.

As previously defined the q's equal the total number of moles of traced sodium transported across the boundary. For convenience, the observed values of $q_A - q_B$ are listed in Table I together with those calculated by means of the equation[1]

$$q_A - q_B = Q't. \qquad (2)$$

The data in Table I include five pairs of identical experiments. In four of these, the q values agree within 5 percent, in the fifth, by 10 percent. In view of the experimental technique, especially the method of forming the initial discontinuity in tracer concentration, we consider this accuracy satisfactory.

It should also be mentioned that with one exception the observed values of the q's lie between those calculated for $k=0$ and $k=\infty$, as would be expected. Of course, this is not a severe test of the data, especially for large times, but at least it indicates qualitatively that we are dealing with an exchange phenomenon.

TABLE II. Observed and calculated $q_A - q_B$ *vs* time slopes.

Series	$d(q_A-q_B)/dt \times 10^7$ moles/min	$Q' \times 10^7$ moles/min
1	−6.7	−6.1
2	−5.8	−5.4
3	−3.1	−3.2
4	—	0.34
5	1.8	1.4
6	2.7	2.6
7	4.3	4.5

THE QUANTITY $q_A - q_B$ AS A FUNCTION OF TIME

In agreement with Eq. (2), the plots of $q_A - q_B$ *vs* time are straight lines with slopes nearly equal to Q' in every case.[5] As can be seen from Table I and Fig. 1, the differences between the individual observed and calculated values of $q_A - q_B$ are greater than 10 percent in only a few instances.

TABLE III. Numerical values of k in liters/equiv. min as computed from the ratio q_A/q_B.

Series	1	2	3	5	6	7
% Neutralization	78.7	74.9	64.2	47.2	39.7	36.5
c	0.0396	0.0396	0.0263	0.0396	0.0263	0.0396
Time min						
20			5			
30	30					
40		14	12	13	13	2
60	16	7				2
80		5	7	2	4	4
90	9					
120	7	4	6	0.6	1	1

The experimental accuracy appears to be considerably better for the relatively large values of q than for the small ones. In view of the nature of the experiment, this is not surprising. In Table II the slopes of the best straight lines are compared with Q'.

The agreement between $d(q_A - q_B)/dt$ and Q' is generally satisfactory. For experiment 4, where $\alpha = 0.92$, q_A and q_B are nearly equal, so their difference is subject to a large percentage error. Even in this unfavorable case, as can be seen from Fig. 1, the individual values of $q_A - q_B$ are of the right order of magnitude.

THE MAGNITUDE OF k

When the values of q_A and q_B listed in Table I are plotted against t, we find that the points can almost

[5] The fact that $q_A - q_B = Q't$ does not of itself prove the general validity of our theory of the exchange process. It does, however, serve to verify a limited portion thereof.

always be connected fairly well by straight lines through the origin. In several cases the short time points (20 to 40 minutes) fall below the straight lines.

Now it can be seen from the following equations,[1]

$$q_A=\frac{Q't}{1-\alpha}[1+\alpha H(\eta_0, \alpha)] \quad (3)$$

$$q_B=\frac{\alpha Q't}{1-\alpha}[1+H(\eta_0, \alpha)], \quad (4)$$

and from inspection of the numerical values[1] of $H(\eta_0, \alpha)$ that the curves for q_A and q_B plotted against time should be concave downward or in the limit, linear. However, the observed curves, as mentioned above, usually appear to be concave upward. Qualitatively, the k's computed from the short-time points should then be too large relative to those computed from the long-time points. While the short-time points are probably less reliable than those corresponding to longer times because of background correction, filling error, etc., the fact that they are quite consistently low warrants some explanation, which will be given later.

Values of k can be computed from the ratio q_A/q_B as follows. $H(\eta_0, \alpha)$ is found from the following equation:

$$H(\eta_0, \alpha)=\frac{1/\alpha-q_A/q_B}{q_A/q_B-1}. \quad (5)$$

Then η_0 is found from a plot of $H(\eta_0, \alpha)$ against η for the given experimental value of α. This plot can be made from data given in Table I of the preceding article.[1] η_0 and k are related by the following expressions:

$$\eta_0=\frac{\Lambda_{Na}rftk}{\Lambda_{Na}+\Lambda_p}. \quad (6)$$

Thus k can be found from η_0 and the other known values discussed in connection with Eq. (1). The results of this calculation are shown in Table III. With two exceptions, Series 3 and 7, k decreases with increase in time, although in most instances k is constant within a factor of two over the range 60 to 120 minutes. It should also be pointed out that the value of k is quite sensitive to errors in the q's and α. For the larger values of k in Table III, $H(\eta_0, \alpha)$ varies weakly with η_0; consequently, a small error in H can give rise to a large error in the calculated value for η_0.

By assuming values of k, q_A and q_B have been calculated from Eqs. (3) and (4). The proper value of η_0 is found from Eq. (6); then $H(\eta_0, \alpha)$ is found from the plots described above. The data are generally represented rather well by this method of computation, which is apparently not so sensitive to errors as is Eq. (5). By successive trials, the values of k that best represent the data are obtained, and these "best" average values of k are probably accurate within a factor of about two. They are summarized in Table IV.

In Fig. 2 are given three illustrative examples of q_A and q_B plots. For this purpose we have chosen Series 1, for which agreement between theory and experiment is poor, and Series 7, for which the agreement is good. These results can also be seen in Table III, where the range of k values for Series 1 is found to be much larger than for Series 7.

TABLE IV. Average k values determined graphically.

Series	% Neut.	Polymer conc. equiv./liter	k liters/equiv. min
1	78.7	0.0396	8
2	74.9	0.0396	4
3	64.2	0.0263	5
5	47.2	0.0396	1
6	39.7	0.0263	2
7	36.5	0.0396	2

For Series 1, Fig. 2(A), it is possible to choose k so that the calculated curves for q_A and q_B closely approximate the observed values for 90 and 120 minutes, but the short-time points (30 and 60 minutes) fall well below these curves. For Series 7, Fig. 2(B) and 2(C), the q *vs* t plots are given for two values of k, to show how well k can be determined by the graphical method. The curves in Fig. 2(B) correspond to $k=2.0$, which we have taken as the best value, while the curves in Fig. 2(C) correspond to $k=1.3$. It will be seen that the curves in Fig. 2(B) fit the data appreciably better than do those in Fig. 2(C).

It appears from Table IV, that k exhibits considerably variation in value, with possibly some tendency to

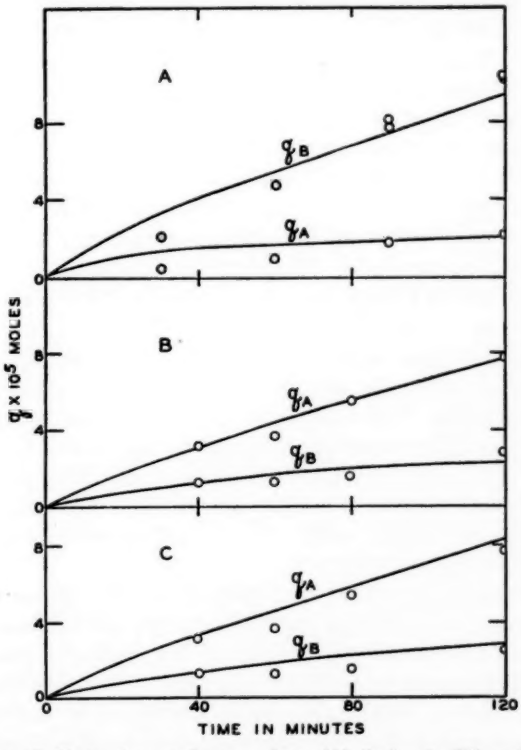

FIG. 2. Pots of q_A and q_B *vs* time. (A) Series 1; (B) and (C) Series 7. Circles represent experimental points; curves are drawn from calculated values.

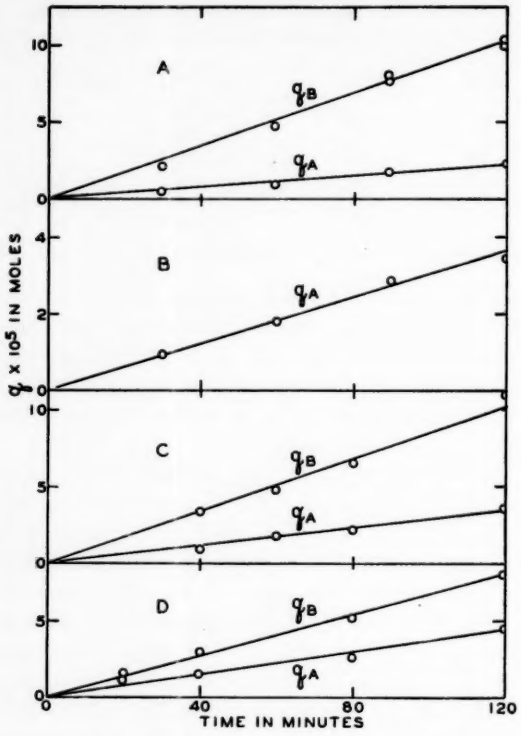

FIG. 3. q_A and q_B *vs* time. Lines are drawn to fit data as well as possible. (A) Series 1; (B) Series 4; (C) Series 2; (D) Series 3.

increase with increasing neutralization. This trend is not conclusive nor will we attempt to offer any detailed explanation for it. It is of interest to note, however, that the values of k indicate second-order reactions which require about 5 minutes for half the exchange to be complete for the concentrations employed. This suggests that the exchange process is actually much slower than one might surmise. It is evident that many of the sodium ions bound to the polyacrylate anions are held fairly tightly and can escape from the sphere of influence only with some difficulty.

EXTENSION TO THE CASE OF TWO EXCHANGE REACTIONS

The foregoing results show that the assumption of a single ion exchange rate is not entirely satisfactory in describing the observed results. It was mentioned earlier that the initial exchange appears to take place faster than that which occurs in the later stages. In an effort to account for this behavior, we shall now consider an alternative model which is a combination of two simpler ones.

Let us suppose that a significant fraction of the sodium ions bound to the polyacrylate ions are present as a cloud surrounding it outside of the central polymer ion. The remainder of the sodium ions will be assumed to be tied up within the core of the negative ion. We can now expect that the outer sodium ions will exchange at an exceedingly rapid rate, whereas those in the interior will exchange very slowly. An artificial, although instructive model, consists of assuming two classes of ions, one which exchanges infinitely fast, and the other infinitely slowly.

For such a model, let us suppose that there are p_{21} bound sodium ions that exchange at a rate governed by k_1, and p_{22} bound sodium ions that exchange at a rate governed by a constant k_2. Then the exchange equations are as follows:

$$\begin{aligned}
-n_1\partial\rho_1/\partial t &= n_1v_1\partial\rho_1/\partial x + n_1n_2p_{21}k_1(\rho_1-\rho_{21}) \\
&\quad + n_1n_2p_{22}(\rho_1-\rho_{22}) \\
-n_2p_{21}\partial\rho_{21}/\partial t &= n_2p_{21}v_2\partial\rho_{21}/\partial x - n_1n_2p_{21}k_1(\rho_1-\rho_{21}) \\
-n_2p_{22}\partial\rho_{22}/\partial t &= n_2p_{22}v_2\partial\rho_{22}/\partial x - n_1n_2p_{22}k_2(\rho_1-\rho_{22}).
\end{aligned} \tag{7}$$

In the limit as $k_1\rightarrow\infty$, $\rho_1\rightarrow\rho_{21}$, so upon adding the first two equations in (7) we obtain

$$\begin{aligned}
-(n_1+n_2p_{21})\partial\rho_1/\partial t &= (n_1v_1+n_2p_{21}v_2)\partial\rho_1/\partial x \\
&\quad + n_1n_2p_{22}k_2(\rho_1-\rho_{22}) \\
-n_2p_{22}\partial\rho_{22}/\partial t &= n_2p_{22}v_2\partial\rho_{22}/\partial x \\
&\quad - n_1n_2p_{22}k_2(\rho_1-\rho_{22}).
\end{aligned} \tag{8}$$

The linear transformations

$$\begin{aligned}
\xi' &= \gamma(x-v_2t)/(\beta-v_2) \\
\eta' &= -k_2n_1(x-\beta t)/(\beta-v_2),
\end{aligned}$$

where

$$\begin{aligned}
\beta &= (n_1v_1+n_2p_{21}v_2)/(n_1+n_2p_{21}) \\
\gamma &= k_2p_{22}n_1n_2/(n_1+n_2p_{21})
\end{aligned}$$

reduce Eqs. (8) to the form

$$\begin{aligned}
\partial\rho_1/\partial\xi' &= \rho_{22}-\rho_1 \\
-\partial\rho_{22}/\partial\eta' &= \rho_{22}-\rho_1.
\end{aligned} \tag{9}$$

On carrying through the computation of q_A and q_B as before we find that (3) and (4) formally still hold providing we replace

$$\begin{aligned}
J_1 &\text{ by } J_1+J_{21}, \\
J_2 &\text{ by } J_{22}, \\
k &\text{ by } k_2.
\end{aligned}$$

The new equations are

$$q_A = \frac{Q't}{1-\alpha'}[1+\alpha' H(\eta_0', \alpha')], \tag{10}$$

$$q_B = \frac{\alpha' Q't}{1-\alpha'}[1+H(\eta_0', \alpha')], \tag{11}$$

TABLE V. Comparison of the flow ratio α' computed from Eqs. (12) and (13). The ratio of fast to slow exchanging sodium ions p_{21}/p_{22}.

Series	% Neut.	dq_A/dt $\times10^7$	dq_B/dt $\times10^7$	$Q'\times10^7$	α' Eq. (12)	α' Eq. (13)	p_{21}/p_{22}
1	78.7	1.8	8.6	−6.10	4.5	3.4	1.6
2	74.9	3.0	8.5	−5.41	2.8	2.8	1.3
3	64.2	3.9	6.7	−3.23	1.8	1.9	1.1
4	54.7	3.0	2.6	0.34	1.1	1.2	−0.23
5	47.2	4.3	2.7	1.39	0.68	0.66	0.39
6	39.7	5.1	2.3	2.55	0.50	0.45	0.63
7	36.5	6.6	2.1	4.46	0.32	0.32	0.97

where

$$\alpha' = -J_{22}/(J_1+J_{21}),$$
$$\eta_0' = k_2(J_1+J_{21})t/(v_1-v_2),$$
$$Q' = A(J_1+J_{21})(1-\alpha').$$

Up to now we have always considered α to be positive since J_2 and J_1 have opposite signs. Now, however, α' can be negative even though v_1 and v_2 have opposite signs whenever $|J_{21}| > |J_1|$.

The case of $k_2=0$ is of special interest, for then we simply have

$$q_A = Q't/(1-\alpha'), \tag{12}$$

$$q_B = \alpha' Q't/(1-\alpha'). \tag{13}$$

Qualitatively (12) and (13) are in accord with the experiments here reported, for as we noted in the previous section q_A and q_B are approximately linear with t in most instances. Quantitatively it turns out that our data are in excellent agreement with (12) and (13). From plots of the data, such as those in Fig. 3, the slopes, dq_A/dt and dq_B/dt, of the best straight lines, can be determined. Using Q', α' is then computed separately by means of Eqs. (12) and (13). The results of this calculation are shown in Table V. As can be seen, the separate α' values agree closely except for Series 1. Even for Series 4, where q_A and q_B are nearly equal, and the $q_A - q_B$ plot was indeterminate, there is good agreement for the present calculation.

We can also calculate p_{21}/p_{22}, which is the ratio of the number of sodiums that exchange rapidly to the number that exchange slowly. Thus from the definition of α', we find, since $J_{21} = n_2 p_{21} v_2$, that

$$-p_{22} = \alpha' p_{21} + \alpha'(n_1 v_1/n_2 v_2).$$

We can also write Q' in two ways, namely,

$$Q'/A = n_1 v_1 + n_2 v_2 p_{21} + n_2 v_2 p_{22}$$
$$= n_1 v_1(1-\alpha) = (n_1 v_1 + n_2 v_2 p_{21})(1-\alpha'),$$

or

$$p_{21} = [-1+(1-\alpha)/(1-\alpha')](n_1 v_1/n_2 v_2).$$

Combining these expressions for p_{22} and p_{21} we find simply that

$$p_{21}/p_{22} = [(\alpha/\alpha')-1]/(1-\alpha).$$

The values of this ratio are also included in Table V. For Series 4 and 5, α/α' is approximately unity, so the computed values of p_{21}/p_{22} will be particularly sensitive to small errors in the ratio α/α'. For Series 4, the calculation fails and a negative value of p_{21}/p_{22} is obtained. Likewise the value 0.39 for Series 5 might easily be in substantial error. For example, if we arbitrarily use a value of α' 6 percent smaller than 0.67, p_{21}/p_{22} is nearly doubled.

If we disregard the results in the neighborhood of 50 percent neutralization, it appears that the fraction of the bound sodium ions that are in the ionic atmosphere increases with increase in degree of neutralization. On the basis of the calculations that we made in this and the preceding section, there is little doubt that the hypothesis of two exchange processes, one proceeding infinitely fast while the other proceeds infinitely slowly, gives a much better interpretation of our results than does the assumption of a single exchange process. This appears to be a satisfactory outcome because the hypothesis of two exchange rates is physically plausible.

Within the accuracy of our data, the assumption that $k_2=0$ is simply a convenient approximation. Of course, we have tacitly assumed that $k_2>0$ in part of our treatment because initially we let $\rho_1=\rho_{21}=\rho_{22}$ everywhere, if $k_2=0$, ρ_{22} would always be zero. Actually the exchange constant k_2 must be appreciable. To gain some idea of its magnitude we performed the following experiments. Tracer as sodium ions was added to a given polyacrylic acid—sodium hydroxide mixture and in the first instance, the electrolysis was carried out as quickly as possible. In the second instance the tracer—polyacrylic acid—sodium hydroxide mixture was allowed to stand for several days before an identical electrolysis was carried out. q_A and q_B were found to be the same in the two kinds of experiments both at 75 percent and 45 percent neutralization. If k_2 were equal to zero, then q_A should have been the same for both types of experiment, but q_B should have been less in the first instance than in the second. Evidently k_2 is large enough so that during the time of filling and rinsing the cell (15 to 30 minutes) as well as during the time of electrolysis (one hour) the relatively slow exchange proceeds effectively to completion.

Were our data precise enough, at short times we could in principle determine k_2 by means of Eqs. (10) and (11). A k_2 value not equal to zero will give rise to curves for q_A and q_B that are concave downward, but the curvature will be distinctly less marked than is evident in Fig. 2, particularly for high degrees of neutralization where p_{21}/p_{22} is largest. To estimate p_{21}/p_{22} it is reasonable, in the interest of simplicity, to let $k_2=0$ and use the simple Eqs. (12) and (13). What we have done then, is to compute the ratio of fast to slowly exchanging sodiums that would exist if the slow group actually exchanges at zero rate.

For the complicated system polyacrylic acid—sodium hydroxide, it appears that the rate of exchange experiments do not provide us with single exchange constants. Actually we obtain some more interesting information concerning the distribution of bound sodium ions between rapidly and slowly exchanging groups. It is reasonable to identify these as being "outside" the polyacrylate ion (i.e., in its atmosphere) on the one hand and "inside" the ion on the other.

Inter- and Intramolecular Energy Transfer Processes. I. Nitro-Compounds and Hydrocarbons

C. Reid
University of British Columbia, Vancouver, British Columbia, Canada
(Received February 11, 1952)

The addition compounds of aromatic nitro-compounds and hydrocarbons fluoresce appreciably only if the hydrocarbon component itself has a possible transition lying in the region where the nitro-complex might be expected from its absorption to emit. The resulting emission spectrum is very similar to that of the hydrocarbon component but much more strongly allowed. This is attributed to the breaking down of the $S \leftarrow T$ selection rule as the complex dissociates.

INTRODUCTION

THIS is the first of a series of papers dealing with the emission spectroscopy of systems of two components dissolved or suspended in a nonabsorbing rigid medium. It was suggested in a recent letter[1] that the highly efficient process, in which energy absorbed by one component in solution is transferred to and emitted by the second component in microcrystalline form, is due to one of two processes: (a) long-range transfer of the kind suggested by Förster[2] or (b) short-range transfer, the first component being adsorbed on the second. Subsequent work[3] has shown that although in some cases (e.g., anthracene) long-range transfer between identical molecules in solution occurs, transfer between nonidentical molecules is observable only at temperatures low enough for definite molecular association to be brought about by dispersion forces.

Much of this work has been clarified by comparison with a more stable kind of molecular compound formed by aromatic hydrocarbons, namely, the well crystalline nitro-complexes often used for hydrocarbon characterization. Of the complexes examined those with styphnic acid and picric acid are nonfluorescent. The trinitrobenzene complexes, however, almost all emit strongly in the 5000 to 7000A region and are the subject of this paper.

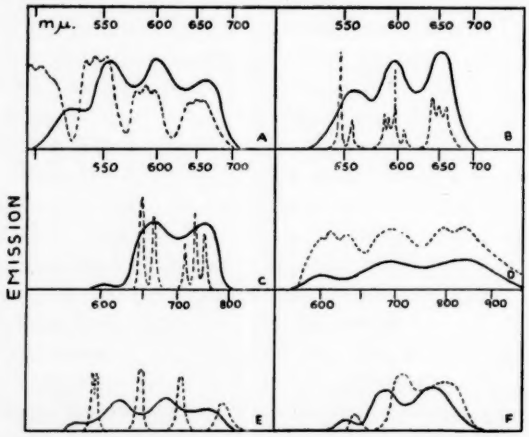

FIG. 1. Solid lines: emission spectra of complexes of hydrocarbons with trinitro benzene. Dotted lines: long-lived triplet emission spectra of the corresponding hydrocarbons alone. *A*: chrysene; *B*: 1,2,5,6 dibenzanthracene; *C*: pyrene; *D*: phenanthrene; *E*: 1,2 benzanthracene; *F*: 9,10 dimethyl 1,2 benzanthracene. All at −180°C.

EXPERIMENTAL

Hydrocarbons were purified by chromatography in Al_2O_3 columns. Trinitrobenzene (cp) was recrystallized several times from ether. Hydrocarbon-T.N.B. complexes were prepared in ether solutions and recrystallized. Solutions in one part ether plus 5 parts isopentane, which mixture forms a clear rigid glass at the temperature of liquid nitrogen, were cooled to −180°C and irradiated with the mercury 3600 line from a General Electric A.H. 6 high pressure mercury arc with suitable filters. Spectra were photographed using a Hilger *E2* spectrograph on Eastman Kodak II F3 or IN plates. Traces of some of the spectra obtained are shown in Fig. 1. Similar results were obtained with fluorene, trans-stilbene, acenaphthene, and with a few heterocyclics, such as acridine.

Absorption spectra of the hydrocarbon complexes were also examined at low temperatures using the same spectrograph. Some of them are given in Fig. 2.

DISCUSSION

The emission spectra show obvious similarities to the well-known long-lived triplet-singlet emission of the pure hydrocarbons, although usually there is a slight shift in the position of the bands and considerable broadening. The emission spectra show no mirror image relationship with the absorption spectra which usually exhibit no trace of vibrational structure (pyrene is an exception). This suggests that the situation is as shown in Fig. 3.

Absorption is to a repulsive state. This is very reasonable since the binding energies of the hydrocarbon complexes are only 2 to 4 kcal in the ground state and explains the absence of vibrational structure in the absorption spectra. The dissociation products are the hydrocarbon in its triplet state and presumably an unexcited trinitrobenzene molecule. However, during the dissociation process the spin selection rule breaks down and the $S \leftarrow T$ process occurs rapidly.* The considerable broadening of the bands is presumably a

[1] M. M. Moodie and C. Reid, J. Chem. Phys. **19**, 986 (1951).
[2] Th. Förster, Ann. Physik **2**, 55 (1948).
[3] M. M. Moodie and C. Reid (to be published).

* Less than 10^{-4} sec.

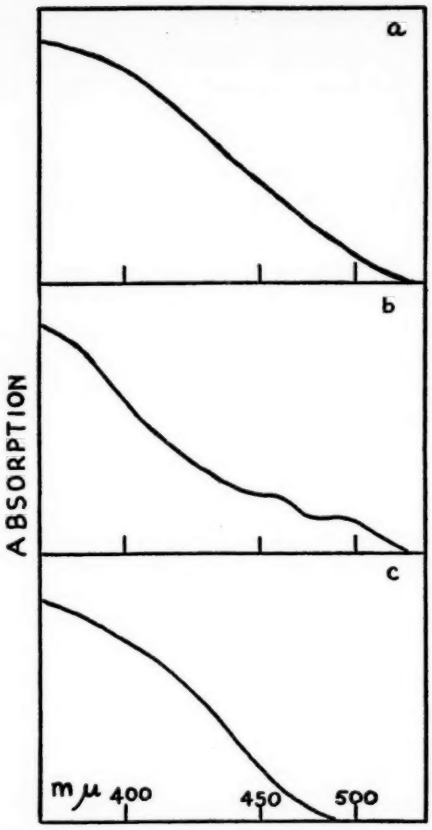

FIG. 2. Onset of absorption in complexes of hydrocarbons and trinitro benzene (a) 1,2,5,6 dibenzanthracene-T.N.B. (b) pyrene-T.N.B. (c) chrysene-T.N.B. Curves give approximate log I_0/I values. Extinction coefficients cannot be given because complexes are partly dissociated in solution.

result of the fact that the energy is a function of the amount of coupling with the trinitrobenzene molecule, and this decreases during the dissociation process. That the emission is due to the hydrocarbon component is consistent with the fact that polynitro compounds themselves are well known for their lack of fluorescence.

A few special cases may be mentioned. The T.N.B.-carbazole complex does not emit appreciably. This is explained by the fact that the carbazole triplet level (4080A) lies at higher energy than that of most of the aromatic hydrocarbons we have considered and the energy, E, in Fig. 3 is less than is required to excite the hydrocarbon triplet level. For the same reason, presumably, the fluorescence yield from the phenanthrene complex (4600A) is very low compared with that of other hydrocarbons.

The case of the anthracene-T.N.B. complex (Fig. 4) requires special mention. It shows a very well-defined emission spectrum beginning at about 5200A and extending into the infrared. The absorption spectra is again a continuum suggesting that the situation should be similar to that of other hydrocarbons. However, the triplet emission[4] is reported as at 6800A. One explanation of this fact might be that the hydrocarbon in the complex is already in the lowest triplet state and is excited to the second triplet level, and the observed emission then corresponds to triplet-triplet emission. A triplet-triplet transition has been found in absorption by McClure[5] and could very well correspond to this emission. If this is the case, however, the anthracene complex is quite different to those formed by most other hydrocarbons. The alternative is that the assigned triplet level is in error. The possibility of the latter will be considered elsewhere.

[4] G. N. Lewis and M. Kasha, J. Am. Chem. Soc. **66**, 2100 (1944).

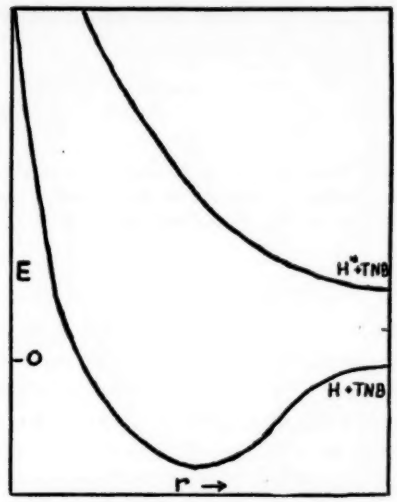

FIG. 3. Ground (H+T.N.B.) and excited (H^*+T.N.B.) states of hydrocarbon-T.N.B. complexes. E=potential energy. r=intermolecular distance.

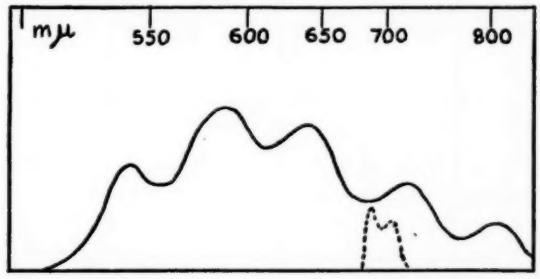

FIG. 4. Solid line: emission spectrum of anthracene-T.N.B. complex. Dotted line: previously reported anthracene triplet emission.

Investigation of molecular complexes of the kind described in this paper promises to provide information about energy levels otherwise difficult to observe because transitions from them to the ground state are highly forbidden. For the dozen or so substances which have been examined, the high frequency limit of the band found in the complex differs on the average by less than 100A from the value found by examination of the hydrocarbon itself.

Note added in proof:—Since the same emission spectrum can be obtained from the crystalline complexes, in which relative movement of the two molecules is largely restricted, such movement is not essential to the mechanism. A considerable field change will nevertheless accompany the switch from the attractive to the repulsive orbital and may be responsible for the breakdown of the $S \leftarrow T$ selection rule.

[5] D. S. McClure, J. Chem. Phys. **19**, 670 (1951).

The Lowest Triplet Levels of Aromatic Hydrocarbons

C. REID
University of British Columbia, Vancouver, British Columbia, Canada
(Received February 11, 1952)

New data for anthracene and naphthacene suggest that the lowest triplet levels of polyacenes are of species ^3L_b. This makes the 39,000 cm^{-1} singlet band of benzene of symmetry B_{2u} as was originally proposed and not B_{1u} as was later suggested.

INTRODUCTION

THERE is some confusion in the literature about the symmetry species of the lowest triplet levels of aromatic hydrocarbons. In a paper correlating hydrocarbon levels Klevens and Platt[1] decided that the triplet levels were probably ^3L_a on the basis of shifts in position parallel to those of the ^1L_a bands in polyacenes. Platt's correlation is shown in Fig. 1. However, for the case of benzene Shull[2] and McClure[3] have pointed out that the triplet level must be $^3B_{2u}$ on the basis of its perturbation by the adjacent $^1B_{1u}$ level. McClure[4] accepted the ^3L_a assignment for the lowest triplet level and consequently had to reverse Klevens and Platt's assignment of the $^1B_{1u}$ level as ^1L_a, and $^1B_{2u}$ as ^1L_b. This assignment had been based on Mayer and Sklar's[5] M.O. calculations.

More recently McClure[6] has assumed all aromatic hydrocarbons to have lowest triplet levels of species ^3L_a.

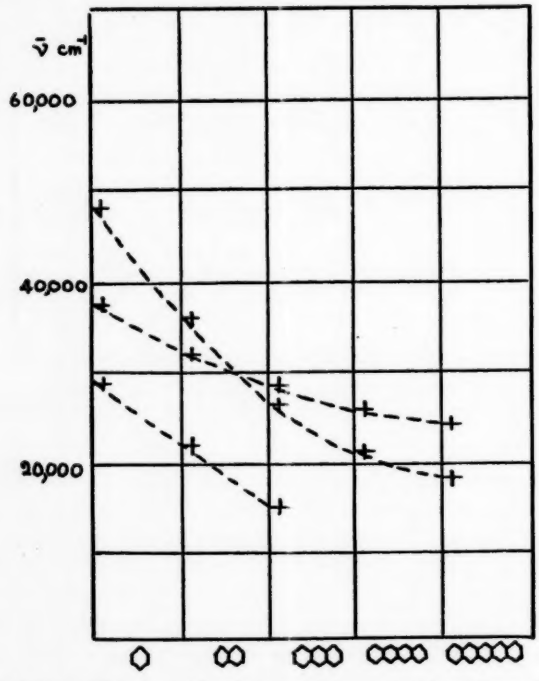

FIG. 1. Correlation of levels in polyancenes—After Klevens and Platt. Triplet level follows ^1L_a rather than ^1L_b and is therefore labeled ^3L_a.

It will be shown on the basis of new experimental results that the lowest triplet levels of the polyacenes are probably of species ^3L_b and that the above reversal is therefore unjustified.

EXPERIMENTAL

(a) Anthracene

The low temperature emission spectrum of the molecular complex of anthracene and trinitrobenzene is shown in Fig. 2. Since it is shown elsewhere[7] that for other hydrocarbon-T.N.B. complexes this emission normally corresponds closely to the triplet level of the hydrocarbon, this is a strong indication that there is an anthracene triplet level in the neighborhood of 19,000 cm^{-1}. However, Kasha[8] has reported a weak emission from anthracene with short wave limit at 14,700 cm^{-1} and has assumed that this is the lowest triplet level. Using very pure anthracene ("scintillation grade" material further purified by repeated chromatography) the author found in this region only a trace so faint as to be very doubtful using exposure times five times as long (24 hours) as that of Kasha with the same plates, slit width, and the same type of source (G.E. AH 6). Neither our faint trace nor Kasha's, from which it differs slightly, looks much like an aromatic hydrocarbon triplet in which usually a vibrational spacing of 1350–1450 cm^{-1} is the most characteristic feature. It is felt, therefore, that this emission may be due to an impurity and that the emission of our hydrocarbon-T.N.B. complex probably does represent that from the lowest triplet level. The average vibrational separation (1400 cm^{-1}) is very close to that found in the triplet emission spectra of naphthalene (1416 cm^{-1}) and naphthacene (1430 cm^{-1}).

Since the failure to reproduce Kasha's result could have been due to poor geometry or lower source intensity (AH 6 arcs vary considerably from one to

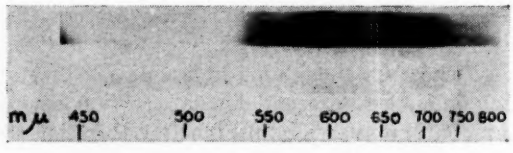

FIG. 2. The emission spectrum of the anthracene-T.N.B. complex at −180°C.

[1] H. B. Klevens and J. R. Platt, J. Chem. Phys. **17**, 470 (1949).
[2] H. Shull, J. Chem. Phys. **17**, 295 (1949).
[3] D. S. McClure, J. Chem. Phys. **17**, 665 (1949).
[4] D. S. McClure, J. Chem. Phys. **17**, 905 (1949).
[5] M. G. Mayer and A. L. Sklar, J. Chem. Phys. **6**, 645 (1938).
[6] D. S. McClure, J. Chem. Phys. **19**, 670 (1951).
[7] C. Reid, J. Chem. Phys. **20**, 1212 (1952).
[8] M. Kasha, J. Am. Chem. Soc. **66**, 2100 (1944).

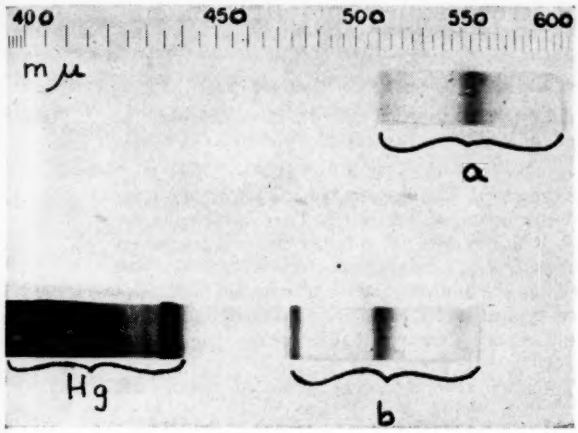

FIG. 3. The emission spectrum of naphthacene at −180°C. (a) with phosphoroscope (b) irradiated continuously.

another), we have considered an alternative possibility. This is that the anthracene-T.N.B. complex contains in its ground state anthracene in a "triplet" form and that this anthracene-T.N.B. complex is excited to the second triplet level. The band system observed could then be the triplet-triplet emission corresponding to the absorption observed by McClure.[6] Triplet-triplet levels have not hitherto been observed in emission, however, and no other hydrocarbons for which the first triplet levels are known with certainty behave in this way. This explanation, therefore, seems unlikely, and it will be assumed that the emission of the complex corresponds to the lowest triplet level.

(b) Naphthacene

Examination of the emission spectrum of naphthacene (chromatographed and recrystallized in an atmosphere of nitrogen) dissolved in a glassy solvent at −180°C shows that there is a long-lived (*ca.* 2 seconds) state lying at 19,650 cm^{-1}, the emission from which is normally masked by the much brighter emission from the singlet state at 21,000 cm^{-1}. In Fig. 3 are shown both the short-lived emission and the long-lived emission photographed using the phosphoroscope with the same sample and the same geometry. Although the positions of the long-lived bands are almost identical with all but one of the short-lived ones, there can be no doubt

TABLE I.

Molecule	^1L_a	^1L_b	Triplet	$^1L_a - T$	$^1L_b - T$
Benzene	48,050	38,000	29,000	19,050	9,000
Naphthalene	34,600	32,000	22,000	12,600	10,000
Anthracene	26,400	28,500	19,000	7,400	9,500
Naphthacene	21,100	27,000	19,600	1,500	7,400
Chrysene	30,200	27,500	20,000	10,200	7,500
Pyrene	29,000	26,800	16,800	12,200	10,000
1,2 benzanthracene	25,800	27,300	16,500	9,300	10,800
1,2,5,6 dibenz-anthracene	c. 27,500	25,500	18,300	9,200	7,200
Phenanthrene	33,000	28,300	21,600	11,400	6,700
Acenaphthene	33,100	29,800	20,800	12,300	9,000

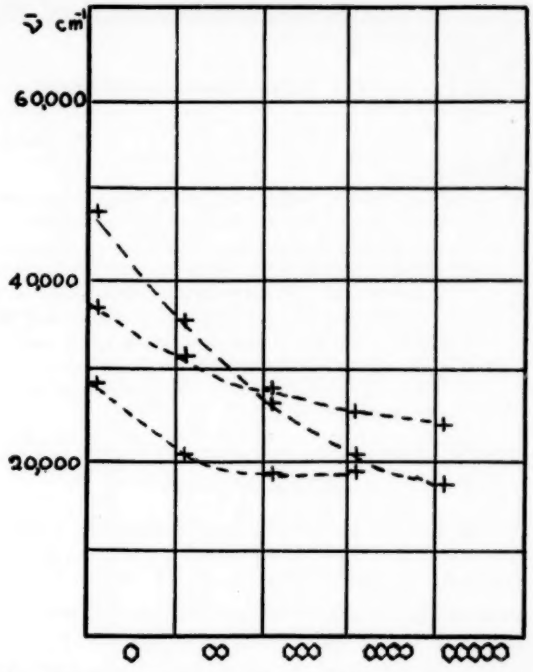

FIG. 4. Corrected correlation of levels in polyacenes. ^3L now follows ^1L_b rather than ^1L_a and is therefore labeled ^3L_b.

that they belong to a different and much more forbidden transition. It is assumed that this must be the lowest $S \leftarrow T$ transition for which such a lifetime is to be expected. No triplet level for naphthacene has been previously reported.

DISCUSSION

If we use the new results for anthracene and naphthacene to make a plot of the polyacene levels, we find the situation shown in Fig. 4. It is clear that the triplet levels are to be correlated with the ^1L_b rather than the ^1L_a levels and are themselves therefore probably ^3L_b.

The argument for benzene is now as follows. Shull has shown that the triplet level is perturbed by a $^1B_{1u}$ level. McClure has proved that the triplet level is therefore $^3B_{2u}$. We now associate this with a ^3L_b state. Accordingly, ^1L_b with the same electron configuration as ^3L_b cannot be the perturbing state which is therefore the ^1L_a second excited singlet level. Shull's analysis therefore shows that the ^1L_a level is $^1B_{1u}$ and the lowest ^1L_b level at 39,000 cm^{-1} is, consequently, of species $^1B_{2u}$ as was originally suggested by Mayer and Sklar.

Whether or not we are justified in carrying over the ^3L_b assignment to nonlinear aromatics is uncertain, but Table I shows that there is at least as much constancy in the ^1L_b-triplet as in the ^1L_a-triplet interval.

The author is indebted to the National Research Council of Canada for a grant in support of this work.

Note added in proof:—Recent work by Mizushima and Koide (private communication from D. S. McClure) suggests that the perturbing singlet responsible for the $S \leftarrow T$ transition in benzene may be of species $^1E_u^+$. If this proves correct, the question of whether $^1B_{1u}$ or $^1B_{2u}$ is the lowest singlet level remains unsettled.

The Statistical Mechanical Theory of Irreversible Condensation. I

HOWARD REISS*
Central Research and Development Department, Celanese Corporation of America, Summit, New Jersey

(Received December 26, 1951)

A theory of nucleation, based on statistical mechanics, is presented. The problem reduces to the computation of the multiple occupation, by molecules, of cells, this being accomplished through the evaluation of the configuration integral for a supersaturated assembly. The new theory does not consider the first fragments of the stable phase formed to be spherical liquid drops. In no place (not even at the nucleus) is it necessary to to consider explicitly phase equilibrium between an embryo and the mother phase. The manifold difficulties connected with this point (in view of the small dimensions of typical nuclei) are therefore obviated. Furthermore, it is possible to define an embryo unambiguously, and in such a manner that its energetic properties can, in principle, be computed. This is not possible in the classical theory.

Certain limitations on the application of Einstein fluctuation theory to supersaturated systems are demonstrated.

I. INTRODUCTION

IF a vapor, free of dust and condensation nuclei, is enclosed in an expansion chamber, one finds, when the expansion is performed, that the vapor does not condense when it becomes saturated. Usually condensation does not occur until the vapor pressure p exceeds the saturation pressure p_∞ by a marked amount. It is apparently an experimental fact that for a given temperature T condensation occurs reproducibly when the *supersaturation ratio* p/p_∞ reaches some definite value, the so-called *critical supersaturation ratio.*

The existence of this critical limit of metastability has provided an intriguing target for quantitative theoretical considerations. It should be noted that one is here confronted with the problem of *irreversible* condensation, sometimes called *nucleation.* Unlike *reversible* condensation the problem of irreversible condensation has not been investigated extensively with the tools of statistical mechanics. A passing acquaintance with the most general treatments of reversible condensation of which, perhaps, the Mayer cluster theory[1] is the most famous, is sufficient to convey the idea that the irreversible counterpart must be very difficult. Therefore, workers in the field have been content to utilize semiphenomenonological models, designed to provide numerical results when used in certain quasi-thermodynamic arguments.

Prominent among these has been the liquid drop model employed by Becker and Doring[2] and Frenkel.[3] With it, the first fragments of the new phase formed are regarded as well-defined spherical liquid drops having the thermodynamic features of macroscopic drops. The concept becomes extremely vague[4] when it is applied to fragments of *nuclear* dimensions containing as few as twenty molecules. It is absolutely meaningless when applied to *embryos* of subnuclear size which are not in phase equilibrium with the mother phase; a privilege reserved for the nuclear fragment alone. For such embryos *surface tension* (an important parameter in the Becker-Doring-Frenkel theory) cannot be defined, even when the embryos are large.

Because of the continuous nature of the transition layer[5–7] separating a liquid from a vapor phase it is impossible to define unambiguously[4] the number of molecules in a small drop.

In view of these inconsistencies it is desirable to develop a more logical theory of nucleation. The natural vehicle for this purpose must still be statistical mechanics. Ideally, the dynamic analog of the Mayer cluster theory is required. However, the former would be fraught with the same, if not more formidable, calculational difficulties as the latter. We should content ourselves with a more middle of the road approach in which a truly statistical theory is developed, but where some rigor is sacrificed in the interest of calculational expediency. The bulk of the following text consists of the development of such a theory.

II. THE STATISTICAL THEORY

The statistical theory will be based on a cell method evaluation of the configuration integral,

$$\Omega=\int\int\cdots\int_V e^{-W/kT}(d\omega)^N \qquad (2.1)$$

for a supersaturated fluid system, enclosed in the volume V and constrained to persist in the metastable state. In (2.1), N is the number of particles in the system, k is the Boltzmann constant, and W is the configurational potential energy, a function of the coordinates of the centers of mass (and, possibly, of the rotational coordinates) of all N molecules. For convenience, we shall assume that the rotational coordinates

* Present address: Bell Telephone Laboratories, Murray Hill, New Jersey.

[1] J. E. Mayer, J. Chem. Phys. **5**, 67, 74 (1937).
[2] R. Becker and Doring, Ann. phys. **24**, 719 (1935).
[3] J. Frenkel, J. Chem. Phys. **7**, 538 (1939); *Kinetic Theory of Liquids* (Oxford University Press, London, 1946), Chap. VII.
[4] F. P. Buff and J. G. Kirkwood, J. Chem. Phys. **18**, 991 (1950).
[5] R. C. Tolman, J. Chem. Phys. **16**, 758 (1948); **17**, 118, 333 (1949).
[6] F. Koenig, J. Chem. Phys. **18**, 449 (1950).
[7] J. G. Kirkwood and F. P. Buff, J. Chem. Phys. **17**, 338 (1949).

do not enter W, since the argument can easily be extended to the case where they do. Then the symbol $d\omega$ stands for the translational volume element of a single molecule in configuration space. In evaluating Ω we shall follow the usual practice of regarding the N molecules as distinguishable, canceling this error by preceding Ω with the factor $1/N!$, whenever Ω is used in a statistical formula.

There are many schemes for evaluating Ω under the most general conditions. One may cite the work of Ursell,[8] Kirkwood,[9] Mayer,[1] and Born and Green.[10] In our case attention will be focused on a supersaturated vapor inside the metastable limit. It is assumed, and it is almost true experimentally, that the vapor in this condition obeys the ideal gas law. Consequently, it will not be necessary to evaluate Ω under general conditions but only under a condition consistent with this law. This statement may seem a bit unsophisticated. It is well known that in an ideal gas interactions between molecules are neglected so that

$$W=0. \tag{2.2}$$

When (2.2) is substituted into (2.1) the familiar result

$$\Omega=V^N \tag{2.3}$$

is obtained where V is the volume of the gas, and one fails to see what else must be done toward evaluating Ω in this instance.

The difficulty is obviated when it is considered that adherence to the ideal gas law is a necessary but not sufficient condition for the absence of molecular interaction. As it will appear later a gas, suitably constrained, will follow this law and yet support moderate interaction. Although this interaction is negligible with respect to the computation of the various macroscopic features of a metastable gas (e.g., p, V, etc.), it is, however, *all important in connection with computations having to do with the collapse of the metastable state.* We are thus confronted with the rather unique circumstance of having an experimental situation requiring a more detailed evaluation of Ω, for a gas following the ideal law, than is contained in (2.3).

At the outset it is important to remember that the evaluation of Ω for temperatures and pressures corresponding to two phase equilibria must lead to an Ω predicting the existence of two phases, unless some sort of internal constraint is applied to the vapor to prevent its condensation.

The following scheme will be adopted in the detailed analysis of Ω. The volume V containing the gas is formally divided into cubical cells, each having the volume

$$\tau=gv, \tag{2.4}$$

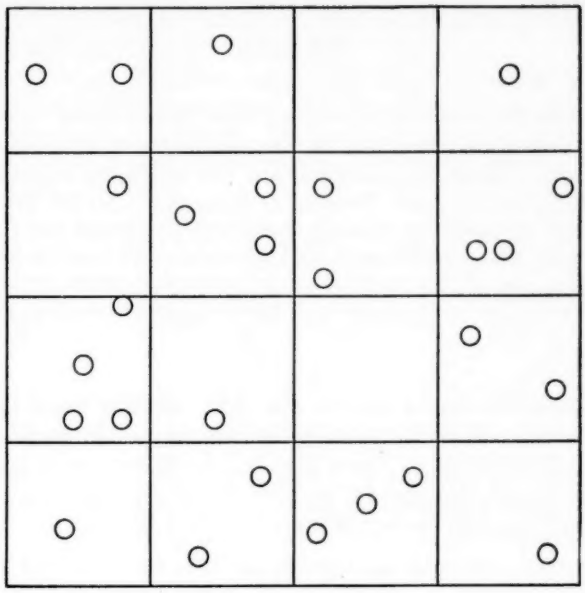

FIG. 1. A configuration picture.

where v is the volume per molecule,

$$v=V/N, \tag{2.5}$$

and g is a positive number which may be greater or less than unity. Now Ω as an integral is really a sum of terms of the type

$$e^{-W/kT}(d\omega)^N. \tag{2.6}$$

We shall call (2.6) a *configuration term.*

The three-dimensional array of cubic cells into which the volume V is divided can be represented by a two-dimensional array as in Fig. 1. If each cell is numbered, it will be possible to specify which cells have given numbers of molecules. A specification of this kind, when it is complete, can be represented by a picture such as the one in Fig. 1 in which molecules are scattered in some definite manner throughout the array of cells. Such a picture will be called a *configuration picture.*

Depending upon the values of the coordinates ω in W, the configuration term (2.6) can be correlated with a definite configuration picture. In fact, a large number of configuration terms will correspond to a single picture, since by a given configuration picture we mean a specification of the numbers of molecules in each cell independent of how the molecules are disposed within their respective cells or of which molecules (regarded as distinguishable) are in what cells. The series of terms belonging to a single picture can be generated in two ways: (a) by disposing the molecules differently within their cells without removing any molecule from any cell, and (b) by permuting the N distinguishable molecules among the various cells without changing the number in each cell. In the usual manner, the con-

[8] H. D. Ursell, Proc. Cambridge Phil. Soc. **23**, 685 (1927).
[9] J. G. Kirkwood, J. Chem. Phys. **3**, 300 (1935).
[10] M. Born and H. S. Green, *A General Kinetic Theory of Liquids* (Cambridge University Press, London, 1949).

figuration energy W can be written as the sum of terms

$$W=\sum_{ij} u_{ij}, \tag{2.7}$$

where the sum extends over all pairs of molecules, i and j, and u_{ij} is a function of the coordinates of molecules i and j alone. Consider the kth cell which for a given configuration term contains x_k molecules. Call the sum of all the terms u_{ij} between molecules in the kth cell u_k. Then, for a given configuration term (2.7) can be replaced by

$$W=\sum_k u_k+\sum_{\substack{\text{between}\\ \text{cells}}} u_{ij}, \tag{2.8}$$

where the second sum on the right refers to those u_{ij} corresponding to interactions between molecules located in different cells. These intercell terms are quite important and cannot be ignored. For the moment, however, we shall neglect them, writing for W

$$W=\sum_k u_k. \tag{2.9}$$

Similar schemes for evaluating Ω are followed whether the intercell terms are neglected or not. By neglecting them, at first, it will be possible to outline the scheme with maximum simplicity. Eventually, of course, they will be included in the development.

When (2.9) is employed (2.6) can be written in the form

$$\prod_k[e^{-u_k/kT}(d\omega)^{x_k}]. \tag{2.10}$$

All the terms of this kind belonging to a given configuration picture can be obtained by following procedures (a) and (b) described above. The application of procedure (a) (disposing the molecules differently within their cells) transforms (2.10) into

$$\prod_k\left[\int\int\cdots\int_{gv} e^{-u_k/kT}(d\omega)^{x_k}\right], \tag{2.11}$$

where the integral is taken over the volume gv of a single cell. The integrals for the individual cells are independent of one another because the intercell terms have been neglected. After the integrations have been carried out the contribution to (2.11) of each cell which contains the same number of molecules, x, ($x_k=x$) will be the same. Therefore, if in the given configuration picture there are $n(x)$ cells containing x molecules, the factors can be collected and (2.11) rewritten as

$$\prod_x\left[\int\int\cdots\int_{gv} e^{-u(x)/kT}(d\omega)^x\right]^{n(x)}. \tag{2.12}$$

A quantity $\langle u(x)\rangle_{Av}$ can be defined by the equation

$$\exp[-\langle u(x)\rangle_{Av}/kT]\int\int\cdots\int_{gv}(d\omega)^x = \int\int\cdots\int \exp[-u(x)/kT](d\omega)^x. \tag{2.13}$$

By differentiating both sides of (2.13) with respect to T it can be shown that

$$\langle u(x)\rangle_{Av}=\frac{\int\int\cdots\int_{gv} u(x)e^{-u(x)/kT}(d\omega)^x}{\int\int\cdots\int_{gv} e^{-u(x)/kT}(d\omega)^x}, \tag{2.14}$$

so that $\langle u(x)\rangle_{Av}$ is the average mutual potential energy of x molecules confined to a cell of volume gv. It is obviously (from (2.14)) temperature dependent.

Substituting (2.13) into (2.12) and using the relation

$$\int\int\cdots\int_{gv}(d\omega)^x=(gv)^x, \tag{2.15}$$

the latter expression becomes

$$\prod_x\{\exp[-\langle u(x)\rangle_{Av}/kT](gv)^x\}^{n(x)}. \tag{2.16}$$

To get the rest of the terms belonging to a single configuration picture procedure (b) (permuting molecules among the various cells) is employed. The number of permutations of N distinguishable molecules among the cells when $n(x)$ of them contain x molecules is

$$N!/\prod_x(x!)^{n(x)}. \tag{2.17}$$

The product of (2.16) by (2.17) is the sum of all the configuration terms belonging to a given configuration picture.

How many different configuration pictures can be formed when $n(x)$ is specified? With reference to Fig. 1, a different configuration picture is formed, each time cells containing unlike numbers of molecules are exchanged. There are

$$V/gv=N/g \tag{2.18}$$

cells. The number of permutations of these, not counting exchanges of cells containing equal numbers x of molecules, is

$$\frac{(N/g)!}{\prod_x n(x)!}. \tag{2.19}$$

The product of (2.16), (2.17), and (2.18) can be written (when Stirling's approximation is used for $n(x)!$) in the following form:

$$\binom{N}{g}!N!\prod_x\left[\frac{\exp[(1-\langle u(x)\rangle_{Av}/kT)](gv)^x}{x!n(x)}\right]^{n(x)}. \tag{2.20}$$

It corresponds to that part of the configuration integral Ω consistent with a given specification of $n(x)$, and, according to a well-known theorem[11] in statistical mechanics, measures the probability of that specification.

[11] Fowler and Guggenheim, *Statistical Thermodynamics* (Cambridge University Press, Cambridge, 1939), p. 254.

The entire configuration integral is obtained by summing (2.20) over all distributions $n(x)$ consistent with the conservation conditions

$$\sum n(x)=\mathcal{N}/g \tag{2.21}$$

$$\sum xn(x)=N. \tag{2.22}$$

Making use of (2.21) and (2.22), the factors e and (gv) in (2.20) may be collected in front of the product sign. When we do this, and sum

$$\Omega=\left(\frac{N}{g}\right)!N!(gv)^N e^{N/g}\sum_{n(x)}\prod_x\left[\frac{\exp[-\langle u(x)\rangle_{Av}/kT]}{x!n(x)}\right]^{n(x)}, \tag{2.23}$$

where the sum is for all $n(x)$ consistent with (2.21) and (2.22). Now all of the terms in the summand are positive, and since N is a very large number, it can be shown, by the usual arguments,[12] that the entire sum is adequately approximated by the largest term. Under this condition the distribution $n(x)$ belonging to largest term (i.e., the most probable distribution) will be indistinguishable from the average or the equilibrium distribution. It is obtained in a straightforward manner by maximizing the typical term in (2.23) with respect to the variations of $n(x)$ consistent with (2.21) and (2.22). This constrained maximization is easily accomplished through the use of undetermined multipliers.[13] The result[14] is

$$n(x)=\lambda\gamma^x\frac{\exp[-\langle u(x)\rangle_{Av}/kT]}{x!}, \tag{2.24}$$

where λ and γ are parameters to be determined by substituting (2.24) into (2.21) and (2.22).

We will pursue the present argument (in which intercell terms have been ignored) no further. Enough has been said to illustrate the manner of evaluation of Ω so that the real case (involving intercell terms) can be understood and treated with facility.

The number $n(x)$ announces that, at any instant, on the average, the molecules of the gas will be distributed among the cells so that $n(x)$ cells will each contain x molecules. Nothing is said about the disposition of the molecules in each cell. It may and will differ from cell to cell so that two cells, both having x molecules, will exhibit entirely dissimilar appearances.

We now turn to the rigorous statistical theory in which the intercell terms are included.

It is convenient to begin with the introduction of a slightly altered notation. Consider the kth cell which contains x molecules. The mutual potential energy denoted by $u(x)$ in the previous treatment will now be denoted by $u_k(x)$. Consider all of the intercell terms between the x molecules in the kth cell and molecules in other cells containing just y molecules. The sum of these terms is denoted by $\varphi_{ky}(x)$. Among the $\varphi_{ky}(x)$ belonging to a given kth cell we only include those terms for which

$$y\leqslant x. \tag{2.25}$$

Terms for which

$$y>x \tag{2.26}$$

will appear among the $\varphi_{ky}(x)$ of another kth cell having a larger value of x. In that case, the symbolic roles of the x and y satisfying (2.26) will be reversed, and the condition (2.25) will still be satisfied for the new kth cell having the larger value of x. With these definitions

$$W=\sum_k[u_k(x)+\sum_{y=0}^{y=x}\varphi_{ky}(x)], \tag{2.27}$$

where it is understood that the x may or may not be different for different kth cells.

Using (2.27) the configuration term becomes

$$\prod_k[\exp\{-[u_k(x)+\sum_{y=0}^{y=x}\varphi_{ky}(x)]/kT\}(d\omega)^x]. \tag{2.28}$$

In the metastable gas, constrained to follow the ideal law, it will appear that the distribution function $n(x)$ has the property

$$n(x+1)\ll n(x). \tag{2.29}$$

It follows that for the collection of cells having a given molecular content x, the number of pairs which can be formed between cells of this collection and other cells whose y's satisfy (2.25) is enormously greater than the number of pairs possible involving value of y satisfying (2.26). Therefore, almost all of the intercell terms involving the collection of cells with x molecules, apiece, are included in the sums

$$\sum_{y=0}^{y=x}\varphi_{ky}(x) \tag{2.30}$$

belonging to k's with the value x in question. The sum of sums (2.30) consistent with a given x is almost the total intercell interaction energy of cells of size x.

Referring to (2.28), the $u_k(x)$ and $\varphi_{ky}(x)$ belonging to cells having x values less than a certain value, say α, will be almost zero for almost all dispositions of the molecules within such cells. In addition, the $\varphi_{ky}(x)$ corresponding to $x>\alpha$, $y<\alpha$ will also represent small interactions. It is possible to write (2.28) in slightly greater detail collecting into groups all factors belonging to the same value of x. Thus, within the approximation

[12] Mayer and Mayer, *Statistical Mechanics* (John Wiley and Sons, Inc., New York, 1940), p. 282.

[13] Sokolnikoff and Sokolnikoff, *Higher Mathematics for Engineers and Physicists* (McGraw-Hill Book Company, Inc., New York, 1941), p. 163.

[14] In a recent paper [Prog. Theor. Phys. **5**, 997 (1950)] Katsura and Fujita obtained an equation identical with (2.24) by considering the multiple occupation of cells. These authors were interested in reversible condensation, and were able to choose their cell size arbitrarily and large enough so that cell interaction terms could be legitimately ignored. As it will appear, in the present case of irreversible condensation, the cell size cannot be chosen arbitrarily, and interaction terms cannot be ignored. On the other hand, we shall be able to evaluate λ and γ, simply, whereas this cannot be done in the reversible case.

just mentioned, (2.28) becomes

$$\prod_{x=0}^{x=\alpha-1} d\omega^{xn(x)}\{\prod_k \exp\{-[u_k(\alpha)+\psi_k(\alpha)]/kT\}(d\omega)^{\alpha}\}$$
$$\cdot\{\prod_k \exp\{-[u_k(\alpha+1)+\psi_k(\alpha+1)]/kT\}(d\omega)^{(\alpha+1)}\}\cdot\{\prod_k \exp\{-[u_k(\alpha+2)+\psi_k(\alpha+2)]/kT\}(d\omega)^{(\alpha+2)}\}\cdots, \quad (2.31)$$

where

$$\psi_k(\alpha+s)=\sum_{y=\alpha}^{y=\alpha+s}\varphi_{ky}(\alpha+s) \quad (2.32)$$

and the symbol $\prod_k$ now means the product of all factors belonging to a given value of x, i.e., α, $\alpha+1$, etc.

Just as in the previous argument in which intercell terms were neglected, it is possible to generate a number of configuration terms consistent with a given configuration picture by moving each group of x molecules about its kth cell. Let us do this in stages, first moving the molecules in all cells with $x<\alpha$, then those in cells with $x=\alpha$, $x=\alpha+1$, etc. in turn. The result of moving those with $x<\alpha$ transforms (2.32) into

$$\prod_{x=0}^{x=\alpha-1}(gv)^{xn(x)}\{\prod_k \exp\{-[u_k(\alpha)+\psi_k(\alpha)]/kT\}(d\omega)^{\alpha}\}\cdots. \quad (2.33)$$

Doing this for $x=\alpha$ affects $u_k(\alpha)+\psi_k(\alpha)$ as well as certain terms in $\psi_k(\alpha+1)$, $\psi_k(\alpha+2)$, etc. The sum of these latter terms which are affected is small compared with $u_k(\alpha)+\psi_k(\alpha)$, in view of (2.29). The result now is

$$\prod_{x=0}^{x=\alpha-1}(gv)^{xn(x)}\exp[-\langle W(\alpha)\rangle_{Av}/kT](gv)^{\alpha n(\alpha)}\cdot\{\prod_k \exp\{-[u_k(\alpha+1)+\psi_k'(\alpha+1)]/kT\}(d\omega)^{(\alpha+1)}\}\cdots, \quad (2.34)$$

in which the prime in $\psi_k'(\alpha+1)$ signifies that the terms in $\psi_k(\alpha+1)$ involving the coordinates of molecules in α-cells do not appear. These terms have been partially affected by the integration so that they (or rather quantities related to them, after integration) appear in $\langle W(\alpha)\rangle_{Av}$ which by the same argument involved in (2.13) is the average sum of the mutual and intercell energies of all the molecules in α-cells, for fixed dispositions of all molecules in cells with $x>\alpha$.

The dispositions of the latter molecules enter $\langle W(\alpha)\rangle_{Av}$ through the terms which have been extracted from the various $\psi_k(\alpha+s)$ to leave $\psi_k'(\alpha+s)$. As we have indicated, because of (2.29), these terms are small beside $u_k(\alpha)+\psi_k(\alpha)$ so that $\langle W(\alpha)\rangle_{Av}$ is only slightly dependent on the dispositions of molecules in cells with $x>\alpha$. We shall *not*, however, neglect this slight dependence.

Set

$$W^*(\alpha)=\sum_k[u_k(\alpha)+\psi_k(\alpha)], \quad (2.35)$$

where the sum is for all values of k consistent with $x=\alpha$. Furthermore, denote by $W'(\alpha)$ the sum of all interactions between cells with $x=\alpha$ and $x>\alpha$, i.e., the terms extracted from $\psi_k'(\alpha+s)$. Then, obviously

$$\langle W(\alpha)\rangle_{Av}=\frac{\int\int\cdots\int_{gv}[W^*(\alpha)+W'(\alpha)]\exp\{-[W^*(\alpha)+W'(\alpha)]/kT\}(d\omega)^{\alpha n(\alpha)}}{\int\int\cdots\int_{gv}\exp\{-[W^*(\alpha)+W'(\alpha)]/kT\}(d\omega)^{\alpha n(\alpha)}}$$
$$=\frac{\int\int\cdots\int_{gv}W^*(\alpha)\exp\{-[W^*(\alpha)+W'(\alpha)]/kT\}(d\omega)^{\alpha n(\alpha)}}{\int\int\cdots\int_{gv}\exp\{-[W^*(\alpha)+W'(\alpha)]/kT\}(d\omega)^{\alpha n(\alpha)}}$$
$$+\frac{\int\int\cdots\int_{gv}W'(\alpha)\exp\{-[W^*(\alpha)+W'(\alpha)]/kT\}(d\omega)^{\alpha n(\alpha)}}{\int\int\cdots\int_{gv}\exp\{-[W^*(\alpha)+W'(\alpha)]/kT\}(d\omega)^{\alpha n(\alpha)}}$$

$$\approx\frac{\int\int\cdots\int_{gv} W^*(\alpha)\exp[-W^*(\alpha)/kT](d\omega)^{\alpha n(\alpha)}}{\int\int\cdots\int_{gv}\exp[-W^*(\alpha)/kT](d\omega)^{\alpha n(\alpha)}}$$

$$+\frac{\int\int\cdots\int_{gv} W'(\alpha)\exp\{-[W^*(\alpha)+W'(\alpha)]/kT\}(d\omega)^{\alpha n(\alpha)}}{\int\int\cdots\int_{gv}\exp\{-[W^*(\alpha)+W'(\alpha)]/kT\}(d\omega)^{\alpha n(\alpha)}}$$

$$=\langle W^*(\alpha)\rangle_{Av}+\langle W'(\alpha)\rangle_{Av}. \quad (2.36)$$

Because of the smallness of $W'(\alpha)$ relative to $W^*(\alpha)$, the approximation leading to $\langle W^*(\alpha)\rangle_{Av}$ is a good one. The errors incurred in eliminating $W'(\alpha)$ from the integral to begin with are small and are made even smaller by the fact that the elimination involves both the integral in the numerator and the one in the denominator. The errors, therefore, tend to cancel. Under this approximation we see that $W^*(\alpha)$ is the average sum of the mutual and intercell energies of α cells *in a gas from which cells with $x>\alpha$ are absent.*

One can define the quantity

$$\langle\omega(\alpha)\rangle_{Av}=[\langle W^*(\alpha)\rangle_{Av}/n(\alpha)], \quad (2.37)$$

the average mutual-intercell energy per α-cell in a gas from which cells with $x>\alpha$ are absent. For such a gas (2.33) is a complete expression (the . . . etc. can be eliminated) and to the extent that the $\psi_k(\alpha)$ for two different k are independent of each other, the integration leading to the equivalent of (2.34) involves a product of integrals. The result is

$$\prod_{x=0}^{x=\alpha-1}(gv)^{xn(x)}\prod_k\{\exp[-\langle\omega_k(\alpha)\rangle_{Av}/kT](gv)^{\alpha}\}, \quad (2.38)$$

where the product is taken over all k consistent with $x=\alpha$. Only a negligible number of $\psi_k(\alpha)$ are interdependent because the frequency with which two α-cells occur in juxtaposition is very low. The product in (2.38) is therefore valid. The obvious correspondence to be gleaned from (2.38) is

$$\langle W^*(\alpha)\rangle_{Av}=n(\alpha)\langle\omega(\alpha)\rangle_{Av}=\sum_k\langle\omega_k(\alpha)\rangle_{Av}$$

or

$$\langle\omega(\alpha)\rangle_{Av}=\frac{\sum_k\langle\omega_k(\alpha)\rangle_{Av}}{n(\alpha)}. \quad (2.39)$$

In other words, $\langle\omega(\alpha)\rangle_{Av}$ is the average mutual-intercell energy per α-cell averaged over the environments of all the α-cells in the configuration picture.

Another interpretation is possible. Imagine a given α-cell to be enclosed by a shell permeable to the molecular force fields but impermeable to matter. Let this shell be immersed in a gas having the same temperature and density as the one for which $\langle\omega(\alpha)\rangle_{Av}$ has been evaluated above. One could then observe the succession, in time, of environments to which this α-cell was subject. The mutual-intercell energy averaged over this succession for a very long period of time would be the same as that averaged, instantaneously, over a large number of α-cells in different environments.

Next, we move the molecules in the $(\alpha+1)$ cells about their respective domains. The integration which must be performed of course involves $\langle W'(\alpha)\rangle_{Av}$.

The result of this integration transforms (2.34) into

$$\prod_{x=0}^{x=\alpha-1}(gv)^{xn(x)}\exp[-\langle W^*(\alpha)\rangle_{Av}/kT](gv)^{\alpha n(\alpha)}\cdot\exp[-\langle W(\alpha+1)\rangle_{Av}/kT](gv)^{(\alpha+1)n(\alpha+1)}$$

$$\cdot\{\prod_k\exp\{-[u_k(\alpha+2)+\psi_k''(\alpha+2)]/kT\}(d\omega)^{\alpha+2}\}\cdots, \quad (2.40)$$

in which the double prime in $\psi_k''(\alpha+2)$ indicates that now interaction terms for *both* α and $\alpha+1$ cells have been extracted from $\psi_k(\alpha+2)$.

By the same argument used in connection with $\langle W(\alpha)\rangle_{Av}$, it is apparent that $\langle W(\alpha+1)\rangle_{Av}$ is virtually independent of the dispositions of molecules in cells with $x>\alpha+1$, and that $\langle W(\alpha+1)\rangle_{Av}$ can be approximated accurately by

$$\langle W(\alpha+1)\rangle_{Av}=\langle W^*(\alpha+1)\rangle_{Av}+\langle W'(\alpha+1)\rangle_{Av}, \quad (2.41)$$

where $\langle W^*(\alpha+1)\rangle_{Av}$ is the average mutual-intercell energy for $(\alpha+1)$ cells in a gas from which cells with $x>\alpha+1$ have been excluded.

Continuing in this manner, (2.33) can finally be written as

$$\prod_x \exp[-\langle W^*(x)\rangle_{Av}/kT](gv)^{xn(x)} = \prod_x[\exp[-\langle\omega(x)\rangle_{Av}/kT](gv)^x]^{n(x)}, \quad (2.42)$$

in which $\langle W^*(x)\rangle_{Av}$ is zero for $x<\alpha$, and $\langle\omega(x)\rangle_{Av}$ is the time average mutual-intercell energy for a shell-enclosed x cell immersed in a gas from which cells containing numbers of molecules greater than x have been excluded.

Actually, since $W'(x)$ is small compared to $W^*(x)$, a good approximation to $\langle\omega(x)\rangle_{Av}$ is obtained if the cell is immersed in a gas (constrained to follow the ideal law and having the same density and temperature as the supersaturated gas in question) from which cells greater than x have not been excluded. This fact will be important in the next section when we want to compare the present theory with the more usual approximate fluctuation theory.

It must be remembered that the validity of (2.41) is contingent upon (2.29), which implies that the $n(x)$ being considered does not vary very much about the equilibrium $n(x)$ for a gas constrained to obey the ideal law.

By multiplying (2.42) by (2.17) we obtain the sum of the configuration terms corresponding to a given configuration picture. A little thought must be exercised in calculating the number of configuration pictures consistent with a given $n(x)$. Certain pictures will be highly organized, in the sense that all cells with a given value of x will be confined to a small region of space. In these pictures [consistent with the same $n(x)$] the environments of the various x cells will be far from random, and the identification of $\langle\omega(x)\rangle_{Av}$ with a time average for a shell-enclosed x cell, immersed in a gas, will not be valid. On the other hand, because of the large numbers of cells involved, configuration pictures with almost the same degree of randomness (the greatest possible randomness) will account for the bulk of all possible pictures. Hence, one can approximate a typical term in Ω by taking the product of (2.42) by (2.19) as well as by (2.17).

The inconsistency introduced by those pictures which are highly organized and hence have different values of $\langle\omega(x)\rangle_{Av}$ will be small. Ω is now given by the counterpart of (2.23) in which $\langle\omega(x)\rangle_{Av}$ replaces $\langle u(x)\rangle_{Av}$. Thus

$$\Omega=\left(\frac{N}{g}\right)!N!(gv)^Ne^{N/v}\sum_{n(x)}\prod_x\left[\frac{\exp[-\langle\omega(x)\rangle_{Av}/kT]}{x!n(x)}\right]^{n(x)}. \quad (2.43)$$

In determining the maximum term of (2.23) subject to (2.21) and (2.22) no difficulty appeared because $u(x)$ was independent of $n(x)$. This is not true of $\langle\omega(x)\rangle_{Av}$ since $n(x)$ determines the average environment of an x cell. However, (2.29) rescues the situation. $\langle\omega(x)\rangle_{Av}$ only includes interactions with cells of smaller x. According to (2.29) the number of these far exceeds the number of cells of size x. Only a small number of the former can fit at one time into the immediate environments of the x cells. As a result, a small variation in some $n(x-s)$ (where s is a positive number less than or equal to x) hardly affects the average environment of an x cell, since that environment is saturated with $(x-s)$ cells, and by (2.29) there are many such cells to spare. Thus, for small variations about the distribution $n(x)$ corresponding to the maximum term, $\langle\omega(x)\rangle_{Av}$ may be considered independent of $n(x)$. These small allowable variations are sufficient for the determination of the maximum. In this manner one obtains the more rigorous analog of (2.24):

$$n(x)=\lambda\gamma^x\frac{\exp[-\langle\omega(x)\rangle_{Av}/kT]}{x!}. \quad (2.44)$$

It is necessary to determine λ and γ by substituting (2.44) into (2.21) and (2.22). Before doing this, we must consider how the supersaturated vapor is to be constrained so that when (2.44) (with λ and γ determined) is substituted into (2.43) the Ω obtained leads to the ideal gas law,

$$pV=NkT. \quad (2.45)$$

In the usual manner[15]

$$p=-\left(\frac{\partial A}{\partial V}\right)_{T,N}=kT\left[\frac{\partial}{\partial V}\left(\ln\frac{\Omega}{N!}\right)\right]_{T,N} \quad (2.46)$$

so that if

$$\Omega=V^N, \quad (2.3)$$

(2.46) reduces to (2.45). Therefore, the most natural constraint will be that which permits (2.44) to yield (2.3) when substituted in (2.43).

We notice that for a truly ideal gas in which $\langle\omega(x)\rangle_{Av}=0$, (2.44) becomes

$$n(x)=\lambda(\gamma^x/x!) \quad (2.47)$$

[15] See reference 12, p. 235.

and (2.47) in (2.21) and (2.22) yields the relations

$$\lambda \sum_0^\infty (\gamma^x/x!) = \lambda e^\gamma = N/g, \tag{2.48}$$

$$\lambda\gamma \sum_1^\infty [\gamma^{(x-1)}/(x-1)!] = \lambda\gamma e^\gamma = N. \tag{2.49}$$

The simultaneous solution of (2.48) and (2.49) determines λ and γ. Thus

$$\gamma = g, \tag{2.50}$$

$$\lambda = (N/g)e^{-g}, \tag{2.51}$$

and (2.47) is

$$n(x) = (N/g)e^{-g}(g^x/x!). \tag{2.52}$$

The substitution of (2.52) into the maximum term of (2.43) [setting $\langle\omega(x)\rangle_{Av}=0$ in (2.43)] produces (2.3), when Stirling's approximation is used to correlate the various factorials and (2.21) and (2.22) are applied. This provides an internal check on the validity of the solution of the combinatorial problem.

Furthermore, it is to be noted that the substitution of (2.44) into the bracketed factor of (2.43) leaves the result

$$\prod_x \left[\frac{\exp[-\langle\omega(x)\rangle_{Av}/kT]}{x!n(x)}\right]^{n(x)} = \prod_x [\lambda^{-1}\gamma^{-x}]^{n(x)}$$

$$= \lambda^{-\Sigma n(x)}\gamma^{-\Sigma x n(x)} = \lambda^{-N/g}\gamma^{-N} \tag{2.53}$$

so that the character of Ω is fully determined by λ and γ. To fulfill (4.3), therefore, the choices (2.50) and (2.51) should still be made. When this is done, (2.44) becomes

$$n(x) = \frac{N}{g} e^{-g} g^x \frac{\exp[-\langle\omega(x)\rangle_{Av}/kT]}{x!}. \tag{2.54}$$

But now (2.48) demands

$$e^g = \sum_0^\infty \frac{g^x}{x!} = \sum_0^h \exp[-\langle\omega(x)\rangle_{Av}/kT]\frac{g^x}{x!}, \tag{2.55}$$

where the upper limit h on the right must be prescribed so that (2.55) holds. Obviously, since $\langle\omega(x)\rangle_{Av}$ is negative (referred to infinite separation of the molecules), if $h\to\infty$, the right member of (2.55) would far exceed the left, and the equation would be impossible. Thus, the internal constraint consistent with the ideal gas law takes the form of a sharp cutoff in the distribution function, $n(x)$ at $x=h$. It is obvious that *some* cutoff is required if only for the preservation of the metastable state. In addition, a cutoff at h preserves the ideal gas law.

With the aid of Stirling's approximation, (2.54) can be written as

$$n(x) = \frac{N}{g} \exp\left\{-\left[kT\left(g - x + x\ln\frac{x}{g}\right) + \langle\omega(x)\rangle_{Av}\right]/kT\right\}. \tag{2.56}$$

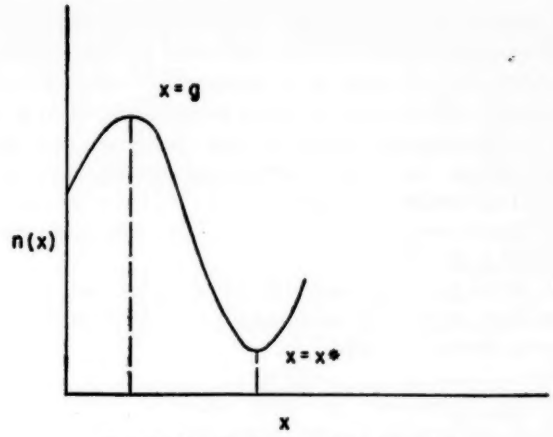

FIG. 2. The distribution function, $n(x)$.

Let us investigate the extremal values of $n(x)$. Thus, we apply the condition

$$[dn(x)/dx] = 0, \tag{2.57}$$

which leads to the result

$$-kT\ln(x/g) = [d\langle\omega(x)\rangle_{Av}/dx]. \tag{2.58}$$

When x is small,

$$\langle\omega(x)\rangle_{Av} = 0 \tag{2.59}$$

and (2.58) becomes

$$-kT\ln(x/g) = 0 \quad \text{or} \quad x = g. \tag{2.60}$$

This corresponds to a maximum of $n(x)$. The number density of molecules in the cell corresponding to this *most probable* cell is

$$x/gv = g/gv = 1/v = N/v, \tag{2.61}$$

i.e., *the average density throughout the gas*. One would have anticipated this result. It provides another check on the validity of our development.

When x is large so that $\langle\omega(x)\rangle_{Av}$ is finite, (2.58) determines a *minimum* of $n(x)$. The value of x for which (2.58) is satisfied, in this case, will be denoted by x^*.

III. THE STATISTICAL THEORY CONTINUED

A plot of $n(x)$ *versus* x, now, looks like the curve of Fig. 2. In the next section it will be demonstrated that cells with $x>x^*$ have more chance of gaining than losing molecules, while the reverse is true for cells with $x<x^*$. It will therefore be convenient to define cells of size x^* as nuclei while defining those of size $x<x^*$ as embryos. In any circumstance, when the rate of production of nuclei is high, the metastable state will collapse.

Nothing yet has been said about the freedom of choice which can be exercised in choosing the magnitude of g. Two important quantities are sensitive to g. These are the values of h determined by (2.55) and of x^* determined by (2.58). If $h<x^*$, then we have no basis for the consideration of nuclei since the distribution formula cuts off before the nuclear size is reached. On

the other hand, if $h>x^*$, the minimum of $n(x)$ will have been exceeded, and (2.29), a condition for the validity of (2.56), will not hold. As a matter of fact, a rough calculation of $\langle\omega(x)\rangle_{Av}$ based upon a uniform distribution of the x molecules on a lattice in a cell in which the molecules attract each other according to the Lennard-Jones-Devonshire potential,[16] shows that the minimum at x^* is extremely sharp so that (2.29) will be *severely* violated if $h>x^*$.

In order to retain the validity of (2.56) and, at the same time, retain its usefulness it thus becomes necessary to choose g so that

$$x^*=h. \tag{3.1}$$

It is interesting to determine whether the requirement $h\leqslant x^*$ imposes an upper or lower limit on the magnitude of g. This can only be accomplished rigorously when $\langle\omega(x)\rangle_{Av}$ has been evaluated. It can, however, be investigated approximately by introducing certain not too unreasonable assumptions concerning $\langle\omega(x)\rangle_{Av}$. Thus, denote $\langle\omega(x)\rangle_{Av}$ evaluated for a cell of volume gv by $\langle\omega_g(x)\rangle_{Av}$. Then, the first assumption is

$$\langle\omega_{2g}(2x)\rangle_{Av}=2\langle\omega_g(x)\rangle_{Av}, \tag{3.2}$$

and the second assumption is

$$\frac{\langle\omega_g(x+1)\rangle_{Av}}{\langle\omega_g(x)\rangle_{Av}}>\frac{\langle\omega_g(x)\rangle_{Av}}{\langle\omega_g(x-1)\rangle_{Av}}. \tag{3.3}$$

Assumption (3.2) corresponds to ignoring the effects of the cell surface, and hence will be more valid for larger values of g. For smaller values of g it is a reasonable "order of magnitude approximation." The relation (3.3) is quite accurate as long as x does not become large enough for the repulsive term in the intermolecular potential to be operative. It certainly is valid up to values of x somewhat greater than x^*.

Using (3.2) in (2.58), one obtains

$$-kT\ln\frac{(2x)^*}{2g}=\frac{d\langle\omega_{2g}[(2x)^*]\rangle_{Av}}{d(2x)}$$
$$=\frac{d2\langle\omega_g(x^*)\rangle_{Av}}{d(2x)}=\frac{d\langle\omega_g(x^*)\rangle_{Av}}{dx}=-kT\ln\frac{x^*}{g}$$

or

$$(2x)^*/2=x^*. \tag{3.4}$$

Doubling the volume of the cell doubles the number of molecules in the nucleus. The size of the nucleus is directly proportional to g.

Now, write (2.55) for cells of size g and $2g$, respectively. Thus

$$e^g=\sum_0^{h_1}\frac{g^x}{x!}\exp[-\langle\omega_g(x)\rangle_{Av}/kT], \tag{3.5}$$

$$e^{2g}=\sum_0^{h_2}\frac{(2g)^x}{x!}\exp[-\langle\omega_{2g}(x)\rangle_{Av}/kT], \tag{3.6}$$

where h_1 and h_2 denote the respective limits. Squaring both sides of (3.5) yields

$$e^{2g}=\sum_{y_1=0}^{y_1=h_1}\sum_{y_2=0}^{y_2=h_1}\frac{g\exp[y_1+y_2]}{y_1!y_2!}$$
$$\times\exp\{-[\langle\omega_g(y_1)\rangle_{Av}+\langle\omega_g(y_2)\rangle_{Av}]/kT\}$$
$$=\sum_{x=0}^{x=2h_1}g^x\sum_{y_1+y_2=x}\frac{\exp\{-[\langle\omega_g(y_1)\rangle_{Av}+\langle\omega_g(y_2)\rangle_{Av}]/kT\}}{y_1!y_2!}, \tag{3.7}$$

where the second sum in (3.7) is carried over all values of y_1 and y_2 whose sum is x.

Because of (3.3) the *smallest* value that

$$-[\langle\omega_g(y_1)\rangle_{Av}+\langle\omega_g(y_2)\rangle_{Av}] \tag{3.8}$$

can have when

$$y_1+y_2=x \tag{3.9}$$

must be

$$-2\langle\omega_g(x/2)\rangle_{Av}. \tag{3.10}$$

Replacing (3.8) by (3.10) and carrying the substitution to (3.7) yields the inequality

$$e^{2g}>\sum_{x=0}^{x=2h_1}g^x\exp\{-2\langle\omega_g(x/2)\rangle_{Av}/kT\}\cdot\sum_{y_1+y_2=x}\frac{1}{y_1!y_2!}. \tag{3.11}$$

From the well-known relation on binomial coefficients

$$\sum_{y_1+y_2=x}\frac{1}{y_1!y_2!}=\frac{2^x}{x!} \tag{3.12}$$

so that (3.12) becomes

$$e^{2g}>\sum_{x=0}^{x=2h_1}\frac{(2g)^x}{x!}\exp[-2\langle\omega_g(x/2)\rangle_{Av}/kT]$$
$$=\sum_{x=0}^{x=2h_1}\frac{(2g)^x}{x!}\exp[-\langle\omega_{2g}(x)\rangle_{Av}/kT], \tag{3.13}$$

the last step resulting from (3.2).

Comparison of (3.13) with (3.6) shows (since all terms in the sum are positive) that

$$2h_1<h_2, \tag{3.14}$$

which means that, unlike x^*, h increases more rapidly than linearly with g. Thus, the requirement $h\leqslant x^*$ imposes an upper limit on g.

Returning to (2.56), it is interesting to compare that equation with the more usual fluctuation theory[17] in which the frequency of occurrence of various inhomogeneities in density is described by a formula similar to (2.56) where the numerator of the exponent is the

[16] Lennard-Jones and Devonshire, Proc. Roy. Soc. (London) **A163**, 53 (1937); **165**, 1 (1938).

[17] A. Einstein, Ann. Physik **33**, 1275 (1910).

isothermal reversible work (at constant volume V) required in the production of the inhomogeneity.

It will be shown that the numerator of the exponent in (2.56) approximates the isothermal, reversible work required in the manufacture of an x cell in the midst of a vapor whose volume is held constant, so that (2.56) agrees, within limits, with fluctuation theory. Before outlining this proof we remark that (2.56) has not been shown to be generally valid, but to be applicable when (2.29) holds, i.e., for that range of g, below some maximum value, in which $x^* \gtrsim h$. This is not at variance with fluctuation theory since the latter is recognized as an approximation subject to limitations. Our detailed analysis merely emphasizes some of the limitations.

In particular, this type of limitation only arises when we apply fluctuation theory to a *supersaturated* system, one for which the minimum x^* exists. Therefore, the present analysis shows that special care must be exercised in applying fluctuation theory in this case.

The upper limit is undoubtedly associated with the fact that supersaturation cannot be maintained in a system enclosing liquid fragments larger than a certain size.

The present analysis also demonstrates clearly that the individual inhomogeneities are not thermodynamic entities (as they are sometimes visualized in fluctuation theory) each of which have the same appearance. Nevertheless, the frequency $n(x)$ is computed using average quantities, and, therefore, on some mean entity.

We close this section by identifying the numerator of the exponent in (2.56) with the isothermal reversible work of formation of an x cell. The cell is formed, reversibly, in four steps.

In the first step x molecules are selected occupying the volume xv in the gas, and their force fields are discharged reversibly so that they become perfectly ideal.

In the second step these idealized molecules are compressed, isothermally and reversibly, to the volume gv. The work of this step is

$$-xkT \ln(gv/xv) = xkT \ln(x/g). \tag{3.15}$$

In the third step the remaining $N-x$ molecules, occupying the volume $V-xv$ are expanded isothermally and reversibly to fill the larger volume $V-gv$ made available by the compression of the x discharged molecules. During this expansion the molecules are ideal in the sense of (2.55). Consequently, the work of this step can be computed. It is

$$\begin{aligned} &-(N-x)kT \ln(V-gv/V-xv) \\ &\qquad -(N-x)kT \ln[1-gv/V] \\ &+(N-x)kT \ln[1-(xv/V)] \\ &\qquad = (N-x)kT[(g-x)/V]v, \end{aligned} \tag{3.16}$$

the last transformation resulting from the fact that

$$gv/V \ll 1, \quad xv/V \ll 1. \tag{3.17}$$

For all practical purposes

$$N-x \approx N \tag{3.18}$$

and it is true that

$$V/v = N. \tag{2.5}$$

Substituting (3.18) and (2.5) into (3.16) yields for the work of the third step

$$kT(g-x). \tag{3.19}$$

Finally, in the fourth step, the x molecules are recharged, reversibly, in their time average positions. The sum of the work of the first and fourth steps is

$$\langle \omega(x) \rangle_{Av}. \tag{3.20}$$

This statement represents an approximation. The work of charging would be $\langle \omega(x) \rangle_{Av}$ strictly, only if cells with more than x molecules were excluded from the surrounding gas. The approximation is again based on the supposition that $W'(x)$ is small compared to $W^*(x)$. The sum of (3.15), (3.19), and (3.20), the work of formation, is the numerator of (2.56).

Since $n(x)$ has a maximum at $x=g$, (2.29) is violated when $x<g$. The difficulty is removed when it is realized that α, defined in (2.31), can be identified conveniently with g.

IV. THE RATE OF NUCLEATION

In Sec. II and III the equilibrium distribution of embryos, $n(x)$, has been computed. The theory for the rate of growth of these embryos can now be developed along lines similar to those proposed by Zeldovich[18] in connection with classical nucleation theory. Like most tractable rate theories it suffers the disadvantage of being an equilibrium[19] theory of rate.

In setting up the rate problem, the number of embryos of size x present during some process of change at the time t will be denoted by $f(x, t)$. This function reduces to $n(x)$ when equilibrium is induced by erecting a formal barrier at $x=h$, preventing the formation of embryos of size $x>h$. The net rate $I(x, t)$ with which embryos of size x become embryos of size $x+1$ is given by

$$I(x, t) = 6(gv)^{\frac{2}{3}}[\beta f(x, t) - \gamma(x+1) f(x+1, t)]. \tag{4.1}$$

Here $6(gv)^{\frac{2}{3}}$ is the surface area of an embryo (the surface of a cell), β is the rate at which single molecules bombard unit area of embryo surface, and $\gamma(x+1)$ is the rate at which single molecules escape unit area of surface for an embryo of size, $x+1$. As an approximation, β may be taken as the familiar quantity

$$\beta = p/(2\pi mkT)^{\frac{1}{2}}, \tag{4.2}$$

where m is the mass of a single molecule and p is the pressure of the supersaturated vapor.

At equilibrium, (4.1) becomes

$$0 = 6(gv)^{\frac{2}{3}}[\beta n(x) - \gamma(x+1) n(x+1)], \tag{4.3}$$

[18] J. Zeldovich, J. Exp. Theoret. Phys. **12**, 525 (1942).
[19] See reference 11, Chap. XII.

the zero arising through application of the principle of detailed balance.[20] It is possible to solve for $\gamma(x+1)$ in this equation. Thus

$$\gamma(x+1)=[\beta n(x)/n(x+1)]. \tag{4.4}$$

When this result is substituted into (4.1) the following expression is obtained:

$$I(x,t)=6\beta(gv)^{\frac{1}{3}}n(x)\left[\frac{f(x,t)}{n(x)}-\frac{f(x+1,t)}{n(x+1)}\right]. \tag{4.5}$$

On regarding x as continuous (4.5) is approximated by

$$I(x,t)=6\beta(gv)^{\frac{1}{3}}n(\partial/\partial x)(f/n). \tag{4.6}$$

Returning to (4.4) and writing it in the following form,

$$[\beta/\gamma(x)]=[n(x)/n(x-1)], \tag{4.7}$$

we see that when $x<x^*$ the right member is less than unity while for $x>x^*$ that member is greater than unity (since $n(x)$ has a minimum at x^*). Consequently, when $x<x^*$, β which measures the probability of growth is less than $\gamma(x)$ which measures the probability of decay, while the reverse is true for $x>x^*$. Cells of size x^* are therefore defined conveniently as nuclei, a fact mentioned in Sec. III.

Now as soon as the transition begins to take place at an appreciable rate (when $I(x,t)$ becomes large), (4.6) becomes meaningless since $n(x)$ is a function of temperature and pressure and these are indefinable for a system undergoing violent change. It is therefore sensible to study the transition rate at values of p/p_∞ inside the metastable limit. In this manner an expression for $I(x^*,t)=I^*$ (the rate at which nuclei are formed) can be obtained, depending upon p/p_∞ and T. As in the classical theory of nucleation, when I^* so calculated is plotted *versus* p/p_∞ for some value of T, a point will be reached at which it suddenly increases from an almost zero to an almost infinite magnitude. It can be assumed that this abrupt change in the magnitude of I^* signalizes the collapse of the metastable state and that the value of p/p_∞ to which it corresponds is the critical supersaturation ratio. The procedure leading to the evaluation of I^* is as follows.

Until p/p_∞ reaches the critical value (inside the metastable limit) the transition occurs so slowly that, relatively, the number of embryos of size g, $f(g,t)$ (i.e., the most probable embryos, at equilibrium, having the gas density) represents an inexhaustible supply. As a result a quasi-steady state is set up in which f for each value of x is independent of time, and I is independent of both x and time. Thus

$$I^*=I=-6\beta(gv)^{\frac{1}{3}}n(d/dx)(f/n). \tag{4.8}$$

Since the transition has not yet occurred in any considerable amount,

$$(f/n)\to 1, \quad x\to g. \tag{4.9}$$

[20] Tolman, *The Principles of Statistical Mechanics* (Oxford, 1938), p. 165.

If the distribution function $n(x)$ is formally extended to values of x far greater than x^* it will pass through a second maximum because of repulsion between molecules. Call the value of x corresponding to this second maximum G. Certainly, inside the metastable limit, there are no embryos of size G present. Thus, as another condition, there arises

$$(f/n)\to 0, \quad x\to G. \tag{4.10}$$

Now (4.8) can be integrated subject to the boundary conditions (4.9) and (4.10). The result is

$$I^*=\left[6\beta(gv)^{\frac{1}{3}}\Big/\int_g^G\frac{dx}{n(x)}\right]. \tag{4.11}$$

The integrand $1/n(x)$ has an *extremely* sharp maximum at x^* so that

$$\frac{1}{n(x)}=\frac{g}{N}\exp\left\{\left[kT\left(g-x^*+x^*\ln\frac{x^*}{g}\right)+\langle\omega(x^*)\rangle_{Av}\right]\Big/kT\right\}$$
$$\cdot\exp\left\{\frac{1}{2}\left[\frac{1}{x^*}+\frac{1}{kT}\frac{d^2\langle\omega(x^*)\rangle_{Av}}{dx^2}\right](x-x^*)^2\right\}$$
$$=(g/N)\exp[W(x^*)/kT]\exp[-\Gamma(x-x^*)^2] \tag{4.12}$$

in which the reversible work, $W(x)$ in the numerator of (2.56), has been replaced by its quadratic approximation about x^*.

Because of the sharpness of the maximum the limits of integration in (4.11) may be extended to $(-\infty,+\infty)$ without loss of rigor, provided that (4.12) is used as the integrand. The final result, then, is

$$I^*=\frac{6N\beta v^{\frac{1}{3}}}{g^{\frac{1}{3}}}(\Gamma/\pi)^{\frac{1}{2}}\exp[-W(x^*)/kT]$$
$$=K\exp[-W(x^*)/kT]. \tag{4.13}$$

The approximation (4.2) for β is not serious since it appears in (4.13) in the coefficient K, a rather insensitive place.

V. DISCUSSION

In the preceding sections a theory of nucleation, based on statistical mechanics, has been presented. This theory does not consider the first fragments of the new phase formed to be spherical liquid drops. In no place (not even at the nucleus) has it been necessary to consider explicity, phase equilibrium between an embryo and the mother phase. The manifold difficulties connected with this point (in view of the small dimensions of typical nuclei) are therefore obviated.

Furthermore, in the preceding development, it has been possible to define an embryo unambiguously, and in such a manner that its energetic properties can, in principle, be computed. This was not possible in the classical theory.

The question of obtaining numerical values for I^* now

arises. The main obstacle to be overcome in this endeavor is the evaluation of $\langle\omega(x)\rangle_{Av}$. As a first step in this direction one might assume that the average distribution of matter in a cell of size x is uniform and that the density of matter changes abruptly at the cell wall to N/V, the uniform density of the surrounding gas. The mutual energy within the cell could then be evaluated in the Lennard-Jones, Devonshire[16] fashion, and the surface effect could be treated by the method of Fowler[21] or Hill.[22] As a next step, the variation of density through the cell wall might be computed using the procedure of Hill[23] or the more elegant, though more difficult, technique of Kirkwood and Buff.[7] The continuous average distribution of matter so obtained could then be used in evaluating the *average* mutual-intercell energy.

In the succeeding papers of this series we shall attempt some of these calculations beginning with simple molecules such as nitrogen where the molecular interation is chiefly of the dispersion type.

[21] See reference 11, p. 445.
[22] T. L. Hill, J. Am. Chem. Soc. **72**, 3923 (1950).
[23] T. L. Hill, J. Chem. Phys. **20**, 141 (1952).

ACKNOWLEDGMENT

The author wishes to express his appreciation to Professor Frank Buff of the University of Rochester, for illuminating discussions in connection with this paper.

THE JOURNAL OF CHEMICAL PHYSICS VOLUME 20, NUMBER 8 AUGUST, 1952

Rotational Isomerism and the Vibrational Spectrum of *Sym*-Dideuterodibromoethane

H. J. BERNSTEIN AND A. D. E. PULLIN,* *National Research Council, Ottawa, Canada*
AND
B. S. RABINOVITCH AND N. R. LARSON,† *University of Washington, Seattle, Washington*

(Received January 29, 1952)

Trans-ethylene-d_2 was brominated by two methods, which involved different stereochemical paths, to give 95 percent *meso*-BrDHC-CHDBr as one product and a mixture of *meso*- and *racemic*-BrDHC-CHDBr as the other. Liquid phase Raman spectra and liquid and solid phase infrared spectra of these materials have been obtained and a tentative assignment of the vibrational frequencies of BrDHC-CHDBr to the *trans* and *skew* configurations of the *meso* and *racemic* compounds has been made.

THE bromation of *trans*-ethylene-d_2 may be carried out to obtain products having different proportions of the *meso* and *racemic* diastereoisomers of *sym*-dideuterodibromoethane. This would facilitate the assignment of the vibrational frequencies in the spectrum of *sym*-dideuterodibromoethane to its diastereoisomers and would simplify the further assignment of frequencies to the rotational isomers of each diastereoisomer.

The heterolytic addition of Br to ethylenic double bonds in polar solvents has been found to yield *trans* addition products preponderantly.[1] Roberts and Kimball[2] have explained this behavior in terms of an initial attack of a bromonium ion on the π-bond of the ethylenic linkage to give a cyclic intermediate (see Fig. 1).

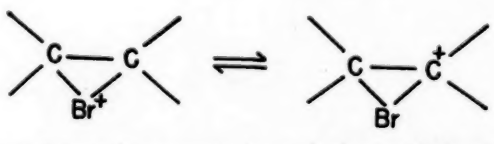

FIG. 1. Schematic representation of the heterolytic bromine addition to a double bond.

The second step is the attraction of a negative Br ion resulting in addition above and below the plane of the C—C bond. With *trans*-dideuteroethylene this would give rise to a centrosymmetrical dibromoethane of point group, $C_i = S_2$.

In nonpolar solvents in the presence of light, however, a mixture of *cis* and *trans* addition products is usually obtained.[3,4] This can be explained by a free radical, homolytic mechanism. A radical is formed when a Br atom forms a bond with one π-orbital as in (a) (see Fig. 2). But there is just as much of the configuration (b) present as of (a). Thus, the next Br (which adds on the *trans* side from steric considerations)

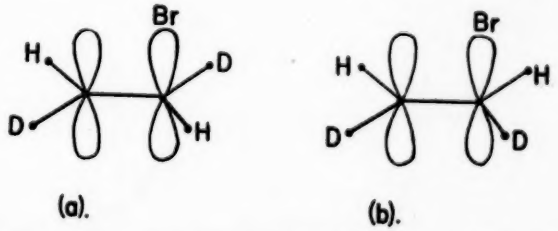

FIG. 2. Schematic representation of the homolytic bromine addition to a double bond.

* National Research Laboratories Postdoctorate Fellow, 1950.
† Postdoctorate Research Fellow, 1950.
[1] P. B. D. De la Mare, Quart. Rev. **3**, 127 (1949).
[2] I. Roberts and G. E. Kimball, J. Am. Chem. Soc. **59**, 947 (1937).
[3] S. Winstein and D. Seymour, J. Am. Chem. Soc. **68**, 119 (1946).
[4] G. W. Wheland, *Advanced Organic Chemistry* (John Wiley and Sons, Inc., New York, New York 1949), p. 298.

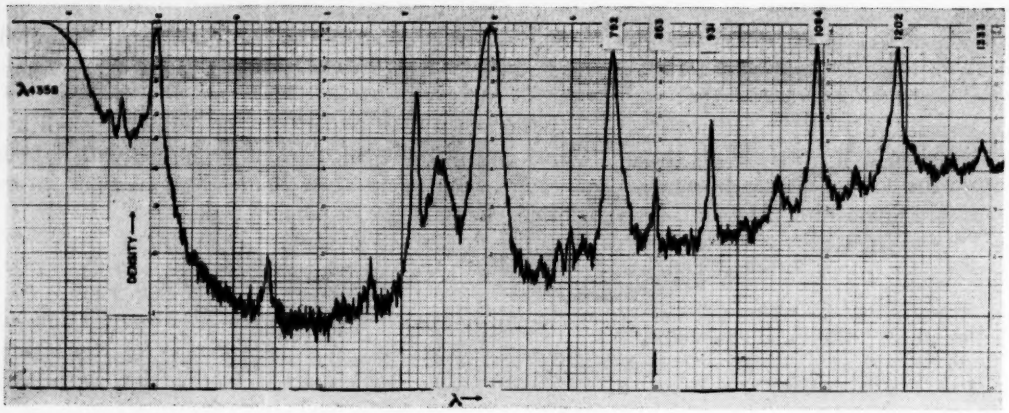

FIG. 3. Raman spectrum of liquid $(CHDBr)_2$ "dark."

gives a *meso* form with the radical of (a) and an active form with the radical of (b), and the result is a 1:1 mixture of these forms. A similar conclusion would be reached if the mechanism were presented in terms of inversion of configuration of a pyramidal free radical resulting from addition of the first Br atom to the double bond.

Trans-ethylene-d_2 has been brominated in the two different ways just discussed and the Raman and infrared spectra of the resulting products examined.

EXPERIMENTAL

Trans-ethylene-d_2 was prepared by the reduction of acetylene-d_2 with chromous chloride.[5] Mass-spectrographic analysis showed that the product was 98.8 percent ethylene-d_2 and that the infrared spectra of the *cis* and *asymmetric* isomers were completely absent.

Two samples of BrDHC-CHDBr were prepared as follows: For the first, the bromination was carried out in 25 cm³ of an aqueous solution saturated with Br and KBr. The solution was first subjected to several alternate freezings, evacuations, and meltings to remove any dissolved O_2. Then 1.5 l. (S.T.P.) of *trans*-ethylene-d_2 was allowed to come in contact with the stirred aqueous solution, which was protected from light and maintained at 0°C. These conditions correspond to the heterolytic mechanism discussed above. The second preparation was performed by carrying out the bromination in CCl_4 solution in the presence of light at room temperature; 1.5 l. (S.T.P.) of *trans*-ethylene-d_2 was brought into contact with 25 cm³ of solvent which contained a small stoichiometric excess of Br. The solution was irradiated during addition with a 500-w tungsten projection lamp. This corresponds to the homolytic reaction.

Both preparations were washed free of Br with 0.5*N* NaOH and dried with $CaCl_2$. Further purification of the two compounds was accomplished by distillation at 1-atmos pressure on a small column having 15 theoretical plates. The materials accepted were center fractions which boiled over a range of 0.2°C.

The Raman spectra of the two liquid samples, hereafter referred to as "dark" and "light," were obtained on Eastman Kodak 103a-J plates after an exposure of approximately 12 hr. The Raman spectrograph used contained 2 EDF3 flint glass, 60° prisms, and was equipped with f/3.5 and f/7.7 camera lenses. Pen-recorded charts of the spectra are shown in Figs. 3 and 4, taken on a Leeds and Northrup microphotometer with a Speedomax Recorder.

The infrared spectra of the liquid samples were obtained with a Perkin-Elmer Infrared Spectrometer (model 12c), used in conjunction with a Brown Recorder. Infrared spectra of the solids also were obtained using

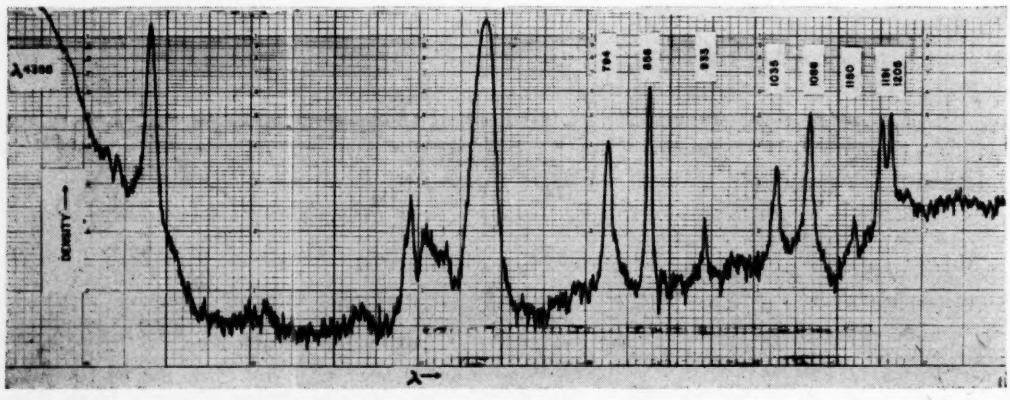

FIG. 4. Raman spectrum of liquid $(CHDBr)_2$ "light."

[5] W. I. Patterson and V. du Vigneaud, J. Biol. Chem. **123**, 327 (1938).

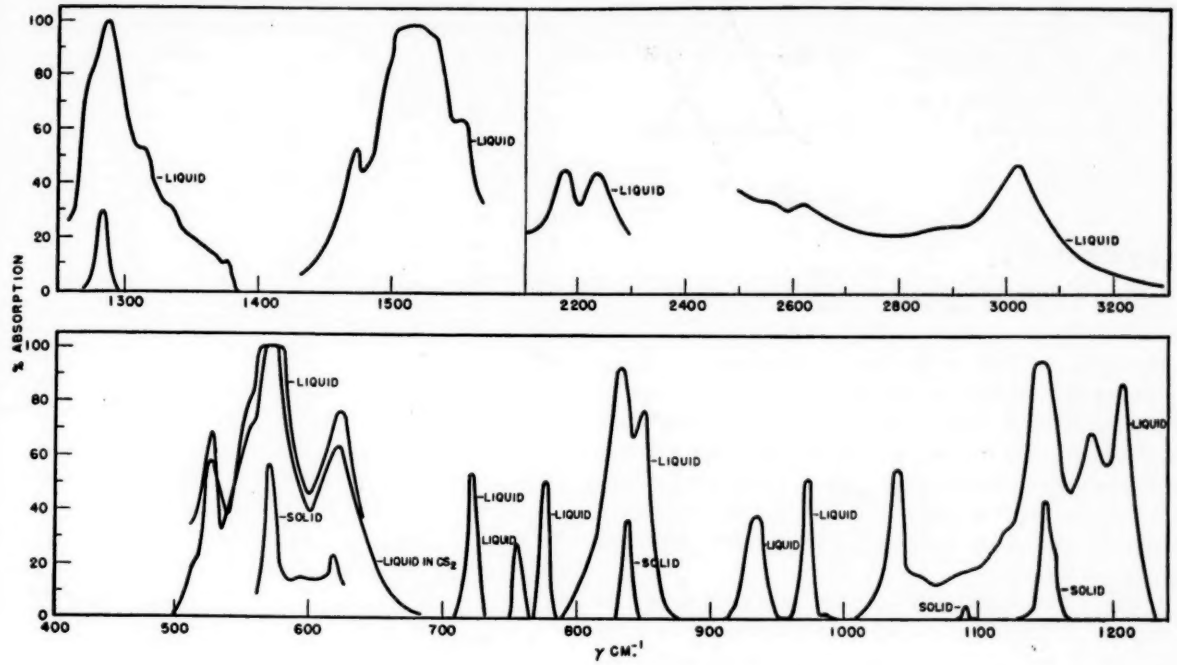

FIG. 5. The infrared spectrum of liquid and solid $(CHDBr)_2$ "dark."

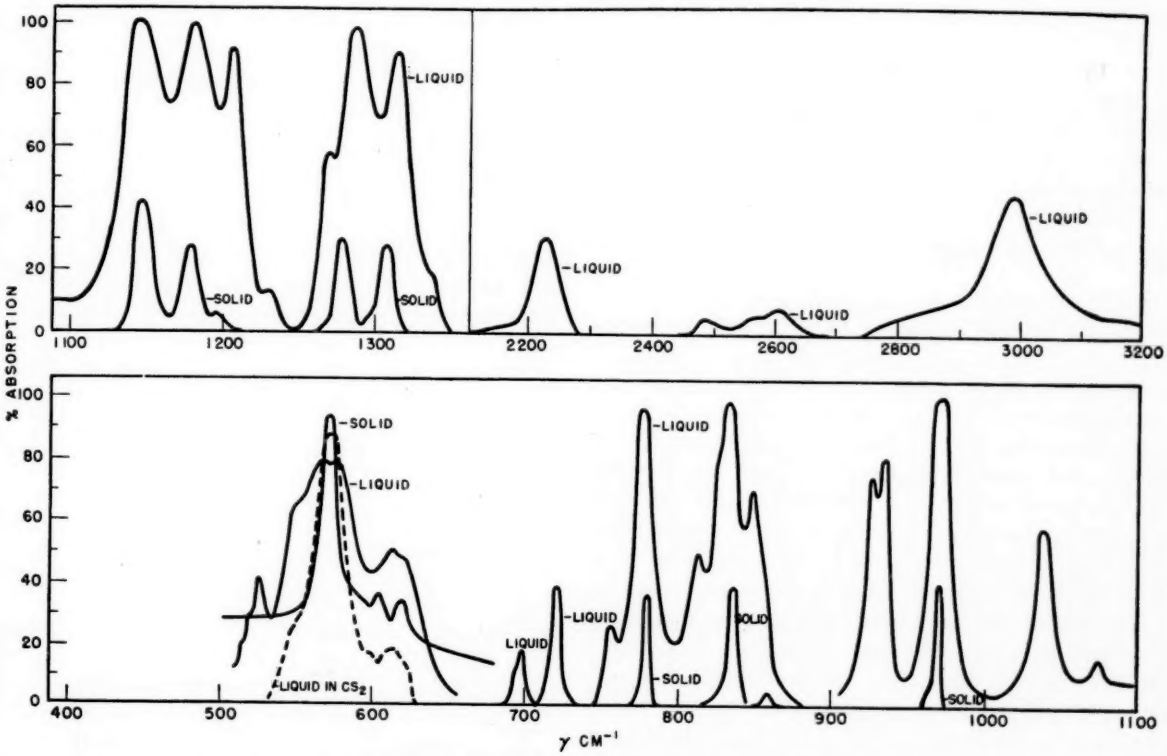

FIG. 6. The infrared spectrum of liquid and solid $(CHDBr)_2$ "light."

the technique and cell described elsewhere.[6] The infrared spectra of the products of the "dark" and 'light" brominations are shown in Figs. 5 and 6.

[6] E. L. Wagner and D. F. Hornig, J. Chem. Phys. **18**, 296 (1950).

RESULTS

It is immediately evident that the spectra of the "light" and "dark" compounds are different. The Raman spectrum of the "light" compound seems to be identical with that obtained for BrDHC-CHDBr by

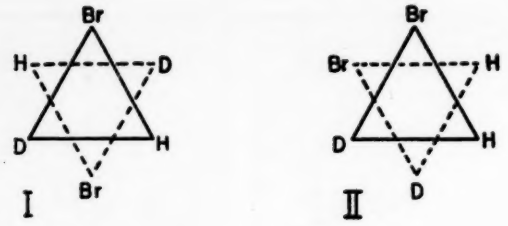

FIG. 7. The rotational isomers of meso $(CHDBr)_2$.

de Hemptinne,[7] both as to lines and intensities. Since the compound studied by de Hemptinne was obtained by the addition of DBr to acetylene it is evident[8] that it will consist of a 1:1 mixture of the *meso* and *racemic* forms, corresponding to our "light" compound. Comparison of the spectra allows one immediately to classify the bands and lines belonging to the *meso* (*m*) and *racemic* (*r*) form.

In Fig. 7 the *meso* form with its rotational isomer is shown and in Fig. 8 an active form with its isomers are shown. It is well known[9] that the solid modification of 1,2-dibromoethylene is made up entirely of the *trans* form. Thus the solid spectrum of the pure *meso* form should be that of configuration I in Fig. 7, whereas the

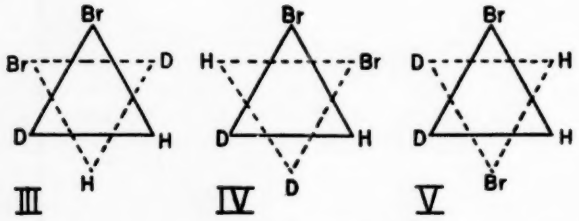

FIG. 8. The rotational isomers of *racemic* $(CHDBr)_2$. III, IV, and V have C_2 symmetry. III and IV have the same energy.

solid spectrum of the pure active form should be that of configuration V. Form I has a center of symmetry, so the vibrations active in Raman effect are inactive in infrared, and vice versa. Form V, however, has the proper symmetry C_2, so all modes should be both Raman and infrared active. However, since the decrease in symmetry from C_i, for form I, to C_2, for form V, is due to the asymmetry of mass in the arrangement of the D and H atoms, the electrical symmetry remaining unchanged, it is expected that those lines allowed for form V under C_2 symmetry, but forbidden under C_i symmetry, will be weak in intensity. On this basis, and guided by the assignments[10] for $BrH_2C\text{-}CH_2Br$ and $BrD_2C\text{-}CD_2Br$, we have made assignments for the *trans* and *skew* forms of *meso* and *racemic* BrDHC-CHDBr. The notation is that used in the previously mentioned work.[10]

[7] M. de Hemptinne, Vol. Comm. V. Henri (Desoer, Liege, 1947), p. 150.
[8] G. J. Szasz, J. Chem. Phys. **18**, 393 (1950).
[9] S. Mizushima and Y. Morino, Proc. Indian Acad. Sci. **8**, 315 (1938).
[10] J. T. Neu and W. D. Gwinn, J. Chem. Phys. **18**, 1642 (1950).

TABLE I. Spectrum of *meso*-BrDHC-CHDBr.

Raman Liq.	Raman Int.	Raman Assign.[a]	Infrared spectrum Liq.	Int.	Assign.[a]	Solid
85	1*b*	ω_{10}	527	*m*	ω_5	
187	8	ν_6	556	*w*	ω_{17}	
334	1*b*	ω_{18}	570	*s*	ν_{17}	570
526	4	ω_5	621	*m*	ν_9	619
553	2	ω_{17}	721	*m*	ω_{13}	
623	10	ν_5	756	*m*	ν_9	
719	0	ω_{13}	833	*s*	ν_8	837
757	0	ω_9	849	*m*	ω_8	
792	5	ν_{13}	934	*m*	ω_{12}	
931	3	ω_{12}	1040	*m*	ω_3	
984	1	ν_4				1093 *vvw*
1068	1	ν_{12}	1144	*s*	ν_{16}	{1150 {1156
1084	6	ν_3	1207	*s*	ω_{16}	
1202	5	ν_2	1287	*s*	ν_{15}	1284
1285	1	ω_2	1331	*w*	ω_{15}	
1332	2	ω_{15}	1474	*m*	$\nu_6+\nu_{15}$	
2154	1	ω_{11}	1509	*s*	$2\omega_9$, and $\omega_6+\omega_2$	
			1550	*m*	$\nu_4+\nu_{17}$	
2195	1	ω_{14}	2177	*m*	ω_{14}	
2212	0	$\omega_2+\omega_{12}$	2235	*m*	ν_{14}	
2230	5	ν_{11}	3020	*m*	ν_7	
2992	5	ν_1, ω_1				

[a] ν, ω are used for the *trans* and *skew* forms, respectively (see Fig. 7).

The high ratio of *m* to *r* in the dark compounds (see below) makes possible a rigorous division of the observed frequencies into those belonging to the *meso* and *racemic* compounds.

The present Raman and infrared data do not enable more than a very tentative assignment to be made, except for the *trans* form of the *meso* compound, for which the center of symmetry ensures the strict applicability of the mutual exclusion rule for Raman and infrared frequencies. The assignment of the remainder of the frequencies observed for the *m* com-

TABLE II. Frequency assignments *meso*-BrDHC-CHDBr.

Trans (C_i) Assign.	Raman	Infrared	*Skew* Assign.	Raman	Infrared
ν_1	2992		ω_1	2992	
ν_2	1202		ω_2	1285	
ν_3	1084		ω_3		1040
ν_4	984		ω_4		
ν_5	623		ω_5	526	527
ν_6	187		ω_6		
ν_7		3020	ω_7		3020
ν_8		833	ω_8		849
ν_9		621	ω_9	757	756
ν_{10}			ω_{10}	85	
ν_{11}	2230		ω_{11}	2154	
ν_{12}	1068		ω_{12}	931	934
ν_{13}	792		ω_{13}	719	721
ν_{14}		2235	ω_{14}	2195	2177
ν_{15}		1287	ω_{15}	1332	1331
ν_{16}		1144	ω_{16}		1207
ν_{17}		570	ω_{17}	553	556
ν_{18}			ω_{18}	334	

TABLE III. Spectrum of BrDHC-CHDBr (*racemic*).

Raman spectrum de Hemptinne[a]				Infrared spectrum			
Liq.	Int.	Assign.[b]	Solid	Liq.	Int.	Assign.[b]	Solid
88	3	ω_{10}		517	*m*	ω_5	
188	10	ν_6		572	*s*	ν_{17}	572
344	½	ω_{18}		612	*w*	ν_5	605, 619
520	2	ω_5		698	*w*	ω_{13}	
543	2	ω_{17}		776	*s*	ν_9	780
610	13	ν_5	610	813	*m*	ω_9	
854	8	ν_{13}	855	860	*w*	ν_{13}	860
1035	5	ν_{12}		927	*s*	ω_{12}	
1045	1	ν_3		970	*s*	ν_8	970
1191	8	ν_2	1191	1075	*w*	ω_3	
1224	½	ω_2		1180	*s*	ν_{16}	1180
1299	½	ω_{15}					1195
2195	1			1215	*w*	ω_{16}	
2214	3	ν_{11} or ν_1		1268	*m*	ω_{15}	
2230	7	ω_{11}		1314	*s*	ν_{15}	1308
2992	5	ν_1 or ν_{11}		2225	*m*	ν_7 or ν_{14}	
3001	5	ω_{14} or ω_7		2480	*w*	ν_2 or ν_{15}	
				2565	*w*		
				2610	*w*		
				2990	*m*	ν_{14} or ν_7	

[a] See reference 7.
[b] ν, ω are used for the *trans* and *skew* forms, respectively.

pound to the *skew* form is less certain, since this form does not possess a center of symmetry, but there is still little choice if the assignment is to be consistent with those for the *skew* forms of BrH_2C-CH_2Br and BrD_2C-CD_2Br.

For the *trans* and *skew* forms of the *racemic* molecule, the position is much less satisfactory. In the *r trans* form, there are strictly only two symmetry types, and although the skeletal frequencies may be expected largely to preserve the same character as in BrH_2C-CH_2Br and BrD_2C-CD_2Br, it is not obvious how far the methylene modes will mix under the lesser symmetry of *racemic*-BrDHC-CHDBr.

TABLE IV. Frequency assignments BrDHC-CHDBr (*racemic*).

Trans			*Skew*[a]		
Assign.	Raman	Infrared	Assign.	Raman	Infrared
ν_1	2992 or 2214		ω_1		
ν_2	1191		ω_2	1224	
ν_3	1045		ω_3		1075
ν_4			ω_4		
ν_5	610	612	ω_5	520	517
ν_6	188		ω_6		
ν_7		2990 or 2225	ω_7		
ν_8		970	ω_8		
ν_9		776	ω_9		813
ν_{10}			ω_{10}	88	
ν_{11}	2214 or 2992		ω_{11}	2230	
ν_{12}	1035		ω_{12}		927
ν_{13}	855	860	ω_{13}		698
ν_{14}		2225 or 2990	ω_{14}	3001	
ν_{15}		1314	ω_{15}	1299	1268
ν_{16}		1180	ω_{16}		1215
ν_{17}		572	ω_{17}	543	
ν_{18}			ω_{18}	344	

[a] There are two *skew* forms corresponding to III and IV of Fig. 8. The requencies given here are probably single for the skeletal vib rations, whereas one would expect the H vibrations to be double. The numbers given indicate the spectral region in which these frequencies are to be found.

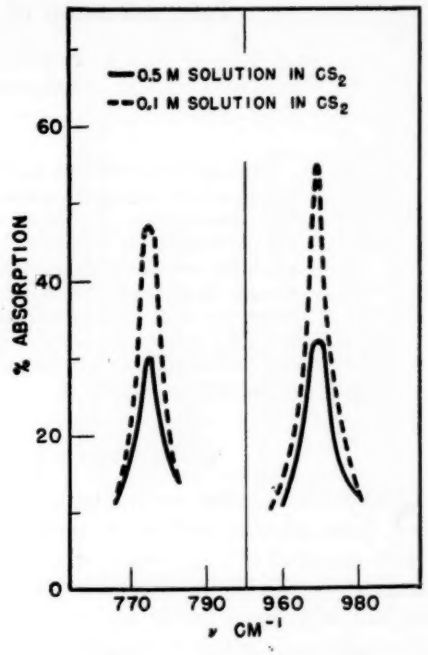

FIG. 9. Estimation of the *racemic* content of the "dark" compound.

It is interesting that while the frequency of the C—C stretching vibration[10] is relatively strong in both *trans*-BrH_2C-CH_2Br (at 1052 cm^{-1}) and *trans*-BrD_2C-CD_2Br (at 907 cm^{-1}) there is no Raman frequency in this range for *racemic*-BrDHC-CHDBr, and only a weak one at 984 cm^{-1} for the *meso* compound. Since the large shift from 1052 in the d_0 compound to 907 in the d_4 compound indicates that considerable H motion is to be associated with this vibration, one does not expect the intensity of this band to remain unaffected by D substitution. The results of the experimental work and assignments are given in Tables I–IV.

Since it has been reasonably well established that the "light" compound is 50 percent *m* and 50 percent *r*, it is apparent from the infrared spectra that the bands at 777 cm^{-1} and 970 cm^{-1} can be used to estimate the quantity of the *r* form in the "dark" compound. In Fig. 9 these bands are shown for a 0.5*M* solution of "dark," and an 0.1*M* solution of "light," in carbon disulfide.

It is readily seen that the "dark" compound contains 95 percent of the *m* form and 5 percent of the *r* form. This correlates with the fact that the (*trans*) reduction of the *meso* form of the dibromide with zinc and water yields 95 percent *trans*-ethylene-d_2.

ACKNOWLEDGMENTS

This work was supported in part under Contract N8 onr-52009 between the ONR and the University of Washington. We wish to thank Dr. Vernon H. Dibeler of the National Bureau of Standards for a mass spectrographic check of the purity of the ethylene-d_2. One of us (B.S.R.) thanks Professor G. B. Kistiakowsky for calling his attention to the work of Patterson and du Vigneaud.

Interdiffusion of Polyvinyl Acetate with a Series of Solvents*

A. T. HUTCHEON,† R. J. KOKES, J. L. HOARD, AND F. A. LONG
Department of Chemistry, Cornell University, Ithaca, New York

(Received October 12, 1951)

The Lamm scale method has been used to follow the interdiffusion of polyvinyl acetate with ethyl acetate, propyl acetate, isopropyl acetate, butyl acetate, and triacetin at 30°C, and with acetone at 20°, 30°, and 40°C. For all these systems the mutual diffusion coefficient attains a maximum value at intermediate polymer concentrations. At a given concentration and temperature the $D(c)$ values are largest with acetone and much the smallest with triacetin, although the relative variation in $D(c)$ over the concentration range is actually largest with the latter. The general variation of $D(c)$ with concentration can be plausibly interpreted in terms of the mass flow-intrinsic diffusion concept introduced by Hartley. For the system acetone—polyvinyl acetate the calculated energy of activation for the diffusion is nearly constant at 1 kcal in the concentration range 0 to 40 grams polymer per 100 cc of solution but then rises rapidly to 10 kcal at 90 grams polymer per 100 cc.

INTRODUCTION

SEVERAL studies dealing with the interdiffusion of high polymer and small molecule solvents have been reported,[1,2,3] but until very recently almost all quantitative examinations have been conducted in the regions of either high or low polymer concentrations. The diffusion coefficient, which is usually concentration dependent, has been evaluated in the dilute region by optical methods employing "schlieren" techniques,[4] interferometry,[5] and the scale method of Lamm.[1] For pure or slightly swollen polymers the diffusion coefficient can be calculated from either the permeability of the polymer to the solvent vapor[6] or the rate of sorption of the vapor by polymer films.[3]

Diffusion studies at intermediate concentrations have been reported recently by Hartley[7,8] and Robinson[5,9] and co-workers. Both groups of investigators agree that since the polymer and small molecule species differ so greatly in size, the rate of true diffusion, i.e., the net rate of transfer resulting from random molecular motion, should be much smaller for polymer than for solvent. However, as the solvent molecules diffuse into the polymer phase its volume must increase, thus producing an apparent diffusion of the polymer species into the solvent phase. The resultant transfer can be regarded as a mass flow of polymer and leads to the concept of an intrinsic diffusion coefficient which may differ greatly from the experimentally determined coefficient for interdiffusion.

This paper presents data for diffusion in the intermediate concentration regions and tests the applicability of some existing theories for the process. The Lamm scale method has been used to determine concentration as a function of the position in the diffusion cell. By subsequent mathematical analysis the diffusion coefficient was evaluated as a function of concentration for the interdiffusion of polyvinyl acetate with ethyl, propyl, isopropyl, and butyl acetates, and with triacetin and acetone. To minimize mechanical strains all experiments except one series with acetone were conducted above the second-order transition temperature of the polymer (28°C).[10]

EXPERIMENTAL PROCEDURE

In the Lamm scale method[11] a uniformly ruled scale is photographed through a diffusion cell. If a refractive index gradient exists within the cell, the rulings appear on the photographic record to be unequally spaced. The magnitude of the apparent shift of a scale line is proportional to the refractive index gradient at the corresponding level in the diffusion medium. From the relation between refractive index and concentration the latter can be evaluated as a function of the cell coordinate.

Monochromatic light, 5461A, from a Mercury A-H4 lamp equipped with suitable filters was employed. The transparent scale was a photograph of a precision scale ruled in millimeters. The diffusion cell was formed by a U-shaped, steel spacer-plate (0.5 mm thick) clamped between two flats of optically polished glass to make a rectangular parallelopiped 0.5×10×50 mm. The cell and scale were mounted on a machined slide so that the distance between them could be varied between 1 and 15 cm. These were placed in an air bath thermostatted to ±0.3°C. A 1-diopter, meniscus lens was "stopped" by a 1.5-cm aperture to give an F number of 67. The distances from scale to lens and lens to photographic plate were both approximately 200 cm.

In order to obtain an initially sharp horizontal boundary between the diffusing species and generally

* This work was carried out as part of a research project sponsored by Army Ordnance.

† Present address: Department of Chemistry, McMaster University, Hamilton, Ontario, Canada.

[1] C. O. Beckmann and J. L. Rosenberg, Ann. N. Y. Acad. Sci. **46**, 329 (1945).
[2] J. Crank and G. S. Park, Trans. Faraday Soc. **45**, 240 (1949).
[3] S. Prager and F. A. Long, J. Am. Chem. Soc. **73**, 4072 (1951).
[4] J. S. L. Philpot, Nature **141**, 283 (1938).
[5] J. Crank and C. Robinson, Proc. Roy. Soc. (London) **A204**, 549 (1951).
[6] P. E. Rouse, J. Am. Chem. Soc. **69**, 1068 (1947).
[7] G. S. Hartley and J. Crank, Trans. Faraday Soc. **45**, 801 (1949).
[8] G. S. Hartley, Trans. Faraday Soc. **45**, 821 (1949).
[9] C. Robinson, Proc. Roy. Soc. (London) **A204**, (1951).
[10] R. H. Wiley and G. M. Brauer, J. Polymer Sci. **4**, 351 (1949).
[11] T. Svedburg and K. O. Pederson, *The Ultracentrifuge* (Clarendon Press, Oxford, England, 1940), p. 254.

to minimize mechanical strains within the polymer when clamped in the cell, the following procedure was adopted. A strip of film slightly thicker than 0.5 mm was cut to fit the bottom third of the cell. The loosely assembled cell was held at 45°C until the film began to flow, at which time all clamps were tightened. After one hour, the cell was cooled and taken apart. The top edge of the film was trimmed to give a straight squared edge, the cell reassembled, held at 45°C in a vacuum oven for several hours, and then stored overnight in an oven at 35°C until the start of the experiment.

For a diffusion run the cell was mounted in the air bath, solvent introduced, the cell closed and sealed with paraffin to prevent evaporation. At definite time intervals, ranging from 5 to 600 hours, photographs were taken of the scale through the diffusion cell. Positions of the scale lines on the photograph were measured with a traveling microscope (carefully set to move along the central axis of the photograph since there was usually an indication of seepage of solvent where the polymer touched the steel) and the scale line displacements recorded.

To determine the concentration cell coordinate relations by the scale method, refractive index and solution density as functions of concentration must be known. A Pulfrich refractometer and specific gravity bottles were used to obtain these data; typical results for the system ethyl acetate—polyvinyl acetate are shown in Fig. 1. Since the refractive index varies almost linearly with concentration only four or five points were determined for solutions in other solvents.

Polyvinyl acetate of commercial grade, AYAT, was obtained from the Carbide and Carbon Chemicals Corporation. The unfractionated material had a viscosity average molecular weight, using the formula of Wagner,[12] of 170,000. The films were prepared by casting from acetone solutions on a mercury surface

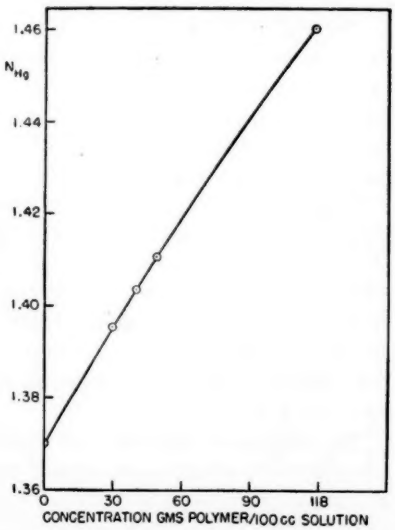

FIG. 1. Refractive index as a function of concentration for ethyl acetate—polyvinyl acetate.

[12] R. H. Wagner, J. Polymer Sci. 2, 21 (1947).

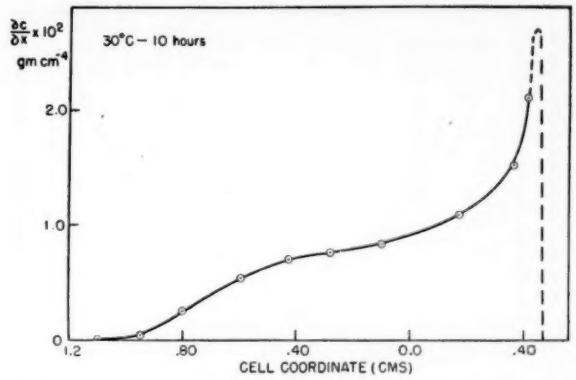

FIG. 2. Concentration gradient as a function of the cell coordinate for acetone—polyvinyl acetate.

in a vacuum desiccator with subsequent slow removal of solvent and drying in a vacuum oven at 45°C. All solvents were reagent grade, distilled and dried.

TREATMENT OF DATA

The refractive index N can be evaluated as a function of height x in the cell by means of the formula,[11]

$$Z = GabdN/dx. \qquad \begin{matrix} G = \text{magnification factor} \\ a = \text{cell thickness} \\ b = \text{cell to scale distance} \\ Z = \text{scale line displacement} \end{matrix} \qquad (1)$$

Upon integration (1) becomes

$$N(x) - N(x_0) = 1/Gab \int_{x_0}^{x} Z dx. \qquad (2)$$

The relation between cell and film coordinates is

$$dx = Fdz, \qquad \begin{matrix} z = \text{film coordinate} \\ x = \text{cell coordinate} \end{matrix} \qquad (3)$$

$$F = l - b/Gl. \qquad l = \text{optical distance from camera objective to scale}$$

This treatment includes approximations which are justifiable only if both $\{adN/dx\}$ and $\{d^2N/dx^2\}$ are sufficiently small. These conditions are met satisfactorily by the apparatus as described except for measurements near the polymer-solution boundary. In this region, as is made evident from inspection of a typical plot (Fig. 2) of concentration gradient against cell coordinate, both dc/dx and d^2c/dx^2 (which are proportional to dN/dx and d^2N/dx^2) are increasing rapidly at the point nearest the polymer-solution boundary where it is still feasible to measure the con centration gradient. Since dc/dx must be zero at the boundary, the qualitative behavior of the dc/dx *vs* x curve can be sketched in as shown. It seems, moreover, that both the height and breadth of the resulting peak in concentration gradient must be fairly substantial since otherwise the area under the dc/dx *vs* x curve over the whole of the diffusion domain will be appreciably smaller than the theoretical value. If the ex-

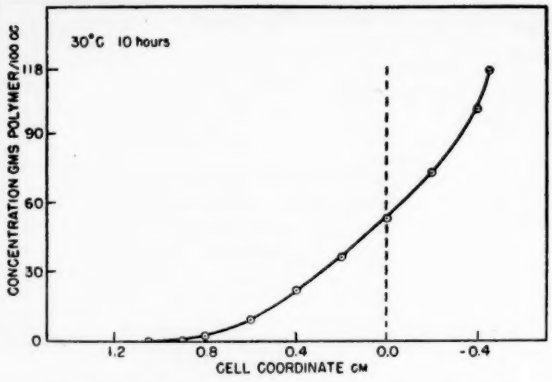

FIG. 3. Concentration-cell coordinate relation for acetone—polyvinyl acetate.

trapolation assumes a peak of minimum area, the discrepancy may be as much as 10 percent.

Graphical integration of the concentration gradient *vs* distance curve gives the concentration as a function of cell coordinate. Figure 3 shows a typical $c-x$ curve.

The infinite solid approximation applies in this case to the evaluation of the diffusion coefficient, $D(c)$ appearing in Fick's Law

$$\partial c/\partial t=\partial/\partial x\{D(c)\partial c/\partial x\}. \tag{4}$$

The Boltzman[13] substitution ($y=x/t^{\frac{1}{2}}$), which requires x to be linear in $t^{\frac{1}{2}}$, was shown experimentally to be valid for these systems. This substitution leads to

$$D(c)dc/dx=\tfrac{1}{2}t\int_0^c xdc. \tag{5}$$

Since both the above integral and the value of dc/dx may be calculated from curves of the sort illustrated in Fig. 3, $D(c)$ may be evaluated immediately once the origin of x is determined. To fix this origin it is noted that dc/dx is zero at both boundaries, and therefore $\int_0^c xdc$, taken over the whole diffusion domain, is zero. It may be demonstrated that the origin of x for the polymer species should not change with time, whereas the origin for the solvent species should move by an amount directly calculable from the volume change occurring upon mixing. In most experiments a small movement of the polymer mathematical boundary was observed, most probably as a consequence of relaxation of mechanical strains within the polymer not entirely removed by the earlier annealing treatment. The effect of this apparent movement appears to be inconsequential in comparison with other sources of experimental error.

The volume change on mixing is so small that mutual diffusion coefficients calculated from solvent and polymer $c-x$ curves obtained in a single experiment agree within the experimental error which, on the basis of repeat runs, appears to be 5 to 10 percent. In subsequent analysis the volume changes on mixing will be neglected (see Hartley and Crank[7]).

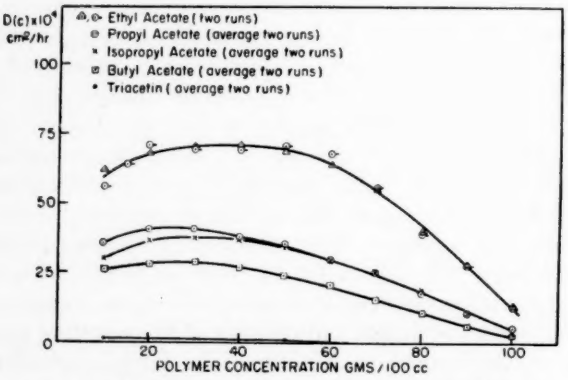

FIG. 4. $D(c)$ as a function of concentration for polyvinyl acetate in several acetate esters.

[13] L. Boltzman, Wied. Ann. **53**, 959 (1894).

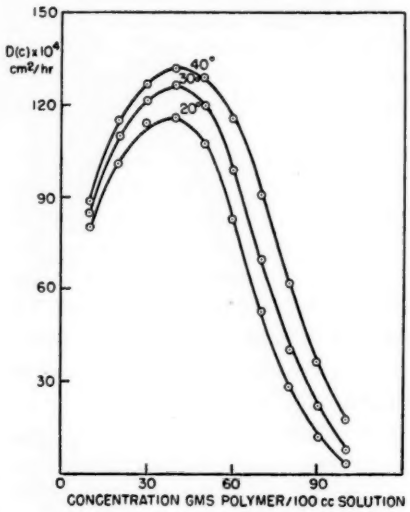

FIG. 5. $D(c)$ for acetone—polyvinyl acetate as a function of temperature and concentration.

RESULTS

For all the systems studied $D(c)$ shows a broad but definite maximum at an intermediate composition lying in the range 30–50 percent of polymer. Considerably lower values are found at both extremes of composition, especially so at the high polymer limit. The values of $D(c)$ for polyvinyl acetate and some acetate esters are shown graphically in Fig. 4; Fig. 5 shows the results for polyvinyl acetate and acetone at three temperatures.

In these figures one observes generally the expected variation in diffusion coefficient with increasing molecular size of the small molecule. In fact, it may be seen from Table I which lists $D(c)$ at several concentrations that D_{max} decreases approximately 100-fold from acetone to triacetin and the values of D for the homologous series of esters decrease as expected from ethyl to butyl acetate.

The difference between the diffusion coefficients of the polyvinyl acetate—isopropyl acetate and polyvinyl acetate *n*-propylacetate systems, Fig. 4, is much smaller than might have been anticipated from studies of sorption of hydrocarbon vapors by polyisobutylene.[3]

For the latter systems $D(c)$ at high polymer concentrations was found to decrease much more with branching than with a corresponding increase in chain length of the small molecule. It may be that the effect of the relatively large carboxyl groups in the acetate esters partially masks the effect of branching in the alkyl group.

The solution process of polyvinyl acetate in triacetin is significantly different from that for the smaller esters. Figure 6 shows c *vs* x curves for several different esters when the lengths of the diffusion domain are roughly comparable. The concentration gradient of triacetin is by far the steepest of the three in the region of large polymer concentration. Consequently, the fraction of the diffusion domain which consists of swollen polymer (arbitrarily defining swollen polymer as solutions of concentration greater than 50 g of polymer/100 cc solution) is least for triacetin. For the homologous series studied a progressively thinner swollen region accompanies solution as the size of the solvent molecule increases. This same result has been observed qualitatively for the dissolution of nitrocellulose and cellulose acetate in a homologous series of solvents.[14] The

TABLE I. $D(c)$ at 30°C as function of solvent and concentration.

Solvent	10^6 $D(c)$, cm²/hr for polymer conc. in g/100 cc			
	20 g/100 cc	40 g/100 cc	70 g/100 cc	90 g/100 cc
Acetone	110	126	70	22
Ethyl acetate	68	70	56	26
Propyl acetate	41	38	25	12
Isopropyl acetate	36	37	25	12
Butyl acetate	28	27	16	6
Triacetin	1.4	1.2	0.51	0.14

mechanism of the dissolution process presumably reflects the variation of $D(c)$ with concentration. As is seen from Table I, the fractional decrease of $D(c)$ in going from the maximum to solutions of large polymer concentration is largest for triacetin, smallest for acetone. It is significant also that the maximum in $D(c)$ shifts to lower polymer concentrations with an increase in size of the solvent molecule.

To investigate the influence of molecular weight of polymer, two fractions of polyvinyl acetate, viscosity average molecular weight 170,000 and 360,000, were studied with *n*-propyl acetate and their diffusion coefficients were calculated. As opposed to the results reported for dilute solutions,[15] it was found that in the concentration range covered in our experiments variations in polymer molecular weight produce a negligibly small change in $D(c)$.

From the data of Fig. 5 one can calculate energies of activation for the interdiffusion of acetone and the polymer using the equation

$$D(c)=D_0\exp[-E^*/RT].$$

[14] J. DeHaan, doctoral thesis (Cornell University, 1949).
[15] A. F. Schreck and S. J. Singer, J. Phys. and Colloid Chem. 54, 1028 (1950).

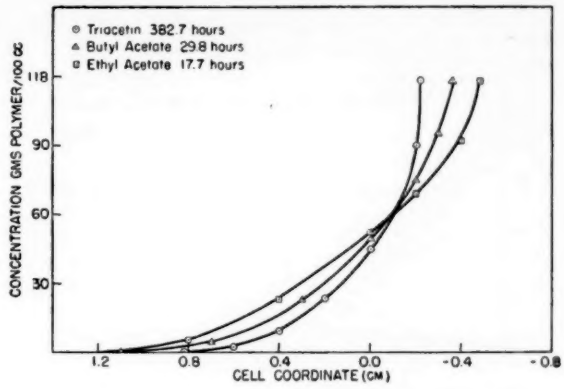

FIG. 6. Concentration-cell coordinate relation for several acetate esters.

Figure 7 gives the results. For the lower polymer concentrations, E^* is practically constant at only about 1 kcal. At a polymer concentration of about 35 g per 100 cc, E^* starts to increase and reaches a value of 10 kcal at a concentration of 90 g/100 cc.

DISCUSSION

Hartley and Crank[7] have analyzed the over-all diffusion process for polymer—small molecule systems in terms of a combination of mass flow and intrinsic diffusion. They have related the mutual diffusion coefficient $D(c)$ to intrinsic diffusion coefficients, $\mathfrak{D}_s$ and $\mathfrak{D}_p$, of the solvent and polymer species, respectively,

$$D(c)=\mathfrak{D}_s+V_s(\mathfrak{D}_p-\mathfrak{D}_s), \qquad (6)$$

where V_s is the volume fraction of solvent. Since $\mathfrak{D}_s$ is assumed to be much larger than $\mathfrak{D}_p$ the second term will be negative; this term represents what Hartley and Crank call the mass flow. It can be interpreted as a flow of the swollen polymer in the direction opposite to the flow of the small molecules, resulting from the expansion of the polymer matrix. In the form above,

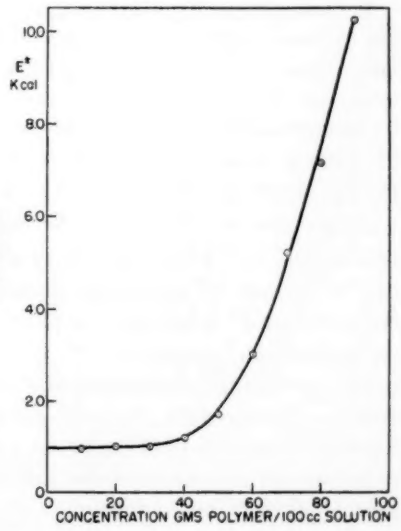

FIG. 7. Activation energy for interdiffusion as a function of concentration for acetone—polyvinyl acetate.

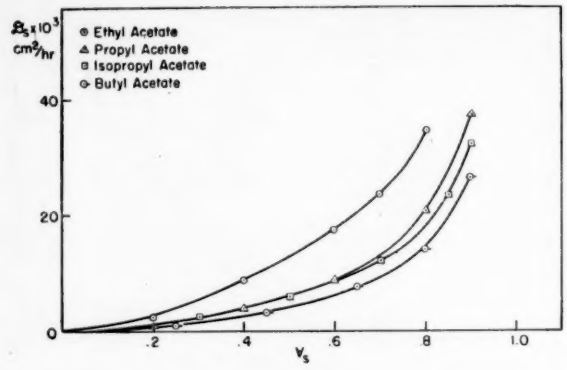

FIG. 8. The intrinsic diffusion coefficient as a function of concentration for several systems.

Eq. (6) cannot easily be applied. However, it is reasonable to assume that at moderate concentrations of polymer the intrinsic diffusion coefficient $\mathfrak{D}_p$ is negligibly small. Then the equation becomes

$$D(c)=(1-V_s)\mathfrak{D}_s. \tag{7}$$

$\mathfrak{D}_s$ would be expected to be virtually independent of size of polymer molecule; in contrast one would expect $\mathfrak{D}_p$ to be strongly dependent on polymer molecular weight. The experimental observation that $D(c)$ is independent of polymer molecular weight in the concentration ranges studied thus supports the assumption involved in Eq. (7).

Several typical plots of $\mathfrak{D}_s$, calculated from Eq. (7) are shown in Fig. 8. For all the systems studied $\mathfrak{D}_s$ increases with increasing volume fraction of small molecule and, in contrast to $D(c)$, no maximum is observed. As one varies the small molecule from acetone to triacetin, the values of $\mathfrak{D}_s$, for a given volume fraction of polymer, decrease strongly just as does $D(c)$ itself. In fact for all the solvents studied, $\log\mathfrak{D}_s$ (at a given volume fraction) decreases almost linearly with molecular weight of the solvent.

It follows from Eq. (7) that energies of activation for the intrinsic diffusion coefficient $\mathfrak{D}_s$ will be identical with those for $D(c)$, assuming only that volume fractions are temperature independent. Hence Fig. 7 may be interpreted as giving values of E^* for the diffusion of acetone molecules into the swollen polymer matrix. On this basis the large variation of E^* with polymer concentration is reasonable. At low polymer concentrations a "hole" for diffusion of an acetone molecule can be formed by movement primarily of small molecules so that E^* is low and constant; for larger polymer concentrations, movement of polymer segments becomes increasingly important and consequently E^* increases. We conclude that the mass flow concept for solvent-polymer interdiffusion is consistent with the experimental observations and permits a fairly specific and satisfactory interpretation.

TABLE II. Viscosities and calculated friction factors for polyvinyl acetate—acetone at 30°C.

V_p	$\log\eta$	$\log f$, calc
0.1	−0.57	14.56
0.2	0.45	14.82
0.3	1.30	15.04
0.4	2.23	15.23
0.5	3.18	15.46
0.6	4.21	15.76
0.7	5.35	16.15

As is well known, a successful quantitative explanation of the diffusion of binary small molecule systems has been developed by expressing the diffusion coefficient as a product of thermodynamic and hydrodynamic factors.[16,17] The resulting equation is

$$D(c)=RT/f[\partial \ln a_s/\partial \ln V_s],$$

where a_s is the activity of the solvent and f is the friction factor. For small molecule systems f is assumed to be proportional to viscosity. However, for the system acetone—polyvinyl acetate the viscosity variation in going from $V_s=0.30$ to $V_s=0.90$ is so large (e.g., $\eta_1/\eta_2=10^6$ whereas $D(c)_1/D(c)_2=4$) that a theory of this sort will fit only if there is a large and quite unlikely compensating variation in the thermodynamic factor. Actually, in terms of the intrinsic diffusion coefficient and mass flow it is not surprising that there is so little correlation between viscosity and diffusion coefficient for these concentrated solutions. For diffusion of the small molecules into the polymer matrix, only motions of the polymer segments are involved whereas for viscous flow there must be an actual displacement of polymer molecules.

Because of uncertainties in the friction factor f one cannot calculate $D(c)$ directly. One can, however, do the inverse, that is, evaluate f as a function of concentration from the experimental $D(c)$. For the system polyvinyl acetate—acetone the thermodynamic factor $(\partial \ln a_s/\partial \ln V_s)$ was evaluated from the Flory-Huggins[18,19] equation,

$$\ln a_s=\ln(V_s)+(1-V_s)+\mu(1-V_s)^2,$$

assuming an average value of 0.35 for the parameter μ.[20] The calculated values of f and the experimentally determined values of η for the concentration range studied are tabulated in Table II. The variation of f with concentration is very marked, although much less so than the variation of the viscosity. A point of some interest is that $\log f/\eta$ is accurately linear with volume fraction, even though $\log\eta$ itself is not.

[16] Glasstone, Laidler, and Eyring, *The Theory of Rate Processes* (McGraw-Hill Book Company, Inc., New York and London, 1941), p. 533.
[17] L. Onsager and R. M. Fuoss, J. Phys. Chem. **36**, 2689 (1932).
[18] P. J. Flory, J. Chem. Phys. **10**, 51 (1942).
[19] M. L. Huggins, J. Chem. Phys. **9**, 440 (1941).
[20] R. J. Kokes, doctoral thesis (Cornell University, 1951).

The Rotation-Vibration Spectra of Allene and Allene-d_4

R. C. LORD AND PUTCHA VENKATESWARLU
Spectroscopy Laboratory, Massachusetts Institute of Technology, Cambridge 39, Massachusetts

(Received February 25, 1952)

The infrared absorption spectra of allene and allene-d_4 vapor have been measured over the spectral range 250–5000 cm^{-1} with a prism spectrometer. The infrared data, together with previously obtained Raman spectra, enable a complete vibrational analysis that satisfies the product rule well for all vibrational species. The torsional vibration is located at 865 cm^{-1} in allene and 615 cm^{-1} in allene-d_4. Fine structure was resolved for all perpendicular fundamental bands except that of the lowest frequency in both compounds. With help of the zeta-sum rule, a modified equation of H. H. Nielsen and the statistical weights of the rotational levels, the fine structure is analyzed to yield a complete set of zeta-values for both molecules and a moderately accurate value for the moment of inertia about the figure axis. The latter gives for the HCH angle the figure 113°±1° if one assumes a C−H distance of 1.071A.

INTRODUCTION

FOR many reasons the rotation-vibration spectra of the allene molecule — $H_2C=C=CH_2$ — are of special interest. It is the smallest molecule with cumulative double bonds, and therefore knowledge of its structure is important. The frequency of its torsional mode of vibration and the size of the H−C−H bond angle are relevant data in the theory of its electronic structure and chemical binding. The unusual possibilities for rotation-vibration interaction in the D_{2d} structure of the molecule make it a nice example for spectroscopic study.

The infrared absorption spectrum of allene vapor has been investigated by Linnett and Avery,[1] Thompson and Harris,[2] and Miller and Thompson.[3] The spectrum of allene in the photographic infrared region was also examined by Eyster.[4] Three of the perpendicular fundamentals were well resolved by Thompson and coworkers,[2,3] but the band centers were not definitely established. The low frequency perpendicular fundamental which was placed at 353 cm^{-1} by earlier work in the Raman effect[1] lies outside the region investigated by previous infrared workers. No data have been published on the infrared spectrum of allene-d_4. Investigation of the infrared and Raman spectra both of allene and allene-d_4 was thought to be desirable to establish the vibrational assignment and the structure without ambiguity. The Raman spectra of these molecules were studied by Lord and Ocampo in this Laboratory,[5] and in the present paper the infrared spectra of allene and allene-d_4 are reported. Together the infrared and Raman data lead to a complete vibrational analysis and a moderately accurate determination of the H−C−H angle.

[1] J. W. Linnett and W. H. Avery, J. Chem. Phys. **6**, 686 (1938).
[2] H. W. Thompson and G. P. Harris, Trans. Faraday Soc. **40**, 295 (1944).
[3] C. H. Miller and H. W. Thompson, Proc. Roy. Soc. (London) **200**, 1 (1949).
[4] E. H. Eyster, J. Chem. Phys. **6**, 580 (1938).
[5] R. C. Lord and J. Ocampo, J. Chem. Phys. **19**, 260 (1951).

EXPERIMENTAL DETAILS

Preparation of Allene and Allene-d_4

The preparation of allene was carried out as usual by the dehalogenation of 2,3-dibromopropene with zinc dust in alcoholic solution.[6] This method will produce allene contaminated with propene if the 2,3-dibromopropene contains a slight amount of 2,3-dibromopropane.[2,6] In the sample of allene for which a Raman spectrum was reported earlier,[5] this contamination resulted in the presence of three weak lines at the points where propene has its most intense Raman lines (920, 1296, and 1646 cm^{-1}). In subsequent preparation of allene by this method, contamination by propene was absent, as shown by the absence from the infrared spectrum of the strong propene bands at 580, 920, and 1646 cm^{-1}. Presumably this means that the 2,3-dibromopropene used in the preparation of the allene on which the infrared studies were made was of higher purity than that from which the Raman sample was prepared.

Allene-d_4 was obtained as a by-product in the preparation of methyl acetylene-d_4, with which it is isomeric. The latter was synthesized in large quantity from the tricarbide of magnesium (Mg_2C_3) by passing deuterium oxide vapor over the carbide at elevated temperatures (>150°C).[7] The presence of allene bands in the spec-

TABLE I. Equilibrium between methyl acetylene and allene.

T°K	$-\Delta(F^0-E_0^0)/T$	K_{eq}(calc)	"K_{obs}"
300	−0.78	0.040	
400	−0.86	0.078	<0.01
523	−0.93	0.123	0.01
623	−0.97	0.157	0.05
800	−1.00	0.209	
1000	−1.00	0.258	

$K_{eq}=p$(allene)$/p$(methyl acetylene)
$\Delta E_0^0=+1689$ cal (reference 10)

[6] See, for example, Kistiakowsky, Ruhoff, Smith, and Vaughn, J. Am. Chem. Soc. **58**, 146 (1936).
[7] See A. W. Baker, doctoral thesis, "The Preparation of Cyclopropane-d_6, etc.," Massachusetts Institute of Technology, Sep-

trum of methyl acetylene prepared in this way was noted, as was an increase in the relative amount of allene when the preparation was carried out at higher temperature (*ca* 350°C). Investigation of the thermodynamics of the isomerization of methyl acetylene to allene shows that increased temperature does indeed favor the conversion.

In Table I are listed the equilibrium constants for the isomerization as calculated from the thermodynamic functions for methyl acetylene[8] and allene,[1] and the heats of hydrogenation of the two compounds.[6,9] It is necessary to change the free energy values tabulated for allene in reference 1 because they were calculated with a symmetry number of 12. This value of the symmetry number is not explicitly mentioned anywhere in reference 1 but is apparent from the equation for the translational and rotational parts of the entropy as well as from the tabulated entropy values. The symmetry number for a D_{2d} structure is 4, and hence the entropy and $-(F^0-E_0^0)/T$ values need to be increased by $R\ln 3$, as was pointed out by Frank-Kamenetzki and Markovich.[10] These authors also computed the value of ΔE_0^0 from which the results of Table I were obtained.

TABLE II. Infrared data for allene vapor (300–6100 cm^{-1}).

Obs. frequency (cm^{-1} in vac.)	Band type[a]	Intensity[b]	Assignment	Calc. freq.[c]	Raman data Freq. (cm^{-1})	Raman data Est'd. int.
354	Not Res.	202	$\nu_{11}(e)$		356	3
			$2\nu_{11}$		707	2 *b*
842	Res.	326	$\nu_{10}(e)$		848	5 *b*
			$\nu_4(b_1)$		865	1
					(920)	Imp.
1015	Res.	64	$\nu_9(e)$		991	3
			$\nu_3(a_1)$		1076	10 pol
			$\nu_4+\nu_{11}(E)$	1221	1226	1
					(1296)	Imp.
			$\nu_9+\nu_{11}$	(1369)	1351	
1384 *b*	*P*					
1398 *s*	*Q*	85	$\nu_7(b_2)$		1421	2
1408 *b*	*R*					
			$\nu_2(a_1)$		1440	9 pol
					(1646)	Imp.
1675 *b*	*P*	184	$2\nu_{10}(B_2)$		1694	
1698 *b*	*R*					
1942.2 *b*	*P*					
1950.2 *s*		1000	$\nu_8+\nu_{11}-\nu_{11}$		1960	
1956.5 *s*	*Q*		$\nu_8(b_2)$			
1970 *b*	*R*					
1996.7.7		7				
2015	Part. Res.	95	$2\nu_9(B_2)$	2030		
			$2\nu_9(A_1)$?	2030	2043	0
2428.5	Res.	7	$\nu_7+\nu_9(E)$	2412		
			$\nu_2+\nu_9(E)$	2455		
2814.5 *b*	*P*					
2826.7 *s*	*Q*	12	$\nu_2+\nu_7(B_2)$	2837		
2840 *b*	*R*					
2869.5 *s*	*Q*	6	$2\nu_2(A_1)$	2880	2861	3
2884.7 *b*	*R*		$\nu_4+2\nu_9(B_2)$	2895		
2920 *b*	*P*					
2932.6 *s*	*Q*	9	$\nu_3+\nu_9+\nu_{10}(B_2)$	2933		
2955		13	$\nu_8+\nu_9(E)$	2973		
			$\nu_1(a_1)$		2996	10 pol
2995.4 *b*	*P*					
3005.4 *s*	*Q*	149	$\nu_5(b_2)$			
2018.5 *b*	*R*					
3085	Res.	50	$\nu_8(e)$		3067	8 *b*
4065	*P*					
4086	*R*	10	$\nu_8+\nu_9(B_2)$	4100		
4156	*b*	1	$\nu_3+\nu_8(E)$	4161		
4229 *b*	*P*					
4255 *b*	*R*	3	$2\nu_2+\nu_7(B)_2$	4278		
4480 *b*	Part. Res.	19	$\nu_7+\nu_8(E)$	4483		
4766 *b*		3	$\nu_8+2\nu_{10}(E)$	4769		
4988 *b*		5	$\nu_8+\nu_8(E)$	5043		
			$\nu_1+\nu_8(B_2)$	4954		
5963 *b*		30	$\nu_1+\nu_5(B_2)$	6000		
6030		1	$\nu_1+\nu_8(E)$	6080		
6141 *b*		17	$2\nu_8(B_2)$	6170		

[a] Abbreviations: *s* = sharp, *b* = broad, *n* = no distinct maximum. *P*, *Q*, and *R* refer to peaks that are *P*, *Q*, and *R* branches, respectively. "Res" means the band is a perpendicular band whose constituent sub-bands have been resolved. The wave-number value given corresponds to the band origin.

[b] The intensity of the strongest band is assumed to be 1000 and the intensities of the other bands are calculated with the assumption that the intensity is proportional to $(1/pl)\log(I_0/I)$ where p and l are pressure and path lengths and where I_0 and I are the incident and transmitted intensities, respectively. Since the width of the bands is not taken into consideration, and the dependence of peak height and slit width used and the effect of pressure broadening on peak heights are neglected, the relative intensities given are quite rough.

[c] Based on harmonic oscillator approximation.

TABLE III. Infrared data for allene-d_4 vapor (250–5000 cm^{-1}).

Obs. frequency (cm^{-1} in vac.)	Band type[a]	Intensity[b]	Assignment	Calc. freq.[c]	Raman data Freq. (cm^{-1})	Raman data Est'd. int.
306 *b*	Not Res.	413	$\nu_{11}(e)$		315	2 *b*
			?		436	0
498 *s*		59	?			
			$\nu_4(b_1)$		615	0
			$2\nu_{11}$			
667	Res.	652	$\nu_{10}(e)$		667	5 *b*
(830)	Part. Res.	128	$\nu_9(e)$		847	2
			$\nu_3(a_1)$		874	10 pol
			$3\nu_{11}$			
			$\nu_4+\nu_{11}$	920	933	3
			$\nu_{10}+\nu_{11}$	982	987	3
1021.9 *b*	*P*					
1034.2 *s*	*Q*	128	$\nu_7(b_2)$		1053	2 *b*
1046.7 *b*	*R*					
1138 *b*		413	$\nu_9+\nu_{11}$	1153	1151	
			$\nu_3+\nu_{11}(E)$	1180		
			$2\nu_4(A_1)$	1230	1203	1
			$\nu_2(a_1)$		1228	8 pol
1325.3 *b*	*P*					
1337.6 *s*	*Q*	156	$2\nu_{10}(B_2)$	1332		
1347 *b*	*R*					
1360 *n*		31	$\nu_7+\nu_{11}(E)$	1340		
1386 *b*	*P*					
1395 *b*	*R*	54	$\nu_9+2\nu_{11}(B_2)$	1417		
			?		1587	3
1905.2 *b*			$\nu_3+\nu_7(B_2)$	1908		
1912.6	*P*					
1914.8 *s*						
1917.2 *s*			$\nu_8+\nu_{11}-\nu_{11}$			
1921.1 *s*	*Q*	1000	$\nu_8(b_2)$			
1930 *b*	*R*					
2069 *b*		31	$2\nu_2+\nu_{11}(E)$	2054	2070	2 *b*
			$\nu_2+\nu_9(E)$	2058		
			$2\nu_7(A_1)$	2106	2120	3 *b*
2130 *b*	Part. Res.	38	$\nu_9+2\nu_{10}(E)$	2164	2152	3
			$\nu_1(a_1)$		2195	10 pol
2204		67	$\nu_8+\nu_{11}(E)$	2227		
2224	*P*					
2229.6	*Q*	183	$\nu_5(b_2)$			
2236.8	*R*					
2267.4		15	$\nu_2+\nu_7(B_2)$	2262		
2276.8		9	?			
2330	Res.	57	$\nu_8(e)$		2304	5 *b*
2603.77 *b*	*P*					
2614.3 *s*	*Q*	16	$\nu_8+\nu_{11}(B_2)$	2636		
2624.7 *b*	*R*					
2780 *b*	*P*					
2790.1 *s*	*Q*	42	$\nu_3+\nu_8(B_2)$	2795		
2800.0 *b*	*R*					
2870.2 *b*		139	$\nu_5+\nu_{10}(E)$	2890		
2947 *b*		31	$\nu_4+\nu_8(E)$	2945		
2981.0	*P*					
2984.9	*Q*	131	$\nu_8+\nu_{10}(B_2)$	2996		
2989.6	*R*		$\nu_1+\nu_9(E)$	3000		
3129 *b*	*P*					
3140	*Q*	45	$\nu_8+\nu_9(B_2)$	3135		
3151 *b*	*R*					
3329 *b*		11	$\nu_7+\nu_8(E)$	3364		
4360		5	$2\nu_7+\nu_8(E)$	4398		
4411 *b*	*P*					
4431 *b*	*R*	28	$\nu_1+\nu_5(B_2)$	4421		
4489 *b*		17	$\nu_1+\nu_8(E)$	4499		
4610 *b*	*P*					
4631.5 *b*	*R*	26	$2\nu_8(B_2)$	4660		

[a], [b], [c] See corresponding notes in Table II.

tember, 1950. The synthesis of methyl acetylene-d_4 will be described in some detail as a part of the publication of this thesis.

[8] B. L. Crawford, Jr., J. Chem. Phys. **8**, 526 (1940); **9**, 69 (1941).

[9] Conn, Kistiakowsky, and Smith, J. Am. Chem. Soc. **61**, 1868 (1939).

[10] D. A. Frank-Kamenetzki and V. G. Markovich, Acta Physico chim. U.R.S.S. **17**, 308 (1942).

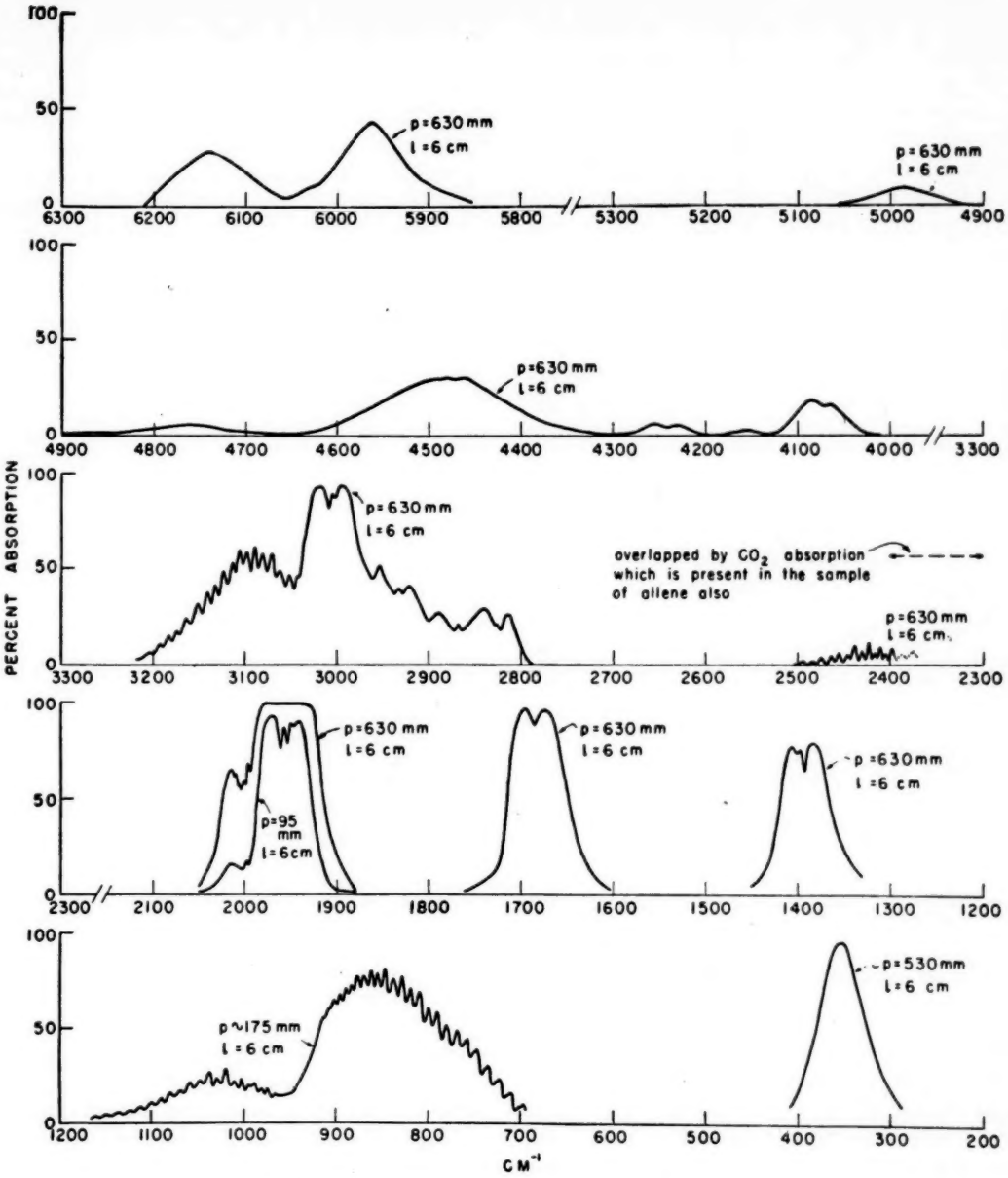
PERCENT ABSORPTION
p=630 mm l=6 cm
p=630 mm l=6 cm
p=630 mm l=6 cm
p=630 mm l=6 cm
overlapped by CO_2 absorption which is present in the sample of allene also
p=630 mm l=6 cm
p=630 mm l=6 cm
p=630 mm l=6 cm
p=630 mm l=6 cm
p=95 mm l=6cm
p~175 mm l=6 cm
p=530mm l=6 cm
CM^{-1}

FIG. 1. Infrared absorption of allene vapor, 300–6100 cm^{-1}.

In the formation of methyl acetylene and allene from Mg_2C_3, there is no assurance that the two are formed in equilibrium amounts, and the experimental evidence is indeed against this.[11] Although the calculated equilibrium at 150°C calls for roughly 10 percent allene, indications are that decidedly less than 1 percent allene is formed. As the temperature is increased, the percentage of allene goes up, the observed rate of increase being much larger than the calculated. However, it may simply be that the higher temperature facilitates isomerization and that the observed increase is attributable entirely to more rapid approach to equilibrium. At the highest temperature where measurement was made, the observed allene concentration was still smaller than calculated by a factor three. Higher temperature studies were ruled out, so far as the purposes of the present investigation were concerned, by the considerable pyrolysis observed for the hydrocarbon products.

In Table I are also given values for the observed ratio "K_{obs}" of allene to methyl acetylene produced by hydrolysis of Mg_2C_3 at the indicated temperatures. The amount of allene was determined by difference in a gas-volumetric procedure in which the methyl acetylene was removed from a fixed volume of vapor mixture by precipitation as the silver complex, and then re-

[11] See J. Ocampo, bachelor's thesis, Massachusetts Institute of Technology, September, 1950.

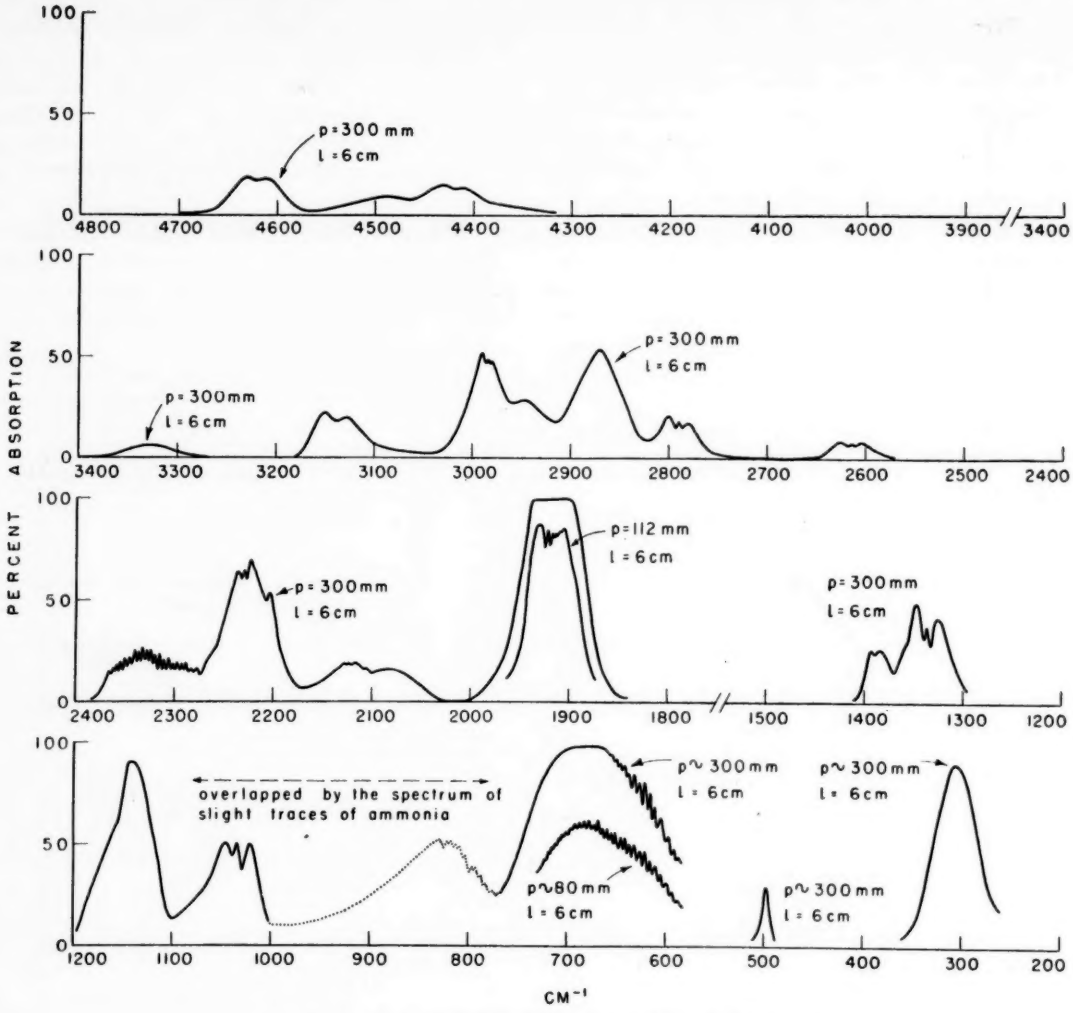

FIG. 2. Infrared absorption of allene-d_4 vapor, 250–5000 cm^{-1}.

generated and measured volumetrically. It is impossible to reconcile the temperature dependence of "K_{obs}" with that of the calculated K_{eq}. In view of the lack of evidence for equilibrium, the "K_{obs}" values merely can be taken as qualitative indication of the preferential formation of methyl acetylene.

Allene-d_4 was separated from methyl acetylene-d_4 by slowly passing a mixture of the two gases formed at 350°C from heavy water and Mg_2C_3 through an ammonical silver nitrate solution.[11] Ammonia was scrubbed from the allene-d_4 by dilute aqueous HCl and then water removed by passage through a drying train. From approximately 40 cc of liquid methyl acetylene-d_4, 2 cc of liquid allene-d_4 were recovered. The Raman spectrum of this material was taken before the ammonia was removed,[11] but the amount of ammonia present was too small to detect in the Raman effect. The infrared studies here reported were carried out after the removal of ammonia and the fact that this removal was incomplete is indicated in Fig. 2.

In the course of the synthesis of cyclopropane-d_6, propene-d_6 was prepared.[7] Comparison of the infrared spectrum of the latter with that of our sample of allene-d_4 showed no contamination of allene-d_4 by propene-d_6. The infrared spectrum also showed that the removal of methyl acetylene-d_4 was complete.

Spectroscopic Procedures

The infrared spectra of gaseous allene and allene-d_4 were recorded with a Perkin-Elmer 12B Spectrometer. This instrument was modified[12] to enable the elimination of water vapor absorption from the spectrum. Spectra were taken with prisms of LiF, CaF_2, NaCl, KBr, and TlBr-TlI ("*KRS*-5"), each prism being used in its region of optimum dispersion. Achieved resolution is very close to 3 cm^{-1} throughout the region 250–3500 cm^{-1}, and the frequency precision is seldom worse than 1 cm^{-1} except possibly above 3200 cm^{-1}. The absorption cell had a path length of 6 cm and windows of potassium iodide. Various gas pressures were used, as indicated in the figures. The spectra are shown in

[12] Lord, McDonald, and Miller, J. Opt. Soc. Am. **42**, 149 (1952).

Figs. 1 and 2, and the frequencies in cm^{-1} tabulated in Tables II and III.

The Raman frequencies, also listed in Tables II and III, are essentially those reported earlier.[5] The low temperature Raman technique and the method of determining the state of depolarization of the Raman lines were those of Lord and Nielsen.[13] Apart from the previously mentioned identification of the Raman lines at 920, 1296, and 1646 cm^{-1} as those of propene and not allene, no serious corrections are required by the results of the present paper in the data of reference 5. There are several lines reported there that have not been found earlier. These lie at 865, 991, 1351, 1421, and 2043 cm^{-1}, and failure of Linnett and Avery[1] to report them is readily understandable from the published microphotometer record of their Raman spectrum. The line at 865 is quite weak and lies rather close to the somewhat broad line at 848, while the line at 1351 is weak and unresolved from the strong 3067 line excited by Hg-4047, which was not filtered out in their work. The 1421 line is not easy to separate from the intense line at 1440, and the 2043 line is extremely weak, though comparable to the 1959 line reported both in reference 1 and 5. The 991 line requires special comment. As excited by Hg-4358, it was obscured on their microphotometer trace by the 1076 line from Hg-4339. It is strong enough, however, to have been found as excited by Hg-4047, but at the precise position on the trace where it should occur, there is a clear-cut line contour labeled, unfortunately but no doubt correctly, "scratch." This point is brought out because the 991 line is later identified as a fundamental.

Discussion of Spectra

The most probable structures for the allene molecule are of symmetry D_{2d} and D_{2h}. The former, which is favored by valence theory, is a symmetrical-top rotator and the latter, an asymmetrical-top rotator. A D_{2h} structure has a center of symmetry, while the D_{2d} structure does not. The infrared evidence is clear-cut that the allene molecule is a prolate symmetrical top, and the considerable number of coincidences between infrared and Raman frequencies rule out a symmetry center. On these general grounds, the D_{2h} structure is rejected, and, as will be shown below, the detailed features of both infrared and Raman spectra are in agreement with D_{2d} symmetry.

An allene molecule of D_{2d} symmetry has three totally symmetrical vibrations (A_1) which are Raman-active and polarized, one torsional vibration of species B_1, which is Raman-active and depolarized, three vibrations of species B_2, which is both infrared and Raman active (depolarized), and four doubly-degenerate vibrations of species E, also infrared and Raman-active (depolarized).[14] Thus all vibrations are Raman-active. The A_1 species can be recognized by its polarized lines, the B_1 species because it is inactive in the infrared, the B_2 species by its parallel infrared bands, and the E species by the perpendicular bands. There is thus a clear-cut means of assigning each observed Raman line and infrared band to its species. When this is done as indicated in Table IV, the resultant frequency values for allene and allene-d_4 satisfy the Teller-Redlich product rule[15] very well.

The fundamental assignment of Table IV is virtually identical with that of reference 1, but in view of the considerably firmer basis provided for it by improved spectroscopic techniques and the data for allene-d_4, some comment is required.

Species A_1

The assignment is definite in view of the polarization measurements on both allene and allene-d_4. The frequency values in allene-d_4, however, indicate that qualitative descriptions such as those in column 3 of Table IV are only approximate. If the 1440 frequency in allene were a pure CH_2 bending, it should shift by $1/\sqrt{2}$ in allene-d_4, or to about 1020 cm^{-1}. Actually the shift is only half this large. The symmetrical C=C=C stretching frequency at 1076, which should be expected to change only slightly in allene-d_4, moves a relatively larger amount. This means that both in allene and in allene-d_4, especially the latter, the actual vibration forms are imprecisely described by the simple labels in column 3.

Species B_1

In reference 1, the torsional frequency was placed in the neighborhood of 820 cm^{-1} from the results of heat capacity measurements, since it was not observed directly. This figure is still approximately valid in view of the unchanged frequency assignment, but receives additional support from the weak but quite definite

TABLE IV. Assignment of fundamental frequencies in allene and allene-d_4 (D_{2d} structure).

Vib'l. species	Freq. no.	Type of vibration	Frequencies in cm^{-1} Allene	Allene-d_4	Product rule τ_{obs}	τ_{calc}
A_1	1	C−H stretching	2996	2195	1.97	2.000
	2	CH_2 bending	1440	1288		
	3	C=C=C stretching	1076	874		
B_1	4	CH_2 torsion	865	615	1.407	1.414
B_2	5	C−H stretching	3005	2230	1.86	1.907
	6	C=C=C stretching	1957	1921		
	7	CH_2 bending	1398	1034		
E	8	C−H stretching	3085	2330	2.43	2.391
	9	CH_2 rocking	1015	830		
	10		842	667		
	11	C=C=C bending	354	306		

[13] R. C. Lord and E. Nielsen, J. Opt. Soc. Am. **40**, 655 (1950); J. Chem. Phys. **19**, 1 (1951).

[14] See G. Herzberg, *Infrared and Raman Spectra* (D. Van Nostrand Company, Inc., New York, 1945), p. 339; see also reference 1 and R. C. Herman and W. H. Shaffer, J. Chem. Phys. **17**, 30 (1949).

[15] See Herzberg, reference 14, p. 231 *ff*; also F. Halverson, Revs. Modern Phys. **19**, 87 (1947).

line at 865 cm^{-1} observed by Lord and Ocampo[5] in the Raman effect. The corresponding line in allene-d_4 should lie at 615 cm^{-1}, and should be weaker by $\sqrt{2}$. A very weak line is observed at this point but unfortunately can be interpreted also as the first overtone of the fundamental at 306 cm^{-1}. In any event, the combined evidence of thermal and spectroscopic data is entirely consistent with the identification of the 865 cm^{-1} line in allene with the torsional vibration.

Species B_2

The values for the B_2 frequencies in Table IV are those observed in the infrared. Corresponding lines have been observed in the Raman effect for ν_6 and ν_7 at 1960 and 1421 in allene and for ν_7 in allene-d_4. The ν_5 fundamentals are obscured in the Raman effect by ν_1, and ν_6 for allene-d_4 was not observed. The vapor-liquid shift for ν_7 is rather considerable, but the ratio of the allene:allene-d_4 values is the same in both phases. Hence the product rule agreement shown in Table IV would be unaffected by the shift. The product rule is useful in deciding between the assignment of the infrared band at 1034 and that at 1138 to ν_7 in allene-d_4.

Species E

The degenerate vibrations are readily located in the infrared by their perpendicular bands. Analysis of these bands, by means of which the vibrational frequencies are obtained, is described below. It leads to the satisfactory location shown in Table IV for the centers of all except the band of ν_9 in allene-d_4. The product rule is reasonably well satisfied for both the infrared and the Raman assignments. However, the sign and magnitude of the discrepancy observed for the Raman-effect values indicate that probably 315 cm^{-1} for ν_{11} in allene-d_4 is in error and should agree more closely with the infrared value of 306. The location of the band origin of ν_9 in allene-d_4 is difficult because of the proximity of the broad band due to ν_{10}. The trace of ammonia previously mentioned also gives some interference. However, the 830 estimate agrees reasonably well with the Raman value of 847.

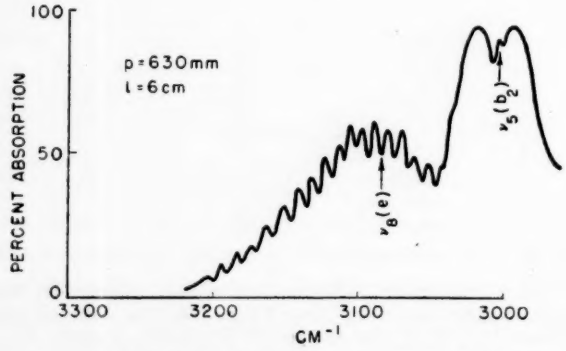

FIG. 3. Rotational structure of perpendicular band ν_8 and parallel band ν_5 in allene.

Analysis of the Rotational Structure

The infrared bands of allene and allene-d_4 are of three kinds: (1) those that show fine structure with alternation of intensity "strong, weak, strong, weak···" for the successive sub-bands. This feature is expected for the perpendicular bands of the symmetrical-top structure, and all such bands are therefore assigned as perpendicular bands; (2) those that show a weak but sharp Q branch with more intense, broad P and R branches. Such bands are of the parallel type, and under lower dispersion show only P and R branches, the weaker Q branch being usually unobservable; (3) those that show an unresolved broad envelope with maximum intensity at the center. These bands are of the perpendicular type, but their constituent sub-bands are too closely spaced for resolution with our instrumental setup.

Parallel Bands

The fine structure of the parallel bands is determined by the large (double) moment of inertia and cannot be resolved with our instrument. However, from a study of the structure of the parallel band $3\nu_5$ in the photographic infrared, Eyster[4] obtained a set of values for the quantities[16] $\Delta_2F''(J)/2(2J+1)$ that had an average value 0.2847 cm^{-1}, which is therefore the value of the rotational constant B'' for allene. From this, $I_B=98.3\times10^{-40}$ g cm^2. If one uses an estimated value of 120° for the HCH angle and 1.071A for the C−H distance (the value in ethylene), one finds the C=C distance as 1.344A. From these approximate values, rough working values of I_B and B for allene-d_4 of 125×10^{-40} g cm^2 and 0.22 cm^{-1}, respectively, are obtained. It will be seen later that these estimates agree closely with the values obtained using a bond angle of 113° determined from the perpendicular-band analysis.

The moment of inertia about the figure axis is similarly estimated to be roughly 5.7×10^{-40} g cm^2, with the result that I_A/I_B is 0.06. So small a ratio means that the integrated intensity of the Q branch is of the order of one-fifth that of the P or R branch.[17] Hence rather good resolution on the part of the prism spectrometer is required to separate the weak Q branch from the P and R components of the parallel bands.

Perpendicular Bands

As was first shown by Teller,[17] the rotational structure of degenerate (i.e., perpendicular) vibrational bands in the infrared is complicated by the existence of angular momentum of vibration. Interaction of this angular momentum with that of molecular rotation about the figure axis introduces a linear term into the rotational energy which contains the interaction constant ζ, the rotational quantum number K, and the

[16] See Herzberg, reference 14, p. 434.

[17] E. Teller, Hand- und Jahrbuch der chem. Physik, **9II**, 28 (1934). See also reference 14, p. 421.

TABLE V. Wave numbers of the sub-bands in $\nu_9(e)$ of allene at 3085 cm^{-1}.

Assignment	ν_{vac} in cm^{-1}	I	$^RQ_K - {}^PQ_K$	$\Delta\nu$	$\frac{^RQ_K - {}^PQ_K}{2K}$	Assignment	ν_{vac} in cm^{-1}	I	$^RQ_K - {}^PQ_K$	$\Delta\nu$	$\frac{^RQ_K - {}^PQ_K}{2K}$
$^RQ_{11}$	3194.2					$^RQ_2$	3107.0	s	36.5	8.7	9.13
$^RQ_{10}$	3184.0			10.2		$^RQ_1$	3098.5	w	18.2	8.5	9.10
$^RQ_9$	3174.7			9.3		$^RQ_0$	3089.5	s		9.0	
$^RQ_8$	3164.2			10.5		$^PQ_1$	3080.3	w		9.2	
$^RQ_7$	3152.0			12.2		$^PQ_2$	3070.5	s		9.8	
$^RQ_6$	3142.5	s	105.9	9.5	8.83	$^PQ_3$	3062.2	w		8.3	
$^RQ_5$	3133.6	w	89.8	8.9	8.98	$^PQ_4$	3052.8	s		9.4	
$^RQ_4$	3124.6	s	71.8	9.0	8.98	$^PQ_5$	3043.8	w		9.0	
$^RQ_3$	3115.7	w	53.5	8.9	8.92	$^PQ_6$	3036.6			7.2	

rotational constant A. ζ can lie between -1 and $+1$ for the first vibrational state. A zero value for ζ means that there is no vibrational angular momentum, and hence that the vibrating electric dipole moment rotates about the symmetry axis at the same rate as the molecule itself. The minus sign corresponds to a speeding-up of the rotation of the vibrating moment about the symmetry axis, and hence to an increase in the rotational spacing in the spectrum. A plus sign gives a retardation of the rotation of the vibrating moment, and a decrease in the rotational spacing.

As a result of this interaction, the equation for the Q branches of the constituent sub-bands of a perpendicular band ($\Delta J=0$, $\Delta K=\pm 1$) takes the form:[18]

$$\nu=\nu_0+[A_v'(1-2\zeta_i)-B_v']\pm 2[A_v'(1-\zeta_i)-B_v']K + [(A_v'-B_v')-(A_v''-B_v'')]K^2, \quad (1)$$

where as usual A and B are the rotational constants for I_A and I_B, $'$ and $''$ refer to the upper and lower vibrational states of the band, and v is the vibrational quantum number for each state. The subscript i designates which doubly-degenerate vibration is concerned, since of course the ζ-values differ for different vibrations. In Eq. (1), the $\pm$ sign indicates the two branches of sub-bands, the $+$ sign giving the R branch ($\Delta K=+1$) and the minus sign the P branch ($\Delta K=-1$).

The form of a perpendicular band given by Eq. (1) and the appropriate Boltzmann factors is that of a broad spread of Q branches with no clear-cut maximum to the band as a whole (see Fig. 4). Hence the numbering of the different Q branches [i.e., assignment of the correct K values of Eq. (1)] and the corresponding location of ν_0 are not immediately obvious. Considerable assistance is offered, however, if there is an alternation of intensity in the Q branches.

Alternation of intensity results from alternation in the statistical weights of the rotational energy levels, which in turn results from molecular symmetry and nuclear spin. Wilson[19] has discussed the group-theoretical procedures for evaluation of statistical weights, and has applied the procedure to various molecules, none, however, of D_{2d} symmetry. By straightforward application of his methods to the D_{2d} model of allene[20] and allene-d_4, for both of which the rotational subgroup is D_2, it can be shown that, apart from the Boltzmann factor, the intensity alternation 10:6 should be observed for sub-bands of even:odd K in allene and 45:36 in allene-d_4.

This alternation is of great help in assigning numbers to the constituent sub-bands and the determination of the band centers. The sub-band with the strongest Q branch is the first in the R branch side (i.e., $^RQ_0$), and the first weak Q branch on the low frequency side of $^RQ_0$ is the first in the P branch ($^PQ_1$). The band center lies between $^RQ_0$ and $^PQ_1$, and the frequencies listed on Tables II-IV for infrared-active vibrations have been determined in this way for all resolved perpendicular bands. As indicated above, the bands at 354 in allene and 306 cm^{-1} in allene-d_4 are not resolved, and hence their centers have been determined from the band maxima, which are to be taken to be the band centers.

The best way to obtain the coefficient of K in Eq. (1) is to plot $^RQ_K - {}^PQ_K$ against K. This plot is a straight line of slope $4[A_v'(1-\zeta_i)-B_v']$. Another method is to average the quantity $(^RQ_K - {}^PQ_K)/2K$. The practical way to obtain the coefficient of K^2 is to plot $^RQ_K + {}^PQ_K$ against K^2. This plot should be a

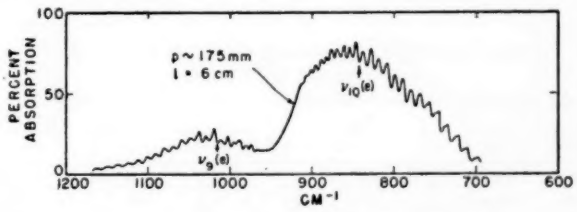

FIG. 4. Rotational structure of perpendicular bands ν_9 and ν_{10} in allene.

[18] See reference 14, p. 429 and Eq. IV, 60.

[19] E. B. Wilson, Jr., J. Chem. Phys. **3**, 276 (1935).

[20] After the present work was completed, the authors learned that Dr. J. de Heer [J. Chem. Phys. **20**, 637 (1952)] had also worked out the statistical weights as well as an equation corresponding to Eq. (5) below. As de Heer points out, there is a difference in appearance of Eq. (5) if one uses the convention $K=K'$ rather than the convention of Herzberg, $K=K''$, as is done here. After correction for this, the two equations are in agreement. However, there are differences in the exact locations of the band centers and in the ζ values. The additional information provided by the allene-d_4 spectrum and the ζ sum rule accounts for these differences. The authors are much indebted to Dr. de Heer for the privilege of seeing his manuscript before it appeared in print.

TABLE VI. Wave numbers of the sub-bands of $\nu_9(e)$ in allene at 1015 cm^{-1}.

Assignment	ν_{vac} in cm^{-1}	I	^RQ_K $-^PQ_K$	$\Delta\nu$	Assignment	ν_{vac} in cm^{-1}	I	$-^RQ_K$ $-^PQ_K$	$\Delta\nu$
$^RQ_{13}$	1161.7	w			$^RQ_2$	1037.8	s	35.1	10.3
$^RQ_{12}$	1149.6	s		12.1	$^RQ_1$	1028.3	w	17.6	9.5
$^RQ_{11}$	1136.9	w		12.7	$^RQ_0$	1019.2	s		9.1
$^RQ_{10}$	1124.2	s		12.7	$^PQ_1$	1010.7	w		8.5
$^RQ_9$	1112.6	w		11.6	$^PQ_2$	1002.7	s		8.0
$^RQ_8$	1101.2	s	140.2	11.4	$^PQ_3$	994.7	w		8.0
$^RQ_7$	1090.4	w	122.7	10.8	$^PQ_4$	987.6	s		7.1
$^RQ_6$	1079.9	s	105.4	10.5	$^PQ_5$	981.0	w		6.6
$^RQ_5$	1069.5	w	88.5	10.4	$^PQ_6$	974.5	s		6.5
$^RQ_4$	1059.2	s	71.6	10.3	$^PQ_7$	967.7			6.8
$^RQ_3$	1048.1	w	53.4	11.1	$^PQ_8$	961.0			6.7

straight line whose slope is $2[(A_v'-B_v')-(A_v''-B_v'')]$.

The wave numbers and the assignment of the sub-bands of the perpendicular band ν_8 at 3085 cm^{-1} are given in Table V and the band is shown in Fig. 3. It will be seen that the spacing is somewhat irregular, for reasons not clear at present. This feature was also pointed out by Miller and Thompson.[3] Nevertheless, the sub-bands can be presented approximately by the formula

$$\nu=3089.0\pm9.0K+0.03K^2. \quad (2)$$

It follows from Eqs. (1) and (2) that

$$2[A_v'(1-\zeta_8)-B_v']=9.0. \quad (3)$$

The case of the bands for ν_9 and ν_{10} at 1015 and 842 cm^{-1}, shown in Fig. 4, is more complicated. Here there is a Coriolis interaction, first described by Nielsen,[21] between the two fundamentals, in addition to that interaction between the degenerate components of each vibration which leads to Eq. (1). If the individual degeneracy of ν_9 and ν_{10} is neglected, the sub-bands of ν_9 and ν_{10} can be represented by

$$\nu=(\nu_9+\nu_{10})/2+(A-B)\pm2(A-B)K \pm\tfrac{1}{2}\{(\nu_9-\nu_{10})^2+4(K\pm1)^2\zeta^2_{9,10}A^2[(\nu_9/\nu_{10})^{\frac{1}{2}} +(\nu_{10}/\nu_9)^{\frac{1}{2}}]^2\}^{\frac{1}{2}}. \quad (4)$$

TABLE VII. Wave numbers of the sub-bands of $\nu_{10}(e)$ in allene at 842.2 cm^{-1}.

Assignment	ν_{vac} in cm^{-1}	I	^RQ_K $-^PQ_K$	$\Delta\nu$	Assignment	ν_{vac} in cm^{-1}	I	$\Delta\nu$
$^RQ_{10}$	913.0	s	167.0		$^PQ_4$	809.5	s	9.9
$^RQ_9$	908.0	w	151.2	5.0	$^PQ_5$	799.7	w	9.8
$^RQ_8$	902.3	s	134.2	5.7	$^PQ_6$	789.3		10.5
$^RQ_7$	896.4	w	117.1	5.9	$^PQ_7$	779.3		10.0
$^RQ_6$	889.8	s	100.5	6.6	$^PQ_8$	768.1		11.2
$^RQ_5$	883.4	w	83.7	6.4	$^PQ_9$	756.8		11.3
$^RQ_4$	876.9	s	67.4	6.5	$^PQ_{10}$	745.9		10.9
$^RQ_3$	869.5	w	50.1	7.4	$^PQ_{11}$	734.3		11.6
$^PQ_2$	862.1	s	33.9	7.4	$^PQ_{12}$	722.2		12.1
$^RQ_1$	854.7	w	16.9	7.4	$^PQ_{13}$	710.8		11.4
$^RQ_0$	846.5	s		8.2	$^PQ_{14}$	699.3		11.5
$^PQ_1$	837.8	w		8.7	$^PQ_{15}$			
$^PQ_2$	828.3	s		9.5	$^PQ_{16}$			
$^PQ_3$	819.4	w		8.9				

[21] H. H. Nielsen, J. Opt. Soc. Am. 34, 521 (1944).

Here $\zeta_{9,10}$ is the constant for the interaction of ν_9 and ν_{10}. The positive sign before the coefficient of the term corresponds to the R branches and the negative sign to the P branches. The positive sign before the final term corresponds to the sub-bands for ν_9, and the negative, to those for ν_{10}. The factor $(K+1)^2$ in the final term goes with the R branches and $(K-1)^2$ with the P branches. As it was in Eq. (1), the parameter K is K'', that is, the value of K in the lower vibrational state. If K is set equal to K', its value in the upper vibrational state, Eq. (4) is changed by replacement of the first positive sign with a negative one, and the $(K\pm1)^2$ term by K^2. It then is identical, apart from symbolism, with Eq. (11) of reference 21. The subscripts and superscripts on A and B have disappeared because the effect of the vibrational state on A and B has been assumed negligibly small.

Nielsen[21] first suggested that the unusual fine structure observed for the 842 and 1015 cm^{-1} bands in allene by Thompson and Harris[2] could be accounted for on the basis of Eq. (4), and Miller and Thompson[3] applied the suggestion to their later and much improved spectra of these bands. However, Eq. (4) does not apply as it stands because each of the vibrations concerned is doubly degenerate. If one takes the Coriolis interaction due to the degeneracy into account, one obtains, instead of Eq. (4),

$$\nu=(\nu_9+\nu_{10})/2+(A-B)-A(\zeta_9+\zeta_{10}) \pm2[(1-\{\zeta_9+\zeta_{10}\}/2)A-B]K\pm1/2[\{\nu_9-\nu_{10} \mp2A(K\pm1)(\zeta_9-\zeta_{10})\}^2+4\zeta^2_{9,10}(K\pm1)^2A^2 \times\{(\nu_9/\nu_{10})^{\frac{1}{2}}+(\nu_{10}/\nu_9)^{\frac{1}{2}}\}^2]^{\frac{1}{2}}. \quad (5)$$

Here ζ_9 and ζ_{10} are the interaction constants for ν_9 and ν_{10}, the first $\pm$ sign gives the P branches $(-)$ and R branches $(+)$, the second $\pm$ sign gives the bands for ν_9 $(+)$ and ν_{10} $(-)$, and the $\pm$ and $\mp$ signs within the square brackets enclosing the last term go with the P branches (lower sign) and R branches (upper sign).[22]

[22] The derivation of Eq. (5) is as follows: Eq. (9) of reference 21, corrected for obvious typographical errors and translated into the notation of the present paper, gives, for $E(\pm)/hc$, the interacting rotational-vibrational levels of ν_9 and ν_{10} in cm^{-1}, the expression

$$E(\pm)/hc=\tfrac{1}{2}\{[E_{1,0}/hc+E_{0,1}/hc]\pm([E_{1,0}/hc-E_{0,1}/hc]^2 +4\zeta^2_{9,10}K'^2A^2[(\nu_9/\nu_{10})^{\frac{1}{2}}+(\nu_{10}/\nu_9)^{\frac{1}{2}}]^2)^{\frac{1}{2}}\}, \quad (a)$$

where $E_{1,0}/hc$ and $E_{0,1}/hc$ are the unperturbed energy terms for the first excited vibrational levels of ν_9 and ν_{10}, K' is the rotational quantum number, and zero-point energy is omitted. If the double degeneracy of ν_9 and ν_{10} is taken into consideration, the unperturbed energy terms can be represented by

$$E_{1,0}/hc=\nu_9+BJ(J+1)+(A-B)K'^2-2AK'\zeta_9 l \quad (b)$$

and

$$E_{0,1}/hc=\nu_{10}+BJ(J+1)+(A-B)K'^2-2AK'\zeta_{10} l. \quad (c)$$

The quantum number l has only the values ±1, depending on whether the vibrational angular momentum $\zeta h/2\pi$ is parallel or antiparallel to the rotational angular momentum. Teller[17] has shown that in perpendicular transitions where the upper level is degenerate, only $+l$ levels combine with the lower (ground) levels for $\Delta K=+1$, and only $-l$ levels for $\Delta K=-1$. The levels

From Eq. (5) it can be seen that for the band due to ν_9, the $\Delta\nu$ between the individual sub-bands of the R branch increases as K increases, but decreases as K increases for the sub-bands of the P branch. The reverse is true of ν_{10}. The constant in Eq. (5)

$$[(\nu_9+\nu_{10})/2+(A-B)-A(\zeta_9+\zeta_{10})]$$

(denoted C below) is given by the average value of the combinations

$$[{}^RQ_K(\nu_9)+{}^RQ_K(\nu_{10})+{}^PQ_K(\nu_9)+{}^PQ_K(\nu_{10})]/4$$

for different K's. This value is 933.2 cm^{-1}. The following relations also can be seen to hold:

$$[{}^RQ_K(\nu_9)+{}^RQ_K(\nu_{10})] = 2C+4[A(1-\{\zeta_9+\zeta_{10}\}/2)-B], \quad (6a)$$

and

$$[{}^PQ_K(\nu_9)+{}^PQ_K(\nu_{10})] = 2C-4[A(1-\{\zeta_9+\zeta_{10}\}/2)-B]. \quad (6b)$$

The slope of the straight lines which we get by plotting the left-hand sides of Eqs. (6) *versus* K will thus give

TABLE VIII. Wave numbers of the sub-bands in $\nu_8(e)$ of allene-d_4 at 2330 cm^{-1}.

Assignment	ν_{vac} in cm^{-1}	I	$\Delta\nu$	$\frac{{}^RQ_K-{}^PQ_K}{2K}$	Assignment	ν_{vac} in cm^{-1}	I	$\Delta\nu$
${}^RQ_8$	2365.7	s	3.6	4.31	${}^PQ_3$	2319.5	w	4.2
${}^RQ_7$	2362.1	w	3.6	4.37	${}^PQ_4$	2314.8	s	4.7
${}^RQ_6$	2358.1	s	4.0	4.37	${}^PQ_5$	2310.2	w	4.6
${}^RQ_5$	2353.9	w	4.2	4.37	${}^PQ_6$	2305.6	s	4.6
${}^RQ_4$	2349.4	s	4.5	4.33	${}^PQ_7$	2300.9	w	4.6
${}^RQ_3$	2345.0	w	4.4	4.25	${}^PQ_8$	2296.7	s	4.2
${}^RQ_2$	2340.9	s	4.1	4.3	${}^PQ_9$	2292.2	w	4.5
${}^RQ_1$	2336.3	w	4.6	4.15	${}^PQ_{10}$	2288.0	s	4.2
${}^RQ_0$	2332.1	s	4.2		${}^PQ_{11}$	2283.5	w	4.5
${}^PQ_1$	2328.0	w	4.1					
${}^PQ_2$	2323.7	s	4.3					

the coefficient of K in Eq. (5), apart from a factor two. From the lines given in Tables VI and VII, this procedure gives

$$2[A(1-\{\zeta_9+\zeta_{10}\}/2)-B]=8.55. \quad (7)$$

Finally, from analogous combination relations and the above results, there follows the numerical formula

$$\nu=933.2\pm8.55K\pm\tfrac{1}{2}[\{172.8\mp0.4(K\pm1)\}^2 +135(K\pm1)^2]^{\frac{1}{2}}. \quad (8)$$

Equation (8) represents well the sub-bands of ν_9 and

of the ground term $E_{0,0}$ are given by

$$E_{0,0}/hc=BJ(J+1)+(A-B)K''^2. \quad (d)$$

When Eqs. (b) and (c) are substituted in Eq. (a) the correct set of levels for the interacting degenerate vibrations is obtained. The frequencies for allowed transitions from the ground levels (d) to this set of levels are then given by Eq. (5).

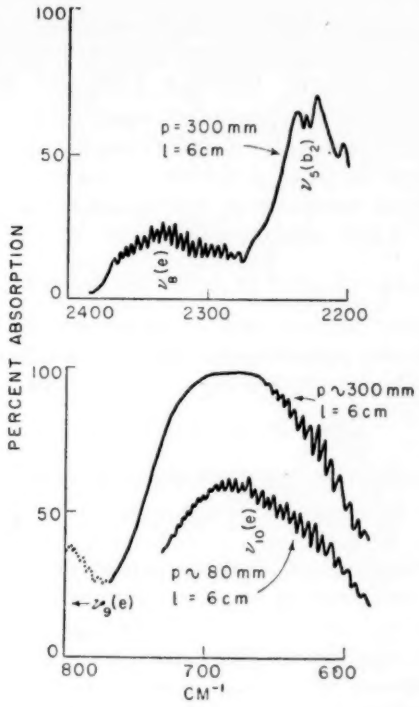

FIG. 5. Rotational structure of bands in allene-d_4. Upper: Perpendicular ν_8 and parallel ν_5. Lower: Perpendicular ν_{10}.

ν_{10}. A comparison of Eqs. (5) and (8) shows

$$2A(\zeta_9-\zeta_{10})=0.4 \quad (9)$$

$$4A^2\zeta_{9,10}^2[(\nu_9/\nu_{10})^{\frac{1}{2}}+(\nu_{10}/\nu_9)^{\frac{1}{2}}]^2=135, \quad (10)$$

$$2A\zeta_{9,10}=5.78. \quad (11)$$

It can also be seen from Eqs. (5) and (8) that when K is very large (i.e., when $\{172.8\mp0.4(K\pm1)\}^2\ll135(K\pm1)^2$), $\Delta\nu$ approaches limiting values in both the P and R branches of ν_9 and ν_{10}. The limiting value for the R branch of ν_9 and the P branch of ν_{10} is $2[A(1-\{\zeta_9+\zeta_{10}\}/2)-B]+2A\zeta_{9,10}$. The same expression with the

TABLE IX. Wave numbers of the sub-bands in $\nu_{10}(e)$ of allene-d_4 at 667 cm^{-1}

Assignment	ν_{vac} in cm^{-1}	I	$\Delta\nu$	Assignment	ν_{vac} in cm^{-1}	I	$\Delta\nu$
${}^RQ_{14}$	726.8			${}^PQ_1$	664.1	w	4.9
${}^RQ_{13}$	723.3		3.5	${}^PQ_2$	659.4	s	4.7
${}^RQ_{12}$	719.8		3.5	${}^PQ_3$	654.9	w	4.5
${}^RQ_{11}$	716.3		3.5	${}^PQ_4$	650.7	s	4.2
${}^RQ_{10}$	712.7		3.6	${}^PQ_5$	645.5	w	5.2
${}^RQ_9$	709.0		3.7	${}^PQ_6$	640.7	s	4.8
${}^RQ_8$	705.3		3.7	${}^PQ_7$	635.8	w	4.9
${}^RQ_7$	701.1		4.2	${}^PQ_8$	630.6	s	5.2
${}^RQ_6$	697.0	s	4.1	${}^PQ_9$	625.6	w	5.0
${}^RQ_5$	692.6	w	4.4	${}^PQ_{10}$	620.4	s	5.2
${}^RQ_4$	688.1	s	4.5	${}^PQ_{11}$	615.1		5.3
${}^RQ_3$	683.3	w	4.8	${}^PQ_{12}$	609.6		5.5
${}^RQ_2$	678.4	s	4.9	${}^PQ_{13}$	604.0		5.6
${}^RQ_1$	673.7	w	4.7	${}^PQ_{14}$	597.5		6.5
${}^RQ_0$	669.0	s	4.7	${}^PQ_{15}$	592.2		5.3
				${}^PQ_{16}$	586.6		5.6

last sign negative holds for the P branch of ν_9 and the R branch of ν_{10}. From Eqs. (8) and (11) these values of $\Delta\nu$ are, respectively, 14.3 and 2.77 cm^{-1}. However, they would only be approached experimentally if sub-bands were observed for K values beyond about 35.

The band due to ν_{11} at 354 cm^{-1} is not resolved. Since the achieved resolution of the instrument is 3.5 cm^{-1} or better in this region, we may write

$$2[A(1-\zeta_{11})-B]=\Delta\nu_{11} \quad (0<\Delta\nu_{11}<3.5). \tag{12}$$

The wave numbers and the assignment of the sub-bands of the perpendicular band ν_8 of allene-d_4 are given in Table VIII (see Fig. 5). For this band

$$2[A^*(1-\zeta_8^*)-B^*]=4.35, \tag{13}$$

and the sub-bands can be represented by the equation

$$\nu=2332.1\pm4.35K. \tag{14}$$

The asterisks denote the deuterium compound.

The wave numbers and the assignment of the sub-bands of ν_{10}^* at 667 cm^{-1} in allene-d_4 are given in Table IX (see Fig. 5). One can expect a mutual interaction between ν_9^* and ν_{10}^* in allene-d_4 similar to that of allene. The band ν_9^* at 830 cm^{-1} in allene-d_4 is weak and only partially resolved. Further, it is overlapped to some extent by the spectrum of ammonia which is present as a minor impurity. However, as for ν_{10} in allene, the $\Delta\nu$ of the sub-bands of ν_{10}^* in allene-d_4 appears to be approaching "asymptotic" values in both the P branch and R branch at sufficiently large K values. If this is taken as evidence of interaction between ν_9^* and ν_{10}^* in allene-d_4, then Eq. (5) can be applied to the sub-bands of ν_{10}^*.

As the sub-bands of ν_9^* could not be measured well, the constants in Eq. (5) cannot be obtained very accurately. However, the sub-bands of ν_{10}^* (Table IX) can be fairly well represented by the equation

$$\nu_{10}^*=750.7\pm4.6\pm\tfrac{1}{2}[\{163.0\mp0.2(K\pm1)\}^2 +20(K\pm1)^2]^{\frac{1}{2}}. \tag{15}$$

Equation (15) implies that $\nu_9^*=830$ cm^{-1}, $\nu_{10}^*=667$ cm^{-1}, and

$$2[A^*(1-\{\zeta_9^*+\zeta_{10}^*\}/2)-B^*]=4\ ?, \tag{16}$$

$$2A^*(\zeta_9^*-\zeta_{10}^*)=0.2, \tag{17}$$

TABLE X. Rotational constants and related quantities for allene and allene-d_4.

Quantity	Allene	Allene-d_4
A	5.28 cm^{-1}	2.64 cm^{-1}
B	0.285 cm^{-1}	0.224 cm^{-1}
ζ_8	0.09	0.09
ζ_9	0.16	0.07
ζ_{10}	0.12	0.03
ζ_{11}	0.66	0.86
$\zeta_{9,10}$	0.55	0.42
$\angle$HCH	113°	(Assuming r(C–H)
r(C=C)	1.335A	=1.071A)

and

$$\{2\zeta_{9,10}^*A^*[(\nu_9/\nu_{10})^{\frac{1}{2}}+(\nu_{10}/\nu_9)^{\frac{1}{2}}]\}^2=20. \tag{18}$$

The band for ν_{11}^* at 306 cm^{-1} was not resolved. Therefore, as before,

$$2[A^*(1-\zeta_{11}^*)-B^*]=\Delta\nu_{11}^* \quad (0<\Delta\nu_{11}^*<3.5). \tag{19}$$

Determination of A and the ζ-Values

Use of the foregoing numerical relations among the rotational spacings to determine the constant A and the ζ-values can be made with the help of the ζ-sum rule of Teller.[17] As Teller and also Dennison[23] have pointed out, the ζ-sum for the vibrations of a given symmetry species in a molecule is independent of the nature of the molecular potential system provided it is harmonic. Hence the ζ-sum can be determined by assuming special force fields for the molecule (Dennison's "limiting force fields," for example) that yield individual ζ-values easily, and then summing.

By application of the limiting-force-field type of reasoning to the D_{2d} model for allene,[24] it can be shown that

$$\sum_i\zeta_i=1+B/2A, \tag{20}$$

where the sum is taken over the four vibrations of species E. From Eq. (20) and the various equations relating the ζ-values and the rotational constants A and B to the fine-structure spacings $\Delta\nu_i$, simple addition leads to the results

$$6A-9B=26.1+\Delta\nu_{11}, \tag{21a}$$

$$6A^*-9B^*=13.55+\Delta\nu_{11}^*. \tag{21b}$$

The asterisk denotes allene-d_4, and the symbols $\Delta\nu_{11}$ and $\Delta\nu_{11}^*$ appear on the right-hand side because, as was stated above, these quantities could not be measured experimentally with the prism instrument. Since $A=2A^*$, B has been evaluated[4] as 0.285 cm^{-1}, and B^* can be reasonably estimated as 0.22 cm^{-1}, it follows that

$$\Delta\nu_{11}-2\Delta\nu_{11}^*=2.4 \text{ cm}^{-1}. \tag{22}$$

The error in Eq. (22) is hard to estimate, but is probably not larger than 0.5 cm^{-1}. From the achieved resolution of the prism instrument on the water-vapor bands near 350 cm^{-1} it can safely be concluded that $\Delta\nu_{11}$ experimentally is smaller than 3.5 cm^{-1}. Therefore, from Eq. (22), $\Delta\nu_{11}=3.0\pm0.6$ and $\Delta\nu_{11}^*=0.3\pm0.3$ cm^{-1}. From this value of $\Delta\nu_{11}$ and the value of B,

[23] See, for example D. M. Dennison and M. Johnston, Phys. Rev. 47, 93 (1935); 48, 868 (1935).

[24] It has not been plainly stated heretofore, so far as the writers can find, that the ζ-sums need not be computed on an *ad hoc* basis for each molecule by the limiting-force-field method, but can be determined as readily on general grounds as can the number of vibrations of a given symmetry species. Tables for determination of the latter quantities (such as Tables 34–36 of reference 14) have been in the literature for some time. The preparation of analogous tables for the ζ-sums of axially symmetrical molecules is entirely feasible.

TABLE XI. Wave numbers of resolved sub-bands of the combination band in allene at 2420.9 cm^{-1}.

Assignment	ν_{vac} in cm^{-1}	Int.	$\Delta\nu$	$^RQ_K - {}^PQ_K$	$\frac{(^RQ_K - {}^PQ_K)}{2K}$	Assignment	ν_{vac} in cm^{-1}	Int.	$\Delta\nu$
$^RQ_8$	(2495.0)			120.4	7.5	$^PQ_2$	2410.9	s	6.5
$^RQ_7$	(2484.4)		10.6	104.8	7.5	$^PQ_3$	2404.8	w	6.1
$^RQ_6$	2474.9	s	9.6	88.9	7.4	$^PQ_4$	2398.2	s	6.6
$^RQ_5$	2465.6	w	9.3	...			...		
$^RQ_4$	2456.1	s	9.5	57.9	7.4	$^PQ_6$	2386.0[a]	s	2×6.1
$^RQ_3$	2447.0	w	9.1	42.2	7.0	$^PQ_7$	2379.6[a]		6.4
$^RQ_2$	2439.3	s	7.7	28.4	7.1	$^PQ_8$	2375.3[a]		4.3
$^RQ_1$	2431.3	w	8.0	13.9	7.0				
$^RQ_0$	2424.3	s	7.0						
$^PQ_1$	2417.4	w	6.9						

[a] Beginning with $^PQ_6$, the sub-bands are overlapped by CO_2-absorption (present in the sample). There appear to be several more sub-bands below 2375 cm^{-1}.

A is found to be 5.28±0.1 cm^{-1}, whence $A^*=2.64$ ±0.05. If these values of A and A^* are now substituted back into Eqs. (7)–(13), (16)–(19) for the $\Delta\nu_i$, along with B and B^*, the ζ-values listed in Table X are obtained.

Most of the overtone and combination bands can be satisfactorily assigned, as shown in Tables II and III. Some of these have been resolved and, in conjunction with the constants A and B, can also yield information about the ζ-values. In Table XI are listed the wave numbers of the sub-bands of the perpendicular band at 2420.9 cm^{-1}, which is well resolved. They can be represented by the formula

$$\nu = 2424.3 \pm 7.3K \pm 0.17K^2. \quad (23)$$

This band could be $\nu_7+\nu_9(E)$ or $\nu_2+\nu_9(E)$. In either event, $\Delta\nu$ and ζ would be the same as for the fundamental band of ν_9 apart from anharmonicity and the dependence of A and B on the vibrational state. Equation (23) gives $\zeta_9=0.26$, whereas from the fundamental it is 0.16. Most of the discrepancy has to be ascribed to a combination of experimental error and anharmonicity, because the difference between A' and A'', as shown by the coefficient of K^2 in Eq. (23), is too small and in the wrong direction to explain it. Another possibility is that the band is $3\nu_{10}(E)$. In this case the ζ-value is not necessarily the same as that of the fundamental (ζ_{10} =0.12), but the anharmonicity would have to be rather large. $2\nu_{10}(B_2)$ is found with considerable intensity in both allene and allene-d_4, and $3\nu_{10}$ in the latter would probably be obscured by ν_6.

The combination band $2\nu_{10}+\nu_{11}(E)$ at 2015 cm^{-1} in allene is partially resolved. The spacing is irregular and the average $\Delta\nu$ is 3.4 cm^{-1}. This value is consistent with that estimated from the sum rule and other relations to be 3.0±0.6 cm^{-1} for $\Delta\nu_{11}$.

The equilibrium value of A in allene depends on two parameters, the C−H distance and the HCH angle, and since neither of these changes in allene-d_4, of course A^*, as indicated above, is the same as A except for the factor two from the D:H mass ratio. Hence to find either parameter from A, the other must be known. The safest procedure appears to be to assume the value of the C−H distance to be the same as that in ethylene, since small changes in the C−H distance are accompanied by large changes in the C−H stretching frequency, and in ethylene and allene the C−H frequencies are very nearly the same. If r(C−H) is assumed equal to 1.071A, the HCH angle is found to be 113°±1° from $A=5.28\pm0.1$ cm^{-1}. From this angle and the B value, r(C=C) is 1.335A. Finally I_B and B for allene-d_4 turn out to be 124.9×10^{-40} g cm^2 and 0.224 cm^{-1}, respectively, in good consistency with the rough working values used for these constants.

It is perhaps worth noting that the large number of ζ-values (six independent values, in principle) and vibrational frequencies of the E species would be more than enough for a calculation of the complete set of potential constants, ten in all, for this species. The ζ's are not too accurately known, however, from the present work, and hence the constants would perhaps suffer somewhat in accuracy also. A similar calculation for ethane using the frequencies and ζ-values from ethane and ethane-d_6 has recently been made by Hansen and Dennison.[24]

ACKNOWLEDGMENT

The authors wish to acknowledge the support of the Office of Ordnance Research (Contract DA-19-020-ORD-896, Project TB5-0002 (5)), under whose auspices the present work was completed. Heavy water was obtained by allocation from the AEC, whose cooperation is gratefully acknowledged.

[24] G. E. Hansen and D. M. Dennison, J. Chem. Phys. **20**, 313 (1952).

Spectroscopic Studies in the Near Ultraviolet of the Three Isomeric Dimethylbenzene Vapors.* II. Absorption Spectra of Meta and Ortho Dimethylbenzene†

C. D. COOPER‡ AND H. SPONER
Department of Physics, Duke University, Durham, North Carolina

(Received March 24, 1952)

The vapor absorption spectra of meta- and ortho-xylene were obtained with a 3-meter grating spectrograph. The *m*-xylene spectrum has the least number of bands and the most diffuse appearance. Its 0, 0 band is located at 36955 cm^{-1}. The *o*-xylene spectrum consists of many very sharp bands, several of which must be assigned to $v-v$ transitions. Its 0, 0 band is found at 37308 cm^{-1}. Vibrational frequencies of 965, 675 and 470 cm^{-1} are found in the upper level of the meta-spectrum and are correlated with the ground-state frequencies of 995, 725, and 510 cm^{-1}. In the ortho spectrum ground-state vibrational frequencies of 1233, 1054, and 736 cm^{-1} are correlated with the excited state values 1195, 939, and 692 cm^{-1}, respectively. Assignments of the different frequencies are discussed. The Tesla luminescence spectrum of meta-xylene is interpreted along with the absorption spectrum.

INTRODUCTION

THE first paper of this series[1] called I in this paper dealt with the absorption and fluorescence spectra of para-xylene vapor. In the present paper, experimental data pertaining to the vapor absorption spectra of ortho- and meta-xylene (dimethylbenzene) will be presented along with an interpretation of these spectra and the corresponding Tesla luminescence spectrum of meta-xylene reported by McVicker, Marsh, and Stewart.[2] References to earlier related spectroscopic work were given in I.

EXPERIMENTAL DETAILS

The spectrographic equipment and experimental procedure used to photograph and measure the ortho- and meta-xylene spectra were the same as those described in I for obtaining the para-spectrum. Samples of both compounds were purchased from the National Bureau of Standards. The ortho-xylene had a 0.010 ± 0.007 mole percent impurity and the meta-xylene a 0.17 ± 0.07 mole percent impurity. Vapor pressures of the compounds were obtained from the work of Stuckey and Saylor.[3]

EXPERIMENTAL RESULTS

The near ultraviolet absorption spectra of meta- and ortho-dimethylbenzene lie in the region between 2820 and 2350A. These spectra were studied in dependence of the pressure of the substance for temperatures ranging between $-40°$ and 100°C. With path lengths of 75 cm the most detailed spectrograms were obtained for both compounds at 0°C. Even though some of the frequency differences are found to be roughly the same for both spectra, their general appearance is considerably different due to the diffuseness of the meta spectrum and the lack of similarity in the reoccurring groups of bands which are characteristic of each spectrum.

The meta-xylene bands are broad, diffuse, do not have definite heads, and usually appear in pairs about 65 cm^{-1} apart. A close inspection of the plates with a microscope reveals that the bands contain fine structure even though they are diffuse. The appearance of the bands in pairs of equal intensity is evident at the lowest reservoir temperature, $-40°$C (0.06 mm Hg), at which bands were detectable. For this temperature three groups of bands are observed with the center of the short wavelength band in each group appearing at 2705A (36,955 cm^{-1}), 3671A (37,425 cm^{-1}), and 2636A (37,920 cm^{-1}). At a higher temperature, $-20°$C (0.37 mm Hg), these band groups are accompanied by a very weak but similar "doublet" spaced about 160 cm^{-1} to the red and by an extremely weak band spaced 110 cm^{-1} to the red. For the same temperature two other doublets appear, one at 2652A (37,690 cm^{-1}) and another at 2624A (38,100 cm^{-1}), and a broad single band is found at 2617A (38,205 cm^{-1}). With a further increase in the temperature of the reservoir other bands appear toward the violet as may be seen in Fig. 1; also three definite weak doublets are discernible on the red side of the 36,955 cm^{-1} band with the one at 2759 (36,230 cm^{-1}) appearing as the strongest.

In contrast to the meta spectrum the bands of the ortho-xylene spectrum are narrow, have sharp heads, and are degraded toward the red. The repeated groups of this spectrum are made up of many narrow bands, and in some cases these groups overlap. In Fig. 2 we see that at least the main features of the well-developed group at 2679.6A (37,308 cm^{-1}) are repeated in the groups at 2647.3A (37,815 cm^{-1}), 2630.8A (38,000 cm^{-1}), and 2596.4A (38,503 cm^{-1}). The group at 2613.8A (38,247 cm^{-1}) resembles the above groups but it has been found to be slightly different. When the spectrogram obtained for a substance temperature of $-40°$C (0.03 mm

* This work was assisted by the ONR under contract N6ori-107, Task Order I, with Duke University.

† Based on part of a thesis submitted in partial fulfillment of the requirement for the degree of Doctor of Philosophy in the Graduate School of Arts and Sciences of Duke University in 1950.

‡ Present address: Physics Department, University of Georgia, Athens, Georgia.

[1] C. D. Cooper and M. L. N. Sastri, J. Chem. Phys. **20**, 607 (1952).

[2] McVicker, Marsh, and Stewart, J. Chem. Soc. **125**, 1743 (1924).

[3] J. M. Stuckey and J. H. Saylor, J. Am. Chem. Soc. **62**, 2922 (1940).

Hg) is examined, all of the first four groups mentioned above are present and each consists of three bands. In each group the two bands of longest wavelength are separated from the one on the violet side by 76 and 131 cm^{-1}. The band at 38,247 cm^{-1} is also present at this temperature, but with a companion 60 cm^{-1} toward the red. At $-20°C$ (0.28 mm Hg) a companion appears 60 cm^{-1} to the red also in the first four groups. Above $-5°C$ (0.92 mm Hg) other weak bands are found in the above groups as can be seen in Table II and Fig. 2. The sharpness of the individual bands allows in some cases to distinguish fine bands, separated from each other by 3 to 5 wave numbers and giving the impression of band heads.

As in the other two spectra the ortho-xylene spectrum, when fully developed, contains many bands toward shorter wavelengths; however, in ortho-xylene the group character of the spectrum becomes lost because of diffuseness and an accidental, almost equal spacing between adjacent bands with not so much intensity variation. At the long wavelength end of the spectrum the weak, temperature dependent, bands on the red side of the 37,308 cm^{-1} group were difficult to measure because of an increasing diffuseness of the spectrum with temperature.

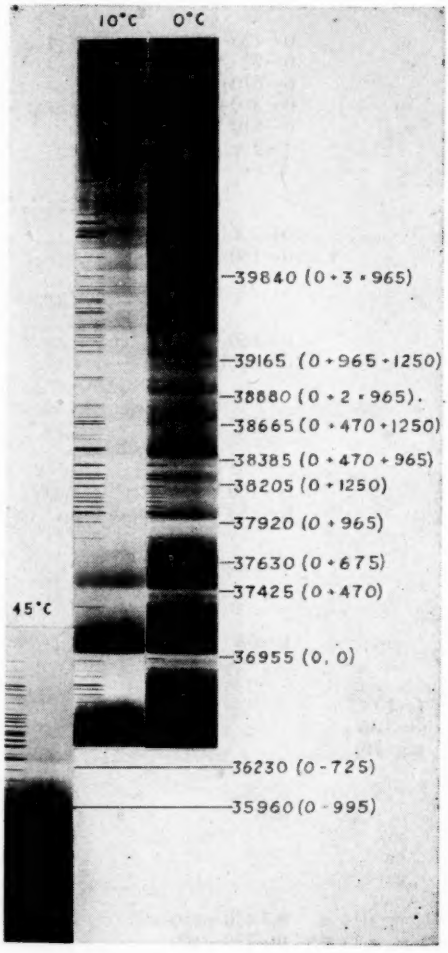

FIG. 1. Absorption spectrum of meta-xylene vapor.

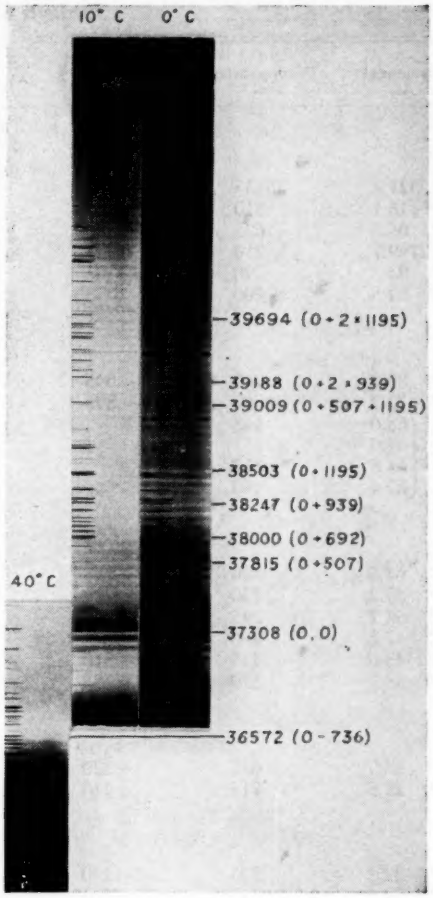

FIG. 2. Absorption spectrum of ortho-xylene vapor.

For both meta- and ortho-xylenes there is another absorption system around 2100A which is separate from the one discussed above. A study of this system with ultraviolet sensitized plates revealed only the edge of a continuous absorption which gradually moves toward the red with increasing temperatures. This edge was found around 2100A at $-60°C$ of the reservoir and around 2300A for 40°C. Above 50°C this system merges with the one at longer wavelengths.

The measured bands and pertinent information pertaining thereto are presented in Tables I and II, for

TABLE I. Absorption bands of meta-xylene.

Wavelength A	Wavenumber cm^{-1}	Separation from 0, 0 36955 cm^{-1}	Intensity			Assignments
			$t=45°C$ $p=24.5$ mm Hg	$t=60°C$ $p=49.5$ mm Hg	$t=70°C$ $p=76.1$ mm Hg	
*2821.3	35435	−1520			ew	0−2×725−65
* 15.1	510	−1445			ew	0−2×725
* 05.5	635	−1320			ew	0−1245−65
*2799.7	710	−1245		ew	vw	0−725−510; 0−1245
* 93.3	790	−1165		ew		0−995−160
* 84.8	900	−1055	ew	m		0−995−65
					$t=35°C$ $p=14.5$ mm Hg	
* 80.2	960	−995	vw	m	ew	0−995
* 72.2	36060	−895	vw		ew	0−725−160
65.6	148		vw			
64.9	157		m			
63.8	171		m			
62.4	190		m			
				$t=20°C$ $p=6.26$ mm Hg		
* 63.8	170	−785	m	ew	m	0−725−65
* 59.2	230	−725	m	mw	s	0−725
* 54.2	295	−660	vw			0−510−160
* 47.8	380	−575		ew	m	0−510−65
* 43.0	445	−510		m	s	0−510
* 33.7	570	−385		ew		0−2×160−65
				$t=0°C$ $p=1.71$ mm Hg		
* 28.9	635	−320		ew		0−2×160
* 22.8	715	−240		vw		0−160−65
			$t=-10°C$ $p=0.82$ mm Hg			
* 22.2	725	−230	ew			0−160−65; 0−226?
* 20.6	745	−210	ew			0−2×110
18.4	775			ew		
17.2	792		vw	w		
17.0	794			w		
16.1	807		vw	w		
15.3	817			ew		
* 16.9	795	−160	vw	w		0−160
* 13.1	845	−110		w		0−110
11.2	873		ew	ew		
10.2	887		m	ms		
09.1	902		m	ms		
08.4	911			ms		
07.9	918					
* 09.7	895	−60	m	s		0−65
06.3	940		ew	vw		
05.4	952		vs	vs		
					$t=10°C$ $p=3.36$ mm Hg	
04.4	966		vs	vs		
03.7	975		ew			
* 05.1	955	0	vs	vs		0, 0
* 00.2	37025	70		ew	vw	
*2694.6	100	145			ew	
* 93.2	120	165		ew	ew	
* 91.2	145	190			ew	
* 87.4	200	245	ew	vw	m	0+470−160−65
* 83.0	260	305	ew	vw	s	0+470−160
77.5	337			vw		
76.5	351			ms		
75.0	372			ms		
74.0	386			vw		
* 76.1	355	400	mw	ms		0+470−65
72.6	406			ew		
71.5	421			s		
70.3	438			s		
69.4	450			vw		
* 71.3	425	470	s	s	vs	0+470
* 66.1	495	540	ew	ew	w	

TABLE I.—*Continued.*

Wavelength A	Wavenumber cm^{-1}	Separation from 0, 0 36955 cm^{-1}	Intensity			Assignments
* 61.6	560	605	ew	ew	vw	0+675−65
* 60.1	580	625		ew	vw	0+735−110
58.0	611			ew		
56.9	627			mw		
55.9	641			mw		
55.3	649			ew		
* 56.7	630	675	mw	mw	mw	0+735−65; 0+675
* 52.5	690	735	vw	vw	mw	0+735; 0+965−160−65
* 47.5	760	805		w		0+965−160
* 43.8	815	860		w		0+965−110
42.3	835		ew	ew		
41.4	847		mw	m		
40.5	860		mw	m		
39.6	873		ew	m		
39.3	878		ew	ew		
* 40.8	855	900	mw	m		0+965−65
37.7	901		ew	ew		
36.4	919		vs	s		
35.2	936		s	s		
34.4	948		ew	ew		
* 36.3	920	965	vs	s		0+965
* 27.9	38040	1085	ew	ew		0+1145−65; 0+675+470−65
* 24.0	100	1145	ew	ew		0+1145; 0+675+470
18.0	186		ew	ew		
16.8	203		m	m		
15.9	216		mw	m		
15.1	228		vw			
* 16.8	205	1250	m	m		0+1250
* 08.7	320	1365	mw	s		0+470+965−65
05.4	370		ew	ew		
04.7	381		m	s		
03.5	398		mw	s		
02.8	409			ew		
* 04.3	385	1430	m	s		0+470+965
*2594.2	535	1580	ew	ew		0+675+965−65
91.6	575			ew		
90.5	591		mw	mw		
89.5	606		mw	mw		
88.4	622			ew		
* 90.1	595	1640	mw	mw		0+470+1250−65; 0+675+965
86.2	655		ew			
85.4	667		w			
84.5	681		w			
83.7	693		ew			
* 85.4	665	1710	mw	mw		0+470+1250
* 75.5	815	1860	ew	ew		0+2×965−65
72.2	866		ew	ew		
71.1	882		m	m		
70.4	893		mw	m		
69.9	900		ew	ew		
* 71.2	880	1925	m	m		0+2×965; 0+675+1250
* 63.3	39000	2045	vw	vw		0+965+1145−65
* 59.6	055	2100	w	ew		0+965+1145; 0+470+675+965
53.7	147			ew		
52.7	162		mw	mw		
51.6	179		mw	mw		
51.2	185		ew			
* 52.5	165	2210	mw	mw		0+965+1250
* 44.8	285	2330	w	mw	s	0+470+2×965−65
* 40.7	345	2390	w	mw	s	0+470+2×965; 0+470+675+1250
* 27.0	560	2605	ew	vw	mw	0+470+965+1250−65; 0+675+2×965
* 22.7	630	2675	ew	vw	mw	0+470+965+1250
* 13.9	765	2810			ew	0+3×965−65
* 09.2	840	2885		ew	m	0+3×965; 0+675+965+1250
* 02.1	955	3000			vw	0+2×965+1145−65
*2498.0	40020	3065		ew	m	0+2×965+1145; 0+470+675+2×965
* 91.5	125	3170		ew	mw	0+2×965+1250
* 84.1	245	3290		ew	m	0+470+3×965−65

TABLE I.—*Continued.*

Wavelength A	Wavenumber cm^{-1}	Separation from 0, 0 36955 cm^{-1}	Intensity			Assignments
* 80.3	305	3350		ew	m	0+470+3×965; 0+470+675+965+1250
* 74.6	400	3445			vw	
* 73.2	420	3465			vw	
* 71.6	445	3490			vw	
* 67.0	525	3570			vw	0+470+2×965+1250−65; 0+675+3×965
* 62.8	590	3635			vw	0+470+2×965+1250
* 57.2	685	3730			vw	
* 54.2	735	3780			ew	0+4×965−65
* 50.2	800	3845			vw	0+4×965; 0+675+2×965+1250
* 39.3	985	4030			ew	0+3×965+1145
			$t=20°C$ $p=6.26$ mm Hg			
* 33.9	41075	4120	vw		ew	0+3×965+1250
* 26.1	205	4250	vw		ew	0+470+4×965−65
* 22.6	265	4310	mw		ew	0+470+4×965
* 16.8	365	4410			ew	
* 09.8	485	4530	ew			
* 05.7	555	4600	ew			
* 00.3	650	4695	ew			
*2393.8	760	4805	ew			0+5×965
				$t=35°C$ $p=14.5$ mm Hg		
* 83.3	945	4990	ew	ew		
* 68.0	42215	5360	ew	ew		

TABLE II. Absorption bands of ortho-xylene.

Wavelength A	Wavenumber cm^{-1}	Separation from 0, 0 37308 cm^{-1}	Intensity			Assignments
			$t=55°C$ $p=32.0$ mm Hg	$t=65°C$ $p=51.0$ mm Hg	$t=70°C$ $p=63.2$ mm Hg	
2782.0	35935	−1373		ew	ew	0−1373
76.8	36002	−1306		ew	ew	
72.0	064	−1244	ew	ew		
71.2	075	−1233	ew			0−1222
68.8	106	−1202	ew			
67.2	127	−1181	vw			
64.4	164	−1144	ew			
					$t=50°C$ $p=25.52$ mm Hg	
62.7	186	−1122	mw		ew	
58.8	237	−1071			ew	
57.5	254	−1054	m		ew	0−1054
54.4	295	−1013			vw	
				$t=40°C$ $p=15.41$ mm Hg		
53.4	308	−1000		ew	vw	
52.7	317	−991	m	ew	ew	0−985
50.5	346	−962			ew	0−736−3×76
47.7	383	−925		ew	s	0−736−189
44.8	422	−886			s	0−736−2×76
			$t=25°C$ $p=6.70$ mm Hg			
43.2	443	−865	ew	w	vw	0−736−60−72
42.4	454	−854		ew		0−736−2×60
40.3	482	−826		ew		0−736−90
39.7	490	−818		vw		0−736−81
39.0	499	−809	mw	vs		0−736−72
38.1	511	−797		w		0−736−60
33.5	572	−736	s	vs		0−736
					$t=10°C$ $p=2.65$ mm Hg	
33.3	575	−733	ew		vw	0−578−2×76

TABLE II.—*Continued.*

Wavelength A	Wavenumber cm^{-1}	Separation from 0, 0 37308 cm^{-1}	Intensity			Assignments
			$t=5°C$ $p=2.10$ mm Hg			
27.7	650	−658	ew			0−578−81; 0−503−2×76
26.4	668	−640	ew			0−578−60
21.8	730	−578	ms	ew	mw	0−578; 0−503−76
16.2	805	−503		vw	vw	0−503
14.8	824	−484		ew	ew	
12.3	858	−450		ew		
09.9	891	−417		ew		
			$t=0°C$ $p=1.33$ mm Hg			
01.9	37001	−307	ew	ew		0−4×76
2698.5	047	−261	vw			0−2×131
97.6	060	−248	w	mw		0−2×126; 0−255
96.0	081	−227	w	mw		0−3×76
93.3	119	−189	w	mw		0−131−60
91.3	146	−162	vw			0−162
90.7	155	−153	w			0−2×76
89.9	166	−142	vw			0−2×72
89.0	177	−131	m			0−131; 0−60−72
88.7	182	−126		mw		0−126
88.2	188	−120	ew	vw		0−2×60
85.1	232	−76	vs			0−76
84.8	235	−73	ms	vs		0−72
83.9	248	−60	s	vs		0−60
83.6	252	−56	ew	vw		0−56
79.6	308	0	vs	vs		0, 0
79.4	311	3	ew	vw		0−503+507
77.1	343	35		ew		
74.4	381	73		ew		
71.7	418	110	vw	ew		0+582+692
66.1	497	189		ew		0−503+692; 0+189
63.5	533	225		ew		
61.3	564	256	vw	vw		
57.6	617	309	m			
57.0	625	317	mw			0+507−131−60
54.4	662	354	vw			0+507−2×76
53.9	670	362	mw			0+507−2×72
52.9	683	375	s			0+507−131; 0+507−60−72
51.8	699	391	vw			0+507−2×60
49.4	734	426	mw			0+507−81
48.9	740	432	vs			0+507−76
47.8	756	448	vs			0+507−60
47.3	815	507	vs			0+507
40.1	868	560	vw			0+692−131; 0+692−60−72
36.1	924	616	s			0+692−76
35.8	928	620	ew			0+692−72
34.9	941	633	m			0+692−60
30.8	38000	692	vs			0+692
22.1	127	819	m			0+939−2×60
19.2	168	860	ew			0+939−81
18.7	176	868	s			0+939−72
17.9	187	879	s			0+939−60
14.7	234	926	ew			0+1001−75?
13.8	247	939	vs			0+939
13.0	259	951	ew			
09.6	309	1001	m			0+1001?; 0+1195−2×60−72
06.6	353	1045	ew			0+1195−2×76
05.4	371	1063	m			0+1195−131; 0+1195−60−72
04.2	388	1080	mw			0+1195−2×60
02.1	419	1111	vw			0+1195−80
01.5	428	1120	vs			0+1195−76
00.3	446	1138	s			0+1195−60
2596.4	503	1195	vs			0+1195
92.6	560	1252	ew			
87.9	630	1322	w			0+507+939−60−72
84.3	684	1376	mw			0+507+939−76
83.5	695	1387	ew			0+2×692; 0+507+939−60
80.1	747	1439	mw			0+692+939−2×60−72
79.3	759	1451	w			0+507+939
75.5	816	1508	mw			0+507+1195−2×60−72; 0+692+939−60−72

TABLE II.—*Continued.*

Wavelength A	Wavenumber cm^{-1}	Separation from 0, 0 37308 cm^{-1}	Intensity	Assignments
71.5	876	1568	s	0+507+1195−60−72; 0+692+939−72
71.3	879	1571	w	0+692+939−60
67.1	942	1634	s	0+507+1195−76; 0+692+939
66.6	951	1643	m	0+507+1195−60
63.5	998	1690	m	0+692+1195−2×60−72
62.7	39009	1701	m	0+507+1195
59.5	058	1750	vw	0+2×939−60−72
55.7	116	1808	m	0+2×939−72
54.4	136	1828	mw	0+692+1195−60
51.0	188	1880	m	0+2×939
50.6	195	1887	m	0+692+1195
42.6	318	2010	mw	
39.2	371	2063	m	
38.4	383	2075	w	
34.9	437	2129	m	0+1195+939
34.4	446	2138	mw	
30.5	507	2199	mw	
26.3	572	2264	mw	
23.4	618	2310	mw	
22.3	634	2326	w	
18.5	694	2386	w	0+2×1195
15.5	742	2434	ew	
10.3	824	2516	vw	
07.1	875	2567	vw	
02.6	947	2639	vw	0+507+1195+939
00.0	988	2680	ew	
2499.1	40002	2694	vw	
94.3	080	2772	w	
90.9	134	2826	w $t=10°C$ $p=2.65$ mm Hg	0+692+1195+939
* 87.3	190	2882	ew	0+507+2×1195
* 83.6	250	2942	vw	
* 80.9	295	2987	vw	
* 79.8	315	3007	ew	
* 76.9	360	3052	ew	
* 76.0	375	3067	vw	
* 75.5	385	3077	ew	
* 71.9	440	3132	ew	
* 68.2	505	3197	vw	
* 67.3	520	3212	ew	
* 64.8	560	3252	ew	
60.1	638	3330	vw	0+2×1195+939
* 56.8	690	3382	ew	
52.8	757	3449	ew	
48.7	826	3518	ew	
45.4	881	3573	ew	0+3×1195
* 42.0	940	3632	ew	
* 38.8	990	3682	ew	
* 37.9	41005	3697	mw	
* 35.3	050	3742	mw	
* 30.9	125	3817	ew	
* 27.1	190	3882	vw	
* 23.7	245	3937	m	
* 20.0	310	4002	m	0+3×939+1195; 0+2×1195+939+692
* 16.2	375	4067	mw	
* 12.9	430	4122	vw	
* 09.2	495	4187	mw	
* 06.2	545	4237	vw	
* 05.2	560	4252	mw	0+2×1195+2×939
* 01.5	630	4322	ew	
*2398.7	675	4367	ew	
* 97.7	695	4387	ew	
* 94.2	755	4447	ew	
* 90.7	815	4507	ew	
* 87.7	870	4562	ew	
* 83.8	935	4627	ew	
* 81.3	980	4672	ew	
* 80.3	42000	4692	ew	

meta- and ortho-xylene, respectively. The first column contains wavelengths which correspond to the heads of the bands except where they are preceded by an asterisk. Those so marked represent the center of the absorption band. In Table I the wavelengths enclosed by brackets represent the variations of intensity within the broad diffuse meta-xylene bands. The center of these bands, which were used for the calculations, are recorded directly beneath such groups. Wave numbers, as obtained from Kayser's tables, are given in column two while column three presents the separation of the designated from the 0,0 band. Wave numbers are accurate to within 2 or 3 cm^{-1} except those for bands marked with an asterisk which are given only to the nearest five cm^{-1}. Column four contains intensity data obtained by visual means for different temperatures and pressures. The following intensity scale of eight steps was used: ew—extremely weak, vw—very weak, w—weak, mw—medium weak, m—medium, ms—medium strong, s—strong, and vs—very strong. Assignments and remarks are included in the fifth column of the tables.

DISCUSSION AND ANALYSIS

A. Meta-Xylene

If we treat the CH_3 groups as single atoms then meta-xylene has C_{2v} symmetry. This same symmetry is possessed by toluene, but the twofold axis is oriented differently. In both cases the z axis is perpendicular to the plane of the ring, but in toluene the twofold y axis is directed along the line of the $C-CH_3$ bond, while in meta-xylene the twofold axis bisects the angle formed by the two lines which pass through the respective $C-CH_3$ bonds. In the more symmetric 1, 3, 5 trimethylbenzene (mesitylene) which belongs to the point group D_{3h}, the twofold axis is directed along one $C-CH_3$ bond and bisects the angle between the other two. Mesitylene is of interest here because of the meta-orientations of the CH_3 groups. The near ultraviolet spectrum of mesitylene has been interpreted by Sponer and Stallcup[4] as a forbidden transition ($^1A_1'-{}^1A_1'$) made allowed by a vibration of symmetry ϵ'. In contrast, the meta-xylene spectrum is allowed ($^1A_1-{}^1B_1$) with a transition moment along the x axis; nevertheless, a striking resemblance has been observed between the two spectra. Bands of both spectra are diffuse and appear in pairs; also each spectrum has maximum absorption coefficient of about 250 and their oscillator strengths f are not very different. The meta-xylene spectrum has a little higher intensity than that of mesitylene.

In discussing the meta-xylene bands the wavenumbers referring to the centers of the bands will be used, but it must be kept in mind that most of the bands are about 20 cm^{-1} in width and do not form heads. This not only influences the accuracy of the assignments but also introduces in places some uncertainty in the interpretation. The band at 2705A (36,955 cm^{-1}) is chosen as the 0, 0 band. Only the frequency of 965 cm^{-1} has been found to definitely form a progression in the meta-spectrum. However, a progression of the 470 cm^{-1} frequency may be masked by the strong 965 band. Members of the 965 progression are found at 37,920, 38,880, 39,840, 40,800, and 41,760 cm^{-1}. For higher members than the first of this progression the double bands are no longer of equal intensity; instead, the long wavelength component of each "doublet" becomes progressively weaker for higher members. This upper state frequency of 965 cm^{-1} is easily correlated with the ground-state value of 995 cm^{-1} as represented by the band at 35,960 cm^{-1}. Further the Raman spectrum[6] has a strong polarized line at 999 cm^{-1}, and a frequency of 1010 cm^{-1} has been found in the emission spectrum produced by a Tesla discharge through meta-xylene vapor.[2] Then without doubt, the 995 and 965 values observed in the absorption spectrum correspond to the ground- and excited-state frequencies of a totally symmetric carbon vibration. It takes the place of the "breathing" vibration of 992 cm^{-1} in benzene and may well be "derived" from this vibration.[6]

Two other bands of medium intensity are found at 38,205 and 38,100 cm^{-1} which have upper state frequencies of 1250 and 1145 cm^{-1}. These frequencies are not found in progressions, but they do appear in combinations with members of the 965 progression. Also bands appear which may be explained as combinations of 1250 plus 470, and 1250 plus 470 plus 965. These bands involving the 470 frequency are always double, but the bands representing the frequency 1250 cm^{-1}, and combinations of the 1250 value with members of the 965 progression are the only ones in the entire spectrum which are not accompanied by long wavelength companions. The ground-state frequencies corresponding to the excited-state values of 1250 and 1145 cm^{-1} cannot be ascertained with certainty. Several possibilities of interpretation offer themselves. In analogy to meta-dichlorobenzene,[7] the three upper state frequencies 965, 1145, and 1250 cm^{-1} may be assigned to symmetric carbon vibrations, and the latter two may be taken to correspond to the ground-state values 1249 and 1264 cm^{-1} which appear in Raman lines of medium intensity with a joint depolarization factor of 0.10. However, if we follow a recent discussion given in the case of benzotrifluoride,[8] the symmetric bending vibration of the CH_3 group represented by the strong polarized Raman line at 1375 cm^{-1} might show up excited in the electronic absorption spectrum with a value of 1250 in the upper state. Third, the 1145 may not be a carbon vibration but either the combination 675+470 or the

[4] H. Sponer and M. J. Stallcup, paper in V. Henri Memorial Volume, *Contributions à l'Etude de la Structure Moléculaire, Desoir* (Liège, 1948), p. 222.

[5] E. Herz, Monatsh. Chem. **74**, 160 (1942).

[6] K. S. Pitzer and D. W. Scott, J. Am. Chem. Soc. **65**, 803 (1943).

[7] H. Sponer, Revs. Modern Phys. **14**, 225 (1942).

[8] H. Sponer and D. S. Lowe, J. Opt. Soc. Am. **39**, 840 (1949).

C—CH_3 vibration for which a ground-state value of 1249 had been chosen by Pitzer and Scott.[6] It seems, on the other hand, that Kohlrausch prefers a correlation of the strong polarized Raman line of 724 to this vibrational mode which he derives from the totally symmetric benzene vibration of 992 cm^{-1}. The ambiguity of interpretation just demonstrated is typical of much analysis work. A definite assignment of the 1250 and 1145 frequencies should be postponed until more data are available from many more related molecules.

The 724 frequency is observed in the band 36,230 cm^{-1} which is the strongest band found in this region. Its counterpart in the excited state can be chosen from weak bands only. The band 37,630 was picked which is 675 cm^{-1} toward the violet from the 0, 0 band. The situation met here, namely, a vibration which belongs to a very strong Raman line and appears strongly in the ground but weakly in the excited electronic state, has been encountered before in respect to the C—Cl valence vibration of the monochlorobenzene and meta-dichlorobenzene.[9] As seen from Table I, the bands 38,595, 39,560, and 40,525 can then be explained as combinations of 675 with the 965 progression, and 675+470 may be represented by the band 38,100. The combination 675+1250 would then coincide with a band representing 2×965. In such a case, the short wavelength component of the "doublet" members of the 965 cm^{-1} progression should be stronger than the long wavelength component for all members except the first. This is exactly what is observed.

The vibration of 470 cm^{-1} was taken from the band at 37,425 cm^{-1} and correlated with the ground-state frequency of 510 cm^{-1} represented by the weak band at 36,445 cm^{-1}. Raman lines have been observed[10] at 515 and 536 cm^{-1} with a combined depolarization factor of 0.33; however, Herz[11] lists the 515 as depolarized and associates the 536 with the 0.33 depolarization factor. The 536 Raman line is twice as intense as the 515 line. In the infrared spectrum both the 515 and 536 cm^{-1} frequencies have been observed by Plyler.[12] Following Pitzer and Scott[6] he assigned the 515 value to the β_1 component and the 536 value to the α_1 component resulting from the 600 ϵ_g^+ benzene vibration. The same assignment of the 515 value had been chosen here and it is in excellent agreement with the similar assignment of 516 to class ϵ' in mesitylene. In fact, if we assume that the migration of electrons from the CH_3 group into the ring is weak and then consider the vibration forms of symmetry ϵ_g^+ in benzene it can be seen that the corresponding degenerate ϵ' vibration in mesitylene should have about the same frequency as the nontotally symmetric component β_1 in meta-xylene since the third methyl group of mesitylene does not take part in the vibration. Further check on the above assignment is obtained from the chloro substituted benzenes. In meta-dichlorobenzene the β_1 (from ϵ_g^+ benzene) vibration is 428 while the ϵ' (ϵ_g^+) vibration is 425 in 1, 3, 5 trichlorobenzene.[13] Because of the breadth and diffuseness of the ultraviolet absorption bands we have assumed that bands involving the 515 and 536 cm^{-1} vibration are indistinguishable. The same is true for bands involving the upper state frequencies of these vibrations. Therefore, it is not expected that the so-called forbidden part of the spectrum would be observed, for it would be masked by bands involving combinations of the α_1 (ϵ_g^+) and other totally symmetric vibrations.

A brief comparison of the interpretations given for the meta-xylene and mesitylene spectra may be in order. The 0, 0 band of meta-xylene at 36,955 cm^{-1} is only 45 cm^{-1} from the position of the 0, 1 band in mesitylene (37,000 cm^{-1}). The 965 and 1250 separations in meta-xylene may be correlated with the vibrations 968 and 1300 in mesitylene. The similarity of the spectra is further enhanced by the almost identical separation, 65 cm^{-1} in meta-xylene and 68 cm^{-1} in mesitylene, occurring between the diffuse double bands found in each spectrum. In both cases these small frequency differences are probably produced by a $v-v$ transition of a low-lying, nontotally symmetric vibration. Two such vibrations which were suggested for mesitylene, are represented in the 229 and 275 depolarized Raman lines. Corresponding Raman values occur at 226 and 277 cm^{-1} in meta-xylene.§ Only the first band toward the violet from the 0, 0 band in meta-xylene (0, 0+470) and from the 0, 1 band in mesitylene (0, 1+555) are of different origin as might be expected from the different character of the spectra (allowed and forbidden.)

It is suggested that the diffuseness of the meta-xylene and mesitylene bands is caused in part by overlapping $v-v$ transitions and in part by the internal rotation of the CH_3 group. In meta-xylene the potential restricting such rotation is only about 500 cal/mole,[6] so the group may experience almost free rotation causing a broadening of the bands. The $v-v$ transitions will involve not only the same vibration in the two states but also different vibrations in the upper and lower states, although probably to a lesser degree. Another factor contributing to the diffuseness is the overlapping of the gross and fine structure resulting from rotations about the different axes. From the small restricting potential in para-xylene,[6] which is about the same as in the meta isomer, we might expect diffuseness in the para spectrum, too. Actually the para bands are slightly diffuse but to a much lesser extent than the meta bands. In ortho-xylene where the CH_3 groups are on adjacent

[9] H. Sponer and S. H. Wollman, J. Chem. Phys. **9**, 816 (1941).
[10] Reference 5, Table 7.
[11] Reference 5, p. 161.
[12] E. K. Plyler, Disc. Faraday Soc. **9**, 100 (1950).
[13] H. Sponer and M. B. Hall, Paper in V. Henri Memorial Volume, *Contributions à l'Etude de la Structure Moléculaire, Desoir* (Liège, 1948), p. 211.

§ Herz questioned his depolarization measurements of these lines, 0.66 for 226 and 0.61 for 277, because of interference from the exciting line. L. Simons [Soc. Sci. Fenn., Comm. Phys. Math VI, No. 13 (1932)] obtained the following depolarization factors: For 201 combined with 226, $\rho=0.89$, and for 277, $\rho=0.90$.

TABLE III. Absorption spectrum of solid meta-xylene.[a]

Amorphous state −180°C				Crystalline state −180°C		
Wave number (cm^{-1})		Separation from 0, 0 36,810 cm^{-1}	Assignments	Wave number (cm^{-1})		Separation from 0, 0 36,455 cm^{-1}
36450–700	(1)	−275				
720–900	(10)	0	0, 0	36410–500	(4)	0
37150 edge 300 max. 400 edge	(7)	490	470	770 edge 900 max. 37020 edge	(8)	445
700 edge 800 max. 850 edge	(9)	990	965	140–180 280–360 500–600	(2) (9) (5)	705 865 1095
38060	(1)	1250	1250	740–38060	(3)	1445
220–320	(3)	1460	470+965	38200–340	(10)	1815
500–580	(2)	1730	470+1250	500–600	(2)	2095
680–780	(2)	1920	2×965	680–780	(3)	2275
960	(1)	2150		900–39060	(3)	2525
39260	(1)	2450	470+2×965	39160–300	(3)	2775
470	(1)	2660	470+965+1250	560	(1)	3105

[a] Results of A. Kronenberger, Z. Physik **63**, 494 (1930).

carbon atoms, the bands are very sharp and narrow. We would expect interaction between the methyl groups and a much higher potential barrier. Pitzer and Scott[6] have obtained an approximate value of 2000 cal/mole. It may be added for comparison that none of the dichlorobenzene spectra shows noticeable diffuseness.

The absorption spectrum of meta-xylene has been obtained by Kronenberger[14] in the solid state at −180°C and at −259°C. Although an absorption spectrum at a low temperature becomes simpler due to a decrease in thermal excitation of vibrations and rotations, it becomes on the other hand more complicated because of appearing lattice vibrations. For example, the structure of the main bands in benzene at −259°C was attributed to superposition of crystalline frequencies.[15] The absorption in meta-xylene was taken at −180°C for both the amorphous and crystalline state and at −259°C for the crystalline state. It does not show a sharpness or structure like the benzene or chlorobenzene bands[12] at −259°C. For the amorphous state, the bands are broader and more diffuse than the corresponding vapor bands, and the spectrum is shifted about 150 cm^{-1} to the red, but otherwise it is very similar. The spectrum in the crystalline state at −180°C is also composed of broad bands and their frequency separations from the 0, 0 band (band of longest wavelength at 36,410–500 cm^{-1}) are slightly different from those found in the vapor spectrum. The entire spectrum is shifted about 500 cm^{-1} to the red from its position in the vapor. Kronenberger's data are exhibited in Table III. The intensities are included in parentheses alongside the wave numbers and in the adjacent column, for each state, the frequency difference between the centers of each band and the center of the 0, 0 band, in our interpretation, is given. Assignments added for the amorphous state are those found for the vapor spectrum (Table I). The agreement is good if we note the broadness of the observed bands. It should be mentioned that the first band 36,450–700 is actually only a slight step-out on the envelope of the strong 36,720–900 band.

For the lower temperature of −259°C (data not given in Table III) the 0, 0 band is unchanged, but the frequency separations are found to be still a little lower than those at −180°C. Most of the bands are split in three components about 60 cm^{-1} apart for this temperature, but the strong bands at 36,400–470, 37,230–320, and 38,140–280 are not, and are actually broader than the corresponding bands found at 36,955, 37,920, and 38,880 cm^{-1} in the vapor spectrum.

Using the interpretation given here for the ultraviolet vapor absorption spectrum, the prominent Tesla luminescence bands, which were measured by McVicker, Marsh, and Stewart,[2] are easily explained. If the 36,960 cm^{-1} band is chosen as the 0, 0 band, the bands toward the red are found to involve ground-state frequencies of 510, 725, 995, and 1245 cm^{-1} as expected. The 37,400 band is interpreted as a transition from the 470 cm^{-1} level in the excited state to the vibrationless ground state.

B. Ortho-Xylene

The numerous closely spaced fine bands of the ortho-xylene spectrum give it an appearance entirely different from that of the spectra of the other two isomers. Actually, the structure observed in the meta bands indicates that such fine bands would also occur in this spectrum if the bands were not diffuse. Furthermore, for ortho-xylene with its fairly large restricting potential of internal rotation the group C_{2v}* is a poorer approximation to the actual molecular symmetry than C_{2v} and D_{2h} for the other xylenes, so that practically all vibrational combinations may occur superposed on the pure electronic transion. However, since the strong bands will be those expected for C_{2v}* symmetry, the spectrum will

[14] A. Kronenberger, Z. Physik **63**, 494 (1930).
[15] Sponer, Nordheim, Sklar, and Teller, J. Chem. Phys. **7**, 207 (1939).

be discussed from this point of view. The transition is $^1A_1 - {}^1A_1$. It is allowed with the transition moment in the x direction.

As stated previously, the strong sharp bands of ortho-xylene appear in characteristic groups which are repeated. The most detail is observed in the strong group of longest wavelength. Of this group the strong band on the short wavelength side at 2679.6A (37,308 cm^{-1}) is chosen as the 0, 0 band. The band of shortest wavelength in the fluorescence spectrum has been measured by Marsh[16] to be 2680A (37,300 cm^{-1}). It is a strong band. He also found the violet edge in the Tesla luminescence to have the same value. These observations support the above choice for the 0, 0 band.

Due to the overlapping of band groups, some of the bands may be explained in more than one way. Generally, the bands will be assigned using the smallest possible number of fundamental frequencies, but some other possible assignments will be discussed.

In the Raman spectrum of ortho-xylene strong, polarized lines of 1222, 1052, 733, and 582 cm^{-1} have been reported.[17] In the absorption spectrum, bands on the red side of the 0, 0 band were very difficult to measure because of a partial masking by the continuous background; however, many weak bands were measured. More prominent bands at 36,075, 36,254, 36,572, and 36,730 cm^{-1} are separated from the 0, 0 band by 1233, 1054, 736, and 578 cm^{-1}, and these separations are correlated with the Raman frequencies mentioned before. All the prominent bands in the absorption spectrum which are found between 37,308 cm^{-1} (0, 0 band) and 38,503 cm^{-1} can be explained as belonging to groups which have their band of shortest wavelength located at 38,503, 38,247, 38,000, and 37,815 cm^{-1}. Their respective separations from the 0, 0 band are 1195, 939, 692, and 507 cm^{-1}. These upper-state frequencies are correlated here with the ground-state values of 1233, 1054, 736, and 582 cm^{-1}. The frequencies 1195, 939, and 692 do form progressions, and the second member of each respective progression is located at 39,694, 39,188, and 38,695 cm^{-1}. Assignments of the 1233, 1054, and 736 frequencies to definite modes of vibration are not unambiguous,[6,17] but they do involve totally symmetric carbon ring vibrations and the $C-CH_3$ valence vibration. It is necessary to study further these uncertain assignments, and we hope to do so.

An assignment different from the correlation 939 (upper state) -1054 (lower state) just mentioned is possible for the 939 frequency. A polarized Raman line at 985 cm^{-1}, which is only one-fifth as intense as the 1052 line, could be associated with the 939 upper-state frequency. Also, the band at 36,317 cm^{-1}, could represent the ground-state frequency of 991 cm^{-1}. If this is true, the band of medium intensity at 38,309 cm^{-1}, which previously has been assumed to be associated with the 1195 group, could instead represent a fundamental vibration of 1001 cm^{-1} in the upper state. In this case the ground-state vibration corresponding to the 1001 frequency would be connected with the 1054 separation. An inducement for this assignment is that in ortho-dichlorobenzene the upper-state frequencies of 1089, 957, and 944 cm^{-1} have been assigned[7] to totally symmetric carbon vibrations. Arguments against a similar assignment here are that the 1001 frequency does not form a progression nor does it combine with the 939 frequency. Also the observed intensities fit the first assignment better where the 1001 band was considered part of the 1195 band group.

The 507 cm^{-1} frequency in the upper state with its corresponding ground-state value of 578 cm^{-1} is assigned to the α_1 ($\epsilon_g{}^+$) vibration. The β_1 component of the $\epsilon_g{}^+$ (606 cm^{-1}) benzene vibration has been identified[6] as the depolarized Raman line of 505 cm^{-1} and the absorption band appearing at 36,805 cm^{-1}, that is 503 cm^{-1} distant from the 0, 0 band toward longer wavelengths, is correlated with it. This vibration has not been observed with certainty in the upper electronic state but may practically coincide with one of the companions on the long wave side of the 507 band.

We whall now consider the long wavelength companions which accompany the strong bands discussed above. At least fifteen such companions were found on the red side of the 0, 0 band. A smaller number than this appears in the other repeated groups. As stated previously, the groups are all similar except for the one at 38,247 cm^{-1}.

Notable bands which accompany the 0, 0 band are separated from it by 60, 72, 76, 126, and 131 cm^{-1}. Tentative assignments will be suggested for some of these bands, but there are not enough data available to make definite assignments.

The 37,248 and 37,188 cm^{-1} bands in the first group represent separations of 60 and 2×60 cm^{-1}. Their intensity indicates that they may involve ground-state vibrations of about 300 and 2×300 cm^{-1}. The measured Raman value nearest 300 is the 255 cm^{-1} line. It may correspond to our 248 separation found from the band 37,060. Herz[17] has assigned this frequency to an out-of-plane vibration of the ring of symmetry class β_2 or α_2. The bands 37,248 and 37,188 cm^{-1} may be produced by $v-v$ transitions ($v=1$ and 2) between 248 in the ground state and 188 in the upper state. Since these vibrations appear singly excited, they would then have to be of symmetry character β_2.

The band at 37,235 cm^{-1} which represents the 72 cm^{-1} separation is produced perhaps by a $v-v$ transition between the ground-state vibration 578 cm^{-1} and upper-state vibration 507 cm^{-1} of the α_1 ($\epsilon_g{}^+$) vibration. The intensity of this band and the one at 37,166 cm^{-1}, which has a separation 2×72, is a little high for such an assignment, but not high enough to make the assignment untenable.

The band which is separated 76 cm^{-1} from the 0, 0 band, is as strong as the 0, 0 band; so it is probably

[16] J. K. Marsh, Phil. Mag. 49, 971 (1925).
[17] E. Herz, Monatsh. Chem. 76, 1 (1947).

produced by a low-lying vibration. Four members of this $v-v$ transition ($v=1$, 2, 3, and 4) are observed with separation 76, 2×76, 3×76, and 4×76 cm^{-1}. They are represented by the bands at 37,232, 37,155, 37,081, and 37,001 cm^{-1}, respectively. It is possible that the depolarized Raman line of 178 cm^{-1} may be associated with this transition.

In addition to the above bands which accompany the 0, 0 band, a very weak band is found at 37,311 cm^{-1}, which is 3 cm^{-1} on the violet side of the 0, 0 band. This band may be produced by a transition from the (β_1) 503 cm^{-1} ground-state level to the (α_1) 507 cm^{-1} upper-state level. This transition would have a moment in the y direction. The band 0−56 may be the result of a superposition of this 503→507 transition on the one producing the separation of 60 cm^{-1}. Although a similar correlation fits numerically for the separations 72 and 76, and 126 and 131 (see Table II), the intensities of these bands are rather high for such an interpretation, which is therefore considered as quite uncertain. It is also possible that some of these frequency differences are connected with rotational structure.

Other transitions involving a different ground and upper state vibration are represented, for example, by the bands, at 37,418 and 37,497 cm^{-1}. These transitions are 0−582→0+692 and 0−503→0+692.

On the basis of the above interpretation most of the prominent bands have been assigned in Table II.

Marsh observed only four bands in the fluorescence spectrum[16] and five bands in the emission spectrum produced by a Tesla discharge[2] through ortho-xylene vapor. Doubtlessly, other expected bands were masked by the continuous spectrum he reported in this region. The fluorescence and Tesla luminescence data are so meager it would not be informative enough to include them in this report.

THE JOURNAL OF CHEMICAL PHYSICS VOLUME 20, NUMBER 8 AUGUST, 1952

Some Statistical Mechanical Models of Elastic Polyelectrolytes and Proteins

TERRELL L. HILL
Naval Medical Research Institute, Bethesda, Maryland
(Received January 14, 1952)

Three statistical mechanical models are developed for use in connection with the problem of muscle action. In addition, the models should apply to certain other systems, for example, polyelectrolyte fibers or gels, fibrous proteins in general, and ion exchange resins.

The first model is a statistical mechanical version of the "autone" model of Varga, Szent-Gyorgyi, Gergely, and Laki, but we extend the theory to include the effect of an adsorbed substance (e.g., ATP) on the length of the elastic element.

The second model is a charged rubber-like cylindrical fiber. The charges on the molecular chains of the network may be permanent or may result from the adsorption of ions from solution (e.g., hydrogen ions, or ATP). The approximate free energy of the system is computed by combining the Flory-Rehner swelling theory, the Fowler-Langmuir adsorption model, and an electrostatic free energy based on a "smeared" uniform charge density inside the fiber (electrolyte is also present), as suggested by the work of Hermans and Overbeeck. If the radius of the cylinder is large compared to the radius of the Debye-Hückel ionic atmosphere, it is not necessary to linearize the Boltzmann factor in the Poisson-Boltzmann equation. From the free energy of the system one obtains the interconnected pressure-volume, length-tension and adsorption isotherm relations. Important special cases are isotropic swelling (zero tension) with the gel under pressure or not, and the elasticity of the fiber (with adsorption) under zero pressure. When the fiber is constrained to a constant radius, it is possible to get a phase change in the length-tension curve (see below).

The third model is an equilibrium statistical theory of the well-known $\alpha-\beta$ transformation in fibrous proteins (such as keratin and myosin). Adsorption of ions from solution and electrostatic effects can be included here as well as in the preceding model, but the discussion is concerned primarily with an analysis of the elasticity of a sheet of polypeptide chains with α- and β-units statistically scrambled, taking into account as a nearest-neighbor problem in statistical mechanics (using the quasi-chemical method) lateral $\beta-\beta$ hydrogen bonds and vertical $\alpha-\alpha$ hydrogen bonds. From the theory it would appear that critical phenomena, phase changes (for example, a considerable increase in length at constant tension, representing a phase change from primarily vertical $\alpha-\alpha$ crystallization to primarily lateral $\beta-\beta$ crystallization) and hysteresis are to be expected. These phenomena are observed experimentally, though modified in most cases by superimposed non equilibrium effects. It is pointed out that a fiber operating (on stretching and retraction) between the two "ends" of a phase change would be particularly suitable in the muscle problem, because of the sensitivity of the length of the fiber at constant tension to small changes in environment (e.g., pH).

Although a few illustrative examples are given, further applications are reserved for a later paper.

I. INTRODUCTION

IN another paper[1] the thermodynamics of free energy transfer in muscle has been discussed for a certain class of models of muscle action.[2] The essential structural feature involved in the free energy transfer is an elastic fiber which can shorten on adsorbing a solute (for example, adenosine triphosphate, ATP) from solution. In order to apply the thermodynamics to the muscle problem, in a detailed way, explicit statistical models of such a fiber must be available. The purpose of the present paper is to provide three such models (Morales and Botts[2] have discussed another related

[1] T. L. Hill and M. F. Morales, Arch. Biochem. and Biophys. (to be published).

[2] For example, M. F. Morales and D. J. Botts, Arch. Biochem. and Biophys. (to be published). See also J. Riseman and J. G. Kirkwood, J. Am. Chem. Soc. **70**, 2820 (1948).

model. Also, the earlier work of Riseman and Kirkwood[2] should be mentioned.) The actual numerical applications of the statistical equations will be presented elsewhere.[3]

In addition to the particular application which stimulated this work, it is believed that the results of Secs. III and IV, particularly, will be useful in connection with work on polyelectrolyte fibers and gels (including ion exchange resins) and fibrous proteins in general, respectively.

II. THE "AUTONE" MODEL

Here we consider the fiber to be made up of independent parallel molecular chains. Each chain consists of B *macromolecular* units or "autones" linked together. An autone can exist in a short ("contracted") state of length l_α or a long ("relaxed") state of length l_β, and an equilibrium exists between the two states. This model, in quasi-thermodynamic form, has been used before.[4] We give a statistical treatment here and extend the model to take into account the effect of *variable* amounts of an adsorbed substance (e.g., ATP) on the length of the chain. It will be noticed that the treatment in this section is rather formal and general and could apply to several different specific molecular theories (e.g., electrostatic forces could play essentially the same role here as in Secs. III and IV, although the formalism is different).

We need consider only a single chain. Let B_α autones be in the state α and $B-B_\alpha$ in the state β, so that the length of the chain is

$$l=l_\alpha B_\alpha+l_\beta(B-B_\alpha). \tag{1}$$

The length is thus essentially determined by the value of B_α. Let $J_\alpha(T)$ and $J_\beta(T)$ be the partition functions of individual autones in states α and β, respectively. These quantities take into account both energy and entropy (e.g., number of molecular configurations) contributions to the relative stability of the two types of unit. Similarly, let $j_\alpha(T)$ and $j_\beta(T)$ be the partition functions (including energy and entropy of adsorption) of an individual adsorbed molecule on the two types of unit, respectively. For example, if $j_\alpha > j_\beta$, adsorption is stronger on α units than on β (hence adsorption will result in some $\beta\rightarrow\alpha$ and a shortening of the chain). We assume that there are x equivalent and independent adsorption sites on each autone. Interactions between adsorbed molecules are neglected. Suppose N molecules are adsorbed, N_α on α-autones and $N-N_\alpha$ on β-autones. Then the complete partition function for the chain is

$$Q(l, N, T)=\sum_{N_\alpha} q(N_\alpha, l, N, T), \tag{2}$$

$$q=\frac{B!}{B_\alpha!B_\beta!}\cdot\frac{(xB_\alpha)!}{N_\alpha!(xB_\alpha-N_\alpha)!}\cdot\frac{(xB_\beta)!}{N_\beta!(xB_\beta-N_\beta)!}J_\alpha^{B_\alpha}J_\beta^{B_\beta}j_\alpha^{N_\alpha}j_\beta^{N_\beta},$$

$$B_\beta\equiv B-B_\alpha, \quad N_\beta\equiv N-N_\alpha,$$

where $B_\alpha(l)$ is given by Eq. (1). The three combinatorial expressions are, respectively, the number of ways of arranging B_α and B_β autones of the two types, the number of ways of distributing N_α adsorbed molecules on xB_α sites, and the number of ways of distributing N_β adsorbed molecules on xB_β sites.

As usual, we can set Q equal to the maximum term in the sum in Eq. (2). By using the Stirling approximation, the required value of N_α for given l, N, T is found from

$$(\partial \ln q/\partial N_\alpha)_{B_\alpha, N, T}=0 \tag{3}$$

to be given by

$$\frac{N_\alpha(xB_\beta-N_\beta)}{N_\beta(xB_\alpha-N_\alpha)}=j_{\alpha\beta}; \quad j_{\alpha\beta}\equiv j_\alpha/j_\beta. \tag{4}$$

This is a quadratic equation which can be solved for N_α.

We have[5]

$$dA=-SdT+\tau dl+\mu dN,$$
$$A=-kT\ln Q, \tag{5}$$

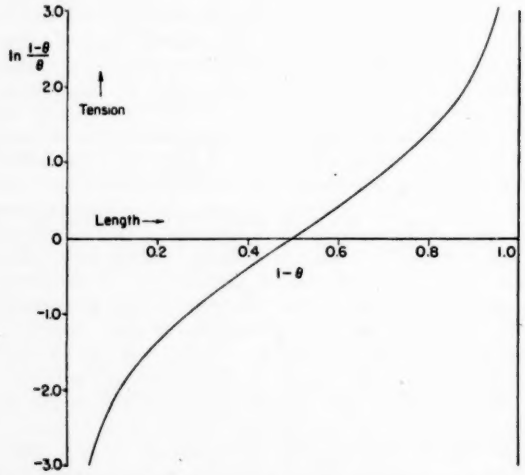

FIG. 1. Length-tension curve at constant c (Eq. (12a)). $\tau=0$ in equation below determines rest length.

$$\ln\frac{1-\theta}{\theta}=\frac{\tau(l_\beta-l_\alpha)}{kT}-\ln\left(\frac{1+cf_\alpha}{1+cf_\beta}\right)^x J_{\alpha\beta}$$

$$1-\theta=\frac{l-Bl_\alpha}{B(l_\beta-l_\alpha)}.$$

[3] T. L. Hill, Trans. Faraday Soc. (to be published).

[4] L. Varga, Hung. Acta Physiol. **1**, 1 (1946); A. Szent-Gyorgyi, Biol. Bull. **96**, 140 (1949); J. Gergely, Enzymologia **14**, 220 (1950); J. Gergely and K. Laki, Enzymologia **15**, 272 (1950). The model is due originally to Laki.

[5] T. L. Hill, J. Chem. Phys. **18**, 791 (1950).

where τ is the tension (strictly, force). Then

$$\tau=-kT\left(\frac{\partial \ln Q}{\partial l}\right)_{N,T}=-kT\frac{dB_\alpha}{dl}\left(\frac{\partial \ln q}{\partial B_\alpha}\right)_{N_\alpha,N,T}, \tag{6}$$

$$\frac{\tau(l_\beta-l_\alpha)}{kT}=\ln\frac{B_\beta}{B_\alpha}\left[\frac{(xB_\beta-N_\beta)B_\alpha}{(xB_\alpha-N_\alpha)B_\beta}\right]^x J_{\alpha\beta};\quad J_{\alpha\beta}\equiv J_\alpha/J_\beta \tag{7a}$$

$$=\ln\frac{B_\beta}{B_\alpha}\left(\frac{N_\beta B_\alpha j_{\alpha\beta}}{N_\alpha B_\beta}\right)^x J_{\alpha\beta}. \tag{7b}$$

By using Eqs. (1) and (4), Eq. (7) gives us $\tau=\tau(l, N, T)$. Also

$$\mu=-kT\left(\frac{\partial \ln Q}{\partial N}\right)_{l,T}=-kT\left(\frac{\partial \ln q}{\partial N}\right)_{N_\alpha,B_\alpha,T} \tag{8}$$

$$-\frac{\mu}{kT}=\ln\left(\frac{xB_\beta-N_\beta}{N_\beta}\right)j_\beta=\ln\left(\frac{xB_\alpha-N_\alpha}{N_\alpha}\right)j_\alpha$$
$$=-\frac{1}{kT}[\mu^0(T,P)+kT\ln c], \tag{9}$$

where c is the concentration (more rigorously, the activity) of the adsorbate in solution, and $\mu^0(T, P)$ is the standard chemical potential in solution. If we define

$$f_\alpha\equiv j_\alpha\exp(\mu^0/kT),$$
$$f_\beta\equiv j_\beta\exp(\mu^0/kT),$$

Eq. (9) becomes

$$N_\alpha=xB_\alpha f_\alpha c/(1+f_\alpha c), \tag{10}$$

$$N_\beta=xB_\beta f_\beta c/(1+f_\beta c). \tag{11}$$

These are, of course, "Langmuir" adsorption isotherms. On substituting these expressions in Eq. (7a) and using Eq. (1), we find

$$\frac{\tau(l_\beta-l_\alpha)}{kT}=\ln\frac{1-\theta}{\theta}\left(\frac{1+cf_\alpha}{1+cf_\beta}\right)^x J_{\alpha\beta};\quad \theta\equiv B_\alpha/B \tag{12a}$$

$$=\ln\frac{l-Bl_\alpha}{Bl_\beta-l}\left(\frac{1+cf_\alpha}{1+cf_\beta}\right)^x J_{\alpha\beta}. \tag{12b}$$

This gives $\tau=\tau(l, c, T)$. We can also obtain $l(\tau, c, T)$

$$\frac{l}{B}=\frac{l_\alpha J_{\alpha\beta}(1+cf_\alpha)^z+l_\beta z(1+cf_\beta)^x}{J_{\alpha\beta}(1+cf_\alpha)^z+z(1+cf_\beta)^x}$$
$$z\equiv\exp[\tau(l_\beta-l_\alpha)/kT]. \tag{13}$$

Equation (13) has the form of a weighted mean of l_α and l_β, the qualitative significance of the "weights" being obvious.

Figure 1 shows the form of the length-tension curve at constant c according to Eq. (12). An s-shaped curve may or may not be obtained, depending on the location of $\tau=0$. Figure 2 is an illustrative numerical example showing how l can depend on c at constant τ, according to Eq. (13).

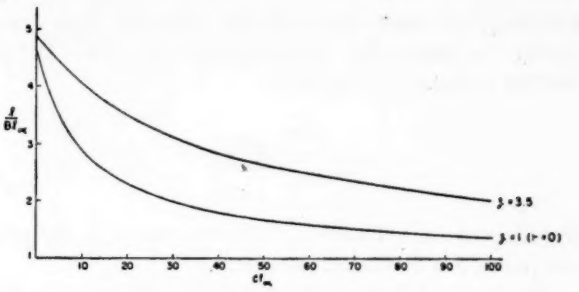

FIG. 2. Shortening of chain with increasing c at constant τ (Eq. (13)) in the arbitrary special case $x=1$, $l_\beta/l_\alpha=5$, $J_{\alpha\beta}=\frac{1}{10}$ (β units more "stable" than α) and $f_\beta=0$ (no adsorption on β units). The $z=1$ curve gives the rest length as a function of c.

The treatment of Gergely and Laki[4,6] corresponds in our notation to the special case $c=\infty$ (actomyosin saturated with ATP)

$$\frac{\tau(l_\beta-l_\alpha)}{kT}=\ln\frac{l-Bl_\alpha}{Bl_\beta-l}\cdot\frac{J_{\alpha\beta}f_\alpha{}^x}{f_\beta{}^x}. \tag{14}$$

This is also formally identical with the $c=0$ case (replace $J_{\alpha\beta}f_\alpha{}^x/f_\beta{}^x$ by $J_{\alpha\beta}$).

III. CHARGED RUBBER-LIKE CYLINDRICAL FIBER

Consider a very long cylinder (we neglect end effects) of rubber-like material of length l, radius R and volume V, immersed in an electrolytic solution. The intrinsic elastic and swelling properties of this molecular network (i.e., in the presence of solution but in the absence of charges on the network) are treated using the theories[7] of Wall, Flory and Rehner, and Flory. Attached at random along the various molecular chains of the network are n charges ϵ. Also, there are B equivalent sites for adsorption in the sample and N molecules are adsorbed. Each adsorbed molecule carries with it a charge $m\epsilon$. Aside from electrostatic forces, the adsorbed molecules do not interact and the nature of the specific binding at the adsorption sites is assumed independent of l, V, and total charge. The total charge in the volume V is $n^*\epsilon\equiv n\epsilon+Nm\epsilon$. We make the simplifying assumption that the resulting charge density $\rho\epsilon=n^*\epsilon/V$ is *uniform*. Solvent (of dielectric constant D) and electrolyte are free to penetrate inside the cylinder. In the

[6] It should be pointed out that (1) the "rest length" referred to by Gergely and Laki is the maximum length Bl_β ($\theta=0$) and not the elastic rest length ($\tau=0$) used here; and (2) the application made by Gergely and Laki is to an (enzymatic) steady-state condition (see reference 2).

[7] F. T. Wall, J. Chem. Phys. **10**, 485 (1942); **11**, 527 (1943); P. J. Flory and J. Rehner, J. Chem. Phys. **11**, 512, 521 (1943); **12**, 412 (1944); P. J. Flory, Chem. Revs. **35**, 51 (1944); J. Chem. Phys. **18**, 108, 112 (1950). See also Kuhn, Pasternak, and Kuhn, Helv. Chim. Acta **30**, 1705 (1947); J. J. Hermans, Trans. Faraday Soc. **43**, 591 (1947); H. J. White and H. Eyring, Textile Research J. **17**, 523 (1947); L. R. G. Treloar, Proc. Roy. Soc. (London) **200A**, 176 (1950).

solution, far from the cylinder, ions of type i and charge ϵ_i have the concentration c_i. The Debye-Hückel constant κ is given by

$$\kappa^2=\frac{4\pi}{DkT}\sum_i c_i\epsilon_i^2.$$

Refinements of the electrostatic treatment in the present paper are discussed elsewhere.[3]

The particular application we have in mind is that the n charges are, say,[2] $-COOCa^+$ and $-NH_3^+$ (n constant; this is not quite the same as pH constant—see below) and $m\cong -4$(ATP). Adsorption of ATP reduces the positive charge and will cause contraction of the fiber[1,2] at constant tension. Other examples: (a) In a strong polyelectrolyte fiber or gel, adsorption may be absent, $N=0$; and (b) in a weak acidic polyelectrolyte fiber or gel n would be, say, the total number of carboxyl groups, $\epsilon=-|$electronic charge$|$ for $-COO^-$, and N the number of "adsorbed" hydrogen ions ($m=-1$, $B=n$). The experiments of Katchalsky and Kuhn[8] on this kind of system are well known. If there are several different types of groups for "adsorbing" protons, Langmuir adsorption on a "heterogeneous surface" can be introduced with no difficulty.[9] Also, adsorption of, for example, ATP at constant or variable pH can be given similar treatment by using mixed Langmuir adsorption (ATP and H^+) on two different sets of sites, both species contributing to n^* and therefore influencing each other's adsorption.

We now derive an *approximate* expression for the Helmholtz free energy A of this system (cylinder plus solution) in the state l, V, n, N, κ, using isothermal processes at temperature T. As an initial reference state we take (a) the "dry" network at pressure P, tension $\tau=0$, volume V_0, length l_0, radius R_0, $N=0$, and $\epsilon=0$ (i.e., discharge the charges on the network) plus (b) a sufficient volume of solution at pressure P. The free energy of the initial state is A_0. The "dry" network and the solution are both assumed incompressible (see below), and, on mixing, the two volumes are assumed additive. The solution is treated as a one-component solvent (with volume per molecule v_0) in the entropy of mixing expression below.

When applied to a protein (or related substances), the equations below will be more suitable if the "dry" network is understood to include, as part of the protein, water relatively strongly bound on polar groups. Thus, on adsorption of water vapor by proteins, there is apparently first localized adsorption on specific sites, followed by "solution" adsorption.[9a] For convenience we take as our initial reference state protein with specific sites already filled. The adsorption problem itself, including length-tension effects in the cross-linked case, will be treated elsewhere.[9b]

Consider the following processes:

(1) Dry network at P, etc., $+N_s$ molecules of solution at P (from (b) above)$\rightarrow$swollen network with l and V, where $V=V_0+N_sv_0$.

(2) Addition of N discharged adsorbate molecules to the network (not from the solution—the adsorption equilibrium is considered frozen, for example by a membrane impermeable to adsorbate, until process (4)).

(3) The network and the N adsorbed molecules are gradually charged up from $\epsilon=0$ to ϵ, keeping l and V constant. We neglect the influence of this charging process on the relative probabilities of various configurations involved in process (1).

(4) We let A refer to the free energy of the system for an arbitrary value of N and let A_{eq} refer to the system when the value of N in (2) is chosen so that the chemical potential of adsorbate on the network (after charging in (3)) is just equal to its chemical potential in solution. In this case we can unfreeze the adsorption equilibrium without any further free energy change.

There are two contributions[7] to ΔA_1, mixing of solution with network and deformation of the network. Suppose the network consists of ν chains, each containing Z "statistical" segments of volume βv_0 (hence $V_0=Z\nu\beta v_0$). In the Flory-Huggins polymer solution theory, the entropy of mixing ν polymer molecules (not in a network) with N_s solvent molecules is

$$\Delta S_{mix}=-k\left[(N_s/\beta)\ln\frac{N_s}{N_s+Z\nu\beta}+\nu\ln\frac{Z\nu\beta}{N_s+Z\nu\beta}\right]. \quad (15)$$

A network is essentially a single molecule so that the desired result in the present application follows formally from Eq. (15) on letting $\nu\rightarrow 0$ keeping $Z\nu\beta$ constant (Hermans[7])

$$\Delta S_{mix}=-\frac{N_sk}{\beta}\ln\frac{N_s}{N_s+Z\nu\beta}=-\frac{(V-V_0)k}{v_0\beta}\ln\frac{V-V_0}{V}. \quad (16)$$

As in the Flory-Huggins theory a van Laar "heat" of mixing (actually including an entropy contribution) term is added, so that

$$\Delta A_{mix}=B'V_0\left(\frac{V-V_0}{V}\right)+\frac{(V-V_0)kT}{v_0\beta}\ln\frac{V-V_0}{V}, \quad (17)$$

where B' is a constant. The entropy of deformation of the network we obtain from Wall's theory[7] (Eq. (29) of his paper III) as modified by Flory[7] to take account of the volume dependence of the entropy of cross-

[8] For example, A. Katchalsky, Experientia **5**, 319 (1949); Kuhn, Hargitay, Katchalsky, and Eisenberg, Nature **165**, 514 (1950).

[9] T. L. Hill, J. Chem. Phys. **17**, 762 (1949).

[9a] A. D. McLaren and J. W. Rowen, J. Polymer Sci. **7**, 289 (1951).

[9b] T. L. Hill and J. W. Rowen, J. Polymer Sci. (to be published).

linking. We have

$$\Delta A_{\text{def}} = -T\Delta S_{\text{def}} = \frac{-\nu kT}{\gamma^2}\left(\frac{3}{2}\gamma^2 - \frac{\alpha^2}{2} - \frac{V}{V_0\alpha} + \frac{2\gamma^2}{f}\ln\frac{V}{V_0}\right)$$

$$\alpha \equiv l/l_0, \tag{18}$$

where f is Flory's "functionality" of the cross-links in the network, and the cross-links are assumed to have been formed in the presence of diluent at a volume $V_0\gamma^3$. For large extensions, the Gaussian distribution, on which this equation is based, can be refined, as is well known, but we omit this refinement for the present. Further equations will be restricted to the usual special case $f=4$, $\gamma=1$; the extension of these equations to the general case is trivial. Wall's treatment[7] corresponds formally to the case $\gamma=1$, $f=2$.

Incidentally, in applying Eq. (18) to dry polymer, it is implicit that an additional term representing the virtual incompressibility ($V=V_0$) of the polymer should be present. Boggs[9c] has treated this point explicitly, using the Lennard-Jones and Devonshire theory of liquids.

Then

$$\Delta A_1 = \Delta A_{\text{mix}} + \Delta A_{\text{def}}. \tag{19}$$

Apart from electrostatic effects, the partition function associated with the N adsorbed molecules is (see Eq. (2))

$$Q = B!j^N/[N!(B-N)!], \tag{20}$$

so that

$$\Delta A_2 = -kT[B\ln B - N\ln N - (B-N)\ln(B-N) + N\ln j]. \tag{21}$$

(It would be more correct to write j' here—the partition function for an isolated *uncharged* adsorbed molecule—and include a term $-NkT\ln(j/j')$ in ΔA_3, but the final result is the same.)

There are two cases for which we wish to calculate ΔA_3. Before considering these it is convenient to discuss the thermodynamics applying to both cases. Figure 3(a) shows *schematically* the most general experimental arrangement of interest in the present paper. The solution and fiber are connected by a membrane or porous plug permeable to solution, and an incompressible, inert fluid surrounds but does not penetrate the fiber. P is, for example, the constant atmospheric pressure while p is an adjustable pressure. A_{eq} is the Helmholtz free energy of solution plus fiber, at equilibrium. If we pass to a neighboring equilibrium state

$$dA_{\text{eq}} = -SdT + \tau dl - (p-P)dV$$
$$\tau \equiv (\partial A_{\text{eq}}/\partial l)_{T,V}, \text{ etc.} \tag{22}$$

Alternatively, from

$$A = A_0 + \Delta A_1 + \Delta A_2 + \Delta A_3 \tag{23}$$

[9c] F. W. Boggs (personal communication) and J. Chem. Phys. **20**, 632 (1952).

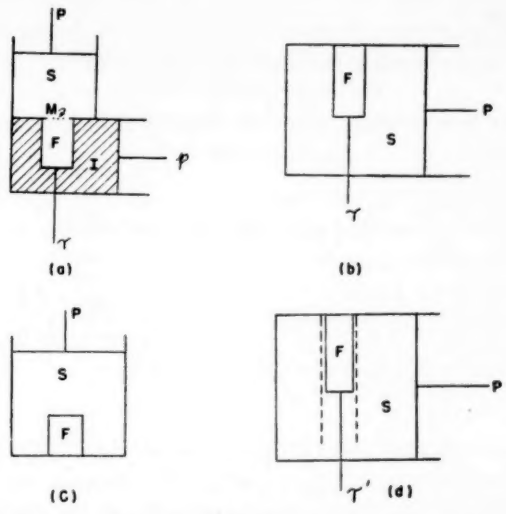

FIG. 3. (a) General schematic experimental arrangement. S=solution, F=fiber, I=inert fluid, M=membrane permeable to solution but not fiber material, P, p=pressures, and τ=tension. (b) Special case with fiber immersed in solution, and no inert fluid. (c) Special case of freely swelling network (fiber). (d) Special case of fiber restricted to constant radius.

we obtain

$$dA_{\text{eq}} = \left(\frac{\partial A}{\partial T}\right)_{V,l,N} dT + \left(\frac{\partial A}{\partial l}\right)_{T,V,N} dl + \left(\frac{\partial A}{\partial V}\right)_{T,l,N} dV + \left(\frac{\partial A}{\partial N}\right)_{T,V,l} dN - \mu dN. \tag{24}$$

The last term must be added in this equilibrium process since the increment in the number of adsorbed molecules, dN, comes from the solution and not from outside the system as in process (2) above. Further, at equilibrium,

$$\mu = \left(\frac{\partial A}{\partial N}\right)_{T,V,l}, \tag{25}$$

so the last two terms in Eq. (24) drop out. Hence, comparing Eqs. (22) and (24),

$$\tau = \left(\frac{\partial A}{\partial l}\right)_{T,V,N}, \quad p-P = \left(\frac{\partial A}{\partial V}\right)_{T,l,N}, \text{ etc.} \tag{26}$$

Let τ_i and p_i' ($i=1, 2, 3$) be the contributions to τ and $p-P$ arising from ΔA_i in Eqs. (23) and (26). Then we find

$$\tau_2 = p_2' = 0 \tag{27}$$

and

$$\tau_1 = \frac{\nu kT}{l_0}\left(\alpha - \frac{1}{\nu\alpha^2}\right) \tag{28}$$

$$p_1' = \frac{kT}{v_0\beta}\left[\frac{1}{Z}\left(\frac{\nu}{2} - \frac{1}{\alpha}\right) - \frac{K}{2}v^2 - v - \ln(1-v)\right], \tag{29}$$

where

$$v \equiv V_0/V \quad \text{and} \quad K \equiv 2B'v_0\beta/kT. \tag{30}$$

We now consider ΔA_3. The Poisson-Boltzmann equation is

$$\nabla^2\psi = -\frac{4\pi}{D_i}[\rho\epsilon + \textstyle\sum_i \epsilon_i c_i(1-v)\exp(-\epsilon_i\psi/kT)] \quad 0 \leqslant r < R \tag{31}$$

$$= -\frac{4\pi}{D}\textstyle\sum_i \epsilon_i c_i \exp(-\epsilon_i\psi/kT) \quad r > R, \tag{32}$$

where r is the perpendicular distance from the axis of the cylinder. D_i and $1-v$ in Eq. (31) take care, approximately, of the effect of the network on the dielectric constant and average local electrolyte concentration inside the cylinder.

We must distinguish two cases here. If $R \gg 1/\kappa$, for example if the cylinder has an essentially macroscopic radius, it is not necessary to make the usual Debye-Hückel linear approximation if a single symmetrical electrolyte is used. If $R \gtrsim 1/\kappa$, one must linearize the Debye-Hückel differential equation in order to solve it.[10]

A. Cylinder of Small Radius

On linearizing, Eqs. (31) and (32) become

$$\nabla^2\psi = -\frac{4\pi\rho\epsilon}{D_i} + a^2\kappa^2\psi \quad 0 \leqslant r < R \tag{33}$$

$$= \kappa^2\psi \quad r > R \tag{34}$$

$$a^2 \equiv D(1-v)/D_i$$

If the continuity of ψ and $D(d\psi/dr)$ at $r=R$ is used, the solution[11] of Eqs. (33) and (34) is

$$\psi(x) = \frac{4\pi\rho\epsilon}{D(1-v)\kappa^2}\left[1 - \frac{K_1(s)I_0(ax)}{I_0(as)K_1(s) + K_0(s)I_1(as)(D_i a/D)}\right] \quad 0 \leqslant x \leqslant s \tag{35}$$

$$= \frac{4\pi\rho\epsilon}{D(1-v)\kappa^2} \cdot \frac{I_1(as)(D_i a/D)K_0(x)}{I_0(as)K_1(s) + K_0(s)I_1(as)(D_i a/D)} \quad x \geqslant s \tag{36}$$

$$x \equiv \kappa r, \quad s \equiv \kappa R,$$

where $I_n(x)$ and $K_n(x)$ are modified Bessel functions of the first and second kinds, respectively. The electrostatic free energy of charging the network at constant T, l, and V is

$$\Delta A_3 = \int_{\lambda=0}^{1}\int_{r=0}^{R} 2\pi r l dr \cdot \rho\epsilon d\lambda \cdot \psi(\epsilon\lambda, r) \tag{37}$$

$$= \frac{2\pi n^{*2}\epsilon^2}{D\kappa^2(V-V_0)} \times \left\{1 - \frac{2I_1(as)K_1(s)}{as[I_0(as)K_1(s) + K_0(s)I_1(as)(D_i a/D)]}\right\}. \tag{38}$$

By using $R=(V/\pi l)^{\frac{1}{2}}$, the definition of a, and making some choice for the function $D_i(v)$, Eq. (38) can be differentiated to give τ_3 and p_3'; but for simplicity we confine ourselves here to the important special case $V \gg V_0$, i.e., we put $v=0$, $D=D_i$, $a=1$. Then

$$\Delta A_3 = \frac{2\pi n^{*2}\epsilon^2}{D\kappa^2 V}[1 - 2I_1(s)K_1(s)], \tag{39}$$

$$\tau_3 = \frac{2\pi\epsilon^2 n^{*2}}{D\kappa^2 Vl}[I_1(s)K_1'(s) + K_1(s)I_1'(s)]s, \tag{40}$$

$$p_3' = \frac{2\pi\epsilon^2 n^{*2}}{D\kappa^2 V^2}\{1 - 2I_1(s)K_1(s) + s[I_1(s)K_1'(s) + K_1(s)I_1'(s)]\}, \tag{41}$$

$$s = \kappa(V/\pi l)^{\frac{1}{2}}.$$

The adsorption isotherm, from Eqs. (9), (21), and (39), is

$$fc = \frac{N}{B-N}\exp\left\{\frac{4\pi\epsilon^2 n^* m}{D\kappa^2 VkT}[1 - 2I_1(s)K_1(s)]\right\} \tag{42}$$

$$f \equiv j\exp(\mu^0/kT),$$

where, it should be remembered, n^* depends on N. It will be noticed that there is the implicit simplification that the extent of adsorption is independent of r. $(R \gtrsim 1/\kappa)$.

Finally, we remark that if we let[12] $\kappa R \to \infty$ in Eqs. (35)–(42), we use

$$K_1(s) \to \left(\frac{\pi}{2s}\right)^{\frac{1}{2}} e^{-s}$$

$$1 - 2I_1(s)K_1(s) \to 1 \tag{43}$$

$$s[I_1(s)K_1'(s) + K_1(s)I_1'(s)] \to 0.$$

[10] See, however, Fuoss, Katchalsky, and Lifson, Proc. Nat. Acad. Sci. **37**, 579 (1951).

[11] T. L. Hill, J. Chem. Phys. **17**, 1125 (1949).

[12] Compare J. J. Hermans and J. Th. G. Overbeeck, Rec. Trav. Chim. **67**, 761 (1948), Appendix I. The electrostatic theory in the present paper is similar to that given by Hermans and Overbeeck, except for geometry (R small) and nonlinearizing the Boltzmann factor (R large). Incidentally, we are investigating two refinements of the Hermans and Overbeeck theory, namely, use of an ellipsoidal model instead of a sphere (to allow following the transition from a sphere to a rod on adding charges) and inclusion of the appropriate Flory-Rehner free energy of mixing terms for a single polymer molecule (P. J. Flory, J. Chem. Phys. **17**, 303 (1949)). See T. L. Hill, J. Chem. Phys. **20**, 1173 (1952).

B. Cylinder of Large Radius (Donnan Equilibrium)

Because of the assumed large radius, edge effects near $r=R$ are negligible in ΔA_3 and hence we can put $\psi=$constant in Eq. (31). Hence (note that D_i drops out)

$$\rho\epsilon+\sum_i \epsilon_i c_i(1-v)\exp(-\epsilon_i\psi/kT)=0. \tag{44}$$

In the linear approximation,

$$\psi=\frac{\rho\epsilon kT}{(1-v)\sum_i \epsilon_i^2 c_i}=\frac{4\pi\rho\epsilon}{D(1-v)\kappa^2} \tag{45}$$

in agreement with Eq. (35) ($x=0$, $s\to\infty$; see Eq. (43)). In the nonlinear case, for a single symmetrical electrolyte[13] (we take, to be specific, $c_2=c_1$, $\epsilon_1=-\epsilon_2=\epsilon$)

$$\psi=\frac{kT}{\epsilon}\sinh^{-1}\frac{\rho}{2c_1(1-v)}. \tag{46}$$

We now calculate ΔA_3 by gradually charging up the n^* charges on the molecular network:

$$\Delta A_3=\int_0^1 n^*\cdot\epsilon d\lambda\cdot\psi(\rho\lambda)=n^*kT\left\{\sinh^{-1}\frac{n^*}{2c_1(V-V_0)}\right.$$
$$\left.-\left[1+\left(\frac{2c_1(V-V_0)}{n^*}\right)^2\right]^{\frac{1}{2}}+\frac{2c_1(V-V_0)}{n^*}\right\}. \tag{47}$$

Then

$$\tau_3=0 \tag{48}$$

$$p_3'=-2c_1kT\left\{1-\left[1+\left(\frac{n^*}{2c_1(V-V_0)}\right)^2\right]^{\frac{1}{2}}\right\} \tag{49}$$

$$fc=\frac{N}{B-N}\exp\left[m\sinh^{-1}\frac{n^*}{2c_1(V-V_0)}\right] \tag{50}$$

$$=\frac{N}{B-N}\exp(m\epsilon\psi/kT). \tag{51}$$

Equation (51) is similar to the Stern equation.[14]

Equations (35)–(42) and Eqs. (46)–(51) of course converge to the same results for $\kappa R\to\infty$ in the former equations and $n^*\to 0$ or $c_1\to\infty$ in the latter ($1-v$ is omitted in Eqs. (39)–(43)).

This completes the formal, approximate solution of the problem of the present section. The interrelations between length, tension, volume, pressure, electrolyte concentration, adsorbate concentration, amount of adsorption, etc., are contained in the above equations. However, we shall discuss further in the present paper only certain important special cases.

Special Cases

(*1*) $p=P$. The case of most interest is perhaps the one shown in Fig. 3(b). The total volume of the system is constant so that l is the only external thermodynamic variable. The volume V of the cylinder plays the role of a parameter with respect to which A_{eq} is minimized at constant T and l. That is,

$$(\partial A_{eq}/\partial V)_{T,l}=0. \tag{52}$$

But from Eq. (22) this is just the condition $p=P$. Then

$$p_1'+p_3'=0. \tag{53}$$

Equation (53) represents the balance between the elastic resistance of the network to expansion (first term in Eq. (29)) on the one hand and the osmotic pressure of the network (last three terms in Eq. (29)) plus the osmotic pressure of the ions[12] (p_3') tending to increase V, on the other. In the more general situation ($p\neq P$), the elastic resistance of the network and $p-P$ are together balanced by the osmotic pressures

$$p-P+(-p_{\text{elastic}})=\Pi_{\text{osm. network}}+\Pi_{\text{osm. ions}},$$

where

$$\Pi_{\text{osm. network}}+p_{\text{elastic}}=p_1'$$
$$\Pi_{\text{osm. ions}}=p_3'.$$

From Eq. (53) we can get, for example, $v(\alpha)$ to be substituted for v in $\tau=\tau_1+\tau_3$, giving $\tau(\alpha)$ (constant N and T).

(*2*) $p=P$, $\tau=0$, $R\gg 1/\kappa$. Unless the cylinder is large, swelling (with $\tau=0$) is not isotropic (Eq. (40)). With $R\gg 1/\kappa$, $\tau=0$ in Eq. (28) gives $\alpha=1/v^{\frac{1}{3}}$ (isotropic swelling). Using this relation to eliminate α in Eq. (53), the resulting equation determines the equilibrium swelling of the free network (Fig. 3(c)), including the electrostatic contribution. If we put $n^*=0$, the result is of course $p_1'=0$ (with $\alpha=1/v^{\frac{1}{3}}$), i.e., free swelling (Fig. 3(c)) in the absence of charges on the network.[7]

(*3*) $p=P$, $R\gg 1/\kappa$, $v\ll 1$, $\epsilon\psi/kT\ll 1$. This is the case of a highly swollen large cylinder which may be under tension (Fig. 3(b)), using the linear approximation. We have from Eqs. (28), (29), and (41)

$$t\equiv\frac{\tau l_0}{\nu kT}=\alpha-\frac{1}{v\alpha^2} \tag{54}$$

$$0=\frac{v}{2}-\frac{1}{\alpha}+\frac{v^2}{2}\cdot Z(1-K)+qv^2 \tag{55}$$

$$q\equiv\frac{2\pi n^{*2}\epsilon^2}{D\kappa^2\nu V_0 kT}=\frac{n^{*2}\epsilon^2}{2\nu V_0\sum_i c_i\epsilon_i^2}.$$

[13] The ion being adsorbed is of course part of the electrolyte hence this simplification (single symmetrical electrolyte) may not be possible in some cases. In ATP adsorption, the concentration of ATP in solution is in general low enough to neglect its contribution as part of the electrolyte (this neglect is of course not necessary when the linear approximation is used).

[14] See E. J. W. Verwey and J. Th. G. Overbeeck, *Theory of the Stability of Lyophobic Colloids* (Elsevier Publishing Company, Amsterdam, Holland, 1948), Eq. (17).

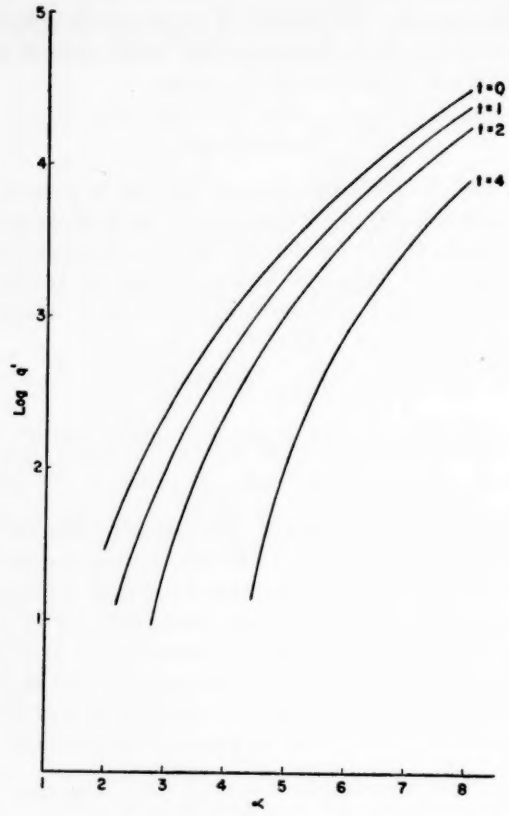

FIG. 4. Relation between q' and α at constant tension, in the special case (3) (Eq. (57)). Equation (56) gives the degree of lateral swelling. The $t=0$ curve is the isotropic swelling case (also gives "rest length").

Usually $v/2$ will be negligible compared with $1/\alpha$ in Eq. (55). Defining

$$\delta^2 \equiv 1/v\alpha, \quad q' \equiv q+\tfrac{1}{2}Z(1-K)$$

($\delta = R/R_0$ is the lateral swelling factor analogous to α (longitudinal)), Eq. (55) can be written

$$\delta^2 = \left[1+\left(1+\frac{16q'}{\alpha}\right)^{\frac{1}{2}}\right]\Big/4. \tag{56}$$

Eliminate δ^2 from Eq. (54) by using Eq. (56), and it is found that

$$\alpha^2(\alpha-t)[\alpha(\alpha-t)-(1/2)] = q'. \tag{57}$$

Equation (57) shows, for example (Fig. 4), how α depends on n^*, the effective number of charges, at constant t and other parameters. A new stretching factor (replacing α) can be defined as $\alpha(q', t)/\alpha(q', 0)$, if desired.

If we put $t=0$ (isotropic swelling), $n^*=0$ and neglect $1/2$ compared to α^2 in Eq. (57),

$$v_1^{5/3} = 1/\tfrac{1}{2}Z(1-K), \tag{58}$$

which is the Flory and Rehner[7] result (using $v_1 = V_0/V_1$ to denote the swelling with $n^*=0$). Comparing with the swelling when $n^*>0$,

$$\left(\frac{v_1}{v}\right)^{5/3} = \frac{q+\frac{1}{2}Z(1-K)}{\frac{1}{2}Z(1-K)}. \tag{59}$$

Put $\sum_i c_i\epsilon_i^2 = 2c_1\epsilon^2$ in q; then

$$q = \frac{(n^*/V_0)^2}{(\nu/V_0)\cdot 4c_1} = \frac{Z}{4c_1v_0\beta x^2}, \tag{60}$$

where there is a charge ϵ, on the average, at every xth segment along the chains. Then

$$\left(\frac{v_1}{v}\right)^{5/3} = 1+\frac{1}{2c_1v_0\beta x^2(1-K)}. \tag{61}$$

As a numerical example, taking water as solvent (to obtain v_0), $K=0.5$, $\beta=1$, $c_1=0.15$M uni-univalent electrolyte, and $x=3$ and 10:

$$\begin{aligned} &x=3: \quad v_1/v=9.432; \quad \alpha/\alpha_1=(v_1/v)^{\frac{1}{2}}=2.113 \\ &x=10: \quad v_1/v=2.531; \quad \alpha/\alpha_1=1.363. \end{aligned} \tag{62}$$

Also,

$$\frac{\epsilon\psi}{kT} = \frac{n^*}{2c_1V} = \frac{v}{2c_1xv_0\beta}. \tag{63}$$

If we take $Z=400$ in this example, Eq. (58) gives $1/v_1 = 15.85$ and

$$\begin{aligned} \frac{\epsilon\psi}{kT} &= 0.412 \quad x=3 \\ &= 0.461 \quad x=10. \end{aligned} \tag{64}$$

As will be seen below, the linear approximation is rather accurate in this case. (Actually, $\epsilon\psi/kT \ll 1$ means roughly $\epsilon\psi/kT < \frac{1}{2}$, to a good approximation.)

(4) $p=P$, $R \gg 1/\kappa$, $v \ll 1$. We do not make the linear approximation here. If we neglect $v/2$ compared to $1/\alpha$ in Eq. (29), and use Eq. (49), we obtain instead of Eq. (56)

$$\delta^4 = \frac{2(1+a)d+a^2b+a[a^2b^2+4d(d+b+ab)]^{\frac{1}{2}}}{2(1+2a)}$$

$$a \equiv \frac{2c_1V_0\alpha}{\nu}, \quad b \equiv \frac{n^{*2}}{4c_1^2V_0^2\alpha^2}, \quad d \equiv \frac{1}{2}\frac{Z(1-K)}{\alpha}. \tag{65}$$

Substitution of δ^2 from Eq. (65) in Eq. (54) gives t (or α) as a function of α (or t), ν/V_0c_1, n^*/V_0c_1 and $Z(1-K)$. In the isotropic swelling case ($t=0$, $\delta=\alpha$), Eq. (65) gives α or v as a function of ν/V_0c_1, n^*/V_0c_1 and $Z(1-K)$, and reduces to Eqs. (58) and (59) as special cases. In the numerical example of Eqs. (62) and (64),

Eqs. (46) and (65) give for comparison

$$x=3: \quad \frac{\alpha}{\alpha_1}=2.096; \quad \epsilon\psi/kT=0.411$$
$$x=10: \quad \frac{\alpha}{\alpha_1}=1.352; \quad \epsilon\psi/kT=0.457. \tag{66}$$

(5) $R=constant$. Suppose there is a rigid membrane, sheath, or other mechanism forcing $R=R^*=$ constant. Then (Fig. 3(d)) Eq. (22) becomes

$$dA_{eq}=-SdT+\tau' dl, \tag{67}$$

where τ' is the tension that would be observed experimentally. In Eq. (24), $dV=\pi R^{*2}dl$ so that

$$\tau'=(\partial A/\partial l)_{T,V,N}+\pi R^{*2}(\partial A/\partial V)_{T,l,N} \tag{68}$$

or

$$\tau'=\tau-\pi R^{*2}(p-P). \tag{69}$$

In using previously derived results for τ and $p-P$ we replace R by R^* and V by $\pi R^{*2}l$ (or v by $1/\alpha\delta^{*2}$, where $\delta^*=R^*/R_0$). An interesting property of Eq. (69) (not found in the case $p=P$) is the occurrence of a phase change in the length-tension curve for appropriate values of the parameters (see Sec. IV). This phase change is related to the splitting of polymer solutions into two phases as observed experimentally in suitable cases and as predicted by the Flory-Huggins theory. Incidentally, a similar phase change is encountered in a model consisting of a bundle of uncross-linked parallel (when extended) molecular chains, immersed in an electrolyte solution, and attached to the two ends of the cylinder containing the bundle. For reasonable values of Z, the values of K leading to a phase change (in both cases above) are of just the order of magnitude deduced by Rowen and Simha[14a] from an analysis of the sorption of water vapor by wool, collagen, and serum albumin, which fact may be of significance in the muscle problem (see Sec. IV). These cases will be discussed in more detail elsewhere[3] (critical constants, effect of charges, etc.).

(6) $\tau=0$, $R\gg 1/\kappa$. Isotropic volume changes under pressure may be observed experimentally using, for example, mercury as the inert nonpenetrating fluid[15] (Fig. 3(a) with $\tau=0$). The equation of state, from Eqs. (29) and (49), is

$$p-P=\frac{\nu kT}{V}\left\{\frac{1}{2}-\left(\frac{V}{V_0}\right)^{\frac{1}{3}}-Z\left[\frac{K}{2}\frac{V_0}{V}+1+\frac{V}{V_0}\ln\left(1-\frac{V_0}{V}\right)\right]\right\}-2c_1kT\left\{1-\left[1+\left(\frac{n^*}{2c_1(V-V_0)}\right)^2\right]^{\frac{1}{2}}\right\}. \tag{70}$$

In the special case $v\ll 1$, and using the linear approximation, Eq. (70) simplifies to

$$p-P=\frac{\nu kT}{V}\left[q'\frac{V_0}{V}-\left(\frac{V}{V_0}\right)^{\frac{1}{3}}\right]. \tag{71}$$

Equations (58) and (59) are special cases ($p=P$) of Eq. (71). The pressure difference necessary, because of charges on the network, to maintain the volume V_1 (Eq. (58)) is

$$p-P=(\nu kT/V_1)\cdot qv_1. \tag{72}$$

IV. FIBROUS PROTEINS

We give here an approximate equilibrium statistical theory of the well-known $\alpha-\beta$ transformation[16–18] based, necessarily, on a rather idealized model. We shall consider below that charges are distributed on the protein and that adsorbed molecules contribute additional charges, but for clarity we give first the theory taking into account hydrogen bonds only. The intrachain hydrogen bonds in the α-structure we shall call "vertical" and the interchain hydrogen bonds in the β-structure "lateral." A given molecular chain is considered in general to have α- and β-units statistically scrambled.[19] This is in formal analogy with the autone discussion of Sec. II, but here the units (see below) are of ordinary molecular size (several amino acid residues) whereas in Sec. II an autone is macromolecular: The hydrogen bonds being discussed here could all be *inside* a single autone; and in the autone theory, a macromolecular unit can have just two lengths (long or short) while here a macromolecular unit (made up of a very large number of α- and β-units) can vary essentially continuously in length.

Cellulose has certain structural features in common with the fibrous proteins and a related treatment of the elasticity of this substance might be given.

We are aware that most length-tension experiments on fibrous proteins are carried out in such a way that there are nonequilibrium effects (e.g., retarded elastic response) superimposed on the equilibrium phenomena. The present theory is strictly applicable in the limit of infinitely slow extension and retraction and in the absence of any irreversible flow. Also, since we do not include S−S cross-linking in the model, the theory is more suitable when applied, for example, to wool fibers treated chemically to eliminate S−S bonds.

Various suggestions about the α-structure have been made in which, for example, each amino acid residue has a hydrogen bond with its two first (nearest) neighbor residues,[17] or with the two second neighbors,[17] third neighbors,[18] or fifth neighbors[18] (in general, xth neigh-

[14a] J. W. Rowen and R. Simha, J. Phys. and Colloid Chem. **53**, 921 (1949).

[15] A. Katchalsky, American Chemical Society meeting, September, 1951. This paper included both experimental and theoretical developments for this case (with $N=0$).

[16] W. T. Astbury, Proc. Roy. Soc. (London) **134B**, 303 (1947).

[17] M. L. Huggins, Chem. Revs. **32**, 195 (1943).

[18] L. Pauling and R. B. Corey, Proc. Nat. Acad. Aci. **37**, 261, 729 (1951).

[19] J. Frenkel, *Kinetic Theory of Liquids* (Oxford University Press, London, England, 1946).

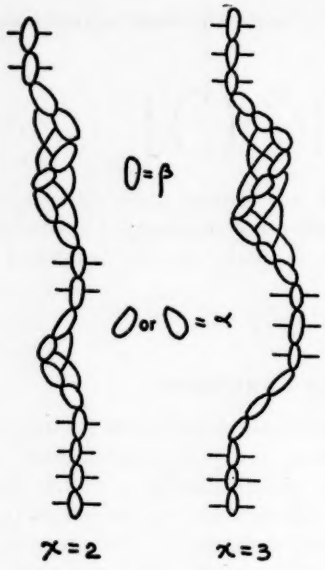

FIG. 5. *Strictly schematic* representation of individual molecular chains to show vertical nearest neighbor interactions between α-units, with $x=2$ and 3. O=one amino acid residue. Horizontal lines from β-units represent possible hydrogen bonds with adjacent chains. Curved lines represent vertical hydrogen bonds.

bors). A third neighbor structure ($x=3$) is believed by Pauling and Corey[18] to be correct. In any case, in order to make the problem tractable, we introduce the simplifying assumption that, in a given chain, amino acid residues occur in groups or units of x, all residues in a unit being α or all β. This reduces the statistical problem to a nearest neighbor interaction problem (Fig. 5).

We retain the notation of Sec. II as far as possible. Suppose we have a sheet of C ($\gg 1$) molecular chains (i.e., each chain has two nearest neighbor chains), each chain containing B/C units, the mean number of units in the α form in each chain being B_α/C. Let $\theta=B_\alpha/B$. Let l_α and l_β be the lengths of α- and β-units, respectively, and let l be the length of the sheet:

$$l=\frac{1}{C}[B_\alpha l_\alpha+(B-B_\alpha)l_\beta] \tag{73a}$$

$$=\frac{B}{C}[l_\alpha+(1-\theta)(l_\beta-l_\alpha)]. \tag{73b}$$

Let $J_\alpha(T)$ and $J_\beta(T)$ be the "internal" partition functions for α and β units (*not* including lateral or vertical interactions between units). Let ω_α be the interaction energy (x hydrogen bonds) between a vertical nearest neighbor pair of α-units.[20] The energy of vertical $\alpha\beta$ and $\beta\beta$ nearest neighbors pairs is taken as zero.[21] Concerning lateral (interchain) interactions, a given unit of one chain has, roughly speaking, a lateral nearest neighbor unit in each of the two nearest neighbor chains. We say "roughly speaking" because, since $l_\alpha \neq l_\beta$, there will not in general be perfect alignment between lateral nearest neighbor units. This complication can be dealt with in special cases, and we treat perhaps the most important example below in detail. For the present, though, we keep the treatment general and assume each unit has two lateral nearest neighbor units as well as two vertical nearest neighbor units. Then we let ω_β be the interaction energy (x hydrogen bonds) between a lateral nearest neighbor pair of β units[20] and we take the energy of lateral $\alpha\beta$ and $\alpha\alpha$ nearest neighbor pairs as zero.[21]

ω_α and ω_β involve x hydrogen bonds each. The magnitudes of ω_α and ω_β will be very sensitive to humidity. In the absence of any water, one would use for each bond the full protein-protein hydrogen bond energy. At the other extreme (the case of interest in muscle), the system is saturated with water and, instead, for each bond, one would use the combination of hydrogen bond energies (protein-protein)+(water-water)−2 (protein-water). This will presumably be a much smaller quantity than (protein-protein). Pauling and Corey[18] suggest 2 kcal/mole. Furthermore, steric interactions (van der Waals attractions and, especially, repulsions) between side chains[18] must be incorporated into the above quantities. J_α and J_β will include any steric effects *within* a unit; ω_α will include steric interactions between vertical nearest neighbor α units[21]; and ω_β will include steric interactions between lateral nearest neighbor β units.[21]

We use the quasi-chemical pair approximation.[22] In a linear system (each element with two nearest neighbor elements; e.g., for a single isolated chain here) the quasi-chemical pair treatment is in fact exact (Ising model). When extended in the usual way[22] to a two-dimensional system, each element with four nearest neighbor elements, the implicit approximation involved can be shown to be that the two (vertical and lateral) linear systems behave independently of each other. This is the approximation we make. A more refined method would be to use larger groups of units, for example, squares of four.[23–26]

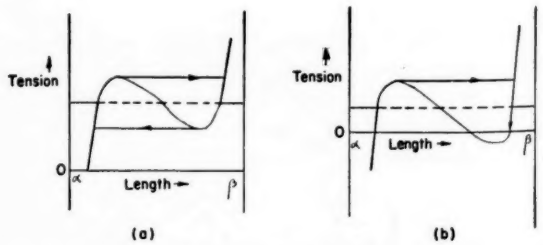

FIG. 6. Schematic illustrative length-tension curves predicted by theory (below critical temperature). Dotted lines=stable equilibrium path. Arrows indicate hysteresis. In case (b), on releasing the tension, the system may become "frozen" in a near-β state.

[20] Actually, ω_α and ω_β (below) can be free energies (including entropy terms) without changing the equations below. See E. A. Guggenheim, Trans. Faraday Soc. 44, 1007 (1948).

[21] This restriction is made for simplicity but is not necessary. See Appendix I.

[22] R. H. Fowler and E. A. Guggenheim, *Statistical Thermodynamics* (The Cambridge University Press, Cambridge, England, 1939).

[23] E. A. Guggenheim, Proc. Roy. Soc. (London) **183A**, 213 (1944); E. A. Guggenheim and M. L. McGlashan, Proc. Roy. Soc. (London) **206A**, 335 (1951); Trans. Faraday Soc. **47**, 929 (1951). We believe the criticism of our paper (see reference 26) by Guggen-

In a given configuration with B_α α units out of a total of B units, let $B_{\alpha\alpha}$ be the number of vertical pairs of nearest neighbor units both α, and similarly for $B_{\alpha\beta}$ and $B_{\beta\beta}$; and let $B_{\alpha\alpha'}$, $B_{\alpha\beta'}$, and $B_{\beta\beta'}$ have the same meaning for lateral pairs. Let $y_\alpha \equiv \exp(-\omega_\alpha/kT)$ and $y_\beta \equiv \exp(-\omega_\beta/kT)$. Then for given B_α (i.e., for a given length—Eq. (73a)) and T, the partition function is[26,27]

$$Q=\sum_{B\alpha\alpha}\sum_{B\alpha\alpha'} q(B_\alpha, B_{\alpha\alpha}, B_{\alpha\alpha'}, T) \tag{74}$$

$$q=\frac{(B-B_\alpha)!B_\alpha!}{B_{\alpha\alpha}!(B-2B_\alpha+B_{\alpha\alpha})![(B_\alpha-B_{\alpha\alpha})!]^2}$$

$$\cdot\frac{(B-B_\alpha)!B_\alpha!}{B_{\alpha\alpha'}!(B-2B_\alpha+B_{\alpha\alpha'})![(B_\alpha-B_{\alpha\alpha'})!]^2}$$

$$\times\frac{B_\alpha!(B-B_\alpha)!}{B!}y_\alpha^{B_{\alpha\alpha}}y_\beta^{B-2B_\alpha+B_{\alpha\alpha'}}$$

$$\times J_\alpha^{B_\alpha}J_\beta^{B-B_\alpha}.$$

We replace the sum in Eq. (74) by its maximum term

$$\left(\frac{\partial \ln q}{\partial B_{\alpha\alpha}}\right)_{B_{\alpha\alpha'},B_\alpha,T}=0;\quad \left(\frac{\partial \ln q}{\partial B_{\alpha\alpha'}}\right)_{B_{\alpha\alpha},B_\alpha,T}=0. \tag{75}$$

Equations (75) give the quasi-chemical relations

$$\frac{4B_{\alpha\alpha}B_{\beta\beta}}{B_{\alpha\beta}^2}=y_\alpha;\quad \frac{4B_{\alpha\alpha'}B_{\beta\beta'}}{B_{\alpha\beta'}}=y_\beta. \tag{76}$$

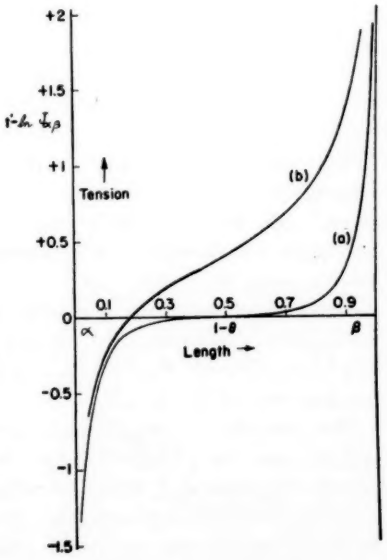

FIG. 7. (a) Critical length-tension curve ($y_\alpha=y_\beta=4$) from Eq. (78). (b) Length-tension curve for $y_\alpha=y_\beta=4$ from Eq. (90), taking into account imperfect lateral alignment.

heim and McGlashan to be incorrect. This point will be discussed elsewhere.

[24] C. N. Yang, J. Chem. Phys. **13**, 66 (1945).
[25] Y. Y. Li, Phys. Rev. **76**, 972 (1949).
[26] T. L. Hill, J. Chem. Phys. **18**, 988 (1950).
[27] T. S. Chang, Proc. Cambridge Phil. Soc. **35**, 265 (1939).

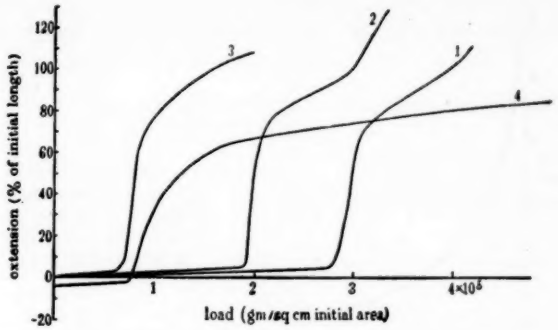

FIG. 8. Length-tension curves (1), (2), and (3), of oriented myosin strips compared with that of "generalized" Cotswold wool (4). (Experiments of H. J. Woods, reproduced from Astbury and Dickinson (see reference 30).)

If Eqs. (76) are used, the tension is

$$\tau=-kT\left(\frac{\partial \ln Q}{\partial l}\right)_T=-kT\frac{dB_\alpha}{dl}\left(\frac{\partial \ln q}{\partial B_\alpha}\right)_{B_{\alpha\alpha},B_{\alpha\alpha'},T}$$

$$=\frac{CkT}{l_\beta-l_\alpha}\ln\left(\frac{B_\alpha}{B-B_\alpha}\right)^3\left(\frac{2B_{\beta\beta}}{B_{\alpha\beta}}\right)^2\left(\frac{B_{\alpha\beta'}}{2B_{\alpha\alpha'}}\right)^2 J_{\alpha\beta} \tag{77}$$

or[22]

$$t'=\ln\frac{\theta}{1-\theta}\left(\frac{\eta_\alpha+1-2\theta}{\eta_\beta-1+2\theta}\right)^2 J_{\alpha\beta}$$

$$t'\equiv\tau(l_\beta-l_\alpha)/CkT \tag{78}$$

$$\eta_\alpha^2\equiv 1-4\theta(1-\theta)(1-y_\alpha);$$

$$\eta_\beta^2\equiv 1-4\theta(1-\theta)(1-y_\beta).$$

If $\omega_\alpha=\omega_\beta=0$ (i.e., $\eta_\alpha=\eta_\beta=1$), Eq. (78) reduces to Eq. (12a) with $c=0$, as it should (Fig. 1).

Curves of t' *versus* $1-\theta$ (linearly related to l through Eq. (73b)) show a familiar type of critical behavior.[28] For negative ω_α and ω_β, at low enough temperatures a loop is obtained (Fig. 6) which corresponds physically (if the stable equilibrium path is followed) to a sudden jump in $1-\theta$ (or l) at constant τ (i.e., a change from predominantly vertical "crystallization" (α) to predominantly lateral "crystallization" (β)). Strong hydrogen bonds (low humidity) favor this type of behavior, which experimentally often manifests itself in metastable states and hysteresis (Fig. 6).[29,30]

[28] Reference 22, p. 432.
[29] T. L. Hill, J. Chem. Phys. **15**, 767 (1947), discusses the relation between "loops" and hysteresis.
[30] For example, H. B. Bull and M. Gutmann, J. Am. Chem. Soc. **66**, 1253 (1944); H. B. Bull, J. Am. Chem. Soc. **67**, 533 (1945); T. Alfrey, *Mechanical Behavior of High Polymers* (Interscience Publishers, Inc., New York, 1948); H. R. Kruyt, Colloid Science, Vol. II (Elsevier Publishing Company, Inc., Amsterdam, Holland, 1949); J. B. Speakman, J. Text. Inst. **24**, 273 (1933); J. B. Speakman and M. C. Hirst, Trans. Faraday Soc. **29**, 148 (1933); H. Burte and G. Halsey, Textile Research J. **17**, 465 (1947); W. T. Astbury and S. Dickinson, Proc. Roy. Soc. (London) **129B**, 307 (1940); J. B. Speakman and L. Peters, J. Text. Inst. **39**, 253 (1948).

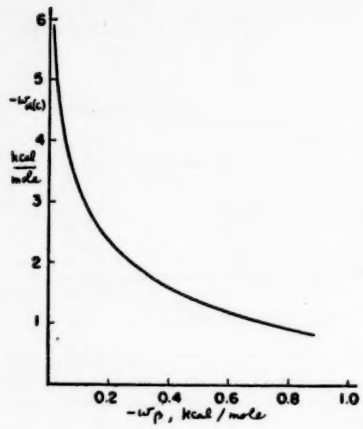

FIG. 9. Value of $-\omega_\alpha(c)$ necessary to give critical length-tension curve at 310°K, as a function of $-\omega_\beta$.

The hysteresis which is observed experimentally may be associated both with this "phase change" and with rate processes (above), as an illustration of Alfrey's[30] general discussion of this question. An explanation of observed hysteresis loops (Speakman[30]) on the equilibrium theory alone certainly does not seem to be possible.

Alfrey[30] and Burte and Halsey[30] have discussed qualitatively the tendency of crystallization or other cooperative phenomena to give *s*-shaped or horizontal length-tension curves (Figs. 6 and 7), as found in the present theory. Experimentally, practically horizontal curves have been observed (Astbury and Dickinson[30]) in myosin (Fig. 8) and rather flat curves are very common in wool (e.g., Fig. 8). (In Fig. 8 ordinate and abscissa are exchanged so "horizontal" becomes "vertical.") One would not expect *completely* horizontal curves in any case because of the non-uniformity of structure in the fiber sample. Astbury and Dickinson[30] verified by x-ray measurements that the $\alpha-\beta$ transition is actually associated with the horizontal region of the length-tension curve. There seems little doubt that a cooperative phenomenon is involved even though non-equilibrium effects complicate matters.

If it should turn out that the $\alpha-\beta$ transition (or other mechanism involving a cooperative phenomenon) is actually operative in the muscle action problem (see below), a horizontal region of easy extensibility could have considerable physiological significance. Thus, for example, a small change in the state of charge on the fiber could produce a relatively great change in length at constant tension (e.g., Eqs. (69) and (102)). A fiber operating between the two ends of a phase change region (Fig. 6) would appear to be an ideally sensitive system in this physiological application.

On returning to Eq. (78), it is easy to see that l' is an odd function of $\theta-\frac{1}{2}$. By equating $dl'/d\theta$ and $d^2l'/d\theta^2$ to zero, the critical point is found to be

$$\theta_c=\tfrac{1}{2} \tag{79a}$$

$$1=\exp(\omega_\alpha/2kT)_c+\exp(\omega_\beta/2kT)_c. \tag{79b}$$

As an example of Eqs. (78) and (79) we show a critical length-tension curve ($y_\alpha=y_\beta=4$) in Fig. 7. In this symmetrical case, taking $T=310°\text{K}$, $-\omega_c=850$ cal/mole. Usually we expect $y_\alpha>y_\beta$ because of the importance of steric repulsion of side chains in the β configuration. The *effective* value of $-\omega_\beta$ is further reduced here because of the neglect of imperfect lateral alignment (see below). Figure 9 shows the value of $-\omega_{\alpha(c)}$ necessary, at 310°K, to give a critical length-tension curve, as a function of $-\omega_\beta$. $-\omega_{\alpha(c)}=\infty$ for $-\omega_\beta=0$, and in this case the quasi-chemical method is exact (lateral alignment doesn't enter). We may conclude that $T=310°\text{K}$ may be above or below the critical temperature in actual cases of interest, depending on steric repulsions, humidity, etc.

Finally, we note that the value of θ (or l) at $\tau=0$ depends on $J_{\alpha\beta}$ (e.g., Figs. 6 and 7). In particular, *s*-shaped length-tension curves (above the critical temperature) may or may not be obtained depending on $J_{\alpha\beta}$ (e.g., Figs. 1 and 7). Also, from Eq. (78), the inflection point is located at

$$\theta=\tfrac{1}{2},\quad l'=\ln\frac{y_\alpha}{y_\beta}J_{\alpha\beta}. \tag{80}$$

When a loop is obtained, this is the value of l' at which the jump in l occurs.

Lateral Alignment in a Special Case

Because $l_\alpha\neq l_\beta$, lateral "nearest neighbor" β-units will not in general be perfectly aligned though the hydrogen bond energy will give extra weight to aligned pairs through an appropriate Boltzmann factor (below). This imperfect alignment will reduce the *effective* value of $-\omega_\beta$ in the treatment above, and will involve structural distortion (so that hydrogen bonds can be formed) analogous to that suggested by Pauling and Corey[18] because of steric hindrance. A further complication of a similar nature, according to the Pauling and Corey structures, would be the transformation of a "pleated sheet" (β) into a double row of α-chains. Lateral hydrogen bonds would be geometrically inhibited in a double row structure, or in a hybrid double row-pleated sheet structure (intermediate θ), resulting in additional distortion and further reduction of the effective value of $-\omega_\beta$ (in fact, making $-\omega_\beta$ a decreasing function of θ).

We consider a simple but, fortunately, important special case in which we treat lateral alignment explicitly (instead of in terms of reduction of the effective $-\omega_\beta$ in the preceding analysis). Even this case leads to rather complicated equations. Suppose $l_\beta=2l_\alpha$ (this is almost the situation in keratin and myosin[18]) and let us ignore structural distortions and the double row-pleated sheet difficulty just mentioned. We use an extension of the quasi-chemical pair method. Vertical interactions are treated as before. The various types,

numbers and energies of lateral pairs are shown in Fig. 10. For reasons similar to those encountered elsewhere,[26] it is not possible to set up a configurational expression leading to the correct quasi-chemical relations if both $\omega_\beta^*\neq 0$ and $\omega_\beta\neq 0$. For simplicity we take $\omega_\beta^*=0$ in the following quasi-chemical analysis.[30a]

We have

$$2B_{\alpha\alpha}'+B_{\alpha\beta}'=2B_\alpha \tag{81}$$

$$B_{\alpha\beta}'+2B_{\beta\beta}^*+4B_{\beta\beta}'=4(B-B_\alpha). \tag{82}$$

In a completely random lateral distribution of B_α α units among B total units, one finds

$$B_{\alpha\beta}'=\frac{4\theta(1-\theta)B}{2-\theta} \qquad B_{\beta\beta}^*=\frac{2(1-\theta)^2B}{2-\theta}$$

$$B_{\alpha\alpha}'=\frac{\theta^2B}{2-\theta} \qquad B_{\beta\beta}'=\frac{(1-\theta)^2B}{2-\theta}. \tag{83}$$

Then

$$(B_{\alpha\beta}'/4)^2/B_{\alpha\alpha}'(B_{\beta\beta}^*/2)=1 \tag{84a}$$

$$(B_{\alpha\beta}'/4)^2/B_{\alpha\alpha}'B_{\beta\beta}'=1. \tag{84b}$$

With $\omega_\beta\neq 0$, Eq. (84b) becomes in the quasi-chemical approximation

$$(B_{\alpha\beta}'/4)^2/B_{\alpha\alpha}'B_{\beta\beta}'=1/y_\beta. \tag{85}$$

Our problem is now to write down, as an approximation, a configurational expression of the usual type[26,27] which leads to Eqs. (84a) and (85) for lateral interactions,

$$(B_{\alpha\beta}/2)^2/B_{\alpha\alpha}B_{\beta\beta}=1/y_\alpha \tag{86}$$

for vertical interactions, and to Eq. (12a) (with $c=0$) when $\omega_\alpha=\omega_\beta=0$. Omitting details, the complete partition function, including the required configurational expression is found to be

$$Q=\sum_{B_{\alpha\alpha}}\sum_{B_{\beta\beta}^*}\sum_{B_{\beta\beta}'} q(B_\alpha, B_{\alpha\alpha}, B_{\beta\beta}^*, B_{\beta\beta}', T), \tag{87}$$

$$q=\frac{(B-B_\alpha)!B_\alpha!}{B_{\alpha\alpha}!(B-2B_\alpha+B_{\alpha\alpha})![(B_\alpha-B_{\alpha\alpha})!]^2}\cdot\left[\frac{(2B-B_\alpha)!}{B_{\alpha\alpha}'![(B_{\alpha\beta}'/4)!]^4[(B_{\beta\beta}^*/2)!]^2(B_{\beta\beta}'!)^2}\right]^{\frac{1}{2}}\times\frac{(B-B_\alpha)!B_\alpha!}{B!}\cdot\frac{(B-B_\alpha)!B!}{(2B-B_\alpha)!}\times y_\alpha^{B\alpha\alpha}y_\beta^{B\beta\beta'}J_\alpha^{B\alpha}J_\beta^{B-B_\alpha}, \tag{88}$$

where $B_{\alpha\alpha}'$ and $B_{\alpha\beta}'$ are given as functions of B, B_α, $B_{\beta\beta}^*$, and $B_{\beta\beta}'$ by Eqs. (81) and (82). To find the maximum value of q we write

$$\frac{\partial \ln q}{\partial B_{\alpha\alpha}}=0; \quad \frac{\partial \ln q}{\partial B_{\beta\beta}^*}=0; \quad \frac{\partial \ln q}{\partial B_{\beta\beta}'}=0. \tag{89}$$

These give, respectively, Eqs. (86), (84a), and (85). From Eqs. (77) and (88),

$$t'=\ln\frac{1-\theta}{\theta}\left[\frac{\eta_\alpha+1-2\theta}{2(1-\theta)}\right]^2\times\left[\frac{16(2-\theta)\theta^3}{(\gamma+2-\theta)(\gamma-2+3\theta)^3}\right]^{\frac{1}{2}}J_{\alpha\beta}, \tag{90}$$

where

$$\gamma^2=(2-\theta)^2-4\theta(1-\theta)(1-y_\beta). \tag{91}$$

Equations (78) and (90) agree, as they should, when $\omega_\beta=0$.

We have not found simple symmetry and critical properties for Eq. (90). However, as an example, the length-tension curve from Eq. (90) for $y_\alpha=y_\beta=4$ is given in Fig. 7. On comparison with the other curve in the figure (Eq. (78)), it is apparent that taking into account imperfect alignment reduces the contribution of lateral $\beta\beta$ interactions to a cooperative $\alpha\rightarrow\beta$ transformation, as expected. In fact, $y_\alpha=4$ and $y_\beta=2.69$ in Eq. (78) give the same value (0.395) of $t'-\ln J_{\alpha\beta}$ at $\theta=\frac{1}{2}$ as Eq. (90) with $y_\alpha=y_\beta=4$. This effect of imperfect lateral alignment will be more pronounced in cases where l_β/l_α is not an integer or simple ratio.

Bragg-Williams Approximation[22]

Simple equations, which may be useful for semi-quantitative purposes, are obtained if we assume a *random* distribution of α- and β-units in order to calculate interaction energies. The equations also follow as a limiting case of the quasi-chemical approximation if we retain only the linear terms in expanding y_α, y_β, and

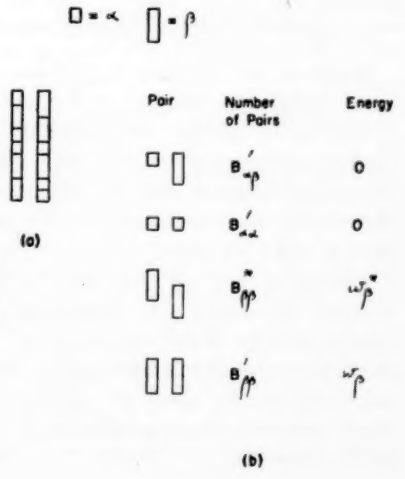

FIG. 10. (a) Parts of two parallel chains with the length of a β-unit equal to the length of two α units. (b) Types, numbers, and energies of different kinds of lateral nearest neighbor pairs.

[30a] As an alternative to considering only the case $\omega_\beta^*=0$ as in the text, one can follow the same procedure as in reference 26. That is, although the quasi-chemical relations obtained will not involve ω_β^* in a completely satisfactory way, we can use the $\omega_\beta^*=0$ quasi-chemical configurational expression of Eq. (88) and still take $\omega_\beta^*\neq 0$. In this case an additional factor $y_\beta^{*B_{\beta\beta}^*}$ is inserted in Eq. (88), where $y_\beta^*\equiv\exp(-\omega_\beta^*/kT)$ (Fig. 10). The only effect on Eq. (90) is to replace y_β in γ by $y_\beta+y_\beta^*-1$.

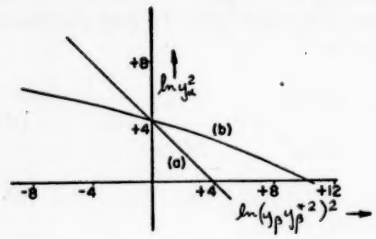

FIG. 11. Relation between y_α and $y_\beta y_\beta^{*2}$ at critical point according to (a) Eq. (94) and (b) Eq. (95). With $\omega_\beta^*=0$ and $y_\beta>1$, a larger value of y_α is needed to obtain a critical length-tension curve if imperfect lateral alignment is taken into account (b).

y_β^*.[30a] The results are

$$t'=\ln\frac{1-\theta}{\theta}y_\alpha{}^{2\theta}y_\beta{}^{2\theta-2}J_{\alpha\beta} \tag{92}$$

instead of Eq. (78), and

$$t'=\ln\frac{1-\theta}{\theta}y_\alpha{}^{2\theta}(y_\beta y_\beta{}^{*2})^{-(3-\theta)(1-\theta)/(2-\theta)^2}J_{\alpha\beta} \tag{93}$$

replacing Eq. (90). Equation (92) has the critical properties

$$\theta_c=\tfrac{1}{2} \tag{94a}$$

$$-\left(\frac{\omega_\alpha}{kT}\right)_c-\left(\frac{\omega_\beta}{kT}\right)_c=2 \tag{94b}$$

and Eq. (93)

$$\ln y_{\alpha(c)}{}^2=\frac{-(\theta_c{}^2+2\theta_c-2)}{3\theta_c{}^2(1-\theta_c)^2} \tag{95a}$$

$$\ln(y_\beta y_\beta{}^{*2})_c{}^2=\frac{(2-\theta_c)^4(2\theta_c-1)}{3\theta_c{}^2(1-\theta_c)^2}. \tag{95b}$$

With $\omega_\beta^*=0$, Fig. 11, based on Eqs. (94) and (95), shows the same effect of taking into account lateral alignment as mentioned above.

With $x=3$, it would be reasonable to take $\omega_\beta^*=\frac{1}{3}\omega_\beta$ (one hydrogen bond). See Appendix II.

Introduction of Charges and Adsorption

Suppose on the sheet of C chains (immersed in solution) there are n charges, and N molecules adsorbed on B^0 sites, as in Sec. III (see also Appendix II). The chains are assumed to stay at a fixed lateral distance from each other during stretching so that the width of the sheet, d, is a constant. We neglect edge effects (i.e., d and l are large).

Following Sec. III, we consider three successive isothermal processes: (1) stretching of the sheet to a length l, with $N=0$ and $\epsilon=0$; (2) adsorbing N discharged molecules from outside the system; and (3) charging up the sheet at constant l. The volume of sheet plus surrounding solution is considered constant in all processes.

Then (see Sec. III)

$$dA_{eq}=-SdT+\tau dl \tag{96}$$

$$A=A_1(l,T)+\Delta A_2(N,T)+\Delta A_3(N,l,T) \tag{97}$$

$$\tau=(\partial A/\partial l)_{N,T} \tag{98}$$

$$\mu=(\partial A/\partial N)_{l,T}, \tag{99}$$

where $A_1=-kT\ln Q$ (Sec. IV) and ΔA_2 is given by Eq. (21).

(1) We calculate ΔA_3 first assuming the sheets are far apart compared to $1/\kappa$ and hence are essentially independent. As a first approximation, if we consider the sheet as a plane of negligible thickness and uniform surface charge density $n^*\epsilon/ld$, and write $\sum_i c_i\epsilon_i{}^2=2c_1\epsilon^2$, we can use the simple theory of the flat double layer (Gouy-Chapman) in Verwey and Overbeek,[31] except for the fact that here electrolyte can be on both sides of the sheet. Making this modification, the electric potential at the sheet is

$$\psi_0(\lambda)=\frac{2kT}{\epsilon}\sinh^{-1}\frac{\kappa n^*\lambda}{8ldc_1} \tag{100}$$

and

$$\Delta A_3=\int_0^1\psi_0(\lambda)n^*\epsilon d\lambda$$

$$=2n^*kT\left\{\sinh^{-1}\frac{\kappa n^*}{8ldc_1}-\left[1+\left(\frac{8ldc_1}{\kappa n^*}\right)^2\right]^{\frac{1}{2}}+\frac{8ldc_1}{\kappa n^*}\right\}, \tag{101}$$

which is of the same form as Eq. (47) for a uniform three-dimensional charge density with penetrating electrolyte. Then, from Eqs. (97)–(99),

$$\tau=\tau_1+\frac{16c_1dkT}{\kappa}\left\{1-\left[1+\left(\frac{\kappa n^*}{8ldc_1}\right)^2\right]^{\frac{1}{2}}\right\} \tag{102}$$

$$fc=\frac{N}{B^0-N}\exp\left(2m\sinh^{-1}\frac{\kappa n^*}{8ldc_1}\right) \tag{103}$$

$$=\frac{N}{B^0-N}\exp\left[\frac{m\epsilon\psi_0(1)}{kT}\right], \tag{104}$$

where τ_1 is given by Eqs. (78), (90), (92), or (93). τ_3, the electrostatic part of τ in Eq. (102), is negative because of the repulsion between charges (τ_3 varies as $-l^{-2}$ at constant n^* in the linear approximation) and has the effect of lowering the critical temperatures (i.e., decreasing the cooperative effect) discussed above in connection with τ_1 alone.

(2) For a system of many parallel sheets close together (and a fixed distance apart) an analogous treat-

[31] Reference 14, p. 25.

ment can in principle be given based on Eqs. (32) and (34) of Verwey and Overbeeck[14] (properly modified as in (1)). Instead, for this case, we use the much simpler but reasonable approach of assuming that the sheets of length l and *total* number of chains C occupy (with solution) a cylinder of radius R (a constant)$\gg 1/\kappa$, and that the n^* charges are distributed with uniform volume density throughout the cylinder (as in Sec. III). Then the volume of the cylinder is $V=\pi R^2 l$ and let V_0/V be the volume fraction of the cylinder occupied by protein, where V_0 is a constant. The arrangement is as in Fig. 3(d), with the total volume of the system constant. Equations (97)–(99) apply here with ΔA_3 given by Eq. (47) (recalling $V=\pi R^2 l$, $R=$constant). Then (compare Eq. (69)

$$\tau=\tau_1+2c_1\pi R^2 kT\left\{1-\left[1+\left(\frac{n^*}{2c_1(V-V_0)}\right)^2\right]^{\frac{1}{2}}\right\} \quad (105)$$

$$fc=\frac{N}{B^0-N}\exp\left[m\sinh^{-1}\frac{n^*}{2c_1(V-V_0)}\right]. \quad (106)$$

These equations are very similar to Eqs. (102) and (103).

Muscle Contraction

Pauling and Corey[32] have indicated how the $\beta\rightarrow\alpha$ transformation can be consistent with x-ray results[16] on contracting muscle. On the other hand, Astbury[16] considers that both relaxed and contracted muscle are in the α-form. We merely remark here that if contraction does take place by an *additional* coiling up of Astbury's α-chains, this model could be included in Sec. III, each "molecular chain" of the network representing one or a bundle of α-chains (see also the "parallel chain" model, Sec. III(5)). A more general theory (now being investigated) would use the network configurational elasticity at small extensions and gradually involve the $\alpha\rightarrow\beta$ transformation within individual "chains" at larger extensions. We may mention that on purely *configurational* grounds it is very much "easier" to extend a network of coiled polymer molecules than it is to extend "$\alpha-\beta$" chains; but an $\alpha-\beta$ phase change can reverse this.

ACKNOWLEDGMENT

The author is greatly indebted to Dr. M. F. Morales for very many stimulating and informative discussions, and has had the benefit of helpful suggestions by Drs. K. Laki, P. J. Flory, and J. W. Rowen.

APPENDIX I

If we write

$$\omega_\alpha=\omega_{\alpha\alpha}+\omega_{\beta\beta}-2\omega_{\alpha\beta},$$

$$\omega_\beta=\omega_{\alpha\alpha'}+\omega_{\beta\beta'}-2\omega_{\alpha\beta'},$$

with obvious notation (formerly $\omega_\alpha=\omega_{\alpha\alpha}$, $\omega_\beta=\omega_{\beta\beta'}$), and modify Eq. (74) accordingly, Eq. (77) becomes

$$\tau=\frac{CkT}{l_\beta-l_\alpha}\ln\left(\frac{B_\alpha}{B-B_\alpha}\right)^3\left(\frac{2B_{\beta\beta}}{B_{\alpha\beta}}\right)^2\left(\frac{B_{\alpha\beta'}}{2B_{\alpha\alpha'}}\right)^2 J_{\alpha\beta}\left(\frac{y_{\alpha\beta}y_{\alpha\alpha'}}{y_{\beta\beta}y_{\alpha\beta'}}\right)^2. \quad (107)$$

This tension differs from Eq. (77), formally, only by a constant, hence the critical properties are the same in the two cases. The well-known adsorption problem[22] on a square lattice with $\omega_\alpha=\omega_{\alpha\alpha}=\omega_\beta=\omega_{\alpha\alpha'}$ is essentially a special case.

APPENDIX II

The remarks of Pauling and Corey[18] and Pryor[33] have suggested the following illustrative model as an alternative to electrostatic models. Consider the "lateral alignment" case above with $x=3$ (ω_α and ω_β refer to three hydrogen bonds each) and $\omega_\beta^*=\frac{1}{3}\omega_\beta$ (one hydrogen bond). Suppose there is a substance in solution which can form a hydrogen bond (i.e., be adsorbed) with any of the six $-C=O$ or $-N-H$ groups of a β-unit. When such a bond (or bonds) is made with one (or both) of the two groups of a potential $\beta\beta$ lateral hydrogen bond between chains, the latter bond cannot be formed. This effect therefore tends to weaken the β-structure. However, there is an associated configurational effect favoring the β-structure: the more β-units, the greater the number of absorption sites (compare Sec. II).

We use the Bragg-Williams approximation for simplicity. If there are B_α α units, and N molecules adsorbed (on 6 $(B-B_\alpha)$ sites), the probability a given site is occupied by an adsorbed molecule is $N/6(B-B_\alpha)$. Consider a given $\beta\beta$ hydrogen bond when $N=0$. With N molecules adsorbed, the probability this $\beta\beta$ bond has not yet been destroyed is $\{1-[N/6(B-B_\alpha)]\}^2$. The partition function is then (see Sec. IV)

$$Q(l,T)=\frac{B!}{B_\alpha!(B-B_\alpha)!}\cdot\frac{[6(B-B_\alpha)]!j^N}{N![6(B-B_\alpha)-N]!}\times y_\alpha{}^{B\alpha\alpha}y_\beta{}^{W_1}J_\alpha{}^{B\alpha}J_\beta{}^{B-B_\alpha} \quad (108)$$

$$W_1=(B_{\beta\beta'}+\tfrac{1}{3}B_{\beta\beta^*})\left[1-\frac{N}{6(B-B_\alpha)}\right]^2$$

$$B_{\alpha\alpha}=B_\alpha{}^2/B$$

$$B_{\beta\beta'}=(B-B_\alpha)^2/(2B-B_\alpha)$$

$$B_{\beta\beta^*}=2(B-B_\alpha)^2/(2B-B_\alpha)$$

and

$$\tau=\frac{CkT}{l_\beta-l_\alpha}\ln\frac{1-\theta}{\theta}\left[\frac{1-\theta-(N/6B)}{1-\theta}\right]^6 y_\alpha{}^{2\theta}y_\beta{}^{W_2}J_{\alpha\beta} \quad (109)$$

$$W_2=-\frac{5}{3}\frac{[1-\theta-(N/6B)][3-\theta+(N/6B)]}{(2-\theta)^2}$$

$$fc=\frac{N/6B}{1-\theta-(N/6B)}y_\beta{}^{\{5[1-\theta-(N/6B)]/9(2-\theta)\}}. \quad (110)$$

The y_β factor in Eq. (110) reduces the amount of adsorption for a given c, because of the effective "repulsion" of adsorbed molecules associated with breaking $\beta\beta$ bonds. The significance of Eq. (109) is seen from

$$B\left(\frac{\partial t'}{\partial N}\right)_l=-\frac{1}{1-\theta-(N/6B)}+\frac{5}{9}\frac{[1+(N/6B)]}{(2-\theta)^2}\ln y_\beta. \quad (111)$$

Thus, increasing the number of adsorbed molecules at constant l tends to cause an increase in tension (or a contraction at constant tension) because of the $\beta\beta$ bond breaking effect (second term on right) but the configurational effect (first term on right) is in the opposite direction (lengthening at constant tension increases the number of β-units and therefore adsorption sites). Which term in Eq. (111) predominates depends on the particular case.

Electric charges (as determined by pH, for example) can be introduced here as before, in accordance with the suggestion of Pauling and Corey.[18]

[32] L. Pauling and R. B. Corey, Nature **168**, 550 (1951).

[33] M. G. M. Pryor, *Progress in Biophysics*, edited by J. A. V Butler and J. T. Randall (Butterworth-Springer, Ltd., 1950), Vol. I.

THE JOURNAL OF CHEMICAL PHYSICS VOLUME 20, NUMBER 8 AUGUST, 1952

The Quantum-Mechanical Partition Function

H. S. GREEN
University of Adelaide, South Australia
(Received February 5, 1952)

An exact evaluation is attempted of the quantum-mechanical partition function for an assembly of similar particles with central interaction. Quantum-mechanical analogs of the classical cluster integrals are derived and evaluated as far as required to determine the virial coefficients. It is shown that the results are particularly well adapted for computation at very low temperatures.

1. INTRODUCTION

THE fundamental problem of quantum statistical mechanics is the evaluation of the partition function

$$Q=\sum_S \exp(-\beta E_S), \tag{1}$$

where $\beta=1/(kT)$, T is the absolute temperature, and E_S is the energy of the system considered in a state S. The summation is over all states, so that at first sight it might appear that one had to determine all the energy levels E_S, defined as the eigenvalues of the Hamiltonian operator H:

$$H\Psi_S(x)=E_S\Psi_S(x), \tag{2}$$

together with the degeneracy of each level. For systems of any degree of complexity, this is an obviously impracticable task.

The difficulty can, however, be avoided if the density matrix, given under conditions of thermodynamical equilibrium by

$$\rho(x, x_0)=\sum_S \exp(-\beta E_S)\Psi_S(x)\Psi_S(x_0) \tag{3}$$

is known. For, assuming that the wave functions $\Psi_S(x)$ are normalized, one will have, instead of (1),

$$Q=\int \rho(x, x)dx. \tag{4}$$

To determine ρ, one has, on differentiating (3) with respect to β, Bloch's well-known equation

$$\partial\rho/\partial\beta=-\sum_S \exp(-\beta E_S)E_S\Psi_S(x)\Psi_S(x_0)=-H\rho; \tag{5}$$

this has to be supplemented by the boundary condition

$$\rho=\sum_S\Psi_S(x)\Psi_S(x_0)=\delta(x-x_0) \quad \text{when} \quad \beta=0. \tag{6}$$

In this paper, a method of solution of Eq. (5) will be given for a system of interacting particles. The total potential energy $\Phi(x)$ of the system is assumed to be a function of the position vectors $x^{(1)}, x^{(2)}, \cdots, x^{(N)}$ of the particles; the Hamiltonian operator is then

$$H=-\tfrac{1}{2}[(\partial^2/\partial x^{(1)2})+\cdots+(\partial^2/\partial x^{(N)2})]+\Phi(x), \tag{7}$$

if units are chosen so that Planck's constant and the molecular mass are both unity.

The idea of using Bloch's equation in this connection has been used by various authors, in particular by Uhlenbeck and Beth (1936, 1937)[1] to determine quantum-mechanical corrections to the virial coefficients. Their method was, however, based on an expansion in powers of Planck's constant, which fails at low temperatures. In a recent paper (Green, 1951[2]) the author noticed that a "perturbation" expansion appeared to be more suitable in the low temperature range, and, starting from an equation due to Wigner (1932),[3] derived the first two terms in such an expansion. Bloch's equation has a decided advantage over Wigner's, so that it is now possible to evaluate the general term in the perturbation series and to sum the series. The result is more tractable than that obtained recently by Goldberger and Adams (1952)[4]; these authors indeed obtained an expression for the general term of the series for the density matrix, but in an operational form not easy to evaluate. It can, however, be seen that the expression which they obtain for the "diagonal element" $\rho(x, x)$ of the density matrix is equivalent to that which one obtains on setting $x_0=x$ in the more complicated (23) of the two forms of the density matrix given below.

In the present work, the analysis is carried far enough to evaluate, for an arbitrary potential function, the coefficients in Mayer's series

$$p=\beta^{-1}\sum b_m z^m,$$

which gives the pressure as a function of the activity z. From these the virial coefficients are easily determined in the usual way.

The values of a number of definite integrals are required in the course of the work; these are derived in a short appendix.

2. SOLUTION OF THE BLOCH EQUATIONS

For brevity, in this section $\int dx$ and $\int d\xi$ will indicate integrations with respect to all the coordinates $x^{(1)}\cdots x^{(N)}$ and velocities $\xi^{(1)}\cdots\xi^{(N)}$, respectively; and expressions such as ξ^2 and $x\cdot\xi$ will represent $\xi^{(1)2}+\cdots+\xi^{(N)2}$ and $x^{(1)}\cdot\xi^{(1)}+\cdots+x^{(N)}\cdot\xi^{(N)}$, respectively.

It will be supposed that the potential energy $\Phi(x)$

[1] G. E. Uhlenbeck and E. Beth, Physica **3**, 729 (1936). G. E. Uhlenbeck and E. Beth, Physica **4**, 915 (1937).
[2] H. S. Green, J. Chem. Phys. **19**, 955 (1951).
[3] E. P. Wigner, Phys. Rev. **40**, 749 (1932).
[4] M. L. Goldberger and E. N. Adams, J. Chem. Phys. **20**, 240 (1952).

becomes very large or infinite when any of the N particles lie outside a certain volume V, in which the particles are then effectively contained. As a consequence, $\rho(x, x_0)$ will tend to zero when any of the coordinates $x^{(i)}$ or $x_0{}^{(i)}$ passes outside this volume, and the Fourier transform

$$\bar{\rho}(\xi, x_0)=\int dx e^{ix\cdot\xi}\rho(x, x_0) \tag{8}$$

will exist. On account of (6)

$$\bar{\rho}=\exp(i\xi\cdot x_0) \quad \text{when} \quad \beta=0. \tag{9}$$

It follows from (5) and (7) that $\bar{\rho}$ satisfies

$$[\partial\bar{\rho}(\xi)/\partial\bar{\beta}]=-\tfrac{1}{2}\xi^2\bar{\rho}(\xi)+\int dx\Phi(x)\int d\xi_1$$

$$\times\exp\{ix\cdot(\xi-\xi_1)\}\bar{\rho}(\xi_1)/(2\pi)^{3N}. \tag{10}$$

Now let $\bar{\rho}$ be regarded as a function of β, and define the Laplace transform

$$\sigma(E)=\int_0^\infty d\beta e^{-\beta E}\bar{\rho}(\beta). \tag{11}$$

Using (9) one has

$$\int_0^\infty d\beta e^{-\beta E}(\partial\bar{\rho}/\partial\beta)=-\exp(ix_0\cdot\xi)+E\sigma;$$

so (10) gives

$$(E+\tfrac{1}{2}\xi^2)\sigma(\xi)=\exp(i\xi\cdot x_0)-\int dx\Phi(x)d\xi_1$$

$$\times\exp\{ix\cdot(\xi-\xi_1)\}\sigma(\xi_1)(2\pi)^{3N}. \tag{12}$$

The last equation is readily solved by an iterative procedure; if

$$L(x)=\int d\xi\,\exp ix\cdot\xi/\{(2\pi)^{3N}(E+\tfrac{1}{2}\xi^2)\}, \tag{13}$$

then

$$\sigma(\xi)=\frac{\exp(ix_0\cdot\xi)}{E+\frac{1}{2}\xi^2}-\int dx_1L(x_0-x_1)\frac{\exp(ix_1\cdot\xi)}{E+\frac{1}{2}\xi^2}+\cdots. \tag{14}$$

Thus

$$=\frac{1}{2\pi i}\int_{c-i\infty}^{c+i\infty}dEe^{\beta E}\frac{1}{(2\pi)^{3N}}\int d\xi e^{-ix\cdot\xi}\sigma$$

$$=\frac{1}{2\pi i}\int dEe^{\beta E}\Big\{L(x_0-x)-\int dx_1L(x_0-x_1)$$

$$\times\Phi(x_1)L(x_1-x)+\cdots\Big\}, \tag{15}$$

where the kth term is

$$\rho_k(x, x_0)=(2\pi i)^{-1}\int dEe^{\beta E}\int\prod_{l=1}^{k}\{-dx_l\Phi(x_l)$$

$$\times L(x_l-x_{l-1})\}L(x_k-x). \tag{16}$$

The $3N$-fold integral (13) is evaluated in the appendix, where it is shown that, for an odd value $2M+1$ of N,

$$L(x)=\left(\frac{1}{2\pi R}\frac{d}{dR}\right)^{3M}\frac{\exp-[R(2E)^{\frac{1}{2}}]}{2\pi R}, \quad R=(x^2)^{\frac{1}{2}}, \tag{17}$$

and in general L can be expressed in terms of a Bessel function of imaginary argument and order $\frac{1}{2}(3N-2)$. There is obviously no restriction in supposing the number of particles to be odd, so for simplicity that will be done. The next step is then the evaluation of the inverse Laplace transform in (16). Let

$$s_l=\{(x_l-x_{l-1})^2\}^{\frac{1}{2}}; \tag{18}$$

then, as shown in the appendix,

$$(2\pi i)^{-1}\int_{c-i\infty}^{c+i\infty}dEe^{\beta E}\exp-[(2E)^{\frac{1}{2}}\sum_{l=1}^{k+1}s_l]$$

$$=\frac{2\pi\sum s_l}{(2\pi\beta)^{\frac{1}{2}}}\exp-\frac{(\sum s_l)^2}{2\beta}. \tag{19}$$

Hence, substituting (17) into (16), one obtains*

$$\rho_k(x, x_0)=\int\prod_{l=1}^{k}\{-dx_l\Phi(x_l)\}\prod_{l=1}^{k+1}\left(\frac{1}{2\pi s_l}\frac{\partial}{\partial s_l}\right)^{3M}$$

$$\times\frac{(\sum 2\pi s_l)\exp-(\sum s_l)^2/2\beta}{(2\pi\beta)^{\frac{1}{2}}(\prod 2\pi s_l)}, \tag{20}$$

where, one the right-hand side, the x_{k+1} in s_{k+1} is identified with x. This is evidently the simplest result of general validity which can be obtained without knowledge of the structure of the potential energy function Φ. A somewhat more complicated formula is useful in subsequent calculations; this is obtained by substituting in (20) an identity which is also proved in the appendix, namely,

$$\frac{(\sum 2\pi s_l)\exp-(\sum s_l)^2/2\beta}{(2\pi\beta)^{\frac{1}{2}}(\prod 2\pi s_l)}$$

$$=\beta^k\int dv_1\cdots\int dv_k\prod_{l=1}^{k+1}\frac{\exp\{-s_l^2/2\beta(v_l-v_{l-1})\}}{\{2\pi\beta(v_l-v_{l-1})\}^{\frac{1}{2}}}, \tag{21}$$

which holds when the integrations are carried out sub-

* The differential operators $(2\pi s_l)^{-1}\partial/\partial s_l$ all commute, so the following expression is quite unambiguous.

ject to the restriction

$$0=v_0\leqq v_1\leqq\cdots\leqq v_k\leqq v_{k+1}=1. \tag{22}$$

When this is substituted into (20), one has finally

$$\rho=\sum_{k=0}^{\infty}\rho_k,$$

$$\rho_\kappa(x,x_0)=\int^k\prod_{l=1}^{k}\{-\beta dx_l\Phi(x_l)\}\int dv_1\cdots$$

$$\times\int dv_k\prod_{l=1}^{k+1}\frac{\exp\{-(x_l-x_{l-1})^2/2\beta(v_l-v_{l-1})\}}{\{2\pi\beta(v_l-v_{l-1})\}^{3N/2}}. \tag{23}$$

3. REDUCTION OF THE DENSITY MATRIX

Now it will be supposed that $\Phi(x)$ has the form

$$\Phi(x)=\sum_{j=1}^{N}\sum_{i=1}^{j}\phi(x^{(j)}-x^{(i)})+\sum_{i=1}^{N}\chi(x^{(i)}), \tag{24}$$

where the first term represents the mutual interaction of the particles, and the second term the high potential barrier which prevents the particles from penetrating beyond the confines of the volume V. As $\chi(x^{(i)})$ vanishes within this volume, it will be neglected on the understanding that space-like integrals are limited to the interior of the volume. It should be noticed further that $\phi(r)$ must not be more singular than r^{-2} at $r=0$; otherwise there is a lack of definition of the Hamiltonian operator (7).

On substituting (24) in (23), it is convenient to use the identity

$$\prod_{l=1}^{k}\phi(x_l)=(k!)^{-1}\sum\nolimits_{\text{perm}}\prod_{l=1}^{k}\phi(x_l), \tag{25}$$

where $\sum_{\text{perm}}$ indicates the sum of all permutations of the suffixes $1\cdots k$ attached to the coordinates. The typical term in the expansion of the product is then

$$T_k{}^{(ab)\cdots(yz)}=(k!)^{-1}\sum\nolimits_{\text{perm}}\phi(r_1{}^{(ab)})\cdots\phi(r_k{}^{(yz)}), \tag{26}$$

and

$$r_l{}^{(ij)}=x_l{}^{(j)}-x_l{}^{(i)},$$

$$\rho_k(x,x_0)=(\sum_{b}^{N}\sum_{a}^{b})\cdots(\sum_{z}^{N}\sum_{y}^{z})I_{k(N)}{}^{(ab)\cdots(yz)},$$

$$I_{k(N)}{}^{(ab)\cdots(yz)}=\int^k\prod_{l=1}^{k}(-\beta dx_l)T_k{}^{(ab)\cdots(yz)}\int dv_1\cdots$$

$$\times\int dv_k\prod_{l=1}^{k+1}\frac{\exp\{-(x_l-x_{l-1})^2/2\beta(v_l-v_{l-1})\}}{\{2\pi\beta(v_l-v_{l-1})\}^{3N/2}}. \tag{27}$$

The integrations with respect to the coordinates $x^{(\alpha)}$ not included among the $x^{(a)}, x^{(b)}, \cdots, x^{(y)}, x^{(z)}$ can be performed immediately. For, if

$$e(x,v)=(2\pi\beta v)^{-\frac{3}{2}}\exp(-x^2/2\beta v),$$

$$\int e(x_l{}^{(\alpha)}-x_m{}^{(\alpha)},\quad v_l-v_m)e(x_m{}^{(\alpha)}-x_n{}^{(\alpha)},$$

$$v_m-v_n)dx_m{}^{(\alpha)}=e(x_l{}^{(\alpha)}-x_n{}^{(\alpha)},\quad v_l-v_n). \tag{28}$$

So the result is

$$I_{k(N)}{}^{(ab)\cdots(yz)}=I_{k(n)}{}^{(ab)\cdots(yz)}\prod_{\alpha}e(x^{(\alpha)}-x_0{}^{(\alpha)},1), \tag{29}$$

where n is the number of different coordinates among $x^{(a)}\cdots x^{(z)}$. If one writes

$$I_{0(1)}{}^{(\alpha)}=e(x^{(\alpha)}-x_0{}^{(\alpha)},1)$$

$$=(2\pi\beta)^{-\frac{3}{2}}\exp-(x^\alpha-x_0{}^\alpha)^2/2\pi\beta, \tag{30}$$

this result may be written in the form

$$I_{k(N)}{}^{(ab)\cdots(yz)}=I_{k(n)}{}^{(ab)\cdots(yz)}\prod_{\alpha}I_{0(1)}{}^{(\alpha)} \tag{31}$$

where each superfix $1\cdots N$ makes at least one appearance.

It will now be supposed that the pairs of associated coordinates $x^{(a)}$ and $x^{(b)}$, $x^{(c)}$ and $x^{(d)}$, etc., separate into two groups, each of which contains no coordinate in common with the other. If there are m different coordinates and q pairs in the first group, it may be shown that

$$k!I_{k(n)}{}^{(ab)\cdots(yz)}=q!I_{q(m)}{}^{(ab)\cdots(yh)}(k-q)!$$

$$\times I_{k-q(n-m)}{}^{(ij)\cdots(yz)}. \tag{32}$$

For, from (26) one has

$$k!T_k{}^{(ab)\cdots(yz)}=\sum\nolimits_{\text{part}}q!T_q{}^{(ab)\cdots(yh)}(k-q)!$$

$$\times T_{k-q}{}^{(ij)\cdots(yz)}, \tag{33}$$

where $\sum_{\text{part}}$ indicates the sum of all partitions of the suffixes $1\cdots k$ among the two groups of coordinates. By using Eq. (28), one may reduce the integral $I_{k(n)}{}^{(ab)\cdots(yz)}$ to the form

$$(k!)^{-1}\int dv_1\cdots\int dv_k\sum\nolimits_{\text{part}}q!$$

$$\times J_{q(m)}{}^{(ab)\cdots(yh)}(v)(k-q)!J_{k-q(n-m)}{}^{(ij)\cdots(yz)}(v), \tag{34}$$

where $J_{q(m)}{}^{(ab)\cdots(yh)}(v)$ is an integral similar to $I_{q(m)}{}^{(ab)\cdots(yh)}$, as defined by (28), except that the integrations with respect to the v_l are omitted. The $\sum_{\text{part}}$ now operates on the suffixes attached to the v's contained in $J_{q(m)}$ and $J_{k-q(n-m)}$. At this stage, the v's continue to satisfy (22); but if, in each term of the summation in (34), one interchanges the suffixes under the signs of integration so that $J_{q(m)}$ is always a function of $v_1\cdots v_q$, and $J_{k-q(n-m)}$ of $v_{q+1}\cdots v_k$, the condi-

tion (22) no longer holds: Instead, one has

$$\begin{aligned} 0=v_0\leqq v_1\leqq\cdots\leqq v_q\leqq v_{k+1}=1 \\ 0=v_0\leqq v_{q+1}\leqq\cdots\leqq v_k\leqq v_{k+1}=1, \end{aligned} \tag{35}$$

together with various other inequalities between v's in the two groups, which vary from term to term of the summation. However, the effect of the summation is to remove these latter restrictions by extending the ranges of integration to all values of the v's which satisfy (35). The result (32) is thereby established.

A device will now be introduced similar to that employed by Mayer (1937, 1938)[5] in his theory of condensation.[5] The integral $I_{k(n)}{}^{(ab)\cdots(yz)}$ is associated with a configuration of n particles, situated at the points $x^{(a)}$, $x^{(b)}$, etc., the k pairs $x^{(a)}$ and $x^{(b)}$, $x^{(c)}$ and $x^{(d)}$, etc., being joined by "bonds." A configuration completely connected by these bonds is called a "cluster." As a limiting case, the expression (30) may be associated with a "cluster" containing only one molecule, at $x^{(a)}$.

By repeated application of (30), $I_{k(n)}{}^{(ab)\cdots(yz)}$ may be expressed in terms of the integrals associated with the various clusters of particles into which the original configuration of n particles resolves. If there are ν clusters, containing $w_1, w_2, \cdots, w_\nu$ particles and $q_1, q_2, \cdots, q_\nu$ bonds, respectively, the product of the $I_{q(w)}$'s is divided by the number of partitions $[k!/(q_1!q_2!\cdots q!)]$ of the k bonds among the clusters. This divisor is, however, canceled, on insertion of $I_{k(N)}$ in the expression (27) for ρ_k, by an identical factor obtained by collecting equal terms under the multiple summation. One therefore obtains finally

$$\rho_k(x, x_0)=\sum{}^{(k)}\prod_{q(w)} I_{q(w)}, \tag{36}$$

where $\sum^{(k)}$ indicates the sum of all different products obtained by distributing the k bonds among the N particles. Configurations in which two or more bonds connect the same pair of particles are admissible.

4. THE PARTITION FUNCTION

It should be observed at this stage that the result (36) is strictly correct only for ideal assemblies satisfying classical statistics. This is a consequence of the supposition, embodied in the boundary condition (6), that

$$\sum_S \Psi_S(x)\Psi_S(x_0)=\delta(x-x_0), \tag{37}$$

which would not be true if only the symmetrized wave functions required by quantum statistics were included in the summation. There is, however, a simple way of obtaining the density matrix for quantum statistics from that for classical statistics. The author has considered the corrections required for Bose and Fermi statistics elsewhere [Green (1951)[2]] and shown that they are (1) negligible above a certain temperature T_c, and (2) approximately additive to the corrections introduced by quantum mechanics below this temperature. Pending a more exact treatment, one may therefore proceed as if classical statistics were always applicable and insert the known corrections for quantum statistics as required.

The partition function, for classical statistics, is obtained from (4) with the help of (27) and (36). One has

$$Q=\sum_{k=0}\sum{}^{(k)}\prod_{q(w)} I_{q(w)}(x_0=x)dx. \tag{38}$$

If

$$w!Vb_w=(2\pi\beta)^{3w/2}\sum_q\int I_{q(w)}(x_0=x)dx \tag{39}$$

is defined as the sum of all the integrals associated with a cluster of w particles, irrespective of the number of bonds connecting them, the coefficient of

$$(Vb_1)^{k_1}(2!Vb_2)^{k_2}\cdots(N!Vb_N)^{k_N}$$

in Eq. (38) for Q will be

$$\frac{(2\pi\beta)^{-3N/2}}{k_1!k_2!\cdots k_N!}\,\frac{N!}{(1!)^{k_1}(2!)^{k_2}\cdots(N!)^{k_N}},$$

if

$$\sum_w wk_w=N \tag{40}$$

and zero otherwise. Hence, Q is the coefficient of z^N in the expansion of $(2\pi\beta)^{-3N/2}N!\exp\sum_w(Vb_wz^w)$ in powers of z. The b's are evidently identical with those defined by Uhlenbeck and Kahn (1938) by analogy with Mayer's theory, but, so far as the author is aware, no one has previously derived explicit expressions for them. From (27) and (39), this may now be done. One has, with the help of (26)

$$b_w=\sum_q\int_0^1 dw_1\int_{v_1}^1 dv_2\cdots\int_{v_{q-1}}^1 dv_q(q!)^{-1}\sum\nolimits_{\text{perm}}c_{q(w)}, \tag{41}$$

where

$$\begin{aligned} m!Vc_{q(w)}=(2\pi\beta)^{3w/2}\int^q\prod_{l=1}^{a}\Big[-\beta dx_l\phi(r_l) \\ \times\frac{\exp\{-\sum(x_l-x_{l-1})^2/2\beta(v_l-v_{l-1})\}}{\{2\pi\beta(v_l-v_{l-1})\}^{3w/2}}\Big]. \end{aligned} \tag{42}$$

In (41), $\sum_{\text{perm}}$ applies to the ordering of the suffixes of the vectors r_l, which coincide with the bonds connecting the particles of the cluster. In (42), x_0 is now identified with x_q, and v_0 with v_{q-1}.

In evaluating (42), note that the bonds are numbered 1, $2\cdots q$, and that r_l connects the particles at $x^{(i,l)}$ and $x^{(j,l)}$. The number of the bond, meeting at $x^{(i,l)}$, next below l, will be denoted by (bl); and that of the bond, meeting at $x^{(j,l)}$, next below l, will be denoted by (lb). In case there is no bond whose number is less

[5] J. E. Mayer, J. Chem. Phys. **5**, 67 (1937); J. E. Mayer and S. F. Harrison, **6**, 87, 101 (1938). The method here adopted is more closely analogous to that of S. F. Streeter and J. E. Mayer, J. Chem. Phys. **7**, 1025 (1939).

than l meeting at $x^{(i,l)}$, suppose the highest number of all bonds meeting at the point is m; then $x_{(bl)}{}^{(i)}$ will mean $x_m{}^{(i)}$, and $v_{(bl)}$ will mean v_m-1; a similar interpretation is given to $v_{(lb)}$ and $x_{(lb)}{}^{(j)}$ when there is no bond with number less than l meeting at $x^{(j,l)}$. One may now perform all the integrations in (42), with the help of (28), except those relating to the coordinates $x_l{}^{(i,l)}$ and $x_l{}^{(j,l)}$ $(l=1, 2, \cdots, q)$. After writing

$$y_l=\tfrac{1}{2}(x_l{}^{(i,l)}+x_l{}^{(j,l)}), \tag{43}$$

one has

$$m!Vc_{q(m)}=(2\pi\beta)^{3m/2}\int\prod_{l=1}^{q}\{-\beta dr_l dy_l\phi(r_l)$$
$$\times e(y_l-y_{(bl)}-s_{(bl)l},\, v_l-v_{(bl)})$$
$$\times e(y_l-y_{(lb)}+s_{l(lb)},\, v_l-v_{(lb)})\}, \tag{44}$$
$$s_{(bl)l}=\tfrac{1}{2}(r_l\pm r_{(bl)}),\quad s_{lr lb)}=\tfrac{1}{2}(r_l\pm r_{(lb)}),$$

where $e(x, v)$ is defined in (28). The ambiguities of sign are removed by the observation that the vector $s_{(bl)l}$ joins the ends of $r_{l(bl)}$ and r_l which do not meet at $x_l{}^{(i,l)}$, and $s_{(lb)}$ joins the ends of r_l and $r_{(lb)}$ which do not meet at $x_l{}^{(j,l)}$.

The final reduction of the integral in (44) requires the performance of the integrations with respect to the y_l. Since only differences of the y's occur, the integration with respect to one of them (say y_q) yields a factor V canceling the one on the left-hand side of that equation; and the other integrations may be performed giving y_q any constant value (say 0). If $m=(bl)$, write $l=(am)$; and if $m=(lb)$, write $l=(ma)$. Write also

$$u_m=(v_l-v_m)^{-1}; \tag{45}$$

the exponent of the integral is then

$$-\sum_l\{u_{l(bl)}(y_l-y_{(bl)}-s_{(bl)l})^2$$
$$+u_{l(lb)}(y_l-y_{(lb)}+s_{l(lb)})^2\}/2\beta$$
$$-(\sum_l\sum_m f_{lm}y_l\cdot y_m+2\sum f_l\cdot y_l+g)/2\beta, \tag{46}$$

where

$$f_{lm}=u_{l(bl)}+u_{l(lb)}+u_{(al)l}+u_{(la)l},\quad l=m$$
$$=-u_{lm}(\delta_{(bl)m}+\delta_{(lb)m})-u_{ml}(\delta_{(bm)l}+\delta_{(mb)l}),\quad l\neq m$$
$$f_l=-u_{l(bl)}s_{(bl)l}+u_{l(lb)}s_{l(lb)}+u_{(al)l}s_{l(al)}-u_{(la)l}s_{(la)l}$$
$$g=\sum_{l=1}^{q}(u_{l(bl)}s_{(bl)l}{}^2+u_{l(lb)}s_{(lb)l}{}^2). \tag{47}$$

The result of performing the integrations is therefore

$$w!c_{q(w)}=(2\pi\beta)^{3w/2}\int\prod_{l=1}^{q}\left\{-\frac{\beta dr_l\phi(r_l)u_{l(bl)}{}^{\frac{1}{2}}u_{l(lb)}{}^{\frac{1}{2}}}{(2\pi\beta)^{\frac{1}{2}}}\right\}$$
$$\times\frac{\exp(-F/2\beta f)}{(2\pi\beta f)^{\frac{1}{2}}}, \tag{48}$$

where f is the determinant $|f_{lm}|$ of the matrix f_{lm} with $q-1$ rows and columns, and

$$F=\begin{vmatrix} f_{lm} & f_m \\ f_l & g \end{vmatrix} \tag{49}$$

is the determinant of the matrix obtained by "embroidering" f_{lm} with an additional row and column consisting of the vectors $f_l(l=1, 2, \cdots, q-1)$ and the scalar g—products of vectors being interpreted as scalar products wherever they occur. These determinants depend, of course, on the structure of the cluster with which $c_{q(m)}$ is associated.

It is not hard to convince oneself that, in the case of an "reducible" cluster, i.e., one consisting of two or more part connected by only one particle, the integral (48) always factorizes into simpler integrals associated with the irreducible components. It is not, however, obvious that the integral (41) factorizes in a similar way, and perhaps it does not do so in general. However this may be, it is simpler in the quantum theory to define the "irreducible cluster integrals" β_l as those which satisfy the simultaneous equations

$$m^2b_m=\sum_r\frac{(m\beta_1)^{r_1}}{r_1!}\frac{(m\beta_0)^{r_2}}{r_2!}\cdots\frac{(m\beta_{m-1})^{r_{m-1}}}{r_{m-1}!}. \tag{50}$$

One has, for example,

$$\sum_l lr_l=m-1,$$
$$\beta_1=2b_2$$
$$\beta_2=3(b_3-2b_2{}^2). \tag{51}$$

It is known from Mayer's work that these are the second and third virial coeficients, respectively. As a first application of the present theory, the series which represent them will be evaluated in the next section.

5. THE VIRIAL COEFFICIENTS

The evaluation of b_2 from (41) will now be completed. Setting $w=2$, one obtains from (47)

$$f_{ll}=2(u_{ll-1}+u_{l+1l})$$
$$f_{ll-1}=f_{l-1l}=-2u_{ll-1}$$
$$f=2^{q-1}(\prod_{l=1}^{q}u_{ll-1})(\prod_{l=1}^{q}u_{ll-1})$$
$$=2^{q-1}\prod u_{ll-1}$$
$$f_l=0;\quad F/f=g=\tfrac{1}{2}\quad u_{ll-1}(r_l-r_{l-1})^2, \tag{52}$$

so

$$2c_q(2)=(4\pi\beta)^{\frac{1}{2}}\int\prod_{l=1}^{q}[-\beta dr_l\phi(r_l)er_l-r_{l-1},$$
$$2(v_l-v_{l-1})]. \tag{53}$$

The integrations required by the formula (41) can be performed; for, since $c_q(2)$ depends only on the differ-

ences $v_l - v_{l-1}$ $(l=1, 2, \cdots, k-1)$ and is invariant under a cyclic permutation of these variables, one has

$$\int_0^1 dv_1 \int_{v_1}^1 dv_2 \cdots \int_{v_{q-1}}^1 dv_q c_q(2) = q^{-1} \int_0^1 dw_2 \int_{w_2}^1 dw_3 \cdots \int_{w_{k-1}}^1 dw_k c_q, \quad (2)$$

where $w_l = v_l - v_1$. This integral can be simplified by applying again the identity (21); it reduces to

$$q^{-1} \int^q \prod\{-dr_l \phi(r_l)/4\pi t_l\} \sum (4\pi t_l) \exp -(\sum t_l)^2/4\beta, \quad (54)$$

where

$$\begin{aligned} t_1 &= |r_1 - r_q|, \\ t_l &= |r_l - r_{l-1}| \quad (l=2, \cdots q). \end{aligned} \quad (55)$$

Hence (41) gives

$$2b_2 = \beta \sum_{q=1}^{\infty} q^{-1} \int^q \prod\{-dr_l \phi(r_l)/4\pi t_l\} (\sum 4\pi t_l) \times \exp\{-(\sum t_l)^2/4\beta\}. \quad (56)$$

It has already been supposed that $\phi(r)$ is not more singular than r^{-2} at $r=0$, so each integral in the series converges. At very low temperatures, b_2 is given by

$$2b_2 = \beta \sum_{q=1}^{\infty} \int^q \prod\{-dr_l \phi(r_l)/4\pi t_l\} 4\pi t_l \times \{1 - (\sum t_l)^2/4\beta\} + 0(\beta^{-1}). \quad (57)$$

It is worth noting that the value at absolute zero can be obtained by observing that the function

$$\nu(r_1) = 1 + \sum_{q=2}^{\infty} \int^{q-1} \prod_{l=2}^{q} \{-dr_l \phi(r_l)/4\pi t_l\} \quad (58)$$

satisfies the two-particle Schrödinger equation

$$(1/r)(d^2/dr^2)\{r\nu(r)\} = \phi(r)\nu(r) \quad (59)$$

and is, in fact, that solution which approaches the value 1 as $r \to \infty$. But clearly, from (57),

$$2b_0 = \beta \left\{ \int \nu(r)\phi(r)dr + 0(\beta^{-1}) \right\}. \quad (60)$$

Thus, an elementary solution of the Schrödinger equation gives the second virial coefficient for very low temperatures almost immediately.

The evaluation of b_3 is more complicated, and here only the first terms in the perturbation series will be considered. The irreducible triangular cluster will be considered first; one has

$$\begin{aligned} f &= u_{12}u_{21}u_{23}u_{32}u_{31}u_{13}\{(u_{12}u_{21})^{-1} \\ &\quad + (u_{23}u_{32})^{-1} + (u_{31}u_{13})^{-1}\}, \quad (61) \\ F &= u_{12}u_{21}u_{23}u_{32}u_{31}u_{13}(r_1+r_2+r_3)^2, \end{aligned}$$

so the contribution of this cluster to $3!c_{3(3)}$ is

$$\int^3 \prod\{-\beta dr_l \phi(r_l)\} e(r_1+r_0+r_3, \alpha_3),$$

$$\alpha_3 = (v_2-v_1)(1-v_2+v_1) + (v_3-v_2)(1-v_3+v_2) + (v_3-v_1)(1-v_3+v_1). \quad (62)$$

Now, by some elementary transformations one has

$$\int_0^1 dv_1 \int_{v_1}^1 dv_2 \int_{v_2}^1 dv_3 e(r, \alpha_3) = 3^{-\frac{1}{2}} \int_0^{\pi/3} d\theta \int_{\frac{1}{3}(1-\frac{1}{4}\sec^2\theta)}^{\frac{1}{4}} d\alpha \; e(r, \alpha) \quad (63)$$

so the contribution to b_3 of the cluster considered is

$$(3!)\sqrt{3}^{-1} \int^3 \prod\{-b dr_l \phi(r_l)\} \times \int_0^{\pi/3} d\theta \int_{\frac{1}{3}(1-\frac{1}{4}\sec^2\theta)}^{\frac{1}{4}} d\alpha \; e(r_1+r_2+r_3, \alpha). \quad (64)$$

It can be shown that this approaches a value proportional to β as $\beta \to \infty$.

There remains to be considered the reducible clusters formed by three molecules. There are three configurations with one particle joined to each of the others by a single bond; these all give $f = u_{12}u_{21}$ and $F=0$, so

$$3!c_{2(3)} = \left\{ \beta \int \phi(r)dr \right\}^2. \quad (65)$$

The contribution to b_3 of this term is then

$$\frac{1}{2}\left\{ \beta \int \phi(r)dr \right\}^2.$$

This removes from β_3, expressed as in (51), the term proportional to β^2 arising from the square of b_2, at least as far as terms proportional to the square of the force constant are concerned. Most probably the same cancellation occurs in terms of higher order, so that β_2, like β_1, is proportional to β at very low temperatures. A likely hypothesis is that all the virial coefficients are inversely proportional to the temperature near absolute zero, so that the pressure depends on the density alone. The verification of this hypothesis will require a more extended evaluation of the virial coefficients, based on the method of this paper.

APPENDIX

It is required first to evaluate the integral

$$L_N(x, \eta) = 2 \int \frac{d^N\xi}{(2\pi)^{3N}} \frac{\exp(ix\xi)}{\eta^2 + \xi^2}, \quad \eta = (2E)^{\frac{1}{2}}. \quad (66)$$

This is obviously a function of the length $r_N=(x^2)^{\frac{1}{2}}$ of the vector x with $3N$ components; also it satisfies the differential equation

$$(\partial^2 L_N/\partial x^2)=\eta^2 L_N \tag{67}$$

except for $r_N=0$. Writing, therefore,

$$L_N=2\eta^{3N-2}k_N(\eta r_N), \tag{68}$$

one obtains

$$sk_N''(s)+(3N-1)k_N'(s)-k_N(s)=0. \tag{69}$$

The solution of this equation which is proportional to s^{2-3N} for small values of s is

$$k_N(s)=c_N s^{(2-3N)/2}K_{(3N-2)/2}(s), \tag{70}$$

where c_N is a constant and K_n is the Bessel function of imaginary argument and order n. With Basset's normalization[6]

$$\lim_{s\to 0} s^n K_n(s)=2^{n-1}\Gamma(n). \tag{71}$$

The value of the constant c_N can thus be determined by the relations

$$L_N(x,0)=2c_N r_N{}^{(2-3N)}\cdot 2^{(3N-2)/2}\Gamma(3N-2)/2$$

$$=2\int \frac{d^N\xi}{(2\pi)^{3N}}\frac{\exp(ix\cdot\xi)}{\xi^2},$$

$$\int L_N(x,0)dx^{(N)}=L_{N-1}(x,0). \tag{72}$$

Since

$$\Gamma(3N-2)/2\int r_N{}^{(2-3N)}dx^{(N)}=\pi^{\frac{3}{2}}\Gamma(3N-5)/2r_N{}^{(5-3N)},$$

this gives $(2\pi)^{\frac{1}{2}}c_N=c_{N-1}$, and as

$$L_1(x)=2c_1(\eta/r_1)^{\frac{1}{2}}K_{\frac{1}{2}}(\eta r_1)=(2\pi r_1)^{-1}\exp(-\eta, r_1), \tag{73}$$

one has

$$c_1=(2\pi)^{-\frac{3}{2}}$$

and

$$c_N=(2\pi)^{-3N/2}. \tag{74}$$

Hence

$$L_N(x,\eta)=2(2\pi)^{-3N/2}(\eta/r_N)^{(3N-2)/2}K_{(3N-2)/2}(\eta r_N). \tag{75}$$

To obtain the expression (17) in the text for odd values of N, one makes use of the well-known recurrence relation

$$(d/ds)\{s^n K_n(s)\}=s^n K_{n-1}(s)$$

satisfied by the Bessel functions. This, together with (75) above, enables one to express L_N in the required form.

The Laplace transform

$$\frac{1}{2\pi i}\int_{c+i\infty}^{c-i\infty} dE\exp[\beta E-\alpha(2E)^{\frac{1}{2}}]$$

is easily evaluated by deforming the path of integration to pass from $-\infty$ along the real axis, round the origin in a positive direction, and back to $-\infty$. If $-\pi\leqq\arg E<\pi$, the above integral reduces to

$$\frac{1}{2\pi i}\int_{-\infty}^{0}\{\exp[\beta E+i\alpha(-2E)^{\frac{1}{2}}]-\exp[\beta E-i\alpha(-2E)^{\frac{1}{2}}]\}dE$$

or

$$\pi^{-1}\int_0^\infty \exp(-\tfrac{1}{2}\beta k^2)\sin(\alpha k)kdk$$

on substituting $k^2=-2E$. This is

$$-\frac{1}{2\pi}\frac{\partial}{\partial\alpha}\int_{-\infty}^{\infty}\exp(-\tfrac{1}{2}\beta k^2)\cos(\alpha k)dk$$

$$=2\pi(2\pi\beta)^{-\frac{3}{2}}\alpha\exp(-\alpha^2/2\beta),$$

the result required in the text.

To establish the identity (21), consider first the case $k=1$. One has

$$\exp(s_1^2+s_2^2)/2\beta\int_0^1 dv\{v(1-v)\}^{\frac{1}{2}}$$

$$\times\exp-\{s_1^2/v+s_2^2/(1-v)\}/2\beta$$

$$=2\int_0^\infty duu^{-2}(1+u^2)\exp-(s_1^2/u^2+u^2s_2^2)/2\beta \tag{76}$$

by the substitution $v/(1-v)=u^2$. Now by putting $w=s_1u$ and $w=s_2/u$ one has

$$\int_0^\infty dw\exp(w^2+s_1^2s_2^2/w^2)/2\beta$$

$$=s_1\int_0^\infty du\exp-(s_1^2u^2+s_2^2/u^2)/2\beta$$

$$=s_2\int_0^\infty duu^{-2}\exp-(s_1^2u^2+s_2^2/u^2)/2\beta,$$

so the above integral is

$$2(s_1+s_2)/s_1s_2\int_0^\infty dw\exp-(w^2+s_1^2s_2^2/w^2)/2\beta.$$

Now if

$$f(\theta)=\int_0^\infty dw\exp-(w^2+\theta^2/w^2)/2\beta,$$

one has

$$f(0)=\tfrac{1}{2}(2\pi\beta)^{\frac{1}{2}};$$

also,

$$f'(\theta)=-f(\theta)/\beta$$

[6] J. M. Basset, Proc. Cambridge Phil. Soc. 6, 11 (1889).

so

$$f(\theta)=\tfrac{1}{2}(2\pi\beta)^{\frac{1}{2}}\exp(-\theta/\beta).$$

Thus the integrals of (76) reduce to

$$(s_1+s_2)\cdot(2\pi\beta)^{\frac{1}{2}}\exp(-s_1s_2/\beta)/s_1s_2.$$

This proves the desired result for $k=1$. For higher values of k, one proceeds by induction. Assuming the formula (21) of the text to be correct, replace s_{k+1} by $s_{k+1}+s_{k+2}$, and use the result for $k=1$ to express $\exp\{-(s_{k+1}+s_{k+2})^2/2\beta(1-v_k)\}$ in the form

$$(2\pi\beta)^{-\frac{1}{2}}(1-v_k)^{-\frac{1}{2}}(s_{k+1}^{-1}+s_{k+2}^{-1})\int_0^1 dv$$
$$\times\exp\{-[s_{k+1}^2/v+s_{k+2}^2/(1-v)]/2\beta(1-v_k)\}.$$

If one now writes $v(1-v_k)=v_{k+1}-v_k$ so $(1-v)(1-v_k)=1-v_{k+1}$, the formula is verified for the higher value $k+1$ of k. Thus the conditions for mathematical induction are satisfied.

THE JOURNAL OF CHEMICAL PHYSICS VOLUME 20, NUMBER 8 AUGUST, 1952

Markoff Random Processes and the Statistical Mechanics of Time-Dependent Phenomena*†

MELVILLE S. GREEN
Institute for Fluid Dynamics and Applied Mathematics, University of Maryland, College Park, Maryland
(Received February 11, 1952)

Two principles of a statistical mechanics of time-dependent phenomena are proposed and argued for. The first states that the proper mathematical object to describe the physical situation is the stationary random process specified by the ensemble of time series $a_i(X_t)i=1\cdots s$ and the distribution $\rho(X)$. The set phase functions $a_i(X)i=1\cdots s$ represent the set of grossly observable features of the system. X_t is the image of the phase X after time t. $\rho(X)$ is a stationary distribution. The second principle is concerned with the very common case in which the phenomenological equations are of the first order in time and states that in this case the random process in question is a Markoff process. A Fokker-Planck equation is derived for the process, and an entropy is defined and is shown always to increase. Phenomenological equations are derived as a first approximation to the Markoff process. These involve a certain matrix ξ_{ij} which is shown to satisfy symmetry relations which are a generalization of Onsager's. The theory is applied to the uniformization of the direction of momentum of a particle on a two-dimensional torus subject to a small perturbing potential.

THE principles of statistical mechanics as developed by Boltzmann and Gibbs were designed to give a mechanical and molecular basis for the laws of phenomenological thermodynamics and to provide means to calculate grossly observable quantities from known or assumed properties of molecules. The first principle of the theory is the identification of the time average of certain functions of the phase of a mechanical model with the values that the grossly observable properties of an isolated physical system assume after a long enough time. The second is the identification of time averages with phase space averages as justified by the ergodic theory. The fact that physical systems contain large numbers of molecules means that the dispersion of the gross variables is very small, and therefore that it is very improbable that a value of the gross variables different from the phase space average will be observed.

The problem with which this paper will be concerned is the extension of the principles of statistical mechanics so as to give a mechanical and molecular basis for phenomenological laws of time-dependent nonequilibrium phenomena and to provide the means to calculate the time behavior of grossly observable quantities from known or assumed properties of molecules. This problem has, of course, not been without quite good answers in certain special cases. Thus the Maxwell-Boltzmann kinetic theory of gases gives a good answer for gases at low densities. The electron theory of metals gives a good answer for electrical properties of metals. Eyring's theory of absolute reaction rates deals with the problem of chemical reactions in gases. Each of these theories, however, is limited to a much smaller group of systems than that to which equilibrium statistical mechanics applies.

Latterly there have been some works which have tried to answer the problem for more general systems. Peierls has given a theory of the conduction of heat in nonmetallic crystals. Eyring has extended the ideas of his chemical rate theory to deal with such processes as diffusion and viscosity in condensed phases.[1] On different principles Born and H. S. Green have given a kinetic theory of liquids using the so-called superposition principle for the distribution of groups of three particles.[2] In general these works have been concerned

* This paper has been submitted in partial fulfillment of the requirements for the degree of Doctor of Philosophy at Princeton University.

† Supported in part by the ONR.

[1] Glasstone, Laidler, and Eyring, *Theory of Rate Processes* (McGraw-Hill Book Company, Inc., New York, 1941).

[2] M. Born and H. S. Green, Proc. Roy. Soc. (London) **A188**, 10 (1946); **189**, 103 (1947); **190**, 455 (1947).

with particular models and more or less restricted classes of systems.

Works which have stated principles which are independent of particular models are Onsager's theory of microscopic reversibility,[3,4] and the work of Richardson[5] on Markoff processes and irreversible phenomena. Kirkwood's statistical mechanical theory of transport processes,[6] based on the idea of diffusion in the phase space of n-uples of particles, is intended to apply to all states of aggregation. Peierls' theory of heat conduction, while concerned with a particular model is based on an idea (the Fokker-Planck equation of a random process) which we wish to generalize and discuss independently of a model.[7]

In the main body of the present paper we will propose and argue for some of the principles of a statistical mechanics of time-dependent phenomena independent of a particular model. Some of these principles are implicit or explicit in the above works, particularly those mentioned in the preceding paragraph. We will propose them and argue for them in their most general form. In an appendix we will discuss a specific example which can be shown explicitly to exhibit the behavior which we assert in the main body. As an answer to our problem, the set of principles to be stated is incomplete in that there is no principle which plays the role of the ergodic principle in the equilibrium theory, i.e., of allowing the calculation of physical properties without explicit knowledge of the solutions of the equations of motion. In the present paper we do not, for the time being, consider quantum mechanics.

A. GROSS VARIABLES AND RANDOM PROCESSES

Let us have before us a few typical time-dependent phenomena in systems of large numbers of particles. Such are, for example, the motion of a viscous fluid, the conduction of heat, chemical reactions. We are interested in understanding the time behavior of certain grossly observable quantities which can be expressed as functions $a_i(X)$ of the phase X of the mechanical model which we know or assume to represent our system. Such quantities are the local velocity in the case of the viscous fluid, the local temperature in the case of heat conduction, the mole fractions of the several species in chemical reactions. We will call these quantities gross variables as opposed to the microscopic variables, the positions and momenta of all the particles.

So far as can be observed with large scale methods the gross variables are smoothly varying, definite functions of the time which are reproduced in each repetition of the same conditions. A metal bar heated in the same manner on different occasions cools down in the same way. From a more fundamental point of view, however, we know that the gross variables are subject to rapidly varying fluctuations which are not reproduced on successive repetition of the same conditions, but which are very difficult to observe because large fluctuations are extremely improbable. If we are to give complete theoretical description of the grossly observable quantities we must include these rapidly varying fluctuations. Since from this more fundamental point of view the gross variables are not definite functions of the time we must consider the ensemble of all possible functions which can represent the time behavior of the gross variables given, of course, the mechanical model which we take to represent our physical system. In order to be able to say which of these functions are likely to be observed we must introduce a probability into this ensemble. In the current language of mathematics we must consider the gross variables to be represented by a *random process.*

In mathematical symbols, we are concerned with certain functions of the phase $a_i(X)$ $i=1\cdots s$ which we call gross variables. Let X_t be the image of the phase X after time t, i.e., X_t is the phase of our dynamical system at time t if its phase at 0 was X. At time t the gross variables will have the values $a_i(X_t)$. We will obtain the ensemble of all possible functions which can represent the time behavior of the a_i if we let X vary over all possible phases. To introduce a probability into this ensemble of functions means to give a probability distribution to the initial phases X. The ensemble of functions $a_i(X_t)$ together with the distribution of the initial phases X is a random process.[8]

Given this random process we are able to answer questions of the following type: What is the probability of observing a set of values of the $a_i(X_t)$ such that

$$\begin{aligned} &a_i^{(1)} \leqq a_i(X_{t_1}) \leqq a_i^{(1)} + \Delta a_i^{(1)} \qquad i=1\cdots s \\ &a_i^{(2)} \leqq a_i(X_{t_2}) \leqq a_i^{(2)} + \Delta a_i^{(2)} \\ &\quad \cdot \quad \cdot \quad \cdot \quad \cdot \quad \cdot \quad \cdot \quad \cdot \quad \cdot \\ &a_i^{(r)} \leqq a_i(X_{t_r}) \leqq a_i^{(r)} + \Delta a_i^{(r)} ? \end{aligned} \tag{1}$$

We will indicate such a distribution by

$$\rho_r(a_i^{(1)}\, t_1 \cdots a_i^{(r)}\, t_r)\Delta a_1^{(1)} \cdots \Delta a_s^{(r)}. \tag{2}$$

This is the so-called joint distribution of the gross variables at times $t_1 \cdots t_r$. Until now we have not specified the distribution of the initial phases. We can make a further specification of our random processes by noting that we do not observe a different time behavior for the distribution of the gross variables at different epochs. In the current language of mathematics our random process must be stationary. The joint distributions should remain unchanged when each of the times of observation are changed by the same constant amount. The necessary and sufficient condition for this

[3] L. Onsager, Phys. Rev. **37**, 405 (1931); **38**, 2265 (1931).
[4] H. B. G. Casimir, Revs. Modern Phys. **17**, 343 (1945).
[5] J. Richardson, unpublished lecture delivered at a Symposium on Non-Equilibrium Statistical Mechanics, Meeting of Fluid Dynamics Section. American Physical Society, University of Virginia, December 28–30, 1949.
[6] J. G. Kirkwood, J. Chem. Phys. **14**, 180 (1946).
[7] R. Peierls, Ann. Physik **3**, 1055 (1929).
[8] Ming Chen Wang and G. E. Uhlenbeck, Revs. Modern Phys. **17**, 323 (1945). See also C. Shannon, *The Mathematical Theory of Communication* (University of Illinois Press, Urbana, 1949).

is that the distribution of initial phases should be a function of the single-valued integrals of motion of the dynamical system, the energy, and possibly the linear and angular momentum. In what follows we shall suppose the energy is the only one-valued integral of motion.

There are no other general principles which allow us to define our random process more precisely. Which function of the energy we choose as the distribution of the initial phases depends on what knowledge we have of the energy of the system. It is, however, expedient to consider the random processes in which the distribution of the initial phases is that corresponding to a microcanonical ensemble of energy E. If $\rho_E(X)$ is the distribution of initial phases,

$$\rho_E(X)=\delta(H(X)-E)/W(E), \tag{3}$$

where δ is the Dirac delta-"function," and $W(E)dE$ is the phase volume contained between two adjacent surfaces of constant energy corresponding to E and $E+dE$. A random process with such a distribution of initial phases has, according to the ergodic theorem, a certain homogeneity in the sense that each representative of the ensemble of functions $a_i(X)$ has the same properties over long stretches of time except for a set of functions of probability zero. More precisely for almost every X (or except for a set of X's of probability zero) the fraction of the time t out of a stretch of length T which satisfies the inequalities

$$\begin{aligned} a_i^{(1)} \leqq a_i(X_{t+t_1}) \leqq a_i^{(1)}+\Delta a_i^{(1)} \\ a_i^{(2)} \leqq a_i(X_{t+t_2}) \leqq a_i^{(2)}+\Delta a_i^{(2)} \\ \cdot \quad \cdot \quad \cdot \quad \cdot \quad \cdot \quad \cdot \quad \cdot \quad \cdot \\ a_i^{(r)} \leqq a_i(X_{t+t_r}) \leqq a_i^{(r)}+\Delta a_i^{(r)} \end{aligned} \tag{4}$$

approaches the same limit as T approaches infinity. The common limit is the joint distribution (2) for the process. We can consider a random process with any distribution of the energy to be a linear combination of such homogeneous parts.

We wish to propose as a first principle that *the appropriate objects of study of a statistical mechanics of time-dependent phenomena are the random processes $a_i(X_t)$ with initial distribution of X, $\rho_E(X)$, for all energies of interest and for all gross variables of interest.* We note that the distribution function $\rho_1(a_i t)$ is independent of time because of the stationary character of our random processes. It contains all the information considered in equilibrium statistical mechanics. The distribution functions $\rho_2(a_i^{(1)}t_1, a_i^{(2)}, t_2)$, $\rho_3(a_i^{(1)}t_1, a_i^{(2)}t_2, a_i^{(3)}t_3)$ etc., are indeed time-dependent and are the special objects of a statistical mechanics of time-dependent phenomena.

B. COMPLETE SETS OF GROSS VARIABLES

One of the facts to be explained by a statistical mechanics of time-dependent phenomena is that in certain systems the time-behavior of the gross variables as observed with large scale methods can be represented very well by differential equations which are of the first order in the time. Thus the Navier-Stokes equation, the phenomenological equation of heat conduction and the equations expressing the rate of a chemical reaction in terms of the concentrations of the species are of this kind. Another way of expressing this fact is that if the values of the gross variables are fixed at one time they are determined for all times thereafter.

This circumstance is, of course, not the case for all systems and for all choices of gross variables. Systems exhibiting combined viscous and elastic effects may require a complete knowledge of the past history in order to predict the future behavior. Moreover, even for such phenomena as heat conduction we cannot predict the future from the present unless we have enough knowledge of the present. If we know only the temperature at the ends of a metal bar, we cannot predict the future course even of the temperature at the ends. If for a particular system there is a set of gross variables which is such that from the large scale point of view the knowledge of the present values of these variables at one time determines their values at all times thereafter, we will call such a set of gross variables a complete set.

As an example of a complete set of gross variables consider the case of the motion of a viscous fluid. According to the phenomenological equations of motion a knowledge of the three components of the local momentum density and the local particle and energy densities at every point of the fluid at one time determines these quantities at all later times. Because of the discrete structure of the system there is a certain indefiniteness in the usual definition of local density as the limit of the average density of an arbitrarily small volume. If, however, we are willing to ignore inhomogeneities of size smaller than, say, one millimeter we can divide the space occupied by the fluid into cubical cells of size one millimeter and take as our complete set of gross variables the momentum, energy, and number of particles in each cell divided by the volume of the cell. Our definition is, of course, not unique. We would get a different, but equally satisfactory set of gross variables if we chose any cell size large enough to contain a large number of molecules but small compared to the size of the inhomogeneities in which we are interested.

One of the important problems of the theory is to define the conditions under which a system has a complete set of gross variables and to give a rule for determining them. In what follows we will have something more to say about this problem. For the present we wish to note that in the above case the five quantities momentum, energy, and number of particles would be the only one-valued integrals of motion if there were no interaction between cells.

In the remainder of this paper we will consider only systems which have a complete set of gross variables. We will discuss the special properties of the random processes associated with complete sets of gross variables.

C. MARKOFF PROCESSES

We have characterized the random processes with which we are concerned by specifying an ensemble of functions of the time $a_i(X_t)$ together with the distribution $\rho(X)$ of the parameter X. Another way of characterizing a random process is to give all the joint distribution functions $\rho_r(a_i^{(1)}t_1\cdots a_i^{(r)}t_r)$. These distribution functions are not all independent. In fact we have

$$\rho_{r-1}(a_i^{(1)}t_1\cdots a_i^{(r-1)}t_{r-1})$$

$$=\int \rho_r(a_i^{(1)}t_1\cdots a_i^{(r-1)}t_{r-1}, a_i^{(r)}t_r)da_i^{(r)}, \quad (5a)$$

$$\int \rho_r(a_i^{(1)}t_1\cdots a_i^{(r)}t_r)da_1^{(1)}\cdots da_s^{(r)}=1. \quad (5b)$$

This characterization is perhaps more suitable for our purposes because we are usually interested in the values of the a_i at only a few distinct times, usually the present and one future time.

There is another set of functions derivable from the joint distributions which express the physical circumstances even more directly. These are the so-called transition probabilities.

$$T(a_i^{(-u)}t_{-u}, \cdots a_i^{(-1)}t_{-u}, a_i^{(0)}t_0/a_i^{(1)}t_1\cdots a_i^{(r)}t^{(r)}) \quad (6)$$

is the conditional probability that the gross variables have the values $a_i^{(1)}$ at $t_1\cdots a_i^{(r)}$ at t_r if we know that they had the values $a_i^{(-u)}$ at t_{-r}, $\cdots a_i^{(0)}$ at t_0. We can express the transition probabilities (6) as

$$\frac{\rho_{r+u+1}(a_i^{(-u)}t_{-u}\cdots a_i^{(r)}t_r)}{\rho_{u+1}(a_i^{(-u)}t_{-u}\cdots a_i^{(0)}t_0)}. \quad (7)$$

We wish to examine these transition probabilities along with our large scale physical knowledge in order to reduce the range of possibilities for the random processes associated with complete sets of gross variables.[8]

First let us consider the transition probability $T(a_i^{(0)}t_0/a_i, t)$. This expresses our knowledge of the gross variables a_i at time t when we know certainly that they had the values $a_i^{(0)}$ at t_0. Since a_i is certainly equal to $a_i^{(0)}$ when $t=t_0$ we must have $T(a_i^{(0)}t_0/a_it_0)=\delta(a_i-a_i^{(0)})$. In most cases the fluctuations in the gross variables are very small and the probability that the gross variables are observably different from one particular set of values $\bar{a}_i(a_i^{(0)}, t-t_0)$ must be very small. In other words $T(a_i^{(0)}t_0/a_it)$ must be very sharply peaked around the representative values $\bar{a}_i(a_i^{(0)}, t-t_0)$ which depend on the $a_i^{(0)}$ and on $t-t_0$. We may take for $\bar{a}_i$ the conditional mean of a_i:

$$\bar{a}_i=\langle a_i\rangle=\int da_i\cdots da_s a_i T(a_i^{(0)}t_0/a_it), \; i=1\cdots s. \quad (8)$$

The $\langle a_i\rangle$ are the values of the gross variables observed with large scale methods. They are evidently approximate solutions of the phenomenological equations of motion

$$d\langle a_i\rangle/dt=v(\langle a_i\rangle) \quad i=1\cdots s \quad (9)$$

with

$$v(\langle a_i\rangle)=\lim_{t-t_0\to 0}(\bar{a}_i(\langle a_i\rangle, t-t_0)-\langle a_i\rangle)/(t-t_0). \quad (9a)$$

Large scale observations do not give us a great deal of information about the transition probabilities in which information about more than one time is assumed to be known. Thus to determine $T(a_i^{(-1)}t_{-1}, a_i^{(0)}t_0/a_it)$ we are supposed to know the values of the gross variables at times t_{-1}, t_0, and t. Since, however, the distributions of the gross variables are very sharply peaked functions we cannot hope to have information about $T(a_i^{(-1)}t_{-1}, a_i^{(0)}t_0/a_it)$ except for values of $a_i^{(-1)}$, $a_i^{(0)}$, a_i which are solutions or the phenomenological equations of motion (9) for times t_{-1}, t_0, and t, respectively. For a complete knowledge of T we must have knowledge of the a_i when we have previously observed values of $a_i^{(-1)}$ at t_{-1} and of $a_i^{(0)}$ at t_0 which are considerable fluctuations from a solution of (9).

There is reason to believe, however, that physical systems with complete sets of gross variables "forget" their past history. If we produce an arbitrary past history by artificial means, i.e., by acting on the system from the outside, the behavior of the system after the outside influence has been stopped depends only on the state of the system at the time of stopping. Thus, if our metal bar is heated up at a varying rate and then isolated, its temperature distribution as a function of time depends only on the temperature distribution at the time of isolation. There must be, of course, a short time after isolation during which the past history has some influence because of the continuity of physical phenomena. Evidently this time is short compared to times measurable by large scale methods.

The situation in which there is an outside influence is not at all the same as that in which an *a priori* improbable past history has arisen by a fluctuation from the expected behavior. Indeed as long as external forces are present the Hamiltonian of the system is not the same as the Hamiltonian when the system is isolated. It is not, however, unreasonable to believe that the ability of the system to forget its past history is a property of the part of the Hamiltonian due to internal forces only and therefore belongs to the isolated system as well.

Using the above argument as a suggestion we propose the following hypothesis: the transition probabilities $T(a_i^{(-u)}t_{-u}\cdots a_i^{(0)}t_0/a_it)$ are independent of the arguments $a_it_u\cdots a_it_{-1}$. In symbols

$$T(a_i^{(-u)}t_{-u}\cdots a_i^{(0)}t_0/a_it)=T(a_i^{(0)}t_0/a_it). \quad (10)$$

Random processes for which (10) holds are usually called Markoff processes. There is a qualification of

(10) which we must make because of the continuity of physical phenomena mentioned above. We assume that (10) holds as long as the difference of any two times of observation are not less than a time t which is small compared to times observable with large scale methods. With this qualification, we take as a second principle of the statistical mechanics of time-dependent phenomena that *the random processes associated with a complete set of gross variables are stationary Markoff processes.*

This hypothesis is not new. Peierls[7] has used it in his theory of heat conduction in nonmetallic crystals, while Richardson[5] has proposed it for the general case. We wish to examine the consequences which may be drawn from it. Any final judgment as to its validity will of course depend on how well it serves to explain physical phenomena.

We wish to cite the case of Brownian motion in a field of force as an example of a physical system which has a set gross variables that is a Markoff random process. The system in this case is the Brownian particle plus the molecules of the surrounding fluid. The complete set of gross variables is the position and momentum of the Brownian particle and the total energy of the system. (The total energy determines the temperature of the system, and since it is a constant we need not consider it explicitly in the transition probabilities.) In this case the fluctuations are large enough to be observed with a microscope, and the success of the phenomenological theory of Brownian motion, which assumes a Markoff process for the position and momentum of the Brownian particle, is *a posteriori* proof of the possibility of (10) for a physical system. The case in which there is an external force field is more analogous to the situation we are considering, for then the mean position of the particle, which is the analog of the value $\langle a_i \rangle$ of a gross variable observed with large scale methods, changes with time. In Brownian motion both the expected value and the fluctuations are observable.

A Markoff process has the property that all the transition probabilities and joint distributions are determined by $\rho_1(a_i, t)$ and $T(a_i^{(0)}t_0/a_it)$. In fact from the definition of the transition probabilities we have

$$\begin{aligned}\rho_r(a_i^{(1)}t_1\cdots a_i^{(r)}t_r)&=\rho_{r-1}(a_i^{(1)}t_1\cdots a_i^{(r-1)}t_{r-1})\\&\quad\times T(a_i^{(1)}t_1\cdots a_i^{(r-1)}t_{r-1}/a_i^{(r)}t_r)\\&=\rho_r(a_i^{(1)}t_1\cdots a_i^{(r-1)}t_{r-1})T(a_i^{(r-1)}t_{r-1}/a_i^{(r)}t_r)\end{aligned}\tag{11a}$$

by (10). By successive application of this formula we have

$$\begin{aligned}\rho_r(a_i^{(1)}t_1\cdots a_i^{(r)}t_r)&=\rho_1(a_i^{(1)}t_1)\\&\quad\times T(a_i^{(1)}t_1/a_i^{(2)}t_2)\cdots T(a_i^{(r-1)}t_{r-1}/a_i^{(r)}t_r).\end{aligned}\tag{11b}$$

By the definition of transition probability and (11b)

$$\begin{aligned}T(a_i^{(-u)}t_{-u}\cdots a_i^{(0)}t_0/a_i^{(1)}t_1\cdots a_i^{(r)}t_r)\\=T(a_i^{(0)}t_0/a_i^{(1)}t_1)\cdots T(a_i^{(r-1)}t_{r-1}/a^{(r)}\cdot t_r).\end{aligned}\tag{11c}$$

Thus a Markoff process can be specified by giving, $\rho_1(a_it)$, the distribution function at one time, and the transition probability $T(a_i^{(0)}t_0/a_it)$. This transition probability, however, is not any function of its arguments, but must satisfy certain conditions which are consequences of (5a). We have from (11c) and (5a)

$$\begin{aligned}\int\rho_3(a_i^{(1)}t_1, a_i^{(2)}t_2, a_i^{(3)}t_3)da_i^{(2)}&=\rho_2(a_i^{(1)}t_1, a_i^{(3)}t_3)\\&=\rho_1(a_i^{(1)}t_1)\int T(a_i^{(1)}t_1/a_i^{(2)}t_2)T(a_i^{(2)}t_2/a_i^{(3)}t_3)da_i^{(2)},\end{aligned}$$

or dividing by $\rho_1(a_i^{(1)}t_1)$,

$$\begin{aligned}&T(a_i^{(1)}t_1/a_i^{(3)}t_3)\\&\quad=\int T(a_i^{(1)}t_1/a_i^{(2)}t_2)T(a_i^{(2)}t_2/a_i^{(3)}t_3)da_i^{(2)}\end{aligned}\tag{12}$$

for all t_1, t_2, t_3. Again we have

$$\begin{aligned}\int\rho_2(a_i^{(1)}t_1, a_i^{(2)}t_2)da_i^{(1)}&=\rho_1(a_i^{(2)}t_2)\\&=\int\rho_1(a_i^{(1)}t_1)T(a_i^{(1)}t_1/a_i^{(2)}t_2)da_i^{(1)}.\end{aligned}$$

Now, because our random processes are stationary, the distribution function at one time is actually independent of the time and we should write it $\rho_1(a_i)$. We have

$$\rho_1(a_i^{(2)})=\int\rho_1(a_i^{(1)})T(a_i^{(1)}t_1/a_i^{(2)}t_2)da_i\tag{13}$$

for all t_1 and t_2. Equation (12) is a linear integral equation for $T(a_i^{(1)}t_1/a_it)$ considered as a function of the a_i with $T(a_i^{(2)}t_2/a_i^{(3)}t_3)$ as kernel. Equation (13) states that this kernel has the proper function $\rho_1(a_i)$ with proper value 1 for all t_2, t_3. Equations (12) and (13) are sufficient to satisfy all the Eqs. (5a). We can specify a Markoff process by giving the distribution $\rho_1(a_i)$ and a transition probability $T(a_i^{(1)}t_1/a_i^{(2)}t_2)$ which satisfies (12) and (13). The distribution function $\rho_1(a_i)$ can be determined by the methods of equilibrium statistical mechanics. To determine $T(a_i^{(1)}t_1/a_i^{(2)}t_2)$ is the special problem of the present theory.

D. THE FOKKER-PLANCK EQUATION

In the mathematical theory of Markoff processes it is shown that (12) is equivalent to a differential equation

$$\frac{\partial}{\partial t}T(a_i^{(0)}t_0/a_it)=\mathfrak{L}T(a_i^{(0)}t_0/a_it)\tag{14}$$

together with the boundary condition $T(a_i^{(0)}t_0/a_it)\rightarrow\delta(a_i-a_i^{(0)})$ as $t\rightarrow t_0$. $\mathfrak{L}$ is a linear operator on T considered as a function of the a_i. In general, $\mathfrak{L}$ is an integral operator. Under conditions, which act to rule out the possibility that the $a_i(x_k)$ have sharp discontinuities,

however, $\mathfrak{L}$ will be a differential operator. We will not prove this statement here but will rather give the form of $\mathfrak{L}$ in this case and the conditions for its validity.[9] $\mathfrak{L}$ will have the form

$$\frac{\partial T}{\partial t}=\sum_{ij}\frac{\partial}{\partial a_i}\left(-\bar{v}_i(a_k)T+\frac{\partial}{\partial a_j}\bar{\xi}_{ij}(a_k)T\right)\quad i,j=1\cdots s, \tag{15}$$

where $\bar{v}_i(a_k)$, $\bar{\xi}_{ij}(a_k)$ are defined as

$$\bar{v}_i(a_k^{(0)})=\lim_{t-t_0\to 0}(t-t_0)^{-1}\times\int(a_i-a_i^{(0)})T(a_k^{(0)}t_0/a_kt)da_k \tag{16a}$$

$$2\bar{\xi}_{ij}(a_k)=\lim_{t-t_0\to 0}(t-t_0)^{-1}\times\int(a_i-a_i^{(0)})(a_j-a_j^{(0)})T(a_k^{(0)}t/a_kt)da_k. \tag{16b}$$

The condition that $\mathfrak{L}$ should be of this form is that for the corresponding third-order moments

$$\lim_{t-t_0\to 0}(t-t_0)^{-1}\times\int|(a_i-a_i^{(0)})(a_j-a_j^{(0)})(a_k-a_k^{(0)})|Tda_k=0.$$

The $\bar{v}_i(a_k)$ can be interpreted as the components of the velocity of the center of gravity of the distribution T, while the $\bar{\xi}_{ij}(a_k)$ measure the rate spreading of the distribution. The condition on the third-order moments can be interpreted to mean that this spreading must not take place too rapidly. Equation (15) is the well-known Fokker-Planck equation. Two special cases of this equation are the diffusion equations in phase space and inconfiguration space for a Brownian particle.

We propose now to derive expressions for the $\bar{v}_i(a_k)$ and $\bar{\xi}_{ij}(a_k)$ by a method used by Kirkwood to obtain an expression for the friction constant in Brownian motion.[6] Before we do this, however, let us consider the kinds of phase functions which can conceivably make up a complete set of gross variables. It is clear that the Hamiltonian function, $H(X)$ must be one of the members of a complete set or at least must be expressible as a function of the members of the set.

$$H(X)=E(a_1(X)\cdots a_s(X)). \tag{17}$$

Indeed if (17) is not the case there are many values of the energy consistent with a particular set of values of the a_i. If a particular set of values of the a_i is observed, we do not know which of the ergodic parts of the ensemble of functions $a_i(X_t)$ includes the particular function $a_i(t)$ which represents the future behavior of the system. Since a different set of values of the a_i can be expected for each of the ergodic parts, we do not have enough information to predict the future course of the a_i, and our set of gross variables will not be a complete set.

Now we have pointed out that for the particular case of the motion of a viscous fluid the members of the complete set of gross variables are in a certain sense approximate single-valued integrals of motion. The Hamiltonian in this case is a simple sum function of the energy of the cells. We believe that this circumstance is quite general. More precisely, a set of functions which contains not only the Hamiltonian, but all the *approximate* single-valued integrals of motion will be complete.

Let us suppose in fact that each of our gross variables is in some sense an approximate single-valued integral of motion and consider the part of the phase space in which the inequalities

$$a_i\leqslant a_i(X)\leqslant a_i+\Delta a_i\qquad i=1\cdots s \tag{18}$$

are satisfied. Any definition of approximate integral of motion must imply that if X satisfies (17) X_t will satisfy (17) for a relatively long time thereafter. Now the rates of change of the $a_i(X)$ will be certain phase functions $v_i(X)$ (the Poisson bracket expressions of a_i and the Hamiltonian) which will not in general be constant in the region (18). The change in an a_i, $\Delta a_i=a_i(X_T)-a_i(X)$, will be the time-integral of $v_i(X_t)$

$$\Delta a_i=\int_0^T v_i(X_t)dt. \tag{19}$$

If the set of functions a_i were all of the *exact* single-valued integrals of motion the ergodic theorem tells us that except for phases X contained in a small volume of (17) this integral is very nearly $\langle v_i\rangle T$ where $\langle v_i\rangle$ is the mean of the function $v_i(X)$ in the region (17).[10,11] We suppose that this statement remains true for times not too long even when the a_i are merely *approximate* integrals of motion. This means that if the $a_i(X_t)$ have values a_i at 0 they will almost certainly have the values $a_i+\langle v_i\rangle T$ at time T. This is precisely the kind of behavior asserted of complete sets of gross variables. Moreover, if we know in addition the values of the a_i at t_{-1}, this means that the phase of our system satisfies inequalities

$$a_i^{(-1)}\leqslant a_i(X_{t_{-1}})\leqslant a_i^{(-1)}+\Delta a_i^{(-1)}, \tag{20}$$

as well as (19), i.e., the phase of our system is known to be in a certain part of the region defined by (18). Since the above statement holds for almost all X's we can expect that it holds for this part as well. Thus, unless the part of (18) where (20) is satisfied coincides with

[9] S. Chandrasekhar, Revs. Modern Phys. **15**, 1 (1943).

[10] A proof of (15) together with a precise statement of the conditions for its validity is given by A. Kolmogoroff, Math. Ann. **104**, 415 (1931).

[11] We will use the notation $\langle Q\rangle$ to indicate the mean value of the phase function $Q(X)$ in the shell ensemble where the $a_i(X)$ have constant values a_i. This average is in general a function of the constant values a_i. Whenever necessary we will indicate the particular shell ensemble in which the average is to be taken by suitable subscripts.

the part of (18) where time-average does not equal phase-space average, knowledge of the a_i in the past does not change their future expectation values.

This argument is not, of course, meant to be rigorous. Nevertheless it points the way to a characterization of complete sets of gross variables, and gives the very useful approximation $\bar{v}_i \cong \langle v_i \rangle$. This approximation is often used tacitly in discussions of time-dependent phenomena. When applied to the case of fluid motion, it leads to the usual equations of motion without the viscosity and heat conduction terms. We will show later that quite generally this approximation does not give an account of irreversible processes.

Let us consider the first and second moments of the

$$\Delta a_i = a_i(X_T) - a_i(X) = \int_0^T v_i(X_\tau) ds.$$

In order to calculate the quantities $\bar{v}_i$ and ξ_{ij} we must take averages for all phases which satisfy (18). If we write $E(X; a_i, \Delta a_i)$ for the characteristic function[12] of the set of X's where (18) is satisfied we have

$$\langle \Delta a_i \rangle = \lim_{\Delta a_k \to 0} \int_0^T d\tau \int v_i(X_\tau) E(X; a_k, \Delta a_k) dX / w(a_1 \cdots a_s) \Delta a_1 \cdots a_s, \tag{21a}$$

$$\langle \Delta a_i \Delta a_j \rangle = \lim_{\Delta a_k \to 0} \int_0^T \int_0^T d\tau d\tau' \int v_i(X_\tau) v(X_{\tau'}) E(X; a_k, \Delta a_k) / w(a_i \cdots a_s) \Delta a_1 \cdots \Delta a_s, \tag{21b}$$

where $w(a_1 \cdots a_s)\Delta a_1 \cdots \Delta a_s$ is the volume of phase space where (17) is satisfied. Equations (21a), (21b) are special cases of integrals of the following type:

$$\int_0^T d\tau \int v_i(X_\tau) \varphi[A(X)] dX \tag{22a}$$

$$\int_0^T \int_0^T d\tau d\tau' \int v_i(X_\tau) v_j(X_{\tau'}) \varphi[A(X)] dX, \tag{22b}$$

where we have written $A(X)$ for the set of functions $a_1(X) \cdots a_s(X)$. We will obtain a general formula for such expressions which we will then apply to (21a) and (21b). Let us divide the region of integration over $d\tau d\tau'$ in (22b) into two parts, the part where $\tau' > \tau$ and the part where $\tau > \tau'$. In the second part we rename the variables so that $\tau \to \tau'$, $\tau' \to \tau$. We obtain thus for (22b)

$$\int_0^T d\tau' \int_0^{\tau'} d\tau \int (v_i(X_\tau) v_j(X_{\tau'}) + v_j(X_\tau) v_i(X_{\tau'}) \varphi[A(X)]) dX. \tag{22c}$$

We see that (22c) is the sum of two terms, one for the indices (i, j), and one for the indices (j, i). Henceforth we will not write the second term, but simply remember to include both in our final formulas. We now change the variable of integration from X to $Y = X_t$. Since our equations of motion are in Hamiltonian form, the Jacobian of this transformation is 1. We have for (22a) and (22c)

$$\int_0^T d\tau \int v_i(Y) \varphi[A(Y_{-\tau})] dY, \tag{23a}$$

$$\int_0^T d\tau' \int_0^{\tau'} d\tau \int v_i(Y) v_j(Y_{\tau'-\tau}) \varphi[A(Y_{-\tau})] dY. \tag{23b}$$

We note that in (23a) and (23b) the a_i are taken at the time $-\tau$ which is different from 0 by an amount which is less than T, a macroscopically short time. Since the a_i have been assumed to be approximate integrals of motion the differences,

$$a_i(X_0) - a_i(X_{-\tau}) = \int_{-\tau}^0 v_i(X_\sigma) d\sigma$$

can be considered to be small. It is a reasonable procedure therefore to expand $\varphi[A(Y_{-\tau})]$ in a power series in the Δa_i. If we do this we obtain for (23a)

$$\int_0^T d\tau \int v_i(Y) \varphi[A(Y)] dY - \sum_k \int_0^T d\tau \int_{-\tau}^0 d\sigma v_i(Y) v_k(Y_\sigma) \varphi_k[A(Y)] dY + \tag{24a}$$

etc. $\varphi_k(A)$ is the partial derivative of φ with respect to a_k. The terms we have not written involve products of more than two v_i's. Since we have assumed that the v_i are small these terms are of higher order than those we have written and we will provisionally neglect such terms in all our formulas in this paper. To this approximation (23b) becomes

$$\int_0^T d\tau' \int_0^{\tau'} d\tau \int v_i(Y) v_j(Y_{\tau'-\tau}) \varphi[A(Y)] dY. \tag{24b}$$

We note that averages such as $\langle \Delta a_i \Delta a_j \Delta a_k \rangle$ involve products of more than two v_i's and we are consistent in neglecting them.

[12] The characteristic function of a set is the function which has the value 1 for all points in the set, and zero elsewhere.

We have

$$\int_0^T d\tau \int v_i(Y_\tau)\varphi[A(Y)]dY = \int \Delta a_i \varphi[A(Y)]dY$$

$$= \int \langle \Delta a_i \rangle \varphi(A) w(A) dA, \quad (25a)$$

$$\int_0^T d\tau \int_0^T d\tau' \int v_i(Y_\tau) v_j(Y_{\tau'}) \varphi[A(Y)]dY$$

$$= \int \Delta a_i \Delta a_j \varphi[A(Y)]dY$$

$$= \int \langle \Delta a_i \Delta a_j \rangle w(A)\varphi(A)dA, \quad (25b)$$

with $A=(a_1\cdots a_s)$, $dA=da_1\cdots da_s$. From (24a) and (24b) we have

$$\int \langle \Delta a_i \rangle \varphi(A) w(A) dA = \int_0^T d\tau \int \langle v_i \rangle w(A)\varphi(A)dA$$

$$-\sum_k \int_0^T d\tau \int_{-\tau}^0 d\sigma \langle v_i v_k(\sigma)\rangle w(A)\varphi_k(A)dA, \quad (26a)$$

$$\int \langle \Delta a_i \Delta a_j \rangle \varphi(A) w(A) dA = \int_0^T d\tau' \int_0^{\tau'} d\tau [\langle v_i v_j(\tau'-\tau)\rangle$$

$$+\langle v_j v_i(\tau'-\tau)\rangle] w(A)\varphi(A)dA. \quad (26b)$$

By partial integration we obtain for (25a)

$$\int \langle \Delta a_i \rangle \varphi(A) w(A) dA = \int_0^T d\tau \int \langle v_i \rangle w(A)\varphi(A)dA$$

$$+\frac{\partial}{\partial a_k}\int_0^T d\tau \int_{-\tau}^0 d\sigma \int \langle v_i v_k(\sigma)\rangle w(A)\varphi(A)dA. \quad (26c)$$

Since $\varphi(A)$ is arbitrary we obtain

$$\langle \Delta a_i \rangle = \langle v_i \rangle T + w^{-1}\frac{\partial}{\partial a_k} w \int_0^T d\tau \int_{-\tau}^0 d\sigma \langle v_i v_k(\sigma)\rangle, \quad (27a)$$

$$\langle \Delta a_i \Delta a_j \rangle = \int_0^T d\tau' \int_0^{\tau'} d\tau [\langle v_i v_j(\tau'-\tau)\rangle$$

$$+\langle v_j v_i(\tau'-\tau)\rangle]. \quad (27b)$$

We see that the first term on the right in (27a) is the first approximation we have already given. The second term on the right in (27a) and two terms on the right in (27b) all involve time-integrals of the expressions $\langle v_i v_j(\sigma)\rangle$. Now if the a_i were all actual integrals of motion of the system the expressions would be equal to the time-averages

$$\lim_{T\to\infty} T^{-1}\int_0^T v_i(X_\tau)v_j(X_{\tau+\sigma})d\tau, \quad (28)$$

which is an element of the autocorrelation matrix of the functions $v_1(X_\tau)\cdots v_s(X_\tau)$. Under the actual circumstances it is not unreasonable to expect that the quantities $\langle v_i v_j(\sigma)\rangle$ behave like the elements $w_{ij}(\sigma)$ of an autocorrelation matrix. In Appendix I we will discuss the following properties of such a matrix:

(a) for $\sigma=0$, $w_{ij}(0)=\langle v_i v_j\rangle$,
(b) for $\sigma\to\infty$, $\lim_{\sigma\to\infty} w_{ij}(\sigma)=\langle v_i\rangle\langle v_j\rangle$,
(c) $w_{ij}(-\sigma)=w_{ji}(\sigma)$,
(d) under certain circumstances the integral

$$\int_0^\infty [\langle v_i v_j(\sigma)\rangle - \langle v_i\rangle\langle v_j\rangle]d\sigma = \xi_{ij}$$

exists.

If we assume these properties for the quantities $\langle v_i v_j(\sigma)\rangle$ and that the integral in (d) converges to ξ_{ij} for σ greater than a certain macroscopically short time θ we obtain

$$\langle \Delta a_i \rangle = T\left[\langle v_i\rangle + w^{-1}\sum_k \frac{\partial}{\partial a_k} w\xi_{ki}\right], \quad (29a)$$

$$\Delta a_i \Delta a_i = T[\xi_{ij}+\xi_{ji}] = 2T\xi_{ij}. \quad (29b)$$

Equations (29a) and (29b) are correct to terms of the order T. The paradox of neglecting terms of order T^2 compared to terms of order T can be resolved if we remember that while T must be large compared to θ it is still a macroscopically short time. Substituting these expressions into (16a) and (16b) we obtain the Fokker-Planck equation:

$$\frac{\partial T}{\partial t} = \sum_i \frac{\partial}{\partial a_i}\left[\left(\langle v_i\rangle + \sum_j w^{-1}\frac{\partial}{\partial a_j} w\xi_{ij}\right)T + \sum_j \frac{\partial}{\partial a_j}\xi_{ij}T\right]. \quad (30)$$

E. THE PHENOMENOLOGICAL EQUATIONS OF MOTION

If we multiply (30) by a_k and integrate over dA we will obtain an expression for the rate of change of the expectation value $\langle a_k\rangle$. After two partial integrations we obtain

$$\frac{d}{dt}\langle a_k\rangle = \int \left(\langle v_k\rangle + \sum_j w^{-1}\frac{\partial}{2a_j} w\xi_{jk}\right)TdA$$

$$= \int \left(\langle v_k\rangle + \sum_j \xi_{jk}\frac{\partial}{\partial a_j}\log w + \sum_j \frac{\partial}{\partial a_j}\xi_{jk}\right)TdA. \quad (31)$$

If the expression in parentheses is a slowly varying function of the a_i, and if T is sharply peaked around the

values $\langle a_i\rangle$ we obtain the ordinary differential equations

$$\frac{d}{dt}\langle a_k\rangle=\left(\langle v_k\rangle+\sum_j \xi_{jk}\frac{\partial}{\partial a_j}\log w+\sum_j \frac{\partial}{\partial a_j}\xi_{jk}\right)\Bigg|_{\langle a_1\rangle\cdots\langle a_s\rangle}. \quad (32)$$

The expression in parentheses is evaluated at the expectation values $\langle a_1\rangle\cdots\langle a_s\rangle$. These are the phenomenological equations of motion.

F. THE EQUILIBRIUM SOLUTION

If we multiply (30) by $\rho_1(a_i^{(0)})$, where the $a_i^{(0)}$ are the values of the gross variables at t_0 and integrate over $da_1^{(0)}\cdots da_s^{(0)}$, we see from (18) that $\rho_1(a_i)$ must be a solution of (30). Since $\rho_1(a_i)$ is independent of the time we have

$$0=\frac{\partial\rho_1}{\partial t}=\sum_k \frac{\partial}{\partial a_k}\left[-\left(\langle v_k\rangle+\sum_j w^{-1}\frac{\partial}{\partial a_j}w\xi_{jk}\right)\rho_1+\sum_j \frac{\partial}{\partial a_j}\xi_{jk}\rho_1\right]. \quad (33)$$

Now $\rho_1(a_i)$ must be of the form $w(A)\psi[E(A)]$ where $\psi[E(A)]$ is determined by the distribution of the energy $E[A(X)]=H(X)$. We wish to show that any function of the form $w(A)\psi[E(A)]$ is a solution of (30). We may transform (30) by inserting ξ_{jk} for $\bar{\xi}$ in the last term (since ξ_{jk} is symmetric in j and k). We have

$$\frac{\partial\rho_1}{\partial t}=\sum_k \frac{\partial}{\partial a_k}\rho_1\left[-\langle v_i\rangle+\sum_j \frac{\partial}{\partial a_j}\xi_{jk}\log\frac{\rho}{w}\right]=0. \quad (34)$$

Substituting $w(A)\psi[E(A)]$ for ρ_1 we have for the left-hand side of (31),

$$\sum_k \frac{\partial}{\partial a_k}w\psi\left\{-\langle v_k\rangle+\sum_j \frac{\partial}{\partial a_j}\frac{\partial\log\psi}{\partial E}\left[\xi_{jk}\frac{\partial E}{\partial a_j}\right]\right\}.$$

We will show that both the expression in square brackets and the first term are zero.

We have

$$0=\Delta E=E[A(X)]-E[A(X_T)]=\sum_j \frac{\partial E}{\partial a_j}\Delta a_j=\sum_j \frac{\partial E}{\partial a_j}\int_{-T}^{0} v_j(\sigma)d\sigma.$$

If we multiply (32) by $v_k(0)$ and integrate over the region (18) we obtain

$$\sum_j \frac{\partial E}{\partial a_j}\int_T^0 \langle v_j(\sigma)v_k\rangle d\sigma=0$$

and by the definition of ξ_{jk}

$$\sum_j \frac{\partial E}{\partial a_j}\xi_{jk}=0. \quad (35)$$

Moreover, we will show in Appendix II that if $P(Xt)$ is a solution of the Liouville equation

$$\frac{\partial}{\partial t}\langle P\rangle w=-\sum_k \frac{\partial}{\partial a_k}w\langle v_k P\rangle. \quad (36)$$

Since $\psi[E(A(X))]$ is such a solution, we have

$$0=\frac{\partial}{\partial t}\psi w=-\sum_k \frac{\partial}{\partial a_k}\langle v_k\rangle w. \quad (37)$$

G. THE INCREASE OF ENTROPY

Up to the present we have been concerned with the solutions of (30) which approach $\delta(a_i-a_i^{(0)})$ as $t\to 0$. These are to be interpreted as giving the distribution of the a_i when we know that they certainly had the values $a_i^{(0)}$ at $t=0$. Equation (30), however, has solutions which approach an arbitrary distribution $\rho_0(A)$ as $t\to 0$. These solutions must be interpreted as giving the distribution of the a_i at t when their distribution at 0 is $\rho_0(A)$.[13]

We can associate with such a solution $\rho(A,t)$ a quantity

$$S=-\int \rho\log\rho/w dA, \quad (38)$$

which is analogous to the quantity

$$S'=-\int P(X)\log P(X)dX, \quad (39)$$

which Gibbs has identified with the entropy (for a system of units in which Boltzmann's constant = 1) of phenomenological thermodynamics.[14] $P(X)$ is a distribution in phase space. Indeed if $P(X)$ is a distribution which gives an equal probability to equal volumes contained in the same region (18), i.e., if $P(X)$ is a function of the gross variables we have

$$P(X)=\rho[A(X)]/w[A(X)], \quad (40)$$

where $P(A)$ is the distribution of the gross variables corresponding to $P(X)$ and

$$S'=S.$$

[13] We note that the transition probability T is not a genuine function since $T=0$ unless $E(a_i^{(0)})=E(a_i)$. We can, however, express T in terms of delta-"functions." All formal operations can then be carried out using the rules for delta-"functions."

[14] J. W. Gibbs, *Elementary Principles of Statistical Mechanics* (Yale University Press, New Haven, 1902).

In general if $P(X)$ is not a function of the a_i we have

$$S=-\int P(X)\log\langle P(X)\rangle dX.$$

We wish to show that S always increases unless $\rho(A)$ is an equilibrium distribution. Firstly if $\rho_1(A)$ is an equilibrium distribution,

$$S_{EQ}=-\int\rho_1(A)\log\frac{\rho_1(A)}{w(A)}dA$$

is greater than S for any ρ having the same distribution of energy. For any $\rho(A)$ the distribution of energy is

$$\chi(E)=\lim_{\Delta E\to 0}\Delta E^{-1}\int_{E\leq E(A)\leq E+\Delta E}\rho(A)dA. \quad (41)$$

For an equilibrium distribution $\rho_1(A)=w(A)\psi[E(A)]$ this expression is

$$\chi(E)=\psi(E)\lim_{\Delta E\to 0}(\Delta E^{-1})\int_{E\leq E(A)\leq E+\Delta E}w(A)dA$$
$$=\psi(E)U(E).$$

In terms of $\chi(E)$ and $w(E)$ we have for an equilibrium distribution

$$\rho_1(A)=\chi(E)w(A)/U(E). \quad (42)$$

We have

$$S_{EQ}-S=-\int\left[\rho_1(A)\log\frac{\chi(E)}{U(E)}-\rho(A)\log\frac{\rho(A)}{w(A)}\right]dA,$$

and since $\rho(A)$ has the same distribution of energy $\chi(E)$ as $\rho_1(A)$, we can write this as

$$S_{EQ}-S=-\int\rho(A)\log\rho_1(A)/\rho(A)dA.$$

Since $\rho_1(A)$ and $\rho(A)$ are both distributions we have

$$\int\rho(A)(\rho_1(A)/\rho(A)-1)dA=0.$$

Adding the latter to the former we have

$$S_{EQ}-S=\int\rho(A)(-\log\rho_1(A)/\rho(A)$$
$$+\rho_1(A)/\rho(A)-1)dA. \quad (43)$$

The quantity in the parenthesis is of the form $(x-1-\log x)$ which is always positive unless $x=0$. $S_{EQ}>S$ unless $\rho(A)=\rho_1(A)$.

Returning now to the rate of change of S we have

$$\frac{dS}{dt}=-\int\frac{\partial\rho}{\partial t}\log\frac{\rho}{w}dA-\int\frac{\partial\rho}{\partial t}dA$$
$$=-\int\frac{\partial\rho}{\partial t}\log\frac{\rho}{w}dA. \quad (44)$$

If we write the Fokker-Planck equation in the form (31) we have

$$\frac{\partial\rho}{\partial t}=\sum_k\frac{\partial}{\partial a_k}\rho\left[-\langle v_k\rangle+\sum_i\frac{\partial}{\partial a_j}\xi_{jk}\log\frac{\rho}{w}\right]. \quad (45)$$

Introducing this expression for $\partial\rho/\partial t$ into (44) and performing a partial integration, we obtain

$$\frac{dS}{dt}=-\sum_k\int\rho\langle v_k\rangle\frac{\partial}{\partial a_k}\log\frac{\rho}{w}dA$$
$$+\sum_{jk}\int\rho\xi_{jk}\frac{\partial}{\partial a_k}\log\frac{\rho}{w}\frac{\partial}{\partial a_j}\log\frac{\rho}{w}dA. \quad (46)$$

The integrand in the first term can be written

$$\sum_k\frac{\partial}{\partial a_k}\rho\langle v_k\rangle-\frac{\rho}{W}\frac{\partial}{\partial a_k}w\langle v_k\rangle$$

and applying (36) for the case in which $P(X)=1$ we see that this integrand is the divergence of a vector that vanishes for large values of the a_i and the first term is zero. We have

$$\frac{dS}{dt}=\int\rho\sum_{jk}\xi_{jk}\frac{\partial}{\partial a_j}\log\frac{\rho}{w}\frac{\partial}{\partial a_j}\log\frac{\rho}{w}dA. \quad (47)$$

Now the matrix ξ_{jk} is the limit of the matrix $\Delta t^{-1}\langle\Delta a_j\Delta a_k\rangle$ which must be at least positive semi-definite, and if this limit exists must be semi-definite as well. This means that any quadratic form

$$\sum_{jk}Z_jZ_k\xi_{jk}\geqslant 0.$$

From (32) we see that this form is zero if and only if $Z_j=c(a_1\cdots a_s)\partial E/\partial a_j$. The quantity S always increases unless

$$\partial\log(\rho/w)/\partial a_j=c(a_1\cdots a_s)\partial E/\partial a_j.$$

This can only be true if ρ has the form

$$\rho(A)=w(A)\psi[E(A)].$$

We have stated that the approximation $\bar{v}_i=\langle v_i\rangle$ does not give an account of irreversible phenomena. This approximation amounts to the setting of $\xi_{jk}=0$. The rate of increase of S is then zero. Moreover the Fokker-

Planck equation becomes

$$\frac{\partial \rho}{\partial t}+\frac{\partial}{\partial a_k}\langle v_k\rangle\rho=0. \tag{48}$$

This equation is of the same form as the Liouville equation with $W(A)$ playing the role of the volume in phase space, and like the Liouville equation has solutions which are linear combinations of purely oscillatory functions of the time. Only if ξ_{ij} is not equal to zero does the Fokker-Planck have solutions which die out with increasing time.[15]

H. ONSAGER'S RECIPROCAL RELATIONS

Equations (32) have a form which is very similar to the form which Onsager assumed in his discussion of reciprocal relations between the phenomenological constants of irreversible phenomena.[3,4] Indeed if the $\langle v_k\rangle$ are identically zero and ξ_{jk} are constants the phenomenological equations have precisely Onsager's form

$$da_k/dt=\xi_{jk}\partial \log w/\partial a_j. \tag{49}$$

This suggests that the ξ_{jk} obey certain reciprocal relations which reduce to Onsager's when (49) is valid.

Onsager's theory depends on the fact that the Hamiltonian function is a symmetric function of the momenta. If we write $-X$ for the phase in which each of the momentum components of X is changed to its negative, while all of the coordinate components remain unchanged, we can express this symmetry by the relation

$$H(-X)=H(X). \tag{50}$$

Equation (49) has the consequence that if the phase X goes into the phase X_t in time t, the phase $-X_t$ goes into the phase $-X$ in the same time. Symbolically

$$[-X_t]_t=-X. \tag{51}$$

Onsager's relations are supposed to hold for cases in which all of the gross variables are either symmetric or antisymmetric functions of the momenta. If we call the symmetric functions α_κ and the antisymmetric functions β_μ we have

$$\begin{aligned}\alpha_\kappa(-X)&=\alpha_\kappa(X) &&\kappa=1\cdots m\\ \beta_\mu(-X)&=-\beta_\mu(X) &&\mu=1\cdots n.\end{aligned}$$

In what follows we will use the indices κ, λ for the α's and μ, ν for the β's. We will use the symbols α for the set of symmetric functions and β for the set of antisymmetric functions.

We will derive symmetry relations for $W(\alpha,\beta)$, $\rho_1(\alpha,\beta)$, $\langle v_\kappa\rangle_{\alpha\beta}$, $\rho_2(\alpha^{(1)},\beta^{(1)}t_1,\ \alpha^{(2)},\beta^{(2)}t_2)$,

$$T(\alpha^{(1)},\beta^{(1)}t_1/\alpha^{(2)},\beta^{(2)}t_2),\ \xi_{\kappa\lambda}(\alpha,\beta).$$

[15] For a discussion of the spectral analysis of the motion of a probability distribution in phase space see B. O. Koopman, Proc. Nat. Acad. Sci. **17**, 315 (1931).

We have

$$w(\alpha,-\beta)\Delta\alpha\Delta\beta=\int_R dX,$$

where R is the region where

$$\begin{aligned}\alpha_\kappa\leqq\alpha_\kappa(X)\leqq\alpha_\kappa+\Delta\alpha_\kappa &&\kappa=1\cdots m\\ -\beta_\mu\leqq\beta_\kappa(X)\leqq-\beta_\mu+\Delta\beta_\mu &&\mu=1\cdots n.\end{aligned}$$

If we change the region of integration to $X'=-X$ we have

$$w(\alpha,-\beta)\Delta\alpha\Delta\beta=\int_{R'} dX,$$

where R' is the region where

$$\begin{aligned}\alpha_\kappa\leqq\alpha_\kappa(-X')\leqq\alpha_\kappa+\Delta\alpha_\kappa &&\kappa=1\cdots m,\\ -\beta_\mu\leqq\beta_\mu(-X')\leqq-\beta_\mu+\Delta\beta_\mu &&\mu=1\cdots n.\end{aligned}$$

By the symmetry properties of the α's and β's this region is the same as the region where

$$\begin{aligned}\alpha_\kappa\leqq\alpha_\kappa(X')\leqq\alpha_\kappa+\Delta\alpha_\kappa &&\kappa=1\cdots m\\ \beta_\mu-\Delta\beta_\mu\leqq\beta_\mu(X')\leqq\beta_\mu &&\mu=1\cdots n.\end{aligned}$$

Thus we have

$$w(\alpha,-\beta)=w(\alpha,\beta). \tag{52}$$

Since $\rho_1(\alpha,\beta)=w(\alpha,\beta)\psi[E(\alpha,\beta)]$ and since

$$\begin{aligned}E[\alpha(X),\beta(X)]&=H(X)=H(-X)\\ &=E[\alpha(-X),\beta(-X)]=E[\alpha(X),-\beta(X)],\end{aligned}$$

we have the symmetry relation

$$\rho_1(\alpha,-\beta)=\rho_1(\alpha,\beta). \tag{53}$$

Similarly for $\langle v_\kappa\rangle$ we have

$$\langle v_\kappa\rangle_{\alpha,-\beta}w(\alpha,-\beta)\Delta\alpha\Delta\beta=\int_R v_\kappa(X)dX,$$

and making the transformation from X to X',

$$\langle v_\kappa\rangle_{\alpha,-\beta}w(\alpha,-\beta)\Delta\alpha\Delta\beta=\int_{R'} v_\kappa(-X')dX'.$$

Now

$$\begin{aligned}v_\kappa(X')&=\frac{d}{dt}\alpha_\kappa(X_t')\Big|_{t=0}\\ v_\kappa(-X)&=\frac{d}{dt}\alpha_\kappa[(-X)_t]\Big|_{t=0}\\ &=\frac{d}{dt}\alpha_\kappa(-X_{-t})\Big|_{t=0}\\ &=-v_\kappa(X')\end{aligned}$$

from (49) and the symmetry properties of α_κ. Thus a v corresponding to an α is an antisymmetric function and

$$\langle v_\kappa\rangle_{\alpha,-\beta}=-\langle v_\kappa\rangle_{\alpha,\beta}. \tag{54a}$$

A similar argument shows that a v_μ is a symmetric function and

$$\langle v_\mu\rangle_{\alpha,-\beta}=\langle v_\mu\rangle_{\alpha,-\beta}. \tag{54b}$$

To derive the symmetry relations for

$$\rho_2(\alpha^{(1)}\beta^{(1)}t_1,\alpha^{(2)},\beta^{(2)}t_2)$$

we express this distribution as

$$\Delta\alpha^{-1}\Delta\beta^{-1}\int_{R''}\psi[H(X)]dX,$$

where $\psi[H(X)]$ is the distribution of initial phases (section A) and R'' is now the region where

$$\begin{aligned}\alpha_\kappa^{(1)}\leqq\alpha_\kappa(Xt_1)\leqq\alpha_\kappa^{(1)}+\Delta\alpha_\kappa^{(1)} &\qquad \kappa=1\cdots m\\ \beta_\mu^{(1)}\leqq\beta_\mu(Xt_1)\leqq\beta_\mu^{(1)}+\Delta\beta_\mu^{(1)} &\qquad \mu=1\cdots n\end{aligned}$$

and

$$\begin{aligned}\alpha_\kappa^{(2)}\leqq\alpha_\kappa(Xt_2)\leqq\alpha_\kappa^{(2)}+\Delta\alpha_\kappa^{(2)}\\ \beta_\mu^{(2)}\leqq\beta_\mu(Xt_2)\leqq\beta_\mu^{(2)}+\Delta\beta_\mu^{(2)}.\end{aligned}$$

If we change our variable of integration to $X'=-X$ we must integrate over the region R''' where

$$\begin{aligned}\alpha_\kappa^{(1)}\leqq\alpha_\kappa[(-Xt_1')]\leqq\alpha_\kappa^{(1)}+\Delta\alpha_\kappa^{(1)} &\qquad \kappa=1\cdots m\\ \beta_\mu^{(1)}\leqq\beta_\mu[(-Xt_1')]\leqq\beta_\mu^{(1)}+\Delta\beta_\mu^{(1)} &\qquad \mu=1\cdots n\end{aligned}$$

and

$$\begin{aligned}\alpha_\kappa^{(2)}\leqq\alpha_\kappa[(-X')t_2]\leqq\alpha_\kappa^{(2)}+\Delta\alpha_\kappa^{(2)}\\ \beta_\mu^{(2)}\leqq\beta_\mu[(-X')t_2]\leqq\alpha_\kappa^{(2)}+\Delta\beta_\mu^{(2)}.\end{aligned}$$

Since by (49) $(-X')t_1=-X_{-t_1}'$, $(-X')t_2=(-X')_{-t_2}$ and by the symmetry properties of the α's and β's, R''' is the region which defines $\rho_2(\alpha^{(1)},-\beta^{(1)}-t_1,\alpha^{(2)},-\beta^{(2)}-t_2)$. Moreover $\psi[H(X)]$ is invariant under the change of variables. Thus we have

$$\rho_2(\alpha^{(1)},\beta^{(1)}t_1,\alpha^{(2)},-\beta^{(2)}t_2)=\rho_2(\alpha^{(1)},\beta^{(1)}-t_1,\alpha^{(2)},\beta^{(2)},-t_2).$$

We can put this relation in a more perspicuous form if we recall that ρ_2 is actually a function of t_2-t_1 and since $(-t_2)-(-t_1)=t_1-t_2$ we have (54)

$$\rho_2(\alpha^{(1)},-\beta^{(1)}t_1,\alpha^{(2)},-\beta^{(2)}t_2)=\rho_2(\alpha^{(1)},\beta^{(1)}t_2,\alpha^{(2)},\beta^{(2)},t_1). \tag{55}$$

We can obtain the symmetry relation for

$$T(\alpha^{(1)},\beta^{(1)}t_1/\alpha^{(2)},\beta^{(2)}t_2)$$

by expressing (51) in terms of the distribution function ρ_1 and the transition probabilities. We have

$$\rho_1(\alpha^{(1)},-\beta^{(1)})T(\alpha^{(1)},-\beta^{(1)}t_1/\alpha^{(2)},-\beta^{(2)}t_2)=\rho_1(\alpha^{(2)},\beta^{(2)})T(\alpha^{(2)},\beta^{(2)}t_1/\alpha^{(1)},\beta^{(1)}t_2),$$

and remembering that $T=0$ unless $E(\alpha^{(1)},\beta^{(1)})=E(\alpha^{(2)},\beta^{(2)})$ we obtain

$$w(\alpha^{(1)},-\beta^{(1)})T(\alpha^{(1)},-\beta^{(1)}t_1/\alpha^{(2)}-\beta^{(2)}t_2)=w(\alpha^{(2)},\beta^{(2)})T(\alpha^{(2)},\beta^{(2)}t_1/\alpha^{(1)},\beta^{(1)}t_2).$$

Let us now consider the symmetry properties of the $\xi_{\kappa\lambda}(\alpha,\beta)$. We have

$$\begin{aligned}\langle v_\kappa v_\lambda(\sigma)\rangle_{\alpha,-\beta}w(\alpha,-\beta)\Delta\alpha\Delta\beta&=\int_R v_\kappa(X)v_\lambda(X_\sigma)dX\\ &=\int_{R'}v_\kappa(-X')v_\lambda(-[(-X')_\sigma])dX'\\ &=\int_{R'}v_\kappa(-X')v_\lambda(-X'_{-\sigma})dX'\\ &=\int_{R'}v_\kappa(X')v_\lambda(X_{-\sigma}')dX=\int_{R'}v_\lambda(X')v_\kappa(X_\sigma')dX'.\end{aligned}$$

Remembering the property (c) of the elements of the autocorrelation matrix, we have

$$\xi_{\kappa\lambda}(\alpha_1-\beta)=\xi_{\lambda\kappa}(\alpha,\beta). \tag{56a}$$

A similar argument gives

$$\xi_{\kappa\mu}(\alpha,-\beta)=-\xi_{\mu\kappa}(\alpha,\beta) \tag{56b}$$

and

$$\xi_{\mu\nu}(\alpha,-\beta)=\xi_{\nu\mu}(\alpha,\beta). \tag{56c}$$

APPENDIX I

In this appendix we will consider the properties (a), (b), (c), (d), of the elements of the autocorrelation matrix. We will discuss these properties under the hypothesis that the $a_i(X)$ are all the single-valued integrals of motion of the system. Property (a) is of course an obvious consequence of the definition (28). If property (b) holds for all functions $Q(X)$, $P(X)$ the system is said to have the mixing property.[16] The significance of this term is that if $Q(X)$ is the characteristic function of a region R of phase space and $P(X)$, a probability density, property (b) means that the total probability given to the region R by the probability density $P(X_\sigma)$ approaches the ratio of the volume of R to the volume of the shell ensemble where the a_i have constant values. In other words the probability density $P(X_\sigma)$ approaches (in the sense of weak convergence)[16,17] a uniform distribution in the shell ensemble. This property has not been proved for any real dynamical system. It is known, however, that if the a_i are all the single-valued integrals of motion, and if there are no angle variables, property (c) holds in a wider sense; namely,

$$\lim_{T\to\infty}T^{-1}\int_0^T|w_{ij}(\sigma)-\langle v_i\rangle\langle v_j\rangle|^2d\sigma=0. \tag{57}$$

This means that $w_{ij}(\sigma)-\langle v_i\rangle\langle v_j\rangle$ can differ significantly from zero only during a very small fraction of a long interval. A system for which (57) is true for all phase functions $Q(X)$, $P(X)$ is said to have the mixing prop-

[16] E. Hopf, *Ergodentheorie* (Chelsea Publishing Company, New York, 1948).

[17] J. v. Neuman, Proc. Nat. Acad. Sci. **18**, 70 (1932).

erty in the wider sense. Since the existence of angle variables is an unusual circumstance for a dynamical system we can assume that (*b*) is true in the wider sense (57).

To prove (*c*) we turn to the definition (28):

$$w_{ij}(-\sigma)=\lim_{T\to\infty}T^{-1}\int_0^T v_i(X_\tau)v_j(X_{\tau-\sigma})d\tau$$

$$=\lim_{T\to\infty}T^{-1}\int_{-\sigma}^{T-\sigma} v_i(X_{\tau'+\sigma})v_j(X_{\tau'})d\tau' \quad (58)$$

$$=\lim_{T\to\infty}T^{-1}\int_0^T v_i(X_{\tau'+\sigma})v_j(X_{\tau'})d_{\tau'}$$

$$=w_{ji}(\sigma).$$

To prove (d) is a more difficult problem even when it is known that the system has the mixing property. Indeed it is probable that (d) is not true in the sense stated. We wish, however, to discuss the existence of the integral in (d) by relating it to the spectral analysis of the random process $(v_1(\sigma)\cdots v_s(\sigma))$. We suppose that the mean of each v_i is zero. According to Wiener[18] the autocorrelation matrix can be represented as the Fourier transform of another matrix, $S_{ij}(\omega)$, the so-called coherency matrix. The coherency matrix is Hermitian and is a function of an angular frequency. Its chief significance is that the spectral intensity distribution of any linear combination $v(\sigma)=\sum_i c_i v(\sigma_1)$ of the functions $v_i(\sigma)$ can be represented as a linear combination of the $S_{ij}(\omega)$. If $\Delta S=S(\omega_2)-S(\omega_1)$ is the total spectral intensity of $\nu(\sigma)$ between the angular frequencies ω_2 and ω_1 then

$$\Delta S(\omega)=\sum_{ij} c_i c_j^*\Delta S_{ij}(\omega). \quad (59)$$

The spectral energy of $v(\sigma)$ is related to its autocorrelation function $w(\sigma)$,

$$w(\sigma)=(2\pi)^{-1}\int_{-\infty}^{+\infty}\exp -i\omega\sigma dS(\omega). \quad (60)$$

Similarly

$$w_{ij}(\sigma)=(2\pi)^{-1}\int_{-\infty}^{+\infty}\exp -i\omega\sigma dS_{ij}(\omega). \quad (61)$$

The integrals in (60), (61) are to be interpreted as Stieltjes integrals since the S_{ij} need not be differentiable or even continuous. We wish, however, to consider cases in which $(d/d\omega)S_{ij}(\omega)=s_{ij}(\omega)$ exists. In this case we may speak of a density of spectral energy in the neighborhood of zero. We have now

$$w_{ij}(\sigma)=(2\pi)^{-1}\int_{-\infty}^{+\infty}\exp -i\omega\sigma s_{ij}(\omega)d\omega. \quad (62)$$

[18] N. Wiener, Acta Mathematica **55**, 117 (1930).

Then

$$\xi_{ij}=\lim_{T\to\infty}\int_0^T w_{ij}(\sigma)d\sigma$$

$$=\lim_{T\to\infty}(2\pi)^{-1}\int_{-\infty}^{+\infty}\frac{\exp -i\omega T-1}{-i\omega}s_{ij}(\omega)d\omega$$

$$=\lim_{T\to\infty}(2\pi)^{-1}\left[\int_{+\infty}^{+\infty}\frac{\sin\omega T}{\omega}s_{ij}(\omega)d\omega\right.$$

$$\left.+\int_{-\infty}^{+\infty}\frac{1-\cos\omega T}{i\omega}s_{ij}(\omega)d\omega\right].$$

Now w_{ij} is real, and therefore $s_{ij}(-\omega)=s_{ij}^*(\omega)$. In other words if we break s_{ij} up into its real and imaginary parts, $s_{ij}(\omega)=u_{ij}(\omega)+iv_{ij}(\omega)$, we have $u_{ij}(-\omega)=u_{ij}(\omega)$, $v_{ij}(-\omega)=-v_{ij}(\omega)$. Moreover, $u_{ji}=u_{ij}$, $v_{ji}=-v_{ij}$. Proceeding to the limit, the first term is $\frac{1}{2}u_{ij}(0)$ since $v_{ij}(0)=0$. The second term will involve only the antisymmetric part of w_{ij} since $\omega^{-1}(1-\cos\omega T)$ is antisymmetric. Since $\cos\omega T$ is a more and more rapidly oscillating function of ω for large T, we have

$$\xi_{ij}=\tfrac{1}{2}u_{ij}(0)+\int_{-\infty}^{+\infty}\omega^{-1}v_{ij}(\omega)d\omega. \quad (63)$$

We have not attempted a rigorous derivation of (63). We may suppose, however, that if the quantities on the right exist in some sense, ξ_{ij} will exist in a corresponding sense. In Appendix III we will give an example in which, while the spectral intensity $S_{ij}(\omega)$ is discontinuous the expression $(2\omega)^{-1}[S_{ij}(\omega)-S_{ij}(-\omega)]$ has a quite definite value for ω small, but not too small.

APPENDIX II

In this appendix we wish to prove Eq. (36) of Sec. F. Let $P(X,t)$ be a solution of Liouville's equation

$$\frac{\partial P}{\partial t}+\sum_r u_r\frac{\partial P}{\partial x_r}. \quad r=1\cdots N; \quad (64)$$

the x_r are the components of X while the $u_r(X)$ are the corresponding rates of change. N is the number of degrees of freedom. The dynamical equations of motion are

$$\frac{d}{dt}x_r=u_r(X). \quad (65)$$

The $u_r(X)$ satisfy the partial differential equation

$$\sum_r\frac{\partial u_r}{\partial x_r}=0. \quad (66)$$

We have by (66)

$$\frac{\partial P}{\partial t}=-\sum_r\frac{\partial}{\partial x_r}u_r P. \quad (67)$$

Let us multiply (66) by an arbitrary function, $\varphi[A(X)]$, of the gross variables, and integrate over the whole phase space. We have

$$\frac{d}{dt}\int P(X,t)\varphi[A(X)]dX = -\sum_r \int \varphi[A(X)]\frac{\partial}{\partial x_r}u_r P(X,t)dX \quad (68)$$

$$= \sum_k \int \varphi_k[A(X)]\left\{\sum_r \frac{\partial a_k}{\partial x_r}u_r\right\}P(X,t)dX,$$

$$\varphi_k = \frac{\partial \varphi(A)}{\partial a_k}.$$

The second equation is derived from the first by a partial integration. The quantity in the curved bracket is precisely $v_k(X)$ since from (65)

$$v_k = \frac{d}{dt}a_k = \sum_r \frac{\partial a_k}{\partial x_r}\frac{dx_r}{at} = \sum_r \frac{\partial a_k}{\partial x_r}u_r.$$

Thus, integrating over regions (18) and then over dA we have

$$\frac{d}{dt}\int \varphi(A)\langle P(X,t)\rangle w(A)dA = \sum_k \int \varphi_k(A)\langle v_k P\rangle w(A)dA.$$

A second partial integration yields

$$\int \varphi(A)\frac{\partial}{\partial t}\langle P(X,t)\rangle w(A)dA = -\sum_k \int \varphi(A)\frac{\partial}{\partial a_k}\langle v_k P\rangle w(A)dA.$$

Since $\varphi(A)$ is an arbitrary function,

$$\frac{\partial}{\partial t}\langle P\rangle = -w^{-1}\sum_k \frac{\partial}{\partial a_k}\langle v_k P\rangle w. \quad (69)$$

For the case $\rho = 1$ this becomes

$$\frac{\partial}{\partial a_k}\langle v_k\rangle w = 0. \quad (70)$$

APPENDIX III

In the course of our arguments thus far we have not been able to prove many of our statements by rigorous mathematical methods. It will therefore be very worth while to examine an example which, while it is not very physical, can be carried through in all its details. The example which we will consider is the motion of a particle on a two-dimensional torus, i.e., on a square $0 \leqslant x_1 \leqslant a$, $0 \leqslant x_2 \leqslant a$ in which the points $(x_1, a)(a, x_2)$ are considered to be identical to the points $(x_1, 0), (0, x_2)$, respectively. If there are no forces acting on the particle, the trajectories will be segments of straight lines parallel to the vector $(p_1 p_2)$, where p_1, p_2 are the components of the momentum of the particle. If p_1 and p_2 are not commensurable, the trajectory will cover the torus everywhere densely. p_1 and p_2 will be two independent integrals of motion and the energy will be

$$E(p_1 p_2) = (2M)^{-1}(p_1^2 + p_2^2), \quad (71)$$

where M is the mass of the particle.

Let us now consider the case in which there is a small perturbing force field with a potential $V(x_1 x_2)$ acting on the particle. p_1 and p_2 will no longer be integrals of motion, and after a long enough time the direction of $(p_1 p_2)$ will have all possible values with equal probability. Since (71) will still be approximately true, the magnitude of $(p_1 p_2)$ will be approximately constant. Moreover, if V is small enough p_1 and p_2 will be approximate integrals of motion and we may expect that the analysis of the main part of this paper will apply. We take p_1 and p_2 to be the gross variables. Equation (71) expresses the energy as a function of the gross variables.

The equations of motion will be

$$\frac{dx_1}{dt} = \frac{p_1}{M} \qquad \frac{dp_1}{dt} = -\frac{\partial V}{\partial x_1},$$
$$\frac{dx_2}{dt} = \frac{p_2}{M} \qquad \frac{dp_2}{dt} = -\frac{\partial V}{\partial x_2}. \quad (72)$$

Let us express V as a double Fourier series with common period a.

$$V(x_1 x_2) = \sum_{m_1=-\infty}^{\infty}\sum_{m_2=-\infty}^{\infty} V_{m_1 m_2}\exp 2\pi i/a(m_1 x_1 + m_2 x_2); \quad (73)$$

we have

$$F_1 = -\frac{\partial V}{\partial x_1} = -\frac{2\pi i}{a}\sum_{m_1,m_2} m_1 V_{m_1 m_2} \times \exp\frac{2\pi i}{a}(m_1 x_1 + m_2 x_2) \quad (74a)$$

$$F_2 = -\frac{\partial V}{\partial x_2} = -\frac{2\pi i}{a}\sum_{m_1,m_2} m_2 V_{m_1 m_2} \times \exp\frac{2\pi i}{a}(m_1 x_1 + m_2 x_2). \quad (74b)$$

We are interested in the autocorrelation matrix of F_1 and F_2. To determine this we will need to know x_1, x_2 as functions of t. It will be sufficient for our purposes to take

$$x_1(t) = x_1(0) + \frac{p_1}{M}t \text{ modulo } a,$$
$$x_2(t) = x_2(0) + \frac{p_1}{M}t \text{ modulo } a. \quad (75)$$

We have then

$$\langle F_iF_j(\sigma)\rangle=\frac{4\pi}{a^2}\sum_{m_1,m_2} m_im_j|V_{m_1m_2}|^2 \times\exp\frac{2\pi i}{aM}(m_1p_1+m_2p_2)d\sigma. \quad (76)$$

The spectrum of F_1, F_2 will thus, to this approximation, contain frequencies of the form $m_1\omega_1+m_2\omega_2$ with $\omega_1=2\pi p_1/aM$, $\omega_2=2\pi p_2/aM$. ω_1 and ω_2 will be of the order of the reciprocal of the time the particle takes to cross the torus. Now let us specialize the potential $V(x_1x_2)$ to be such that $V_{m_1m_2}=V_0$ if $m_1^2+m_2^2\leqslant m^2$, $V_{m_1m_2}=0$ if $m_1^2+m_2^2\geqslant m^2$ where m is a large integer to be specified later. We can suppose that this situation is realized physically by a random distribution of scattering centers of average size am^{-1}.

Let us consider the integral

$$\int_0^T\langle F_iF_j(\sigma)\rangle d\sigma=\frac{4\pi V_0^2}{a^2}\sum_{m_1^2+m_2^2\leq m^2} m_im_j \times\frac{\sin(m_1\omega_1+m_2\omega_2)T}{m_1\omega_1+m_2\omega_2}. \quad (77)$$

For times T such that $mT(\omega_1^2+\omega_2^2)^{-\frac{1}{2}}\ll 1$ this has the value

$$T\langle F_iF_j\rangle\cong\frac{4\pi^2V_0^2}{a^2}T\int_{m_1^2+m_2^2\leq m^2} m_im_jdm_1dm_2 =\frac{\pi^3V_0^2}{a^2}m^4T\delta_{ij}. \quad (78)$$

For times T large compared to $m^{-1}(\omega_1^2+\omega_2^2)^{-\frac{1}{2}}$, Eq. (63) of Appendix I gives us an expression for this integral in terms of the density of spectral energy in the neighborhood of zero. Now clearly the quantity $\Delta\omega^{-1}n(\Delta\omega)$, where $n(\Delta\omega)$ is the number of terms in (76) with frequencies less in absolute value than $\frac{1}{2}\Delta\omega$, does not approach a limit as $\Delta\omega\to 0$. However, if ω_1 and ω_2 are not commensurable this quantity will have a fairly constant value so long as $n(\Delta\omega)$ is large compared to 1. We have for $n(\Delta\omega)$

$$n(\omega)=\int_{-m\omega_2(\omega_1^2+\omega_2^2)^{-\frac{1}{2}}}^{+m\omega_2(\omega_1^2+\omega_2^2)^{-\frac{1}{2}}}dm_1\int_{-\frac{1}{2}\frac{\Delta\omega}{\omega_2}-\frac{m_1\omega_1}{\omega_2}}^{\frac{1}{2}\frac{\Delta\omega}{\omega_2}-\frac{m_1\omega_1}{\omega_2}}dm_2 =\frac{2\Delta\omega m}{(\omega_1^2+\omega_2^2)^{\frac{1}{2}}}. \quad (79)$$

If ω_1 and ω_2 are commensurable the quantity $\Delta\omega^{-1}n(\Delta\omega)$ will have a fairly constant value as long as the common measure of ω_1 and ω_2 is small compared to $\Delta\omega$. Thus for times T such that

$$m^{-1}\theta\ll T\ll m\theta, \quad (80)$$

where $\theta=(\omega_1^2+\omega_2^2)$ is the time for the particle to cross the torus, will have the value

$$\frac{4\pi^2V_0^2}{a^2}\cdot\int_{-\infty}^{+\infty}\frac{\sin\omega T}{\omega}d\omega\cdot\Delta\omega^{-1} \times\int_{-m\omega_2(\omega_1^2+\omega_2^2)^{-\frac{1}{2}}}^{m\omega_2(\omega_1^2+\omega_2^2)^{-\frac{1}{2}}}\int_{\omega_2^{-1}(-m_1\omega_1-\frac{1}{2}\Delta\omega)}^{\omega_2^{-1}(-m_1\omega_1+\frac{1}{2}\Delta\omega)} m_im_jdm_1d =\frac{8}{3}\frac{V_0^2}{a^2}\pi^3m^3\cdot\theta(\delta_{ij}-\omega_i\omega_j\theta^2). \quad (81)$$

Expressing θ in terms of p_1 and p_2 we have

$$\xi_{ij}=Dp^{-3}(p^2\delta_{ij}-p_ip_j), \quad (82)$$

where $p=(p_1^2+p_2^2)^{-\frac{1}{2}}$ and $D=4/3\pi^2V_0^2/aMm^3$. We are now in a position to write down the Fokker-Planck equation. From (73a) and (73b) we see that $\langle F_1\rangle=\langle F_2\rangle=0$ while $w(p_1p_2)=a^2=$constant. We have

$$\sum_i\frac{\partial}{\partial p_i}\xi_{ij}=-p_jp^{-3}D \quad (83)$$

and the Fokker-Planck equation is

$$\frac{\partial\rho}{\partial t}=D\sum_j\frac{\partial}{\partial p_j}\left[-p_jp^{-3}\rho+\sum_k\frac{\partial}{\partial p_k}p^{-3}(p^2\delta_{jk}-p_jp_k)\rho\right]. \quad (84)$$

If we make the transformation of variable $p_1=p\cos\varphi$, $p_2=p\sin\varphi$ $\rho'=p\rho$, we obtain (84) in the more transparent form

$$\partial\rho'/\partial t=p^{-3}D\partial^2\rho'/\partial\theta^2. \quad (85)$$

We see that we can represent the random process of the components of momentum of the particle as a simple diffusion process in the angle φ with diffusion constant Dp^{-3}.

p^3D^{-1} has the dimensions of a time and can be interpreted as the time for the direction of the momentum to become uniformly distributed. If our analysis of the problem is to have sense, this time must be long compared the time for ξ_{ij} to converge to (82), i.e., $m^{-1}\theta$ but small compared to time for which (82) ceases to be valid, i.e., $m\theta$. We must have the inequalities

$$\frac{m^{-1}aM}{p}\ll\frac{p^3a}{V_0^2Mm^3}\ll\frac{aM}{p}m$$

or

$$m^{-1}\gg V_0Mp^{-2}\gg m^{-2}. \quad (86)$$

We see the V_0 must be a rather small fraction of the kinetic energy of the particle.

Viscosities of Some Lower Aliphatic Alcohols at Constant Volume

A. JOBLING,* *Department of Inorganic and Physical Chemistry, Imperial College of Science and Technology, London, England*

AND

A. S. C. LAWRENCE, *Chemistry Department, The University, Sheffield, England*

(Received February 29, 1952)

From an analysis of all the published experimental data for methyl, ethyl, *n*-propyl, *iso*butyl, and *n*-octadecyl alcohols, it is shown that, even for these compounds, at constant volume $\log\eta$ is a rectilinear function of $1/T$ and the general pattern of behavior is similar to that described previously. $\mathcal{E}_v$, the energy of activation of viscous flow at constant volume, is plotted as a function of volume, and the curve for ethyl alcohol shows an apparently anomalous minimum.

IT has been demonstrated recently[1] both by direct experiment and by analysis of published viscosity and compressibility data, that at constant volume there is a rectilinear relation between $\log\eta$ and $1/T$ for a number of simple organic liquids. It has been shown that this is to be expected from a study of the fuller viscosity theories of Andrade[2,3] and Eyring[4] and that the slope of the $\log\eta-1/T$ isochore is a measure of $\mathcal{E}_v$, the energy of activation of viscous flow at constant volume, which is a function of volume.

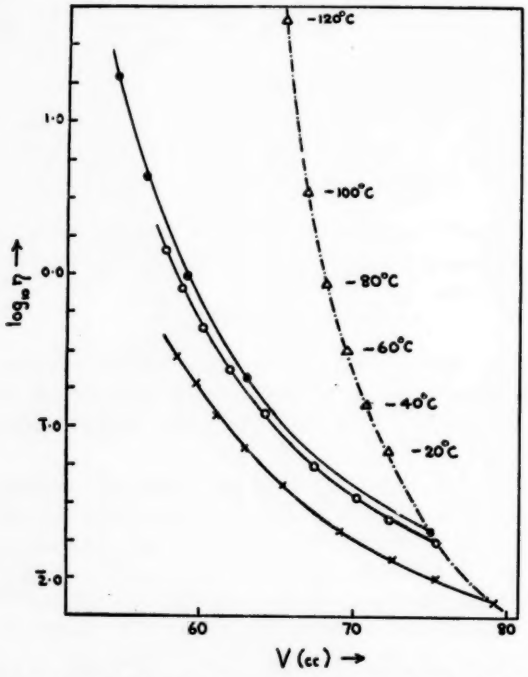

FIG. 1. $\text{Log}_{10}\eta$ (η in poises) as a function of molecular volume, V at constant temperature (*n*-propyl alcohol). ●, Bridgman, 24°C [P. W. Bridgman, Proc. Am. Acad. Arts Sci. **77**, 115 (1949)]; ○, Bridgman, 30°C (reference 5); ×, Bridgman, 75°C (reference 5); △, atmospheric pressure, various observers.

Strong evidence for the correctness of the general scheme of viscous behavior outlined in the previous paper is the fact that the behavior of those lower aliphatic alcohols for which sufficient experimental evidence is available is found to conform to a similar pattern. The $\log\eta-1/T$ isochores are again rectilinear but activation energies calculated from them are much larger than those of the corresponding paraffins.

Figure 1 shows the variation of $\log\eta$ with molecular volume at constant temperature for *n*-propyl alcohol, a typical example. From this, the variation of viscosity with temperature at constant volume is obtained by interpolation (Fig. 2; compare the corresponding Figs. 8 and 9 of the previous paper[1]).

Bridgman's measurements[5] of the viscosity of ethyl alcohol at high pressures are supplemented by those of Faust[6] at pressures up to about 3000 atmos but the

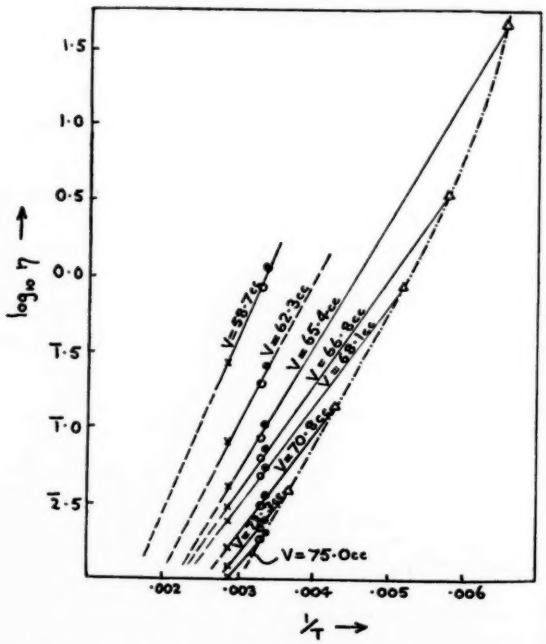

FIG. 2. $\text{Log}_{10}\eta$ (η in poises) as a function of $1/T$ at constant molecular volume V (*n*-propyl alcohol). Legend as in Fig. 1.

* Senior Student, Royal Commission for the Exhibition of 1851.

[1] A. Jobling and A. S. C. Lawrence, Proc. Roy. Soc. (London) **A206**, 257 (1951).

[2] E. N. daC. Andrade, Phil. Mag. **17**, 497 (1934).

[3] E. N. daC. Andrade, Phil. Mag. **17**, 698 (1934).

[4] Eyring, Glasstone, and Laidler, *Theory of Rate Processes* (McGraw-Hill Book Company, Inc., New York, 1941), Chapter IX.

[5] P. W. Bridgman, Proc. Am. Acad. Arts Sci. **61**, 57 (1926).

[6] O. Faust, Z. physik. Chem. **86**, 479 (1914).

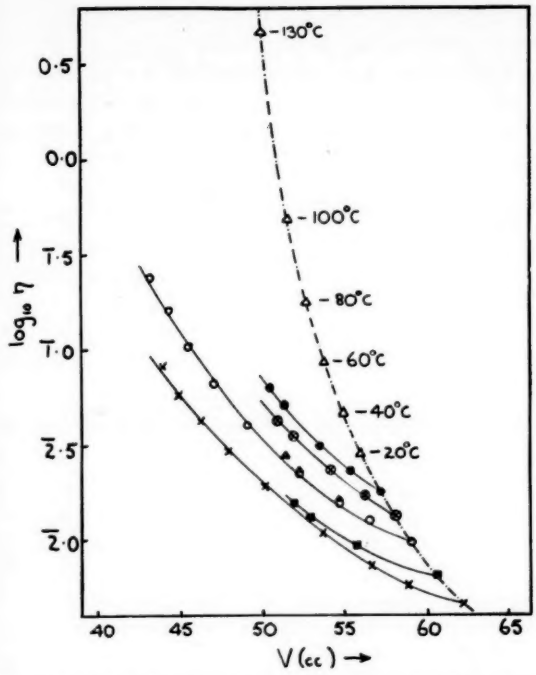

FIG. 3. $\text{Log}_{10}\eta$ (η in poises) as a function of molecular volume V at constant temperature (ethyl alcohol). ○, Bridgman, 30°C; ×, Bridgman, 75°C; ●, Faust, 0°C; ⊗, Faust, 15.1°C; ▲, Faust, 30°C; ■, Faust, 53.5°C; △, various observers, atmospheric pressure and different temperatures.

agreement is not very good. Bridgman[7] has discussed the disparity. The two sets of observations have been combined with various atmospheric pressure measure-

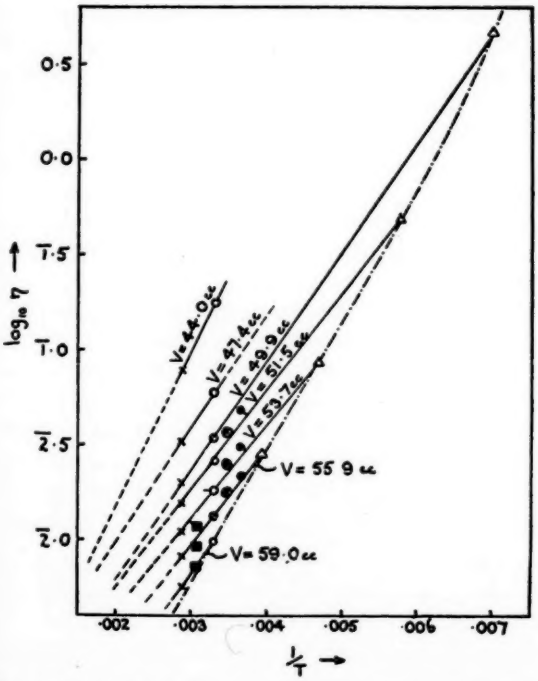

FIG. 4. $\text{Log}_{10}\eta$ (η in poises) as a function of $1/T$ at constant molecular volume V (ethyl alcohol). Legend as in Fig. 3.

[7] P. W. Bridgman, *Physics of High Pressure* (Bell and Company, London, 1949).

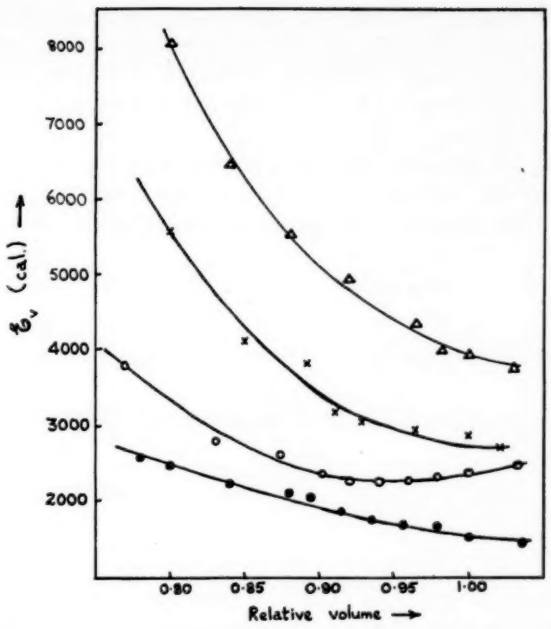

FIG. 5. $\mathcal{E}_v$ as a function of relative volume (volume relative to that at 0°C and 1 atmos pressure). ●, methyl alcohol; ○, ethyl alcohol; ×, *n*-propyl alcohol; △, *iso*-butyl alcohol.

ments in Figs. 3 and 4 to illustrate the lack of agreement. The particular importance of the behavior of ethyl alcohol will be made evident later.

Energies of activation of viscous flow at constant volume $\mathcal{E}_v$, calculated from the isochores of Figs. 2 and 4, are plotted as functions of relative volume in Fig. 5 together with the corresponding curves for methyl and *iso*-butyl alcohols. The literature references to all the relevant experimental work on these four alcohols are listed in Table I.

The reason for the minimum in the $\mathcal{E}_v$ volume curve for ethyl alcohol is not clear. It should be borne in mind that the accuracy with which $\mathcal{E}_v$ can be calculated is greatly reduced at the higher volumes where the isochores are short and errors in the determination of the viscosity are more significant. Bridgman[5] has stated

TABLE I. Viscosities and volumes of liquids at different temperatures and pressures—collected references.

Substance	Viscosity at high pressures	Volume at high pressures	Viscosity at low temperatures at atmospheric pressure	Density
MeOH	a, b	d	e, g	i
EtOH	b, c	d	f, g	i
Pr^nOH	a, b	d	f, g, h	j
Bu^iOH	b	d	f, g	j

[a] P. W. Bridgman, Proc. Am. Acad. Arts Sci. **77**, 115 (1949).
[b] See reference 5.
[c] See reference 7.
[d] P. W. Bridgman, Proc. Am. Acad. Arts Sci. **49**, 3 (1913).
[e] S. Mitsukuri and T. Tonomura, Proc. Imp. Acad. Japan **3**, 155 (1927).
[f] S. Mitsukuri and T. Tonomura, Proc. Imp. Acad. Japan **5**, 23 (1929).
[g] M. A. Veksler, J. Exp. Theor. Phys. USSR **9**, 616 (1939).
[h] G. Tammann and W. Hesse, Z. anorg. u. allgem. Chem. **156**, 245 (1926).
[i] W. Seitz and G. Lechner, Ann. Physik **49**, 93 (1916).
[j] S. Mitsukuri and Y. Kitano, Proc. Imp. Acad. Japan **5**, 21 (1929).

this region, and for other liquids slight deviations of his measurements from those of other workers were noted previously. However, the depth of the minimum seems too large to be accounted for entirely by experimental error.

If the effect is genuine, it is surprising that it is not observed for methyl alcohol also, since there is some that his experimental errors are probably greatest in rather uncertain evidence that a part of the $\mathcal{E}_v$ volume curve for water also has a positive slope.

Straight lines are also obtained on plotting $\log\eta$ against $1/T$ from the experimental data of Van Wijk, Van der Veen, Brinkman, and Seeder[8] for *n*-octadecyl alcohol.

[8] Van Wijk, Van der Veen, Brinkman, and Seeder, Physica 7, 45 (1940).

THE JOURNAL OF CHEMICAL PHYSICS VOLUME 20, NUMBER 8 AUGUST, 1952

The X-Ray *K* Absorption Edges of Covalently Bonded Cr, Mn, Fe, and Ni*

G. MITCHELL† AND W. W. BEEMAN
Department of Physics, University of Wisconsin, Madison, Wisconsin

(Received December 10, 1951)

We discuss some recently measured absorption edges of covalent nickel complexes and edges of Cr, Mn, and Fe in similar complexes already in the literature. Low energy absorption (generally resolved as a line) is observed in all complexes where empty $4p$ orbital is expected from chemical or magnetic data. From the position of the line it is concluded that the metal ion is near neutral in the covalent complex. Where the $4p$ orbital is completely used in bonding, no low energy absorption line is observed. The method may be useful as an additional experimental check on the assignment of bonding orbitals.

INTRODUCTION

THE elements of the first transition series and their compounds have been studied by a great many x-ray spectroscopists. We will confine the present discussion to the *K* edges[1,2] which lie in the nonvacuum region at 1 or 2A. The following results will be useful.

In the pure metals the absorption coefficient increases gradually, with increasing photon energy, from a low value where no *K* shell ionization occurs to a maximum, some nine times greater, where *K* electrons are being excited into the empty $4p$ band of the metal. This region of the principal absorption increase has an energy extent of 15 or 20 ev in the elements under consideration. It is followed by a series of relatively small maxima and minima of the absorption coefficient which extend for 200 or 300 ev. This is the region of the Kronig structure[3] with which we are not primarily concerned.

A fairly standard example of a metal absorption edge in the region of present interest is that of Ni in Fig. 1. In general, no strong absorption lines are found before the main $4p$ absorption at 15 or 20 ev. The natural width of the *K* excited state and a smaller contribution from the finite resolution of the crystals used in the x-ray monochromator combine to limit the resolution in these spectra to about 2 ev. However, since the absorption curve can be considered to be the sum of a large number of overlapping resonance lines of known shape, each of half-width 2 ev, analysis in terms of such lines will sometimes reveal finer detail. In particular one expects[4] and finds[1] the initial absorption (near zero ev in Fig. 1) to follow an arctangent curve. The point of inflection of the arctangent gives the photon energy necessary to excite a *K* electron into the first empty level of the Fermi distribution. This energy is conveniently chosen as a zero for a discussion of absorption edge structure close to the edge since only very rarely does an absorption of lower energy occur in any of the compounds of the element. The point of inflection can be located to about one-half ev in most cases.

The structure of the metal edges can be qualitatively understood[1] in terms of the electron band structure of the metal. In a few other simple cases a qualitative or semi-quantitative discussion of absorption structure within 15 or 20 ev of the edge is available. Parratt[5] measured the *K* edge of argon gas and found a number of absorption lines which he identified as $1s\rightarrow np$ transitions, $n=4$, 5, 6, etc. Bearden and Beeman[6] measured the edges of Ni^{++}, Cu^{++}, and Zn^{++} in aqueous solution and found two absorption lines whose separation agreed with the assignments $1s\rightarrow4p$ and an unresolved $1s\rightarrow np$, $n=5$, 6, 7, etc. to the transitions. In addition the expected separation of the $1s\rightarrow4p$ line of the ion from the

* Supported by the ONR and the Wisconsin Alumni Research Foundation.

† Now with the Capehart-Farnsworth Corporation, Fort Wayne, Indiana.

[1] W. W. Beeman and H. Friedman, Phys. Rev. **56**, 392 (1939).

[2] V. H. Sanner, thesis (Uppsala, Sweden, 1941). See also Y. Cauchois, *Les Spectra des Rayons X et la Structure Electronique de la Matiere* (Gauthier-Villars, Paris, 1948).

[3] R. de L Kronig, Z. Physik **75**, 191 (1932).

[4] Richtmyer, Barnes, and Ramberg, Phys. Rev. **46**, 843 (1934).

[5] L. G. Parratt, Phys. Rev. **56**, 295 (1939).

[6] W. W. Beeman and J. A. Bearden, Phys. Rev. **61**, 455 (1942).

lowest transition in the metal (the inflection point) could be calculated from optical term values. The experimental separation agreed with that calculated.

Monovalent copper in the cuprous halides was investigated, by Beeman, Forss, and Humphrey.[7] As with Cu^{++} a strong $1s \rightarrow 4p$ line was found. It occurs about 10 ev, below the same transition in Cu^{++} in agreement with calculation.

In summary then, the absorption edges of free atoms or of ions in solution and in the simpler ionic compounds consist of a strong $1s \rightarrow 4p$ line followed by weaker lines made up of partially resolved transitions to higher p states. The lines are usually without subsidiary structure but, except for argon gas, are much broader than the radiation plus Auger width of the K excited state. The broadening results from interaction with the unfilled $3d$ shell, Stark splitting, and also, in crystals, to interaction with the other metal ions of the lattice (band formation). The positions of the lines agree well with the calculations for isolated ions. In terms of our energy scale $1s \rightarrow 4p$ for Ni^{++} and Cu^{++} is at about 17 ev, for Cu^{+} at 7 ev, and Mn^{++} 14 ev.[8] The $1s \rightarrow 4p$ transition in an isolated copper atom would be expected at about 4 ev. Details may be found in the cited references.

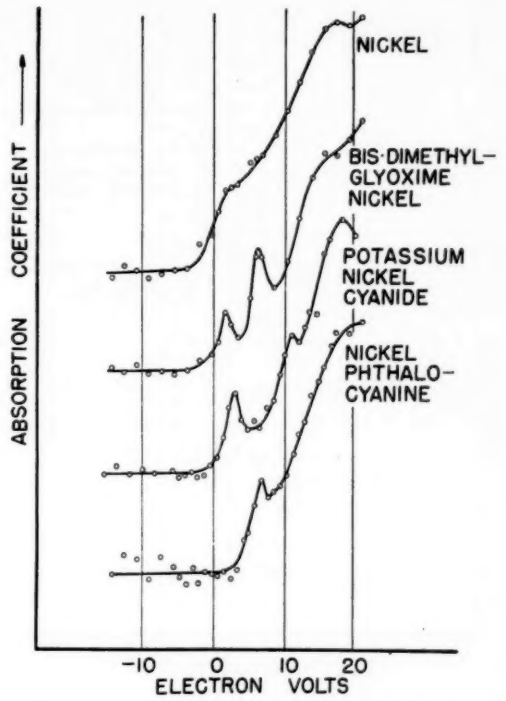

FIG. 1. X-ray absorption curves of nickel metal and three covalent nickel compounds with square symmetry.

DISCUSSION

In general the absorption edges of covalently bonded atoms show quite characteristic and not easily explained structures. Often a narrow intense absorption line is observed at a low energy, about where the $1s \rightarrow 4p$ transition in the neutral atom would be expected. Such a line was first observed by Coster[9] in the Mn edge of $KMnO_4$. Beyond the line the absorption in these compounds increases gradually and reaches a maximum value at 15 or 20 ev.

In the discussion to follow we wish to associate the presence or absence of low energy absorption with the presence or absence of unfilled $4p$ orbital. In the compounds discussed, the central absorbing atom is either four or six coordinated. The bonding orbitals are dsp^2 for planar four coordination, sd^3 or sp^3 for tetrahedral coordination, and d^2sp^3 for octahedral six coordination. The subject has been quite completely discussed by Pauling[10] and others from the chemical viewpoint.

From the orbital assignments we expect low energy absorption for planar complexes and for tetrahedral complexes, involving at least some sd^3 bonding. No low energy absorption is expected for the octahedral complexes.

The experimental data confirm these expectations. However, some assumptions deserving discussion are implicit in the use of the electronic structure of the initial state, before the photon absorption, in the discussion of absorption edge structure. In the final state a $1s$ electron has been excited to an optical level, and we are actually concerned with the wave functions and energy levels of a system with one more electron than is involved in the treatment of the chemical binding of the system.

It is probable that the original configuration of the nuclei will not be stable with the extra electron. However, the Franck-Condon principle requires that the electronic structure of the final state be determined by the original nuclear configuration. Some broadening of absorption lines might be expected but a rough estimate shows this to be small. Nuclear vibrational amplitudes at room temperature will be of the order of 0.1A. Slopes of potential curves in the final state will not be more than a few ev per A, so line broadenings of the order of a few tenths of an electron volt will result. This is small compared to the 2 ev line breadth from other causes.

A more important effect is the change in potential resulting from the absorption. The shielding effect of a $1s$ electron is radically different from that of the same electron in an optical orbit. The excitation may increase the effective Z by almost unity for some of the outer electrons and therefore decrease the radial extent of their wave functions. We do not expect such changes to invalidate our use of the ground-state wave functions since we are mainly interested in whether or not an atomic orbital is used in bonding. This depends both on

[7] Beeman, Forss, and Humphrey, Phys. Rev. **67**, 217 (1945).
[8] H. Hanson and W. W. Beeman, Phys. Rev. **76**, 118 (1949).
[9] D. Coster, Z. Physik **25**, 83 (1924).
[10] L. Pauling, *The Nature of the Chemical Bond* (Cornell University Press, Ithaca, New York, 1939); Y. K. Sirkin and M. E. Dyatkina, *Structure of Molecules and the Chemical Bond* (Interscience Publishers, Inc., New York, 1950).

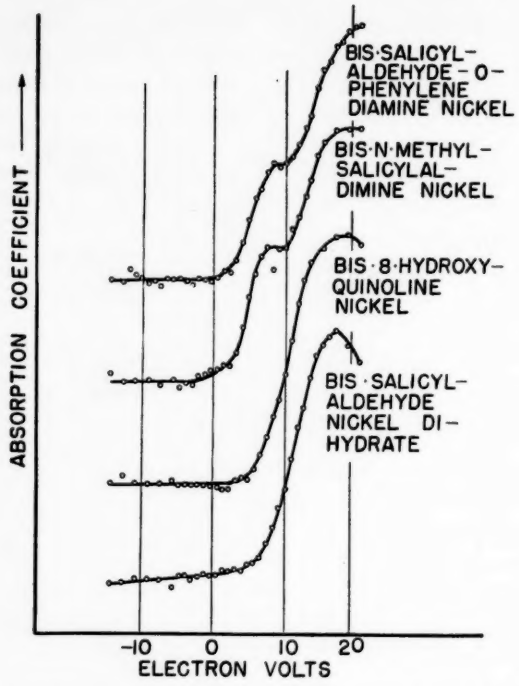

FIG. 2. X-ray absorption curves of four covalent nickel compounds. The upper two have square symmetry, the lower two tetrahedral.

the energy of the orbital and on the space symmetry of the potential. For potential changes no larger than those resulting from the excitation of one of a considerable collection of electrons, the symmetry, which remains constant, should be the predominant influence. Where resonance between several different types of bonds is possible, the replacement of an atom by the one of next higher atomic number (which to a good approximation is the effect of the x-ray excitation) might appreciably change the relative contributions made by the various bond types.

Finally mention must be made of the fact that when low energy absorption lines are observed they are quite narrow, seldom more than twice the natural line width. This is first an indication that in some molecules at least, in agreement with our estimate, nuclear motion is not an important source of line broadening. Secondly, it shows that the causes of line broadening in ions in solution and ionic compounds are not present in the covalent complexes. Among these are interaction with partially filled shells, Stark splitting, and band formation. In most cases the magnetic moment of the complex is zero before the absorption and thus there are no uncompensated spins (except that of the remaining $1s$ electron, which gives a negligible splitting) for the excited electron to interact with. Band formation tends to be small because of high dilution of the absorbing atoms in the crystal. Identical absorbing atoms will be separated by at least a double layer of the immediately coordinated groups as well as by the cations and water which may be incorporated in the crystal.

Most of the absorption lines which have been observed are in the energy range 0 to 10 ev. If we assume that the energy of a nonbonding $4p$ orbital will be determined mainly by the degree of ionization of the absorbing atom, then the results indicate that the atom is neutral or at most singly ionized. This is in agreement with chemical expectations.

We will now discuss the available experimental material.

Chromium

The K absorption edge of chromium in the metal and in $K_2Cr_2O_4$ has been measured by Sanner[2] and by Kiestra.[11] The latter investigator also measured $K_2Cr_2O_7$. In both crystals a narrow intense absorption line is observed. It occurs at about 4.0 ev in K_2CrO_4 and 5.0 ev in $K_2Cr_2O_7$. The line is somewhat more intense in the former compound. In fact, in the center of the line, the absorption coefficient reaches a higher value than in any other part of the K edge. The line absorption is thus stronger than that observed in the nickel compounds of Figs. 1 and 2. There is evidence of a second much weaker line at 12.0 ev in both of the chromates. Beyond this line the absorption rapidly increases to a plateau at about 20 ev which presumably corresponds to complete ejection of the K electron from the complex.

The structure of the $CrO_4^=$ radical is discussed in the book of Syrkin and Dyatkina[10] (p. 355). The configuration is tetrahedral, the magnetic moment zero. The bonding is principally sd^3 with some admixture of ionic structures involving singly or doubly charged chromium. All of the $4p$ orbitals are empty, and thus the strong absorption line may be explained. Since the line is at low energy, the ionic structures do not make a large contribution to bonding. Of course, in view of the previous discussion, what is really established is that in a complex with Cr replaced by a manganese-like atom the ionic structures do not make a large contribution to bonding.

Manganese

Crystalline K_2MnO_4 and $KMnO_4$ were measured by Hanson and Beeman[8] and $KMnO_4$ in aqueous solution by Shurman (unpublished). Both complexes are tetrahedral. The magnetic moment of $KMnO_4$ is zero, that of K_2MnO_4 corresponds to the spin magnetic moment of one unpaired electron. Both show strong low energy absorption lines, $KMnO_4$ at 4 ev and K_2MnO_4 at 3 ev. It is interesting that the line absorption of K_2MnO_4 is less intense and at lower energies than that of $KMnO_4$. The extra electron of $MnO_4^=$ cannot be assigned without making use of $4p$ orbitals. This will weaken the absorption and, because of additional shielding, move it to somewhat lower energies compared to MnO_4^-. $KMnO_4$ in solid and solution give identical absorption

[11] Dr. S. Kiestra (private communication).

edges through the line absorption and up to about 15 ev. This is strong evidence that the excited $1s$ electron remains bound to the complex in this energy region.

Iron

Iron in the metal and several compounds has been measured by Yoshida.[12] The compounds included potassium, ammonium and calcium ferrocyanide, and the three corresponding ferricyanides. In each case the iron is surrounded octahedrally by six cyanide groups. The bonding is d^2sp^3 and as expected no low energy absorption was observed. A fairly sharp absorption maximum at 16 or 17 ev was observed in each of these compounds. This may represent a transition to $5p$ states as proposed by Yoshida or it may correspond to a release of the $1s$ electron from the complex. The absorption maximum occurred at slightly lower energy in the ferrocyanide than in the corresponding ferricyanide.

When only a high energy absorption maximum is observed it is possible to say that the absorbing atom cannot possess empty $4p$ orbital and at the same time be near neutral. It is not easy on the basis of the x-ray evidence alone to rule out the chemically improbable ionic structure, since a $4p$ absorption in doubly or triply ionized iron would be near the observed energy region. However, if the binding is ionic one expects a larger energy shift of the absorption maximum from ferrous to ferric compounds than is observed in the ferro- and ferricyanides. Yoshida measured several ionic compounds of iron and found the $4p$ absorption of ferrous iron about 7 ev lower than that of ferric iron. The shift of the absorption maximum (presumably not $4p$) between the ferro- and ferricyanides averages less than 2 ev.

Nickel

We have recently measured a number of covalent nickel compounds. The compounds are listed in Table I and the absorption curves given in Figs. 1 and 2.

An attempt was made to get examples of both the planar four coordinated dsp^2 hybridization and the tetrahedral sp^3 hybridization. A discussion of such compounds has been given by Pauling[10] (Chap. III). Most of the structures given in Table I have been determined by magnetic moment measurements although x-ray evidence (crystallographic) is available for the planar configuration of nickel phthalocyanine. In some cases chemical evidence based on the existence of isomers is available.

The references of Table I give further information on the structure of these compounds. The four nearest neighbors of the nickel are identical in each of the compounds of Table I except for the fourth, fifth, and sixth where the nearest neighbors are two oxygen and two nitrogen atoms.

[12] S. Yoshida, Sci. Papers Inst. Phys. Chem. Research (Tokyo) 38, 272 (1941).

TABLE I.

Compound	Hybridization
Bis-dimethyl-glyoxime nickel[a]	dsp^2
Potassium nickel cyanide[b]	dsp^2
Nickel phthalocyanine[c]	dsp^2
Bis-salicylaldehyde-*o*-phenylene dimine nickel[a]	dsp^2
Bis-*N*-methyl salicylal-dimine nickel[a]	dsp^2
Bis-8-hydroxyquinoline nickel[a]	sp^3
Bis-salicylaldehyde nickel dihydrate[a]	sp^3

[a] J. B. Willis and D. P. Mellor, J. Am. Chem. Soc. **69**, 1237 (1947).
[b] L. Pauling, *Nature of the Chemical Bond* (Cornell University Press, Ithaca, New York, 1948).
[c] J. M. Robertson, J. Chem. Soc. 615 (1935).

It is seen in Figs. 1 and 2 that low energy absorption is observed in the square coordinated compounds but not in the tetrahedral in agreement with the assignment of bonding orbitals. There is an actual resolution of absorption lines only in the first three compounds of Table I. The fourth and fifth show considerable absorption at 7 or 8 ev and the failure to resolve lines may be related to the lack of a fourfold symmetry in the nearest neighbors of the absorbing atom. The reasons for the line doubling in bis-dimethyl glyoxime nickel and potassium nickel cyanide are not understood.

EXPERIMENTAL

The nickel absorption curves were taken with a double calcite crystal spectrometer with Geiger counter registration. The techniques have been described in previous publications.[7,8] The 1–1 width of the crystals at the Ni K edge was about 13.0 seconds.

The points drawn in Figs. 1 and 2 are from single runs. However, each sample was run at least four times and the solid curves represent structure obtained in every run. It is, of course, considerably more difficult to get good data on molecules with large organic residues than it is on those in which the absorbing atom is present in high concentration.

SUMMARY

An empirical correlation has been established between low energy K edge absorption and empty $4p$ orbital in seventeen covalent complexes of elements of the first transition series. The correlation depends on the assumption that the tetrahedral bonding orbitals in Cr and Mn are largely sd^3, and in Ni almost completely sp^3.

It is a pleasure to express our thanks to Professor J. C. Bailar, Jr., of the University of Illinois who furnished many of the compounds measured in this research.

A Calculation of the Static Dielectric Constant of Ice

J. G. POWLES
Frick Chemical Laboratory, University of Princeton, Princeton, New Jersey
(Received March 14, 1952)

A calculation is made of the static dielectric constant of ice using only simple molecular data and with well-defined assumptions as to the possibilities of molecular movement in the crystal. The paper serves as an illustration of the procedure for calculating static dielectric constants, and it results in a numerical value of this quantity for ice which is in reasonable agreement with experiment.

INTRODUCTION

THE static dielectric constant of ice is calculated making use of Fröhlich's general theory of the static dielectric constant[1] and using Pauling's model for ice.[2] In this model it is assumed that the water molecules in an ice crystal considered as a group can take up only certain configurations as a result of their interactions. The static dielectric constant is obtained for two cases, (1) assuming all the configurations to be of equal probability, as did Pauling; in this case a computationally exact result is obtained; (2) including the effect of electrostatic interaction on the probability of the configurations; in this case the accuracy of the result is somewhat difficult to estimate. The two values obtained straddle the experimental results and show that refinement of the calculation is likely to lead to a value in good agreement with experiment.

1. THE FORMULA FOR THE STATIC DIELECTRIC CONSTANT

In ice the oxygen atoms are arranged in a lattice of hexagonal symmetry. There are therefore two principal dielectric constants, which we call ϵ_c for the hexagonal axes and ϵ_a for any axis at right angles. It is evidently not correct to use the expression given by Fröhlich for isotropic materials, but we shall consider this formula first and the required modifications to it later.

Fröhlich considers a spherical region inside the specimen large enough for the material outside to be treated macroscopically. Within this sphere one chooses a smaller region in any position not close to the surface which has the electric moment $m(x_j)$ when the elementary charges within it are fixed in positions characterized by x_j. The average moment of the sphere, immersed in its own medium, when x_j is fixed is called $m^*(x_j)$. More specifically,

$$m^*(x_j)=\int M(X)\exp(-U(X)/kT)\cdot dX_j \Big/ \int \exp(-U(X)/kT)dX_j, \quad (1.1)$$

where $M(X)$ is the moment of the whole sphere when the elementary charges are in configuration X and the energy of the system is $U(X)$, the integration being carried out over all X provided that the charges in m are fixed at x_j.

The average of $m\cdot m^*$ for all possible x_j, taking due account of the probability of each configuration, gives $\langle m\cdot m^*\rangle_{Av}$. The static dielectric constant is then related to this microscopic quantity as follows:

$$\epsilon_s-n^2=3\epsilon_s/(2\epsilon_s+n^2)\cdot 4\pi N_0/3\cdot\left(\frac{n^2+2}{3}\right)^2\frac{\langle m\cdot m^*\rangle_{Av}}{kT}, \quad (1.2)$$

in which ϵ_s is the static dielectric constant, n^2 is the dielectric constant due to electronic polarization and N_0 the number of small regions per unit volume. Equation (1.2) is a specialized form of the general equation in which the electronic polarization (corresponding to n^2) is treated macroscopically and in the calculation of $\langle m\cdot m^*\rangle_{Av}$ vacuum dipole moments are used. The latter is only strictly true if the molecule may be considered as a point dipole embedded in a sphere of uniform polarizability corresponding to n^2.

The validity of (1.2) required that certain conditions be fulfilled, namely:

(1) The group of molecules must be spherical, although deviations of molecular magnitude are permissible.

(2) The sphere must be so large that the material outside it is adequately characterized by its macroscopic dielectric constant. In this case $\langle m\cdot m^*\rangle_{Av}$ and, hence, ϵ_s is independent of the size of the sphere.

(3) $\langle m\cdot m^*\rangle_{Av}$ should be independent of the position of the small region within the sphere provided it is not near the surface.

Alternatively, one may consider a spherical group of molecules in vacuum, and in this case also a quantity which we call $\langle m\cdot m_{vac}{}^*\rangle_{Av}$ may be obtained in an analogous manner. However, the relation between this microscopic quantity and the macroscopic dielectric constant is now

$$\frac{\epsilon_s-n^2}{\epsilon_s+2}=\frac{4\pi}{3}\cdot\frac{(n^2+2)}{3}\cdot N_0\cdot\frac{\langle m\cdot m_{vac}{}^*\rangle_{Av}}{kT}. \quad (1.3)$$

[1] H. Fröhlich, Trans. Faraday Soc. 44, 238 (1949); *Theory of Dielectrics* (Oxford University Press, London, 1949), p. 36.
[2] L. Pauling, J. Am. Chem. Soc. 57, 2680 (1935).

This equation is again a special case in which the electronic polarization has been treated macroscopically, and the polarization of the molecules by neighbors is treated as in (1.2). The conditions of validity of (1.3) are as for (1.2), except that condition (2) must be that the sphere of molecules is so large that the addition of another "shell" of molecules may be accounted for satisfactorily macroscopically.

The difference between $\langle m\cdot m^*\rangle_{Av}$ and $\langle m\cdot m_{vac}{}^*\rangle_{Av}$ arises from the different values taken up by $U(X)$ in Eq. (1.1).

Equation (1.2) requires modification for an anisotropic material such as ice.[3] If ϵ_k, $k=1$, 2, or 3, are the principal dielectric constants, then the large region should be an ellipsoid with its principal axes parallel to the principal dielectric axes and of length proportional to $\sqrt{\epsilon_k}$ in the k-axis. One then has for the ϵ_k, corresponding to (1.2):

$$\epsilon_k-1=\frac{3\epsilon_k}{2\epsilon_k+1}\cdot\frac{4\pi N_0}{3}\cdot\frac{3\langle m_k m_k{}^*\rangle_{Av}}{kT},\quad k=1,\ 2\text{ or }3,\quad (1.4)\dagger$$

where m_k and $m_k{}^*$ are the components of m and m^* in the k axis and for the ellipsoidal region.

In practice, the shape of the ellipsoid must be modified until the values of the $\langle m_k m_k{}^*\rangle_{Av}$ and the ϵ_k in (1.4) are consistent. However, an estimate of the anisotropy may be obtained by taking a spherical region and noting the dependence of $\langle m_k m_k{}^*\rangle_{Av}$ on the axis. In Sec. 3 we shall find that the anisotropy is probably quite small, and we shall use Eq. (1.2), hence a sphere, in order to obtain an average value ϵ_s for the dielectric constant. Since the anisotropy is not large, the direct comparison of ϵ_s and the measured dielectric constant (of a mass of small crystals) is legitimate. No reliable estimate of the anisotropy results from Sec. 4.

An equation corresponding to (1.4) can be obtained for the "free" ellipsoid.

2. THE STRUCTURE OF ICE AND PAULING'S CONFIGURATIONS

The crystalline structure of ice is a four coordinated lattice in which the oxygen nuclei have the arrangement of the silicon atoms in the tridymite form of silica.[4] A projection of a portion of an ice crystal, showing the arrangement of the oxygen atoms only, is given in Fig. 1; it also shows the puckered hexagons, typical of the structure. Neutron diffraction data on ice (actually heavy ice) show that the hydrogen nuclei are in positions such that each oxygen atom is surrounded tetrahedrally by four half-hydrogen nuclei.[5] The neutron diffraction

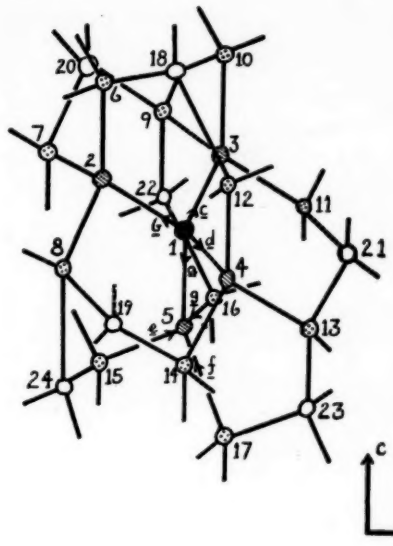

FIG. 1. Projection of portion of ice crystal showing oxygen nuclei only.

experiments are not able to distinguish between a static disordered structure and a dynamic one of the oscillatory type.

Pauling[2] has proposed in order to explain the residual entropy of ice at low temperatures that the crystal can take up, with equal probability, any of a number of configurations consistent with the conditions that there is only one proton between any two oxygen atoms nearer the one than the other and that at any instant there are two protons near each oxygen atom. In this paper a calculation of the static dielectric constant is based on this fluctuating structure proposed by Pauling. We shall not be concerned here as to how one configuration changes to another, whether by rotation of molecules or by proton exchange or both, but merely that all such configurations are taken up with a probability depending on the energy of the configuration. For ice, therefore, the integrals in (1.1) become sums, and we write

$$m^*(x_j)=\sum_i M_i e^{-U_i/kT}/\sum_i e^{-U_i/kT},\qquad (1.1)'$$

where i defines the configuration.

Pauling obtains the experimental value for the residual entropy of ice by assuming that all the configurations are taken up with equal probability. Although this is a very difficult assumption to justify, we shall first calculate the static dielectric constant making this same assumption, i.e., U_i is constant for all i in (1.1)'. We find in Sec. 3 that it is possible to compute accurately in this case the value of $\langle m\cdot m^*\rangle_{Av}$ and inserting this in Eq. (1.2) gives ϵ_s. Later in Sec. 4 we take a more realistic case in which the relative probability of the configurations is determined by the intermolecular electrostatic interaction, since once the configurations are assumed these are the only forces leading to dependence of U_i on i. It is found that the computation can only be carried out

[3] J. G. Powles, E. R. A. Report, *L/T*, 269 (1951); Trans. Faraday Soc. (to be published).

† This is the general form in which induced moments are included in m_k and $m_k{}^*$; allowance for the electronic polarization macroscopically leads to a less simple equation than (1.2), and we do not discuss it here since we shall not employ Eq. (1.4) in the calculations.

[4] W. H. Barnes, Proc. Roy. Soc. (London) **A125**, 670 (1929).

[5] Wollan, Davidson, and Shull, Phys. Rev. **75**, 1348 (1949).

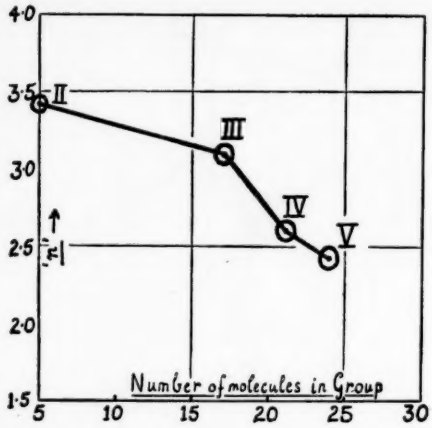

FIG. 2. Average number of positions per molecule as a function of the size of the group.

approximately, but, nevertheless, it shows that the assumption of equal probabilities for the different configurations is not such a ridiculous one as it may seem at first sight.

We assume further that the dipole moment of the water molecule in ice is the same as that of the free molecule apart from polarization by surrounding molecules. The total dipole moment μ_v may be conveniently resolved for the purpose of computation into two elementary moments μ_b directed along the lines joining the oxygen and hydrogen nuclei which are inclined at the tetrahedral angle ($109\frac{1}{2}°$), and therefore $\mu_b/\mu_v = \sqrt{3}/2$. The neutron diffraction experiments[5] are not yet able to determine the HOH angle of the water molecule in ice (private communication from Dr. C. G. Shull).

3. THE COMPUTATION OF $\langle m\cdot m^*\rangle_{Av}$ ASSUMING ALL CONFIGURATIONS OF EQUAL PROBABILITY

(a) Central Molecule as Unit for m

We take as the small unit m, one water molecule, and calculate successive approximations to the dielectric constant as the size of the larger region or "group" of molecules is increased.

In illustration of the calculation of $\langle m\cdot m^*\rangle_{Av}$ take first a single molecule as the group such as molecule 1‡ in Fig. 1. For this molecule there are four possible directions of the elementary dipoles a, b, c, and d. All possible directions in the ice crystal are given by including the vectors e, f, and g. The molecule can take up any one of six positions when its dipole moment is $m=(a+b)$ etc. For this group $m^*=m$ for all m, and all m are of equal probability; hence,

$$\langle m\cdot m^*\rangle_{Av}=(4/3)\mu_b{}^2=\mu_v{}^2. \qquad (3.1)$$

It is convenient to consider the value of $\langle m\cdot m^*\rangle_{Av}/\mu_v{}^2\equiv F$ (and later $3\langle m_i m_i^*\rangle_{Av}/\mu_v{}^2\equiv F_i$) since this quantity is roughly proportional to ϵ_s in ice because $\epsilon_s\gg n^2$. The same result as (3.1) is obtained for freely rotating molecules, and (2.2) is then Onsager's equation.[6]

‡ Only the oxygen atoms are shown and they are not to scale.

[6] L. Onsager, J. Am. Chem. Soc. **58**, 1486 (1936).

F is easily calculated for a central molecule and its four nearest neighbors (Group *II*, molecules 1–5 in Fig. 1), and we find $F=2.33$. This corresponds to Kirkwood's calculation for water,[7] except that we have fixed the directions of the outermost bonds in directions appropriate for ice.

It is interesting to note that for any fixed position of the central dipole, the dipole moments in the acceptor directions to the other two neighbors are also fixed. Hence, the contribution of the first layer of *bonds* to m^* is, for example,

$$a+b-c-d=2(a+b)=2\mu_v; \quad \text{therefore,} \quad F=2.$$

The difference between this value and that for a large group gives, therefore, the effect of the outer bonds.

It is appropriate at this stage to consider how nearly our small groups approach in properties those of a macroscopic crystal. The number of available configurations $\mathfrak{N}$ of a crystal of N molecules approaches $(3/2)^N$ if N is large, or $n=(\mathfrak{N})^{1/N}\rightarrow\frac{3}{2}$. For small N, $n>\frac{3}{2}$, e.g., for Group *II* $n\simeq 3.5$. Values of n are given in Fig. 2. Even for our largest group n is far from its asymptotic value 1.5; in spite of this we shall show that for Group *V* the material outside the group may be treated macroscopically.

Adding twelve second-nearest neighbors gives Group *III* containing seventeen molecules (1–17 in Fig. 1), and the calculation is still comparatively simple since each "leg" of the group may be treated independently. The group is still isotropic, and we find $F=2.78$. This figure is still not suitable for computation of ϵ_s since there is no marked improvement in "n" in passing from Group *II* to Group *III*; neither has the characteristic structure of ice, built up of puckered hexagons, yet appeared. For Group *III* $\mathfrak{N}=2.5\times 10^8$.

Adding four third-nearest neighbors (18, 19, 20, and 21 in Fig. 1) to *III* gives *IV* with a marked reduction in "n," and six hexagons appear. Now, however, computational difficulties have greatly increased as a result of the interconnection of different parts of the group.

We have developed special methods to deal with this situation, which consist essentially in breaking down the group into smaller portions so that the enumeration of the configurations becomes less laborious. Even by this method the work required becomes prohibitive for groups of more than 24 molecules. The amount of calculation can often be reduced by symmetry considerations; for instance, Groups *IV* and *V* are symmetrical about the c axis. One need only calculate m^*, therefore, for two m, e.g., $m_1=(a+b)$ and $m_2=(c+d)$.

We find for Group *IV*:

$$m_1{}^*=2.98a+2.44b \quad \text{and} \quad m_2{}^*=-(2.96a+2.44b+0.03c).$$

The fact that $m_1{}^*\simeq -m_2{}^*$ is not fortuitous since m_2 may be obtained from m_1 by reversal of the four bonds surrounding the central molecule. If we further reverse all bonds throughout the group, there is a one-to-one

[7] J. G. Kirkwood, J. Chem. Phys. **7**, 911 (1939).

correspondence of each configuration contributing to m_1^* and m_2^*, except at the surface of the group where we must count only bond moments directed outwards (bond moments directed inwards arise from protons in the "continuum"). However, if the group is large enough, the contribution of the outermost bonds to m^* will be negligible. The numerical similarity of m_1^* and m_2^* is therefore an indication that our group is getting large enough.§ Again m and m^* are not parallel, which indicates anisotropic properties. We find

$$F_c=3.25, \quad F_a=2.44, \quad \text{and} \quad F=2.70.$$

The true anisotropy may well not be as great as implied by these figures, since Group *IV* has a lower portion which deviates from the spherical form and is, moreover, not well connected with the upper part of the group. These faults are remedied in Group *V*.

Group *V* includes molecules 1–24. In view of our experience with Group *IV* we calculate m for $m_1=(a+b)$ only. The final result is

$$F_c=2.62, \quad F_a=2.71, \quad \text{and} \quad F=2.65.$$

In this case the anisotropy of $\langle m_i m_i^* \rangle_{Av}$ is much smaller, and its magnitude evidently depends rather critically both on the accuracy of computation and on the shape of the group chosen. It seems probable in view of the results for Group *V* that the anisotropy of ice is not large, but we are unable to give a specific value. This being so, it is convenient to consider the values of F that are plotted in Fig. 3, as a function of the number of molecules in the group. For Group *V* the asymptotic value is almost reached. Little improvement in accuracy can be expected unless a considerably larger group is taken, and then the computation required becomes prohibitive. In view of other possible sources of error (Sec. 6) a more exact calculation of F is unnecessary.

(b) Off-Central Unit for m

As stated in Sec. 1, $\langle m \cdot m^* \rangle_{Av}$ should be independent of the position of the reference unit defining m. We have therefore calculated F taking as the reference unit the molecule below the one previously used (molecule 5 of Fig. 1) and the result is given in Fig. 3. This reference molecule is not the next best after the central molecule, but it is suitable for computation on account of its symmetrical position. For Group *V*, the new F is only $6\frac{1}{2}$ percent below the value for the central molecule. We conclude, therefore, that the result for a group of this size is substantially independent of the reference molecule chosen (excluding molecules at the surface of the group).

(c) A Two-Layer Approximation for m

It was pointed out in Sec. 3(a) that the first layer of bonds alone gives $F=2$. The calculation may be extended to include the second layer, and this has been done for Groups *III*, *IV*, and *V*. This quantity should also approach an asymptotic value but different from that of Secs. 3(a) and (b). Figure 3 shows that this is so, and for Group *V* the difference from the correct value is only 3 percent. This suggests that the first two layers of bonds gives a good approximation to the dielectric constant of ice, although interactions have to be accounted for out to the third nearest neighbors.

§ $m \cdot m^*$ is necessarily independent of m in the very symmetrical Groups *II* and *III*.

4. COMPUTATION OF $\langle m \cdot m^* \rangle_{Av}$ WITHOUT THE ASSUMPTION OF EQUAL PROBABILITIES

The energy U_i in (1.1)′ may be divided into two parts (1) that due to interactions of molecules within the sphere, $U_{i\,\mathrm{int}}$, and (2) that due to the interaction of these same molecules with the material outside, $U_{i\,\mathrm{ext}}$:

$$U_i=U_{i\,\mathrm{int}}+U_{i\,\mathrm{ext}}. \tag{4.1}$$

For the free sphere $U_{i\,\mathrm{ext}}=0$ and since most of the computational difficulty arises in the evaluation of $U_{i\,\mathrm{ext}}$, it might seem preferable to calculate ϵ_s using (1.3). However, inspection of (1.3) shows that for large ϵ_s, as in ice, the left-hand side approaches a limiting value, and ϵ_s is very sensitive to an error in $\langle m \cdot m_{\mathrm{vac}}^* \rangle_{Av}$ and also to the way in which the electronic polarization is accounted for. This may be particularly serious for a small group in vacuum. On the other hand, Eq. (1.2) for $\epsilon_s \gg n^2$ shows that ϵ_s is almost proportional to $\langle m \cdot m^* \rangle_{Av}$.

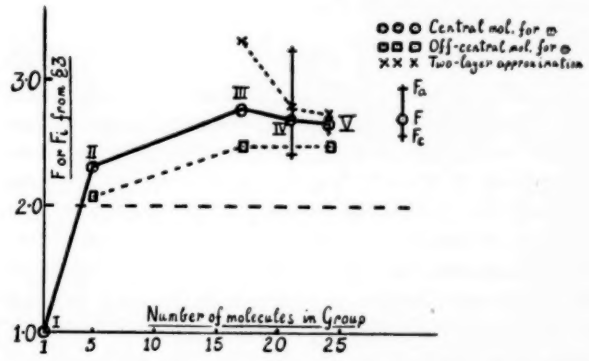

FIG. 3. Variation of F with size of group assuming all configurations of equal probability.

The difference between (1.2) and (1.3) illustrates the importance of the term $U_{i\,\mathrm{ext}}$ in (4.1). Insertion of the experimentally determined quantities in (1.2) and (1.3) gives for $\epsilon_s=80$ the experimental values

$$F=\langle m \cdot m^* \rangle_{Av}/\mu_v^2=2.9$$

and

$$F_{\mathrm{vac}}=\langle m \cdot m_{\mathrm{vac}}^* \rangle_{Av}/\mu_v^2=0.19 \text{ at } 0°\mathrm{C}. \tag{4.2}$$

We shall now follow the same procedure as in Sec. 3 of calculating F (and F_{vac}) and taking groups of molecules of gradually increasing size and obtain asymptotic values.

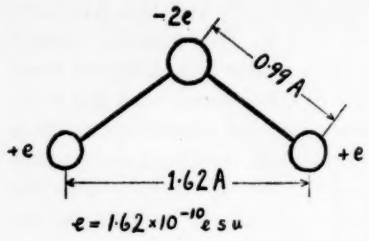

FIG. 4. Point charge model for the water molecule.

(a) Group *II*, 5 Molecules

Consider first the calculation of $U_{i\,\mathrm{int}}$. It is evident from a study of the molecular arrangement that the differences in energy for different configurations may be ascribed to the change in electrostatic energy alone. In order to calculate the change in $U_{i\,\mathrm{int}}$ with configuration we shall use the point charge model of the molecule shown in Fig. 4. This is a somewhat simpler model than those used to calculate the heat of sublimation of ice etc.,[8–10] but it has the advantage that many of the interaction energy terms remain the same for all configurations. The only important contribution to $U_{i\,\mathrm{int}}$ is that resulting from the interaction of nearest neighbors both because of the greater separation of second-nearest neighbors (although the terms are more numerous) and because this interaction energy is reduced roughly by a factor $1/n^2$, since the interacting molecules are separated by other polarizable molecules. $U_{i\,\mathrm{int}}$ can therefore be calculated exactly for the 81 configurations of the five molecule group—consistent with a given model of the molecule. F_{vac} may then be found

$$F_{\mathrm{vac}}=0.76. \tag{4.3}$$

The calculation of $U_{i\,\mathrm{ext}}$ is more difficult. If the sphere is uniformly polarized and of total dipole moment M, then the reaction field due to the material outside the sphere is $2(\epsilon-1)/(2\epsilon+1)\cdot M/R^3$ where R is the radius of the sphere. The energy of the sphere on this account is therefore $-M^2/R^3$ if $\epsilon\gg1$. However, the material outside the sphere is polarized by the dipole distribution M, and it may be shown that this requires an energy $\frac{1}{2}M^2/R^3$. Finally, therefore,

$$U_{i\,\mathrm{ext}}=-\tfrac{1}{2}M_i^2/R^3. \tag{4.4}$$

Using Eq. (4.4) m^* can be calculated for $\epsilon_s\gg1$ exactly for the five-molecule group by enumerating each of the 81 terms and using (1.1)′. This gives

$$F=4.7. \tag{4.5}$$

The approximate results (4.3) and (4.5) show clearly the difference between the free and immersed spheres. For the immersed sphere the reaction of the surroundings on the sphere increases the probability of configurations of large dipole moment, and since in a small group these all have their dipole moment roughly parallel to m, a large value of F results. In a larger group larger values of M_i occur, but there are many configurations for which M_i is not in the direction of m and in taking the average F does not become inordinately large; in fact, it approaches an asymptotic value as the size of the sphere is increased. There are, however, other factors which modify this simple picture, and these are considered later. On the other hand, for the free sphere, in general, configurations of low dipole moment have the lowest energies and this leads to the low numerical value for F_{vac}.

(b) Group *III*, 17 Molecules

The 5-molecule group is evidently too small, and as in Sec. 3 we proceed to the 17-molecule group. Considerable computational difficulties arise as the configurations are very numerous. It is necessary, moreover, to investigate the validity of (4.4) giving the energy $U_{i\,\mathrm{ext}}$.

Consider first the "*free* sphere." A first approximation for F_{vac} may be obtained by assuming that the configurations of any one of the outer twelve molecules is determined solely by the configuration and interaction energy with the inner molecule to which it is attached, e.g., molecule 7 in Fig. 1 is determined by molecule 2. For any configuration j of the five inner molecules taken as a group, we get an average moment $\bar{M}_j$ to add to M_j and an average energy $\bar{U}_{j\,\mathrm{int}}$ to add to $U_{j\,\mathrm{int}}$; we then use $(M_j+\bar{M}_j)$ and $(U_{j\,\mathrm{int}}+\bar{U}_{j\,\mathrm{int}})$ in (1.1)′ in place of M_i and $U_{i\,\mathrm{int}}$. Taking first the most probable configuration of the five-molecule group and then the next most probable and so on, m^* may be found to a sufficient approximation without evaluating all 81 configurations. This leads to $F_{\mathrm{vac}}=1.1$. This is evidently a poor approximation, and we now calculate new values of $\bar{M}_j$ and $\bar{U}_j$ taking the outer molecules in groups of three attached to each of the inner molecules, e.g., 6, 7, and 8 attached to 2. For a given orientation of 2 there are 27 configurations of the triplet 6, 7, and 8, and we determine the mean moment and energy and also for the other triplets, in order to determine the $\bar{M}_j$ and $\bar{U}_j$ for all j. Only a few calculations of this sort have to be made since other results can be derived by suitable rotations. The new values of $(M_j+\bar{M}_j)$ and $(U_j+\bar{U}_j)$ are then used in (1.1)′, and we find $F_{\mathrm{vac}}=0.04$. In judging these results we must compare the *differences* from the experimental value (for $\epsilon_s=80$), i.e., 0.9 for the first approximation and -0.15 for the second; hence, the latter is a much improved value. F_{vac} is rather sensitive both to the exact molecular model assumed and to the accuracy of the computation, as it must be since m^* is the resultant of a rather delicate balance of large terms. We shall therefore be satisfied in finding the correct order of magnitude since it cannot in any case lead to an accurate value of ϵ_s.

For the *immersed* sphere the evaluation of all the configurations is evidently quite impracticable. We have therefore made a similar approximation to that for the free sphere; that is to say, we have assumed that the

[8] E. Bauer and M. Magat, J. phys. et radium (7) **9**, 319 (1938).
[9] J. S. Rowlinson, Trans. Faraday Soc. **47**, 120 (1951).
[10] J. A. Pople, Proc. Roy. Soc. (London) **205**, 163 (1951).

configuration of the outer molecules is determined by that of the inner one to which it is attached to obtain $\bar{M}_j$ and $\bar{U}_{j\,\mathrm{int}}$. The energy of any configuration j of the inner five molecules is then taken to be

$$U_j=(U_{j\,\mathrm{int}}+\bar{U}_{j\,\mathrm{int}})-(1/2R^3)\cdot(M_j+\bar{M}_j)^2, \quad (4.6)$$

with the appropriate value of R. We then have

$$m^*=\sum_j (M_j+\bar{M}_j) \times\exp(-U_j/kT)/\sum_j \exp(-U_j/kT), \quad (4.7)$$

and we find

$$F=3.5.$$

This calculation underestimates the terms in (1.1)′ having high moment values, so that in so far as (4.4) is correct our result is low (although it is still higher than the experimental value). It is found that the U_{ext} term is, in general, more important than U_{int}.

Consider now the validity of (4.4). In the case of ice the delineation of a sphere about the 17-molecule group is rather arbitrary. The dependence of the result on the magnitude of "R" in (4.4) is illustrated in Table II(a). A more serious objection is that (4.4) is only valid if the sphere is uniformly polarized. (It is also true if there is a point dipole of the same moment at the center of the sphere[11] or if the spherical cavity contains a uniformly polarized sphere of the same total moment but of smaller radius.) Inspection of Fig. 1, shows that the polarization of the groups of molecules with which we are concerned is manifestly non-uniform. In order to investigate this, we have calculated the energy $U_{i\,\mathrm{ext}}$ for the simple case of seven dipoles, one at the center of the spherical cavity and the six others in the six positions $(\pm d, \pm d, \pm d)$. It is found (Fig. 5) that when the dipoles all point in the same direction Eq. (4.4) is valid for this group of dipoles for $d/R<\frac{1}{2}$ (corresponding to a uniformly polarized sphere of radius smaller than the cavity radius).‖ However, the introduction of non-uniformity by turning one of the dipoles increases the numerical value of the energy relative to that given by (4.4) so that the configurations of high dipole moment are relatively less favored than would be expected from (4.4). There is little doubt that a similar result would be obtained with an arrangement of dipoles as in ice. A further factor is that the molecules themselves cannot be approximated by point dipoles and this would lead again to the sphere possessing quadrupole and higher moments. It must be concluded, therefore, that use of (4.4) attributes too great an importance to the configurations of high dipole moment. However, the approximation involved in using (4.7) has just the reverse effect in that it attributes too little importance to configurations of high dipole moment while assuming that (4.4) is correct. The two errors are therefore compensatory, and the resultant value of F is not necessarily a poor approximation. It would be necessary to take a larger group to obtain a satisfactory appraisal of the situation.

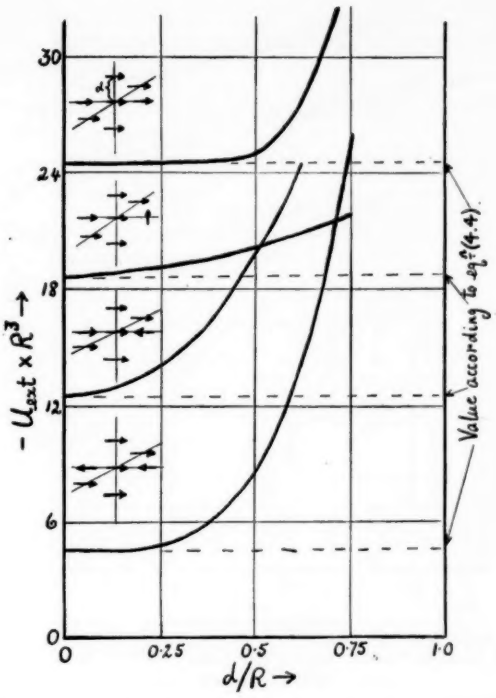

FIG. 5. Dependence of U_{ext} (see Eq. (4.1)) on the arrangement of dipoles within the sphere.

TABLE I. Comparison of experimental values of F_{vac}, F and "n" with those calculated in Sec. 4 for 0°C.

		Experimental values for $\epsilon_s=80$	Theoretical values for Group *II* (5 molecules)	Theoretical values for Group *III* (17 molecules) using $R^3/a^3=7$
	F_{vac}	0.19	0.76	1st approx., 1.1 2nd approx., 0.04
	F	2.9	4.7	3.5
"n"	for free sphere	1.5	2.3	1.9
	for immersed sphere	1.5	1.7	1.8

It seems, therefore, that introducing electrostatic interaction does not invalidate the assumption that the configurations are of equal probability to the extent that might first have been anticipated. The result of Sec. 3 is still valuable in that it is probably a lower limit to F, and it shows in addition that not much further variation in F is to be expected in taking a larger group than 17 molecules.

The possibility of anisotropy introduces a further uncertainty.

The entropy values derived in a similar manner to

[11] See reference 1, p. 165.

‖ When $d/R>\frac{1}{2}$, this arrangement is no longer even approximately a region of uniform polarization, and we ought to take a larger number of dipoles distributed through the volume.

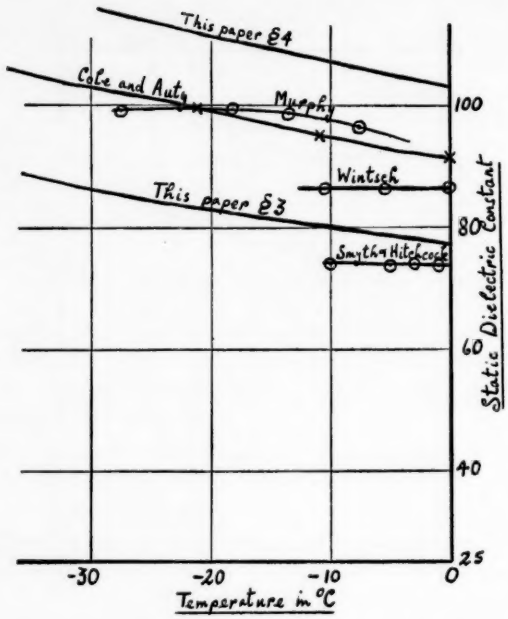

FIG. 6. Comparison of experimental and theoretical values of the static dielectric constant of ice.

that employed in Sec. 3 are not far removed from Pauling's value, again illustrating that the assumption of equal probabilities of configurations in a large group is not a bad approximation, at least for the calculation of residual entropy.

5. COMPARISON WITH EXPERIMENT

The value of F obtained in Sec. 3 is independent of temperature and together with $\mu_v=1.85$ Debye and $n^2=1.72$ in (1.2)′ gives

$$\epsilon_s=20{,}500/T+1.7; \quad \text{thus,} \quad \epsilon_s=77.3 \text{ at } 0°\text{C}.$$

F from Sec. 4 is slightly temperature dependent (Table II(b)). We find $\epsilon_s=103$ at 0°C.

These values are compared with the experimental ones[12–15] in Fig. 6.

Table III gives the experimental values of F calculated from the experimental results of Cole and Auty[15] which seem to be the best available at present. F is seen to be substantially independent of temperature, and this is in agreement with our results of Sec. 4 (and of course of Sec. 3). The fact that our results show the correct variation of ϵ_s with temperature is important in view of their poor absolute accuracy. Measurements at even lower temperatures would be very desirable.

TABLE II. Effect of choice of R and of temperature on F for Group *III*.

(a) Effect of R at 0°C.				(b) Effect of temperature when $R^3/a^3=7$.			
R^3/a^3	5	7	9	Temp. °C	0	−30	−60
F	3.7	3.5	3.4	F	3.5_2	3.5_7	3.5_8

6. DISCUSSION AND CONCLUSIONS

There are a number of factors that can lead to error in the numerical results obtained.

It has been assumed that the dipole moment of the water molecule in ice (apart from polarization by surrounding molecules) is the same as that in the free molecule in spite of a possible change in HOH angle. If it is assumed that the elementary moment μ_b is unchanged, the calculated values of ϵ_s are some 9 percent lower.

Equation (1.2) involves the assumption that the water molecule may be considered as a point dipole immersed in a sphere of polarizability corresponding to n^2. Although this can hardly be true for H_2O, a more precise calculation of the polarization of a given molecule by its neighbors, similar to that given by Kirkwood,[7] suggests that the representation of this effect by the inclusion of the factor $[(n^2+2)/3]^2$ in (1.2) is a good approximation.

The advantage of the calculation in Sec. 3 is that it gives a result which is computationally exact since we have complied very closely with the conditions laid down in Sec. 1. The calculation in Sec. 4 suggests that the result in Sec. 3 is a lower limit to the true value.

In introducing the interaction energies we have not been able to obtain a result whose accuracy is known. It is evident, however, that the true value is not far removed from that given in Sec. 4 and suggests that the assumptions used are essentially valid. These may be summarized by saying that ice can take up a number of configurations as envisaged by Pauling and that the probability of any one of these configurations is determined by essentially electrostatic forces calculated assuming a point charge model for the water molecule.

A recent report that ice is piezoelectric and possibly ferroelectric[16] is difficult to reconcile with the present paper. The possibility is not, however, excluded because the procedure for calculating the static dielectric constant would then be quite different. There would, however, be some difficulty in explaining the residual entropy.

TABLE III. Variation of F with temperature from experimental data of Cole and Auty.

Temperature in °C	0	−10.8	−20.9	−44.7	−65.8
F from data of Cole and Auty[15]	3.19	3.19	3.23	3.05	3.54

[12] C. P. Smyth and C. S. Hitchcock, J. Am. Chem. Soc. **54**, 4631 (1932).
[13] H. Wintsch, Helv. Phys. Acta **5**, 126 (1932).
[14] E. J. Murphy, Trans. Electrochem. Soc. **65**, 309 (1934).
[15] Robert P. Auty and Robert H. Cole, J. Chem. Phys. **20**, 1309 (1952).
[16] F. Rossman, Experientia **6**, 182 (1951).

ACKNOWLEDGMENTS

This work was carried out in part at the University of Liverpool under the supervision of Professor H. Fröhlich and with the financial assistance of the "Electrical Research Association" and in part at Princeton University with Professor C. P. Smyth. The author is grateful for a Visiting Fellowship supported by a Grant-in-Aid to the Chemistry Department of Princeton University from E. I. du Pont de Nemours & Company.

The author wishes to acknowledge the stimulus he received in being able to consult Dr. J. A. Schellman's thesis on the dielectric properties of ice (Princeton, 1950).

THE JOURNAL OF CHEMICAL PHYSICS VOLUME 20, NUMBER 8 AUGUST, 1952

Dielectric Properties of Ice and Solid D_2O*

ROBERT P. AUTY† AND ROBERT H. COLE
Metcalf Research Laboratory, Brown University, Providence, Rhode Island

(Received February 1, 1952)

Complex dielectric constants have been measured for ice from the melting point to −65°C, and for solid D_2O to −35°C, by a combination of bridge and transient methods. For both, the dispersion is described by the simple Debye formula, and the relaxation times τ by the simple rate expression $\tau = A \exp(B/RT)$. For ice, $A = 5.3 \times 10^{-16}$ sec, $B = 13.2$ kcal/mole; and for solid D_2O, $A = 7.7 \times 10^{-16}$ sec, $B = 13.4$ kcal/mole. The equilibrium dielectric constant for ice is 91.5 at 0°C and increases at lower temperatures; the values for solid D_2O are only slightly smaller. Measures taken to minimize errors from voids in the sample and direct current conductance are discussed.

I. INTRODUCTION

SINCE the original investigations of Errera[1] in 1924, a number of workers have reported results of dielectric constant measurements on ice at audio- and radio-frequencies. The agreement among these is rather poor, the values given for equilibrium dielectric constants near the melting point ranging from 70 to 95, and the reported relaxation frequencies varying by as much as 40 percent at −20°C and having rather different temperature dependences. In addition to these discrepancies, most of the measurements did not extend to sufficiently low frequencies to define the equilibrium dielectric constant with any accuracy except near the melting point, nor is it possible to decide from them if the relaxation process is really accurately described by the familiar dispersion and absorption equations originally described by Debye.

Two principal sources of systematic error have been suggested as causes for the discrepancies mentioned: voids or flaws in the solid dielectric, and the presence of conducting impurity. The first of these is ordinarily supposed to lead to dielectric constant and loss values which are too small, although one can readily show that too large values are also possible if the dielectric possesses appreciable direct current conductivity. The increase in apparent dielectric constant and loss, especially at low frequencies, as a result of dc conductance, was shown directly by Smyth and Hitchcock[2] by the addition of a small concentration of KCl to the liquid water before freezing. As a result they took especial precautions to obtain water of high purity and found rather smaller values of dielectric constant than other workers. Murphy's[3] measurements are more comprehensive from the point of view of frequency and temperature range and give considerably larger static values, but were obtained using distilled water not further purified. The question as to whether the differences are occasioned by sample inhomogeneity or by conductance effects or both is thus unanswered.

In view of recent interest in the magnitude of the equilibrium constant of ice and in the relaxation process by which it is realized, the work reported here was undertaken with the especial aim of precluding errors from either of the possible causes mentioned. To minimize formation or development of voids and cracks, two special forms of cells were used. In both of these, the process of freezing the sample between the measuring electrodes could be observed and readily controlled, and the electrodes could follow the subsequent contraction of the sample on cooling.

The possibility of ambiguity or errors arising from anisotropy and preferred crystallite orientations in the specimens was investigated by examining a sample between crossed polaroids which was grown under similar conditions. This showed the visibly clear mass to consist of aggregates of single crystals extending through the sample in the direction of the lines of force, with no preferred orientation of their crystalline axes. This is a reasonable consequence of the freezing process employed, and together with the excellent agreement

* This paper is based on a thesis presented by R. P. Auty in partial fulfillment of the requirements for the degree of Doctor of Philosophy in the Graduate School of Brown University.

† Present address: Dow Chemical Company, Midland, Michigan.

[1] J. Errera, J. Phys. (U.S.S.R.) **5**, 304 (1924).

[2] C. P. Smyth and C. S. Hitchcock, J. Am. Chem. Soc. **54**, 4631 (1932).

[3] E. J. Murphy, Trans. Electrochem. Soc. **65**, 309 (1934).

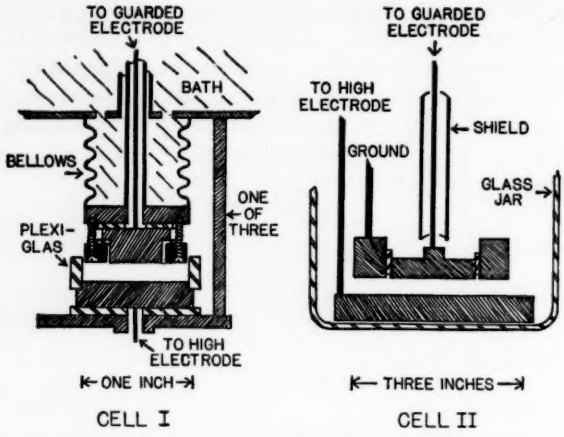

FIG. 1. Drawing of essential features of the two cells used.

between measurements on different samples leads to the conclusion that the results are characteristic of a mass of randomly oriented crystals.

II. EXPERIMENTAL METHODS

A. Electrical

The wide-range conductance-capacitance bridge used has been described in detail elsewhere[4] as has the method for recording transient polarization.[5] Of some importance for the success of the cell arrangements used is the fact that both instruments are intended for cells employing guard electrodes in which only a limited, well-defined volume of dielectric is measured, and can be used to measure capacitances as small as 1 $\mu\mu$f with reasonable precision.

Temperatures were measured by copper-constantan thermocouples in the grounded guard electrodes of the cells and a Leeds and Northrup Type K potentiometer. Temperature control to 0.1°C was effected by adding powdered dry ice to acetone baths in thermal contact with the cells, and all measurements were made as a function of frequency or time at each of a number of constant temperatures.

B. Cells

The essential features of the two cells employed are shown in the drawings of Fig. 1. In cell I, the low potential electrode and the surrounding guard electrode are attached to a Hydron metal bellows mounted on a copper can, and the bellows can be held in compression by the screw and nut arrangement. The high potential electrode is attached rigidly to the base of the can holding the bath liquid by support rods, and insulated from its supporting frame by a Teflon washer. A Plexiglas ring contains the liquid to be frozen, and permits observation of the process through the windows in an outer container.

In cell I, the water was first frozen, then allowed to melt until a clear layer of ice developed at the upper electrodes only. On cooling, this layer grew as a clear solid, except for a few small trapped bubbles, until the electrode space was filled. The bellows compression was then released to permit the upper electrode to follow subsequent contraction of the sample. Electrode spacings from 5 mm to 10 mm were used, corresponding to air capacitances in the range 0.60 $\mu\mu$f to 0.36 $\mu\mu$f for the low potential electrode diameter of 21 mm.

Although this cell gave satisfactory results for large dielectric constants and required only a small quantity of sample, the relatively narrow guard ring led to some uncertainty in cell capacitance for dielectric constants less than about ten with the gaps of several millimeters needed for negligible conductance effects. To insure that no serious errors were so incurred, cell II (Fig. 1) was also used. In this cell the guarded electrode assembly was supported, until the sample was frozen, by German silver tubes clamped by set screws to a Plexiglas cover on the glass container. Then, by loosening the set screws, the electrode was allowed to rest freely on the frozen sample. The guarded electrode diameter is 43.6 mm and the guard ring width is 9.6 mm, giving air capacitances in the range 1.5 to 2.5 $\mu\mu$f for the separations of 8 to 5 mm used.

In cell II, which was placed in a large Dewar containing an acetone bath, freezing began at the bottom and continued until a solid clear layer filled the electrode space. The sample was thus formed in quite a different fashion than in cell I.

In both cells, frozen samples could be cooled for some distance below the melting point before any cracks appeared. When these did develop, they invariably began at or beyond the outside periphery of the electrodes in a direction parallel to the lines of force. At temperatures as low as −50°C no change in capacitance was observed when these occurred, indicating that their effect was confined to the guarded region of the sample. At lower temperatures some nonreproducibility was encountered, which was minimized if the sample was cooled still further and allowed to warm slowly to the temperature of interest. Even so, the lowest temperature for which reliable data could be obtained was defined primarily by strain effects rather than electrical measurement limitations, even though the time scale of the relaxation process becomes very long.

C. Preparation and Handling of Materials

Because of the possible serious effects of even small amounts of conducting impurity, some effort was devoted to insuring cleanliness of the cell. Thorough steaming of all parts of the cells to come in contact with the liquids was followed by prolonged soaking in conductivity water. When equilibrium was reached, specific conductances for the liquid of the order of $1-3\times10^{-6}$ mho/cm were realized. After freezing, much

[4] R. H. Cole and P. M. Gross, Jr., Rev. Sci. Instr. **20**, 252 (1949).
[5] Davidson, Auty, and Cole, Rev. Sci. Instr. **22**, 678 (1951).

smaller but measurable dc conductances were observed of the order 1×10^{-9} mho/cm or less at the melting point. Further evidence as to purity is the fact that consistent data showing no sign of "premelting" were obtained only 0.1° below the melting point.

In cell I, all metal surfaces (brass) in contact with liquid were heavily gold plated, and this procedure was planned for cell II until it was found that prolonged cleaning and soaking of the brass electrodes gave consistent dielectric data and as good conductance behavior as was possible in cell I. The agreement of data from the two cells is thus evidence that the nature of the electrodes had no effect.

III. EXPERIMENTAL ERRORS

The errors resulting from voids and electrode polarization are conveniently shown by considering the complex dielectric constant loci found when their effects are significant. As is well known, simple theories of dielectric relaxation predict a complex dielectric constant ϵ^* of the form

$$\epsilon^*=\epsilon'-i\epsilon''=\epsilon_\infty+(\epsilon_0-\epsilon_\infty)/(1+i\omega\tau), \qquad (1)$$

where ϵ_0 and ϵ_∞ are the equilibrium and limiting high frequency values, $\omega=2\pi$ frequency, and τ is a relaxation time. The complex plane locus of ϵ^* is then a semicircle as shown in Fig. 2.

A. Sample Interface

The various curves of Fig. 2 show for solid H_2O at −10°C the observed deviations from the true locus (curve *b*) as a result of an interface which developed to the extent of about half the electrode area across one sample normal to the lines of force (curve *a*), and as results of electrode space charge effects occasioned by sample conductance (curves *c* and *d*). Considering first curve *a*, one can readily show that the effect is just what one expects from an air gap of fractional width δ in series with the dielectric and condenser plates, the apparent dielectric constant ϵ_{app}^* being given by the series condenser formula

$$\frac{1}{\epsilon_{app}^*}=\frac{1-\delta}{\epsilon^*}+\delta. \qquad (2)$$

The complex locus of ϵ_{app}^* is easily shown from this to be a semicircle but the apparent values of ϵ_0, ϵ_∞, and τ are all too small. The order of the errors incurred for high dielectric constants can be seen from the fact that the observed values represented by curve *a* are accounted for quantitatively by an air gap of average width, δ, 1/300 of the electrode separation.

This particular form of void in the sample is, of course, the most serious one, but one can see very easily by approximate calculations for other forms of defect that rather minute cracks can have serious effects if they lie across the lines of force. That this sort of thing can and does happen in dielectric measurements on solids has often been recognized, but often is not considered as carefully as it should be.

B. DC Conductance

The effect of dc conductance indicated by curves *c*, *d* is not simply an additive one to make the observed loss, expressed by ϵ'', too large, as the apparent values of ϵ' are also too large, the errors in both quantities increasing at low frequencies. That the larger apparent dielectric constants are not real, but rather result from conditions at the electrode-dielectric interface, was established by the fact that they decreased with increasing electrode separation. For the conductances involved here, negligible error in ϵ' resulted if the spacing exceeded 6 mm, as was verified by measurements using spacings as large as 10 mm. What might be called the "direct" conductance error, namely the additive contribution to ϵ'' from dc conductance, was corrected for by subtraction of the measured limiting low frequency conductance G_{dc} from values $G(\omega)$ at higher frequencies, the expression used being

$$\epsilon''=(G(\omega)-G_{dc})/\omega C_0,$$

the values of G being expressed in $\mu\mu$mho and of cell capacitance C_0 in $\mu\mu$f. The value G_{dc} for the results reported here never exceeded one percent of the total absorption conductance realized in the limit $\omega=\infty$.

Both the magnitude and insidious nature of errors from sample inhomogeneity or electrode effects are evident from Fig. 2. The locus for the cracked sample is identical in form with the true curve, as are curves *c* and *d* for frequencies above 600 and 1500 *c/s*, but the values of ϵ' and ϵ'', even for points on the loci, are in error by as much as thirty percent.

C. Other Errors

We believe that errors resulting from faulty samples or space-charge limited conductance are small in our

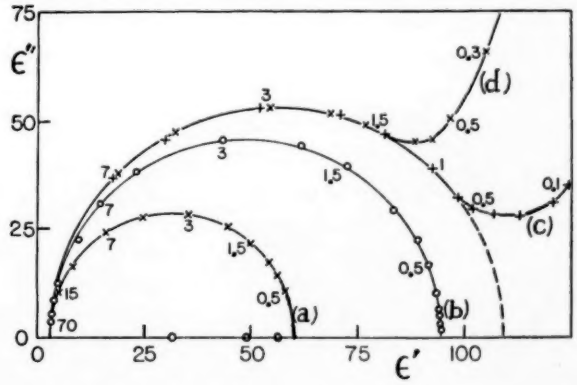

FIG. 2. Complex plane dielectric constants of ice samples at −10.8°C. Curve (*a*), sample with interface parallel to electrodes; curve (*b*), true locus; curves (*c*) and (*d*), samples with electrode polarization arising from dc conductance. Numbers beside points are frequencies in kc/sec.

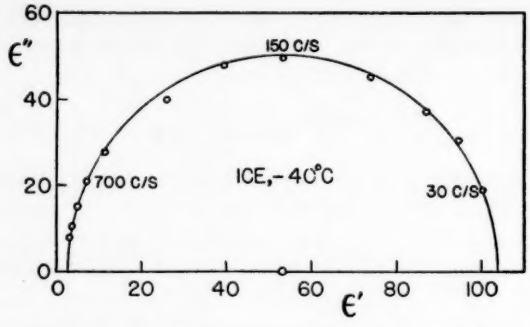

FIG. 3. Complex dielectric constant of ice at −40°C.

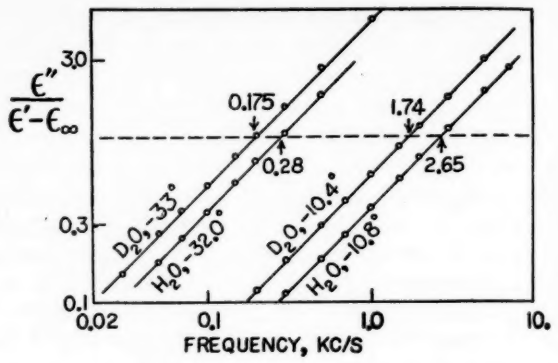

FIG. 4. Plots for determining relaxation times in ice and solid D_2O at −10 and −32°C. The intercepts with the dashed line give the critical frequencies in kc/sec indicated.

results. The accuracy of the data reported here is limited primarily by slight uncertainties in the cell constants, measurement and control of temperatures, and frequencies of the bridge oscillator. A reasonable figure for accuracies of equilibrium dielectric constants ϵ_0 and relaxation times τ is of the order 2–3 percent.

IV. RESULTS

In the measurements reported, some ten runs at temperatures in the range −0.1 to −65°C were made on solid H_2O and three on solid D_2O in the range +1° to −35°C. The reproducibility of data is illustrated in Table I, in which are given values of ϵ', ϵ'' at half the frequencies of measurement for three samples at −10.8°C. Some of these data were used in plotting curve *b* of Fig. 2. The data are evidently in good agreement, except for slight incipient electrode effects at the lowest frequencies for the third run. In Fig. 3 are plotted data for ϵ' and ϵ'' at −40°C, the lowest temperature for which the bridge measurements sufficed to define the complex plane locus adequately, and in this case also a semicircle fits the results within experimental error.

The fact that the bridge data are quantitatively fitted by the simple dispersion Eq. (1) has been further confirmed by an analysis which explicitly verifies the frequency dependence of ϵ^* and also serves to determine the relaxation time τ. From Eq. (1), it is readily shown that what might be called the dipole loss factor $\tan\varphi$ is given by

$$\tan\varphi=\epsilon''/(\epsilon'-\epsilon_\infty)=\omega\tau. \tag{3}$$

From this equation, a plot of experimental values of $\tan\varphi$ *versus* frequency should give a straight line, and the frequency f_c for which $\tan\varphi=1$ gives the relaxation time τ from the relation, $\tau=1/2\pi f_c$. Plots of this kind for solid H_2O and D_2O at two temperatures are shown in Fig. 4, log scales of $\tan\varphi$ and frequency f being used to represent the data symmetrically. The data are fitted without systematic deviation by the straight lines drawn with the unit slope required by Eq. (3). The definitely larger values of τ for D_2O as compared with those for H_2O at the same temperatures are also apparent.

At temperatures much below −40°C, the lowest frequency of bridge measurement (20 counts/sec) was too high to give reliable values of ϵ_0 and τ; hence the transient method already mentioned was used. In effect, this method gives a record of transient charge following application of a step voltage to the dielectric, or what might be called the "transient dielectric constant," $\epsilon(t)$, which for a dielectric satisfying Eq. (1) is readily shown to be given by

$$\epsilon(t)=\epsilon_\infty+(\epsilon_0-\epsilon_\infty)[1-\exp(-t/\tau)]. \tag{4}$$

After correction for dc conductance, the value of ϵ_0 is given by the final equilibrium charge, of ϵ_∞ by the initial value and of τ by the time for $\epsilon(t)$, to reach a value $1/e$ short of the final value, if the data are fitted by Eq. (4), as was true in all cases. The bridge and transient methods gave results in agreement at −50°C and the latter was used at lower temperatures.

Representative values of ϵ_0, ϵ_∞, and τ at several temperatures are listed in Table II for solid H_2O and D_2O. Plots of $\log\tau$ *versus* reciprocal temperature are given in Fig. 5. The data for τ are fitted within their accuracy over the range of temperatures by rate expressions of the form $\tau=A\exp(B/RT)$, the constants A and B having the values $A=5.30\times10^{-6}$ sec, $B=13.25$ kcal/mole for H_2O and $A=7.7\times10^{-16}$ sec, $B=13.4$ kcal/mole for D_2O.

TABLE I. Dielectric constant data for ice at −10.8°C.

	Run 1		Run 2		Run 3	
Electrode spacing	0.52 cm		0.64 cm		0.79 cm	
Specific conductance	2.1×10^{-10} mho/cm		1.9×10^{-10} mho/cm		7.4×10^{-10} mho/cm	
Frequency f	ϵ'	ϵ''	ϵ'	ϵ''	ϵ'	ϵ''
50 counts/sec	94.8	1.7	95.0	2.0	97.5[a]	...
100	94.6	3.2	94.6	3.6	95.4[a]	3.5
200	94.1	6.4	94.0	6.8	94.2	6.9
500	91.6	16.4	91.3	16.8	91.3	16.9
1 kc/sec	83.4	29.1	83.0	30.3	83.1	30.2
2	61.7	44.3	60.6	44.1	61.1	44.5
5	23.0	38.3	22.5	37.8	23.2	39.3
10	9.55	22.9	9.50	22.8	9.55	23.1
20	4.75	12.2	4.71	11.9	4.76	12.1
50	3.32	5.0	3.28	4.9	3.29	5.0

[a] Incipient electrode polarization makes ϵ' large.

TABLE II. Parameters of dielectric relaxation formula for ice and solid D_2O.

(a) Ice				(b) Solid D_2O			
t°C	ϵ_0	ϵ_∞	τ ($\times 10^5$ sec)	t°C	ϵ_0	ϵ_∞	τ ($\times 10^5$ sec)
− 0.1	91.5	3.10	2.2	1.2	90	3.06	3.4
−10.8	95.0	3.08	6.0	−2.7	89.0	3.06	5.0
−20.9	97.4	3.10	16.4	−10.4	92.0	3.03	9.15
−32.0	100	3.00	57	−21.7	95.5	3.06	33
−44.7	104	3.10	252	−27.3	97.9	3.03	48
−56.8	114	3.1	1200	−33.0	100	3.03	91
−65.8	133	3.1	4500				

The values of relaxation time τ found for H_2O are in fair agreement with the results of Smyth and Hitchcock and of Murphy, but differ considerably from those of Wintsch.[6] In any such comparisons, differences in definition of τ should be noted. We have here computed τ from the central frequency of the dispersion region, but a number of other workers express their results by a "Lorentz-field corrected" τ_D differing from ours by the factor $(\epsilon_0+2)/(\epsilon_\infty+2)$ which is of dubious significance.

V. DISCUSSION

The values of equilibrium dielectric constant ϵ_0 near the melting point are larger than those reported by most other workers, but are a little smaller than those of Murphy.[3] The value of 91.5 at 0°C is definitely larger than the figure for water at 0°C, despite the decrease in density on freezing, and increasingly large values are found as the temperature is decreased if sufficient time is allowed for equilibrium.

The large values of ϵ_0 indicate both the existence of a strong local coordination of neighboring molecules in the lattice and the existence of mechanisms by which their rearrangement in an external electric field can be accomplished. For an adequate model of the molecule and its environment, the theories of Kirkwood[7] and Fröhlich[8] provided a basis for calculation of the equilibrium dielectric constant. Calculations of this kind have been made by Powles[9] on the basis of Pauling's model for ice,[10] in which those configurations are permitted which place two hydrogen atoms close to each oxygen atom and two close to its four nearest oxygen neighbors. The complexity of properly taking account of electrostatic interactions makes the calculations necessarily approximate. They do show, however, that values comparable with the observed can be obtained on the basis of a point charge electrostatic model, and indicate that all configurations compatible with two protons near and two far from any oxygen atom are realized with comparable, if not substantially equal,

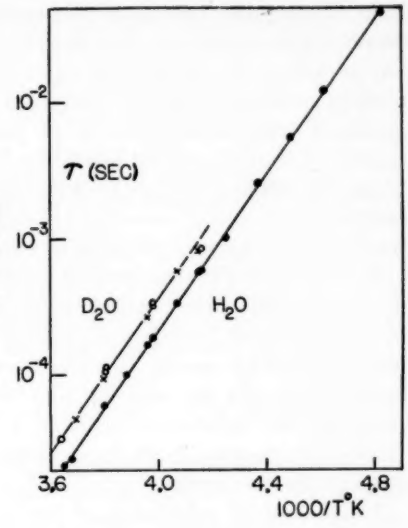

FIG. 5. Relaxation times of ice and solid D_2O (log scale) as a function of reciprocal of absolute temperature ($1000/T$).

probability. This raises the question, implicit in any case in the fact that the equilibrium dielectric constant is so large, of how necessary proton displacements to realize the different configurations can occur.

In an ideal lattice, displacements by proton shifts from one bond to another, no matter how devised, either have improbable energy requirements or lead to no net polarization. If instead one supposes that the displacements occur by proton shifts from one oxygen atom to another, as considered in some detail by Latimer,[11] equally serious difficulties with energy requirements, absence of net polarization, or the improbable consequence of a space-charge type of polarization are encountered.

The difficulties with various such mechanisms have been examined in detail by Schellman,[12] who proposes, as a way out of the difficulty, that actually one has missing bonds between a few of the oxygen atoms from lattice defects or vacancies, and that molecular reorientations through the lattice are then made possible by propagation of the missing bonds.

Although the experimental data on the relaxation process in ice of themselves give no decisive confirmation of any of these various points of view, they do show well-defined and experimentally simple behavior. The frequency dependence of the dispersion is quantitatively described by a single relaxation time over the temperature range studied, from which one infers that a single simple mechanism is probably involved, a situation not often encountered in real dielectrics. The temperature dependence of the relaxation times is accurately described by a simple unimolecular rate law, again suggesting a simple mechanism. Any intrinsic volume conductance in ice is very minute, which argues against proton jumps followed by molecular reorienta-

[6] H. Wintsch, Helv. Phys. Acta **5**, 126 (1932).
[7] J. G. Kirkwood, J. Chem. Phys. **7**, 911 (1939).
[8] H. Fröhlich, *Theory of Dielectrics* (Oxford University Press, New York, 1949).
[9] J. G. Powles, J. Chem. Phys. **20**, 1302 (1952).
[10] L. Pauling, *Nature of the Chemical Bond* (Cornell University Press, Ithaca, New York, 1939), p. 281.
[11] W. M. Latimer, Chem. Rev. **44**, 59 (1949).
[12] J. A. Schellman, Ph.D. thesis (Princeton University Press, Princeton, New Jersey, 1951); see also J. A. Schellman and W. Kauzmann, Phys. Rev. **82**, 315 (1951).

tions. The equilibrium dielectric constant increases with decreasing temperature. One should not expect this for any processes involving transitions to metastable equilibrium positions of higher energy, as is the case for the model of relative orientations of molecular pairs discussed by Bauer[13] and for ionization by proton transfer. Thus, the general picture of polarization by molecular reorientation made possible by lattice imperfections seems the most reasonable one yet proposed.

From Fig. 5 it is apparent that the relaxation process is considerably slower in heavy ice at all temperatures of measurement, a difference which could arise from larger activation energy B, lower frequency factor $1/A$, or both. Because the data for τ are over a quite limited range of the significant variable $1/T$ in the case of heavy ice, caution must be exercised in deciding between these possibilities.

Least squares treatment of the data gives a larger value of A for D_2O than for H_2O and a slightly larger activation energy. That the activation energies should be nearly the same is understandable if essentially the same electrostatic configurations are involved, and the difference of 0.25 kcal/mole is in the proper direction to be explained as resulting from a difference of zero point energies.

The ratio of the constants A calculated from the best fits of the data is 1.5, but the precision of the measurements is not good enough to establish decisively the difference from the value unity‡ one would expect from absolute rate theory. If the value of A for D_2O is assumed to be the same as for H_2O, the best, slightly larger, value of activation energy to fit the data gives slightly poorer agreement as judged by the mean-square deviation. The improvement by using the least squares fitted value of A is, however, too small to be considered significant. A more accurate determination from more extensive data would be of some interest in deciding whether the conventional calculation of the frequency factor, which leads to no isotope effect, is adequate in the present case.

A proper interpretation of the absolute values of the parameters A and B for the relaxation process must await a theory in which the mechanism of dissipation of energy into lattice modes is adequately represented, but Schellman's observation[12] that an activation energy of 13 kcal/mole corresponds to breaking of three hydrogen bonds on the basis of 4.5 kcal/mole bond energy in ice[10] seems pertinent.

The behavior of the equilibrium dielectric constant with decreasing temperature deserves mention. There is no evidence of approach to any finite limiting value, rather the increase becomes more marked. As discussed below, difficulties encountered in obtaining reproducible results below $-60°C$ appear to be related to strain in the sample, and as a result we felt that continuing to still lower temperatures was unwarranted without careful study and better mechanical state of the sample. The present results thus give no indication of the limiting behavior as the temperature approaches absolute zero, a subject which merits further study when suitable experimental procedures have been devised.

In two recent papers,[14] Murphy has discussed an interpretation of his measurements of high frequency absorption conductance in ice in terms of two absorption processes in ice, the first corresponding to volume polarization dominant at temperatures not too far below the melting point. The existence of a second process was inferred from the fact that for temperatures below about $-35°C$, his observed high frequency conductances were larger than continuation of the high temperature rate law would give, and could be represented by a second rate law with smaller activation energy.

In our measurements, we have found no evidence for the coexistence of two absorption processes, but have found that the frequency range of dispersion was in several cases displaced to higher frequencies than predicted by the rate expression at temperatures below $-50°C$, by amounts depending on the sample and its previous thermal history. These displacements gave rise to larger values of high frequency conductance§ as reported by Murphy, but the dispersion was still quantitatively described by the Debye equations (1) with smaller values of τ, and the equilibrium dielectric constant values found were essentially the same. We found that these values of τ were not reproducible from one sample to another, and moreover, that values fitting the higher temperature behavior resulted in some cases from "annealing" the samples by holding them at still lower temperatures for a few hours.

As a result of these observations, we conclude that the effects must have resulted from strains or dislocations developed on cooling the sample which could be partially or wholly relieved, and that there are no indications of a second relaxation process.

We are indebted to Professor Kauzmann for helpful discussion, and to Drs. Powles and Schellman for permission to quote some of their results.

[13] E. Bauer, Cahiers phys. **20**, 1 (1944); **21**, 37 (1944).

‡ It should be recognized that seemingly large changes of the constant A correspond to small differences in $\log A$, which is the quantity directly derived from the measurements.

[14] E. J. Murphy, J. Chem. Phys. **19**, 1516 (1951); Phys. Rev. **79**, 396 (1950); see also E. J. Murphy and S. O. Morgan, Bell System Tech. J. **38**, 502 (1939).

§ This follows from the fact that the absorption conductance is proportional to $\omega\epsilon''$, which in the limit $\omega\tau \gg 1$ has the value $(\epsilon_0 - \epsilon_\infty)/\tau$ for a single relaxation time.

The Absolute Quantum Yields of the Fluorescence of Chlorophyll Solutions*

LESLIE S. FORSTER† AND ROBERT LIVINGSTON
School of Chemistry, Institute of Technology, University of Minnesota, Minneapolis, Minnesota
(Received February 18, 1952)

An integrating sphere has been adapted to the measurement of the quantum yield of the fluorescence of solutions of pigments. The intensities of the fluorescence and of the absorbed light were determined separately with a thermopile.

Chlorophylls *a* and *b* dissolved in various solvents have been studied with this apparatus over a range of concentrations, and the measured yields corrected for autoabsorption. The yield for chlorophyll *a* is 0.25 and is in general independent of solvent and excitation wavelength. The yield for chlorophyll *b* is 0.11 for ether solutions and 0.06 for methanol solutions. The absolute fluorescent yields of solutions of fluorescein, eosine, magdala red, and rubrene were also measured. These results are in reasonable agreement with the published values of the yields for the same compounds.

INTRODUCTION

IT appears plausible that some insight into the primary act of photosynthesis[1] can be obtained from a study of the photochemical properties of homogeneous solutions of purified chlorophyll. While the absolute quantum yield of fluorescence is an important property of this type, the commonly accepted value of ten percent is based upon a rough estimate[2] in which apparently no attempt was made to correct for autoabsorption or to distinguish between chlorophylls *a* and *b*.

Few reliable determinations of absolute fluorescent yields have been published. Vavilov[3] made the first measurements of the absolute yields of fluorescent dye solutions. He compared visually the fluorescent intensity with the intensity of light scattered by a "perfect" diffuser. These comparisons were made for small wavelength intervals, covering the entire fluorescent band, and the total fluorescent intensity was obtained by summation. The method is difficult and laborious, and the apparent reliability of his results is a tribute to his skill and care.

For wavelengths shorter than 4400A the necessity for this summation over wavelength may be avoided by the use of Bowen's[4] ingenious "relative quantum counter." This consists of a phototube provided with a strongly absorbent, fluorescent filter. The output of the phototube is proportional only to the total number of quanta striking the filter per second.

Almy and Gillette[5] determined the absolute yield for biacetyl vapor by directly measuring the light absorbed in a small volume and the fluorescence emitted from this volume in a small solid angle. These authors demonstrated that great care must be taken to minimize the errors due both to the estimation of the solid angle and to the calibration of a selective detector, such as a phototube.

In all of the aforementioned measurements it was assumed that the fluorescence was emitted uniformly in all directions. However, if the degree of polarization[6] differs from zero, the angular distribution is not uniform throughout the solution. In principle, these errors due to non-uniform distribution can be eliminated by using an integrating sphere, and the errors inherent in the calibration of a selective receiver can be avoided by employing a thermopile.

EXPERIMENTAL METHODS AND MATERIALS

Materials

Chlorophylls *a* and *b* were prepared by a modification[7] of the method of Zscheile and Comar.[8] Pheophytin *a* was prepared by treating chlorophyll *a* with hydrogen chloride, tenfold in excess of the stoichiometric amount. The resulting pheophytin was purified chromatographically on powdered sugar using petroleum ether *A* containing 0.5 percent of isopropanol as the developer. Pure samples of magdala red and of rubrene were kindly furnished by Professor E. J. Bowen (Oxford). The mesoporphyrin dimethyl ester was prepared and purified by Dr. Schwartz of the University of Minnesota Medical School. The eosine was a purified[9] sample, and the fluorescein which was Eastman Kodak reagent grade material was used without further purifications. The several solvents were all carefully dried and fractionated shortly before use.

* This work was supported in part by the ONR (Contract N6ori-212, Task Order I. Project NR 059, 028) to whom the authors are indebted. This paper is based upon a dissertation submitted by L. S. Forster to the Faculty of the Graduate School of the University of Minnesota in partial fulfillment of the requirements for the degree of Doctor of Philosophy. During the academic year 1950–1951, L. S. Forster was the recipient of a fellowship supported by the Shell Oil Company.

† Present address: Department of Chemistry, University of Rochester, Rochester, New York.

[1] E. I. Rabinowitch, *Photosynthesis* (Interscience Publishers, Inc., New York, 1945), Vol. I; R. Livingston, *Photosynthesis in Plants* (Iowa State College Press, Ames, Iowa, 1949), Chapter 7.

[2] J. A. Prins, Nature **134**, 457 (1934).

[3] S. I. Vavilov, Z. Physik **22**, 266 (1924).

[4] E. J. Bowen and J. W. Sawtell, Trans. Faraday Soc. **33**, 1425 (1937).

[5] G. M. Almy and P. R. Gillette, J. Chem. Phys. **11**, 188 (1943).

[6] P. Pringsheim, *Fluorescence and Phosphorescence* (Interscience Publishers, Inc., New York, 1949); T. Förster, *Fluorezenz Organischer Verbindungen* (Vandenhoek und Ruprecht, Göttingen, 1951).

[7] Livingston, Sickle, and Uchiyama, J. Phys. & Colloid Chem. **51**, 775 (1947).

[8] F. P. Zscheile and C. L. Comar, Botan. Gaz. **102**, 463 (1941).

[9] F. Hurd and R. Livingston, J. Phys. Chem. **44**, 865 (1940).

Apparatus

The apparatus is shown diagrammatically in Fig. 1.[10] For exciting light of wavelength less than 6000A, the light source (A) was a GE AH6 high pressure mercury arc, provided with a heat absorbing filter (B) consisting of 2.5 cm of saturated copper sulfate solution. When red exciting light was desired, the light source was a 1000-watt tungsten projection lamp,[11] and the copper sulfate solution was replaced by a saturated ferrous ammonium sulfate solution. The spherical glass condensing lens (C)

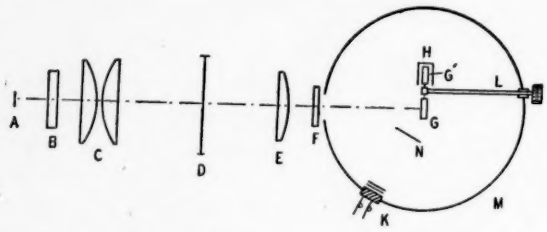

FIG. 1. Schematic diagram of the integration sphere and auxiliary apparatus.

was followed by a shutter (D). Since the image of the AH6 arc was several times longer than it was wide, a cylindrical lens (E) was introduced to render the spot of light falling on the cell (G) roughly circular. The desired spectral region was selected by an appropriate interference or Wratten filter (F) before the beam entered the sphere through a circular opening 3.2 cm in diameter. The sphere, which was 45.5 cm in diameter, was lined with barium sulfate, a highly reflective matt surface. The two glass cells (G and G′) were so mounted on a rod (L) that either cell could be rotated, reproducibly, into the light beam, the other cell disappearing into a whited cell holder (H). A Moll surface thermopile (K) was placed in a bushing in the sphere wall in such a manner that it received light reflected from a fixed portion of the wall. A whited screen (N) prevented direct radiation from the cell striking the thermopile.

The thermopile was used as a null instrument, its output being opposed by a potential obtained from a Leeds and Northrup K-2 potentiometer and dropped across a voltage divider having a ratio of 1:1000. The response of the L and N *HS* galvanometer (whose sensitivity was 0.17 microvolts per mm) in the thermopile circuit was amplified by a simple optical electronic amplifier.[10,12] With this galvanometer and amplifier an unbalance of 0.01 microvolt in the thermopile circuit could be readily detected.

[10] For additional details see Ph.D. thesis, Leslie S. Forster, University of Minnesota, 1951. Available on microfilm from University Microfilms, Ann Arbor, Michigan.

[11] J. McBrady and R. Livingston, J. Phys. & Colloid Chem. **52**, 662 (1948).

[12] Mueller, Garman, and Droz, *Experimental Electronics* (Prentice-Hall, Inc., New York, 1942).

Standard Procedure

In order to measure the intensity of the light absorbed by the solution a filter was placed in front of the photocell. This filter transmitted a large fraction of the exciting light and was opaque to the fluorescent light. Under these conditions the change in thermopile output, which occurred when a cell containing the solution was substituted for one containing the solvent, was proportional to the "total intensity" (ergs/sec) of absorbed light. The following filters were used: for the chlorophylls, pheophytin, mesoporphyrin, and rubrene—Corning #9788; for fluorescein and eosine—Wratten #34A; and for magdala red—Wratten #40. Similarly, the total intensity of the fluorescent light was determined by placing a cut-off filter which transmitted uniformly and efficiently in the range covered by the fluorescent band but which strongly absorbed the exciting light. The following filters were used: for the chlorophylls, pheophytin, mesoporphyrin, and rubrene —Corning #3484; for fluorescein and eosine—Wratten #5; and for magdala red—Wratten #22. In all cases a thin plate of clear glass was placed between the thermopile surface and the cut-off filter. Since the glass strongly absorbed long wavelength infrared, it eliminated a troublesome drift which was caused by the heating of the first filter by the light which it absorbed.

METHODS OF CALCULATION

Light emitted by a source at the center of a closed sphere undergoes an infinite number of reflections before being absorbed by the wall. It has been demonstrated[13] for such a system that the indirect illumination E, (i.e., the light which has been reflected one or more times) striking any area of the wall is given by the following expression:

$$E=cI[1/\alpha-1] \tag{1}$$

or for small values of α,

$$E\cong cI/\alpha, \tag{2}$$

where I is the intensity of the source, α is the absorption coefficient of the wall, and c is a constant of proportionality. The indirect light is uniformly distributed, despite any lack of uniformity in the angular distribution of the emitted light.

In the present experiments the sample (or solvent) vessel may be treated as the light source.[10,14] The intensity T' of the light which strikes the front surface of the thermopile filter is

$$T'\cong cI/\alpha. \tag{3}$$

When the filter which transmits the exciting light is in place, the intensity T_E striking the thermopile proper can be written

$$T_E\cong cG_EI_E/\alpha_E, \tag{4}$$

[13] E. B. Rosa and A. H. Taylor, Natl. Bur. Standards, Sci. Paper 447 (1922).

[14] B. Kok, Enzymologia **13**, 1 (1948).

where the subscript E refers to light having the wavelength of the exciting beam, and G_E is the transmission coefficient of the thermopile filter for this light. Similarly when the filter which transmits the fluorescent light is used,

$$T_F \cong cG_F I_F/\alpha_F. \tag{5}$$

The intensity T_A of the light absorbed by the pigment is proportional to the difference in intensity

$$T_E(\text{solvent}) - T_E(\text{sample})$$

striking the thermopile when the solvent cell is substituted for the sample cell. Since the output of the thermopile is directly proportional to the intensity of the light falling on its surface, the difference in thermopile output A, corresponding to the substitution of the cells, is given by the following relation:

$$A \cong c'G_E I_A/\alpha_E \tag{6}$$

or

$$I_A \cong A\alpha_E/c'G_E.$$

Similarly, if F is the change in thermopile response corresponding to the substitution of the solvent cell for the sample cell when the filter which transmits the fluorescent light is in place,

$$I_F \cong F\alpha_F/c'G_F. \tag{7}$$

By definition the energy yield of fluorescence is I_F/I_A, and the quantum yield of fluorescence φ is

$$\varphi = I_F\lambda_F/I_A\lambda_E.$$

Accordingly, the quantum yield is related to the measured quantities as follows:

$$\varphi = F\lambda_F\alpha_F G_E/A\lambda_E\alpha_E G_F. \tag{8}$$

Since the fluorescence is emitted over a wavelength interval, Eq. 8 should be written

$$\varphi = \frac{FG_E}{AG_f\alpha_F\lambda_E} \cdot \frac{\int \alpha_F(\lambda) I_F(\lambda)\lambda_F d\lambda}{\int I_F(\lambda) d\lambda}, \tag{9}$$

the integration being carried over the entire fluorescence band. Fortunately, the product $\alpha_F(\lambda)\lambda_F$ was constant within one percent over the wavelength interval 5000 to 7200A, and Eq. 8 is sufficiently accurate for the present purpose.

The transmission coefficients G_E and G_F were measured directly with a Beckman spectrophotometer. The factor α_F/α_E was evaluated for various wavelengths, by comparing the response of the thermopile in the sphere to that of a second thermopile which was placed to intercept the incident beam as it entered the sphere.[10] The thermopile filter and the cells were removed when the comparison was made.

ERRORS

The experimental determinations of α_F/α_E have a probable error of about seven percent. The probable error of G_E/G_F is less than one percent and that of F/A in most cases is five percent. The probable error in φ resulting from random errors is then less than ten percent.

Systematic errors arise because the sphere is non-ideal. If the wall pigment is not a perfect scatterer, the non-uniform distribution of light emitted from the "source" can influence the measurements. Since direct light does not reach the thermopile and light which has suffered more than one reflection is uniformly distributed, such an error can only be due to light which has undergone only one reflection. The contribution of the first reflection to the total indirect illumination has been shown[13] to be equal to α, which for the present measurements is 0.05. Even if the distribution of the exciting light were such that none of the once-reflected light reached the thermopile and the distribution of fluorescence were uniform, this error could not exceed five percent. A rough analysis indicates that the measured values of φ may be from one to three percent too high due to this error.

Other systematic errors are also introduced by imperfections in the sphere. If the sphere contains an object whose absorption coefficient is α' and which intercepts a fraction β of the directly emitted light, it will absorb the fraction $\alpha'\beta$ of this light. The various fittings inside the sphere were coated with a white enamel whose absorption coefficient was about 0.10. Estimated values of β for absorption and fluorescence measurements are, respectively, 0.10 and 0.15. The fraction of indirect illumination intercepted would be very nearly the same for both measurements and accordingly does not affect the measured values of φ. The presence of these objects would be expected to reduce the measured yield by less than one percent.

Holes in the wall must be considered as areas of zero reflection coefficient. Walsh[15] has shown that the percent reduction r in the illumination within the sphere due to a hole is

$$r = \frac{[\theta + (1-\alpha)(B-\theta)]}{\alpha} 100,$$

where B is the ratio of the area of the hole to the area of the sphere, and θ is the fraction of the directly emitted light which falls upon the hole. In the absorption measurements no direct light falls upon the hole and $\theta_A = 0$. In the fluorescence measurements the angular distribution is approximately uniform and $\theta_F = B$. In spite of this difference in initial distribution the value of r is about two percent for both the absorption and fluorescence measurements, and the effect on φ is accordingly negligible.

The effect of incomplete shielding of the sample cell by the cell house has been considered and found to be negligible. Some of the fluorescent light may be reflected by the cell holder back into the sample cell and

[15] J. W. T. Walsh, *Photometry* (Constable, London, 1926).

TABLE I. Absolute quantum yields of fluorescence at 25°C.

Dye	Solvent	Exciting wavelength, A	Conc., g/cc	φ	Authors
Fluorescein	Aq. NaOH	4360	4×10^{-5}	0.77 ± 0.06	F and L
Fluorescein	Aq. NaOH	4360	1×10^{-5}	0.79 ± 0.06	F and L
Fluorescein	Aq. NaOH			0.84	V(3)
Fluorescein	Aq. NaOH			0.85	H(16)
Fluorescein	Aq. NaOH			1.05	G and S-G(17)
Fluorescein	Aq. NaOH			0.85	U and LaM(18)
Eosin	Water	4360	1×10^{-5}	0.12 ± 0.02	F and L
Eosin	Water			0.16	V
Magdala Red	Ethanol	5460	1×10^{-4}	0.43 ± 0.03	F and L
Magdala Red	Ethanol	5460	1×10^{-5}	0.49 ± 0.04	F and L
Magdala Red	Ethanol			0.56	V
Rubrene	*n*-Heptane	4360	1×10^{-5}	1.02 ± 0.08[a]	F and L
Rubrene	*n*-Heptane			1.0[b]	B(19)

[a] This measurement was made in oxygen-free solution.
[b] This estimate is relative to Vavilov's value for magdala red.

be partially absorbed. This error should be negligible in those yields that were obtained by extrapolation to zero concentration, but directly measured yields may be about five percent too low.

EXPERIMENTAL RESULTS

As a check on the reliability of our experimental method we have redetermined the absolute quantum yields of solutions of compounds whose values have been determined by other investigators. These results and the corresponding previously published values are given in Table I.[16–19] The published values have in several cases been given as energy yields. In these instances a conversion to quantum yields has been made before tabulation in Table I. None of the quantum yields determined by us have been corrected for autoabsorption and accordingly are too low, especially where the observed yield is small. The agreement between the present values and the more reliable of those previously published is quite satisfactory. Since the substances were chosen to cover a wide range of absolute yields and of wavelengths, the general reliability of the method and of the published results appears to be confirmed by these measurements.

The results for the chlorophylls, pheophytin *a*, and mesoporphyrin dimethyl ester are listed in the following table. All measurements were made in oxygen-free solutions, approximately at 25°C. The exciting light was of λ4360A for the chlorophylls and of 4060A for pheophytin and mesoporphyrin. The values of the quantum yields decrease with increasing concentration presumably, in these dilute solutions, due only to autoabsorption. An approximate analysis[10] of this effect indicates that at low concentrations

$$\varphi/\varphi_0 \cong 1-Um,$$

where m is the molarity and U is a factor which can be evaluated (graphically) if the absorption and emission curves are known. For ether solutions of the chlorophylls this information is available,[8,20] and such an evaluation of U leads to a value of φ at infinite dilution (i.e., φ^0) of 0.025. Graphical extrapolation of the data to $m=0$ leads to the value 0.24 of φ^0 which is given in Table II. The value of φ^0 for chlorophyll *a* in methanol was also obtained by graphical extrapolation. For the other solvents where data was insufficient to permit extrapolation, φ^0 was computed on the assumption that U is inversely proportional to the difference between the absorption and fluorescence maxima. For pheophytin *a* and mesoporphyrin the effect of autoabsorption appears to be small, and it is probably justifiable to assume that the values of φ^0 are 0.14 ± 0.03 and 0.10 ± 0.03, respectively.

TABLE II. Absolute quantum yields for chlorophyll and related compounds.

Pigment	Solvent	Molarity $\times10^6$	φ
Chlorophyll *a*	Methanol	20.0	0.15 ± 0.02
Chlorophyll *a*	Methanol	14.0	0.14 ± 0.02
Chlorophyll *a*	Methanol	11.0	0.17 ± 0.02
Chlorophyll *a*	Methanol	10.0	0.18 ± 0.02
Chlorophyll *a*	Methanol	8.6	0.17 ± 0.02
Chlorophyll *a*	Methanol	6.2	0.18 ± 0.02
Chlorophyll *a*	Methanol	5.5	0.21 ± 0.02
Chlorophyll *a*	Methanol	2.7	0.21 ± 0.02
Chlorophyll *a*	Methanol	(0)	0.24 ± 0.02[a]
Chlorophyll *a*	Ethyl ether	21.0	0.15 ± 0.02
Chlorophyll *a*	Ethyl ether	7.2	0.20 ± 0.02
Chlorophyll *a*	Ethyl ether	5.0	0.20 ± 0.02
Chlorophyll *a*	Ethyl ether	2.3	0.22 ± 0.02
Chlorophyll *a*	Ethyl ether	(0)	0.24 ± 0.02[a]
Chlorophyll *a*	Acetone	9.7	0.21 ± 0.02
Chlorophyll *a*	Acetone	3.3	0.24 ± 0.02
Chlorophyll *a*	Acetone	(0)	0.26 ± 0.04[a]
Chlorophyll *a*	Benzene (wet)[b]	5.5	0.23 ± 0.02
Chlorophyll *a*	Benzene	(0)	0.26 ± 0.04[a]
Chlorophyll *a*	Cyclohexanol	5.0	0.20 ± 0.02
Chlorophyll *a*	Cyclohexanol	(0)	0.26 ± 0.04[a]
Chlorophyll *b*	Methanol	15.0	0.043 ± 0.005
Chlorophyll *b*	Methanol	6.5	0.048 ± 0.007
Chlorophyll *b*	Methanol	(0)	0.06 ± 0.01[a]
Chlorophyll *b*	Ethyl ether	12.0	0.090 ± 0.010
Chlorophyll *b*	Ethyl ether	9.0	0.074 ± 0.007
Chlorophyll *b*	Ethyl ether	(0)	0.11 ± 0.01[a]
Pheophytin *a*	Methanol	10.0	0.14 ± 0.02
Pheophytin *a*	Methanol	2.5	0.13 ± 0.03
Mesoporphyrin	Benzene	20.0	0.10 ± 0.03
Mesoporphyrin	Benzene	10.0	0.10 ± 0.03

[a] These are computed values of φ^0.
[b] Livingston, Watson, and McArdle, J. Am. Chem. Soc. **71**, 1542 (1949).

EFFECT OF WAVELENGTH OF EXCITING LIGHT

It has been reported[21,22] that the fluorescence yield of chlorophyll is about twofold greater when red rather than blue exciting light is used. This claim is based upon preliminary results obtained by Dr. W. Watson in this laboratory. Since this finding differs from those obtained with solutions of fluorescein, etc.,[6] whose quantum yield is largely independent of wavelength, it was

[16] H. Hellstrom, Arkiv. Kemi, Mineral. Geol. **12A**, 17 (1937).
[17] I. C. Ghosh and S. B. Sen-Gupta, Z. Physik. Chem. **B41**, 117 (1938).
[18] J. Umberger and V. LaMer, J. Am. Chem. Soc. **67**, 1099 (1945).
[19] E. J. Bowen and D. Norton, Trans. Faraday Soc. **35**, 44 (1939).
[20] F. P. Zscheile and D. Harris, J. Phys. Chem. **47**, 623 (1943).
[21] E. I. Rabinowitch, *Photosynthesis* (Interscience Publishers, Inc., New York, 1951), Vol. II, part 1.
[22] R. Livingston, J. Soc. Dyers and Colourists **65**, 781 (1949).

thought worthwhile to repeat the measurements under better experimental conditions.

The procedure used with exciting light of λ4360A could not be employed since there is a strong overlap between the fluorescence and the red-absorption bands. The following indirect method[10] was employed. The first step was to determine F (in the following indicated as F_b) as before. Keeping the incident radiation constant, the thermopile was replaced with a photocell fitted with a Wratten 88A filter, and the change in photocell output P_b, corresponding to the substitution of the sample cell for the solvent cell, was determined. The Wratten 88A filter transmits appreciably only at wavelengths greater than 7200A. A 1000-watt incandescent projection lamp provided with a red-transmitting interference filter was substituted for the 4360A source. The change in output, corresponding to the replacement of the solvent by the sample cell, was then determined severally by the thermopile-filter and photocell-filter combinations used before. These quantities are designated, respectively, as R and P_r.

Zscheile and Harris[20] observed that the fluorescence spectra of the chlorophylls are independent of the wavelength of the exciting light. We may assume, therefore, that the relative (total) fluorescent intensities for blue and red excitation are equal to the ratio of the corresponding photocell response differences.

$$F_r/F_b=P_r/P_b. \tag{10}$$

Since in these experiments the average wavelengths of the absorbed and emitted light are nearly coincident,

$$\varphi\cong F_r/A_r. \tag{11}$$

The measured quantity R is equal to the intensity of the light absorbed minus that emitted

$$R=A_r-F_r=A_r(1-\varphi). \tag{12}$$

Combining Eqs. (10), (11), and (12), we obtain the following relation with the aid of which φ may be computed in terms of measured quantities:

$$\varphi=\frac{F_bP_r}{RP_b}\left(1+\frac{F_bP_r}{RP_b}\right)^{-1}. \tag{13}$$

The extrapolated values φ^0 given in Table III were calculated from the values of φ (corresponding to concentrations ranging from 6×10^{-6} to $1.4\times10^{-5}m$) using the very probable assumption that $(\varphi/\varphi_0)\text{red}=(\varphi/\varphi_0)\text{blue}$.

It is apparent that, with the exception of the experiment made with the interference filter having a transmission maximum at λ6980A, there is no appreciable effect of the exciting wavelength upon the yield. This conclusion was confirmed by a more direct but less accurate method which is discussed in reference 10. The falling off of the yield, when exciting light of wavelength greater than the fluorescent maximum is employed, has been observed[6] for several different dye solutions. While its explanation is not apparent, it is certainly not a unique characteristic of chlorophyll.

DISCUSSION

The absolute quantum yields of the fluorescence of infinitely dilute solutions of chlorophylls *a* and *b* in etheral solutions are 0.25 and 0.10, respectively. While these values are distinctly greater than Prins' estimate[2] of 0.1 (for a mixture of chlorophylls *a* and *b*?), this discrepancy is not surprising in view of the apparent crudity of the earlier experiments.

It is somewhat surprising that the yield for chlorophyll *a* is the same for several different solvents, while that for chlorophyll *b* is 40 percent less in methanol than it is in ether. This may be related to the relatively large effect of changing solvent upon the absorption spectrum of chlorophyll *b*.[23]

The present results which indicate that the quantum yield for chlorophyll fluorescence is independent of the wavelength of the exciting light (for wavelengths shorter than that of the emission maximum of chlorophyll) is consistent with the reports[6] of earlier measurements on the fluorescence of dye solutions. They demonstrate that a chlorophyll molecule in its second excited (singlet) state reverts to the first excited singlet state, by a process of internal conversion in a very short time, probably less than 10^{-10} second. The probability of a nonradiative transition from the second excited (singlet) state to a triplet or any other nonemissive state must be relatively very small.

At first sight the present relatively high fluorescent yield for chlorophyll solutions appears incompatible with the observed quantum yields of (practically) unity for chlorophyll-sensitized reactions, whose reactants do not strongly quench fluorescence. The inconsistency is probably more apparent than real. Due to the severe limitations of the Warburg respirometer method, which was used in the photochemical studies,[24] rela-

TABLE III. Effect of the wavelength of the exciting light upon the quantum yield of fluorescence.

Pigment	Solvent	Exciting wavelength, A	φ^0
Chlorophyll *a*	MeOH	4360	0.24±0.02
Chlorophyll *a*	MeOH	~6275	0.24±0.03
Chlorophyll *a*	MeOH	~6440	0.25±0.04
Chlorophyll *a*	MeOH	~6620	0.26±0.03
Chlorophyll *a*	MeOH	~6980	0.11±0.04
Chlorophyll *a*	Et_2O	4358	0.24±0.02
Chlorophyll *a*	Et_2O	~6275	0.21±0.03
Chlorophyll *a*	Et_2O	~6440	0.24±0.03
Chlorophyll *a*	Et_2O	~6620	0.24±0.03
Chlorophyll *b*	Et_2O	4358	0.11±0.01
Chlorophyll *b*	Et_2O	~6440	0.11±0.02

[23] D. G. Harris and F. P. Zscheile, Botan. Gaz. **104**, 515 (1943).
[24] H. Gaffron, Ber. deut. chem. Ges. **60B**, 755 (1927).

tively high concentrations of chlorophyll were used. In most of the measurements the concentration was greater than $10^{-3}m$. At such high concentrations the autoabsorption of chlorophyll fluorescence is very efficient and may well have reduced the escape (as fluorescent light) of energy of excitation by a factor of four or more. When this effect is taken into consideration the fluorescence and photochemical yields appear to be consistent within their limits of accuracy.

ACKNOWLEDGMENT

The authors wish to acknowledge gratefully the following assistance which they received during the course of the work. Dr. John Wertz of this department was of material aid in the elimination of several experimental difficulties, Professor E. J. Bowen of Oxford University placed samples of rubrene and magdala red at our disposal, and Dr. S. Schwartz of the Medical Department of the University of Minnesota furnished the purified sample of mesoporphyrin dimethyl ester.

THE JOURNAL OF CHEMICAL PHYSICS VOLUME 20, NUMBER 8 AUGUST, 1952

On the Calculation of Diffusion Coefficients from Sorption Data

JENN LIN HWANG
Physics Department, Taiwan University, Taipeh, Formosa, China
(Received January 8, 1952)

The general equation of diffusion in which the diffusion coefficient $D(c)$ is given by $D_0(1+\alpha c+\beta c^2+\cdots)$, where $\alpha, \beta\cdots$ are small, can be solved by the method of successive approximation: The solution has the form

$$c(\xi)=c_0(1-\Phi(\xi))+c_0^2\alpha\psi(\xi)+c_0^3[\alpha^2\chi_1(\xi)+\beta\chi_2(\xi)]+\cdots,$$

where $\Phi(\xi)$ is the error function and $\psi(\xi)$, $\chi_1(\xi)\cdots$ may be computed by numerical integrations. On the other hand, one knows from the sorption experiments the quantities defined by $Kc_0=2D_0^{\frac{1}{2}}\int_0^\infty c(\xi)d\xi$ as a function of c_0. Thus, by the above solution one may obtain a set of linear equations, from which the constants $D_0, \alpha, \beta\cdots$ can be found with a reasonable amount of labor.

For practical purposes it would be necessary to tabulate the functions $\psi(\xi)$, $\chi_1(\xi)$, $\cdots$, because they are needed for all the problems of this kind.

INTRODUCTION

IN a process of sorption the weight of vapor taken up by some material can be measured with high accuracy in a simple way.[1] For this reason, several investigators[1–3] have attempted to determine the dependence of the diffusion coefficient on concentration, by making use of these sorption data. Of these methods, the step function method devised by Prager[1] seems most tractable, but, unfortunately, it becomes inapplicable in the region of higher concentrations.

This paper presents an alternative method based upon an approximate formal solution of the diffusion equation.

FORMAL SOLUTION OF THE DIFFUSION EQUATION

If a substance is placed in an atmosphere of the vapor at a pressure p so as to make the diffusion take place only from one surface, then the diffusion equation takes the form

$$\frac{\partial c}{\partial t}=\frac{\partial}{\partial x}\left[D(c)\frac{\partial c}{\partial x}\right]. \tag{1}$$

Before the concentration on the opposite side of the surface attains an appreciable value, we may regard the substance as a semi-infinite solid, so that the boundary and initial conditions are

$$c(0, t)=c_0, \quad c(\infty, t)=0$$
$$c(x, 0)=0. \tag{1a}$$

Here, $c(x, t)$ is the concentration of the vapor at time t and a distance x into the substance normal to the surface, $D(c)$ is the diffusion coefficient, and c_0 is the equilibrium concentration corresponding to the pressure p of the vapor.

Assuming $D(c)$ in the form

$$D(c)=D_0(1+\alpha c+\beta c^2+\gamma c^3+\cdots), \tag{2}$$

where $\alpha, \beta, \gamma\cdots$ are small quantities, Eq. (1) with the boundary conditions (1a) may be solved by the method of successive approximations.[4,5,6] If we introduce the new variable $\xi=x/2(D_0t)^{\frac{1}{2}}$, Eq. (1) may be written as an

[1] S. Prager, J. Chem. Phys. **19**, 537 (1951).
[2] J. Crank and G. S. Park, Trans. Faraday Soc. **45**, 240 (1949).
[3] J. Crank and M. E. Henry, Trans. Faraday Soc. **45**, 636 (1949); **45**, 1119 (1949).

[4] H. Bateman, *Partial Differential Equations of Mathematical Physics* (Cambridge University Press, London, England, 1932), p. 497.
[5] K. Hidaka, *Methods of Numerical Integrations* (Iwanami Book Store, Tokyo, Japan, 1943), Vol. 2, p. 43.
[6] K. Hidaka, Geophys. Mag. Central Meteorol. Observ., Japan **5**, 361 (1932). He solved the equation $c_0\rho_0(1+\beta\theta)\partial\theta/\partial t=\partial[K_0(1+\alpha\theta)\partial\theta/\partial x]\partial x$ appearing in the problem of the heat conduction in a semi-infinite solid.

ordinary differential equation

$$\frac{d}{d\xi}\left\{(1+\alpha c+\beta c^2+\gamma c^3+\cdots)\frac{dc}{d\xi}\right\}+2\xi\frac{dc}{d\xi}=0 \qquad (3)$$

with the conditions

$$c(0)=c_0, \quad c(\infty)=0. \qquad (3a)$$

To solve Eq. (3), we assume that $c(\xi)$ can be expanded in ascending powers of c_0, i.e.,

$$c(\xi)=c_0\theta_1(\xi)+c_0^2\theta_2(\xi)+c_0^3\theta_3(\xi)+\cdots,* \qquad (4)$$

where $\theta_1(\xi)$, $\theta_2(\xi)\cdots$ are all functions of ξ, and satisfy the following conditions:

$$\left.\begin{aligned}&\theta_1(0)=1 \qquad \theta_1(\infty)=0\\&\theta_2(0)=\theta_2(\infty)=0\\&\theta_3(0)=\theta_3(\infty)=0\\&\cdots\cdots\cdots\cdots\cdots\cdots\end{aligned}\right\}. \qquad (4a)$$

Substituting (4) in (3) and equating the coefficients of $c_0, c_0^2, c_0^3\cdots$ to zero, we have

$$\frac{d^2\theta_1}{d\xi^2}+2\xi\frac{d\theta_1}{d\xi}=0 \qquad (5)$$

$$\frac{d^2\theta_2}{d\xi^2}+2\xi\frac{d\theta_2}{d\xi}=-\frac{\alpha}{2}\frac{d^2\theta_1^2}{d\xi^2} \qquad (5a)$$

$$\frac{d^2\theta_3}{d\xi^2}+2\xi\frac{d\theta_3}{d\xi}=-\alpha\frac{d^2\theta_1\theta_2}{d\xi^2}-\frac{\beta}{3}\frac{d^2\theta_1^3}{d\xi^2} \qquad (5b)$$

$$\frac{d^2\theta_4}{d\xi^2}+2\xi\frac{d\theta_4}{d\xi}=-\alpha\frac{d^2}{d\xi^2}(\theta_1\theta_3+\tfrac{1}{2}\theta_2^2)-\beta\frac{d^2\theta_1^2\theta_2}{d\xi^2}-\frac{\gamma}{4}\frac{d^2\theta_1^4}{d\xi^2} \qquad (5c)$$

$$\cdots\cdots\cdots\cdots\cdots\cdots\cdots\cdots\cdots\cdots$$

with the boundary conditions (4a).

The integral of Eq. (5) is evidently

$$\theta_1=1-\Phi(\xi), \qquad (6)$$

where

$$\Phi(\xi)=(2/\pi^{\frac{1}{2}})\int_0^\xi \exp(-\lambda^2)d\lambda. \qquad (7)$$

Hence, the first approximation to $c(\xi)$ is

$$c(\xi)=c_0(1-\Phi(\xi)),$$

which exactly coincides with the solution of the case of no concentration dependence $D(c)=D_0$.

When one substitutes (6) into (5a),

$$\frac{d^2\theta_2}{d\xi^2}+2\xi\frac{d\theta_2}{d\xi}=-4\alpha\left[\frac{\xi}{\pi^{\frac{1}{2}}}(1-\Phi(\xi))\times\exp(-\xi^2)+\frac{\exp(-2\xi^2)}{\pi}\right]. \qquad (8)$$

To solve this equation put

$$d\theta_2/d\xi=u(\xi)\cdot v(\xi); \qquad (9)$$

then we have

$$v\frac{du}{d\xi}+u\left(\frac{dv}{d\xi}+2\xi v\right)=-4\alpha\left[\frac{\xi}{\pi^{\frac{1}{2}}}(1-\Phi(\xi))\exp(-\xi^2)+\frac{\exp(-2\xi^2)}{\pi}\right]. \qquad (10)$$

Determining v by $dv/d\xi+2\xi v=0$, we get $v=\exp(-\xi^2)$. Substituting in (10), we have

$$\frac{du}{d\xi}=-4\alpha\left[\frac{\xi}{\pi^{\frac{1}{2}}}(1-\Phi(\xi))+\frac{\exp(-\xi^2)}{\pi}\right],$$

and

$$u=-\frac{2\alpha\xi^2}{\pi^{\frac{1}{2}}}+\frac{4\alpha}{\pi^{\frac{1}{2}}}\int_0^\xi \lambda\Phi(\lambda)d\lambda-\frac{2\alpha}{\pi^{\frac{1}{2}}}\cdot\Phi(\xi)+c',$$

where c' is an integration constant. Then from (9)

$$\frac{d\theta_2}{d\xi}=-\frac{2\alpha\xi^2}{\pi^{\frac{1}{2}}}\exp(-\xi^2)+\frac{4\alpha}{\pi^{\frac{1}{2}}}\exp(-\xi^2)\times\int_0^\xi \lambda\Phi(\lambda)d\lambda-\frac{2\alpha}{\pi^{\frac{1}{2}}}\exp(-\xi^2)\cdot\Phi(\xi)+c'\exp(-\xi^2).$$

The general integral of θ_2 is, therefore,

$$\theta_2=-\frac{2\alpha}{\pi^{\frac{1}{2}}}\int_0^\xi \lambda^2\exp(-\lambda^2)d\lambda+\frac{4\alpha}{\pi^{\frac{1}{2}}}\int_0^\xi \exp(-\lambda^2)d\lambda\times\int_0^\lambda s\Phi(s)ds-\frac{2\alpha}{\pi^{\frac{1}{2}}}\int_0^\xi \Phi(\lambda)\exp(-\lambda^2)d\lambda+c_1\Phi(\xi)+c_2,$$

where c_1, c_2 are constants of integration.

Now with the relations

$$\int_0^\xi \lambda^2\exp(-\lambda^2)d\lambda=-\frac{\xi}{2}\exp(-\xi^2)+\frac{\pi^{\frac{1}{2}}}{4}\Phi(\xi)$$

$$\int_0^\xi \lambda\Phi(\lambda)d\lambda=\frac{\xi^2}{2}\Phi(\xi)+\frac{\xi}{2\pi^{\frac{1}{2}}}\exp(-\xi^2)-\tfrac{1}{4}\Phi(\xi)$$

$$\int^\xi \exp(-\lambda^2)d\lambda\int_0^\lambda s\Phi(s)ds=-\frac{\xi^2}{4}\exp(-\xi^2)\Phi(\xi)-\frac{\exp(-2\xi^2)}{4\pi^{\frac{1}{2}}}+\frac{1}{4\pi^{\frac{1}{2}}}$$

$$\int_0^\xi \exp(-\lambda^2)\Phi(\lambda)d\lambda=\frac{\pi^{\frac{1}{2}}}{4}(\Phi(\xi))^2,$$

the expression for θ_2 which satisfies the condition (4a)

* Some descriptions concerning the proof of the convergence of this series are seen in reference 4.

becomes

$$\theta_2=\alpha\left\{\left[\frac{\xi}{\pi^{\frac{1}{2}}}\exp(-\xi^2)+\frac{1}{\pi}+\tfrac{1}{2}\Phi(\xi)\right]\times[1-\Phi(\xi)]-\frac{\exp(-2\xi^2)}{\pi}\right\}$$

$$=\alpha\psi(\xi). \tag{11}$$

Substituting (6) and (11) in (5b) and repeating the same procedure, one would obtain the higher approximations in the form†

$$\theta_3=\alpha^2\chi_1(\xi)+\beta\chi_2(\xi),$$
$$\theta_4=\alpha^3\Omega_1(\xi)+\alpha\beta\Omega_2(\xi)+\gamma\Omega_3(\xi)$$
$$\cdots\cdots\cdots\cdots\cdots\cdots;$$

therefore, the approximate formal solution of (1) with (1a) is given by

$$c(\xi)=c_0(1-\Phi(\xi))+c_0^2\alpha\psi(\xi)+c_0^3[\alpha^2\chi_1(\xi)+\beta\chi_2(\xi)]+c_0^4[\alpha^3\Omega_1(\xi)+\alpha\beta\Omega_2(\xi)+\gamma\Omega_3(\xi)]+\cdots, \tag{12}$$

where the analytical expression of function, $\chi_1(\xi)$, $\chi_2(\xi)$, $\Omega_1(\xi)\cdots$, is in general very complicated. We therefore evaluate all θ_n's ($n=2, 3\cdots$), by numerical integration and tabulate the functions $\psi(\xi), \chi_1(\xi), \chi_2(\xi)\cdots$ against ξ. Since the Eqs. (5a), (5b), $\cdots$ all have the same form,

$$\frac{d^2\theta_n}{d\xi^2}+2\xi\frac{d\theta_n}{d\xi}=R_n(\xi)\quad(n=2, 3, 4\cdots)$$
$$\theta_n(0)=\theta_n(\infty)=0, \tag{13}$$

their solution may be obtained by the same approach as that used from (9) to (11), and it takes the form

$$\theta_n(\xi)=\int_0^\xi \exp(-\lambda^2)d\lambda\int_0^\lambda R_n(s)\exp(s^2)ds-\Phi(\xi)\times\int_0^\infty \exp(-\lambda^2)d\lambda\int_0^\lambda R_n(s)\exp(s^2)ds. \tag{14}$$

† Using Eq. (14),

$$\theta_3=\int_0^\xi \exp(-\lambda^2)d\lambda\int_0^\lambda\left\{-\alpha[\alpha\psi(\eta)(1-\Phi(\eta))]''-\frac{\beta}{3}(1-\Phi(\eta))''\right\}\exp(\eta^2)d\eta-\Phi(\xi)\int_0^\infty \exp(-\lambda^2)d\lambda\times\int_0^\lambda\left\{-\alpha[\alpha\psi(\eta)(1-\Phi(\eta))]''-\frac{\beta}{3}(1-\Phi(\eta))''\right\}\exp(\eta^2)d\eta$$
$$=-\alpha^2\left\{\int_0^\xi \exp(-\lambda^2)d\lambda\int_0^\lambda[\psi(\eta)(1-\Phi(\eta))]''\exp(\eta^2)d\eta-\Phi(\xi)\times\int_0^\infty \exp(-\lambda^2)d\lambda\int^\lambda[\psi(\eta)(1-\Phi(\eta))]''\exp(\eta^2)d\eta\right\}$$
$$-\frac{\beta}{3}\left\{\int_0^\xi \exp(-\lambda^2)d\lambda\int_0^\lambda(1-\Phi(\eta))''\exp(\eta^2)d\eta-\Phi(\xi)\times\int_0^\infty \exp(-\lambda^2)d\lambda\int_0^\lambda(1-\Phi(\eta))''\exp(\eta^2)d\eta\right\}$$
$$=\alpha^2\chi_1(\xi)+\beta\chi_2(\xi).$$

Some remarks concerning the mechanical quadrature of (14) will be found at the end of this paper.

Here, it must be remarked that each of the functions $\psi(\xi)$, $\chi_1(\xi)$, $\chi_2(\xi)\cdots$ in the Eq. (12) is independent of the coefficients D_0, α, $\beta\cdots$; this is the very thing that makes it possible to determine the diffusion coefficient $D(c)$.

DETERMINATION OF $D(c)$ FROM SORPTION DATA

If S is the area of the surface normal to the direction of diffusion, the weight Q_{c_0} of the vapor taken up by the substance becomes, with our assumptions,

$$Q_{c_0}=S\int_0^l c(x, t)dx=S\int_0^\infty c(x, t)dx,$$

a function of t for a given value of equilibrium concentration c_0. Since $\xi=x/2(D_0t)^{\frac{1}{2}}$,

$$Q_{c_0}(t)=2D_0^{\frac{1}{2}}t^{\frac{1}{2}}\cdot S\int_0^\infty c(\xi)d\xi=St^{\frac{1}{2}}\cdot K_{c_0},$$

where

$$K_{c_0}=2D_0^{\frac{1}{2}}\int_0^\infty c(\xi)d\xi \tag{15}$$

may be found from the initial slope of the plotting of Q_{c_0} against $t^{\frac{1}{2}}$.

Substituting (12) in (15) yields

$$K_{c_0}=2D_0^{\frac{1}{2}}\int_0^\infty c(\xi)d\xi$$
$$=2D_0^{\frac{1}{2}}\left\{c_0\int_0^\infty(1-\Phi(\xi))d\xi+c_0^2\alpha\int_0^\infty\psi(\xi)d\xi+c_0^3\left[\alpha^2\int_0^\infty\chi_1(\xi)d\xi+\beta\int_0^\infty\chi_2(\xi)d\xi\right]+\cdots\right\}$$
$$=2D_0^{\frac{1}{2}}\{c_0A+c_0^2B\alpha+c_0^3[C_1\alpha^2+C_2\beta]+c_0^4[D_1\alpha^3+D_2\alpha\beta+D_3\gamma]+\cdots\}, \tag{16}$$

where

$$A=\int_0^\infty(1-\Phi(\xi))d\xi,\quad B=\int_0^\infty\psi(\xi)d\xi,\quad C_1=\int_0^\infty\chi_1(\xi)d\xi,\cdots \tag{17}$$

may be computed by numerical integration.

Now, our problem is to find the coefficients D_0, α, $\beta\cdots$ from this information. For the various values of c_0 and K_{c_0}, say $c_0(n)$ and $K_{c_0(n)}$ ($n=1, 2, 3\cdots$), we can establish a simultaneous linear system

$$K_{c_0(n)}=a_nx_1+b_nx_2+c_nx_3+d_nx_4+\cdots,\quad(n=1, 2, 3\cdots) \tag{16a}$$

where $x_1=D_0^{\frac{1}{2}}$, $x_2=D_0^{\frac{1}{2}}\alpha$, $x_3=D_0^{\frac{1}{2}}\alpha^2$, $x_4=D_0^{\frac{1}{2}}\beta\cdots$ are the unknowns, and $a_n=2Ac_0(n)$, $b_n=2Bc_0^2(n)$, $c_n=2C_1c_0^3(n)$, $d_n=2C_2c_0^3(n)\cdots$ are the coefficients. The number of unknowns of this system is apparently large, but those which we really want are only the first few ones, D_0, α, $\beta\cdots$. Thus, the solution is not so laborious.

CONCLUDING REMARKS

In the process of numerical evaluation of the integrals (14),

$$\theta_n(\xi)=\int_0^{\xi}\exp(-\lambda^2)d\lambda\int_0^{\lambda}R_n(s)\exp(s^2)ds-\Phi(\xi)\times\int_0^{\infty}\exp(-\lambda^2)d\lambda\int_0^{\lambda}R_n(s)\exp(s^2)ds,$$

we should avoid the numerical differentiation for the computation of $R_n(\xi)$ because its accuracy is far less than that of integration. We would rather choose the following scheme. Suppose we want to calculate $\theta_2(\xi)$, and the values of

$$R_2(\xi)=-(\alpha/2)d^2\theta_1^2/d\xi^2$$

are desired; then, since

$$\frac{d^2\theta_i^n}{d\xi^2}=n\theta_i^{n-2}\left[(n-1)\left(\frac{d\theta_i}{d\xi}\right)^2+\theta_i\frac{d^2\theta_i}{d\xi^2}\right], \tag{18}$$

and

$$\frac{d^2\theta_1^n}{d\xi^2}=4n[1-\Phi(\xi)]^{n-2}\cdot\left[\frac{n-1}{\pi}\exp(-2\xi^2)+\frac{\xi}{\pi^{\frac{1}{2}}}(1-\Phi(\xi))\exp(-\xi^2)\right], \tag{19}$$

there is no question in computing $R_2(\xi)$. But, if we are going to calculate $\theta_3(\xi)$ and need the values

$$R_3(\xi)=-\alpha\frac{d^2\theta_1\theta_2}{d\xi^2}-\frac{\beta}{3}\frac{d^2\theta_1^2}{d\xi_1^2}$$

a question would arise in finding $d^2\theta_1\theta_2/d\xi^2$, since $\theta_2(\xi)$ is given in the form of a table. However, this question can be easily settled. Since

$$\frac{d^2\theta_i^n\theta_j}{d\xi^2}=n(n-1)\theta_i^{n-2}\theta_j\left(\frac{d\theta_i}{d\xi}\right)^2+2n\theta_i^{n-1}\frac{d\theta_i}{d\xi}\frac{d\theta_j}{d\xi}+n\theta_i^{n-1}\theta_j\frac{d^2\theta_i}{d\xi^2}+\theta_i^n\frac{d^2\theta_j}{d\xi^2} \tag{20}$$

$$\frac{d^2\theta_1\theta_2}{d\xi^2}=2\frac{d\theta_1}{d\xi}\frac{d\theta_2}{d\xi}+\theta_2\frac{d^2\theta_1}{d\xi^2}+\theta_1\frac{d^2\theta_2}{d\xi^2}$$

and

$$\frac{d\theta_2}{d\xi}=\exp(-\xi^2)\int_0^{\xi}R_2(\lambda)\exp(\lambda^2)d\lambda+\frac{2\exp(-\xi^2)}{\pi^{\frac{1}{2}}}\times\int_0^{\infty}\exp(-\lambda^2)d\lambda\int_0^{\lambda}R_2(s)\exp(s^2)ds$$

$$\frac{d^2\theta_2}{d\xi^2}=-2\xi\exp(-\xi^2)\int_0^{\xi}R_2(\lambda)\exp(\lambda^2)d\lambda+R_2(\xi)-\frac{4\xi\exp(-\xi^2)}{\pi^{\frac{1}{2}}}\int_0^{\infty}\exp(-\lambda^2)d\lambda\int_0^{\lambda}R_2(s)\exp(s^2)ds,$$

$d^2\theta_1\theta_2/d\xi^2$ could be computed from the course of calculating $\theta_2(\xi)$. In a similar way, the other $R_n(\xi)$'s may also be computed to any accuracy, for the derivatives appearing in $R_4(\xi)$, $R_5(\xi)\cdots$ always take the forms of (18), (19) and (20).

Needless to say, if the coefficients D_0, α, $\beta\cdots$ were determined, the approximate solution of $c(x/t^{\frac{1}{2}})$ could be immediately written down, and the results might be compared with those of other methods.[1,2,3]

The values of the functions $1-\Phi(\xi)$, $\psi(\xi)$, $\chi(\xi)$, $\Omega(\xi)\cdots$ together with their integrals (17) are obviously universal for all problems of this kind. In other words, if once they are calculated, we can use them in any particular problem.

As we lack adequate calculating equipment, we cannot carry out the necessary numerical computations that would give our method a practical value.

Letters to the Editor

THIS section will accept reports of new work, provided these are terse and contain few figures, and especially few half-tone cuts. The Editorial Board will not hold itself responsible for opinions expressed by the correspondents. Contributions to this section should not exceed 600 words in length and must reach the office of the Editor not later than the 15th of the second month preceding that of the issue in which the Letter is to appear. No proof will be sent to the authors. A publication charge of $10.00 per Letter is made which, when honored, will entitle the Institution to 100 free reprints.

The Infrared Spectrum of Methyltrichlorosilane

LOUIS BURNELLE AND JULES DUCHESNE
Department of Chemical Physics, University of Liège, Liège, Belgium
(Received June 16, 1952)

IN recent papers by Anspach, Duchesne, Monfils, and Roosens,[1] various silane derivatives have been studied by either Raman or infrared spectroscopy. In this note further results which have been obtained in the study of the infrared spectrum of methyltrichlorosilane will be given. The spectra were recorded on a Perkin-Elmer spectrometer (Model 12 C) using NaCl and KBr prisms, and on a Beckman spectrometer equipped with LiF optics. Measurements were made on the substance in both gaseous and dissolved states. An absorbing path of 9 cm with pressures varying from 3 to 150 mm Hg was used for the vapor. For the solutions in CS_2 and CCl_4 cell thicknesses of 0.1 and 1 mm were used, and the concentrations were 10 and 50 percent, respectively.

The molecule CH_3SiCl_3 belongs to the point group C_{3v} whether the two groups have staggered or eclipsed structures. According to group theory, it is easily shown that these structures give rise to five totally symmetric vibrations A_1, six doubly degenerate vibrations E, and the twisting vibration A_2. Except for the last one, all are active in the infrared as well as in the Raman spectrum. The assignment to the normal modes is given in Table I together with a comparison between the Raman frequencies of Shimanouchi, Tsuchiya, and Mikawa[2] and the present infrared measurements.

The infrared frequency values in Table I refer to the gaseous state except for 2915 cm^{-1} which corresponds to a very weak absorption band which appeared only in the solutions. There is satisfactory agreement between the Raman and infrared results. Shimanouchi, Tsuchiya, and Mikawa also observed the frequencies 2912, 1265, 2983, and 1405 cm^{-1} in their Raman experiments. Because these authors did not make any assignment, these frequencies have been omitted from Table I. They can be identified with ν_1, ν_2, ν_7, and ν_8 in the infrared spectrum. A shift towards higher frequencies of up to about 10 cm^{-1} occurs on going from the liquid to the gas, except in the case of ν_7 which is shifted in the opposite direction. The ν_9 vibration has been identified with a band at 807 cm^{-1} in the infrared spectrum. No corresponding line is present in the Raman effect. However, Goubeau, Siebert, and Winterwerb[3] have observed a line at 805 cm^{-1} on their Raman plates. They did not make any assignment of this line as they suggest that it is of questionable origin and perhaps should be ascribed to an impurity. The fact that this band is very intense in the infrared spectrum and that no decrease in its intensity was observed by repeated fractionations of the compound seems, however, to be greatly in favor of its belonging to CH_3SiCl_3.

TABLE I. Assignment of fundamentals of CH_3SiCl_3.

Normal modes	Notation	ν in cm^{-1} infrared data (present work)	ν in cm^{-1} Raman data (liq.) Shimanouchi, Tsuchiya, Mikawa
Symmetric CH stretching	$\nu_1(a_1)$	2915	···
Symmetric CH_3 deformation	$\nu_2(a_1)$	1271	···
Symmetric Si−C stretching	$\nu_3(a_1)$	764	761
Symmetric Si−Cl stretching	$\nu_4(a_1)$	457	450
Symmetric $SiCl_3$ deformation	$\nu_5(a_1)$	···	229
Twisting	$\nu_6(a_2)$	···	···
Degenerate CH stretching	$\nu_7(e)$	2977	···
Degenerate CH_3 deformation	$\nu_8(e)$	1416	···
Degenerate CH_3 rocking	$\nu_9(e)$	807	···
Degenerate Si−Cl stretching	$\nu_{10}(e)$	578	576
Degenerate $SiCl_3$ deformation	$\nu_{11}(e)$	···	164
Degenerate $SiCl_3$ rocking	$\nu_{12}(e)$	···	229

Besides the fundamentals discussed, the following overtone and combination bands have been recorded: 967, 1033, 1163, 1531, 1718, 2016, 2055, 2662, 2822, 3140. These bands, except 967 and 1163 cm^{-1}, correspond to the dissolved state and all of them could be interpreted according to Table I as $\nu_9+\nu_{11}$, $\nu_5+\nu_9$, $2\nu_{10}$, $2\nu_5$, $\nu_2+\nu_4$, $\nu_2+\nu_3$, $\nu_2+\nu_9$, $\nu_3+\nu_3$, $2\nu_8$, $\nu_7+\nu_{11}$, respectively.

We are greatly indebted to Professor E. Rochow, who generously gave us a sample of methyltrichlorosilane. We also wish to express our gratitude to Professor L. D'Or for kindly putting at our disposal the spectrometers and to Mrs. Jachner and Dr. G. Michel for help during the laboratory work.

[1] C. Anspach and J. Duchesne, J. Chem. Phys. **16**, 1006 (1948); **17**, 110 (1949); J. Duchesne and A. Monfils, J. Chem. Phys. **16**, 1009 (1948); **17**, 110 (1949); A. Monfils, J. Chem. Phys. **19**, 138 (1951); A. Roosens, thesis, University of Liège, Liège, Belgium (1951).
[2] Shimanouchi, Tsuchiya, and Mikawa, J. Chem. Phys. **18**, 1306 (1950).
[3] Goubeau, Siebert, and Winterwerb, Z. anorg. Chem. **259**, 240 (1949).

The Effect of the Isomeric Transition in Br^{80} on Its Reactivity with the Tetrachlorides of Carbon, Silicon, Germanium, and Tin

C. C. COFFIN AND W. D. JAMIESON
Department of Chemistry, Dalhousie University, Halifax, Nova Scotia
(Received June 16, 1952)

THE effect of the isomeric transition in Br^{80} on its reactivity with the tetrachlorides of carbon, silicon, germanium, and tin in the liquid state at room temperature has been studied in this laboratory. The main object of the work was to see if the ratios of chemical to nuclear events (reaction efficiencies) could be correlated with any of those properties of the tetrachlorides which might be expected to have a bearing on their reactivities with "hot" bromine atoms. No obvious parallel between the transient equilibrium amounts of 20-min Br^{80} activity acquired by the different tetrachlorides and any one of their properties likely to be chemically significant has been noted. This work, which is planned to include the halides of other elements, has had to be temporarily suspended, and it is considered advisable to present the results in summary at this time.

As these tetrachlorides (except CCl_4) are readily hydrolyzed, all operations in which they were involved were carried out in vacuum or in an atmosphere of dry nitrogen. Radiobromine was prepared by overnight irradiation of 8 kg of ethylene dibromide with a 500-mg Ra-Be neutron source. The aqueous extract (with NaBr carrier) was rapidly evaporated to a volume of about 1 ml from which free bromine was obtained by oxidation with $KBrO_3$ and H_3PO_4. This "tagged" bromine was swept over phosphorus pentoxide with a stream of dry nitrogen, condensed in dry ice and distilled to a liquid air trap, where it was degassed by repeated melting and freezing in vacuum. From here it was evaporated into a measuring volume and condensed into a bulb containing the already distilled and degassed tetrachloride.

After the sealed-off reaction bulb (containing about 1 millimole of bromine and from 2 to 20 ml of tetrachloride) had remained in the dark at room temperature for about two hours, it was opened and its contents divided into two parts. One of these, the reaction mixture, was counted in a jacketed G-M tube at intervals extending over a period of more than twenty-four hours. The other was freed from elemental bromine by distilling from metallic

TABLE I. Some properties and reactivities of CCl_4, $SiCl_4$, and $GeCl_4$.

1 Compound	2 Reaction efficiency	3 Number of experiments	4 Bond strength kcal/g atom	5 Bond character % ionic	6 Liquid density at 20°C
CCl_4	0.32 (±0.04)	12	66	12	1.60
$SiCl_4$	0.44 (±0.03)	7	85	41	1.48
$GeCl_4$	0.19 (±0.01)	5	104	52	1.88

mercury in a stream of nitrogen at atmospheric pressure or by rapid passage in vacuum through a tube packed with freshly amalgamated copper wool. This bromine-free portion which (except for $SnCl_4$) never showed other than the 20-min activity was counted at intervals over a period of about two hours, and, as in the case of the reaction mixture, its activity at the time of bromine removal was obtained by extrapolation. Counts were made in the same G-M tube and where necessary were corrected for the 36-hr Br^{82} activity.

Column 2 of Table I gives the reaction efficiencies for the first three compounds of the series. Stannic chloride is not included because the effect, if any, of the isomeric transition is entirely masked by an exchange reaction which is complete in less than two hours at room temperature. This is probably due to the formation of an ionizable complex made possible by the large volume and coordination number of the central atom.

Of the three compounds listed such internal molecular properties, e.g., bond strength (column 4) and ionic character (column 5), as might be expected to affect the replaceability of Cl by Br atoms do not show any evidence of falling in line with the values in column 2. A comparison of the latter with the appropriate activation energies, if such data existed, would probably be of greater significance.

Those properties of a medium which determine whether or not a cooling atom and its associated molecular fragments will remain within reaction distance of one another should be of importance in this connection. There is indeed experimental evidence on this point. In recent papers Willard and co-workers[1,2] have shown that the reaction of certain high energy radioactive halogen atoms with carbon tetrahalide (e.g., CCl_3Br) solvents increases as the temperature is lowered. The fact that this increase roughly parallels that of the solvent density suggests that it may be due to more effective "caging" of potential reactants at the greater densities. As is evident from Table I, the reaction efficiencies in the compounds studied here also vary regularly with their densities (column 6), but in the opposite direction to that observed by Willard.

Financial aid from the National Research Council of Canada and a scholarship from the Government of Nova Scotia is gratefully acknowledged.

[1] Goldhaber, Chiang, and Willard, J. Am. Chem. Soc. **73**, 2271 (1951).
[2] S. Goldhaber and J. E. Willard, J. Am. Chem. Soc. **74**, 318 (1952).

Isotope Effects in the Exchange Reaction between Uncomplexed Carbonate-Bicarbonate Ions and Carbonate-*Bis*-Ethylenediamine-Cobalt (III) Ion

PETER E. YANKWICH AND JOHN E. MCNAMARA
Department of Chemistry, University of Illinois, Urbana, Illinois
(Received May 29, 1952)

STRANKS and Harris[1] have determined the equilibrium constant under a variety of conditions for the isotopic exchange reaction

$$Co(NH_3)_4C^nO_3^+ + HC^{14}O_3^- = HC^nO_3^- + Co(NH_3)_4C^{14}O_3^+, \quad (1)$$

where n represents the normal admixture of stable carbon nuclides; K was found to be 0.875 ± 0.002 at 0°C and 0.900 ± 0.004 at 30°C.

In the course of an investigation[2] into the kinetics and mechanism of the similar exchange reaction

$$Co(en)_2C^nO_3^+ + HC^xO_3^- = HC^nO_3^- + Co(en)_2C^xO_3^+, \quad (2)$$

where x is 13 or 14, we have had occasion to determine both the equilibrium constants and the relative rates of exchange for C^{13} and C^{14} tracer nuclides. Results were analyzed from twenty-four runs at 25.0°C which involved variations in concentrations over the following ranges: complex, 0.01–0.05 molar; free carbonate + bicarbonate, 0.01–0.05 molar; hydrogen ion, 2×10^{-11}–9×10^{-10} molar. Carbon 13 concentrations were determined with a Consolidated-Nier Isotope-Ratio Mass Spectrometer; carbon 14 specific activities were determined with an Applied Physics Corporation Vibrating-Reed Electrometer. At least ten exchange half-times elapsed before the samples for equilibrium constant determination were taken.[3]

The equilibrium constants found for reaction (2) are C^{13} exchange—$0.99_1\pm0.01_4$; C^{14} exchange—$0.99_0\pm0.01_9$. The average ratio of rates of exchange was $1.03_3\pm0.02_8$, the lighter isotope exchanging the more rapidly;[4] since line drawing or fitting operations were involved in the determination of this quantity, it is subject to a rather larger error than the equilibrium constant values.

If one ascribes the difference between equilibrium constants for reactions (1) and (2) entirely to differences in lability of the exchanging ligand in the complex ions, one would expect more rapid exchange in the *bis*-ethylenediamine system. When data for similar runs in the tetramine system are examined, it is found that the exchange of C^{14} in the wholly bidentate system is faster, sometimes by a factor as large as 2. It is interesting to note that information concerning the exchange of *two* tracer nuclides enables one to predict with some accuracy the rate of the unobservable exchange reaction in which $x=n$, the normal isotope mixture.

[1] D. R. Stranks and G. M. Harris, J. Chem. Phys. **19**, 257 (1951); Symposium on Electron Transfer and Isotopic Reactions, University of Notre Dame, June 11–13, 1952.
[2] Supported by the AEC.
[3] The kinetics of reaction (2) bear little resemblance to those reported for reaction (1) by Harris and Stranks, Trans. Faraday Soc. **48**, 137 (1952). A complete report on the kinetics investigations is in preparation.
[4] The appended errors are standard deviations.

The Dielectric Constant of Some Chlorine Derivatives of Ethane in the Liquid and the Solid States

MASASI YASUMI AND MICHIO SHIRAI
Institute of Science and Technology, University of Tokyo, Tokyo, Japan
(Received June 5, 1952)

DIELECTIC constant ϵ of 1,2-dichloroethane, pentachloroethane, 1,1,2,2-tetrachloroethane and 1,1,1,2-tetrachloroethane were measured in the liquid and the solid states. Measurements were made at the frequency of 2 megacycles with resonance method and at the frequency of 2 kilocycles with alter-

TABLE I.

1,2-dichloroethane										
temp. (°C)	−50	−40	−38	−36	−35	−34	−32	−20	0	20
ϵ	2.74	3.04	3.29	3.61	3.75	14.99	14.80	13.72	11.96	10.60
pentachloroethane										
t	−50	−40	−30	−28	−10	10				
ϵ	2.62	2.62	2.63	4.60	4.20	3.97				
1,1,2,2-tetrachloroethane										
t	−60	−55	−52	−48	−46	−45	−44.5	−44	−42	−30
ϵ	2.77	2.79	2.82	2.95	3.07	3.15	3.24	3.50	14.5	12.9
1,1,1,2-tetrachloroethane										
t	−78	−70	−67	−66	−60	−50	−40			
ϵ	2.65	2.63	2.67	9.22	9.02	8.55	7.93			

nating current bridge. Both of the values were fairly consistent, and we can conclude that the dispersion effect does not exist.

The results are shown in Table I.

As shown in the tables the values for these four substances are considerably great in the liquid state, but very small in the solid state.

By crystallization, the value of ϵ for pentachloroethane suddenly falls to a very small value of 2.7 which remains constant down to very low temperatures. Similar behavior is observed for 1,1,1,2-tetrachloroethane.

On the other hand, the value for 1,2-dichloroethane falls from 14.8 to 3.8 by crystallization and decreases continuously in the range of 10°C below the melting point until it attains a constant value of 2.75. A similar result is obtained for 1,1,2,2-tetrachloroethane.

The small values of ϵ for these four substances in the solid state suggests that the rotation of the molecules as a whole in the crystal are hindered almost completely.

In the liquid state 1,2-dichloroethane and 1,1,2,2-tetrachloroethane have two forms, i.e., *trans* and the *gauche*. In the solid state, however, only the *trans* molecules exist. Therefore, electric polarization of these substances in the solid state may be due to the oscillations of electrons and atoms, i.e., electronic and atomic polarization. The greatest contribution to the atomic polarization is made by the internal hindered rotation, for the latter has low frequency and is optically active.

At the melting point these molecules may oscillate like the *trans* molecules in the liquid state. As the temperature is lowered, the field due to neighboring molecules becomes stronger and the frequency of the internal rotation becomes greater. Therefore, the lower the temperature the smaller the atomic polarization and dielectric constant.

On the other hand, the hindered internal rotations in the molecules of pentachloroethane and 1,1,1,2-tetrachloroethane are optically inactive if we assume that the H−C−C− plane of pentachloroethane and one of the H−C−C− planes of 1,1,1,2-tetrachloroethane are fixed in space, respectively, so that they have no contribution to the atomic polarization and the dielectric constant. If the internal rotations in the molecules of 1,2-dichloroethane and 1,1,2,2-tetrachloroethane take place about the −C−C− axis, the calculated frequencies at their melting points in the solid state are as follows:

33 cm^{-1} for 1,2-dichloroethane,
23 cm^{-1} for 1,1,2,2-tetrachloroethane.

The assumption in the above calculation is so approximate that the values obtained above may be considered to give only the order of magnitude.

Detailed discussion will appear elsewhere.

Absorption Spectra of Crystalline Chlorophyll Derivatives

EARL E. JACOBS AND A. STANLEY HOLT
Photosynthesis Research Project, Department of Botany, University of Illinois, Urbana, Illinois
(Received June 16, 1952)

CHLOROPHYLLS have not been successfully crystallized, but alkyl chlorophyllides, in which the long phytyl side chain is replaced by a methyl or ethyl group, are crystallizable. Colloidal suspensions of chlorophyllide crystals were prepared by diluting acetonic solutions with water. The size of the crystals could be varied by changing the concentration of chlorophyllide and the amount of water added.

The suspensions did not settle appreciably and their absorption spectrum could be measured in transmitted light. Scattering did not affect the results strongly, as indicated by good transparency of the crystal suspension in the green (Fig. 1.) The shaded area is a rough estimate of the contribution of scattering. It is highest in the two absorption bands because it is caused mainly by reflections from crystal surfaces.

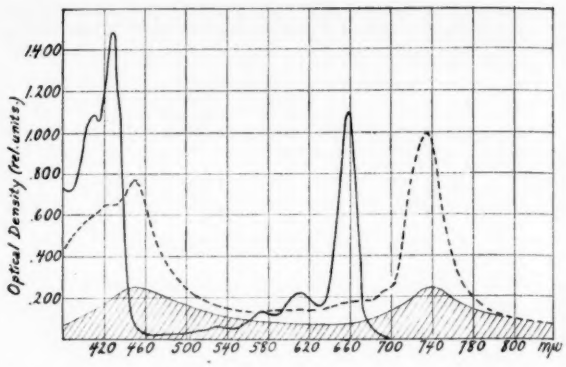

FIG. 1. Extinction curves of ethyl chlorophyllide in acetone (solid line) and in microcrystals (dashed line). Shaded area: estimated contribution of scattering to the crystal extinction curve.

The absorption spectra of the crystals differ significantly from the solution spectra. Figure 1 shows that the red band of microcrystalline ethyl chlorophyllide *a* is shifted far to the red compared to its position in acetone (658 mμ). The exact position and shape of the bands depends on the size of the crystals. A limit is reached when the crystals exceed a certain size; the red peak is then stabilized at about 745 mμ. The crystals to which Fig. 1 refers are equilateral triangular plates, not much under 1μ in two dimensions, but with a much smaller (and variable) thickness; their red peak lies at 738 mμ.

More properly, comparison should be made not with acetonic solution but with isolated chlorophyllide molecules. The position of the red band has been extrapolated by Katz and Wassink (1939) to approximately 648 mμ for chlorophyll *a* vapor; the same value should be approximately correct also for ethyl chlorophyllide *a*. Transition from free molecule to crystal thus causes the red band of ethyl chlorophyllide *a* to shift by 97 (±5) mμ, or about 2300 cm^{-1}.

This shift can be attributed to resonance interaction between identical chromophores arranged in a regular array. The same phenomenon also can be described in terms of excitation energy migration through this array. This interpretation explains the above-mentioned observations (to be described in detail later) that the band gradually shifts toward longer waves with increasing dimensions of the crystal.

A similar explanation has been given to the spectra of linear polymers (one-dimensional crystals) of cyanine dyes (Manly, Scheibe), and to the ultraviolet absorption spectra of naphthalene and anthracene crystals (Davydov).

The response of the blue-violet band ("Soret band") of chlorophyllide to crystallization is more complex than that of the red band, because of its doublet structure. In Fig. 1 it appears as if both components have been shifted by about 1500 cm^{-1} towards the red, without change in relative intensity. However, the relative intensity of the two components is quite different in smaller crystals. It has been suggested that these components correspond to dipole vibrations in two mutually perpendicular directions in the porphin plane; this would make their different behavior in the crystal lattice plausible.

Similar transformations have been observed with ethyl chlorophyllide *b*, where the band is shifted from about 630 mμ in vapor and 644 mμ in acetonic solution, to 725 mμ in crystals, and also with the pheophorbides *a* and *b* and with bacterio-chlorophyllide.

These observations offer the possibility of determining from experimental data the resonance energy and the probability of energy exchange between chlorophyll molecules; they are therefore of some interest for the theory of energy transfer in photosynthesis.

This work has been carried out with the assistance of the Office of Naval Research under contract ONR 565(00).

Theory of Catalysis of Nucleation by Surface Patches

DAVID TURNBULL
General Electric Research Laboratory, Schenectady, New York
(Received June 18, 1952)

RECENTLY the kinetics of solidification of small supercooled liquid mercury[1] and tin[2] droplets coated with various films were investigated. In some cases the isothermal data on droplets coated with a given film were satisfactorily described by a single nucleation frequency per area (I_s) or volume. However, for mercury coated with mercury laurate but infected with patches of HgX (an unidentified decomposition product of the laurate) and oxide-coated tin, the fraction x of droplets solidified approached an asymptote $x_a<1$ with increasing time t that was larger the greater the supercooling ΔT.

To explain $x_a<1$ Kimball[3] proposed that each droplet contained on the average m units or patches equally effective in catalyzing crystal nucleation. If m is of the order unity or less there will be marked variations between significant fractions of the sample in the number of patches per droplet. Assuming a Poisson distribution of patches among uniform droplets Kimball derived

$$dx/(1-x)dt=f=cm\exp(-ct), \tag{1}$$

where c is the nucleation frequency per patch and $m=-\ln(1-x_a)$.

Pound and La Mer[2] found that $x=f(t)$ approximately followed Eq. (1) but with m increasing with ΔT. The Kimball theory provides no explanation for the dependence of m on ΔT or why m should often be of the order unity. To explain these results we propose the following hypotheses: (1) The radius R of a patch is of the order of the critical radius r^* for the growth of a nucleus into the supercooled liquid. (2) There exists a statistical distribution of patch sizes described by $n_A=f(R)$, where n_A is the number of patches per area with radius $\geqslant R$. No transformation nuclei can form from patches for which $R<r^*$; hence, when $R=r^*$, $n_A a_D=m$, where a_D is the area of the droplet.

In order to describe their data Pound and La Mer found it necessary to assume a steady nucleation frequency per droplet ν, in addition to patch nucleation. Equation (1) then becomes

$$f=cm\exp(-ct)+\nu, \tag{2}$$

or

$$\ln(f-\nu)=\ln(cm)-ct. \tag{3}$$

By suitable selection of ν, good straight line relations were obtained between $\ln(f-\nu)$ and t for four of Pound and La Mer's isotherms, corresponding to the largest ΔT's. c and m were evaluated from the constants of these lines. From the variation of c with ΔT and assuming $a_p^*\sim10^{-13}$ cm^{-2}, where a_p^* is the area of a patch of radius r^*, we find for the nucleation frequency (I_p) per area of patch surface

$$c/a_p^*=I_p=10^{21\pm6}\exp[-1.74\times10^6/(\Delta F_v)^2kT]\ \text{cm}^{-2}\ \text{sec}^{-1},$$

where ΔF_v is the bulk free energy (ergs) of transformation per volume (cm)^3. Assuming that ν is due to heterogeneous nucleation on the inactive part of the droplet surface we find from the dependence of ν on ΔT

$$\nu/a_D=I_s=10^{23.4\pm6}\exp[-2.60\times10^6/(\Delta F_v)^2kT]\ \text{cm}^{-2}\ \text{sec}^{-1}.$$

The values of the pre-exponential terms in the expressions for I_p and I_s are in good agreement with the value $10^{27.5}$ cm^{-2} sec^{-1} predicted by the theory of heterogeneous nucleation.[4] From the dependence of m on ΔT,

$$m=6.22\times10^{-13}\exp[0.238\Delta T],$$

and assuming $r^*=-2\sigma/\Delta F_v$, where σ is the liquid-solid interfacial energy estimated by Pound and La Mer, we obtain

$$n_A=1.41\times10^{-6}\exp[3.14\times10^{-6}/R]\ \text{cm}^{-2}.$$

c for HgX is very large so that the patches are covered with crystalline mercury before any are supercritical. Patches of radius R become transformation nuclei immediately when the temperature is lowered sufficiently so that $r^*\geqslant R$. Hence $x\rightarrow x_a$ immediately with little isothermal time dependence. This mode of nucleation is "athermal" and is analogous to athermal nucleation[5] in the martensite type of transformation in crystalline media. c cannot be evaluated but $n_A=f(R)$ was obtained from $x_a=f(\Delta T)$ measured for a dispersion in which 42 percent of the droplets were infected with HgX. The distribution was described by

$$dn_A/dR=7.7\times10^{11}\exp[-1.80\times10^{12}(R-R_m)^2],$$

where $R_m=3.3\times10^{-6}$ cm and $n_A=5.3\times10^5$ cm^{-2} at $R=R_m$. The σ-value from an earlier publication[1] was used in this calculation.

The author gratefully acknowledges valuable conversations on this subject with E. W. Hart of this laboratory.

[1] D. Turnbull, J. Chem. Phys. **20**, 411 (1952).
[2] G. M. Pound and V. K. La Mer, J. Am. Chem. Soc. **74**, 2323 (1952).
[3] G. E. Kimball, private communication to Pound and La Mer, see reference 2.
[4] D. Turnbull, J. Appl. Phys. **21**, 1022 (1950).
[5] Fisher, Hollomon, and Turnbull, Trans. Am. Inst. Mining Met. Engrs. **185**, 691 (1949).

An Effect of the Anion on the Conductive Properties of Triphenylmethane Dye Salts*

R. C. NELSON
Department of Physics, Ohio State University, Columbus, Ohio
(Received May 23, 1952)

THE chlorides of crystal violet (XV)Cl and methyl violet (MV)Cl have previously been reported to be photoconductive and to have very large dark resistivities.[1,2] The bisulfates of these dyes (DY)HSO_4, show about the same order of dark resistivity as the chlorides but very much less photoeffect. Surprisingly, it has been found that the normal sulfates $(DY)_2SO_4$ and oxalates $(DY)_2C_2O_4$ are not only very strongly photoconductive in visible light but have also a rather low dark resistivity, $\sim10^5$ ohm·cm, as against $\sim10^{11}$ ohm·cm for the chlorides. For the dark conduction the thermal activation energies are $(MV)_2SO_4$, 0.39 ev; $(XV)_2SO_4$, 0.36 ev; $(MV)_2C_2O_4$, 0.31 ev; $(XV)_2C_2O_4$, 0.28 ev.

In their general behavior the sulfates and oxalates are very much alike. When prepared as a thin continuous film on glass by evaporation of an aqueous or alcoholic solution, they show the characteristic bright yellow-green metallic luster displayed by the chloride. A preparation strongly illuminated with a 100-watt incandescent bulb shows a conductance about three times the dark conductance. In its general features the photoconductivity resembles that of the chlorides; after a brief illumination the initial decay rate is rapid, but when the cell has been exposed to light long enough to have come to a steady state, perhaps half an hour, the decay is very slow. If the photoconductance is considered to be in parallel with the dark conductance, its decay from the steady state obeys a second-order law; that is,

$$(K_t-K_d)^{-1}-(K_0-K_d)^{-1}=mt,$$

where K_d is the dark conductance and m the rate constant. For a cell having a dark resistance of a megohm and a resistance illuminated of 0.3 megohm, m is $\sim$200 ohms/sec.

After the solid dye film has been formed, irreversible decay of dark conductivity takes place in the presence of air or oxygen. All of the dark conductivity may be destroyed in this way, but under certain circumstances $\sim$10 percent of the photoconductivity may remain. The dark conductivity may also be destroyed thermally. For $(MV)_2SO_4$ this process is of the second order with respect to conductance and has a heat of activation of approximately 30 kcal. In 48 hours at 100°C the dark conductance of a preparation went from $3\cdot10^{-6}$ mho to $<10^{-9}$ mho, while the photoconductance was still $>10^{-8}$ mho.

Measurements on several preparations of $(MV)_2SO_4$ show it to obey Ohm's law to within 1 percent for fields from 0.125 v/cm to 1100 v/cm.

The thermoelectric powers of these materials lie close to -0.15 mv/°C and being negative, indicate conduction predominantly by electrons.†

It is difficult to understand the semiconductivity of the dye sulfates and oxalates in terms of a picture in which the conduction band is associated with the ionic domains of the film structure, as was earlier proposed by the writer.[2] Extensive studies of the kinetics of the build-up and decay of photoconductivity in the chlorides made at this laboratory have also cast doubt upon this hypothesis, and it now seems more likely that in the triphenylmethane dyes the conduction band is an extended mutual excited state of the dye cations. On this basis the sulfate or oxalate ion becomes a donor "impurity" level in the ordinary terminology of semiconductivity, and the primary process is the thermal excitation of an electron to the conduction band. This view is supported by the fact that a chloride film containing 5 percent of the oxalate shows a markedly lowered dark resistivity, $\sim 10^7$ ohm·cm.

The writer wishes to acknowledge his indebtedness to Dr. Josef de Heer and Dr. J. W. Weigl for profitable discussions of these problems.

* This work was supported by the Charles F. Kettering Foundation.
† The measurements of thermoelectric power were made by Mr. Clifford Schroeder in this laboratory. He has also found consistently negative values for (XV)Cl, indicating electron conduction for this substance as well, in contrast to the writer's earlier statement (see reference 2) made on the basis of rather crude preliminary experiments.

[1] A. T. Vartanyan, J. Phys. Chem. (U.S.S.R.) **20**, 1065 (1946); Chem. Abstracts **41**, 2988 (1947).
[2] R. C. Nelson, J. Chem. Phys. **19**, 798 (1951).

Influence of Chain Length on the Symmetry of Conjugated Molecules

J. D. DUNITZ
Chemical Crystallography Laboratory, University Museum, Oxford, England
AND
L. E. ORGEL
Magdalen College, Oxford, England
(Received June 5, 1952)

FAIRLY detailed crystal structure analyses have been carried out for the dihydrates of oxalic acid, acetylene dicarboxylic acid, and diacetylene dicarboxylic acid;[1] the three structures are very similar with the exception of one important feature—the first two molecules are coplanar (symmetry C_{2h}), while the third deviates markedly from coplanarity, opposite carboxyl groups being inclined to one another at an angle of about 57° (symmetry C_2). This difference is emphasized by a change in space group, from $P2_1/a(C_{2h}^5)$ to $I2/c(C_{2h}^6)$ and a doubling of the unit-cell size.

One might reasonably expect that, as the two carboxyl groups become more distant from one another, the dependence of the molecular energy on their relative orientation should decrease, and this expectation is confirmed by a simple molecular orbital calculation. We neglect resonance within the carboxyl group and regard the carbonyl bond as a carbon-carbon double bond. We do not believe that quantitatively significant results could be obtained by the inclusion of various refinements, and we have therefore restricted ourselves to this over-simplified model.

The molecular symmetries C_{2h} or C_2 will result from alternative methods of combination of the π_y and π_z atomic orbitals into molecular orbitals, as shown in Fig. 1. We have calculated the delocalization energies for both configurations, and we find that the energy difference decreases rapidly as the number of triple bonds is increased; the extra stability of C_{2h} is 0.47β for oxalic acid, 0.04β for acetylene dicarboxylic acid, and only 0.01β for diacetylene dicarboxylic acid.

A somewhat similarly simplified model is applicable to the series $CH_2(C)_nCH_2$, where the preferred molecular symmetry is D_{2h} or D_{2d}, according as n is even or odd. Although the ground state of the unfavorable configuration is now a triplet, it is still found that the energy difference between D_{2h} and D_{2d} decreases to zero as n increases, but much more slowly than for the acetylenes. Thus, D_{2d} is favored by 1.17β for $n=1$ (allene) and by 0.24β for $n=11$; D_{2h} is favored by 2.0β for $n=0$ (ethylene), by 0.82β for $n=2$, and by 0.22β for $n=12$. Experimental evidence for the molecular symmetries of the higher members of this series is, however, not available.

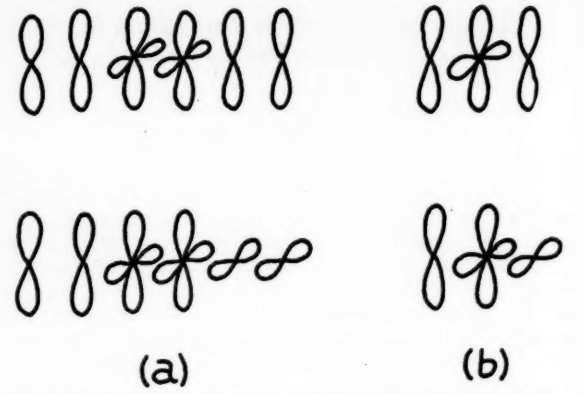

FIG. 1. Alternative arrangements of π_y and π_z atomic orbitals, leading to molecules of differing symmetries, (a) acetylene dicarboxylic acid, (b) allene.

In general, in such molecules containing only a short conjugated chain, we expect molecular energies to determine the configuration in the crystal; as the chain length increases, the influence of intermolecular forces (packing considerations, hydrogen bonds, etc.) is likely to become more important in determining the molecular configuration.

One further point of interest emerges from our calculation. The x-ray analysis gave the length of the central bond of diacetylene dicarboxylic acid, formally a single bond, as 1.33 ± 0.02A, the distance customarily adopted as the double bond standard. For this bond our simplified model ascribes a bond order 1.976 and 1.966 for the C_{2h} and C_2 configurations, respectively.

[1] J. D. Dunitz and J. M. Robertson, J. Chem. Soc. **1947**, 142, 148, 1145.

Errata: The Physical Properties of Molecules in Relation to Their Structure. I. Relations between Additive Molecular Properties in Several Homologous Series

[J. Chem. Phys. **20**, 263 (1952)]

H. J. BERNSTEIN
Division of Chemistry, National Research Council, Ottawa, Canada

AN error has been found in Table IV on page 265 for the substituted ethanes. There should be an entry of 3 under AYY_2 for $P1,1,1,C_2X_3Y_3$, whereas the entry under AXY_2 should be zero instead of 3. In the left-hand column on page 265 lines 13 and 14 under the table should be deleted. In line 7 under the table in the right-hand column on page 265 read "of the five unknowns, PC_2X_6, α, β, γ, and δ," instead of "of the six unknowns, PC_2X_6, α, β, γ, δ, and ϵ. In Table V at the top of page 266 there should be zero and 3 under α and β, respectively, for $P1,1,1,C_2X_2Y_2$ instead of 1 and 2; also the entire column under ϵ is to be deleted. In line 21 under the table of the right-hand column on page 266 read "α, β, γ, and δ" instead of "α, β, γ, δ, and ϵ." In line 25 and 26 under the table of the right-hand column on page 266 read "may be reduced to 4 of the 5 given above, namely, PC_2H_6, α, β, and γ or δ" instead of "may be reduced to 5 of the 6 given above, namely, PC_2H_6, α, β, ϵ, and γ or δ."

This simplifies the relations for the substituted ethanes by reducing the number of unknowns by one, since ϵ is to be replaced by $\alpha-\beta$.

Effect of Various Gases on Potassium Ion Emission from Hot Platinum

CHARLES F. ROBINSON
Consolidated Engineering Corporation, Pasadena 8, California
(Received May 7, 1952)

BRADY and Zemany[1] have published a paper on this subject in which they state, "A proof that the oxygen did not cause the potassium to be emitted in a non-ionized state was obtained by turning on the ionizing mechanism of the mass spectrometer with oxygen in the system. There was no change in the potassium peak height."

This argument seems to have overlooked a tremendous difference in the efficiencies of the two ionization processes involved here, the first being direct emission of potassium ions from a heated platinum surface and proceeding with an efficiency approaching 100 percent[2] and the second of which, being ionization by electron impact with the vapor phase, proceeds at an efficiency that in a typical mass spectrometer is well below 10^{-4} for permanent gases and that may be orders of magnitude lower for condensable or reactive vapors such as potassium vapor. Consequently, a confident assertion of a negative result in the experiment described here would require detection of a change in the potassium peak height which might well be beyond the current limits of precision in the art of mass spectrometry.

It seems important to point out the weakness of this argument because by so doing, one readmits the possibility that the principal effect of oxygen, CCl_4, and bromine on the platinum filament was so to reduce the work function that the potassium was emitted principally as uncharged atoms, in which case the results would be amenable to simple qualitative explanation.

[1] E. L. Brady and Paul D. Zemany, J. Chem. Phys. **20**, 294 (1952).
[2] I. Langmuir, Revs. Modern Phys. **2**, 123 (1930).

Effect of Various Gases on the Emission of Potassium Ions from Hot Platinum

P. D. ZEMANY AND E. L. BRADY
General Electric Research Laboratory, Schenectady, New York
(Received May 19, 1952)

IT is quite true that failure to detect potassium atoms by measuring the potassium ion current in the mass spectrometer after electron bombardment does not definitely prove their absence, as C. F. Robinson states in the preceding letter. It does, however, put a significant limit on the fraction of atoms that evaporated in the place of ions.

There are, as Robinson points out, two different ionization processes with very different probabilities. These two processes, however, may have very different efficiencies of measurement in the mass spectrometer. In the first case, ions emitted directly from the platinum filament are focused, accelerated, deflected, and finally collected and measured. The potassium ion currents measured here were of the order of 10^{-12} amps. A similar filament, heated to about the same temperature, and hence emitting only potassium ions, when completely surrounded by an ion collector showed currents of the order of 10^{-9} amps, indicating a collection efficiency of 1 in 10^3 for the K^+ ions evaporated from the platinum and collected in the spectrometer.

The second ionization process is that of electron bombardment of neutral atoms to provide ions, and their acceleration, etc., to a final collection and measurement. Experiments recently performed show that about 1 ion in 1.65×10^4 molecules of nitrogen that pass through the spectrometer are collected.[1] This is in agreement with the value of about 10^{-4} given by Robinson.

Potassium atoms evaporated from the filament should behave in much the same manner as nitrogen molecules admitted from outside. Hence, we should collect about 1 ion for every 1.6×10^4 atoms emitted. Since we originally collected only 1 out of 10^3 ions, the ion beam with the spectrometer ionization mechanism turned on should be $\frac{1}{16}$ of the original current. This is about 100 times the minimum detectable current. Since no additional ion current was observed due to the electron beam, not more than a small fraction of the potassium was evaporated as atoms.

Plumlee and Smith[2] in a somewhat similar experimental arrangement noted the evaporation of alkali atoms and ions from nickel. They state, "The alkali metal evaporation was detected roughly as follows from nickel alloys: K^+ above 500°C, Na^+ above 600°C, K° and Na° about 850°C, the evaporation of all species increasing with temperature, and the ratio of the atoms to ions increasing sharply with temperature." In other experiments in this laboratory in an arrangement similar to the one described, where sodium was being observed at a higher temperature, both atoms and ions were noted, in agreement with Plumlee. In our original experiments we would expect to have found the potassium atoms as readily as the sodium atoms, had they been present. Our temperature was presumably too low to cause measurable evaporation of atoms.

It is certainly true that if the emission of potassium ions by heated platinum is governed by the laws of thermionic emission, an hypothesis not yet adequately demonstrated, then the phenomenological explanation of changes of emissivity would be ascribable to changes in work function. The usual effect of oxygen- and halogen-containing compounds is to increase the work function of platinum. It does not follow that any decrease in ion emissivity would be compensated by an increase in atom evaporation, for the two processes are quite different.

Robinson's comments would clearly apply if our experiments involved a constant beam of potassium directed from outside onto a metal surface of known work function. This is not the case here, for the source of ions and geometry of collection have a very important effect on the experimental observations.

[1] P. D. Zemany, J. Appl. Phys. (to be published).
[2] R. H. Plumlee and L. P. Smith, J. Appl. Phys. **21**, 811 (1950).

The Surface Contribution to the Heat Capacities of Solids*

J. T. LAW
Cryogenic Laboratory, The Pennsylvania State College, State College, Pennsylvania
(Received May 23, 1952)

IN view of the recent interest in the contribution of the surface to the heat capacity of solids[1–3] it may be worthwhile to mention the work of Tarrasov.[4,5] He derived equations for the heat capacity of one- and two-dimensional molecules and used the latter to explain the experimental values obtained by Nernst[6] for graphite at temperatures below 100°K.† If an equation of the Montroll type[1] can be fitted to the graphitic results, it should also be applicable to the heat capacities of adsorbed films which are effectively two-dimensional solids of a graphite type. Therefore, an experimental proof of Montroll's equation should be possible.

Tarrasov, using an equation of the form $C_v=86.5(T/\theta)^2$ calculated the values of θ required to reproduce the experimental heat capacities. These are listed [$\theta(T)$] in Table I and may be seen to be remarkably constant. The writer has also calculated θ-values from the experimental data using Montroll's[1] limiting equation of the

TABLE I.

T	C_v (Nernst)	$\theta(T)$	$\theta(M)$	$\theta(D)$
30	0.038	1430	1250	680
40	0.080	1310	1200	720
50	0.127	1300	1200	770
60	0.175	1330	1290	830
70	0.225	1370	1350	890
80	0.275	1410	1400	950
90	0.338	1430	1450	1000

form $C_p=464.5(T/\theta)^3+\gamma(T/\theta)^2$, (where γ is calculated from the ratio of the surface area to the volume of the solid) and the known molecular dimensions of graphite, assuming that the graphite sheets are infinite in area. These values are also listed in Table I [$\theta(M)$] together with those obtained from the Debye equation [$\theta(D)$].

It will be seen that the values from both the equations including a T^2 term are much more constant than those obtained from the Debye equation.

Even the simple T^2 equation used by Tarrasov holds over a wide temperature range. The steady increase in $\theta(M)$ at higher temperatures may be due to the breakdown of the limiting equation as in this region a different $\theta(D)$ is obtained from the limiting and the complete Debye equation.

It may be suggested that an equation of the form $C_p=\alpha T+464.5(T/\theta)^3$ could also be used to explain the experimental results as graphite contains conduction electrons. From the intercept of a plot of C_p/T against T^2 a value of 1.0×10^{-3} was obtained for α. This gave fairly constant values of θ which ranged from 900 to 1100.

From the Sommerfeld[8] equation

$$C_e=3.26\times10^{-5}q^{\frac{1}{3}}(A/\rho)^{\frac{1}{3}}T \text{ cal mole}^{-1}\text{ deg}^{-1},$$

assuming that carbon has two conduction electrons per atom (from the atomic structure the number cannot exceed two) we find that $\alpha=1.36\times10^{-4}$ which is far too small to reproduce the observed change of C_p with temperatures.

Because of the fact that the heat capacity of graphite can best be reproduced by an equation containing a T^2 term, we are at present investigating the heat capacities at liquid helium temperature of films adsorbed on a compressed block of lampblack. As was mentioned above the structure of these films is comparable to the layer structure of graphite.

The major difficulty in heat capacity measurements at liquid helium temperatures is heat transfer through the material. At higher temperatures helium gas can be used as the amount of adsorption is small, but below 4°K almost complete condensation will occur on the solid. Desorption of gas during a measurement may introduce a heat correction which is large compared to the heat capacity.

A block of carbon can be used both as a heater and thermometer. Since the heat will be generated in the adsorbent itself, no exchange gas will be required. The attainment of thermal equilibrium will be limited only by the thermal conductivity of the carbon block which should be quite adequate above 1°K.

* This research was carried out under Contract N6 ONR 269, Task Order X, of the ONR.

† The heat capacities used were not obtained as Tarrasov reported, by Simon and Swein (see reference 7). These workers measured heat capacities of an activated charcoal, which were somewhat higher than the results obtained for graphite.

[1] E. W. Montroll, J. Chem. Phys. **18**, 183 (1950).
[2] Jura, paper presented at the American Chemical Society Meeting, March, 1952.
[3] H. Koppe, J. Chem. Phys. **18**, 638 (1950).
[4] Tarrasov, Compt. rend. U.R.S.S. **46**, 20 (1945).
[5] Tarrasov, Compt. rend. U.R.S.S. **46**, 110 (1945).
[6] Nernst, Ann. d. Phys. **36**, 395 (1911).
[7] Simon and Swein, Z. physik. Chem. **28**, 189 (1935).
[8] Sommerfeld, Z. Physik **47**, 1 (1928).

Some Observations on the Mass Spectrum of CO_2

AMOS S. NEWTON
Radiation Laboratory, University of California, Berkeley, California
(Received May 26, 1952)

IN carefully checking the mass spectral pattern of CO_2 in some experiments in which traces of air impurities were undesirable, it was found that the most carefully purified CO_2 gave a small but definite mass 32 peak, apparently due to O_2^+. Since it is not obvious how an O_2^+ fragment can arise from a rearrangement of the linear CO_2 molecule during fragmentation, this has been investigated further.

TABLE I. Effect of pressure on 32/44 ratio in normal CO_2.

Sample pressure (microns)	Pk. ht. m/q =32	Pk. ht. m/q =22	Pk. ht. m/q =44	Ratios 22/32	Ratios 32/44 ×100
33.7	0.215	22.9	1206	104.5±10	0.0198
39.1	0.255	26.6	1398	106.7±10	0.0203
58.8	0.402	40.2	2100	100.0±7	0.0190
142	0.94	97.5	>3000	103.6±5	0.0197[a]
215	1.49	146.9	>3000	98.6±3	0.0187[a]
251	1.70	170.6	>3000	100.6±2	0.0191[a]

[a] Calculated from 22/44 ratio of 0.0190.

A check of the variation of masses 32/44 ratio with pressure shows no change as illustrated in Table I. In this table the ratio of masses 22/32 and masses 32/44 are both calculated since mass 44 soon goes off scale on the mass spectrometer used (Consolidated Engineering Corporation Model 21–103). However, the constancy of ratio of masses 22/32 and masses 32/44 over a considerable pressure range shows the occurrence of O_2^+ to be independent of pressure, hence a first-order process. Since each figure represents a separate introduction of highly purified carbon dioxide which was further carefully frozen and degassed before introduction, it appears highly unlikely that this represents an oxygen impurity. The instrument used does have a mass 32 background of 0.22 division with no gas in the sample bottles because of a leak in the isatron unit. This is quite reproducible over long time periods and has been subtracted in all figures given since it is independent of pressure in the sample bottle, because it occurs on the high vacuum side of the leak. All measurements of the mass 32 peak were made at 5 times sensitivity (50 μa emission current compared to a normal of 10 μa) and calculated back to normal sensitivity.

The filament represents a possible source of oxygen from some such reaction as $CO_2+MO\rightarrow O_2+CO$, which would give rise to a first-order dependence with pressure and not necessitate postulating a rearrangement. Treatment of the filament overnight with 100 microns of butene-1 in the sample bottle lowered the ratio of 22/32, i.e., raised the 32 peak as shown in Table II. This is in the opposite direction expected from interaction with the filament. The following day the 22/32 ratio was back to its "normal" value of 100.

Through the kind cooperation of Professor Richard Ogg of Stanford University a sample of CO_2 enriched in oxygen 18 was obtained. This contained 13.5 percent O^{18} and only a very small amount was available. While larger samples and higher isotope content would be desirable for a completely unambiguous answer, the results indicate that only half the oxygen of the 32 peak comes from CO_2, the other half arising from some source of normal oxygen. The O^{18} in the sample as measured by the 46/44 ratio was 13.45 percent, while the ratio of oxygen content of the O_2^+ peak from the 34/32 ratio was 6.9±1 percent. A second run gave values of 13.45 percent and 7.7±1 percent, respectively. It is not quite clear where the source of normal oxygen which gives rise to the 32 peak can be, but it is certain that half of it arises from the CO_2 molecule. If carbonization with butene removes oxygen from the filament, this would suggest that the filament is not the source, since the 32 peak actually increased with such treatment. This leaves the instrumental source of oxygen unanswered at the present time.

One feature of the spectrum of $CO^{16}O^{18}$ noted was an apparent discrepancy in the ratios 44/22, $(CO^{16}O^{16})^+/(CO^{16}O^{16})^{++}$ and

TABLE II. Effect of carbonizing spectrometer filament on 22/32 ratio.

Time after butene treatment	Sample pressure (microns)	Pk. ht. m/q =32	Pk. ht. m/q =22	Ratio 22/32
5 min	135	1.31	92.0	81.5±4
30 min	121	0.99	82.4	83.2±4
60 min	118.6	0.92	80.8	87.6±4

46/23, $(CO^{16}O^{18})^+/(CO^{16}O^{18})^{++}$. In two runs, values of 51.05 and 51.76 were found for the ratio of 44/22, while the ratio of 46/23 in these runs was 54.93 and 56.35, respectively, the discrepancy being about 8 percent in each case. This is well outside the experimental error, the pattern stability on normal CO_2 being about 2 percent for the 22 peak over short time intervals, leading to the conclusion that $(CO^{16}O^{18})^{++}$ has about 8 percent lower probability of formation than $(CO^{16}O^{16})^{++}$. Ion discrimination effects[1,2] due to use of voltage scanning were shown to be negligible by use of magnetic scanning for each series of peaks which affected no significant difference in the ratios; and by calculation of the effect from discrimination curves on the 22 and 44 peaks, showing the effect to be negligible on the ratios over the small voltage increments concerned. It is probable that this is due not to a difference in the ionization probability (loss of two electrons) but to the greater probability of fragmentation of the doubly ionized molecule containing O^{18} which is unsymmetrical in character and possesses a small dipole moment and less stability than the symmetrical molecule, thus reducing the effective yield of the 23 peak.

This postulate cannot be checked by the expected augmentation of the 28 or 30 and 16 or 18 peaks by the reaction:

$$CO_2^{++} \rightarrow CO^+ + O^+,$$

since the fragmentation of $(CO^{16}O^{18})^+$ is not identical with that of $(CO^{16}O^{16})^+$; nor is the pattern stability on normal CO_2 sufficient to observe the very small expected increase. The ratio of 48/24 which should be "normal" if the above explanation is correct could not be adequately checked using the above sample. The peaks were small and the reading errors greater than the difference.

The author wishes to thank Professor Richard Ogg of Stanford University for the loan of a sample of enriched CO_2, Mr. Laurin Tolman for the mass spectrometer runs, and Dr. David Stewart of Eastman Kodak Company for the valuable discussions and suggestions on the problem. This work was performed under the auspices of the Atomic Energy Commission.

[1] Clifford E. Berry, Phys. Rev. **78**, 597 (1950).
[2] Oliver A. Shaeffer, U. S. Atomic Energy Commission Document, AECU-971 (Technical Information Service, Oak Ridge, Tennessee, October 17, 1951).

Erratum: Hydrogen Redistribution during Olefin Hydrogenation

[J. Chem. Phys. **20**, 338 (1952)]

C. D. Wagner, J. N. Wilson, J. W. Otvos, and D. P. Stevenson
Shell Development Company, Emeryville, California

It has been called to our attention through correspondence with Professor K. J. Laidler that the use of the term "free valence" in our recent letter on "Hydrogen Redistribution During Olefin Hydrogenation"[1] may have been misleading. Our meaning would have been better conveyed by a more general term such as "hydrogen deficiency." Since Professor Laidler and his co-workers propose in the following letter[2] a mechanism that has much in common with the one we attempted to convey[2] and since our proposed mechanism may be of general importance in the catalytic hydrogenation of olefins, we feel that we should clarify our position.

Our principal conclusions from our experimental findings are:

(1) An important mechanism for alkane formation is the transfer of hydrogen between two chemisorbed alkyl radicals *without the intervention of adsorbed hydrogen atoms.* This process presumably forms desorbed alkane and chemisorbed alkene.

(2) Hydrogen redistribution among adsorbed organic residues can occur *without the intervention of adsorbed hydrogen atoms.* A possible reaction of this sort is alkyl plus alkene to alkene plus alkyl.

(3) Depending on the reaction conditions, type of olefin, and nature of the catalyst surface, elementary reactions directly involving adsorbed hydrogen atoms compete with (1) and (2) in both alkane formation and hydrogen redistribution. Our data are consistent with the possibility that these reactions include those favored in recent discussions of the mechanism of catalytic hydrogenation.[3]

[1] Wagner, Wilson, Otvos, and Stevenson, J. Chem. Phys. **20**, 338 (1952).
[2] Markham, Wall, and Laidler, J. Chem. Phys. **20**, 1331 (1952). We are grateful to Professor Laidler for an opportunity to see this manuscript prior to publication.
[3] Disc. Faraday Soc. **8**, "Heterogeneous Catalysis" (1950).

Mechanisms of Exchange and Hydrogenation Reactions of Olefins

Maria Clare Markham, Mary Colman Wall, and Keith J. Laidler
Department of Chemistry, The Catholic University of America, Washington, D. C.

(Received June 5, 1952)

In a recent letter Wagner, Wilson, Otvos, and Stevenson[1] have proposed a mechanism for exchange and hydrogenation, involving migrations of H and D atoms among adsorbed hydrocarbon residues. The present authors have also formulated the mechanisms of such reactions and have calculated absolute rates which are in excellent agreement with experiment. Our general scheme, which explains the phenomena reported by Wagner *et al.* and all other phenomena of this type of which we are aware, is somewhat different from theirs. Our mechanism, as applied to ethylene, is as follows.

Hydrogen and deuterium are adsorbed as atoms on single surface sites. Ethylene may become adsorbed on bare dual sites,

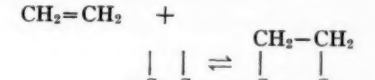

(1)

and in addition may interact with adsorbed H or D to form an adsorbed alkyl radical

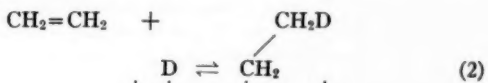

(2)

Adsorbed alkyl radicals may also be formed by interaction between adsorbed ethylene and neighboring adsorbed H or D atoms,

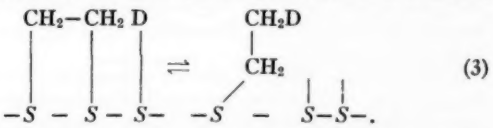

(3)

Surface exchange is assumed to occur by the following type of interaction between alkyls and ethylenes adsorbed in neighboring positions,

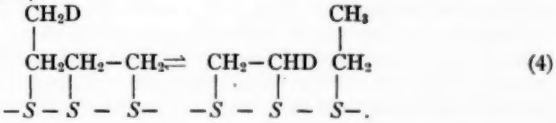

(4)

Ethylene is returned to the gas phase by the reverse of reactions (1) and (2). Ethane is produced in the gas phase by interaction between two alkyl radicals adsorbed on neighboring sites, e.g.,

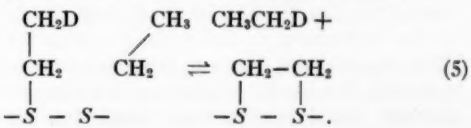

(5)

In addition ethane may be formed under certain conditions by interaction between alkyl and D or H,

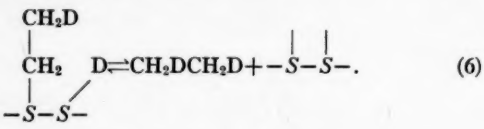

(6)

In permitting independent adsorption of ethylene and deuterium this mechanism is essentially of the Langmuir-Hinshelwood type, in contrast to that of Twigg,[2] and accounts for the falling off of the rate at high ethylene pressures—which certainly occurs at least on some surfaces.[3] The concentration of adsorbed H or D is, at low coverage, proportional to $P_{H_2}^{\frac{1}{2}}$ or $P_{D_2}^{\frac{1}{2}}$ as is also the concentration of ethylene adsorbed as ethyl radicals. The rate of hydrogenation or deuteration, whether it involves reaction (5) or reaction (6), is therefore proportional to p_{H_2} or p_{D_2}. The exchange rate by reaction (4) is proportional to $p_{D_2}^{\frac{1}{2}}$. The order with respect to D_2 is not well established experimentally, but the data[4] are not inconsistent with the square root law, and as will be shown in a later paper absolute rate calculations definitely support this interpretation.

The scheme of reactions considered above differs from that of Twigg mainly in omitting the reaction

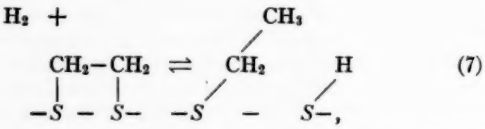

(7)

which according to him is the only reaction by which H_2 or D_2 can become adsorbed. Our reason for omitting this reaction is Beeck's result[5] that the rate is reduced if ethylene is presorbed on the surface; furthermore, the reaction would appear unlikely on steric grounds.

Under some conditions, i.e., at higher temperatures, it appears likely that surface equilibration between H and D occurs rapidly. If the ratio of D to D+H on the surface (in any form) is q, the probability of formation of an ethane containing n D atoms is $(6/n)q^n(1-q)^{6-n}$; for a butane the corresponding probability is $(10/n)q^n(1-q)^{10-n}$. Under the conditions of the experiments of Turkevich, Bonner, Schissler, and Irsa[6] the ratio q is small, and large amounts of C_2H_6 were formed initially in the reaction between C_2H_4 and D_2. The ratio of the initial rates of formation of C_2H_6 and C_2H_5 is $(1-q)^6/6q(1-q)^5=(1-q)/6q$; if q is 0.077 this ratio becomes 2, which is of the order of that found by Turkevich *et al.* In our view the results quoted by Wagner *et al.* are due to the fact that under the conditions of their experiments (they used a large excess of deuterium) their surface D/(D+H) ratio happened to be $\frac{1}{4}$.

Under certain conditions, such as those apparently employed by Wagner *et al.* (with a large excess of deuterium) there is not complete H–D equilibration on the surface. In regions of the surface where there is a large excess of adsorbed deuterium atoms, reaction (6) may occur before equilibration of the alkyl radical has taken place, so that abnormally large amounts of the di-deuterated products are produced.

Wagner *et al.* report that even under conditions where no exchange takes place between D_2 and olefin and D_2 and paraffin, the product of reaction between D_2 and olefin may contain deuterated paraffins containing more than two deuterium atoms. The absence of exchanged olefins under these conditions is explained if the equilibria (1), (2), and (3) are well over to the right at the lower temperatures, so that little gaseous olefin is produced from adsorbed alkyl and little HD is returned to the gas phase; at higher temperatures, on the other hand, the rates of the reverse reactions become appreciable, so that exchange occurs with production of HD in the gas phase. The lack of exchange between D_2 and paraffin is probably because the paraffins are only adsorbed with difficulty. Kemball[7] found that methane adsorption has an energy of activation of 11 kcal and that negligible adsorption of methane occurs at 0°C and below.

Papers dealing with the kinetics and absolute rates of exchange and hydrogenation processes are in preparation.

[1] Wagner, Wilson, Otvos, and Stevenson, J. Chem. Phys. **20**, 338 (1952).
[2] G. H. Twigg, Disc. Faraday Soc. **8**, 152 (1950).
[3] R. N. Pease, J. Am. Chem. Soc. **45**, 1196 (1923) (on copper); A. Farkas and L. Farkas **60**, 20 (1938) (on platinum); O. Toyama, Rev. Phys. Chem. (Japan) **11**, 153 (1937) (on nickel).
[4] G. H. Twigg and E. K. Rideal, Proc. Roy. Soc. (London) **A171**, 55 (1939).
[5] O. Beeck, Disc. Faraday Soc. **8**, 118 (1950).
[6] Turkevich, Bonner, Schissler, and Irsa, Disc. Faraday Soc. **8**, 352 (1950).
[7] C. Kemball, Proc. Roy. Soc. (London) **A207**, 539 (1951).

Evidence for Globulite Molecules in Horse Hemoglobin*

DOROTHY WRINCH
Department of Physics, Smith College, Northampton, Massachusetts
(Received May 22, 1952)

THIS communication discusses evidence in the published sections of Perutz' vector map of crystalline horse methemoglobin[1] regarding the general structure types of the hemoglobin molecules.

Proceeding outwards from the center of the vector map, we encounter two striking features: (1) the shell of below-average density just before 4A and (2) a shell of high density at about 4–6A from the origin, from which certain corridors of slightly above-average density emerge. It was seen that an interpretation of this essentially three-dimensional distribution in terms of the protein molecules would require them to be of impossibly small dimensions; an interpretation was, however, forthcoming in terms of hydrogen-bridged complexes of water molecules, the only other components of the crystal.[2]

Necessarily then proceeding further out for evidence regarding the structural type of the protein component, we remark the uniformly below-average density (apart from the corridors) from 6A to *ca* 9½A in all sections; and the materialization in the 9½–15A region in all sections of domains of above-average density, clustering around, though not completely circumscribing, the origin. Were these domains to cover a spherical shell they could be attributed to distributions within spherical shells of about half the dimensions, suggesting that the backbones of the amino acid residues, which polymerized form the skeletons of the protein molecules, lie within such a shell. This, however, is not the case. All that we remark is the "vestiges" of such a shell which lie in many but not all directions from the origin; that such "vestiges" emerge characteristically in the vector maps of shells which while not spherically symmetrical are globulite in character has, however, been demonstrated for certain hexagonal and rectangular shells in 2 dimensions,[3] for certain polyhedral shells in 3 dimensions,[4] the maxima in these cases lying in the directions of pairs of antipodal sides or faces. It may therefore be suggested that the backbones of the amino acid residues in the hemoglobin molecules form not spherical but globulite or polyhedral shells, for which the inner and outer diameters normal to antipodal faces are at least say 9½A and at most say 15A, respectively. So small a structure can accommodate only a fraction of the 580 amino acid residues[5] estimated for the 66,700 hemoglobin structure. There would therefore be a number of molecules, possibly as many as 12, to correspond to this structure.[6] In this multiplicity of crystallographically independent pairs of molecules, an interpretation of the multiplicity of local maxima in the 5A shell[2] may be sought, in terms of the orientation of some water complexes with respect to each such independently oriented pair. A subsequent publication will discuss the evidence in the vector map regarding the molecular pattern of the structure, i.e., the spatial dispositionof the individual molecules relative to one another. One clue is to be seen in the corridors emerging from the 5A shell. Judging from the results of the x-ray

study of the 29 hydrate of phosphotungstic acid,[7] we would anticipate that the presence and spatial disposition of extended water complexes (in terms of which the corridors have been interpreted[2]) is determined by and will therefore throw light on the placing as well as on the nature of the protein molecules.

A fuller discussion of the structure of the molecules in hemoglobin, in the light of the x-ray work, will appear elsewhere.

* This work is supported by the ONR.
[1] M. F. Perutz, Proc. Roy. Soc. (London) **A195**, 474 (1949).
[2] D. Wrinch, J. Chem. Phys. **20**, 1051 (1952).
[3] D. Wrinch, Phil. Mag. **27**, 111 (1939).
[4] D. Wrinch, Meeting of Am. Assoc. for X-Ray and Electron Diffraction, Ann Arbor, Michigan (1949).
[5] G. R. Tristram, *Haemoglobin* (Interscience Publishers, Inc., New York, 1949), p. 111.
[6] D. Wrinch, Science **115**, 356 (1952).
[7] A. J. Bradley, Proc. Roy. Soc. (London) **A157**, 113 (1936).

Properties of the π Electron Distribution in Conjugated System

H. H. GREENWOOD
Sir John Cass College, Aldgate, London, E.C. 3, England
(Received June 19, 1952)

THE π electron distribution in the molecular orbital treatment of conjugated molecules is usually expressed in terms of the charge density q_r and free valence F_r at the rth atom, and the bond order p_{st} of the bond between adjacent atoms s and t. The simplest treatment takes the Coulomb integrals for all carbon atoms to be equal, of value α_0 say, and the resonance integrals for all bonds to be equal to β. The overlap integral S is put equal to zero. The changes in these quantities due to a change $\delta\alpha_u$ in the Coulomb integral at the uth position given by

$$\alpha_u=\alpha_0+\delta\alpha_u \tag{1}$$

may be written in terms of the expansion formulas

$$\delta A=\sum_{n=1}^{\infty}\frac{1}{n!}\frac{\partial^n A}{\partial\alpha_u{}^n}(\delta\alpha_u)^n, \tag{2}$$

where

$$A\equiv q_r,\ F_r,\ \text{or}\ p_{st}.$$

Coulson and Longuet-Higgins[1] have shown that

$$\frac{\partial q_r}{\partial\alpha_u}=\frac{1}{\pi}\int_{-\infty}^{+\infty}\left[\frac{\Delta_{r,u}(iy)}{\Delta(iy)}\right]^2dy;\quad \frac{\partial p_{st}}{\partial\alpha_u}=-\frac{1}{\pi}\int_{-\infty}^{+\infty}\frac{\Delta_{s,u}(iy)\Delta_{t,u}(iy)}{\Delta^2(iy)}dy, \tag{2'}$$

and Coulson[2] has also given a formula from which it can be deduced that

$$\frac{\partial F_r}{\partial\alpha_u}=-\frac{1}{\pi}\int_{-\infty}^{+\infty}(iy)\left[\frac{\Delta_{r,u}(iy)}{\Delta(iy)}\right]^2dy. \tag{2''}$$

In these formulas $\Delta_{a,b}$ represents the determinant obtained by striking out the ath row and bth column of the secular determinant $\Delta(iy)$ for the unperturbed hydrocarbon. Successive differentiation under the integral sign gives the general differential coefficients

$$\frac{\partial^n q_r}{\partial\alpha_u{}^n}=(-)^{n-1}\frac{n!}{\pi}\int_{-\infty}^{+\infty}\left[\frac{\Delta_{r,u}}{\Delta}\right]^2\left[\frac{\Delta_{u,u}}{\Delta}\right]^{n-1}dy,$$

$$\frac{\partial^n F_r}{\partial\alpha_u{}^n}=(-)^{n}\frac{n!}{\pi}\int_{-\infty}^{+\infty}(iy)\left[\frac{\Delta_{r,u}}{\Delta}\right]^2\left[\frac{\Delta_{u,u}}{\Delta}\right]^{n-1}dy,$$

$$\frac{\partial^n p_{st}}{\partial\alpha_u{}^n}=(-)^{n}\frac{n!}{\pi}\int_{-\infty}^{+\infty}\left[\frac{\Delta_{s,u}\Delta_{t,u}}{\Delta^2}\right]\left[\frac{\Delta_{u,u}}{\Delta}\right]^{n-1}dy,$$

whence

$$\delta q_r=\sum_{n=1}^{\infty}(-)^{n-1}\frac{1}{\pi}\left\{\int_{-\infty}^{+\infty}\left[\frac{\Delta_{r,u}}{\Delta}\right]^2\left[\frac{\Delta_{u,u}}{\Delta}\right]^{n-1}dy\right\}(\delta\alpha_u)^n, \tag{3}$$

$$\delta F_r=\sum_{n=1}^{\infty}(-)^{n-1}\frac{1}{\pi}\left\{\int_{-\infty}^{+\infty}(iy)\left[\frac{\Delta_{r,u}}{\Delta}\right]^2\left[\frac{\Delta_{u,u}}{\Delta}\right]^{n-1}dy\right\}(\delta\alpha_u)^n, \tag{4}$$

$$\delta p_{st}=\sum_{n=1}^{\infty}(-)^{n-1}\frac{1}{\pi}\left\{\int_{-\infty}^{+\infty}\left[\frac{\Delta_{s,u}\Delta_{t,u}}{\Delta^2}\right]\left[\frac{\Delta_{u,u}}{\Delta}\right]^{n-1}dy\right\}(\delta\alpha_u)^n. \tag{5}$$

The properties of the minors of the secular determinants of alternant hydrocarbons have been discussed by Coulson and Longuet-Higgins.[1] Using these we find that the coefficients for which n is even in (3) and odd in (4) and (5) are zero since the corresponding integrands are odd functions of y. In consequence δq_r is an odd function and δF_r, δp_{st} are even functions of $\delta\alpha_u$. It follows also that the variation of the sign of the nonzero terms depends upon the sign of $[\Delta_{u,u}/\Delta]^{n-1}$ which takes alternate signs as n takes alternate values 1, 3, 5, 7, $\cdots$ or 2, 4, 6, 8$\cdots$.

It has been customary to represent approximately the effect of a hetero system in the derivative of a conjugated hydrocarbon by just such a change $\delta\alpha_u$ at the position of substitution, u, the sign of $\delta\alpha_u$ depending upon the electronegativity of the hetero system compared with that of carbon. The dependence of the variations δq_r, δF_r, and δp_{st} upon the change $\delta\alpha_u$ in electronegativity at the position of substitution is of interest in the discussion of the chemical reactivity of conjugated systems. These questions and the relation to Wheland's localization method[3] are being considered elsewhere.[4]

It is interesting to note that the results calculated so far suggest that probably

$$\frac{1}{\pi}\int_{-\infty}^{+\infty}\left|\frac{\Delta_{u,u}}{\Delta}\right|^2dy<1$$

for all conjugated systems. This would guarantee the convergence of (3), (4) and (5) for all $\delta\alpha_u\leq 1$.

[1] C. A. Coulson and H. C. Longuet-Higgins, Proc. Roy. Soc. (London) **A191**, 39 (1947); **A192**, 16 (1948).
[2] C. A. Coulson, J. chim. phys. **45**, 243 (1948).
[3] G. W. Wheland, J. Am. Chem. Soc. **64**, 900 (1942).
[4] H. H. Greenwood, Trans. Faraday Soc. (to be published).

Thermal Conductivity of Solids and Fluids from Studies of Aggregate Matter

H. S. STRICKLER
Wm. H. Singer Memorial Research Laboratory of the Allegheny General Hospital, Pittsburgh, Pennsylvania
(Received April 4, 1952)

IN a previous note,[1] the possibility was indicated of using heat flow studies of aggregate systems to obtain thermal conductivity data of gases at high temperatures. No suitable mathematical function was suggested. Meanwhile, Wilhelm *et al.*[2] used the relation of Schumann and Voss,[3] plus a correction for the heat flow at points of good contact between grains of the aggregate. However, the derivation presented by Schumann and Voss is quite unorthodox. A better defined relation has been given by Eucken and by Russell (see Austin[4]), that of Eucken being based on Maxwell's equation for composite resistivity of a sphere surrounded by a shell of other matter. This equation is written here in the form

$$k=k_fF_1\left[\frac{(3-2P)k_s+2Pk_f}{k_f(3-P)+Pk_s}\right]+F_2, \tag{1}$$

with the coefficients F_1 and F_2 (added by the writer) being functions of surface area and conductivity of the solid material. F_2 is similar to the Δ of Wilhelm *et al.* When k_s, the conductivity of the solid, is much (more than 1,000 times) greater than k_f, the conductivity of the fluid, the bracket τ becomes merely $(3/P)-2$. (P is the porosity.)

For a given aggregate, it then follows that with different fluids

$$k_1-k_2=F_1(k_{f1}\tau_1-k_{f2}\tau_2). \tag{2}$$

In Table I some experimental values are compared with those calculated from Eq. (2), assuming $F_1\simeq 1$. Gas values used are from F. G. Keyes' tabulation, solid conductivities as given by the authors.

Some other data available in these references were not used because the thermal conductivity with H_2 or He would not be at the constant value it would attain at higher pressures. Evidently

TABLE I. $(k_1-k_2)\times10^5$.

System	P	Exptl.	Calc.	Source
Lead:				
H_2–Air	0.4	232	211	Ref. 3
Steel:				
H_2–Air	0.365	206	210	3
SiC:				
H_2–CO_2	0.428	210	173	2
H_2–Air	0.428	198	161	(Kannuluik and
Air–CO_2	0.428	12.1	11.5	Martin)
MgO:				
Air (700°C)	0.515	36.6	33.7	Calc. from 1,
Air (0°C)	0.872	12.4	12.7	F_2 const., $\tau=(3/P)-2$

molecular conduction may be quite appreciable with these gases and fine powders even at one atmosphere. (This was referred to in a somewhat different manner in the first note.[1])

It should be noted that in addition to providing a means of comparing conductivities of fluids, information may be obtained as to the conductivity of solids. The requirement is that one of the fluids (the other could be air) be of reasonably high conductivity (e.g., liquid metals). Such information is definitely needed. For example, the data of Knapp[5] for LiF and Al_2O_3 differ markedly from values recently reported. The writer has utilized the only data known to him as an example. Schumann and Voss give data at $P=0.4$ for lead granules with the fluids H_2O (1), H_2, air. Using Eq. (2) for H_2O (1) and air with $F_1=1$ and τ_2 (for air) as $(3/P)-2$, the writer obtained 9342×10^{-5} cg for lead (experimental value 8430×10^{-5}). This is considered good agreement since the conductivity of liquid water is only 153×10^{-5}.

Probably the accuracy of all such comparisons would be best with smooth particles of reasonably large size (but certainly below 4 mm, see Waddams[6]) and in other than open packing. Furthermore, any change in the surface of the grains should be avoided. Under such conditions F_1 probably would be 1. Radial flow methods would be quite convenient.

[1] H. S. Strickler, J. Chem. Phys. **17**, 427 (1949).
[2] Wilhelm, Johnson, Wynkoop, and Collier, Chem. Eng. Progress **44** (2), 105 (1948).
[3] T. E. W. Schumann and V. Voss, Fuel **13**, 249 (1934).
[4] J. B. Austin, Sympos. Thermal Insul. Materials, American Society for Testing Materials (1939).
[5] W. J. Knapp, J. Am. Ceram. Soc. **26**, 48 (1942).
[6] A. L. Waddams, J. Soc. Chem. Ind. **206**, 337T (1944).

Note on the Free Volume Equation of State for Hard Spheres

WILLIAM W. WOOD
Los Alamos Scientific Laboratory, Los Alamos, New Mexico
(Received June 3, 1952)

BUEHLER, Wentorf, Hirschfelder, and Curtiss[1] have recently discussed in geometric terms the free volume of rigid spheres obtained from the classical Lennard-Jones-Devonshire model in which the nearest-neighbor molecules are fixed at their mean cell positions without, however, introducing the usual "smearing" to obtain spherical cell symmetry. Kirkwood,[2] in his analysis of the foundations of the free volume theory, has shown that this model corresponds to a first approximation to the solution of the following integral equation for the configurational distribution function $\varphi(\mathbf{r})$:

$$\varphi(\mathbf{r})=e^{\beta(\alpha-\psi(\mathbf{r}))},$$
$$\psi(\mathbf{r})=\sum_l\int_{\text{cell}}V_{1l}(\mathbf{R}_{1l}+\mathbf{r}-\mathbf{r}')e^{\beta(\alpha-\psi(\mathbf{r}'))}d\mathbf{v}', \quad (1)$$
$$e^{-\beta\alpha}=\int_{\text{cell}}e^{-\beta\psi(\mathbf{r})}d\mathbf{v}.$$

We have omitted terms involving $\bar{E}$, the energy with all molecules at the centers of their cells, since they vanish for rigid spheres. This choice of $\varphi(\mathbf{r})$ minimizes the configurational Helmholtz free energy per molecule given by

$$A^{(1)}/kT=\int_{\text{cell}}\varphi(\mathbf{r})\log\varphi(\mathbf{r})d\mathbf{v}$$
$$+\beta/2\sum_l\int\int_{\text{cell}}V_{1l}(\mathbf{R}_{1l}+\mathbf{r}-\mathbf{r}')\varphi(\mathbf{r})\varphi(\mathbf{r}')d\mathbf{v}d\mathbf{v}', \quad (2)$$

subject to the assumptions: (1) representation of the potential energy by pairwise interactions; (2) a Hartree-like smoothing of the configurational probability density into a product of functions each depending on the position of a single molecule; (3) single occupancy of cells. The Lennard-Jones-Devonshire theory is obtained by placing $\varphi(\mathbf{r})=\delta(\mathbf{r})$ on the right-hand side of (1) and in the second term on the right-hand side of (2). The sums in Eqs. (1) and (2), formally extending over all the molecules (except the first), may be limited to the nearest-neighbors in the case of hard spheres.

It is the purpose of this note to point out that the system of Eqs. (1) may be solved exactly for rigid spheres. We consider a face-centered cubic lattice, and choose as the cell the dodecahedron Δ of Buehler *et al.* Let us denote the volume of this cell by v_Δ; this is then the range of the integrations denoted in Eqs. (1) and (2). The nearest-neighbor distance and the volume per molecule v are related by $a^3=\sqrt{2}v$. If r_0 denotes the *diameter* of the rigid spheres, the minimum volume per molecule is given by $v_0=r_0^3/\sqrt{2}$.

Our solution for the system of Eqs. (1) is

$$\psi(\mathbf{r})=\begin{cases}0, & \text{if } \mathbf{r} \text{ in } \Delta',\\ \infty, & \text{if } \mathbf{r} \text{ not in } \Delta',\end{cases} \quad (3)$$

where Δ' is a dodecahedron similar to Δ, but with altitude $(a-r_0)/2$ instead of $a/2$. This simple solution was found by an attempt to use the iteration scheme suggested by Kirkwood;[2] the latter does not converge but oscillates around the solution (3). Since the collision spheres of the nearest-neighbors never intersect Δ', we do not need to distinguish among the various cases discussed by Buehler *et al.*[1] The free volume v_f, defined as $v_f=e^{-\beta\alpha}$, is

$$v_f=v_{\Delta'}=(v^{\frac{1}{3}}-v_0^{\frac{1}{3}})^3, \quad (4)$$

and the equation of state is

$$pv/kT=1+\left(\frac{a}{r_0}-1\right)^{-1}. \quad (5)$$

It is interesting that the equation of state (5) is the same as that obtained by the combined "smearing" and delta-function approximations (see reference 1). The correct free energy $A^{(1)}$ actually turns out to be greater than obtained in the usual first (delta-function) approximation because of an inconsistency in the latter: it is actually a combination of the first and next-higher approximations and corresponds to no actual $\varphi(\mathbf{r})$.

I would like to express my thanks to Professor J. G. Kirkwood, with whom I had the opportunity of discussing the material presented here before publication.

[1] Buehler, Wentorf, Hirschfelder, and Curtiss, J. Chem. Phys. **19**, 61 (1951).
[2] J. G. Kirkwood, J. Chem. Phys. **18**, 380 (1950).

Experimental Evidence for Anomalous Population Temperatures of OH in Flames*

S. S. PENNER
Guggenheim Jet Propulsion Center, California Institute of Technology, Pasadena, California
(Received June 3, 1952)

IT is the purpose of this note to present an evaluation of the experimental evidence for and against "anomalous" temperatures of OH in flames. Experimental studies have been carried out on low pressure flames[1,2] and on flames burning at atmospheric pressure.[1,3,4] The results have usually been interpreted by using

relations which are applicable only to isothermal systems. Attempts to correct for self-absorption have been made by using isointensity methods.[3–5] For spectral lines with Doppler contour it has been demonstrated by quantitative calculations that the isointensity methods do not correct for self-absorption unless self-absorption is weak.[6] In particular, Shuler's method,[5] without allowance for the effect of frequency on intensity, has been shown to yield nonlinear plots for strong self-absorption and to be inferior to conventional procedures in the absence of self-absorption.[6] Extensive studies on the effect of self-absorption in falsifying experimental data have been carried out by Cowan and Dieke.[7] We have recently attempted to estimate absolute emission intensities for OH in low pressure flames[8] by using data obtained by Oldenberg and Rieke.[9]

It is commonly acknowledged that the use of the customary isothermal relations may yield plots which are either nonlinear or, if linear, may yield meaningless results. Unfortunately, the matter has been allowed to rest at this point. Thus, it is not uncommon to use relations applicable to isothermal systems with negligible or small self-absorption and to base conclusions on what could be spurious effects. One might, therefore, abort further discussion by noting that claims for the validity of anomalous flame temperatures are based on experimental evidence which is practically uninterpretable in a quantitative and convincing manner. This last statement is especially true for observations made at atmospheric pressure of the "inner cone" of flames, i.e., of the region in which strong temperature gradients exist.† At atmospheric pressure the thickness of the flame front may be no larger than the slit-width of the spectrograph. A significant improvement over this type of investigation has been registered by the low pressure flames of Gaydon and Wolfhard since, at low pressures, temperature gradients normal to the direction of observation can be minimized.

If we neglect, for the time being, the unhappy circumstance that we always observe regions of active combustion through cooler gas layers, there are, to begin with, discrepancies between the conclusions reached by different investigators. For example, Shuler[10] quotes Dieke and Crosswhite as having shown that the "anomalous" intensity distributions of OH observed in some atmospheric pressure flames are principally the result of self-absorption. On the other hand, Gaydon,[11] in summarizing the available information on OH, speaks of effective rotational temperatures for OH around 5700°K at atmospheric pressure and still higher temperatures at very low pressures. The important pioneering work of Gaydon and Wolfhard on low pressure flames has been checked recently; however, the experimental conditions were such that the observed "anomalies" could be explained readily on the basis of self-absorption.[2]

Shuler,[10] in quoting Broida's anomalous rotational temperatures in flames burning at atmospheric pressure, expresses the opinion that "corrections" for self-absorption can be made simply by measuring the intensity of absorption by the flame for continuous radiation. This argument is very weak, however, since absorption measurements for continuous radiation bear a close relation to self-absorption only if the experimental slit-width is small compared to the width of the spectral lines under study. This condition is probably not satisfied in Broida's work in spite of Broida's excellent spectrographic techniques.

The preceding discussion emphasizes the fact that there is at present no direct and unequivocal evidence for the existence of "anomalous" rotational or vibrational temperatures of OH in flames. On the other hand, indirect support for the existence of "anomalies" has been obtained, particularly by Gaydon and Wolfhard.[1] Nevertheless, in view of the ever-present problems arising from the existence of temperature gradients in the field of view and the equally unavoidable possibility for falsification of data as the result of self-absorption, the indirect and inferential evidence is never quite satisfying. Furthermore, even in the absence of analytical treatments on the combined effects of self-absorption and temperature gradients in producing distortions, it is frequently possible to offer plausible explanations for observed data without the invention of "anomalous" rotational temperatures for OH. For example, a decrease in apparent population temperature from the base to the top of a flame may indicate either higher temperatures of OH or else higher concentrations of OH at the base of the flame.‡ Similarly, "normal" temperatures for OH in H_2-O_2 flames but "abnormal" temperatures in the same flames containing a trace of acetylene may indicate either chemiluminescence or else the *initial* production of large quantities of OH as the result of introduction of the acetylene. The calculations on the effect of self-absorption in conventional plots used for the determination of population temperatures in flames,[6] have shown clearly that the apparent rotational temperatures are a very sensitive function of the absolute concentration of OH. Hence, even a relatively small excess of OH at the base of a flame could be responsible for a relatively high value of the population temperature. Perhaps the strongest case for the reality of the "anomalies" can be made on the basis of the increase in rotational temperature with a decrease of pressure. But even this result is not unambiguous without a careful quantitative study of the optical system, of changes in the field of view and of temperature gradients with pressure, etc. Although we have no objections, in principle, against "anomalous" temperatures and no prejudice other than that we believe that "anomalies" should be established beyond any reasonable doubt, it is our considered opinion that the available experimental evidence in support of abnormal rotation or vibration of OH in the $^2\Sigma$ state in flames is not overwhelming.

* Supported by the ONR under Contract Nonr-220(03), NR 015 210.

† No criticism is intended of the valuable work on species identification or basic spectroscopy in which the flame functions only as a means for obtaining suitable conditions for observation of spectra.

‡ Absorption data obtained by Gaydon and Wolfhard show the converse behavior (see reference 1). However, these absorption measurements were performed under such conditions that no quantitative conclusions can be derived from them. The rotational half-width of OH at a pressure of a few mm of Hg must be far less than a few tenths of a wave number. The very important work by Gaydon and Wolfhard on the use of a Fabry-Perot interferometer to obtain line contours for CH suggests that in low pressure flame the spectral lines exhibit a Doppler contour, which is in accord with expectations.

[1] A. G. Gaydon and H. G. Wolfhard, Proc. Roy. Soc. (London) **A194**, 169 (1948); **A199**, 89 (1949); **A201**, 561 (1950); **A201**, 570 (1950); **A202**, 118 (1951); **A205**, 118 (1951); **A208**, 63 (1951).

[2] Penner, Gilbert, and Weber, J. Chem. Phys. **20**, 522 (1952).

[3] G. H. Dieke and H. M. Crosswhite, *The Ultra Violet Bands of* OH, *Fundamental Data*, Bumblebee Series Report No. 87 (Applied Physics Laboratory, The Johns Hopkins University, Silver Spring, Maryland, November, 1948).

[4] H. P. Broida, J. Chem. Phys. **19**, 1385 (1951); H. P. Broida and K. E. Shuler **20**, 168 (1952).

[5] K. E. Shuler, J. Chem. Phys. **18**, 1466 (1950).

[6] S. S. Penner, Technical Report No. 5, Contract Nonr-220(03), NR 015 210, April 1952; for a summary of this work see J. Chem. Phys. **20**, 1334 (1952).

[7] R. D. Cowan and G. H. Dieke, Revs. Modern Phys. **20**, 418 (1948).

[8] S. S. Penner, J. Chem. Phys. **20**, 507 (1952).

[9] O. Oldenberg and F. F. Rieke, J. Chem. Phys. **6**, 439 (1938); R. J. Dwyer and O. Oldenberg, J. Chem. Phys. **12**, 351 (1944).

[10] K. E. Shuler, J. Chem. Phys. **20**, 1176 (1952).

[11] A. G. Gaydon, Quart. Rev., Vol. IV, No. 1, 1950.

Ionic Hydration: An Isotopic Fractionation Technique*

HAROLD M. FEDER AND HENRY TAUBE
George Herbert Jones Laboratory, University of Chicago, Chicago, Illinois
(Received May 27, 1952)

THE determination of ionic hydration is beset with semantic and experimental difficulties.[1] Following Redlich's discussion[2] of molecules *versus* ion pairs, we propose to regard ionic hydrates, $A(H_2O)_n^z$, as existing as definite species in solution if, and only if, characteristic internal vibrations can be detected by spectral or other effects. It has been shown[3] that ions may cause appreciable fractionation of the oxygen isotopes in the water in which they are dissolved. We wish to present some preliminary results indicating the connection between this effect and ionic hydration.

If an ion is hydrated in the sense mentioned above the group vibrations of bound isotopic water molecules will differ in their zero-point vibrational energy levels because of the difference in their masses. It can be readily shown that the effect of such differences is to decrease the activity of heavier species relative to lighter ones, as indicated by the following equation:

$$\alpha\times10^3\equiv1-R/R_0=\Sigma_A m_A n_A(K_A-1)/55.51, \qquad (1)$$

where R = ratio of activity of heavy to light species in the solution, R_0 = ratio of activity of heavy to light species in the absence of solute, m_A = molality of ion A, n_A = hydration number of ion A, K_A = intensity factor K_1/n_a, K_1 being the equilibrium constant for the reaction,[4] $A(H_2O)_n+H_2O^*=A(H_2O)_{n-1}(H_2O^*)+H_2O$, and α = enrichment factor defined by (1).

The assumptions involved in this derivation are: (a) heavy and light water species form an ideal solution; (b) the gross isotopic composition of the water is unchanged by the addition of solute; (c) successive steps of the water replacement reactions differ only by a statistical factor, i.e.,

$$A(H_2O)_n+H_2O^*=A(H_2O)_{n-1}(H_2O^*)+H_2O;\quad K_1=n_AK_A,$$
$$A(H_2O)_{n-1}(H_2O^*)+H_2O^*=A(H_2O)_{n-2}(H_2O^*)_2+H_2O; \qquad (2)$$
$$K_2=(n_A-1)K_A/2,\quad \text{etc.}$$

Experimental.—The isotopic ratio (mass 46/mass 44) in carbon dioxide may be measured with high precision. By maintaining a very large molar ratio of water to carbon dioxide such a measurement faithfully reflects the relative activity of water species via the equilibrium

$$H_2O^{18}(\text{soln.})+CO_2{}^{16}(g)=H_2O^{16}(\text{soln.})+CO^{16}O^{18}(g). \qquad (3)$$

The water used was from a large stock of ordinary distilled water stored in Pyrex. No appreciable change in composition took place over a period of one year. The anhydrous solutes used were vigorously dried and dissolved with minimum exposure to air. Solutions (*ca* 10 grams) were degassed on the vacuum line by repeated cycles of freezing, pumping, and thawing, and carbon dioxide (0.2 millimole) was admitted to the equilibration vessel. After equilibration (5–30 days) at a controlled temperature the gas was sampled, dried, and measured for isotopic ratio.[5] Each solution was compared with pure water for which all the conditions of preparation, equilibration, sampling, and measurement were made as nearly identical as possible. The results are shown graphically in Figs. 1 and 2. The precision (standard deviation) of a single measurement of α is ±0.2. The following single experiments at 25°C are also reported: $[Coen_3]Cl_3$ at 0.4 *m*, $\alpha=0.0$; $Cr(ClO_4)_3$ at *ca* 1 *m*, $\alpha=3.4\pm1.8$[3]; α for $MgCl_2$ and $Mg(ClO_4)_2$, both at 2.84 *m*, differed by less than 0.2.

Discussion.—From these data some conclusions may be tentatively drawn. The approximately linear relation between α and the molality of solute indicates the probable constancy of the hydration numbers of the ions tested to fairly high concentrations. The deviation from linearity for very concentrated solutions may be symptomatic of cooperative effects among the ions prior to the onset of crystallization. The case of hydrochloric acid will require special consideration.

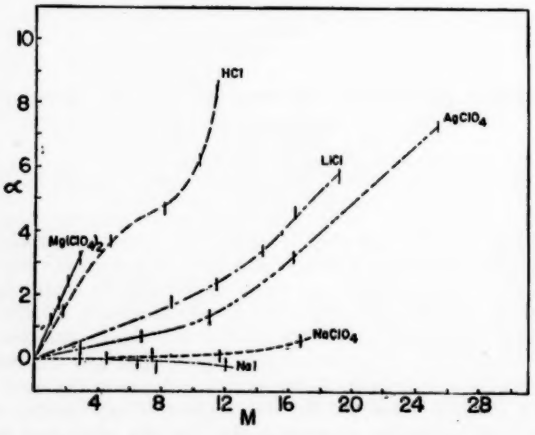

FIG. 1. Enrichment *vs* molality for solutes at 25°C.

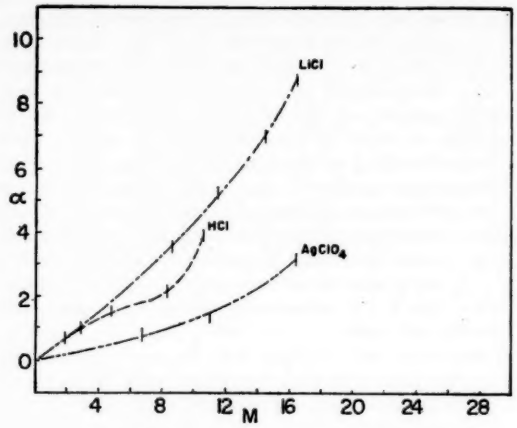

FIG. 2. Enrichment *vs* molality for solutes at 4°C.

A reasonable and consistent distribution of the separate effects due to cations and anions can be made only if the ions ClO_4^-, Cl^-, I^-, Na^+ and $Coen_3^{+3}$ are assumed to be not detectably hydrated in the present sense. From the initial slopes of Figs. 1 and 2 the quantities $n_A(K_A-1)\times10^2$ may be estimated: Li^+ (25°) 1.0; Li^+ (4°), 2.0; Ag^+ (25°) 0.7; Ag^+ (4°) 0.7; H^+ (25°) 4.6; H^+ (4°) 2.0; Mg^{++} (25°) 6.2; Mg^{++} (4°), 7.1; Cr^{+++} (25°), 19±10. The effect exhibits a variation due to ionic charge, radius, and type which is qualitatively reasonable.[6] The experiment with a trivalent cation with a completely filled inner sphere, $(Coen_3)^{+3}$, is particularly significant because it indicates the probable identity of the hydration number and the number of water molecules in the *inner* sphere.

Experimental work is being continued. The theoretical implications of these measurements will be discussed in a future publication.

* This work was supported by funds from the ONR under contract N6-ori-02026.

[1] J. O'M. Bockris, Quart. Rev. **3**, 173 (1949).
[2] O. Redlich, Chem. Revs. **39**, 333 (1946).
[3] J. P. Hunt and H. Taube, J. Chem. Phys. **19**, 602 (1951).
[4] The asterisk indicates the heavier species. All species are in solution.
[5] The authors wish to express their appreciation to Dr. Harold C. Urey and Dr. Samuel Epstein for the use of their precise mass spectrometer.
[6] J. D. Bernal and R. H. Fowler, J. Chem. Phys. **1**, 515 (1933).

Infrared Spectra of Solutions of Iodine in Mesitylene

N. S. HAM, A. L. G. REES, AND A. WALSH
Chemical Physics Section, Division of Industrial Chemistry, Commonwealth Scientific and Industrial Research Organization, Australia
(Received May 26, 1952)

PIMENTEL, Jura, and Grotz[1] have published spectra of mesitylene, with and without iodine in solution, which they offer as evidence for the formation of a complex between mesitylene and iodine. They claim that their spectra support the interpretation of the ultraviolet absorption spectrum of iodine dissolved in mesitylene in terms of a 1:1 solvent-solute complex.[2] Since these results are inconsistent with the infrared spectrum of iodine in benzene[3] and with some recent results on iodine in carbon tetrachloride—benzene solutions in the visible and ultraviolet regions,[4] we have repeated the infrared spectra of mesitylene solutions over the range 2.5μ–15μ.

Mesitylene, as usually supplied, has infrared bands which are not given in the spectrogram issued by the National Bureau of

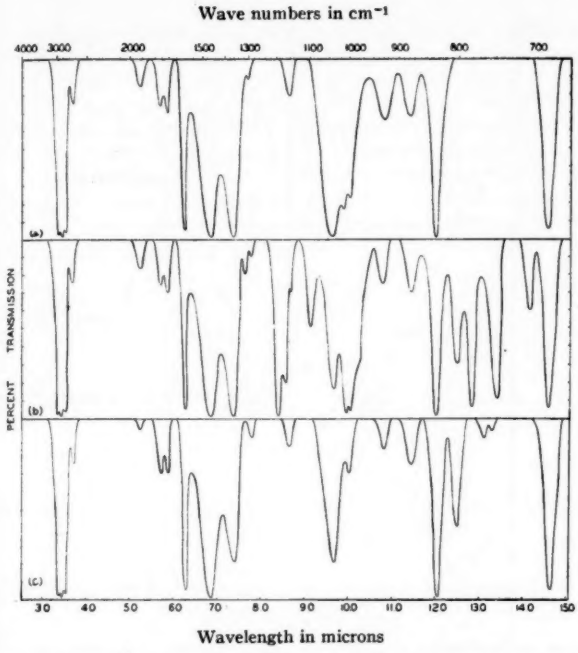

FIG. 1. Infrared absorption spectra of (a) either a purified sample of mesitylene or a saturated solution of iodine in mesitylene, (b) an unpurified sample of mesitylene, (c) a saturated solution of iodine in unpurified mesitylene. Cell thickness 0.05 mm.

Standards.[5] Using such an unpurified sample, a change in the spectrum of mesitylene was observed on the addition of iodine. This change was similar to, but not identical with, that reported by Pimentel, Jura, and Grotz. Mesitylene was therefore purified as follows—a B.D.H. sample was refluxed with dil. H_2SO_4, washed with NaOH and water, shaken with saturated $NaHSO_3$ solution, washed, dried, and fractionated. The middle fraction was sulfonated, the sulfonic acid recrystallized and desulfonated, and the mesitylene steam-distilled under reduced pressure, washed with $NaHCO_3$, dried, and fractionated. This purification was based on a method used by Smith and Cass.[6] The spectrum of purified mesitylene was identical with that given by the National Bureau of Standards.[5]

The spectrum of the saturated solution of iodine in the purified mesitylene was indistinguishable from that of mesitylene. No new bands were observed. (Experimental limits: ± 2 cm^{-1}, ± 3 percent intensity.) The very strong Raman-active totally symmetric stretching vibration at 998 cm^{-1}, which was weak in the infrared spectrum of liquid mesitylene, was not intensified or changed in position on the addition of iodine. The band at 1214 cm^{-1}, which Pimentel, Jura, and Grotz claim to be due to the breakdown of the selection rules in the "complex," was not present in our spectrum. Other new bands and changes in intensities observed by Pimentel, Jura, and Grotz were presumably due to impurities in their mesitylene. In solutions from which a crystalline complex can be isolated (e.g., pyridine), infrared evidence[3] shows that a difference exists between the spectrum of the solvent and that of the solution.

Our results are strong evidence that there is no formation of a 1:1 complex between iodine and mesitylene; they are, however, consistent with the interpretation of solvent effects in terms of the "cage" theory.[7]

[1] Pimentel, Jura, and Grotz, J. Chem. Phys. **19**, 513 (1951).
[2] H. A. Benesi and J. H. Hildebrand, J. Am. Chem. Soc. **71**, 2703 (1949).
[3] Ham, Rees, and Walsh, Nature **168**, 110 (1952).
[4] A. L. G. Rees and J. P. Shelton, in preparation.
[5] "Infrared Spectrograms"—American Petroleum Institute Research Project 44, National Bureau of Standards Chart Nos. 169, 354, and 1104.
[6] L. I. Smith and O. W. Cass, J. Am. Chem. Soc. **54**, 1606 (1932).
[7] N. S. Bayliss and A. L. G. Rees, J. Chem. Phys. **8**, 377 (1940); N. S. Bayliss, Nature **163**, 764 (1949).

Distribution of Segments in a Coiling Polymer Molecule*

P. DEBYE AND F. BUECHE
Department of Chemistry, Cornell University, Ithaca, New York
(Received June 5, 1952)

DURING the past few years it has been customary in many calculations involving coiling polymers to assume that the distribution of segments about the center of mass of the molecule is Gaussian. Until now, no real test of this assumption has been made. In this note we give the equations for the true distribution and show how it deviates from the assumed form.

The calculation of the probability that a single chain segment, say the Kth, is at a vector distance s_k from the center of mass may be carried out along familiar lines. We have done this by use of the Markoff integral method.[1] The result is nearly exact and is limited only by the fact that it makes use of the same assumptions Kuhn[2] employs in obtaining a Gaussian end-to-end distribution. It turns out to be

$$P(s_k)=\{(2/9)\pi R^2[u^3+(1-u)^3]\}^{-\frac{3}{2}}\exp\{-9s_k^2/2R^2[u^3+(1-u)^3]\}.$$

In this expression R^2 is the chain's mean square end-to-end distance and $U\equiv K/N$, where N is the number of segments in the chain. It has been called to our attention that this relation has previously been derived by Isihara.[3]

Since we really wish to know the probability that *any* segment is at a distance s from the center of mass of the molecule, we must integrate the above expression over all segments, i.e., $0\leqslant u\leqslant 1$. This may be done in series form by making the substitution

$$1/\cos^2\phi=u^3+(1-u)^3 \quad 0\leqslant u\leqslant \tfrac{1}{2}.$$

Upon integration one finds the following expressions for the distribution of segments about the center of mass of the molecule:

$$P(s)=4e^{-x}\left[1-\frac{1}{1\cdot 3}(6x)+\frac{1}{1\cdot 3\cdot 5}(6x)^2-\cdots\right]$$

for small $x\equiv 9s^2/2R^2$, and

$$P(s)\cong\frac{2e^{-x}}{3x}\left[1+\frac{1}{2}\left(\frac{1}{3x}\right)+\frac{1\cdot 3}{2\cdot 2}\left(\frac{1}{3x}\right)^2+\frac{1\cdot 3\cdot 5}{2\cdot 2\cdot 2}\left(\frac{1}{3x}\right)^3+\cdots\right]$$

for large X.

These formulas have also been checked by graphical integration. The result is plotted as the solid curve in Fig. 1. For comparison we have also plotted (dashed curve) the common Gaussian distribution usually substituted for the actual one. It is given by

$$(9/\pi R^2)^{\frac{3}{2}}\exp[-9s^2/R^2].$$

As one sees, the agreement is qualitatively satisfactory. However, real discrepancies exist. In particular, the Gaussian form

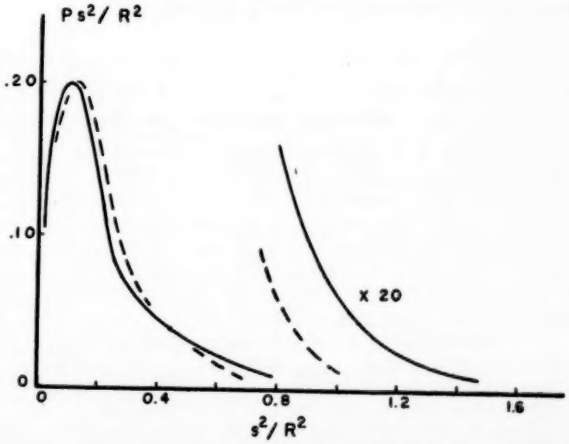

FIG. 1. Theoretical (heavy line) and Gaussian (dashed line) distribution of segments in a coiling polymer molecule.

underestimates the extension of the molecules in space. For most purposes these discrepancies should be only of minor concern. On the other hand, those phenomena which depend seriously on the outer contacts of polymer molecules (such as concentration dependence of viscosity and thermodynamic interactions in good solvents) may be sufficiently sensitive to the segmental distribution to illustrate the invalidity of the Gaussian representation.

* The work discussed herein was performed as a part of a research project sponsored by the Reconstruction Finance Corporation, Synthetic Rubber Division, in connection with the U. S. Government Synthetic Rubber Program.

[1] See, for example, S. Chandrasekhar, Revs. Modern Phys. **15**, 1 (1943).
[2] W. Kuhn, J. Polymer Sci. **1**, 183 (1946).
[3] A. Isihara, J. Phys. Soc. Japan **5**, 201 (1950).

Formula for the Melting Points of Inorganic Compounds of Type MXO_n

SHIZUO FUJIWARA
University of Electro-Communications, Tokyo, Japan
(Received June 6, 1952)

AN empirical expression (1) for the melting points of the inorganic compounds of type MXO_n has been obtained as the function of the ionic radius and the ionic polarizability of the constituent atoms, where M is the cation and XO_n is the anion, e.g., in the case of alkali nitrates, M denotes lithium, sodium, and potassium ion, etc., and XO_n nitrate ion, NO_3^-.

$$T\cdot(\alpha_+-\alpha_-)^{1/6}=a-b(r_-/r_+). \qquad (1)$$

In the expression (1), T is the melting point of the salt in absolute temperature, and α and r represent the polarizability and ionic radius of the ion, respectively. Positive signs are suffixed to α and r of the metal ion M, and negative signs to those of the central ion, $X^{(2n-1)+}$, of the negative ion.

According to the results of the examination of the known data of T,[1,2,3] α,[4,5] and r,[6,7] the values of a and b are characteristic for one series of compounds having different cations and the same anion, and a clear-cut linear correlation expressed as (1) has been obtained. In Table I, the values of a and b for several series of salts are given, and the linearity is shown in Figs. 1 and 2. The polarizabilities of the ion $X^{(2n-1)+}$ are taken as equal as the cubes of the ionic radius of $X^{(2n-1)+}$. Only the polarizability of Si^{4+} in the silicates has been taken as 0.04 (10^{-24} cm^3).[4] When the values of the ionic radius of Al^{3+} and the polarizabilities of cations are taken out of Goldschmidt's data, we can obtain an approximately straight line for the aluminates as is shown in Fig. 2, whereas, when we take those out of data of Pauling and of Fajans and Joos, the presented graph deviates far from a straight line. The melting point values of aluminates taken out of reference 1 are satisfying and those out of reference 2 are not.

TABLE I.[a]

	$M_2O\cdot B_2O_3$	$M_2O\cdot CO_2$	$M_2O\cdot SiO_2$	$MO_2\cdot SiO_2$	$MO_2\cdot SiO_2$
a	0.195	0.178	0.183	0.472	0.975
b	0.482	0.450	0.200	0.904	1.157
		$M_2O\cdot N_2O_5$		$MO\cdot N_2O_5$	
a	$0.113\left[\begin{matrix}\alpha_+(F)\\ r_+(P)\end{matrix}\right]$	$0.097\left[\begin{matrix}\alpha_+(G)\\ r_+(G)\end{matrix}\right]$		$0.175\left[\begin{matrix}\alpha_+(F)\\ r_+(P)\end{matrix}\right]$	
b	1.57	0.440		0.88	
		$M_2O\cdot SO_3$			$MO\cdot SO_3$
a	$0.250\left[\begin{matrix}\alpha_+(F)\\ r_+(P)\end{matrix}\right]$	$0.255\left[\begin{matrix}\alpha_+(F)\\ r_+(G)\end{matrix}\right]$		$0.263\left[\begin{matrix}\alpha_+(G)\\ r_+(G)\end{matrix}\right]$	0.36
b	0.480	0.495		0.666	0.62

[a] Notes of P, F, G suffixed to α_+ and r_+ in the table refer to the author of the data, Pauling, Fajans, and Goldschmidt, respectively. Values of a and b with no reference note are obtained by r_+ and α_+ given by Goldschmidt.

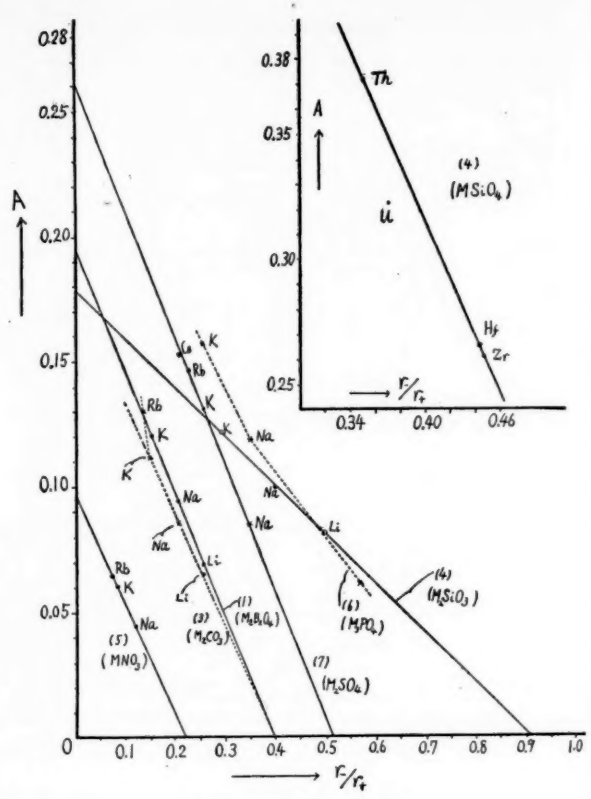

FIG. 1. $A=T\cdot(\alpha_+-\alpha_-)^{1/6}$.

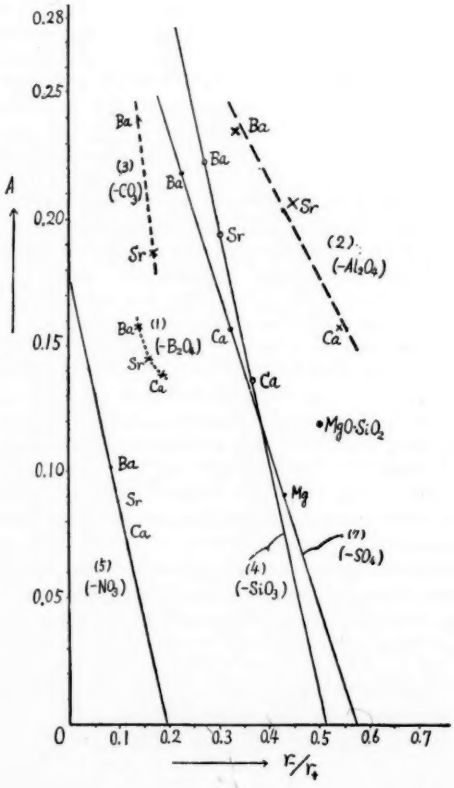

FIG. 2.

The inference of the expression (1) is that T tends to become very large as the polarizabilities approach one another. It is very important that "melting point" is presented as a function of the variables characteristic for atoms, such as ionic radius and polarizability. The more detailed discussion for special compounds is in press now in the Bulletin of the Chemical Society of Japan. The author expresses his sincere thanks to Professor K. Kimura of Tokyo University and Professor G. T. Seaborg of University of California, who have kindly reviewed the advanced copy of this article and given valuable suggestions.

[1] Landolt-Börnstein, Physik.-Chem. Tabellen.
[2] International Critical Tables.
[3] Smithonian Physical Tables, p. 254 (1933).
[4] V. M. Goldschmidt, Geochemische Verteilungsgesetze der Elemente, Vol. 7, 60 (1933).
[5] K. Fajans and G. Joos, Z. Physik. 23, 1 (1924).
[6] V. M. Goldschmidt, Chem. Ber. 60, 1268 (1927).
[7] L. Pauling, J. Am. Chem. Soc. 49, 765 (1927).

The Use of Nuclear Induction in the Kinetic Study of the Reaction $Eu^{+3}+\varepsilon \rightarrow Eu^{+2}$

T. W. Hickmott* and P. W. Selwood
Department of Chemistry, Northwestern University, Evanston, Illinois
(Received June 9, 1952)

Conger and Selwood[1] have shown that the effective magnetic moments of paramagnetic ions in aqueous solution, as computed from proton relaxation times, are subnormal except where spin-orbital coupling is weak or absent. Thus, while the moments of the ions Eu^{+2} and Eu^{+3} as derived from susceptibility measurements at room temperature stand in the ratio 7.9/3.9 = 2.0, the ratio for the same ions as derived from proton relaxation measurements is 3.0/0.20 = 15. This circumstance permits considerable precision in the use of nuclear induction for studying the kinetics of reduction of trivalent europium in solution by metallic zinc. The method may have applications to other systems.

A 0.0550M solution of $EuCl_3$ was prepared by dissolving Eu_2O_3 in dil. HCl. For this experiment to be successful it was essential that the europium be *magnetically* pure, i.e., free from gadolinium.[2] The europium solution was then placed in the nuclear induction apparatus as previously described, and C. P. zinc dust in excess was added to the solution. Stirring was effected by the hydrogen evolved.

The initial proton relaxation time was too long to measure conveniently, but as reduction proceeded a workable range was soon reached. The minimum relaxation time observed corresponded to an effective moment for Eu^{+2} of 2.98 magnetons, in good agreement with the value (3.0) previously reported.[3] The reason for this being less than half the "susceptibility" moment is not yet understood. The experimental results are given in Table I.

According to Bloembergen, Purcell, and Pound[4]

$$1/T_1 = 12\pi^2\gamma^2\eta N\mu^2/5kT^0,$$

where T_1 is the relaxation time, γ the gyromagnetic ratio, η the viscosity, N the concentration of paramagnetic ions, μ the effective moment of the paramagnetic ions, k the Boltzmann constant, and T^0 the temperature. The viscosity of the europium solution was essentially that of water; hence we may write $1/T_1 = CM\mu^2$ where C is a constant and M the molar concentration of the europium. The constant C may be evaluated by calibration of the apparatus with Cu^{+2} ions for which μ will be assumed to be 2.0. Hence $M = 1/(2.98)^2CT_1$. This involves the assumption that the Eu^{+2} ion is solely responsible for changes in T_1. This assumption is valid because of the small influence of Eu^{+3} as compared with that of Eu^{+2}. For instance, a 0.25-millimolar solution of Eu^{+2} would give the same proton relaxation time as a 55-millimolar solution of Eu^{+3}.

TABLE I. The reduction $Eu^{+3} \rightarrow Eu^{+2}$.

Reaction time (sec)	Proton relaxation time (millisec)
90	20.0
150	14.0
195	11.3
255	9.2
360	8.3
390	7.5

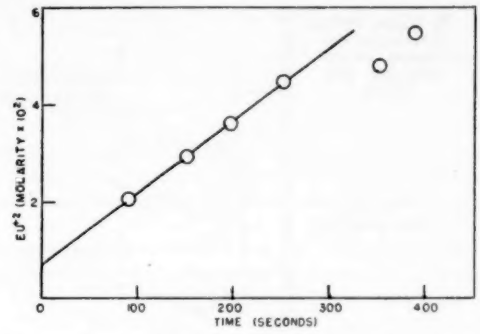

FIG. 1. Concentration of Eu^{+2} as a function of reaction time.

As shown in Fig. 1, a plot of Eu^{+2} concentration against time gives a straight line for the first part of the reaction. This indicates a zero-order reaction, with $k = 1.54 \times 10^{-4}$ moles liters^{-1} secs^{-1}. In view of the large negative free energy change, the reaction on the surface of the zinc should be rapid. The initial rate controlling steps are therefore probably the desorption of Eu^{+2} from the surface and its diffusion through the solution. At a later stage where the reaction is no larger zero-order, the rate controlling process is probably diffusion of reactant on to the zinc surface.

The fact that the intercept on the concentration axis is not zero for zero time is partly due to neglect of the Eu^{+3} contribution to the relaxation time, and partly to the initial rate dependence on diffusion of product.

* Sinclair Refining Company Fellow.
[1] R. L. Conger and P. W. Selwood, J. Chem. Phys. 20, 383 (1952).
[2] B. M. W. Trapnell and P. W. Selwood, Nature 169, 840 (1952).
[3] In reference 1, Table II, μ_N for Eu^{+2} given as 0.30 should be 3.0.
[4] Bloembergen, Purcell, and Pound, Phys. Rev. 73, 679 (1948).

The Thermal and Photochemical Decomposition of H_2O_2 Vapor in the Presence of Foreign Gases

Frank S. Stone* and Hugh S. Taylor
Frick Chemical Laboratory, Princeton University, Princeton, New Jersey
(Received June 19, 1952)

It is generally accepted that the photolysis of H_2O_2 vapor[1] proceeds according to (1),

$$H_2O_2 + h\nu = OH + OH, \qquad (1)$$

and the reaction may be used as a source of hydroxyl radicals.[2] Volman[3] has listed the experimental difficulties encountered in the photolysis of H_2O_2 vapor, and in the present work a compromise was effected by saturating a carrier gas with H_2O_2 vapor in a bubbler at 90°C and then passing the mixture at a high flow rate through an irradiated quartz tube (Fig. 1) contained in a thermostat *BCDE* maintained at temperatures above 90° to prevent condensation. A Hanovia Sc-2537 special quartz mercury vapor discharge tube was used as the source of ultraviolet light.

Thermal decomposition in the quartz vessel, as estimated from volumetric analyses of condensates in F, depended greatly on the rate of transfer of H_2O_2 from A to F (Fig. 2). Figure 3 illustrates the extent of photolysis, over and above the thermal decomposition at 110°C, using a transfer rate of 500 milligrams of H_2O_2 per hour with nitrogen as carrier.

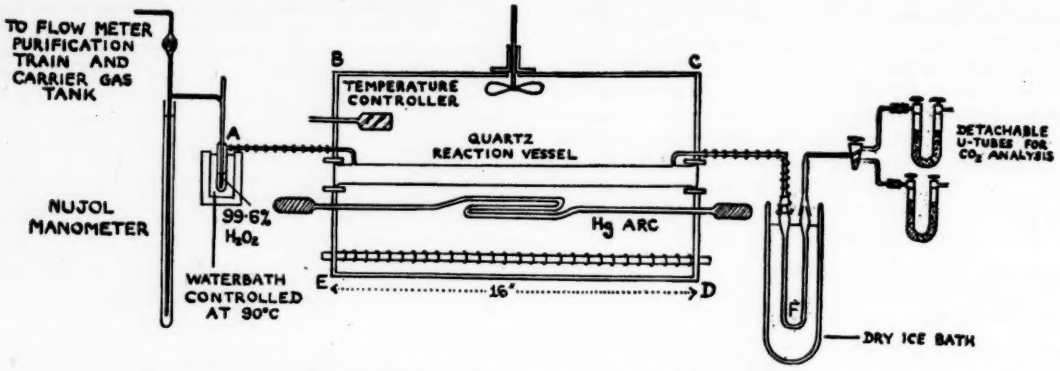

FIG. 1. Flow system for the photolysis of hydrogen peroxide vapor in the presence of a carrier gas.

Nitrogen was replaced by CO as carrier in order to study the reaction of OH radicals with CO. No CO_2 was formed during the dark reaction, but upon irradiation substantial quantities of CO_2 were produced (Table I). CO_2 was estimated gravimetrically by

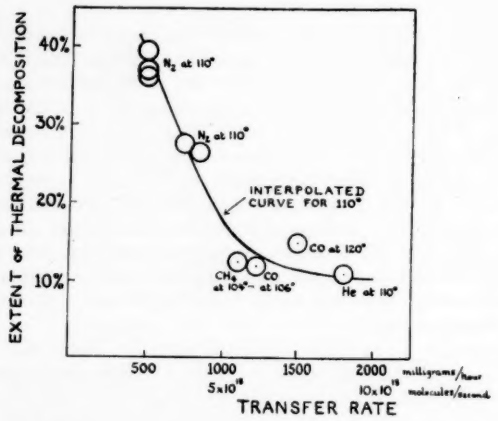

FIG. 2. Thermal decomposition of H_2O_2 vapor as a function of its rate of transfer through the reaction vessel, with different gases as carriers.

absorption in U-tubes containing "Ascarite." A low temperature and a high transfer rate favor a low thermal decomposition. For CO_2 production, however, a compromise between low thermal decomposition and low transfer rate is necessary. The former implies a higher concentration of the absorbing species (*viz.*, undecomposed H_2O_2), and the latter implies a longer time in the absorption path. Both of these factors make for an increased concentration of OH radicals. Temperature has no pronounced effect on the reaction.†

It is possible to make a rough estimate of the number of OH radicals available in these experiments with carbon monoxide. The rate of transfer of H_2O_2 was $6\pm2\times10^{18}$ molecules per second. From an extrapolation of the results with nitrogen (Fig. 3) and from measurements with helium as carrier, it is estimated that about 3 percent of the H_2O_2 would have decomposed photochemically to water if CO had been inert, i.e., 2×10^{17} molecules of water (in addition to "thermal" water) would have left the tube per second, corresponding to a rate of formation of 5.4×10^{16} molecules/sec/cc. But photolytic water is only formed by the reaction

$$OH+H_2O_2=H_2O+HO_2, \quad (2)$$

and apart from recombination this is the only reaction destroying OH, so it is estimated that about 5×10^{16} OH radicals were available for reaction per second per cc.‡

In fact, however, the available OH radicals divide between reactions (2) and (3):

$$OH+CO=CO_2+H. \quad (3)$$

In spite of this, the observed rate of formation of CO_2 (Table I) is greater than the *total* rate at which we estimate OH radicals to be available from (1). Furthermore, analyses of condensates present after irradiation do not favor the suppression of (2). These facts point to some regeneration of OH, and reaction (4) is suggested,

$$HO_2+CO=CO_2+OH, \quad (4)$$

in preference to the usual reaction (5) for disposal of HO_2.

$$HO_2+HO_2=H_2O_2+O_2. \quad (5)$$

Hydrogen atoms from (3) will form HCO,[4] but then since oxygen is present from the thermal decomposition, reaction (6) may be preferred[5] to aldehyde formation:

$$HCO+O_2=CO+HO_2. \quad (6)$$

Hydrogen atoms may also disappear by the fast reaction[6]

$$H+H_2O_2=H_2O+OH. \quad (7)$$

Experiments were also made with methane and with ethane. The condensates obtained during irradiation in each case possessed strong organic odors, indicating that reaction of OH with CH_4 and C_2H_6 had taken place, probably forming alkyl radicals and

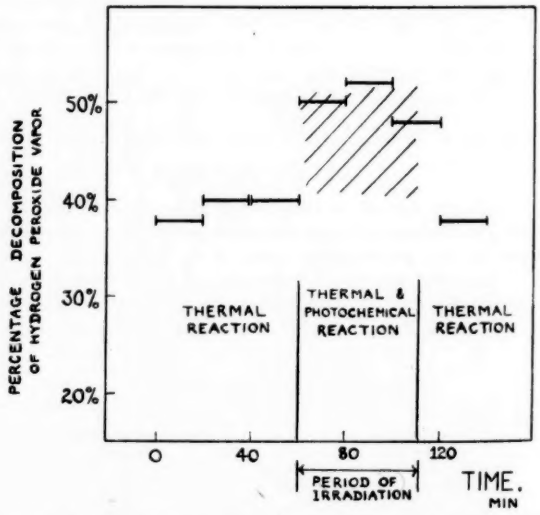

FIG. 3. Thermal and photochemical decomposition of H_2O_2 vapor at 110°C, using nitrogen as carrier gas. Flow rate, 1.7 cc/sec. Rate of transfer of H_2O_2 vapor, 500 milligrams/hr (1×10^{18} molecules/sec). Condensates were analyzed at 20-minute intervals.

TABLE I.

Temperature of reaction vessel (°C)	Extent of thermal decomposition (dark reaction) (%)	H_2O_2 vapor entering reaction vessel (molecules per sec)	CO_2 formed during irradiation (molecules per second per cc)
132	20.5	69×10^{17}	8.7×10^{16}
120	15.3	77×10^{17}	8.1×10^{16}
97	14.3	47×10^{17}	6.8×10^{16}
105	12.0	55×10^{17}	10.5×10^{16}

CO Flow rate = 3.7 cc/sec

water. In neither case could the organic products be identified. Ammonia was also investigated, but the saturated solution in 99.6 percent H_2O_2 became unstable on standing and subsequent agitation produced a violent explosion. It is proposed to make further investigations with these gases.

Our thanks are due to the Buffalo Electrochemical Company, Inc., for a generous gift of concentrated hydrogen peroxide.

* Commonwealth Fund Fellow, 1950–51. Present address: Department of Chemistry, University of Bristol, Bristol, England.
[1] Urey, Dawsey, and Rice, J. Am. Chem. Soc. **51**, 1371 (1929).
[2] von Elbe, J. Am. Chem. Soc. **55**, 62 (1933).
[3] D. H. Volman, J. Chem. Phys. **17**, 947 (1949).
† von Elbe (see reference 2) reported almost twice as much reaction at 40°C as at 27°C. However, as the yields were lower than those reported here by a factor of a thousand, it is likely that the probable error was large.
‡ Recombination of OH does of course occur, but its effect will be similar whether the carrier is active or inert and so it will not modify the number of OH radicals available for reaction.
[4] Frankenburger, Z. Elektrochem. **36**, 757 (1930).
[5] Faltings, Groth, and Harteck, Z. physik. Chem. **B41**, 15 (1938).
[6] Geib and Harteck, Z. physik. Chem. **A170**, 1 (1934).

The Second Virial Coefficient of Benzene

P. G. FRANCIS AND M. L. MCGLASHAN*
Chemistry Department, Reading University, England
AND
S. D. HAMANN AND W. J. MCMANAMEY
C.S.I.R.O., High Pressure Laboratory, Sydney University, Australia
(Received May 26, 1952)

EVERETT and Penney[1] have recently reviewed the experimental data on the second virial coefficient (B) of benzene and drawn attention to the disagreement between the results of different experimenters. This is apparent in Fig. 1 where the values of $-B$ found by Eucken and Meyer[2] and by Baxendale and Enüstün[3] are seen to be considerably larger than those of Lambert, Roberts, Rowlinson, and Wilkinson[4] and of Casado, Massie, and Whytlaw-Gray.[5]

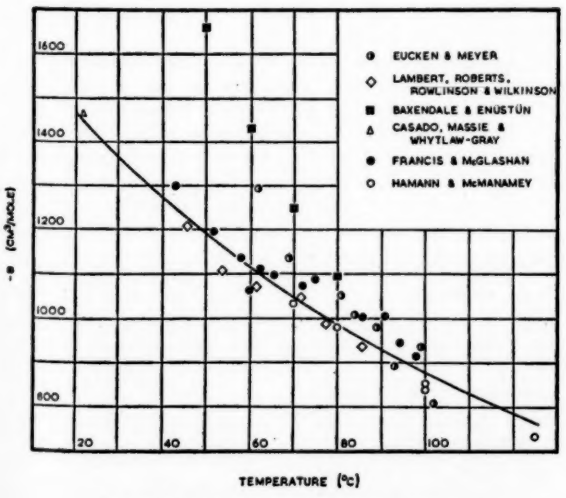

FIG. 1. Second virial coefficient of benzene.

In this note we report two independent series of measurements aimed at resolving these discrepancies.

The measurements at Reading were made in a "Boyle's apparatus" similar to that described by Alexander and Lambert.[6] Two different samples of benzene were used. The first of these was prepared at Reading by treatment with sulfuric acid followed by fractional distillation and then by repeated fractional crystallizations. The purity of the sample so prepared was calculated from the shape of the freezing point curve and was found to be 99.95 ± 0.05 moles percent. The second sample was kindly supplied by Professor J. Timmermans from the Bureau International des Etalons Physico-chimiques in Brussels. Considerable care was taken to de-gas the liquid so as to ensure that a gas-free sample of vapor was introduced into the burette. The results are given below.

Reading sample:

t°C	43.1	51.9	60.0	62.9	65.7	75.1	85.9	94.2	99.1,
$-B$/cm³ mole^{-1}	1300	1198	1064	1112	1099	1090	1004	947	916.

Brussels sample:

t°C	58.1	72.1	90.8,
$-B$/cm³ mole^{-1}	1137	1075	1006.

The measurements at Sydney were made by a comparative method which has been described before.[7]

Mr. I. Brown, C.S.I.R.O., Melbourne, kindly supplied a purified sample of benzene for these determinations. The pressures were between 15 percent and 75 percent of the saturation pressure of benzene, and in this range no virial coefficients higher than the second are needed to describe the behavior of the vapor. The results are given below:

t°C	70	80	100	100	125,
$-B$/cm³ mole^{-1}	1035	971	852	839	733.

Both sets of data have been plotted in the diagram. They lie close to the curve

$$B/\text{cm}^3\ \text{mole}^{-1} = 70 - 13.2\times10^7/T^2,$$

which Everett and Penney selected after rejecting Baxendale and Enüstün's results, and they provide further justification for that choice.

* Now at Canterbury University College, Christchurch, New Zealand.
[1] Everett and Penney, Proc. Roy. Soc. (London) (to be published).
[2] Eucken and Meyer, Z. physik. Chem. **B5**, 452 (1929).
[3] Baxendale and Enüstün, Phil Trans Roy Soc (London) **A243**, 176 (1951).
[4] Lambert, Roberts, Rowlinson, and Wilkinson, Proc Roy Soc (London) **A196**, 113 (1949).
[5] Casado, Massie, and Whytlaw-Gray, Proc. Roy. Soc. (London) **A207**, 483 (1951).
[6] Alexander and Lambert, Trans. Faraday Soc. **37**, 421 (1941).
[7] Hamann and Pearse, Trans. Faraday Soc. **48**, 101 (1952).

A Two-Path Method for Eliminating the Effects of Self-Absorption on Temperature for Isothermal Flames*

S. S. PENNER
Guggenheim Jet Propulsion Center, California Institute of Technology, Pasadena, California
(Received June 3, 1952)

IT is the purpose of the present note to outline a two-path method for the determination of flame temperatures. The method is valid for *isothermal* systems and *spectral lines with Doppler contour*. All errors arising from self-absorption are eliminated. Practical applications are made by determining the ratio of the total intensity observed when the flame is viewed with a cool blackbody as background to the total intensity obtained with a cool mirror as background. For the sake of simplicity it will be assumed that the reflectivity of the mirror is unity. Spectroscopic studies are made in the usual way, i.e., with a low

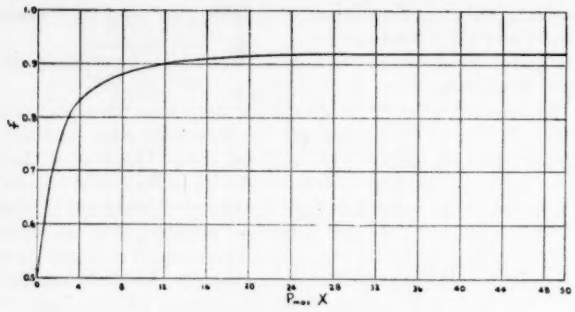

FIG. 1. The quantity $f(P_{max}X)$ as a function of $P_{max}X$ for spectral lines with Doppler contour.

resolution spectrograph since only the *ratios* of total intensities need to be determined. The method is related to a procedure described in a previous publication for spectral lines with resonance contour[1] but differs in so far as it utilizes the fact that observations on visible and ultraviolet spectra are usually made for individual spectral lines. Using the notation of a previous paper,[2] it is found that for spectral lines with Doppler contour the total observable intensity of the line identified by the index K and with center at the frequency ν_{lu} is[3]

$$\{A[\nu_{lu}(K)]\}_1 \simeq R^0(\nu_{lu})(mc^2/2\pi kT\nu_{lu}^2)^{-\frac{1}{2}}[P_{max}(K)X] \times\{\sum_{n=0}^{\infty}[(n+1)^{\frac{1}{2}}(n+1)!]^{-1}[-P_{max}(K)X]^n\}, \quad (1)$$

if the light reaching the receiver traverses the flame only once. If intensities obtained by allowing the light to traverse the flame twice are identified by the subscript 2, then it is evident from Eq. (1) that

$$\{A[\nu_{lu}(K)]\}_1/\{A[\nu_{lu}(K)]\}_2 = f(P_{max}X). \quad (2)$$

The quantity f is plotted as a function of $P_{max}X$ in Fig. 1. But, for spectral lines with Doppler contour and $h\nu_{lu} \gg kT$,[2]

$$P_{max}(K)\,X = \text{constant} \times X \times [g_u(q_{lu})^2]_K \times \exp[-(E_u - h\nu_{lu})/kT].$$

The recommended procedure, subject to the limitations stated earlier, is seen to involve only the measurement of intensity ratios, the determination of $P_{max}(K)X$ from Fig. 1, and the calculation of T from the relation

$$\frac{\partial \ln\{P_{max}(K)X/[g_u(q_{lu})^2]_K\}}{\partial(E_u - h\nu_{lu})} = -1/kT. \quad (3)$$

For isothermal emitters with self-absorption the suggested procedure has the advantage of extreme simplicity. For spectral lines with combined Doppler- and collision-broadening, the quantity f is no longer a universal function of $P_{max}X$ but depends also on the natural damping ratio.

* Supported by ONR under Contract Nonr-220(03), NR 015 210.

[1] S. S. Penner, J. Chem. Phys. **19**, 272, 1434 (1951).
[2] S. S. Penner, J. Chem. Phys. **20**, 507 (1952).
[3] R. Ladenburg, Z. Physik **65**, 200 (1930).

Infiuence of Light on the Secondary Emission in a Low Frequency Electrodeless Discharge: Joshi Effect

A. P. SAXENA
Holkar College, Indore, India
AND
N. A. RAMAIAH
Chemical Laboratories, Benares Hindu University, Banaras, India
(Received May 26, 1952)

THE present communication reports a few significant observations made during the studies of Joshi effect,[1] *viz.*, an instantaneous photovariation (Δi), usually though not invariably diminution ($-\Delta i$), of the current (i) in a low frequency electrodeless discharge in water vapor. Cylindrical (glass) tubes containing pure H_2O vapor were excited by 50-cycle potentials, using external sleeve electrodes; the current structure was investigated by a DuMont cathode-ray oscillograph. The accompanying pair of oscillograms represent a typical group selected out of numerous ones obtained over a wide range of pressure p and applied potential V. Above the "threshold potential" V_m, at which the discharge attained a self-maintained nature, there appeared a few pulses on the otherwise smooth sinusoidal current trace; their number increased markedly with p and V. They were of two types: (a) longer pulses produced presumably due to large number of avalanches created by fast moving electrons emitted from the cathode by γ and $\eta\theta g$ processes,[2,3] and (b) shorter pulses due to avalanches yielded by electrons generated in the vicinity of the cathode by other β processes.[2,3] It was noticed that irradiation diminished the heights of (a) and enhanced the number of (b); (*cf.* the action of transverse magnetic field was to reduce the heights of (b) only).[4] Similar results were recorded in iodine vapor.[5] Under light, the pulses were remarkably of the same height (Fig. 1) as in the well-known Geiger (not self-maintained) region[6]

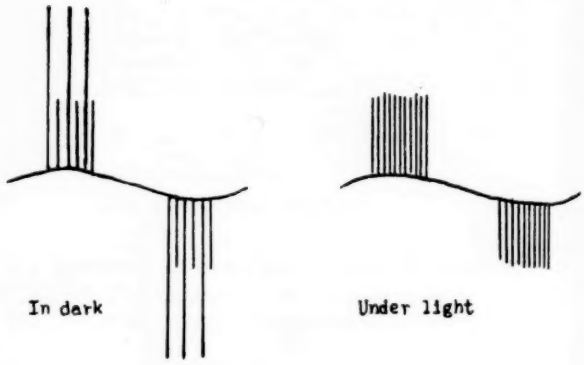

FIG. 1. Current structure in dark and under light (p_{H_2O} = 13.5 mm Hg, 28°C, 1.21 kv).

in which Townsend α-mechanism was but operative. This suggested that the secondary emission from the cathode responsible for the maintenance of the discharge was inhibited by light to give $-\Delta i$; and that the (simultaneous) increase of the number of shorter pulses constituted the positive *effect* $+\Delta i$. When the rms value of i was observed by current detectors like ac microammeter, vacuo-junction, etc., the resultant, $+\Delta i$ or $-\Delta i$ whichever predominated, was noticed.[7,8]

These findings follow from a mechanism suggested simultaneously by Harries and Engel[9] and by one of us[10] (N.A.R.) that surface molecules held by van der Waals forces dissociate under light to yield electronegative atoms or/and radicals which reduce the secondary emission to give $-\Delta i$. The positive *effect* $+\Delta i$ is the result of photo-ionization of pre-excited gas particles in the neighborhood of (and/or on) the cathode.[10]

Grateful thanks are due Professor Joshi of Benares Hindu University for his kind interest in our work.

[1] Joshi, Presidential Address, Proc. Ind. Sci. Congress, Chemical Section (1943).
[2] Loeb, *Fundamental Processes in Electrical Discharge in Gasses* (John Willey & Sons, Inc., New York, 1939); Revs. Modern Phys. **8**, 256 (1936).
[3] Townsend, "Electrons in Gases," Hutchinson's Sci. & Tech. Publications (1947).
[4] Ramaiah, unpublished results.
[5] Jatar, Jour. Sci. Ind. Res. **9B**, 283 (1950).
[6] Korff, *Electrons and Nuclear Counters* (D. Van Nostrand Company, Inc., New York, 1948).
[7] Joshi, Proc. Ind. Sci. Congress, Physical Section, Abstract 25 (1947).
[8] Ramaiah, J. Phys. Chem. **52**, 218 (1952).
[9] Harries and Engel, J. Chem. Phys. **19**, 514 (1951); Proc. Phys. Soc. (London) **64B**, 916 (1951).
[10] Ramaiah, J. Sci. Ind. Res. **10A**, 182 (1951).

Growth of Zinc Sulfide Single Crystals

WM. W. PIPER
General Electric Research Laboratory, Schenectady, New York
(Received May 22, 1952)

PREPARATION of microcrystalline zinc sulfide powder phosphors has long been a well-established art. Bube[1] and others have grown zinc sulfide crystals by a vapor reaction of hydrogen sulfide and zinc. Reynolds and Czyzak[2] have grown single crystals on top of chemically pure grade zinc sulfide powder in a hydrogen sulfide atmosphere.

Report is made here of single crystals grown on a quartz wall from the vapor phase. Pure zinc sulfide single crystals as well as ones incorporating small amounts of copper or silver in the lattice have been grown. The size of the crystals range up to 5 mm in length and 3 mm² in cross section.

The furnace is shown in Fig. 1. A ceramic tube is wound with a tapped platinum ribbon and properly insulated on the outside. Inside the tube two nickel sleeves are suspended with ceramic plugs. A constant flow of nitrogen through the furnace prevents the nickel from oxidizing. Adjustment of the current in various sections of the winding permits independent control of the temperature of each of the sleeves.

Suspended inside the sleeves is an evacuated, sealed quartz bulb containing luminescence-pure zinc sulfide. If a phosphor is desired, a small amount of copper or silver nitrate can be added. Maintaining the lower nickel sleeve at 1170°C to 1200°C allows the powder to vaporize at a reasonable rate. The seeding and growing of single crystals at the top of the bulb depends rather sensitively on the temperature of the quartz walls. The proper temperature varies with the impurities present in the zinc sulfide. The upper nickel sleeve is held at the proper temperature in a range from 1070°C to 1120°C. A single crystal is able to grow about 5 mg/day under favorable conditions. The crystals are essentially wurtzite although crystallographic analysis reveals some disorder in the stacking sequence of the planes perpendicular to the C axis. The fundamental optical absorption edge is at (3.67 ± 0.03) ev.

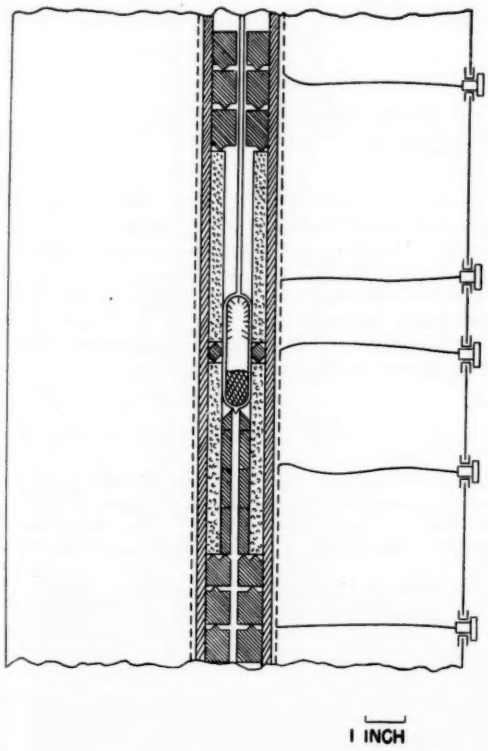

FIG. 1. Cross section of furnace used for growing single crystals of zinc sulfide.

I wish to thank Dr. P. D. Johnson and Dr. J. S. Prener for aid in the early stages of this work, Dr. W. L. Roth for crystallographic analyses, and Dr. F. J. Studer and Miss Gwen Lloyd for absorption measurements.

[1] Richard H. Bube, Phys. Rev. **83**, 393 (1951).
[2] D. C. Reynolds and S. J. Czyzak, Phys. Rev. **79**, 543 (1950).

The Stability of Semiquinones

N. S. HUSH
Department of Physical Chemistry, The University, Manchester, England
(Received May 23, 1952)

IT is well-established that variations in total energy change in reactions of the type

$$\text{quinone}+H_2\rightarrow\text{hydroquinone}$$

over a wide range of quinone/hydroquinone systems are due almost entirely to variations in the change of unsaturation energy accompanying the reduction.[1] Little is as yet known experimentally about the energetics of the separate one-electron steps

$$Q+\tfrac{1}{2}H_2\rightarrow QH,$$
$$QH+\tfrac{1}{2}H_2\rightarrow QH_2,$$

(where Q, QH, and QH_2 are quinone, semiquinone, and hydroquinone, respectively) which together constitute the over-all reaction. It appears, however, that in unsubstituted quinone/hydroquinone systems appreciable concentrations of the semiquinone QH exist in equilibrium with quinone and hydroquinone only when the over-all oxidation potential is low (e.g., 9:10-anthraquinones).[2]

Examination of the change in unsaturation energy accompanying the dismutation reaction

$$2QH\rightarrow Q+QH_2 \qquad \text{(a)}$$

in terms of LCAO MO and perturbation theory suggests that this is indicative of a general trend. Let us take as example the simplest case, where Q and QH_2 are *p*-benzoquinone and *p*-benzohydroquinone, respectively. Q, QH, and QH_2 are isoelectronic with the hydrocarbons benzoquinonedimethane (QDM), and the monocarbanion (MCA) and dicarbanion (DCA) obtained by placing one or two electrons, respectively, in the lowest unoccupied orbital of the dimethane:

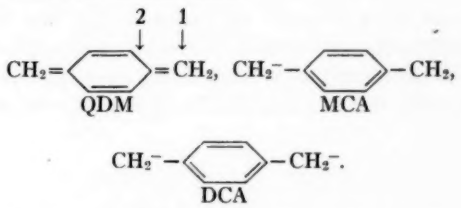

The change in unsaturation energy $\Delta\epsilon'$ for the dismutation reaction analogous to (a) of the hydrocarbon molecules, i.e.,

$$2(\text{MCA})\rightarrow\text{QDM}+\text{DCA}, \qquad \text{(a')}$$

is $\Delta\epsilon'=\epsilon'_{\text{QDM}}+\epsilon'_{\text{DCA}}-2\epsilon'_{\text{MCA}}$, and to the approximation of the LCAO treatment, $\Delta\epsilon'$ is clearly zero. The energies ϵ of the oxygen-containing molecules can, to first-order approximation, be written as[3]

$$\epsilon=\epsilon'+\Sigma_r\, q_r\delta\alpha_r+2\Sigma\Sigma_{r<s}\, p_{rs}\delta\beta_{rs},$$

where ϵ' is the energy, q_r is the π-electron density at atom r, p_{rs} is the mobile order of the $r-s$ bond in the isoelectronic hydrocarbon, and $\delta\alpha_r$ is the difference in Coulomb integral of the

TABLE I. The values of $\Delta\epsilon_{\text{dism.}}$ in the last column are calculated on the assumption that $(\underset{H}{\beta_{OC}}-\beta_{OC}) \approx (\underset{H}{\alpha_O}-\alpha_O) \approx \beta_{CC}$.

System	$c_1^* c_2^*$ [a]	(q_1-1)[a]	$E_0(r)$	$\Delta\epsilon_{\text{dism.}}$ $(\times 1/\beta_{CC})$
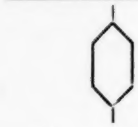	−0.1034	0.665	0.715	0.25
	−0.1105	0.614	0.484	0.17
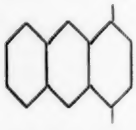	−0.1117	0.597	0.401	0.15
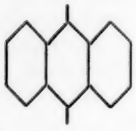	−0.1177	0.554	0.154	0.08

[a] Calculated from the AO coefficients listed by A. Pullman, G. Berthier, and B. Pullman, Bull. Soc. Chim. 450 (1948).

perturbed atom r and atom r in the hydrocarbon, and $\delta\beta_{rs}$ is the difference in resonance integral for atoms r and s.

We shall consider here only alternant molecules and the effects of perturbation only of the Coulomb integral of the extracyclic atoms (1) and of the CC resonance integral between this atom and the ring carbon atom (2) to which it is bonded. It follows immediately that the change of unsaturation energy in the dismutation reaction (a) is, to this approximation,

$$\Delta\epsilon_{\text{dism.}} = 4c_1^* c_2^* (\underset{H}{\beta_{OC}}-\beta_{OC}) + (q_1-1)(\underset{H}{\alpha_O}-\alpha_O), \qquad (1)$$

where c_1^* and c_2^* are the AO coefficients of the lowest unoccupied MO in the quinonedimethane at atoms 1 and 2 and q_1 is the π electron density at atom 1 in the dicarbanion. Equation (1) is a general one, and values of the relevant terms, together with the oxidation-reduction potentials E_0, are shown for some representative systems in Table I.

The main term in Eq. (1) is that in q_1; it is seen that the variation in $c_1^* c_2^*$ is small compared to that in q_1 over this range of molecules. An idea of the magnitude of $(\underset{H}{\alpha_O}-\alpha_O)$ can be obtained from the differences in ionization potential[4] of alcohols (~250 kcal) and of acetone and acetaldehyde (~235 kcal), i.e., 0.7 β_{CC} where β_{CC} is given the usual value 20 kcal/mole. The important point is that, on the reasonable assumption that $(\underset{H}{\alpha_O} > \alpha_O)$, decrease in q_1 leads to increase in stability of the semiquinone relative to quinone and hydroquinone, i.e., to increase in semiquinone formation constant. But as seen from Table I, in these typical systems decrease in q_1 is invariably accompanied by decrease in E_0, the oxidation-reduction potential of the system, so that a steady increase in semiquinone formation constant with decrease in over-all oxidation potential will be expected. As a rough indication of the effect, values of $\Delta\epsilon_{\text{dism.}}$ have been calculated on the assumption that $(\underset{H}{\beta_{OC}}-\beta_{OC}) \approx (\underset{H}{\alpha_O}-\alpha_O) \approx \beta_{CC}$.

This suggests the generalization that in a series of quinone/hydroquinone systems of this type, there is a general tendency for increase in stability of the semiquinone relative to quinone and hydroquinone with decrease in over-all oxidation potential.

[1] M. G. Evans, Trans. Faraday Soc. **42**, 113 (1946); M. Diatkina and J. Syrkin, Acta Physiochim. U.R.S.S. **21**, 921 (1946); M. G. Evans and J. de Heer, Quart. Rev. Chem. Soc. **4**, 94 (1950).
[2] Geake and Lemon, Trans. Faraday Soc. **34**, 1409 (1938).
[3] C. A. Coulson and H. C. Longuet-Higgins, Proc. Roy. Soc. (London) **A191**, 39 (1947).
[4] Diatkina and Syrkin, *Structure of Molecules* (Butterworth, Inc., London, 1950), p. 265.

Preliminary Announcement of the Tenth Annual Pittsburgh Diffraction Conference

THE Tenth Annual Pittsburgh Diffraction Conference will be held at Mellon Institute of Industrial Research, Pittsburgh 13, Pennsylvania, on November 6 and 7, 1952. Technical sessions are being arranged on *Instrumentation and Methods*, *Neutron Diffraction and General Diffraction Studies*. Contributed papers on these and related subjects will be considered in the order in which they are received. Titles should be submitted to the Program Chairman, Mr. R. K. Scott, Hall Laboratories, Inc., Box 1346, Pittsburgh 30, Pennsylvania, before September 1, 1952.

This year's conference will include a symposium of invited papers in the field of *Order-Disorder Studies*.

For further information, and for a copy of the preliminary program when available, write to Mr. E. E. Wicker, U. S. Steel Company, Research and Development Laboratory, 234 Atwood Street, Pittsburgh 13, Pennsylvania.